

PROCEEDINGS OF THE NINTH INTERNATIONAL SYMPOSIUM ON ARTIFICIAL LIFE AND ROBOTICS

(AROB 9th '04)

Vol.2

Jan. 28-Jan. 30, 2004
B-Con Plaza, Beppu, Oita, JAPAN

Supported by · Ministry of Education, Culture, Sports, Science and Technology, Japanese Government (MEXT)
· Air Force Office of Scientific Research, Asian Office of Aerospace Research and Development (AFOSR/AOARD)

Editors : Masanori Sugisaka and Hiroshi Tanaka
ISBN4-9900462-4-2

Proceedings of The Ninth International Symposium on

ARTIFICIAL LIFE AND ROBOTICS

(AROB 9th '04)

January 28-30, 2004
B-Con Plaza, Beppu, Oita, Japan

Editors: Masanori Sugisaka and Hiroshi Tanaka

THE NINTH INTERNATIONAL SYMPOSIUM ON ARTIFICIAL LIFE AND ROBOTICS

(AROB 9th '04)

ORGANIZED BY

Organizing Committee of International Symposium on Artificial Life and Robotics (Department of Electrical and Electronic Engineering, Oita University, Japan)

CO-SPONSORED BY

Santa Fe Institute (SFI, USA)
The Society of Instrument and Control Engineers (SICE, Japan)
The Robotics Society of Japan (RSJ, Japan)
The Institute of Electrical Engineers of Japan (IEEJ, Japan)
Institute of Control, Automation and Systems Engineers (ICASE, Korea)
Chinese Association for Artificial Intelligence (CAAI, China)

COOPERATED BY

The Institute of Systems, Control and Information Engineers (ISCIE)
The Institute of Electronics, Information and Communication Engineers (IEICE)
The Institute of Electrical and Electronics Engineers, Inc.(IEEE Japan Council)
Japan Robot Association (JARA)

SUPPORTED BY

Ministry of Education, Culture, Sports, Science and Technology, Japanese Government (MEXT)
Air Force Office of Scientific Research, Asian Office of Aerospace Research and Development (AFOSR/AOARD)
ISAHAYA ELECTRONICS CORPORATION
MITSUBISHI ELECTRIC CORPORATION ADVANCED TECHNOLOGY R&D CENTER
OITA GAS CO., LTD.
STK TECHNOLOGY CO., LTD.
SANWA SHURUI Co., Ltd.
YATSUSHIKA BREWERY CO., LTD.
Kyushu Bureau of Economy, Trade and Industry, Ministry of Economy, Trade and Industry
OITA PREFECTURE
OITA CITY
Beppu City
The Federation of the Chamber of Commerce and Industry in Oita Prefecture
The Oita Prefectural Organization of the Industrial Groups

KYODO NEWS
JIJI PRESS
OITA GODO SHIMBUNSYA
The Asahi shimbun Company
The Mainichi Newspapers Co.
THE YOMIURI SHIMBUN
The Nishinippon Newspaper Co.
THE NIKKAN KOGYO SHIMBUN, LTD.
Nihon Keizai Shimbun, INC.,
NHK Oita Station
Oita Broadcasting System
Television Oita System
Oita Asahi Broadcasting Co. Ltd.
Oita System Control Research Society

ADVISORY COMMITTE CHAIRMAN

F.Harashima (Tokyo Denki University, Japan)

GENERAL CHAIRMAN

M.Sugisaka (Oita University, Japan)

CO-GENERAL CHAIRMAN (PROGRAM)

H.Tanaka (Tokyo Medical & Dental University, Japan)

CO-CHAIRMAN

J.L.Casti (Santa Fe Institute, USA)

ADVISORY COMMITTEE

F.Harashima (Tokyo Denki University, Japan)
H.Kimura (The University of Tokyo, Japan)
T.Fukuda (Nagoya University, Japan)
S.Ueno (Kyoto University, Japan)
M.Tomizuka(University of California at Berkeley, USA)

INTERNATIONAL ORGANIZING COMMITTEE

K.Aihara (The University of Tokyo, Japan)
W.B.Arthur (Santa Fe Institute, USA)
W.Banzhaf (University of Dortmund, Germany)
C.Barrett (Los Alamos National Laboratory, USA)
M.Bedau (Reed College, USA)
Z.Bubnicki (Wroclaw University of Technology, Poland)
J.L.Casti (Santa Fe Institute, USA)
H.S.Cho (KAIST, Korea)
J.M.Epstein (The Brookings Institution, USA)
T.Fukuda (Nagoya University, Japan)
H.Hashimoto (The University of Tokyo, Japan)

D.J.G.James (Coventry University, UK)
S.Kauffman (Santa Fe Institute, USA)
C.G.Langton (Santa Fe Institute, USA)
M.H.Lee (Pusan National University, Korea)
J.J.Lee (KAIST, Korea)
M.Nakamura (Saga University, Japan)
G.Obinata (Nagoya University, Japan)
S.Rasmussen (Santa Fe Institute, USA)
T.S.Ray (University of Oklahoma, USA)
M.Sugisaka (Oita University, Japan) (Chairman)
H.Tanaka (Tokyo Medical & Dental University, Japan)
C.Taylor (University of California-Los Angeles, USA)
K.Tsuchiya (Kyoto University, Japan)
G.Wang (Tsinghua University, China)
W.R.Wells (University of Nevada-Las Vegas, USA)
Y.G.Zhang (Academia Sinica, China)

INTERNATIONAL PROGRAM COMMITTEE

K.Abe (Tohoku University, Japan)
K.Aihara (The University of Tokyo, Japan) (Co-chairman)
T.Arita (Nagoya University, Japan)
H.Asama (The University of Tokyo, Japan)
M.Bedau (Reed College, USA)
R.Belew (University of California-San Diego, USA)
Z.Bubnicki (Wroclaw University of Technology, Poland)
T.Christaller (Fraunhofer Institute for Autonomous intelligent Systems-AiS)
C.S.Han (Hanyang University, Korea)
I.Harvey (University of Sussex, UK)
H.Hashimoto (The University of Tokyo, Japan)(Co-chairman)
K.Hirasawa (Waseda University, Japan)
H.Hirayama (Asahikawa Medical College, Japan)
N.Honma (Tohoku University, Japan)
T.Ikegami (The University of Tokyo, Japan)
H.Inooka (Tohoku University, Japan)
K.Ito (Tokyo Institute of Technology, Japan)
J.Johnson (The Open University, UK)
Y.Kakazu (Hokkaido University, Japan)
O.Katai (Kyoto University, Japan)
S.Kawaji (Kumamoto University, Japan)
S.Kawata (Tokyo Metropolitan University, Japan)
S.Kitamura (Kobe University, Japan)
T.Kitazoe (University of Miyazaki, Japan)
S.Kumagai (Osaka University, Japan)
J.M.Lee (Pusan National University, Korea)
C.G.Looney (University of Nevada-Reno, USA)
H.H.Lund (University of Southern Denmark, Denmark)
M.Nakamura (Saga University, Japan)
R.Nakatsu (KWANSEI GAKUIN University, Japan)
S.Omatu (Osaka Prefecture University, Japan)

M.Okamoto (Kyushu University, Japan)
R.Pfeifer (University of Zurich-Irchel, Switzerland)
T.S.Ray (University of Oklahoma, USA) (Co- chairman)
T.Sawaragi (Kyoto University, Japan)
T.Shibata (AIST, Japan)
K.Shimohara (ATR, Japan)
M.Sugisaka (Oita University, Japan)
H.Tanaka (Tokyo Medical & Dental University, Japan)
(Chairman)
M.Tanaka-Yamawaki (Tottori University, Japan)
N.Tosa (ATR, Japan)
K.Ueda (The University of Tokyo, Japan)
K.Uosaki (Osaka University, Japan)
H.Wakamatsu (Tokyo Medical & Dental University, Japan)
K.Watanabe (Saga University, Japan)
M.Yano (Tohoku University, Japan)

LOCAL ARRANGEMENT COMMITTEE

X.Feng (University of Singapore, Singapore)
A.Loukianov (Baikal State University of Economy & Law, Russia)
M.Rizon (Northern Malaysia University College of Engineering, Malaysia)
K.Shibata (Oita University, Japan)
M.Sugisaka (Oita University, Japan) (Chairman)
Y.Suzuki (Tokyo Medical & Dental University, Japan)
J.Wang (Oita University, Japan)
X.Wang (Oita Institute of Technology, Japan)

HISTORY

This symposium was founded in 1996 by the support of Science and International Affairs Bureau, Ministry of Education, Culture, Sports Science and Technology, Japanese Government. Since then, this symposium has been held every year at B-Con Plaza, Beppu, Oita, Japan except in Oita, Japan (AROB 5th '00) and in Tokyo, Japan (AROB 6th '01). The ninth symposium will be held on 28-30 January, 2004, at B-Con Plaza, Beppu, Oita, Japan. This symposium invites you all to discuss development of new technologies concerning Artificial Life and Robotics based on simulation and hardware in the twenty first century.

OBJECTIVE

The objective of this symposium is the development of new technologies for artificial life and robotics which have been recently born in Japan and are expected to be applied in various fields. This symposium will discuss new results in the field of artificial life and robotics.

TOPICS

Artificial brain research
Artificial intelligence
Artificial life
Artificial living
Artificial mind research
Bioinformatics chaos
Brain science
Cognitive science evolutionary computations
Complexity
Computer graphics
DNA computing
Fuzzy control
Genetic algorithms
Human-machine cooperative systems
Human-welfare robotics
Innovative computations
Intelligent control and modeling
Micromachines
Micro-robot world cup soccer tournament
Mobile vehicles
Molecular biology
Multi-agent systems
Nano-biology
Nano-robotics
Neural networks
Neurocomputers
Neurocomputing technologies and its application for hardware
Pattern recognition
Robotics
Robust virtual engineering
Virtual reality

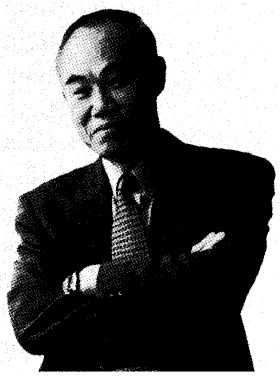
COPYRIGHTS

Accepted papers will be published in the proceeding of AROB and some of high quality papers in the proceeding will be requested to re-submit fir the consideration o publication in an international journal ARTIFICIAL LIFE AND ROBOTICS (Springer) and APPLIED MATHEMATICS AND COMPUTATION (North-Holland). All correspondence related to the symposium should be addressed to AROB Secretariat

Dept. of Electrical and Electronic Engineering,
Oita University
700 Dannoharu, Oita 870-1192, JAPAN
TEL : +81-97-554-7841, FAX : +81-97-554-7818
E-MAIL arobsecr@cc.oita-u.ac.jp
Home Page http://arob.cc.oita-u.ac.jp/

MESSAGE

Masanori Sugisaka
General Chairman of AROB
(Professor, Oita University)



It is my great honor to invite you all to the upcoming International Symposium on Artificial Life and Robotics. The first symposium was held in February (18-20) 1996, B-Con Plaza, Beppu, Oita, Japan. That symposium was organized by Oita University under the sponsorship of the Japanese Ministry of Education, Science, Sports, and Culture (Monbusho), and co-sponsored by Santa Fe Institute (USA), SICE, RSJ, and IEEJ, (Japan). I would like to express my sincere thanks to the Science and Technology Policy Bureau, Ministry of Education, Culture, Sports, Science and Technology (Monkasho), Japanese Government, for their repeated support.
This symposium is supported by Monkasho, Air Force Office of Scientific Research, Asian Office of Aerospace Research and Development (AFOSR/AOARD) and other institutions. The symposium invites you to discuss the development of new technologies in the 21st century, concerning Artificial Life and Robotics, based on simulation and hardware.

We hope that AROB will facilitate the establishment of an international joint research institute on Artificial Life and Robotics. I hope that you will obtain fruitful results from the exchange of ideas during the symposium.

Masanori Sugisaka
M. Sugisaka

December 20, 2003

MESSAGE

Hiroshi Tanaka
Program chairman of AROB
(Professor, Tokyo Medical and Dental University)



On behalf of the program committee, it is truly my great honor to invite you all to the Ninth International Symposium on Artificial Life and Robotics (AROB 9th '04). This symposium is made possible owing to the cooperation of Oita University and Santa Fe Institute. We are also debt to Japanese academic associations such as SICE, RSJ, and several private companies. I would like to express my sincere thanks to all of those who make this symposium possible.

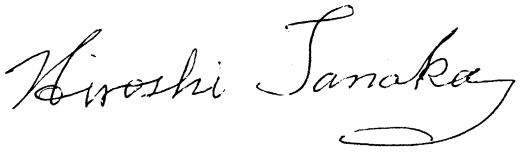
As is needless to say, the complex systems or Alife approach now attracts wide interests as a new paradigm of science and engineering. Take an example in the field of bioscience. The accomplishment of HGP (Human Genome Project) has published the special issue of Nature, and HGP (Human Genome Project), vast amount of genome information brings about not only from human genome but also various species like several bacterias, yeast, warm, fly. However, as a plenty of genome data becomes available, it becomes sincerely recognized that the framework by which these genome data can be understood to make a whole picture of life is critically need thus, in the "post genomic era , the complex systems or Alife approach is now actually expected to be an efficient methodology to integrate this vast amount of data.

This example shows the complex system approach is very promising and becomes widely accepted as a paradigm of next generation of science and engineering. We hope this symposium becomes a forum for exchange of the ideas of the attendants from various fields who are interested in the future possibility of complex systems approach.

I am looking forward to meeting you in Beppu, Oita.

H. Tanaka

December 20, 2003



TIME TABLE

	RoomA	RoomB	RoomC	RoomD
1/27(Tue) 8:00				
13:00	Registration (Registration Desk)			
17:30	Welcome Party (in Hotel Arthur 10th Floor)			
1/28(Wed.) 8:00	Registration (Registration Desk)			
9:00	IPS (4) Chair: J. Wang	IS1 (5) Chair: T. Yamamoto	GS1(6) Chair: P. Sapaty	
10:30	Coffee Break			
10:40				Opening Ceremony
11:00				Plenary Talk Chair J. Johnson PT1 H. H. Lund
12:00	Lunch			
13:00	GS19 (6) Chair: J. Casti	GS13 (5) Chair: W. Wells	IS8 (6) Chair: M. Kono	
14:30	GS9 (4) Chair: M. Rizon	GS24 (4) Chair: J. Johnson	GS6 (4) Chair: H. H. Lund	
15:30	Coffee Break			
15:45	GS4 (6) Chair: C. Tayor	GS21 (7) Chair: D. J. G. James	IS7 (6) Chair: J. M. Lee	
17:30				

GS: General Session IS: Invited Session IPS: Invited Professor's Session PS Poster Session

GS1 Artificial Brain -I
GS2 Artificial Brain- II
GS3 Artificial Intelligence
GS4 Artificial Life-I
GS5 Artificial Life- II
GS6 Artificial Living
GS7 Bioinformatics
GS8 Cognitive Science
GS9 Computer Graphics
GS10 Evolutionary Computations-I
GS11 Evolutionary Computations - II
GS12 Genetic Algorithms
GS13 Human-Machine Cooperative System
GS14 Intelligent Control and Modeling-I
GS15 Intelligent Control and Modeling- II
GS16 Intelligent Control and Modeling- III
GS17 Micro-Robot World Cup-Soccer Tournament
GS18 Molecular Biology-I
GS19 Mobile Vehicles-I
GS20 Mobile Vehicles- II
GS21 Neural Networks
GS22 Robotics-I
GS23 Robotics- II
GS24 Robotics- III
IS1 Soft Robotics and Intelligence
IS2 Artificial and Natural Adaptions
IS3 Biological Information Processing and Control
IS4 Biomimetic Machines and Their Applications
IS5 Intelligent Pattern Classification
IS6 Intelligent Information Retrieval
IS7 Intelligent Mobile Robot
IS8 Computer Vision and Distributed Control Systems
IS9 Molecular Biology- II
IPS Invited Professor's Session
PS Poster Session

	RoomA	RoomB	RoomC	RoomD
1/29(Thu.) 8:00	Registration (Registration Desk)			
9:00	GS12(6) Chair: Y. G. Zhang	GS22 (5) Chair: C. Zhang	GS20 (6) Chair: J. M. Lee	
10:00				
10:30	Coffee Break			
11:00				Plenary Talk Chair D. J. G. James PT2 R. Pfeifer
12:00	Lunch			
13:00	PS (3)	IS3 (5) Chair: K. Abe	IS2 (5) Chair: K. Naitoh	
14:15	Coffee Break			
14:30	GS8 (6) Chair: K. B. Sim	GS14 (5) Chair: Z. Bubnicki	IS5 (4) Chair: S. Omatu	
15:45		GS5 (6) Chair: H. Kashiwagi	GS23 (7) Chair: T. Kubik	
16:00	GS10 (5) Chair: L. Han			
17:30				
18:00	AROB Award Ceremony (Chair: K. Watanabe) Banquet (Hotel Shiragiku)			
20:30				

GS: General Session IS: Invited Session IPS: Invited Professor's Session PS Poster Session

GS1 Artificial Brain-I
GS2 Artificial Brain-II
GS3 Artificial Intelligence
GS4 Artificial Life-I
GS5 Artificial Life-II
GS6 Artificial Living
GS7 Bioinformatics
GS8 Cognitive Science
GS9 Computer Graphics
GS10 Evolutionary Computations-I
GS11 Evolutionary Computations -II
GS12 Genetic Algorithms
GS13 Human-Machine Cooperative System
GS14 Intelligent Control and Modeling-I
GS15 Intelligent Control and Modeling-II
GS16 Intelligent Control and Modeling-III
GS17 Micro-Robot World Cup-Soccer Tournament
GS18 Molecular Biology-I
GS19 Mobile Vehicles-I
GS20 Mobile Vehicles-II
GS21 Neural Networks
GS22 Robotics-I
GS23 Robotics-II
GS24 Robotics-III
IS1 Soft Robotics and Intelligence
IS2 Artificial and Natural Adaptions
IS3 Biological Information Processing and Control
IS4 Biomimetic Machines and Their Applications
IS5 Intelligent Pattern Classification
IS6 Intelligent Information Retrieval
IS7 Intelligent Mobile Robot
IS8 Computer Vision and Distributed Control Systems
IS9 Molecular Biology-II
IPS Invited Professor's Session
PS Poster Session

	RoomA	RoomB	RoomC	RoomD
1/30(Fri.) 8:00	Registration (Registration Desk)			
9:00	GS15 (6) Chair: E. Hayashi	GS3 (5) Chair: T. Yamamoto	GS11 (4) Chair: H. Tanaka	
10:30	Coffee Break			
10:45	IS4 (5) Chair: K. Watanabe	GS2 (4) Chair: T. Arita	IS9 (4) Chair: K. Ohnishi	
12:00	Lunch			
13:00	GS18 (4) Chair: H. Hirayama	GS17 (3) Chair: M. Tanaka-Yamawaki	IS6 (4) Chair: H. Yanagimoto	
14:00	GS7 (4) Chair: K. Uosaki	GS16 (5) Chair: K. Watanabe		
15:15				
15:30	Farewell Party (Room A)			
16:30				

GS: General Session IS: Invited Session IPS: Invited Professor's Session PS Poster Session

GS1 Artificial Brain-I
GS2 Artificial Brain- II
GS3 Artificial Intelligence
GS4 Artificial Life-I
GS5 Artificial Life- II
GS6 Artificial Living
GS7 Bioinformatics
GS8 Cognitive Science
GS9 Computer Graphics
GS10 Evolutionary Computations-I
GS11 Evolutionary Computations - II
GS12 Genetic Algorithms
GS13 Human-Machine Cooperative System
GS14 Intelligent Control and Modeling-I
GS15 Intelligent Control and Modeling- II
GS16 Intelligent Control and Modeling- III
GS17 Micro-Robot World Cup-Soccer Tournament
GS18 Molecular Biology-I
GS19 Mobile Vehicles-I
GS20 Mobile Vehicles- II
GS21 Neural Networks
GS22 Robotics-I
GS23 Robotics- II
GS24 Robotics- III
IS1 Soft Robotics and Intelligence
IS2 Artificial and Natural Adaptions
IS3 Biological Information Processing and Control
IS4 Biomimetic Machines and Their Applications
IS5 Intelligent Pattern Classification
IS6 Intelligent Information Retrieval
IS7 Intelligent Mobile Robot
IS8 Computer Vision and Distributed Control Systems
IS9 Molecular Biology- II
IPS Invited Professor's Session
PS Poster Session

TECHNICAL PAPER INDEX

January 28 (Wednesday)

Room D

11:00~12:00 PT-1 Plenary Talk1
Chair J. Johnson

PT-1 *Re-configurable Robotic Artefacts for Cognitive Rehabilitation and Contextualised Development*
H. H. Lund (University of Southern Denmark, Denmark)

*This talk is a combination of two below papers:
Educational robotics : Manipulative technologies for cognitive rehabilitation ……I-1
H. H. Lund (University of Southern Denmark, Denmark)
P. Marti, V. Palma (University of Siena, Italy)
I-Blocks in an African context ……I-7
H. H. Lund (University of Southern Denmark, Denmark)
M. Vesisenaho (University of Joensuu, Finland)

January 29 (Thursday)

11:00~12:00 PT-2 Plenary Talk2
Chair D. J. G. James

PT-2 *Interacting with the real world - design principles for intelligent systems* ……I-13
R. Pfeifer (University of Zurich, Switzerland, University of Tokyo, Japan)

January 28 (Wednesday)

Room A

9:00~10:30 IPS Invited Professor's Session
Chair: J. Wang (Oita University, Japan)

IPS-1 *Why the future happens* ……I-19
J. L. Casti (Santa Fe Institute, USA)

IPS-2 *Micro-/Nanorobotic system* ……I-24
T. Fukuda, F. Arai, L. Dong (Nagoya University, Japan)

IPS-3 *A mode to create artificial intelligence--from knowledge to intelligence* ……I-28
Y. G. Zhang (Academia Sinica, P.R.China)
M. Sugisaka (Oita University, Japan)

IPS-4 *Robotics in the emergence of complexity science* ……I-32
J. Johnson, P. Iravani (The Open University, UK)

13:00~14:30 GS19 Mobile Vehicles-I
Chair: J. Casti (Santa Fe Institute, USA)

GS19-1 *A navigation scheme for mobile robots using global and local path planning* ……1
G-H. Park, Y-K. Choi (Pusan National University, Korea)
J-H. Park (Jinju National University, Korea)

GS19-2 *Robust acceleration control of wheeled mobile robot moving on rough surface* ……5
M. Wada, M. Oya, H. Honda. T. Kobayashi, H. Ohkawa (Kyushu Institute of Technology, Japan)

GS19-3 *The design of a real-time, multiagent system for controlling distributed devices in an autonomous robot system* ……9
M. Obayashi, H. Nishiyama, F. Mizoguchi (Tokyo University of Science, Japan)

GS19-4 *State observer - Based robust control scheme for wheeled mobile robots* ……13
M. Oya, K. Higashi, M. Wada, T. Kobayashi (Kyushu Institute of Technology, Japan)

GS19-5 *Estimation of vehicle cornering stiffness of using GPS/INS* ……17
M-K. Lee, G. Park, Y-S. Chang, S. Hong, M-H. Lee (Pusan National University, Korea)

GS19-6 *The application of a robot for the construction of curtain wall in a high building* ……21
S-Y. Lee, B-S. Ko, C-S. Han (Hanyang University, Korea)
K-Y. Lee, S-H. Lee (Samsung Corporation, Korea)

14:30~15:30 GS9 Computer Graphics
Chair: M. Rizon (Northern Malaysia University College of Engineering, Malaysia)

GS9-1 *Fingerprint classification method using measurement of ridge energy changes* ……25
K-B. Yoon (Kimpo College, Korea)
C-H. Park (Yonsei University, Korea)

GS9-2 *Generating a virtual human model for a mixed reality space* ……29
I. Yamaguchi, J. K. Tan, S. Ishikawa (Kyushu Institute of Technology, Japan)

GS9-3 *In-vitro experimental results of real-time visual servoing for the laparoscope manipulator* ……33
J-S. Heo, M-S. Kim, Jung-Ju Lee (Korea Advanced Institute of Science and Technology, Korea)

GS9-4 *An efficient fully automatic face tracking using binary template matching* ……37
K-H. An, D-H. Yoo, M-J. Chung (KAIST, Korea)

15:45~17:30 GS4 Artificial Life-I
Chair: C. Tayor (University of California, Los Angels, USA)

GS4-1 *Nonparametric method for nonlinear system identification* ……41
H. Kashiwagi (Kumamoto University, Japan)
Y. Li (University of Glasgow, UK)

GS4-2 *Modelling artificial life by attributed eco-array grammars* ……45
R. Freund, M. Oswald, A. Binder (Vienna University of Technology, Austria)

GS4-3 *Multilayered Discourse in Hyper-comic* ……49
Y. Endo, T. Ogata (Yamanashi University, Japan)

GS4-4 *Implications of the ability to learn simple actions on the efficiency of evolution of social behavior of agents* ……53
I. Tanev (ATR Human Information Science Laboratories, Japan)
K. Shimohara (ATR Human Information Science Laboratories, Kyoto University, Japan)

GS4-5 *An immunity-based approach towards a synthesis of artificial organisms* ……57
T. Mori, Y. Ishida (Toyohashi University of Technology, Japan)

GS4-6 *Fault-tolerance in biological systems simulated on asynchronous cellular automata* ……61
F. Peper (Communications Research Laboratory, Himeji Institute of Technology, Japan)
T. Isokawa, F. Abo, N. Matsui (Himeji Institute of Technology, Japan)
J. Lee, S. Adachi, S. Mashiko (Communications Research Laboratory, Japan)

Room B

9:00~10:30 IS1 Soft Robotics and Intelligence
Chair: T. Yamamoto (University of the Ryukyus, Japan)
Co-Chair: K. Yamada (University of the Ryukyus, Japan)

IS1-1 *A study of a parallelized immune co-evolutionary algorithm for division-of-labor problems* ……67
N. Toma, S. Endo, K. Yamada (University of the Ryukyus, Japan)

IS1-2 *Information separation of position and direction of a robot by two interacting Self-Organizing Maps* ……71
N. Oshiro, K. Kurata (University of the Ryukyus, Japan)

IS1-3 *System identification using dynamical neural network with GA-based training* ……75
K. Nakazono, H. Kinjo (University of the Ryukyus, Japan)
K. Ohnishi (Keio University, Japan)

IS1-4 *Tracking and recognition of moving objects in a monocular image sequence based on visual characteristics* ……79
S. Odo (University of the Ryukyus, Okinawa University, Japan)
K. Hoshino (University of Tsukuba, Japan)
K. Yamada (University of the Ryukyus, Japan)

IS1-5 *Quantitative analysis of relationship between leg movements and subjective impressions in CG animation* ……83
S. Kamisato, S. Odo, K. Yamada, S. Tamaki (University of the Ryukyus, Japan)
K. Hoshino (University of Tsukuba, Japan)

13:00~14:30 GS13 Human-Machine Cooperative System
Chair: W. Wells (University of Nevada, Las Vegas, USA)

GS13-1 *Development of Vietnamese pronunciation training system by DP matching method* ……87
M-T. Nguyen (Tokyo Institute of Technology, Japan)
J. Murakami (Kumamoto National College of Technology, Japan)

GS13-2 *Fault diagnostic of induction motors for equipment reliability and health maintenance based upon fourier and wavelet analysis* ……91
H. Bae, Y-T. Kim, S-H. Lee, S-S. Kim, M-H. Lee (Pusan National University, Korea)

GS13-3 *Interactive musical editing system for supporting human errors and offering personal preferences for an automatic piano* ……95
E. Hayashi, Y. Takamatu (Kyushu Institute of Technology, Japan)
H. Mori (Apex Corporation, Japan)

GS13-4 *Developing potential robots to facilitate humanitarian demining: Challenges, needs and design requirements* ……99
M. K. Habib (Monash University Malaysia, Malaysia)

GS13-5 *Questionnaire results of subjective evaluation of seal robot at the Japan cultural institute in Rome, Italy* ……103
T. Shibata (National Institute of Advanced Industrial Science and Technology, PERESTO, JST, Japan)
K. Wada, K. Tanie (National Institute of Advanced Industrial Science and Technology, University of Tsukuba, Japan)

14:30~15:30 GS24 Robotics-Ⅲ
Chair: J. Johnson (The Open University, UK)

GS24-1 *Intelligent control system based on artificial life* ……107
X. Tu, Y. Yin, G. Zeng, X. Ban (University of Science and Technology Beijing, P.R.China)

GS24-2 *Evolution of a large-scale spiking neural network for robot navigation* ……111
M. Eaton, N. Jordan, J. J. Collins, M. Mansfield (University of Limerick, Ireland)

GS24-3 *High precision and predictive control for linear motor container transport system using DR-FNNs* ……115
J-W. Lee, S-K. Kim, K-S. Lee (Dong-A University, Korea)

GS24-4 *Evocation of robot behaviors based on the affordance of worksite objects* ……119
K. Tani, T. Kawamura (Gifu University, Japan)
H. Yamada (Toyota Industries Corporation, Japan)

15:45~17:30 GS21 Neural Networks
Chair: D. J. G. James (Coventry University, UK)

GS21-1 *Short-term memory circuit using hardware ring neural networks* ……123
N. Sasano, K. Saeki, Y. Sekine (Nihon University, Japan)

GS21-2 *Statistical learning based radial basis function networks for pattern classification* ……128
J-H. Choi (Kimpo College, Korea)
J-H. Lee (Inha University, Korea)
K-W. Rim (Sun Moon University, Korea)

GS21-3 *Evolution of hybrid neural networks using genetic network programming* ……132
D. Li, K. Wada (Kyushu University, Japan)
K. Hirasawa, J. Hu (Waseda University, Japan)

GS21-4 *Auditory evaluation experiments of Japanese vowel synthesized by using cascaded sand-glass type neural network* ……136
M. Kimoto, T. Shimizu, H. Yoshimura, K. Sugata, M. Tanaka (Tottori University, Japan)

GS21-5 *A neural network-based remote guidance interface for rescue robot* ……140
Z. Yang, K. Ito, K. Saijo, A. Gofuku (Okayama University, Japan)
F. Matsuno (University of Electro-Communications, Japan)

GS21-6 *Growing neural network with hidden neurons* ……144
R. Kurino, M. Sugisaka, K. Shibata (Oita University, Japan)

GS21-7 *Backpropagation algorithm for rice yield prediction* ……148
P. Saad, M. Rizon, N. Rusli (Northern Malaysia University College of Engineering, Malaysia)
N. Khairah, A. Bakri (University Technology Malaysia, Malaysia)
S. Sakira (Universiti Utara Malaysia, Malaysia)

Room C

9:00~10:30 GS1 Artificial Brain-I
Chair: P. Sapaty (National Academy of Ukraine, Ukraine)

GS1-1 *Study of artificial brain based on Multi-centrum Self-coordination mechanism* ……152
L. Han (Beijing Technology and Business University, P.R.China)
X. Tu (University of Science and Technology Beijing, P.R.China)

GS1-2 *Dynamic air traffic management using distributed brain concept* ……156
P. Sapaty, V. Klimenko (National Academy of Sciences, Ukraine)
M. Sugisaka (Oita University, Japan)

GS1-3 *Tierra sonification: An audio display system for Tierra* ……160
J. Hart (ATR Human Information Science Laboratories, Japan)
R. Berry (ATR Media Information Science Laboratories, Japan)

GS1-4 *Aspect of non-story processing and film rhetoric composition in the narrative generation mechanism* ……162
A. Kanai (Japan Society for the Promotion of Science, Yamanashi University, Japan)
T. Ogata (Yamanashi University, Japan)

GS1-5 *ATR artificial brain project: Key assumptions and current state* ……166
A. Buller, H. Hemmi, M. Joachimczak, J. Liu, K. Shimohara, A. Stefanski (ATR International, Human Information Science Laboratories, Japan)

GS1-6 *Narrative and music as variation: Transformation of musical structure based on narrative discourse theory* ……170
F. Kobayashi, T. Ogata (Yamanashi University, Japan)

13:00~14:30 IS8 Computer Vision and Distributed Control System
Chair: M. Kono (University of Miyazaki, Japan)
Co-Chair: M. Yokomichi (University of Miyazaki, Japan)

IS8-1 *Autonomous mobile cars on a highway controlled with neural networks* ……174
T. Uemura, T. Kai, T. Shinchi, M. Yokomichi, T. Kitazoe (University of Miyazaki, Japan)

IS8-2 *Stereo matching from color images based on self-organization neural networks* ……178
X. Hua, M. Yokomichi, M. Kono (University of Miyazaki, Japan)

IS8-3 *Stereo correspondence by SVM regression* ……182
H. Sugiyama, M. Yokomichi, X. Hua, M. Kono (University of Miyazaki, Japan)

IS8-4 *Edge detection and curvature calculation in the visual system* ……186
S. Niitsuma, K. Tokunaga (Shizuoka University, Japan)

IS8-5 *Three-dimensional multi-inkdot automata* ……190
T. Makino, H. Okabe, S. Taniguchi, M. Sakamoto (University of Miyazaki, Japan)
K. Inoue (Yamaguchi University, Japan)

IS8-6 *Stabilization of LTI systems with periodic communication constraints by using periodic Kalman filter* ……194
M. Kono, A. Kose, N. Takahashi (University of Miyazaki, Japan)

14:30~15:30 GS6 Artificial Living
Chair: H. H. Lund (University of Southern Denmark, Denmark)

GS6-1 *Design of human support system for smart assistance* ……198
H. Nishiyama, Y. Mine, W. Yamazaki, M. Obayashi, F. Mizoguchi (Tokyo University of Science, Japan)

GS6-2 *Dynamically separating learning algorithm for interactive computers in dynamic environment: Optimization of collective performance in networked computers* ……202
K. Nakayama, K. Shimohara (Kyoto University, ATR Human Information Science Laboratories, Japan)
O. Katai (Kyoto University, Japan)

GS6-3 *On a model of motion sickness induced by coriolis stimuli* ……207
N. Kitayama, M. Tanaka-Yamawaki (Tottori University, Japan)

GS6-4 *Flight control of insects* ……211
T. Ohmi, S. Kuroda (The University of Electro-Communications, Japan)
F. Tanaka (Tokyo University of Science, Japan)
K. Hirasawa (Fluid Technology Co., Ltd., Japan)

15:45~17:30 IS7 Intelligent Mobile Robot
Chair: J-M. Lee (Pusan National University, Korea)

IS7-1 *Environment reconstruction and navigation of a mobile robot using an active vision* ……216
T-S. Jin, J-M. Lee (Pusan National University, Korea)
J-W. Park (Institute of Information Technology Assessment, Korea)

IS7-2 *Trajectory estimation of a moving object using Kohonen Networks* ……221
S-J. Kim, J-H. Lee, J-M. Lee (Pusan National University, Korea)

IS7-3 *Cooperative behavior learning in distributed autonomous robotics system* ……225
C-M. Hwang, J-Y. Kim, D-W. Lee, K-B. Sim (Chung-Ang University, Korea)

IS7-4 *Fingerprint matching algorithm based on the artificial immune system* ……229
J-W. Jeong, T-H. Kim, D-W. Lee, K-B. Sim (Chung-Ang University, Korea)

IS7-5 *Optimal design of the 2-layer fuzzy controller with vision system* ……233
K-S. Byun, K-S. Heo, C-H. Park, K-B. Sim (Chung-Ang University, Korea)

IS7-6 *Discretization of Takagi-Sugeno fuzzy observer-based output-feedback control using intelligent digital redesign* ……237
H-J. Lee, J-B. Park (Yonsei University, Korea)
Y-H. Joo (Kunsan National University, Korea)

January 29 (Thursday)

Room A

9:00~10:30 GS12 Genetic Algorithms
Chair: Y. G. Zhang (Academia Sinica, P.R.China)

GS12-1 *DNA computing for an absolute 1-center problem: An evolutionary approach* ……241
Z. Ibrahim, O. Ono, Y. Tsuboi (Meiji University, Japan)
M. Khalid (Universiti Teknologi Malaysia, Malaysia)

GS12-2 *GA based production simulator by new individual expression, rough crossover and constant individual input* ……245
H. Yamamoto, E. Marui (Gifu University, Japan)

GS12-3 *Object tracking by using additive competitive leaning and shape information* ……249
Y-H. Park, H. Kang (Chung-Ang University, Korea)

GS12-4 *The analysis for the path of an object in earth orbit with genetic algorithms* ……253
R. Goto, Y. Sato (Hosei University, Japan)

GS12-5 *Minimization of the consumption energy of a manipulator using the Genetic Algorithm for obtaining Fourier coefficients of the approximation functions* ……259
Y. Yokose (Kure National College of Technology, Japan)
T. Izumi (Shimane University, Japan)

GS12-6 *Keeping diversity of reference set for keeping diversity of population in distributed genetic algorithms* ……263
T. Nakashima, T. Yoshida, H. Ishibuchi (Osaka Prefecture University, Japan)

13:00~14:15 PS Poster Session

PS-1 *Matching interpretation by utterance interaction on cooperative robot tasks* ……267
T. Kimura, A. Sano (Ryukoku University, Japan)

PS-2 *A subspace-based face detection method using image-size reduction and magnification* ……269
M. Kobayashi, T. Takahashi (Ryukoku University, Japan)

PS-3 *On the stability of a model for interaction between HIV and T-Cell CD4*$^+$ ……271
H. Ueda, Y. Ishida (Toyohashi University of Technology, Japan)

14:30~16:00 GS8 Cognitive Science
Chair: K-B. Sim (Chung-Ang University, Korea)

GS8-1 *Towards fully distributed cognitive systems* ……274
P. Sapaty (National Academy of Sciences, Ukraine)
K. Kawamura (Vanderbilt University, USA)
M. Sugisaka (Oita University, Japan)
R. Finkelstein (Robotic Technology Inc., USA)

GS8-2 *Evolution of biological concept network* ……279
T. Maeshiro (University of Tsukuba, ATR International, Human Information Science Laboratories, Japan)
K. Shimohara (ATR International, Human Information Science Laboratories, Japan)
S. Nakayama (University of Tsukuba, Japan)

GS8-3 *Application of animal feeding behavior learning to a small mobile robot* ……283
N. Sakamoto, H. Kanoh (Meiji University, Japan)

GS8-4 *A genetic algorithm for multiple face detection* ……287
X. Fan (Oita University, Japan)
M. Rizon (Northern Malaysia University College of Engineering, Malaysia)
M. Sugisaka (Oita University, RIKEN, Japan)
H. Kimura (The University of Tokyo, RIKEN, Japan)

GS8-5 *Global identification of complex systems* ……291
J. Swiatek (Wroclaw University of Technology, Poland)

GS8-6 *An experiment of dissimilarity reconstruction in information recommendation* ……295
Z. Kou, T. Ban, C. Zhang, L. Zhuang (Tsinghua University, P.R.China)

16:00~17:30 GS10 Evolutionary Computations-I
Chair: L. Han (Beijing Technology and Business University, P.R.China)

GS10-1 *Length-based DNA computing for 1-pair shortest path problem* ……299
Z. Ibrahim, O. Ono, Y. Tsuboi (Meiji University, Japan)
M. Khalid (Universiti Teknologi Malaysia, Malaysia)

GS10-2 *General protocol for evaluating the degree of occurrence of mis-hybridization* ……303
S. Kashiwamura (Hokkaido University, Japan)
A. Kameda (CREST, Japan Science and Technology Corporation (JST), Japan)
M. Yamamoto (PRESTO, Japan Science and Technology Corporation (JST), Hokkaido University, Japan)
A. Ohuchi (CREST, Japan Science and Technology Corporation (JST), Hokkaido University, Japan)

GS10-3 *A simple model for the evolution of a lexicon* ……309
E. E. Vallejo (Tecnológico de Monterrey, Mexico)
C. E. Taylor (University of California, Los Angeles, USA)

GS10-4 *Evolution of investment strategy in an environment offered by the real tick data* ……313
M. Tanaka-Yamawaki, T. Motoyama (Tottori University, Japan)

GS10-5 *A sub-goals adaptation method for quick reinforcement learning in varied environments* ……317
K. Kondo, K. Yamauchi, T. Omori (Hokkaido University, Japan)

Room B

9:00~10:30 GS22 Robotics-I
Chair: C. Zhang (Tsinghua University, P.R.China)

GS22-1 *Approaching motion control of the Humanoid Robot by using linear visual servoing* ……321
K. Okamoto, K. Yamaguchi, N. Maru (Wakayama University, Japan)

GS22-2 *Design of vision-based motion control system for balloon robot* ……325
H. Kadota, H. Kawamura, M. Yamamoto, A. Ohuchi (Hokkaido University, Japan)
T. Takaya (RICOH SYSTEM KAIHATU COMPANY, LTD., Japan)

GS22-3 *A probabilistic approach to identify environmental models of mobile robots* ……329
K. Kanemoto (Nara Institute of Science and Technology, Japan)
J. Yoshimoto (CREST, Japan Science and Technology Agency, Nara Institute of Science and Technology, Japan)
S. Ishii (Nara Institute of Science and Technology, CREST, Japan Science and Technology Agency, Japan)

GS22-4 *An approximate stability analysis of a robust control DC motor system using higher order derivatives of universal learning networks* ……333
A. Hussein, K. Wada (Kyushu University, Japan)
K. Hirasawa, J. Hu (Waseda University, Japan)

GS22-5 *Experiment of digital RAC for an underwater robot with vertical planar 2-link manipulator* ……337
S. Sagara, K. Shibuya, M. Tamura (Kyushu Institute of Technology, Japan)

13:00~14:15 IS3 Biological Information Processing and Control
Chair: K. Abe (Tohoku University, Japan)
Co-Chair: N. Homma (Tohoku University, Japan)

IS3-1 *Fast Incremental leaning methods inspired by biological learning behavior* ……341
K. Yamauchi, T. Oohira, T. Omori (Hokkaido University, Japan)

IS3-2 *Self-organizing neural networks for concept formation* ……347
N. Homma, M. Sakai, K. Abe (Tohoku University, Japan)

IS3-3 *Discretization of analog communication signals by noise addition in communication learning* ……351
K. Shibata, M. Nakanishi (Oita University, Japan)

IS3-4 *Active and passive dynamics of the head-neck complex in response to vibration* ……355
M. A. Fard, H. Inooka (Tohoku University, Japan)

IS3-5 *A model of bipedal walking controlled by the basal ganglia - brainstem systems* ……359
N. Tomita, M. Yano (Tohoku University, Japan)

14:30~15:45 GS14 Intelligent Control and Modeling-I
Chair: Z. Bubnicki (Wroclaw University of Technology, Poland)

GS14-1 *Computer simulation of an augmented automatic choosing control designed by extremizing a combination of Hamiltonian and Lyapunov functions* ……363
T. Nawata (Kumamoto National College of Technology, Japan)
H. Takata (Kagoshima University, Japan)

GS14-2 *A fully automated and intelligent marine transportation system* ……367
T-H. Nguyen (Hoang Minh JSC, Vietnam)
D-K. Tran, T-Q. Hoang, T-H. Tran, V-T. Bui (Hoang Nguyen Commercial Co., Ltd., Vietnam)
X-T. Cao, D-H. Nguyen, T-N. Hoang, H-S. Pham (Hoang Minh Co., Ltd., Vietnam)
T-M-H. Nguyen, H-S. Dao, V-T. Pham (Manufacture and Service Enterprise, Vietnam)

GS14-3 *Online estimation of ship steering dynamics and its application in designing an optimal autopilot* ……371
M-D. Le (VINASHIN, Vietnam)
C-S. Truong, T-H. Nguyen, T-H. Cao (Hong Thang TST., Vietnam)
H-T. Nguyen, D-T. Nguyen, V-C. Nguyen, V-H. Hoang (C&A Technology Application Support Co., Ltd., Vietnam)

GS14-4 *A design of digital adaptive control systems for space robot manipulators using transpose of Generalized Jacobian Matrix* ……375
Y. Taira (National Fisheries University, Japan)
S. Sagara (Kyushu Institute of Technology, Japan)

GS14-5 *Application of neural network to generation of robot arm trajectory* ……380
S. Imajo, M. Konishi, T. Nishi, J. Imai (Okayama University, Japan)

15:45~17:30 GS5 Artificial Life-Ⅱ
Chair: H. Kashiwagi (Kumamoto University, Japan)

GS5-1 *Formation of agent behavior by adaptive pickup of ambient information with speculative action* ……384
H. Yamagishi, T. Shiose, H. Kawakami, O. Katai (Kyoto University, Japan)

GS5-2 *Construction and verification of DNA hairpin-based RAM* ……388
N. Takahashi (Hokkaido University, Japan)
A. Kameda (CREST, Japan Science and Technology Cooperation (JST), Japan)
M. Yamamoto, A. Ohuchi (Hokkaido University, CREST, Japan Science and Technology Cooperation (JST), Japan)

GS5-3 *The artificial muscle and its application in robot* ……392
M. Sugisaka, H. Zhao, N. Mokhtar (Oita University, Japan)

GS5-4 *Application of uncertain variables to learning process in knowledge-based decision systems* ……396
Z. Bubnicki (Wroclaw University of Technology, Poland)

GS5-5 *Artificial knowledge system consisted of impulse response to change for timing representation* ……400
Y. Amemiya, Y. Yonezawa (Ibaraki University, Japan)

GS5-6 *State estimation of nonlinear stochastic systems by evolution strategies based particle filter* ……406
K. Uosaki, Y. Kimura, T. Hatanaka (Osaka University, Japan)

Room C

9:00~10:30 GS20 Mobile Vehicles- II
Chair: J-M. Lee (Pusan National University, Korea)

GS20-1 *Linear Feature Prediction for confidence estimation of sonar readings in map building* ……410
S. O'Sullivan (IBM Software Group, Ireland)
J. J. Collins, M. Mansfield, D. Haskett, M. Eaton (University of Limerick, Ireland)

GS20-2 *A quantitive evaluation of sonar models and mathematical update methods for map building with mobile robots* ……414
S. O'Sullivan (IBM Software Group, Ireland)
J. J. Collins, M. Mansfield, D. Haskett, M. Eaton (University of Limerick, Ireland)

GS20-3 *Obstacle avoidance strategy for a mobile robot in the guideline navigation* ……419
J. Wang (Oita University, Japan)
H. Kimura (The University of Tokyo, RIKEN, Japan)
M. Sugisaka (Oita University, RIKEN, Japan)

GS20-4 *Fuzzy obstacle avoidance and navigation for mobile robot* ……425
M. Sugisaka, R. Chen (Oita University, Japan)

GS20-5 *Driving control of autonomous vehicle with vision system using Cell Mediated Immune Algorithm (CMIA) controller* ……429
Y-J. Lee (Korea Aviation Polytechnic College, Korea)
S-K. Kim, J-H. Suh, K-S. Lee (Dong-A University, Korea)

GS20-6 *Decentralized control of cooperative 3-wheeled mobile robots using passive velocity field control - Adaptive generation method of desired velocity field -* ……433
J-H. Suh, S-K. Kim, K-S. Lee (Dong-A University, Korea)
Y-J. Lee (Korea Aviation Polytechnic College, Korea)

13:00~14:15 IS2 Artificial and Natural Adaptions
Chair: K. Naitoh (Yamagata University, Japan)
Co-Chair: T. Ohira (Sony Computer Science Laboratories, Japan)

IS2-1 *Diversity and evolutionary implication of Archaea, the third domain of life* ……437
T. Itoh (RIKEN, Japan)

IS2-2 *Self-organizing mechanism of biosystems - Purine and pyrimidine density ratios in tRNA and rRNA -* ……440
K. Naitoh (Yamagata University, Japan)

IS2-3 *Repulsive delayed random walk* ……443
T. Ohira (Sony Computer Science Laboratories, Japan)
T. Hosaka (Tokyo Institute of Technology, Japan)

IS2-4 *Data reduction for 3D visualized data distribution* ……445
H. Miyachi (KGT Inc., Japan)
N. Sakamoto (Kyoto University, Japan)

IS2-5 *Symbiotic fusion of life and artifact - A new possibility of biomass -* ……449
K. Naitoh (Yamagata University, Japan)

14:30~15:45 IS5 Intelligent Pattern Classification
Chair: S. Omatu (Osaka Prefecture University, Japan)

IS5-1 *Evaluation of vibration on many positions by SOM* ……452
N. Kamimoto, Y. Yamada, M. Kitamura (Matsushita Electric Works Ltd., Japan)
K. Nishikawa (Kanazawa University, Japan)

IS5-2 *Separation of acoustic signals of transmission machines by ICA* ……456
N. Kamimoto, Y. Yamada, M. Kitamura (Matsushita Electric Works Ltd., Japan)
K. Nishikawa (Kanazawa University, Japan)

IS5-3 *Intelligent classification of bill money* ……460
S. Omatu (Osaka Prefecture University, Japan)
M. Teranishi (Nara University of Education, Japan)
T. Kosaka (Glory TD Himeji, Japan)

IS5-4 *Removal of environmental noise with adaptive filter* ……464
Y. Kogeichi, S. Omatu (Osaka Prefecture University, Japan)

15:45~17:30 GS23 Robotics-II
Chair: T. Kubik (Wroclaw University of Technology, Poland)

GS23-1 *Quadruped robot positioning control of leg by linear visual servoing* ……468
Y. Inoue, N. Maru (Wakayama University, Japan)

GS23-2 *Evolution of sidewinding locomotion of simulated limbless, wheelless robots* ……472
I. Tanev (ATR Human Information Science Laboratories, Japan)
T. Ray (ATR Human Information Science Laboratories, Japan, The University of Oklahoma, Norman, USA)

GS23-3 *Design of a real time adaptive controller of robot manipulator with eight joint based DSPs* ……476
S-H. Han, H-R. Kim, D-Y. Jung (Kyungnam University, Korea)

GS23-4 *Induction of prototypes in a robotic setting using local search MDL* ……482
G. M. Kobele, J. Riggle, C. Taylor, E. Stabler (University of California, Los Angels, USA)
R. Brooks, D. Friedlander (The Pennsylvania State University, USA)

GS23-5 *Learning of reaching a colored object based on direct-vision-based reinforcement learning and acquired internal representation* ……486
K. Yuki, M. Sugisaka, K. Shibata (Oita University, Japan)

GS23-6 *Optical flow as a tool for optical speed sensor* ……490
T. Kubik (Wroclaw University of Technology, Poland)
M. Sugisaka (Oita University, Japan)

GS23-7 *An assymetric 2-D passive dynamic walker* ……494
N. Mayer, A. A. Forough-Nassiraei, M. Browne (GMD-Japan Research Laboratory Collaboration Center, Japan)
J. M. Herrmann (Universität Göttingen, Germany)
T. Christaller (GMD-Japan Research Laboratory Collaboration Center, Japan, Fraunhofer Institut für Autonome Intelligente Systeme, Germany)

January 30 (Friday)

Room A

9:00~10:30 GS15 Intelligent Control and Modeling-II
Chair: E. Hayashi (Kyushu Institute of Technology, Japan)

GS15-1 *Robot manipulator control using topology representing network according to initial posture* ……498
T. Yamakawa, K. Horio, K. Ueno (Kyushu Institute of Technology, Japan)

GS15-2 *Study on computer simulation system of biological modeling for move-in mud robot* ……502
F. Ren (Harbin University of Science & Technology, P.R.China)
D. Wang, L. Zhang, Q. Meng (Harbin Engineering University, P.R.China)

GS15-3 *Autonomous navigation towards intelligently behaving robots* ……507
M. K. Habib (Monash University Malaysia, Malaysia)

GS15-4 *Speed control of a stepping motor of the electric vehicle based on speed parameters estimation via PWM inverter* ……511
M. Sugisaka, Z. Mbaitiga (Oita University, Japan)

GS15-5 *A robust adaptive direct controller for non-linear first order systems* ……515
M-M. Nguyen (Hoang Minh JSC, Vietnam)
V-L. Nguyen, T-T. Nguyen, V-C. Pham, T-T-H. Do, T-H. Nguyen (Hoa Ban Co., Ltd., Vietnam)
H-B. Nguyen, T-K-H. Nguyen, T-V. Le, Q-S. Nguyen (Phu Bao, Co., Ltd., Vietnam)

GS15-6 *Ships' optimal autopilot using a multivariate auto-regressive exogenous mode* ……519
T-H. Nguyen (Hoang Minh JSC, Vietnam)
T-T. Ha, V-V. Vo, V-T. Nguyen, C. Nguyen (Bac Ninh Consultant and Investment, Co., Ltd., Vietnam)
D-K. Nguyen, T-Q. Pham, M-C. Nguyen, T-M. Nguyen (Tan Viet Hoang, Co., Ltd., Vietnam)

10:45~12:00 IS4 Biomimetic Machines and Their Applications
Chair: K. Watanabe (Saga University, Japan)
Co-Chair: K. Izumi (Saga University, Japan)

IS4-1 *Enhancing awareness in cooperative robots through perceptual anchoring* ……523
S. A. Guirnaldo, K. Watanabe, K. Izumi (Saga University, Japan)

IS4-2 *A study on constructing a neuro-interface using the concept of virtual master-slave system* ……527
R. Syam, K. Watanabe, K. Izumi (Saga University, Japan)

IS4-3 *Neural network approach to acquire the free-gait motion of quadruped robots in obstacle avoidance* ……531
T. Yamaguchi, K. Watanabe, K. Izumi (Saga University, Japan)

IS4-4 *Coordination of voice and visual information for intelligently cooperating between human and robot* ……535
K. Izumi, Y. Tamano, Y. Nose, K. Watanabe (Saga University, Japan)

IS4-5 *Fuzzy hint acquisition for the inverse kinematic solution of redundant manipulators using neural network – Tracking unknown enclosed trajectory-* ……539
S. F. M. Assal, K. Watanabe, K. Izumi (Saga University, Japan)

13:00~14:00 GS18 Molecular Biology-I
Chair: H. Hirayama (Asahikawa Medical College, Japan)

GS18-1 *Statistical micro mechanical method for dynamic kinetic binary interaction among biomolecules with moderate density* ……543
H. Hirayama (Asahikawa Medical College, Japan)

GS18-2 *A cellular automata model for HIV infection and antigenic diversity threshold* ……547
H. Ueda, Y. Ishida (Toyohashi University of Technology, Japan)

GS18-3 *Statistical approach for function classification of proteins in the biological texts* ……551
D-W. Park, H-C. Kwon, M-H. Lee (Pusan National University, Korea)
H-G. Cho (Youngsan University, Korea)

GS18-4 *Chemotaxis of an eukaryotic cell in complex gradients of chemoattractants* ……555
S. I. Nishimura, M. Sasai (Nagoya University, Japan)

14:00~15:15 GS7 Bioinformatics
Chair: K. Uosaki (Osaka University, Japan)

GS7-1 *Time minimum extrinsic blood clotting system as a cascade biosignal transmission* ……559
H. Hirayama (Asahikawa Medical College, Japan)

GS7-2 *Finding evolutional mechanism in financial time series by means of correlation dimension analysis* ……563
M. Tanaka-Yamawaki, H. Tanaka (Tottori University, Japan)

GS7-3 *Gene expression modelling with the use of Boolean network* ……567
T. Kubik (Wroclaw University of Technology, Poland)
M. Sugisaka (Oita University, Japan)

GS7-4 *Chemical genetic programming – Evolutionary optimization of the translation from genotypic strings to phenotypic trees* ……571
W. Piaseczny, H. Suzuki (ATR Human Information Science Labs, Japan)
H. Sawai (Communications Research Laboratory, Japan)

Room B

9:00~10:30 GS3 Artificial Intelligence
Chair: T. Yamamoto (University of the Ryukyus, Japan)

GS3-1 *Efficient method for collecting useful Web pages with the feature of the Web structure* ……575
J. Matsukubo, Y. Hayashi (Japan Advanced Institute of Science and Technology, Japan)

GS3-2 *Toward the consistent simulation of narrative discourse based on narratology* ……579
T. Ogata (Yamanashi University, Japan)

GS3-3 *Extraction of meaningful tables on the Internet* ……585
S-W. Jung, J-H. Kang, K-R. Ryu, H-C. Kwon (Pusan National University, Korea)

GS3-4 *Spatial strategies on a generalized Spatial Prisoner's Dilemma* ……589
Y. Ishida, K. Mori (Toyohashi University of Technology, Japan)

GS3-5 *Transformation of story in the story generation system based on narratology* ……593
T. Ogata, Y. Hosaka (Yamanashi University, Japan)

10:45~12:00 GS2 Artificial Brain-Ⅱ
Chair: T. Arita (Nagoya University, Japan)

GS2-1 *Classification and Combination of perspective in Narrative* ……597
K. Ueda, T. Ogata (Yamanashi University, Japan)

GS2-2 *A robotic approach to emotion from a selectionist perspective* ……601
T. Kato, T. Arita (Nagoya University, Japan)

GS2-3 *Model based recognition for artificial brain* ……605
X. Wang (Tsinghua University, P.R.China, Oita University, Japan)
M. Sugisaka (Oita University, Japan)
W. Xu (Tsinghua University, P.R.China)

GS2-4 *Non-intrusive eye gaze estimation under large head movement using property of projective transform* ……610
D-H. Yoo, M-J. Chung (Korea Advanced Institute of Science and Technology, Korea)

13:00~14:00 GS17 Micro-Robot World Cup-Soccer Tournament
Chair: M. Tanaka-Yamawaki (Tottori University, Japan)

GS17-1 *Developing a benchmarking framework for map building paradigms* ……614
J. J. Collins, M. Eaton, M. Mansfield, D. Haskett (University of Limerick, Ireland)
S. O'Sullivan (IBM Software Group, Ireland)

GS17-2 *Developing a statistical baseline for robot pursuit and evasion using a real world control architecture* ……618
M. Mansfield, J. J. Collins, S. O'Sullivan, M. Eaton, D. Haskett, T. Collins (University of Limerick, Ireland)

GS17-3 *Controlled balanced growth of robot populations* ……622
D. J. G. James (Coventry University, UK)
V. G. Rumchev (Curtin University of Technology, Australia)

14:00~15:15 GS16 Intelligent Control and Modeling-Ⅲ
Chair: K. Watanabe (Saga University, Japan)

GS16-1 *Leak detection in pipelines based on non-negative matrix factorization* ……629
R. Hu, H. Ye (Tsinghua University, P.R.China)

GS16-2 *Acrobot control by learning the switching of multiple controllers* ……633
M. Nishimura (Nara Institute of Science and Technology, Japan)
J. Yoshimoto (CREST, Japan Science and Technology Agency, Nara Institute of Science and Technology, Japan)
S. Ishii (Nara Institute of Science and Technology, CREST, Japan Science and Technology Agency, Japan)

GS16-3 *Real time implementation of visual feedback control for industrial robot manipulator* ……637
S-H. Han, D-Y. Jung, H-R. Kim (Kyungnam University, Korea)
H. Hashimoto (The University of Tokyo, Japan)

GS16-4 *Quality of cascade operations control based on uncertain variables* ……643
D. Orski (Wroclaw University of Technology, Poland)

GS16-5 *On the sub-optimal control of certain nonlinear systems* ……647
W. R. Wells (University of Nevada, Las Vegas, USA)

Room C

9:00~10:30 GS11 Evolutionary Computations-Ⅱ
Chair: H. Tanaka (Tokyo Medical & Dental University, Japan)

GS11-1 *An evolutionary model for 3D agents integrating continuous and plastic development* ……651
A. Matos, T. Arita (Nagoya University, Japan)

GS11-2 *An evolved learning mechanism for teaching a robot to foveate* ……655
G. Gómez (University of Zurich, Switzerland)
P. E. Hotz (University of Zurich, Switzerland, ATR, Japan)

GS11-3 *LQ-learning based on self-organizing classification of sequences* ……659
H-Y. Lee, K. Abe (Tohoku University, Japan)
H. Kamaya (Hachinohe National College of Technology, Japan)

GS11-4 *Occurrence of state confusion in the learning of communication using Q-learning* ……663
M. Nakanishi, M. Sugisaka, K. Shibata (Oita University, Japan)

10:45~12:00 IS9 Molecular Biology-Ⅱ
Chair: K. Ohnishi (Niigata University, Japan)

IS9-1 *Molecular basis underlying social behaviors of honeybees* ……667
H. Takeuchi (The University of Tokyo, Japan)

IS9-2 *Random-walk evolution of protein-sequences analyzed in multi-dimensional pseudo-euclidean sample space spanned by principal coordinate axes. A Study towards constructing multi-dimensional evolutionary tree* ……671
K. Ohnishi, N. Furuichi (Niigata University, Japan)

IS9-3 *Early genesis and evolution of mRNAs and16S rRNA from poly-tRNA ribozymes* ……677
Y. Ishimoto, M. Ohshima, S. Hokari, N. Furuichi, K. Ohnishi (Niigata University, Japan)

IS9-4 *Defence mechanisms of potato : Regulation of RiCDPK, the Ca^{2+}-dependent protein kinase, by the elicitor and suppressor of phytophthora infestans* ……682
N. Furuichi, T. Okuta, A. Hassan, K. Ohnishi, N. Hatsugai (Niigata University, Japan)

13:00~14:00 IS6 Intelligent Information Retrieval
Chair: H. Yanagimoto (Osaka Prefecture University, Japan)

IS6-1 *Extraction of user's interests by ICA and GA for information filtering* ……686
H. Yanagimoto, S. Omatu (Osaka Prefecture University, Japan)

IS6-2 *Recommendation of news articles by consecutive revision with a genetic algorithm* ……690
M. Ikeda, H. Yanagimoto, S. Omatu (Osaka Prefecture University, Japan)

IS6-3 *The proposal for the way to recommend information with ICA* ……694
T. Yokoi, H. Yanagimoto, S. Omatu (Osaka Prefecture University, Japan)

IS6-4 *Construction of a classifier using AdaBoost for information filtering* ……698
H. Yanagimoto, S. Omatu (Osaka Prefecture University, Japan)

Proc. of The Ninth Int. Symp. on Artificial Life and Robotics (AROB 9th '04)
Beppu, Oita, Japan, 28-30 January, 2004

Discretization of Analog Communication Signals by Noise Addition in Communication Learning

Katsunari Shibata(shibata@cc.oita-u.ac.jp) Masanobu Nakanishi
Dept. of Electrical & Electronic Engineering, Oita University, 700 Dannoharu, Oita 870-1192, Japan.

Abstract

Using symbols, our humans can communicate complicated information cleverly with each other. Thinking about the "Symbol Grounding Problem" and the brain structure of the living things, the authors believe that it is the best solution for generating communication to use a neural network that is trained based on reinforcement learning. However, it has been said that neural networks are not good at symbol processing. As the first step of the research of symbol emergence using neural network, this work focused on the necessity of "elimination of noise effect", and it was examined that analog communication signals are binarized in some degree by adding some noise in reinforcement learning-based communication acquisition. It was also observed that when the noise ratio became larger, the degree of the binarization became larger.

1 Introduction

Our humans can communicate complicated information cleverly with each other using symbols. It has been thought that artificial neural networks(ANNs) are good at continuous nonlinear approximation, but are not good at symbol handling or logical processing. In our living things, the functional difference has been pointed out between the left brain and the right brain[1]. Especially, the Broca's area and Wernicke's area that relate deeply to language are located in the left brain[2].

Based on this common knowledge, the idea of the specialization that the ANN corresponding to the right brain is used for pattern processing, and a digital computer corresponding to the left brain is used for logical processing has been accepted generally. However, there is no general idea about what signals should be transferred between the ANN and the computer, and that causes the "symbol grounding problem". Furthermore, it seems strange that the left brain and the right brain looks almost the same in the real brain compared with the difference between the ANN and the digital computer.

We think that this "symbol grounding problem" is very serious. We believe that in order to solve the problem, the pattern processing and the logical processing should not be distinguished, and that is essential to realize intelligence in robots. Accordingly we expect the ANN to do both processing without any discrimination. In our brain also, a natural neural network must process symbols. For this reason, it is very significant to show that the ANN has the ability to discretize analog signals only by applying reinforcement learning. Then, there appears a question "is it true that symbols do not emerge from the ANN through learning?"

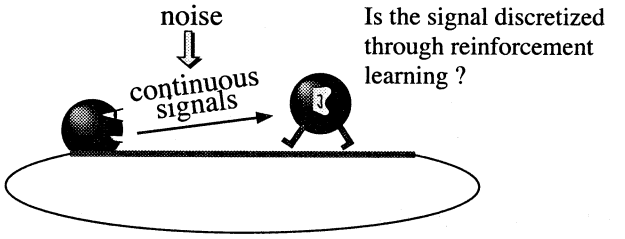


Figure 1: Discretization of communication signals by the addition of noise.

Here, for simplicity, symbols are considered as discretized signals. Then, why do we discretize the communication signals? Considering from necessity, either logical thinking or eliminating noise effect can be one of the reasons. Considering from the structure, associative memory, in other words, fixed-point dynamics can be a solution to realize the discretization. As the first step of the research of symbol emergence, this work focuses on the necessity of "elimination of noise effect", and it is examined whether analog communication signals are discretized or not by adding some noise in reinforcement learning-based communication acquisition.

2 Learning and Task

As a simple communication environment, two agents are assumed. Referring to [3], one of them can transmit some communication signals to the other. They are put on a very simple one-dimensional space as shown in Fig. 1. When the both agents touch together, they get some reward. The transmitting agent cannot move, but can observe the relative location of the opponent, and generates its communication signals by its own neural network. The receiving agent interprets the communication signals and generates its motion command also by its own neural network. It can move according to the motion command. It can-

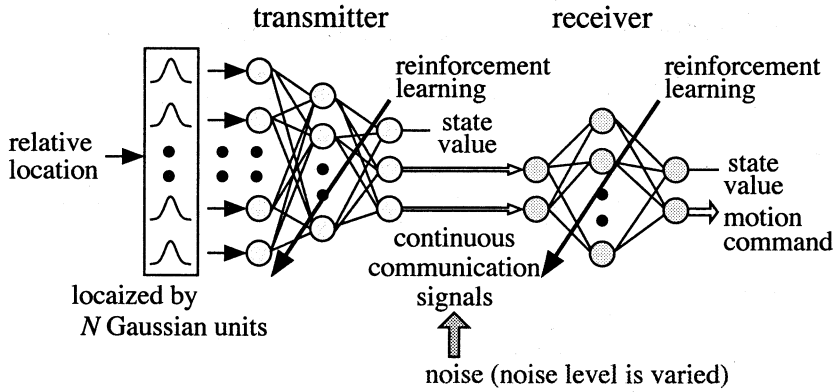


Figure 2: Architecture of each agent and signal flow.

not observe anything except for the communication signals, and cannot transmit anything. Both agents are trained based on reinforcement learning independently. The transmitting agent deals with the communication signals as its actions, while the receiving agent deals with the communication signals as its states.

The transmitting agent is fixed at the left edge on a one-dimensional ring where the left edge is linked to the right edge. The length of the ring is 1.0. The receiving agent is located randomly at every trial. The distance moved is proportional to the motion command that is the sum of the output of the receiver's neural network and a random number as a trial and error factor. The motion command can be negative. When the command is positive, it goes to the right, and when it is negative, it goes to the left. When the distance between the transmitter and receiver is less than some value, they can touch each other and get a reward. However, if the motion command is large though the receiver is close to the transmitting agent, it goes past the transmitter, and they cannot get the reward. Accordingly the receiver's motion should be in a range, and the range is gradually sifted according to the relative receiver's location.

Fig. 2 shows the architecture of each agent and the signal flow. The transmitting agent observes the relative receiver's location, and then the information is localized by N Gaussian units. This helps the neural network to learn a strong nonlinear transformation. The center of each Gaussian is arranged between 0.0 and 1.0 with a constant interval. The size of each Gaussian σ is $1.0/(N-1)$, where N is the number of Gaussian units. The output is described as

$$GS_i(dist) = exp\left(-\frac{1}{2}\left(dist - \frac{i}{N-1}\right)^2\right), \quad (1)$$

where i is the suffix of the Gaussian unit number ($i = 0, 1, 2, .., N-1$), $dist$ is the relative receiver's distance from the transmitter. Here, $N = 30$.

Two or three of the outputs of the transmitting agent are used to decide the communication signals. Each signal is the sum of the corresponding output and a random number as a trial and error factor that is added for reinforcement learning. A noise factor is also added to the signal.

As a reinforcement learning architecture, actor-critic is employed for each agent. One of the outputs of the network is used as critic, and the others are used as actor. The hidden neurons are used in common by both types of outputs. The training signals are computed based on reinforcement learning, and the network is trained based on Back Propagation. TD error $\hat{r}$ is calculated as

$$\hat{r}_t = r_t + \gamma P_t - P_{t-1} \quad (2)$$

where r is the reward, P_t is the critic output, and γ is a discount factor. The critic output is trained by the training signal as

$$P_{s,t-1} = P_{t-1} + \hat{r}_t = r_t + \gamma P_t. \quad (3)$$

The actual motion vector $\mathbf{M}$ is calculated as

$$\mathbf{M}_t = \alpha(2.5\mathbf{A}_t + \mathbf{rnd}_t + \mathbf{n}_t) \quad (4)$$

where $\mathbf{A}$ is the actor output vector, $\mathbf{rnd}$ is the random number vector for the trial and error factor, and $\mathbf{n}$ is the noise vector that is not added in the case of the receiver's motion, but is added in the case of the communication signals. α is a constant. The actor output is trained by the training signal as

$$\mathbf{A}_{s,t-1} = \mathbf{A}_{t-1} + \beta\hat{r}_t\mathbf{rnd}_{t-1} \quad (5)$$

where β is a constant, and it is 0.5 here.

The output function of each hidden or output neuron is a sigmoid function that ranges from -0.5 to 0.5. The upper limit for all the training signals is 0.4, and the lower limit is -0.4 to avoid the saturation area of the sigmoid function. In Eq. (4), by multiplying 2.5 to each actor output, the range becomes from -1.0 to 1.0, and after that, the trial and error factors and noises are added. Here, the trial and error factor is cubed uniform random number whose level, in other words,

whose amplitude is ±0.4 or ±0.6. The noise factor is a uniform random number whose level is varied from ±0.0 to ±1.6 with the interval of 0.2 in the following simulations. When the value becomes larger than 1.0 or less than -1.0, it is returned to 1.0 or -1.0 respectively. Even in the case that the noise factor is always zero, the random number for the trial and error factor is received as a noise for the receiver.

For the critic computation based on TD (Temporal Difference) learning in Eq. (2) and (3), 0.5 is added to the output for the critic actually. The reward that is given to the both agents is 0.9. To generate the communication signal, α in Eq. 4 is 1.0 in the transmitting agent. For the motion command, α is 0.4 or 0.43 in the receiving agent so as that the receiver can touch the transmitter in one step from any locations by an appropriate motion. The number of layers is 3, and the number of neurons in the hidden layer is 10 for both agents.

Two tasks are introduced in this paper. In the first one, the both agents can touch with each other when the distance is less than 0.11, and α in Eq. (4) is 0.4. If the receiver's motion is discretized, no less than 4 levels of output is required. The number of communication signals is two. In the other task, the both agents can touch when the distance is less than 0.08, and α is 0.43. If the receiver's motion is discretized, no less than 6 levels of output is required. The number of communication signals is three.

3 Result

In this communication learning, it was observed whether the transmitted signals became discrete when the noises were added to the communication signals during the learning. The communication signals after learning with no noise are as shown in Fig. 3(a) and those with some noise (level=0.8) are as shown in Fig. 3(b). Fig. 3(c) shows the signals after learning with some noises (level=0.8) in the case of the task with 3 communication signals. Fig. 4 shows the receiver's motion after learning with noise for each of two and three communication signals cases. The sloping lines in Fig. 4 indicate the maximum and minimum limit values of the motion for the receiver to touch the transmitter by the motion. After learning with noise, each communication signal was almost binarized, and only around the boundary of the binary values, the signal took a medium value. However, it is clear that the degree of binarization is larger than in the case of no noise. The receiver's motion is discretized into four levels by the combination of the two binary communication signals in the range between the maximum and the minimum values. The motion is more clearly discretized than the communication signals. The reason might be that the receiver learned to binarize the received signal utilizing non-linear transformation of the neural network. When the number of communication signals is three, the information to generate the motion command is allotted well among three signals.

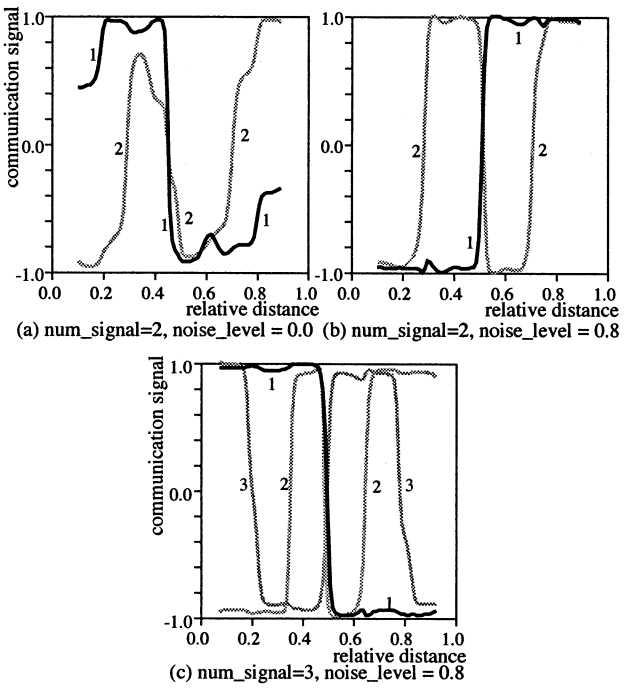


Figure 3: The communication signals as a function of the relative distance. The random number level is 0.4.

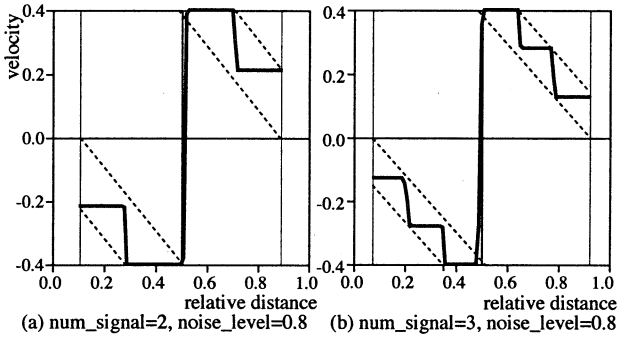


Figure 4: The receiver's motor command as a function of the relative distance. The random number level is 0.4 and the noise level is 0.8.

The relation between the noise range and the discretization was also observed. The degree of binarization that means how the signal is close to 1.0 or -1.0 is defined as

$$bin = \sum_{i}^{Nc} \sum_{j}^{Nd} |com_{i,j}|/(Nc \cdot Nd) \qquad (6)$$

where Nc is the number of communication signal, Nd is the number of sampled relative receiver's locations, and com is the communication signal without the ran-

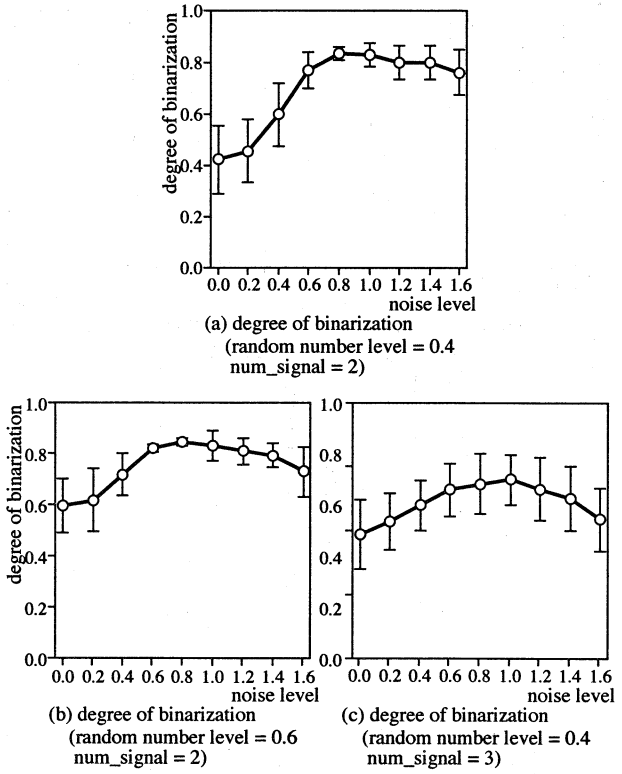


Figure 5: The degree of binarization according to the noise level in the learning phase.

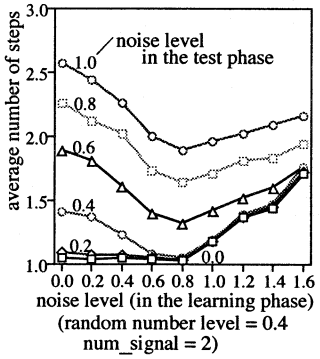


Figure 6: Noise tolerance according to the noise level in the learning phase.

dom number and noise. If the communication signal is always -1.0 or 1.0, the degree becomes the maximum value of 1.0, while if the signal is always 0.0, it becomes the minimum value of 0.0. The degree of binarization according to the noise range is shown in Fig. 5(a). Each small circle shows the average over 50 simulations, and the vertical line shows the standard deviation. It can be seen that when the noise level becomes larger, the degree of binarization becomes larger and the deviation becomes smaller. However, when the noise level becomes larger than 0.8, the degree decreases slightly according to the noise level.

The noise tolerance was also examined. Fig. 6 shows the average steps to the goal as a function of the noise level in the learning phase for each noise level in the test phase after learning. It can be seen that if some noise is added in the test phase, the performance is the best when the noise level in the learning phase is 0.8. It is interesting that under the same condition, the degree of binarization is the maximum. However, when the noise level in the learning phase is larger than 0.8, the performance becomes worse even if the noise level in the test phase is 0.0. This means that the learning itself did not progress by the large noise.

In this simulation, the random number is added to each communication signal other than the noise, but for the receiver, the random number also works as the noise. In order to see the effect of the random number, Fig. 5(b) shows the degree of binarization when the level of the random number is 0.6 on behalf of 0.4. Comparing with Fig. 5(a), the degree is larger when the random number level is larger, and the noise level in the case of the maximum degree of binarization is shifted slightly to be small. It is known that the random number for reinforcement learning also promoting the binarization of the signals.

Fig. 5(c) shows the degree when the number of communication signals is three. It can be also seen that the degree of binarization becomes large according to the noise level and have the maximum value.

4 Conclusion

It was shown that unless the noise level is too large for learning to progress, the communication signal is binarized more, and is tolerant of noise more according to the noise level when the communication signal is generated using a neural network, and the network is trained based on reinforcement learning. The authors think it very significant to show that the signal generated by a neural network is binarized only by reinforcement learning. It is thought that by using a recurrent network, the signal is binarized more clearly.

Acknowledgment

This research was partially supported by the Japan Society for the Promotion of Science, Grants-in-Aid for Scientific Research, #14350227 and #15300064.

References

[1] Sperry, R.W., "Hemisphere Deconnection and Unity in Conscious Awareness", *American Psychologist*, **23**, pp. 723-733, 1968.

[2] Geschwind, N., "Specialization of the Human Brain", In *the Brain*, W.H. Freeman and Company, San Francisco, 1979.

[3] Ono, N, Ohira, T. and Rahmani, A.T., "Emergent Organization of Interspecies Communication in Q-Learning Artificial Organs", *Advances in Artificial Life*, pp.396–405, 1995.

Proc. of The Ninth Int. Symp. on Artificial Life and Robotics (AROB 9th '04)
Beppu, Oita, Japan, 28-30 January, 2004

Active and Passive Dynamics of the Head-Neck Complex in Response to Vibration

Mohammad A. Fard
Tohoku University
Sendai, 980-8579, Japan

Hikaru Inooka
Tohoku University
Sendai, 980-8579, Japan

Abstract

The frequency domain identification method is used to identify the active dynamics of the head-neck complex (HNC) in response to the trunk horizontal (fore-aft) vibration. The passive and the active responses of the HNC to the trunk horizontal vibration are measured. Passive condition indicates the dynamics of the HNC when the volunteer is blindfolded and instructed to be relaxed. While, in the active condition, the subject is instructed to stabilize the head-reference emitted-light to a stationary line. A second order model with passive and active elements is considered for the system in the low frequencies (< 3 Hz). Good consistency obtained between the simulation and the corresponding experimental results. The feedback (active) elements of the HNC model provided significant knowledge about the role of human sensory system on the stabilization of HNC.

1 introduction

The two major mechanisms, responsible for stabilizing the HNC are illustrated in Fig. 1. This schematic drawing indicates that the mechanical properties of the HNC, e.g., the spring and damping coefficients, and the human sensory systems, namely visual, vestibular, and proprioceptive sensory systems, are generally responsible for stabilizing the HNC in response to the vibration [1]. The short latency vestibulocollic reflex (VCR) and cervicocollic reflex (CCR) produce little effective head stabilization when the subject distracted by a mental arithmetic, or advised to relax, and exposed to a random stimulus [1]. There is little knowledge in the literature concerning the elements of the controller that should be considered in the active model. Nevertheless, linear controllers have shown to be quite appropriative in simulating the human postural stability in the upright standing [2]. Such controllers may be sufficient for the HNC, which its active elements, like upright standing posture, responses to the vibration by the use of information received from the sensory systems.

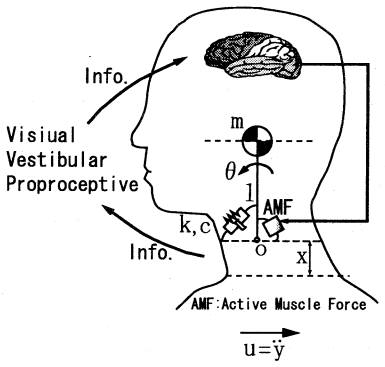


Figure 1: The schematic drawing of passive and active mechanisms responsible for stabilizing the HNC

In this research, a general method is presented to quantify the role of the human sensory systems on stabilizing the HNC. A single-inverted-pendulum model, which has both active and passive elements, is considered for the HNC. Three test conditions are defined. The first is the RLX condition, in which, as explained above, the passive dynamics of the HNC is measured when the subject is exposed to a random phase multisine [3] vibration. Second, in the presence of vision, the closed-loop response of HNC is measured when the subject is instructed to adjust the head-referenced light spot to a stationary target (AV). The third condition is identical to the second one except that the subject is blindfolded so has to imagine the stationary target (AN). It is assumed that the feedback elements are a linear controller. Frequency domain identification method is used to characterize the parameters of the controller. The results, obtained here, are thought to be important data that quantify the two strategies, which are responsible to stabilize the HNC in the mid-sagittal plane.

2 Method

2.1 Experiments

The experiments were conducted using an electro-hydraulic vibrator. Its platform (3 m × 3 m) had a stroke of 30 cm, which had the capability of producing the signals from dc to 30 Hz. A rigid seat was mounted on the platform. The wooden seatback was adjustable in height to cover the posterior part of the trunk for each individual subject (Fig. 2). A surface-mounted accelerometer (Analog Devices ADXL05) was attached to the platform to measure the horizontal acceleration of the input to the HNC. An angular rate sensor (Murata ENC-03J) was applied to measure the HNC angular velocity. This sensor was a lightweight type, pasted on the forehead of the subject to measure mainly in mid-sagittal plane, and to provide high-resolution measures of HNC angular velocity. Care was taken to prevent the skin vibration of the forehead, where the angular rate sensor was attached.

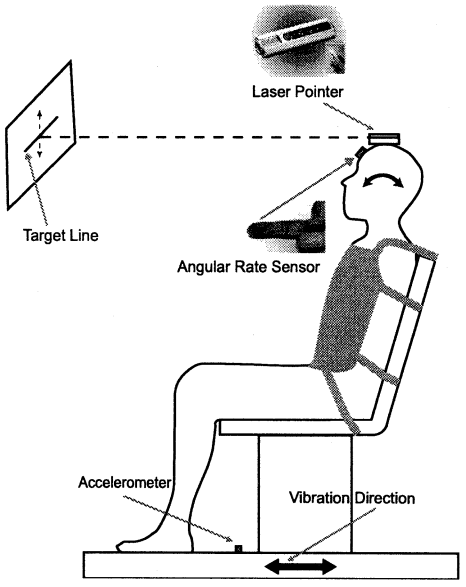


Figure 2: The schematic drawing of the experiment design

Nine male subjects (young and healthy) took part in this study. Their physical characteristics are summarized in Table 1. Each subject placed on the seat and the trunk of subject was tightly fixed to the seatback. This has been done using six straps, which were connected to a strong cloth covering anterior part of the trunk. Three test conditions were studied. The first condition was related to the measurement of the dynamics of the HNC in the RLX condition. Accordingly the subjects were blindfolded and instructed to be relaxed while they were exposed to a non-predictive random vibration. Guitton et al. [1] measured the responses of the HNC in similar conditions. They reported that the contribution of the cervical and vestibular reflexes was negligible in these circumstances. The second and the third test conditions were related to the active (closed loop) responses of the HNC. In the second (AV) condition, the vision was allowed and a lightweight (40 g) laser pointer was fixed on the head by using a lightweight cotton belt (Fig. 2). Care was taken to prevent any relative motion between the head and the laser pointer, while the HNC was vibrating. There was a whiteboard at about 160 cm distance in front of the subject. A horizontal line was considered on the whiteboard as a stationary reference line. The location of the line on the board was adjusted, for the corresponding subject, so as the light of the laser pointer showed exactly the reference line, when there was no vibration from the vibrator (Fig. 2). The subjects were instructed to continuously adjust the light of the laser pointer to the stationary reference-line on the board. For the AV, human uses the vestibular, visual, and proprioceptive sensory feedback to actively response to the vibration. The third experimental condition (AN) was identical to AV except that the subject was blindfolded (no vision), and instructed to adjust the head by imagining both the stationary target and the emitted light. It should be noticed that the experiments of AV condition was done prior to AN. This enabled the subjects to successfully follow the instructions, in AN.

The averaged frequency response function, $\overline{H(\omega_k)}$ is obtained by the division of the averaged output to the averaged input spectra.

$$\overline{H(\omega_k)} = \frac{\overline{Y(\omega_k)}}{\overline{X(\omega_k)}}. \tag{1}$$

where the $\overline{Y(\omega_k)}$ and $\overline{X(\omega_k)}$ are the averaged output and the averaged input spectrum at angular frequency ω_k, which we can derive their values by the use of following equations:

$$\overline{Y(\omega_k)} = \frac{1}{M}\sum_{l=1}^{M} Y^{[l]}(\omega_k) \tag{2}$$

$$\overline{X(\omega_k)} = \frac{1}{M}\sum_{l=1}^{M} X^{[l]}(\omega_k). \tag{3}$$

Table 1: Physical characteristics of subjects. Note that the # sign indicates the subject number

Subject	# 1	# 2	# 3	# 4	# 5	# 6	# 7	# 8	# 9	Mean (SD)
Age(yr)	28	25	31	27	31	24	27	25	23	27(3)
Heig(m)	1.83	1.68	1.79	1.72	1.79	1.64	1.70	1.70	1.80	1.74(0.07)
Wei(kg)	76	56	73	68	75	61	64	64	74	68(7)

2.2 Modeling and Identification of the HNC in the RLX Condition

As we have already mentioned, the behavior of the HNC in the RLX condition can be assumed as an open-loop system. Therefore, we may construct a model for the HNC in accordance with the inertial and viscoelastic parameters. A single-degree-of-freedom model (a two-dimensional inverted pendulum) was then considered as a model for the HNC. This model was constituted of a torsional spring, a torsional damper and a lump mass (Fig. 1). The center of mass was assumed to be exactly over the center of rotation. The center of rotation was located at a distance x from the joint of C7-T1 (Fig. 1). As a convention in this paper, the lower part of the neck that is shown by x is called the lower neck and the other part of the neck that is located over the center of rotation is called the upper neck (Fig. 1). The linearized form of the equation of the system around $\theta = 0$, was obtained in the following form

$$I\ddot{\theta} + c\dot{\theta} + (k - mgl)\theta = ml\ddot{y} \tag{4}$$

where m is the mass of the head and the upper neck, and I is the mass moment of inertia of the head and the upper neck, around the center of rotation o (Fig. 1). The $\ddot{y}$ is the input (acceleration), the l is the distance between center of mass and center of rotation, k indicates the spring factor, c is the damping coefficient, and θ indicates the angular displacement of the system.

The s-domain transfer function $H(s)$ of the system between the HNC angular velocity and input acceleration was obtained from Eq. (4).

$$H(s) = e^{-sT_d} \frac{s}{\alpha s^2 + \beta s + \gamma} \tag{5}$$

where $s = j2\pi f$,

$$\alpha = \frac{I}{ml}, \tag{6}$$

$$\beta = \frac{c}{ml}, \tag{7}$$

$$\gamma = \frac{k - mgl}{ml}. \tag{8}$$

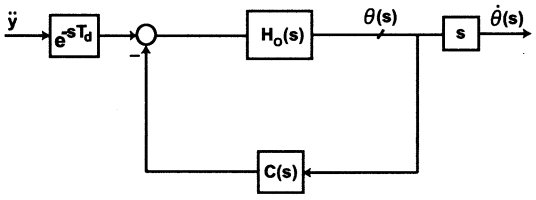


Figure 3: The block diagram of the HNC in the AV and AN conditions

T_d indicates the pure time delay of the system. It is called pure since the delay term e^{-sT_d} can be expressed as a multiplicative term to the rational transfer function Eq. (5).

The α, β, γ, and T_d were the four unknown parameters in the Eq. (5). The pure time delay of system T_d was estimated before the identification.

Frequency domain identification method [3] was used to identify the HNC. In other words, it was attempted to estimate the three unknown parameters, α, β, and γ (Eq. (5)).

2.3 Modeling and Identification of the HNC in the AV and AN conditions

As we have already mentioned, the responses of the HNC in the AV and AN are no longer passive and open loop. However, a feedback system should be considered. This closed-loop behavior of the HNC is related to the human sensory systems. Accordingly, we have shown a schematic draw of the HNC, including the passive and the active elements in the (Fig. 1). The foundamental controller that can be considered for this system are a combination of the P (proportional), I (integral), and D (derivative). It is assumed that the signal that goes to the controller is the feedback of the HNC angular displacement, θ. The block diagram of the system in theses two conditions is shown in the Fig. 3.

The $H_O(s)$ indicates the open-loop transfer function of the HNC between the HNC angular displace-

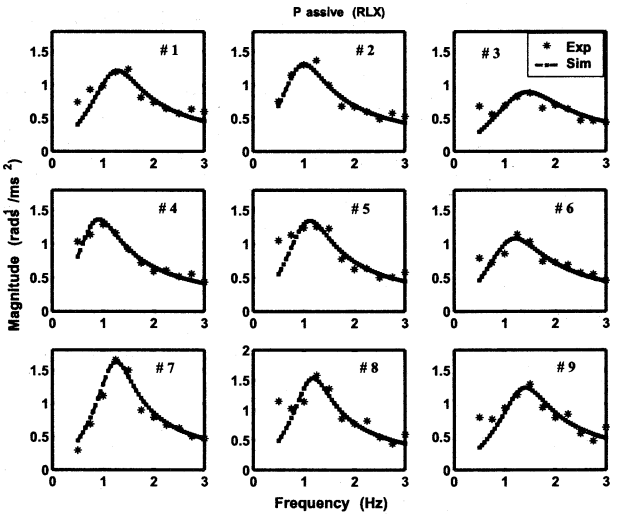


Figure 4: Comparison of the experimental (Exp.) and simulated (Sim.) results of the magnitudes of the HNC transfer functions, corresponding to the nine subjects, in the RLX condition

Table 2: The coefficients of the PD controllers in the AV condition

Subject	# 1	# 2	# 3	# 4	# 5	# 6	# 7	# 8	# 9	Mean (SD)
$(k_p)_{AV}$	0.816	0.468	0.371	1.070	0.798	0.892	1.315	1.383	1.040	0.906 (0.342)
$(k_d)_{AV}$	6.092	4.351	5.110	12.977	9.283	11.642	16.266	16.058	14.614	10.710 (4.689)

ment and the trunk horizontal acceleration. There exist two kinds of delays in this model. The closed-loop transfer function of the HNC, $H_C(s)$, corresponding to the either of the AV or AN conditions, can be obtained as follow:

$$H_C(s) = e^{-sT_d} \frac{s}{\alpha s^2 + (\beta + k_d)s + \gamma + k_P}. \quad (9)$$

3 Results

Frequency response functions of the models, in the RLX, AV, and AN conditions, demonstrated good agreements with the averaged values (Eq. (1)) of the experimentally derived frequency response functions (e.g., Fig. 4). The magnitudes of the averaged frequency response functions, corresponding to the nine subjects were found to be consistent with those of the models.

The coefficients of the P (k_p) and D (k_d) controllers for the AV and AN conditions were also obtained (Table 2). The coefficients of the P and D controllers for the subjects number 2 to 9 were found to be more than the corresponding values in the AN conditions.

Acknowledgements

The authors wish to express their thanks to Professor N. Inoue and Dr. N. Hori of the Department of Architecture and Building Science, Tohoku University, JAPAN, for their collaboration in conducting the experiments. M. A. Fard gratefully acknowledges the support of a JSPS (Japan Society for the Promotion of Science) postdoctoral fellowship.

References

[1] Guitton D, Kearney RE, Wereley N, Peterson BW, Visual, vestibular and voluntary contributions to human head stabilization. Exp Brain Res 64: 59-69, 1986.

[2] Ishida A, Shoji I, Fukuoka Y, Analysis of the postural control system under fixed and sway-referenced support conditions. IEEE Transactions on Biomedical Engineering 44: 331-336, 1997.

[3] Pintelon R and Schoukens J, System identification. A frequency domain approach. IEEE Press, 2001.

Proc. of The Ninth Int. Symp. on Artificial Life and Robotics (AROB 9th '04)
Beppu, Oita, Japan, 28-30 January, 2004

A model of bipedal walking controlled by the basal ganglia - brainstem systems

TOMITA Nozomi, YANO Masafumi
Research Institute of Electrical Communication, Tohoku University,
2-1-1 Katahira, Aoba-ku, Sendai 980-8577, JAPAN
tomita@riec.tohoku.ac.jp

Abstract

We modeled nervous system as a automatic voluntary movement control system, which consists of basal ganglia, midbrain, brainstem, and spinal cord. CPGs generate only phase control information which determines muscle activity pattern. Muscle tone control information is independent of CPGs. Our walking model only needs desired velocity and it can begin to walk from a standstill and change to steady state immediately. Our results suggest that the generated pattern can adopt to unpredictable environment. This model is easily extensible to voluntary movement control model.

Key words: Bipedal walking, Basal ganglia, Brainstem, PPN, CNF/MLR, Central Pattern Generator(CPG)

1 Introduction

Recently the studies of bipedal walking model, there is new approach replaced with the conventional method which is ZMP. In the dynamical systems approach, it is used that passive dynamics of skeletal system or nonlinear interaction among the skeletal system, central pattern generators(CPGs) and environment[1, 2, 3]. The importance of "embodiment" is recognized by these approach. But these walking patterns used dynamical systems approach are merely the results of the nonlinear interaction between the robot and the idealized environments, so it cannot adapt to the unpredictable changing environments such as the real world. We call such environments " indefinite environments". Here we discuss the real-time control of the bipedal robot in the real world.

1.1 Walking models of dynamical systems approach

Taga et al. has proposed a bipedal model constituted of a central pattern generator (CPG), a musculoskeletal system and an environment [1, 2] based on passivewalk[4]. The nonlinear interaction among these three components can produces flexible walking patterns in the sagittal plane, because the CPG as a control system generates various entrainment states depending on the walking velocity and the changes of the environment, termed the global entrainments. This model behaves far more flexible than the passive walking model mentioned above, because the entrained state is restored as far as the perturbation on this system is within the entrainment region.

But some walking model based on this approach, the connections of the CPG are determined ad hoc and remain constant. And these model uniquely determine locomotion rhythm and muscle tones by phase and amplitude of CPG waveform. So locomotion pattern generated these model is not flexible. And it is hard to generate pattern when transient state about the time to begin to walk. So this system is not adaptable to the unexpected changes of the environment.

We modeled nervous system as a automatic voluntary movement control system, which consists of basal ganglia, midbrain, brainstem, and spinal cord. This model based on physiological observation of decerebrate cat[5, 6, 7, 8]. CPGs generate only "phase control information" which determins muscle activity pattern. It descends efferent fiber from CNF/MLR to CPGs. " Muscle tone control information" is independent of CPGs. It descends efferent fiber from PPN to Motoneurons.

2 Model

2.1 Central Pattern Generator Model

In our model we focus on the bipedal walking, so we discuss the control of the motor system after the decision-making, that is, selection of the behavior. The brain stem centers send the velocities of the both sides of the limbs and their muscle tones as the instructions to CPG after coordinating the purposive

movements and the standing posture. In this model the neural network of the control system composed of the brain stem centers and CPG is shown in Fig.1. The CPG send motor outputs to control leg muscles and receive the external afferents as to position, load and force of each muscle. Central pattern generators (CPG) are networks of neurons to control the motor system generating spatio- temporal pattern of neural activities. In this paper, we also construct a coupled nonlinear-oscillator system as the polymorphic network, which can produce various walking pattern by modulating the properties of the composing neurons. We adopt fundamentally their results as schemati-

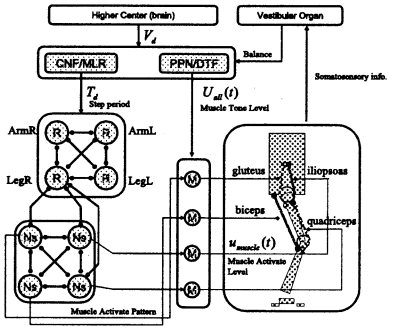


Figure 1: CNS-CPG model for bipedal walking

cally shown in Fig.1. In thoracic ganglion, this signal is transformed into rhythmic wave by rhythmic neuron corresponding to a spiking inter-neuron in the CPG The rhythmic neuron makes direct synaptic connection with non -spiking inter-neuron (NS neuron), which is great important to integrate the information on the states of muscles and inter-segmental pathway. The spatio-temporal patterns of the movement of legs are emerged through the interaction among the NS neurons by integration of the dynamical information feed-backed from the effector organs to content the purpose as the constraints.

The equations of rhythmic neuron(R) and non-spiking neuron(Ns) model have fundamentally the same structure and given by

$$\left.\begin{array}{lcl} \frac{dx(t)}{dt} & = & -y(t) - f(x(t)) \\ & & +Cpl_R + Cpl_{Ns} + Cpl_{MS} \\ \frac{dy(t)}{dt} & = & g(x(t)) + D(t) \\ f(x(t)) & = & A_1 \left\{ \frac{(x-B_1)^3}{3} + C_1 x \right\} \\ g(x(t)) & = & A_2(t)x^3 + B_2 x^2 + C_2 x \end{array}\right\} \quad (1)$$

where Cpl_R, Cpl_{Ns} and Cpl_{MS} are the coupling terms with rhythmic neuron, non-spiking neuron and musclo-skeletal system, respectively. Here, the coupling terms in the equation of the rhythmic neuron are given by,

$$\left.\begin{array}{lcl} Cpl_R^i & = & \sum_j \alpha_R^{ji} \left(x_R^j(t) - x_R^i(t) \right) \\ Cpl_{Ns}^i & = & \sum_k \beta_{Ns}^{ki} \left(x_{Ns}^k(t) \right) \\ Cpl_{MS}^i & = & -k_\theta \theta_{hip}^{ipsi}(t) \end{array}\right\} \quad (2)$$

The coupling terms in the equation of the non-spiking neuron are given by,

$$\left.\begin{array}{lcl} Cpl_R^i & = & \sum_j \beta_R^{ji} \left(x_R^j(t) \right) \\ Cpl_{Ns}^i & = & \sum_k \gamma_{Ns}^{ki} \left(x_{Ns}^k(t) \right) \\ Cpl_{MS}^i & = & 0 \end{array}\right\} \quad (3)$$

where $\alpha(x), \beta(x), \gamma(x)$ are the coupling functions from R to R, R to Ns and Ns to Ns, respectively. The coulpling functions denote the coupling weight and whether the coupling is non rectifier or half-wave rectifier. θ_{hip}^{ipsi} is the ipsilateral hip angle.

2.2 Muscle Model

The dynamical properties of muscle contraction plays essential role for bipedal walking. The muscle model proposed by A.V. Hill[11] has most widely accepted, which can represent a quite precise relationship between the tension development and the shortening velocity, known as force-velocity (P-V) relation. The P-V relation is denoted by

$$P\left(u(t), v(t)\right) = \left\{ \begin{array}{ll} \frac{bP_0 - av}{v+b} u, & v \geq 0 \\ \frac{2P_0 v - bP_0 + av}{v-b} u, & v < 0 \end{array}\right. \quad (4)$$

where v, P_0, a, b and u are the shortening velocity, the maximum tension development, the constant of energy release, the isometric proportional constant and the degree of activation of muscle, respectively. Using the natural length of muscle L_n, the constants a, b are given by $a = 0.25P_0$ and $b = 0.9L_n$, respectively. The energy conversion efficiency performed during muscle contraction η is given by

$$\eta\left(P\left(u(t), v(t)\right), v(t)\right) = \left\{ \begin{array}{ll} \frac{Pv}{Pv + a(v+b)}, & v \geq 0 \\ \frac{Pv}{P(-v) + a(-v+b)}, & v < 0 \end{array}\right. \quad (5)$$

2.3 Control of Muscle Contraction by Moto-Neuron

In our model, each non-spiking neuron is connected to each muscle by one to one through each corresponding moto-neuron. The output of moto-neuron $u(t)$, which determines the activation level of muscle contraction, is given by,

$$\begin{array}{lcl} u_i(t) & = & -k_{v1} H(x_{Ns}^i) v_i - k_{v2} U(t) v_i \\ & & + \sum_j k_f^j H(x_{Ns}^i) f_j(\boldsymbol{v}, \boldsymbol{\eta}) \end{array} \quad (6)$$

where H, v_i and f denote the Heaviside function, the shortening velocity of the corresponding muscle and the constraint of the optimization of energy conversion performed in the muscle, respectively. The first and the second terms of the right side of equation (6) denote the viscosity of the muscle against the external force and one due to the muscle tense of the integrated whole body $U(t)$ which is determined in PPN region in the basal ganglia to take a standing posture, respectively. These viscous properties of muscle are caused from the dynamical and active properties of muscle contraction in response to the changes of the external force.

2.4 Stride determined by balance constraint

To walk at required velocity V_d, there is also an ill-posed problem how to determine the stride and the walking period, since the required velocity is attained with any combination of strides and periods. So we adopt a balance constraint to determine the relation ship between the stride and the walking period. Since the length of the leg during stance phase is constant, the angle θ^d_{leg} between the the swing leg and the direction of the gravity can be written as follows;

$$\theta^d_{leg} = -sgn(v)\left\{\cos^{-1}(\Phi)\right\} - \theta_{v.o} \tag{7}$$

$$\Phi = -\frac{gL^{sw}_{leg}}{v^2} + \frac{1}{v}\sqrt{\frac{gL^{sw\ 2}_{leg}}{v} + V_d^2 + 2gL^{sw}_{leg}}$$

where v is body speed at the last touchdown moment, L^{sw}_{leg} is the swing leg length at the moment and $\theta_{v.o}$ is the angle of the trunk to be obtained the vestibular organ. Step length of this phase is determined by the desired angle and length of the legs as

$$\lambda_{balance} = 2L^{sw}_{leg}\sin\theta^d_{leg}. \tag{8}$$

Applying walking velocity and stride length relation, desired stride period is obtained as

$$T^d_{stride} = \frac{2\lambda_{balance}}{V^d_{body}}. \tag{9}$$

In order to achieve T^d_{stride}, R Neuron is modulated as

$$\Delta A_2 = -k_{A2}(T^d_{stride} - T_{stride}). \tag{10}$$

Since the swing legs should be sufficiently shorter than the stance legs, the desired length of the swing leg is given by,

$$L^d_{leg} = L^{st}_{leg}\left\{\left|\frac{1-\epsilon}{\theta^d_{leg}}\theta_{leg}\right| + \epsilon\right\}, \tag{11}$$

where, ϵ is desired ratio of the swing leg length and the stance one.

3 Results

3.1 Simulation Environment

The results of the computer simulation using a usual personal computer (CPU: Athlon XP1600+, Mem: 512MB, OS: Turbo Linux) are presented. Description and calculation of the mechanics are achieved by the Dynamics Calculation C-library Vortex (Critical Mass Lab.). The musclo-skeletal system and the environment are described by the Vortex.

3.2 Adaptation of Perturbations

Figure 2 show a CPG waveforms and motoneuron acvivate levels. CPG pattern is used only muscle activate pattern by motoneurons. Figure 3 show the stick figure of

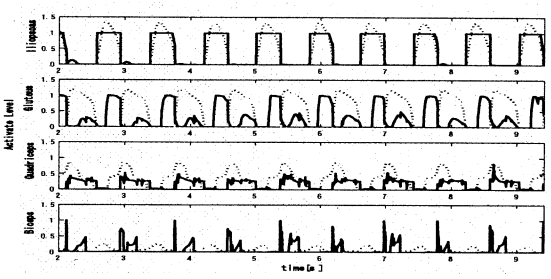


Figure 2: CPG waveform and muscle activate levels of motoneuron. Broken lines are ns neurons pattern. Solid lines are motoneurons activate levels.

our bipedal walking movements on level ground. As shown in Fig. 3-a, the stick figure was traced every 0.1 second and it clearly demonstrates the steady walking. It should be noted that our model can begin to walk from a standstill. The effects of the mechanical perturbations to the right shank at various strength and duration are examined as shown in Fig. 3-b, c. Figure 3-b shows the walking pattern when a force of 100 N in the backward direction for 0.2 sec is applied twice at the timings indicated by bars in the figure. After the first perturbation, the system immediately return to steady state, but the effect of the second perturbation lasts longer than one of the first case, indicating longer restoration time. When a force of 40 N was applied for longer duration of 4 sec, the system is able to return to the steady state (Fig. 3-c).

3.3 Comparison with a Human Walk

In dynamical systems approach, phase plots, phase angle and relative phase have been used to study gait. We compared model walking with human walking by using continuous relative phase(CRP). CRP has been used to study spatial-temporal coordination[12]. In this research,

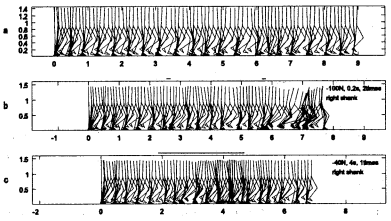


Figure 3: Stick figure of the walking movements. The stick figure was traced every 0.1 second. A: natural walking. B,C: The effects of the mechanical perturbations to the right shank. B: Two perturbations of a force of 100 N in the backward direction for 0.2 sec. Bars at the top indicate perturbation period. C: The bar indicates perturbation period of a force of 40 N for 4 sec.

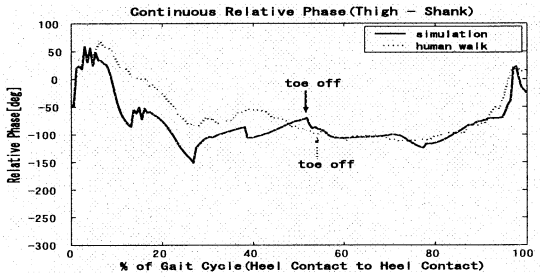


Figure 4: Continuous relative phase of walking for simulation and human. Relative phase wad defined as the thigh phase angle minus the shank phase angle.

the purpose of using CRP was to compare lower extremity coordination in walking at the model and human.

The CRP was defined as the difference between thigh and shank phase angles at each point throughout the stride cycle. Fig.4 is a graphic representation of the typical CRP curves of the model(solid line: 1.3m/s) and the human(broken line:2.2m/s)[12]. Positive CRP indicates that the shank phase angle is in the leading position relative to the thigh phase angle. Horizontal axis is % of Gait Cycle which was defined heel contact to heel contact.

Both those swing phase are similar. Difference of CRPs which is visible to the stance phase is due to that knee of the model flexes about 20 degree when heel strike.

4 Conclusion

In this research, we suggest "basalganglia - brainstem systems". Our strategy proposed in this research for the control of bipedal walking model is quite different from those proposed until now.

Our walking model only needs desired velocity and it can begin to walk from a standstill and change to steady state immediately. A walk is maintained by the real-time control when mechanical perturbations are added to the right shank at various strength and duration. Our results suggest that the generated pattern can adopt to unpredictable environment. This model is easily extensible to voluntary movement control model.

References

[1] G. Taga, Y. Yamaguchi and H. Shimizu : "Self-organized control of bipedal locomotion by neural oscillators." *Biological Cybernetics*, vol.65, pp.147-159, 1991.

[2] G. Taga:"A model of the neuro-musculo-skeletal system for human locomotion II. Real-time adaptability under various costraints", *Biological Cybernetics*, vol.73, pp. 113-121, 1995

[3] H. Kimura, S. Akiyama and K. Sakurama: "Realization of Dynamic Walking and Running of the Quadruped Using Neural Oscillator", *AUTONOMOUS ROBOTS*, Vol.7, No.3, pp. 247-258, 1999

[4] T. McGeer: "Passive Walking With Knees." *Proc.of the 1990 IEEE ICRA*, Vol.3, pp.1640-1645, 1990.

[5] S. Miller & J. Jan der Burg: *Control of posture and locomotion.*, Plenum Press, pp.561-577, 1973.

[6] S. Miller, J. Van Der Burg:"The function of long propriospinal pathways in the co-ordination of quadrupedal stepping in the cat." *Control of posture and locomotion.*(Advances in Behavioral Biology), New York London, Plenum Press, Vol.7, pp.561-577, 1973.

[7] S. Mori : "Integration of posture and locomotion in acute decerebrate cats and in awake, freely moving cats." *Prog. Neurobiol.* 28, pp.161-196, 1987.

[8] K. Takakusaki et al. : "Basal Ganglia Efferents to the Brainstem Centers Controlling Postural Muscle Tone and Locomotion: A New Concept for Understanding Motor Disorders in Basal Ganglia Dysfunction " *Neuroscience*, 119 , pp. 293-08, 2003.

[9] P. A. Getting :"Emerging principles governing the operation of neural networks." *Ann. Rev. Neurosci.*, Vol.12, pp.185-204, 1989.

[10] Y. Makino , M. Akiyama & M. Yano : "Emergent mechanisms in multiple pattern generations of the lobster pyloric network." *Biol. Cybern.* 82, pp.443-454, 2000.

[11] A. V. Hill : "The heat of shortening and the dynamic constants of muscle", *Proc. R. Soc. London Ser. B*,Vol.126, pp.136, 1938.

[12] Li Li, C. H. Elizabeth , van den Bogert, E. C. Graham, E. A. Richard, van Emmerik, J. Hamill : "Coordination patterns of walking and running at similar speed and stride frequency. " *Human Movement Science*, 18, pp.67-85, 1999.

Proc. of The Ninth Int. Symp. on Artificial Life and Robotics (AROB 9th '04)
Beppu, Oita, Japan, 28-30 January, 2004

Computer Simulation of an Augmented Automatic Choosing Control designed by Extremizing a Combination of Hamiltonian and Lyapunov Functions

Toshinori Nawata
Department of Information and Computer Sciences,
Kumamoto National College of Technology,
Kumamoto, Japan. 861-1102

Hitoshi Takata
Department of Electrical and Electronics Engineering,
Faculty of Engineering, Kagoshima University,
Kagoshima, Japan. 890-0065

Abstract

In this paper we consider a nonlinear feedback control called augmented automatic choosing control (AACC) for nonlinear systems. Constant terms which arise from sectionwise linearization of a given nonlinear system are treated as coefficients of a stable zero dynamics. Parameters included in the control are suboptimally selected by extremizing a combination of Hamiltonian and Lyapunov functions with the aid of the genetic algorithm.

1 Introduction

A genetic algorithm (GA)[7] is one of evolutionary computing algorithms in engineering sciences. It has been used to solve such complicated tasks as nonlinear global optimization problems. The purpose of this paper is to present a nonlinear feedback control called AACC (Augmented automatic choosing control), which is designed by making good use of the GA.

Generally, it is easy to design the optimal control laws for linear systems, but it is not so for nonlinear systems, though they have been studied for many years[1]~[6]. One of most popular and practical nonlinear control laws is synthesized by applying a linearization method by Taylor expansion and the linear optimal control method to a given nonlinear system. This is only effective in a small region around the steady state point or in almost linear systems[1]~[3].

To overcome these weakness, the AACC is proposed for nonlinear systems and its design procedure is as follows. Assume that a system is given by a nonlinear differential equation. Choose a separative variable, which makes up nonlinearity of the given system. The domain of the variable is divided into some subdomains. On each subdomain, the system equation is linearized by Taylor expansion around a suitable point so that a constant term is included in it. This constant term is treated as a coefficient of a stable zero dynamics. The given nonlinear system approximately makes up a set of augmented linear systems, to which the optimal linear control theory is applied to get the linear quadratic (LQ) controls. These LQ controls are smoothly united by sigmoid type automatic choosing functions to synthesize a single nonlinear feedback controller.

This controller is of a structure-specified type which has some parameters, such as the number of division of the domain, regions of the subdomains, points of Taylor expansion, gradients of the automatic choosing functions, and so on. These parameters must be selected optimally to be just the controller's fit. Since they lead to a nonlinear optimization problem, we are able to solve it by using the GA suboptimally and successfully. The suboptimal values of these parameters are obtained by extremizing a combination of Hamiltonian and Lyapunov functions in this paper.

This approach is applied to a field excitation control problem of power system to demonstrate the splendidness of the AACC. Simulation results show that the new controller using the GA can improve performance remarkably well.

2 Augmented Automatic Choosing Control

Assume that a nonlinear system is given by

$$\dot{x} = f(x) + g(x)u, \quad x \in \mathbf{D} \tag{1}$$

where $\cdot = d/dt$, $x = [x[1], \cdots, x[n]]^T$ is an n-dimensional state vector, $u = [u[1], \cdots, u[r]]^T$ is an r-dimensional control vector, $f(x) : \mathbf{D} \to R^n$ is a nonlinear vector-valued function with $f(0) = 0$ and is continuously differentiable, $g(x) : \mathbf{D} \to R^{n \times r}$ is a driving matrix with $g(0) \neq 0$ and is continuously differentiable, $\mathbf{D} \subset R^n$ is a domain , and T denotes transpose.

Considering the nonlinearity of the system (1), introduce a vector-valued function $C : \mathbf{D} \to R^L$ which defines the separative variables $\{C_j(x)\}$, where $C = [C_1 \cdots C_j \cdots C_L]^T$ is continuously differentiable. Let D be a domain of C^{-1}. For example, if $x[2]$ is the element which has the highest nonlinearity of (1), then

$$C(x) = x[2] \in D \subset R \quad (L = 1)$$

(see Section 4). The domain D is divided into some subdomains: $D = \cup_{i=0}^{M} D_i$, where $D_M = D - \cup_{i=0}^{M-1} D_i$

and $C^{-1}(D_0) \ni 0$. $D_i(0 \leq i \leq M)$ endowed with a lexicographic order is the Cartesian product $D_i = \Pi_{j=1}^{L}[a_{ij}, b_{ij}]$, where $a_{ij} < b_{ij}$.

Introduce a stable zero dynamics :

$$\dot{x}[n+1] = -\sigma_i x[n+1] \quad (x[n+1](0) \simeq 1,\ 0 < \sigma_i < 1) \tag{2}$$

where the value of σ_i shall be selected so that $\sigma_i = -\dot{x}[n+1]/x[n+1] \leq -\dot{x}[k]/x[k]$ holds for all $k(k = 1, \cdots, n)$. This tries to keep $x[n+1] \simeq 1$ for a good while when the system (1) is not on $C^{-1}(D_0)$.

Combine (1) with (2) to form an augmented system

$$\dot{\mathbf{X}} = \bar{f}(\mathbf{X}) + \bar{g}(\mathbf{X})u \tag{3}$$

where

$$\mathbf{X} = \begin{bmatrix} x \\ x[n+1] \end{bmatrix} \in \mathbf{D} \times R$$

$$\bar{f}(\mathbf{X}) = \begin{bmatrix} f(x) \\ -\sigma_i x[n+1] \end{bmatrix}, \bar{g}(\mathbf{X}) = \begin{bmatrix} g(x) \\ 0 \end{bmatrix}.$$

Let a cost function be

$$J = \frac{1}{2}\int_0^\infty (\mathbf{X}^T\mathbf{Q}\mathbf{X} + u^T\mathbf{R}u)\, dt \tag{4}$$

where

$$\mathbf{Q} = \begin{bmatrix} Q & 0 \\ 0 & q \end{bmatrix}, \quad R \ni q > 0,$$

$Q = Q^T > 0$ and $\mathbf{R} = \mathbf{R}^T > 0$ which denote positive symmetrix matrices. Values of $\mathbf{Q}$ and $\mathbf{R}$ are properly determined based on engineering experience.

On each D_i, the nonlinear system is linearized by the Taylor expansion truncated at the first order about a point $\hat{X}_i \in C^{-1}(D_i)$ and $\hat{X}_0 = 0$:

$$\begin{aligned} f(x) + g(x)u &\simeq A_i x + w_i + B_i u \\ &\simeq A_i x + w_i x[n+1] + B_i u \end{aligned} \tag{5}$$

where

$$\begin{aligned} A_i &= \partial f(x)/\partial x^T|_{x=\hat{X}_i}\ ,\ B_i = g(\hat{X}_i), \\ w_0 &= 0\ ,\ w_i = f(\hat{X}_i) - A_i\hat{X}_i. \end{aligned}$$

That is, an approximation of (3) is

$$\dot{\mathbf{X}} = \bar{A}_i\mathbf{X} + \bar{B}_i u \quad \text{on } C^{-1}(D_i) \times R \tag{6}$$

where

$$\bar{A}_i = \begin{bmatrix} A_i & w_i \\ 0 & -\sigma_i \end{bmatrix}, \bar{B}_i = \begin{bmatrix} B_i \\ 0 \end{bmatrix}.$$

An application of the linear optimal control theory[2] to (4) and (6) yields

$$u_i(\mathbf{X}) = -\mathbf{R}^{-1}\bar{B}_i^T\mathbf{P}_i\mathbf{X} \tag{7}$$

where the $(n+1) \times (n+1)$ matrix $\mathbf{P}_i$ satisfies the Riccati equation :

$$\mathbf{P}_i\bar{A}_i + \bar{A}_i^T\mathbf{P}_i + \mathbf{Q} - \mathbf{P}_i\bar{B}_i\mathbf{R}^{-1}\bar{B}_i^T\mathbf{P}_i = 0. \tag{8}$$

Introduce an automatic choosing function of sigmoid type:

$$\begin{aligned} I_i(x) = \prod_{j=1}^{L}\Bigg\{ & 1 - \frac{1}{1+\exp\left(2N_1\left(C_j(x) - a_{ij}\right)\right)} \\ & - \frac{1}{1+\exp\left(-2N_1\left(C_j(x) - b_{ij}\right)\right)} \Bigg\} \end{aligned} \tag{9}$$

where N_1 is positive real value, $-\infty \leq a_{ij}$ and $b_{ij} \leq \infty$. $I_i(x)$ is analytic and almost unity on $C^{-1}(D_i)$, otherwise almost zero(see Figure 1).

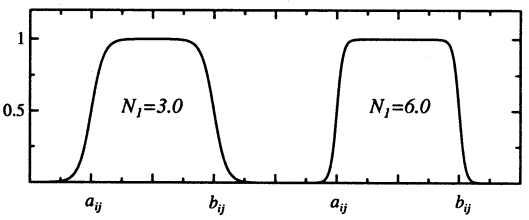


Figure 1: Automatic Choosing Function(N_1=3.0, 6.0)

Uniting $\{u_i(\mathbf{X})\}$ of (7) with $\{I_i(x)\}$ of (9), we have an augmented automatic choosing control

$$u(\mathbf{X}) = \sum_{i=0}^{M} u_i(\mathbf{X})I_i(x). \tag{10}$$

3 Parameter Selection by GA

The Hamiltonian for Eqs.(3) and (4) is given by

$$\begin{aligned} H(\mathbf{X}, u, \lambda) = & \frac{1}{2}\left(\mathbf{X}^T\mathbf{Q}\mathbf{X} + u^T Ru\right) \\ & + \lambda^T\left(\bar{f}(\mathbf{X}) + \bar{g}(\mathbf{X})u\right). \end{aligned} \tag{11}$$

Assume that the adjoint vector $\lambda \in R^{n+1}$ is

$$\lambda(\mathbf{X}) = \sum_{i=0}^{M}\{(\bar{B}_i - \bar{g}(\mathbf{X}))\bar{g}(\mathbf{X})^\dagger + E\}^T\mathbf{P}_i\mathbf{X}I_i(x) \tag{12}$$

where $\bar{g}(\mathbf{X})^\dagger\bar{g}(\mathbf{X}) = E$, E is an appropriate-dimentional unit matrix, $\dagger$ denotes pseudo inverse, and $\mathbf{P}_i$ is the solution of (8).

The necessary condition of the optimality is $\partial H/\partial u = 0$ or $u = -R^{-1}\bar{g}(\mathbf{X})^T\lambda$, which derives Eq.(10) using Eq.(12) and

$$H(\mathbf{X}, u, \lambda) = \frac{1}{2}\mathbf{X}^T\mathbf{Q}\mathbf{X} - \frac{1}{2}u^T Ru + \bar{f}^T(\mathbf{X})\lambda \tag{13}$$

using Eq.(11).

Next, introduce a Lyapunov function candidate:

$$V(\mathbf{X}) = \mathbf{X}^T\Pi(\mathbf{X})\mathbf{X} \tag{14}$$

where

$$\Pi(\mathbf{X}) = \sum_{i=0}^{M}\mathbf{P}_i\Pi_i(x)\ ,$$

$$\Pi_i(x) = \eta_i \prod_{j=1}^{L} \left\{ 1 - \frac{1}{1+\exp\left(2N_2\left(C_j(x)-a_{ij}\right)\right)} - \frac{1}{1+\exp\left(-2N_2\left(C_j(x)-b_{ij}\right)\right)} \right\}, \quad (15)$$

N_2 and η_i are positive real values.

By the Lyapunov's direct method[3], the equilibrium point 0 is uniformly stable on a connected set:

$$\mathbf{D}_V = \left\{ x \in \mathbf{D} : V(\mathbf{X}) < \gamma,\ \dot{V}(\mathbf{X}) < 0 \right\}$$

where

$$\gamma = \inf\left\{ V(\mathbf{X}) : \mathbf{X} \neq 0,\ \dot{V}(\mathbf{X}) = 0 \right\}. \quad (16)$$

In order to design optimal control by Hamiltonian and expand the stable region in the sense of Lyapunov as wide as possible, we define a performance

$$PI = \omega_1 \int_{\mathbf{D}} |H(\mathbf{X}, u, \lambda)| / \mathbf{X}^T \mathbf{X} d\mathbf{X} - \omega_2 \gamma \quad (17)$$

where $\omega_i (\omega_i \geq 0; i = 1, 2)$ is weight.

A set of parameters included in the control (10):

$$\bar{\Omega} = \left\{ M, N_1, N_2, a_{ij}, b_{ij}, \hat{X}_i, \eta_i \right\}$$

is suboptimally selected by minimizing PI with the aid of GA[7] as follows.

<ALGORITHM>

step1:A-priori: Set values $\bar{\Omega}_{apriori}$ appropriately.

step2:Parameter: Choose a subset $\Omega \subset \bar{\Omega}$ to be improved and rewrite it by $\Omega = \{M, N_1, N_2 \cdots\} = \{\alpha_k : k = 1, \cdots, K\}$.

step3:Coding: Represent each α_k with a binary bit string of $\widetilde{L}$ bits and then arrange them into one string of $\widetilde{L}K$ bits.

step4:Initialization: Randomly generate an initial population of $\widetilde{q}$ strings $\{\Omega_p : p = 1, \cdots, \widetilde{q}\}$.

step5:Decoding: Decode each element α_k of Ω_p by $\alpha_k = (\alpha_{k,max} - \alpha_{k,min})\, A_k / \left(2^{\widetilde{L}} - 1\right) + \alpha_{k,min}$ where $\alpha_{k,max}$:maximum, $\alpha_{k,min}$:minimum, and A_k:decimal value of α_k.

step6:Control: Design $u = u(\mathbf{X})_p \quad (p = 1, \cdots, q)$ for Ω_p by using Eq.(10).

step7:Adjoint: Make $\lambda = \lambda(\mathbf{X})_p \quad (p = 1, \cdots, q)$ for Ω_p by using Eq.(12).

step8:Lyapunov function: Make $\gamma = \gamma_p$ $(p = 1, \cdots, \widetilde{q})$ for Ω_p by using Eq.(16).

step9:Fitness value calculation: Calculate

$$PI_p = \omega_1 \int_{\mathbf{D}} \left| \frac{1}{2}\mathbf{X}^T \mathbf{Q} \mathbf{X} - \frac{1}{2} u(\mathbf{X})_p^T R u(\mathbf{X})_p + \bar{f}^T(\mathbf{X}) \lambda(\mathbf{X})_p \right| / \mathbf{X}^T \mathbf{X} d\mathbf{X} - \omega_2 \gamma_p \quad (18)$$

by Eqs.(13) and (17), or fitness $F_p = -PI_p$. Integration of (18) is approximated by a finite sum.

step10:Reproduction: Reproduce each of individual strings with the probability of $F_p / \sum_{j=1}^{\widetilde{q}} F_j$.

step11:Crossover: Pick up two strings and exchange them at a crossing position by a crossover probability P_c.

step12:Mutation: Alter a bit of string (0 or 1) by a mutation probability P_m.

step13:Repetition: Repeat step5~step12 until prespecified G-th generation. If unsatisfied, go to step2.

As a result, we have a suboptimal control $u(\mathbf{X})$ for the string with the best performance over all the past generations.

4 Numerical Example

Consider a field excitation control problem of power system which is described[5][6] by

$$\widetilde{M}\frac{d^2\delta}{dt^2} + \widetilde{D}(\delta)\frac{d\delta}{dt} + P_e(\delta) = P_{in}$$

$$P_e(\delta) = E_I^2 Y_{11} \cos\theta_{11} + E_I \widetilde{V} Y_{12} \cos(\theta_{12} - \delta)$$

$$E_I + T'_{d0}\frac{dE'_q}{dt} = E_{fd}$$

$$E_I = E'_q + (X_d - X'_d) I_d(\delta)$$

$$I_d(\delta) = -E_I Y_{11} \sin\theta_{11} - \widetilde{V} Y_{12} \sin(\theta_{12} - \delta)$$

$$\widetilde{D}(\delta) = \widetilde{V}^2 \left\{ \frac{T''_{d0}(X'_d - X''_d)}{(X'_d + X_e)^2} \sin^2\delta + \frac{T''_{q0}(X_q - X''_q)}{(X_q + X_e)^2} \cos^2\delta \right\},$$

where δ: phase angle, $\dot{\delta}$: rotor speed, $\widetilde{M}$: inertia coefficient, $\widetilde{D}(\delta)$: damping coefficient, P_{in}: mechanical input power, $P_e(\delta)$: generator output power, $\widetilde{V}$: reference bus voltage, E_I: open circuit voltage, and E_{fd}: field excitation voltage. Put $x=[x[1], x[2], x[3]]^T=[E_I - \hat{E}_I, \delta - \hat{\delta}_0, \dot{\delta}]^T$ and $u = E_{fd} - \hat{E}_{fd}$, so that

$$\begin{bmatrix} \dot{x}[1] \\ \dot{x}[2] \\ \dot{x}[3] \end{bmatrix} = \begin{bmatrix} f_1(x) \\ f_2(x) \\ f_3(x) \end{bmatrix} + \begin{bmatrix} g_1(x) \\ 0 \\ 0 \end{bmatrix} u \quad (19)$$

where

$$f_1(x) = -\frac{1}{kT'_{d0}}\left(x[1] + \hat{E}_I\right) + \frac{(X_d - X'_d)\widetilde{V} Y_{12}}{k} x[3] \cos\left(\theta_{12} - x[2] - \hat{\delta}_0\right)$$

$$f_2(x) = x[3]$$

$$f_3(x) = -\frac{\widetilde{V} Y_{12}}{\widetilde{M}}\left(x[1] + \hat{E}_I\right)\cos\left(\theta_{12} - x[2] - \hat{\delta}_0\right) - \frac{Y_{11}\cos\theta_{11}}{\widetilde{M}}\left(x[1] + \hat{E}_I\right)^2 - \frac{\widetilde{D}(x)}{\widetilde{M}} x[3] + \frac{P_{in}}{\widetilde{M}}$$

Table 1: Performances $\widetilde{J}$

Method	$x^T(0)$			
	[0, 0.4, 0]	[0, 0.5, 0]	[0, 1.2, 0]	[0, 1.5, 0]
LOC	0.954	×	×	×
ACC	0.966	5.219	×	×
AACC($\omega_2 = 10$)	0.911	1.205	1.799	×
AACC($\omega_2 = 1000$)	0.970	1.244	2.132	4.573

× : very large value

$$\widetilde{D}(x) = \widetilde{V}^2 \left\{ \frac{T''_{d0}(X'_d - X''_d)}{(X'_d + X_e)^2} \sin^2\left(x[2] + \hat{\delta}_0\right) + \frac{T''_{q0}(X_q - X''_q)}{(X_q + X_e)^2} \cos^2\left(x[2] + \hat{\delta}_0\right) \right\}$$

$$g_1(x) = \frac{1}{kT'_{d0}}, \quad k = 1 + \left(X_d - X'_d\right) Y_{11} \sin\theta_{11}.$$

Parameters are $\widetilde{M} = 0.016095[pu]$, $T'_{d0} = 5.09907[sec]$, $\widetilde{V} = 1.0[pu]$, $P_{in} = 1.2[pu]$, $X_d = 0.875[pu]$, $X'_d = 0.422[pu]$, $Y_{11} = 1.04276[pu]$, $Y_{12} = 1.03084[pu]$, $\theta_{11} = -1.56495[pu]$, $\theta_{12} = 1.56189[pu]$, $X_e = 1.15[pu]$, $X''_d = 0.238[pu]$, $X_q = 0.6[pu]$, $X''_q = 0.3[pu]$, $T''_{d0} = 0.0299[pu]$, $T''_{q0} = 0.02616[pu]$.

Steady state values are $\hat{E}_I = 1.52243[pu]$, $\hat{\delta}_0 = 48.57°$, $\dot{\hat{\delta}}_0 = 0.0[deg/sec]$, $\hat{E}_{fd} = 1.52243[pu]$. Set $\mathbf{X} = [x^T, x[4]]^T = [x[1], x[2], x[3], x[4]]^T$, $n = 3$, $\hat{X}_0 = \hat{\delta}_0 = 48.57°$, $C(x)$=$x[2]$, $L = 1$, $\mathbf{Q}$=diag(1, 1, 1, 1), $\mathbf{R}$=1, $\eta_0 = 1$, $\omega_1 = 1$ and $x[4](0) = 1$. Experiments are carried out for the new control(AACC), the automatic choosing control(ACC)[6], and the ordinary linear optimal control(LOC)[1][2].

1) AACC($\omega_2 = 10$):
The parameters are suboptimally selected along the algorithm of section 3. $\omega_2 = 10$, Ω=$\{M, N_1, N_2, \hat{X}_i, a_{ij}, b_{ij}, \eta_i\}$, $\widetilde{G}$=100, $\widetilde{q}$=100, $\widetilde{L}$=8, P_c=0.8, P_m=0.03, $\mathbf{D}$=[-1,1]×[-1,1.5]×[-5,5]×[0,1.5]. It results that $M = 2$, $N_1 = 3.12$, $N_2 = 7.25$, $\hat{X}_1 = 70°$, $\hat{X}_2 = 95°$, $a = 58.8°$, $b = 93.0°$ and $\eta_1 = \eta_2 = 1.06$.

2) AACC($\omega_2 = 1000$):
The parameters are suboptimally selected by using a similar way of the **AACC**($\omega_2 = 10$). $\omega_2 = 1000$. It results that $M = 3$, $N_1 = 2.94$, $N_2 = 1.21$, $\hat{X}_1 = 80°$, $\hat{X}_2 = 100°$, $\hat{X}_3 = 130°$, $a_1 = 49.2°$, $b_1 = a_2 = 94.8°$, $b_2 = a_3 = 119.7°$ and $\eta_1 = \eta_2 = 2.91$.

3) ACC:
The parameters are suboptimally selected along the algorithm of section 3 when the performance is $PI = -\gamma$. Ω=$\{M, N_1, \hat{X}_i, a_{ij}, b_{ij}\}$. It results that $M = 1$, $N_1 = 8.5$, $\hat{X}_1 = 75°$ and $a_1 = 71.4°$.

Table1 shows performances by the AACC, the ACC and the LOC. The cost function of Table1 is $\widetilde{J} = \frac{1}{2}\int_0^{20} \left(\mathbf{X}^T\mathbf{Q}\mathbf{X} + u^T\mathbf{R}u\right) dt$. These results indicate that the AACC is better than the ACC and the LOC.

5 Conclusions

We have studied an augmented automatic choosing control using zero dynamics for nonlinear systems. This approach have been applied to a field excitation control problem of power system. Simulation results have shown that this controller using the GA can improve performance remarkably well.

References

[1] Y. N. Yu, K. Vongsuriya and L. N. Wedman, "Application of an Optimal Control Theory to a Power System", *IEEE Trans. Power Apparatus and Systems*, 89-1, pp.55–62, 1970.

[2] A. P. Sage and C. C. White III, "Optimum Systems Control (2nd edition)", *Prentice-Hall, Inc.*, 1977.

[3] M. Vidyasagar, "Nonlinear Systems Analysis", *Prentice-Hall, Inc.*, 1978.

[4] A.Isidori, "Nonlinear Control Systems : An Introduction (2nd edition)", *Springer-Verlag*, 1989.

[5] Y.Takagi and T.Shigemasa, "An Application of State-Space Linearization to a Power System Stabilizer", *Proc. 29th CDC*, TA8-1, pp.1553–1558, 1990.

[6] H.Takata, "An Automatic Choosing Control for Nonlinear Systems", *Proc. 35th CDC*, FA10-5, pp.3453–3458, 1996.

[7] D. E. Goldberg, "Genetic Algorithms in Search, Optimization, and Machine Learnings", *Addison-Wesley Pub. Co. Inc.*, 1989.

Proc. of The Ninth Int. Symp. on Artificial Life and Robotics (AROB 9th '04)
Beppu, Oita, Japan, 28-30 January, 2004

A FULLY AUTOMATED AND INTELLIGENT MARINE TRANSPORTATION SYSTEM

Thanh-Ha NGUYEN, *Hoang Minh JSC, Vietnam*
thanhha_hoangminh2003@yahoo.com
Dinh-Khoi TRAN, Thanh-Qui HOANG,
Thi-Ha TRAN, Van-Trieu BUI,
Hoang Nguyen Commercial Co., Ltd., Hanoi, Vietnam

Xuan-Thinh CAO, Duc-Hau NGUYEN,
Thi-Nu HOANG, Hong-Son PHAM,
Hoang Minh Co., Ltd., Hanoi, Vietnam
Thi-Minh-Hue NGUYEN, Hai-Son DAO,
Van-Tan PHAM, *Manufacture and Service Enterprise*

Abstract

This paper presents results of recently carried out studies toward a fully automated and intelligent system for marine transportation, including: current status of Marine Transportation Systems, contents of Virtual Vessel Traffic Service, Intelligent Marine Traffic Systems, Marine Intelligent Transport Systems; a concept of Fully Automated and Intelligent Ships and some advanced technologies for realization of the Fully Automated and Intelligent Marine Transportation System. Main conclusions and further study directions are also pointed out.

Keywords: Marine Intelligent Transportation Systems, Automation and Automatic Control, Marine Transportation System

1 Introduction

In many cases, as in international commerce, there is no alternative to moving goods by water. Waterborne transportation is more fuel-efficient than other transportation modes and reduces propulsion emissions by one-third or more. Transporting bulk goods by water results in a 35 percent reduction in transportation costs, when compared to other modes and the World ocean-borne trade is about 5 billion metric tons and international trade is projected to triple by 2020. To meet this increasing demand, the World New-Building Demand for shipbuilding is projected to be increased by about 15% in the period of 2000-2005.

However, a raising issue is the environmental challenges. The increasing in the number of big disasters has become a worldwide high priority issue and environment protection concerning marine transport has become the most important issue in our today life. How these problems can be solved? How the harmonious coexistence of people, marine transportation and environment can be realized?

Study by researchers worldwide shows that human mistakes contribute about 75-95% of all the reported marine casualties. Therefore the best solution to raise the level of safety (and to protect environment, to make marine transportation systems more efficient) is to build fully automated and intelligent ships. This conclusion does not mean fully automated and intelligent ships can solve any problems of the marine transport, and that should never be expected. However, building that kind of ships is one of the most efficient ways.

Developing of *ITS* – the combination, the "marriage" of information and communication technologies with the vessels should be considered as the main task in realizing the harmonious coexistence of people, marine transport and environment can be realized. Today *ITS* are often seen as the new age transportation systems for land, air, marine and also inland waterway transportation. However, unlike air and land transportation cases, the marine *ITS* are still far from being completed and many research projects have been carried out toward a marine *ITS*. For example, in Japan, a four-year research of Virtual Vessel Traffic Service (*V-VTS*) supported by Ministry of Education, Science, Sports and Culture has been terminated in FY2000 and a new 5-year project of Marine ITS was started by Ministry of Transport of Japan [1].

2 Marine Intelligent Transportation Systems

The Marine *ITS* usually contains supporting systems form shore base, ship operation system and data communication systems [2]. For safety of ship navigation in congested waterways, radar, *LORAN-C, INMARSAT* has been widely used [3], and recently *APPA* or *ECDIS* are added as additional tools. More recently, rapid development in computer and communication technologies has brought various changes in their applications because of the availability, effectiveness and reliability. That leads to several innovations in supporting systems for Marine *ITS*.

2.1 Automatic Identification Systems (AIS) and Visual Vessel Traffic Systems (V-VTS)

AIS are systems used to exchange information in both ship-to-ship and ship-to-shore in congested waterways. AIS help to improve safety of marine navigation. *IMO* requires all ships report the following information through *AIS* at regular interval:

- Static information: call sign, height and width, ship type, antenna's position, *IMO* number;
- Dynamic information such as: standard time, ship's position and heading angle, course on ground, ship's speed, rate of turn, and so on.
- Navigation information: ship's draft, type, departure and destination, waypoints in the course, etc.

- Safety message.

The reporting time depends on the situation of marine navigation.

The V-VTS is a database accessible from network. In this system, ships access to the *V-VTS* through a web browser (such as Internet Explorer or Netscape), each ship sends her information to the *V-VTS* and gets information from/of other ships. Thus, *V-VTS* is similar to the *AIS*, but here the Internet is used for communication. The satellite communication is necessary, and the AIS can be used to build up the *V-VTS*. The Concept of the *V-VTS* is shown in Fig. 1.

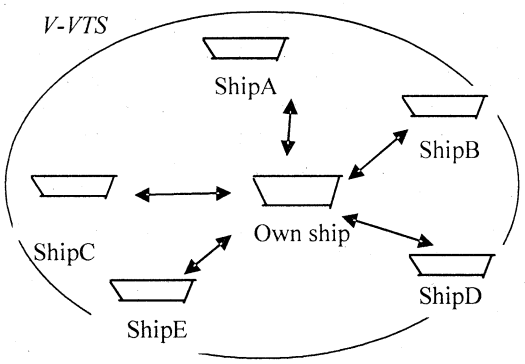


Fig. 1: The *V- VTS* concept

(the arrows show information exchanged between

2.2 Marine IT

The Marine Intelligent Traffic Systems should [1]:

- Provide information of all ships in the area as well as other information such as geographical and environment information;
- Using above-mentioned information to set:
+ Destination and departure gates/ports of each ship;
+ Route of each ship;
+ Waypoints of the route;
- Calculate own ship and target ships' position and behaviors;
- Determine ship steering instruction based on each ship route, plan and technical characteristic as well as environment information;
- Validity the safety of the instruction and after that guides the ships;

2.3 Marine Intelligent Transport

The following three main sub-systems are seen as most important for the Marine *ITS*:

- Collision and grounding avoidance system
- Berth/de-berthing supporting system
- Traffic control system in congested waterways;

There are two stages in building up the above-described systems. First is to make computer simulation systems [4], and after checking the simulation systems carefully, applied them in real ships (second stage). Of course, to be able to use in real navigation and maneuverings, the full scale experiments should also carried out.

3 A Fully Automated and Intelligent Ship

3.1 Concept of a Fully Automated and Intelligent Ship

Recent development of several supporting techniques and new high-tech materials has led to the new concept of a fully automated and intelligent ship [2], [3], [5]. In this study only main systems for ship automatic control displayed described. For more details on current status and future of ship automatic systems please refer to a number of references [3], [5], [6], [7], [8], [9], [10], [11].

3.2 Automatic Systems for Ships in Ocean Navigation

The contents of automatic systems for a fully automated and intelligent ship in ocean navigation will not be so much different from the automatic systems that are used widely in today ships [2]. However, applications of advanced technologies have led to many innovations in those systems, and their quality and level of safety that the new systems can achieve are the most importance.

Supporting system from shore base: Raw data, information not only from considered ship, but also from other surrounding ships, as well as navigation information will be supplied to this system. The system then analyzes and evaluates that information, makes the necessary guide or advice to the shipmasters via satellites or wireless communication [6], [10], [12]. Items included are given in details in [2], [3].

Ship operation system: Up to now the goals of safe and economic navigation have been mainly achieved by human ability based on the screw's knowledge, experience and with the assistance of simple control systems [5]. In the new type of ship, those goals will be achieved by mean of new technologies, especially with help from computer technique [2]. For these purposes, ship operation systems will require software with much more power-full functions [2], [3].

Data communication system: For long time the communication systems for ship navigation have been *DNS*, *Loral-C*, *INMARSAT*, *NNSS*, *GMDSS* and *GPS* recently [2], [3], [9], [10].

3.3 Automatic Systems for Ships in Harbor Maneuvering

Supporting system from harbor: this system mainly used to supply data of harbor and berths, and information about other ships, and may give advice to the pilots or shipmasters.

Ship operation system: Since the most importance goal of harbor maneuvering is to lead the ship enter and berth

(or un-berth and leave harbor) her safely, the automatic system should control the ship motions with high accuracy. The following tasks are suggested for fully automated and intelligent ships while in harbor maneuverings: realize ship position within decimeter level accuracy [10], [11]; evaluate effects of environmental disturbances, overall safety during maneuverings and make right decisions; calculate required forces and moments and allocate them to the tugs in the case of large ship; communicate ship with harbor or berths, tugboats or other ships.

Supporting system from tugboats: Each tug should be equipped with necessary systems to provide satisfactory accuracy of ship controlling. Important issues are systems for communication between ships and tugs, and systems for controlling the tugs timely and accurately.

Data communication system: This system is similar with that used for ship in ocean navigation. The most important function is that this system should supply information so that ship operation system can calculate ship motions (position, velocities and heading angle) with high accuracy. *D-GPS* or *K-GPS* may satisfy this requirement [10], [11], [12], [13].

4 Some Technologies for Realization of a Fully Automated and Intelligent Marine Transportation System

4.1 New advanced techniques, methods and their applications

Measurement of ships' and ship models' motions: To control ships effectively, it is highly desirable to know their maneuvering characters and high accuracy of measurement of ships/ship models' position and motions is required. Using *HALCON* – an image processing software produced by *MVTEC* (German) together with a digital camera, the measurement error was less than 0.35 mm (see Fig. 2). The method was applied to measure ship model motions during tests in towing tank for estimation of ship hydrodynamic coefficients in low speed condition [3], [14] and gave good results. Using *K-GPS* receivers, ship static and dynamic position can be estimated within centimeter level [12], [13] (see Fig. 3 and Fig. 4) and the results can be used for many applications [12], [13], [16].

Methods to estimate ship maneuvering hydrodynamic coefficients and environment's influences: For almost 20 years many methods have been used and developed for the purpose of identification of ship hydrodynamics [17], [18]. Traditional methods such as Least Squares Estimator, Kalman Filter and so on were used to estimate ship maneuvering hydrodynamic coefficients and environment's effects., and a new method has also been developed [12], [14].

4.2 Technological development in response to Environment issues

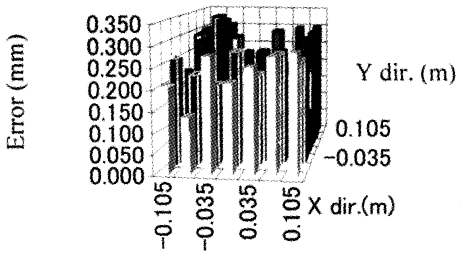


Fig. 2: Error of distance between 2 fixed points

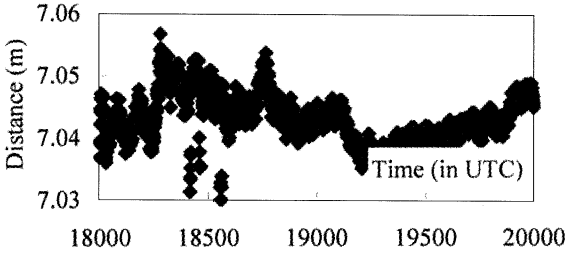


Fig. 3: Distance between 2 static antennas

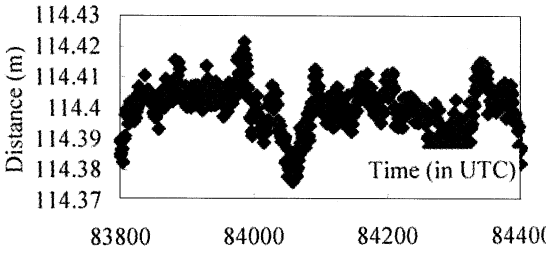


Fig. 4: Distance between 2 moving antennas

The following advanced technologies will significantly reduce the risk of serious accidents and spills:
- Fuel cell development could lead to an environmentally friendly propulsion alternative for the future;
- Full-bottom coverage survey equipment;
- Electronic chart display and information systems;
- Electronic charting systems;
- Vessel traffic services;
- Vessel transponders;
- Real-time acquisition and delivery of data; and
- The differential global positioning system.

5 Conclusions

The concept of Marine ITS were described and its contents have been introduced to realize the harmonious coexistence of people, marine transportation and environment. A concept of a fully automated and intelligent ship to fulfill high requirements of a more economic, safer and cleaner marine transportation system was presented, and the corresponding automatic systems were discussed in details. Further more, some new advanced technologies and methods and their applications in building the fully automated and

intelligent ship were given. Many parts of the discussed ship automatic systems have been successfully carried out using simulation tools, and some even have been put into practice and shown very good results. However, there is still a very long way to complete work of realizing the harmonious coexistence of people, marine transportation and environment. To reach these goals, 2 most important study directions can be pointed out as follows.

(1) Pursuit of greater safety by studying and building fully automated and intelligent ships;

(2) Study toward "environment-friendly ships" in order to solve the marine environment problems;

Abbreviations

GT	Gross Tonnage
TSL	Techno-Super-Liner
SAR	Search And Rescue
DNS	Decca Navigation System
GPS	Global Positioning System
D-GPS	Differential GPS
VTS	Vessel Traffic Service
LORAN	Long Range Navigation
INMARSAT	INternational MAritime SATellite
SMGT	Super Marine Gas Turbine
LSI	Large Scale Integrated Circuits
NNSS	Navy Nav. Satellite System
K-GPS	Kinematic GPS
ITS	Intelligent Transport Systems
AIS	Automatic Identification Systems
IMO	Int. Maritime Organization
ECDIS	Electric Chart Display and Information System
GMDSS	Global Maritime Distress and Safety System

References

[1] Hasegawa, K., Shigemori, Y. and Ichiyama, Y. "Feasibility Study on Intelligent Marine Traffic System", *Proc. 5th IFAC Conf. on Maneuvering and Control of Marine Craft, MCMC2000*, Vol.1, 327-332, 2000.

[2] Le, M-D, Nguyen, D-H. and Chu, C. " Study Toward A 21st Century's Fully Automated Ship", *Proc. of IATSS Symposium, ISSOT'98*, Vol.1, No.1, 58-68, 1998.

[3] Le, M-D and Nguyen, D-H. "On Advanced Supporting Systems and Techniques For A Fully Automated Ship in 21st Century", *Proc. of the 4th Vietnam Conference on Automation*, Vol.1, No.1, 106-111, 2000.

[4] Kuo, P. "A Study on the Safety Evaluation of Ship Maneuvering in Ports - An Introduction of Ship Handling Simulator Studies in Taiwan", *The Journal of Japan Institute of Navigation*, Vol.89, No.1, 1993.

[5] Ijima, Y. and Hayashi, S. "Study Towards a 21st Century Intelligent Ship", *Journal of Institute of Navigation*, Vol.44, No.2, 42-47, 1992.

[6] Hasegawa, K. "Knowledge - Based Automatic Navigation System for Harbor Maneuvering", *Proc. 10th Ship Control Systems Symposium*, Vol. 1, 100-105, 1993.

[7] Kose, K., Fukudo, J., Sugano, K., Akagi, S. and Harada, M. "On a Computer Aided Maneuvering System in Harbors" (in Japanese), *Journal of The Society of Naval Architect of Japan*, Vol.160, No.1, 103-110, 1986.

[8] Koyama, T., Yan, J. and Huan K. A Systematic Study on Automatic Berthing Control (1st Report) (in Japanese), *Journal of The Society of Naval Architect of Japan*, Vol.165, No.3, 201-210, 1989.

[9] Ohtsu, K., Takai, T. and Yoshihisa, H. "A Fully Automatic Berthing Test Using the Training Ship Shioji Maru", *Journal of Institute of Navigation*, Vol.44, No.2, 213-223, 1992.

[10] Takahashi, H., Hagiwara, H., Hayafuji, Y. and Morimitu, K. "Study on Support Systems of Entering a Port for Techno Super Liner" (in Japanese), *The Journal of Japan Institute of Navigation*, Vol.95, No.1, 71-78, 1996.

[11] Takahashi, H., Hagiwara, Itani, K. and Kisaka, T. "Study on Support Systems of Berthing for TSL by RTK/OTF GPS" (in Japanese), *The Journal of Japan Institute of Navigation*, Vol.95, No.1, 79-85, 1996.

[12] Takase, S., Kose, K., Hirata, N., Furumoto, M., Le, D-M and Yamada, T. "Accuracy and Application for Measurement of Ship Motion by Kinematic GPS" (in Japanese), *The Journal of Japan Institute of Navigation*, Vol.97, No.1, 15-22, 1997.

[13] Yamada, T., Nagasawa, A., Takase, S. and Hirata, N. "Precision of Radar Positions Compared with the KGPS Positions" (in Japanese), *The Journal of Japan Institute of Navigation*, Vol.97, No.1, 23-28, 1997.

[14] Le, M-D and Kose, K. "Estimation of Ship Hydrodynamic Coefficients at Low Speed Range and Application to Control Ships", *The Journal of Japan Institute of Navigation*, Vol.103, No.1, 33-39, 2000.

[15] Le, M-D. and Nguyen, D-H. "Estimation of ship hydrodynamic coefficients in harbour manoeuvres and its applications", *Proc. of IFAC Control Applications of Optimisation, CAO2000*, Vol.1, No.1, 227-232, 2000b.

[16] Takase, S., Kose, K., Hirata, N., Furumoto, M., Le, M-D. and Nagasawa, A. "Application of K-GPS for Ship Trial", *Proc. of IFAC Conference, Control Applications in Marine Systems CAMS'98*, Vol.1, No.1, 309-314, 1998.

[17] Abkowits, M. A. "Measurement of Hydrodynamic Characteristics from Ship Maneuvering Trials by System Identification", *Transactions on SNAME*, Vol.88, No.1, 283-318, 1980.

[18] Astrom, K. J. and Kallstrom, C. G "Identification of Ship Steering Dynamics", *Automatica*, Vol.12, No.1, 9-22, 1976.

Proc. of The Ninth Int. Symp. on Artificial Life and Robotics (AROB 9th '04)
Beppu, Oita, Japan, 28-30 January, 2004

ONLINE ESTIMATION OF SHIP STEERING DYNAMICS AND ITS APPLICATION IN DESIGNING AN OPTIMAL AUTOPILOT

Minh - Duc LE, *VINASHIN, Hanoi, Vietnam*
le_minh_duc@yahoo.com
Cong - Son TRUONG, Thi - Huyen NGUYEN,
Thuong - Hai CAO, *Hong Thang TST., Hanoi, Vietnam*

Huu - Thanh NGUYEN, Dinh - Thi NGUYEN,
Van - Cho NGUYEN, Van - Hai HOANG
C&A Technology Application Support Co., Ltd.
inter_conference@yahoo.com

Abstract

Recursive Least Square (RLS) Algorithm applied to a Multivariate Auto-Regressive (MAR) process is used to estimate ship steering dynamics online. The estimation method is then linked to the Linear Quadratic (LQ) Algorithm to design an optimal autopilot for steering ships. The estimation method was applied to several ships and model ships and in all the cases the estimated parameters converged well. The design algorithm was used to construct a tracking system for course keeping and course changing manoeuvres. Simulation results for the ships show the robustness of the estimation method and prove that the autopilot has very good performance.
Keywords: Modeling, estimation and identification, autoregressive models, least-squares algorithm, quadratic control, ship steering dynamics

1 Introduction

Ship steering dynamics is of interest when evaluating ship manoeuvrability as well as when designing ship autopilots and steering systems. Designing a computer-based autopilot for ships is always a challenging task in marine control engineering since ships operating in seawater are often strongly influenced by unpredictable environmental disturbances such as wind, wave and current. Therefore to navigate safely and economically, the ship must have a robust autopilot system with good steering characteristics. To design such a robust computer-based autopilot system that can be adapted well to the changes of the environment a suitable mathematical model representing ship steering dynamics should be constructed. Hence, a suitable estimation method for a chosen model is certainly required.

Methods for determining ship steering dynamics with high accuracy have been of the focus of many studies over a long period of time. Astrom and Kallstrom [1] did the pioneer work in identification of ship steering dynamics. Abkowitz [2] presented results of the identification of ship hydrodynamic characteristics based on Extended Kalman Filter, the results have long been seen as excellent. More recently Le, et al. [3] has proposed a new and effective method for estimation of ship linear hydrodynamic coefficients.

In modern control theory, identification algorithms are often combined with appropriate control laws to construct automatic control systems. In marine control, much research has been carried out in this direction. Several authors have applied stochastic approach to analysis and control of ship motion (see [2], [4], [5], [6], [7]). More recently, Wellstead, et al. [8] combined a self-tuning control algorithm with the RLS algorithm to design control systems. Since then, the self-tuning control algorithm has been developed into a route-tracking controller in the PID form for ships ([9], [10], [11], [12]). Besides this, the RLS algorithm was also combined with an optimal control law to design an adaptive dynamic positioning system for vessels [13].

This paper presents a new method for online estimation of ship steering dynamics and its application to design an optimal autopilot system for ships. Ship steering dynamics is expressed by a MAR model with unknown parameters to be estimated. The RLS algorithm is used as an online estimator to estimate the parameters of the assumed model. The estimated are then used as the input to calculate control gain of the LQ optimal control law for designing the autopilot. The estimation method was applied to estimate steering dynamics of several ships and model ships. The design method was verified by computer simulation of several ships and model ship during course keeping and course changing manoeuvres.

2 Estimation of Ship Steering Dynamics

2.1 RLS algorithm applied to estimate parameters of a MAR model

Ship dynamics can be described by the following state-space equation [1]:

$$\dot{x} = Ex + Fu + De \qquad (1)$$

where x (t), u (t), e (t) are state vector, control vector and disturbance vector, respectively; E , F , D are the corresponding matrices, to be estimated. In this study both x (t), e (t) are assumed to be measured or at least obtained by state estimation.

The above equation can be conveniently expressed by a MAR process of order p:

$$v_i = \omega + \sum_{l=1}^{p} A_l v_{i-l} + \varepsilon_i \,, \; (i = \mathrm{p}, ..., \mathrm{N}) \qquad (2)$$

Here $v_i \in R^m$ is a time series of state vectors, observed as equally spaced instant i ; $\omega \in R^m$ is a parameter vector of intercept terms and is included to allow for a

nonzero mean of time series v_i ; $A_l \in R^{m,m}$ are matrices of unknown (constant) coefficients expressed the process; $\varepsilon_i \in R^m$ are random vectors of noises, with the present of ω , ε_i can be assumed to have zero mean and covariance matrix C . Relations between matrices in formulas (1) and (2) can be easily derived using Multivariate Auto-regressive theory or differential formula.

Denote the augmented state vector by (3) (with n = mp+1) and the augmented coefficient matrix by (4):

$$\upsilon_i=[1^T \; v_{i-1}^T \ldots v_{i-p}^T]^T \in R^n, (i = \text{p}, \ldots, \text{N}) \quad (3)$$

$$A=[\omega \; A_1 \ldots A_p] \in R^{m,n} \quad (4)$$

, the MAR(p) model (2) can be rewritten as:

$$v_i = A\upsilon_i + \varepsilon_i, (i = \text{p}, \ldots, \text{N}) \quad (5)$$

The parameter matrix A can then be estimated using RLS Algorithm with the availability of measurement v_i and υ_i . Introducing the matrices:

$$U=\sum_{i=p}^{N}\upsilon_i\upsilon_i^T \; ; \; W=\sum_{i=p}^{N}v_i\upsilon_i^T \quad (6)$$

, then the best linear unbiased estimate for the matrix A is derived as:

$$\hat{A}=WU^{-1} \quad (7)$$

, and an estimate for the covariance matrix C is given by:

$$\hat{C}=\frac{1}{N-n}\sum_{i=p}^{N}\hat{\varepsilon}_i\hat{\varepsilon}_i^T \text{ with } \hat{\varepsilon}_i=v_i-\hat{A}\upsilon_i \quad (8)$$

In practice, to progressively reduce the emphasis placed on past information a forgetting factor (FF) λ with value between 0.95 to 0.998 was also used [8], [14].

The RLS algorithm applied to estimate ship steering dynamics is summarized as follows.

At time interval i :

(a) Step 1: Form vectors v_i and υ_i using new data according to formulas (2) and (3).

(b) Step 2: Add new values to U and W according to (6), noting that the FF can be used.

(c) Step 3: Calculate the estimates for matrices A and C using formulas (7) and (8).

(d) Step 4: Wait for the next step to elapse and loop back to Step 1 until the end of the estimation process.

2.2 Results of estimation of ship steering dynamics

Usually the input and control variables of the state-space equation (1) expressing ship steering dynamic are chosen as follows: $x=[v\ r\ \psi]^T$ where v, r, ψ respectively are ship sway, angular velocities and heading angle, and $u=\delta$ with δ is the rudder deflection. Since the order of the differential equation (1) is 1, it would be suitable to choose the parameters in equation (2) as: p = 1, m = 4, n = 5. In this case, expressions of vectors v_i and υ_i are derived as follows:

$$v_i=[v_i \; r_i \; \psi_i \; \delta_i]^T \in R^4, (i = \text{p}, \ldots, \text{N}) \quad (9)$$

$$\upsilon_i=[1 \; v_i \; r_i \; \psi_i \; \delta_i]^T \in R^5, (i = \text{p}, \ldots, \text{N}) \quad (10)$$

Parameters of ship steering dynamics then can be estimated using the four steps given in 2.1

Figure 1 shows the time series of the estimated parameters for SR221B, a model ship. Data for the estimation was collected from a 10deg. Zigzag test in a towing tank. Estimation results for a training ship (the Shioji Maru) is shown in Figure 2 and data was collected from a 20deg. Zigzag trial. In these figures, only parameters concerning the input vector x are given, as they are the parameters of the steering dynamics. From both figures, it is clear that the estimated parameters of ship steering dynamics converge very well and this proves the effectiveness of the estimation method.

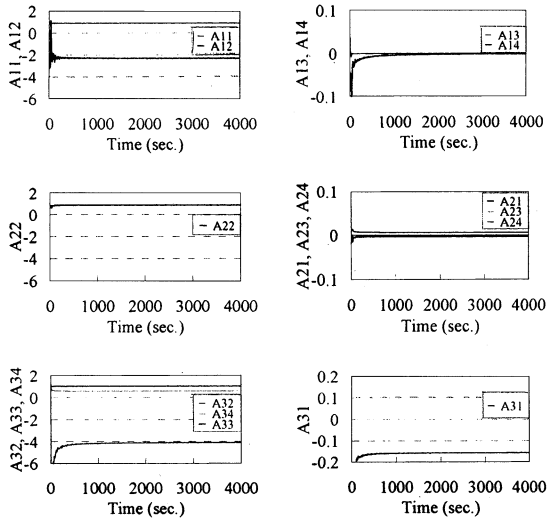


Fig.2. Time series of estimated parameters for the ship Shioji Maru (sampling time = 0.50 sec.)

3 Optimal Autopilot Design

3.1 The LQ optimal control algorithm

Suppose that the output y (t) of the control system (1) is expressed by the following equation:

$$y=Gx+Hu \quad (11)$$

where G and H are corresponding matrices.

To design an optimal controller for tracking a time varying reference (desired) trajectory y_d (t), let define $\tilde{y} = y - y_d$ the trajectory error vector, and

$$J=\sum_{i=0}^{N-p}\left[\tilde{y}^T Q\tilde{y}+u^T Pu\right] \quad (12)$$

the performance index, where $Q \geq 0$ and $P > 0$ are weighting matrices. Solution of the LQ Tracker Problem is a control law that minimizes the performance index

(12) and can be expressed by following equation [7]:

$$u = G_1 x + G_2 y + G_3 e \tag{13}$$

here gain matrices G_1, G_2, G_3 are calculated from:

$$\begin{cases} G_1 = -P^{-1}F^T R \\ G_2 = -P^{-1}F^T (E + FG_1)^{-T} G^T Q \\ G_3 = P^{-1}F^T (E + FG_1)^{-T} RD \end{cases} \tag{14}$$

,with R the solution of the discrete-time Riccati equation:

$$RE + E^T R - RFP^{-1}F^T R + \tilde{Q} = 0 \tag{15}$$

$$\tilde{Q} = G^T QG \tag{16}$$

3.2 Procedure of optimal autopilot design

Equation (13) shows clearly that if the parameters of the state-space equation (1) have been estimated, the optimal solution for the control vector u (t) can be calculated. Therefore, a combination of the estimation method presented in Section 2 and the LQ algorithm could give an approach to designing an optimal autopilot. To design a control system, the input and output variables should be chosen. For ship steering systems v, r, ψ are often chosen as the output variables. Then matrix G is given as:

$$G = \begin{bmatrix} 1 & 0 & 0 \\ 0 & 1 & 0 \\ 0 & 0 & 1 \end{bmatrix} \tag{17}$$

The procedure for designing the optimal autopilot can be summarized by following steps:

At time interval i :

(a) Step 1: Form vectors v_i and υ_i using new data according to formulas (2) and (3), and output vector y.

(b) Step 2: Estimate parameters of MAR process (5) using formulas (6), (7) and (8), then calculate the ship steering dynamics (matrices E, F, D in the state-space equation (1)). Matrix G is given by (17) and matrix H can be easily calculated from matrix A, which has already been estimated in (5).

(c) Step 3: Use the results of Step 2 to find solution equation (15) and then calculate gain matrices G_1, G_2, G_3 according to formula (14).

(d) Step 4: Substitute new values of G_1, G_2, G_3 and the current values of input, output and disturbance vector x_i, u_i, e_i into equation (13) for the new optimal value of the control vector u.

(e) Step 5: Wait for the next step to elapse and loop back to Step 1 until the end of the control process.

Among the practical aspects of designing and implementing such an autopilot, the main task is to choose design parameters such as proper weightings (Q and P) in the performance index function, sampling time and initial parameters during implementing computer simulations and full-scale experiments. The values of Q and P are usually chosen based on the aims of the designing optimal autopilots. For example, when considering the energy saving problem one may choose a large value for P (compared to value of Q) while if the accuracy of the control process is emphasized, the large value should be chosen for Q. Sampling time could be decided based on the allowable rate of rudder deflection and also on a proper sampling rate of measurement equipments. Parameters of ship steering dynamics can be estimated with or without knowing the initial values. Strip theory can be applied to estimate the initial values for the parameters. Fossen [7] gives formulas for this purpose, and the values are highly useful as a priori information for a recursive parameter estimator.

3.3 Simulation results of applying the design method

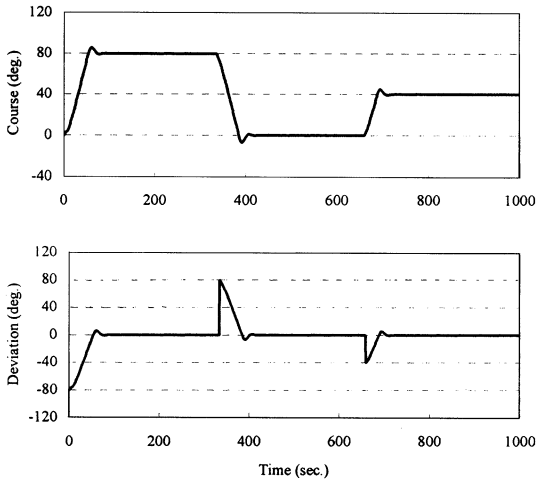


Fig.3. Time series of ship responses (course and deviation) for model ship SR221B during keeping and changing course maneuvers

The procedure of designing an optimal autopilot given in 3.2 was applied to some ships and model ships. and computer simulations of course keeping and course changing manoeuvres using the optimal autopilot were performed for them. Figure 3 gives an example of computer simulation results of the above manoeuvres for the SR221B model ship. The simulation was performed for an 80-0-40 manoeuvre that means the ship starting from zero-degree course was ordered to change to 80-degree course, then to zero-degree course and finally to 40-degree course, after each of the changing course manoeuvres, the ship was ordered to keep the course stable for a period of about 200 seconds. Rudder deflection was limited in the range of -35 to +35 degrees as usually required for most ships. The ship changed to the new course properly and there were only two slight oscillations before stability has achieved. The overshoot that did occur, however, was rather small. The course keeping manoeuvres were performed very well.

3.4 Evaluation of the design algorithm

For a conventional autopilot design approach (such as the PD control law, the SISO MAR model) ship heading is often oscillated several times before achieving stability on the new course. As mentioned above, using the current design algorithm the course-changing manoeuvres were performed rather well: there were very few slight oscillations during each manoeuvre. That means the autopilot design based on the current algorithm has performed better than an autopilot design based on a conventional approach would have.

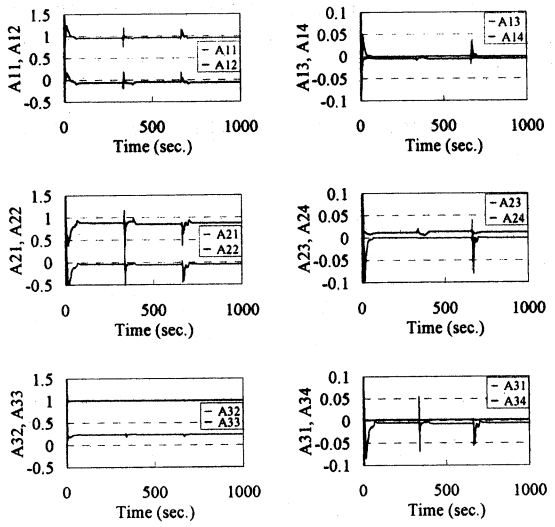


Fig.4. Time series of estimated parameters for the model ship SR221B during course keeping and course changing maneuvers (using autopilot)

In addition, this design algorithm has also proved its robustness as showed in Figure 4. During each of the course changing processes, the parameters of the steering dynamics were changed. At the beginning of the course changing action especially the largest variations in the parameters occurred, however they quickly rebounded (to stable values). This shows that the autopilots could adapt well to environment changes.

4 Conclusions and Future Research

Recursive Least Square (RLS) Algorithm applied to a Multivariate Auto-Regressive (MAR) process was successfully used to estimate ship steering dynamics online. The estimation method was then combined with the Linear Quadratic (LQ) Algorithm to design an optimal autopilot for steering ships. The estimated parameters of steering dynamics for the ships and ship models converged well and computer simulation results showed that using the described design approach, the optimal autopilot had excellent performance both with keeping and changing the courses as desired. Since the method for estimation of ship steering dynamics can be applied both to scale model tests and full scale ship trials, it provides a possibility to analyse effects due to scaling.

To verify the optimal autopilot design approach full-scale trials should also be carried out for investigation of the steering characteristics in practice and its ability to adapt to the environmental. Moreover, it is expected the optimal autopilot will further be developed into an optimal route-tracking controller for ships.

References

[1] Astrom, K.J. and C.G. Kallstrom, "Identification of Ship Steering Dynamics", *Automatica*, **12**, 9-22, Pergamon Press, UK, 1976.

[2]Abkowits, M. A., "Measurement of Hydrodynamic Characteristics from Ship Maneuvering Trials by System Identification", *Transactions on SNAME*, **88**, 283-318, USA, 1980.

[3] Le, M.D, D.H. Nguyen and K. Ohtsu, "A New and Effective Method for Estimation of Ship Hydrodynamic Coefficients". *Proc. of the 4th Vietnam Conference on Automation*, 99-105, 2000.

[4] Ohtsu, K, M. Horigome and G. Kitagawa, "A New Ship's Autopilot Design through a Stochastic Model, *Automatica*, **15**, 255-268, Pergamon, UK, 1979.

[5] Kallstrom, C.G., K.J. Astrom, N.E. Thorell, J. Eriksson and L. Sten, "Adaptive Autopilots for Tankers", *Automatica*, **15**, 241-254, Pergamon Press, UK, 1979.

[6] Holzhuter, T., "A High Precision Track Controller for Ships", *IFAC 11th Triennial World Congress*, 425-430, Talinn, Estonia, Russia, 1990.

[7] Fossen, T.I., "Guidance and Control of Ocean Vehicles", John Wiley and Sons Ltd., UK, 1994.

[8] Wellstead, P.E. and M.B. Zarrop, "Self-tuning Systems: Control and Signal Processing", John Wiley and Sons Ltd., UK, 1991.

[9] Mizuno, H., T. Okawa, I. Komine, N. Mizuno and K. Ohtsu, "Route Tracking System by Adaptive Autopilot", *Proc. of CAMS'89*, 77-82, Copenhagen, Denmark, 1989.

[10] Nguyen, D.H., J.S. Park and K. Ohtsu, "Designs of Self-tuning Control Systems for Ships", *The Journal of Japan Institute of Navigation*, **99**, 235-245, Japan, 1998.

[11] Nguyen, D.H., N. Mizuno and K. Ohtsu, "A Modified Pole Assignment Typed Autopilot for Ships", *The Journal of Japan Institute of Navigation*, **102**, 327-337, Japan, 2000.

[12] Nguyen, D.H. and M.D. Le, "A Challenge to Advanced Autopilot Systems for Ships". *Proc. of the 4th Vietnam Conference on Automation*, 226-232, Hanoi, Vietnam, 2000.

[13] Iida, T., "On an Adaptive Dynamic Positioning System for Vessels" (in Japanese), *Journal of Western Japan Society of Naval Architects*, **213**, 89-96, Japan, 1990.

[14] Hang, C.C., T.H. Lee and W.K. Ho, "Adaptive Control", Instrument Society of America, USA, 1993.

Proc. of The Ninth Int. Symp. on Artificial Life and Robotics (AROB 9th '04)
Beppu, Oita, Japan, 28-30 January, 2004

A Design of Digital Adaptive Control Systems for Space Robot Manipulators Using Transpose of Generalized Jacobian Matrix

Yuichiro Taira
Dept. of Ocean Mechanical Eng.
National Fisheries University
Shimonoseki 759-6595, Japan

Shinichi Sagara
Dept. of Mechanical and Control Eng.
Kyushu Institute of Technology
Tobata, Kitakyushu 804-8550, Japan

Abstract

The authors have proposed a digital control method of space robot manipulators using the transpose of the Generalized Jacobian Matrix. The method, however, is developed on the supposition that all the physical parameters of the robot manipulator are known; therefore, if the end-effector of the manipulator captures an object whose mass is unknown, the stability of the control system cannot be maintained because the physical parameters are changed. This paper presents the adaptive control version.

1 Introduction

Many modeling and control methods of a space robot manipulator with an uncontrolled base, referred to as a free-floating space robot manipulator, have been reported. Masutani et al. [1] have proposed a sensory feedback control method using the transpose of the Generalized Jacobian Matrix (GJM). This is an excellent method, because the inverse of the GJM doesn't need to be used in the control law. The method, however, is developed in a continuous-time domain. In practical systems, digital computers are generally used as controllers; therefore, the stability of the control system must be guaranteed in a discrete-time domain.

The authors have proposed the digital control version [2]. This method, however, is developed on the supposition that all the physical parameters of the robot manipulator are known. In contrast to a Jacobian matrix for a robot manipulator with a fixed base, the GJM includes the dynamic parameters as well as the kinematic parameters. Therefore, if the end-effector of the manipulator captures an object whose mass is unknown, the dynamic parameters of the GJM, such as the mass and moment of inertia, become unknown. In this case, the stability of the control system cannot be maintained because the control law needs the correct parameters of the GJM.

This paper deals with the adaptive control version. In general, an adaptive controller is formed by combining an on-line parameter estimator of physical parameters with a control law developed for known parameters, and the way to select the parameter estimation law leads to two different approaches. In the first approach, the physical parameters are estimated on-line, and the estimates are used to calculate the control law [3]. The stability of the control system is ensured if the estimated parameters converge to the real values. It, however, is generally difficult to guarantee the convergent property. In the second approach, the physical parameters are estimated on-line so that the control system is stable. Therefore, the stability of the control system is guaranteed whether or not the estimated parameters converge to the real values. The digital adaptive control method proposed in this paper is based on the second approach. In this paper, the rigorous stability proofs of the proposed adaptive controller are presented.

2 Discrete-Time Models

2.1 Preliminaries

We consider a free-floating space robot manipulator shown in Fig. 1. It has an uncontrolled base and a n-DOF ($n \geq 6$) manipulator with all revolute joints. The target is stationary in an inertial coordinate frame. The symbols used in this paper are as follows:

[Symbols]

Σ_I: inertial coordinate frame
Σ_B: base coordinate frame
Σ_E: end-effector coordinate frame
Σ_T: target coordinate frame
${}^*\boldsymbol{R}_E$: position vector of Σ_E with respect to Σ_*
${}^*\boldsymbol{R}_T$: position vector of Σ_T with respect to Σ_*
${}^*\boldsymbol{V}_E$: linear velocity vector of Σ_E with respect to Σ_*
${}^*\boldsymbol{\Omega}_E$: angular velocity vector of Σ_E with respect to Σ_*
$\boldsymbol{q}$: angle vector of the joints of the manipulator

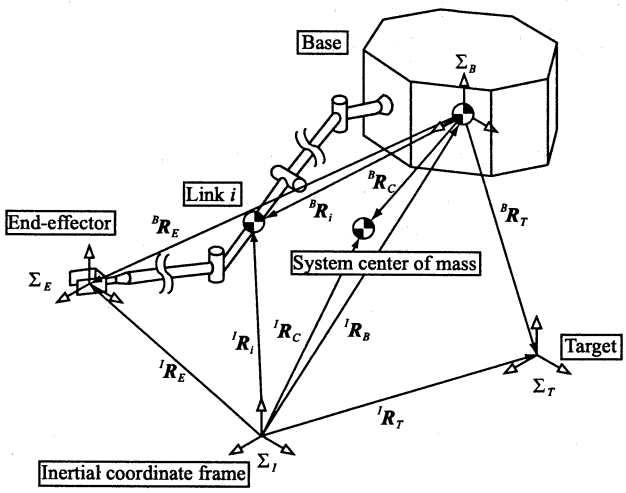


Figure 1: A model of space robot manipulators

$\boldsymbol{\phi}_*$: angle vector representing orientation of Σ_* with respect to Σ_I
$\boldsymbol{\tau}$: torque vector of the joints of the manipulator
$^{**}\boldsymbol{A}_*$: rotation matrix from Σ_* to Σ_{**}
$\boldsymbol{U}_3$: identity matrix ($\in R^{3\times 3}$)
T: sampling period
$\tilde{\boldsymbol{r}}$: skew-symmetric matrix defined as

$$\tilde{\boldsymbol{r}} := \begin{bmatrix} 0 & -z & y \\ z & 0 & -x \\ -y & x & 0 \end{bmatrix}, \quad \boldsymbol{r} = \begin{bmatrix} x \\ y \\ z \end{bmatrix}$$

2.2 Kinematic Models

A discrete-time differential kinematic model is given by the following equations [2]:

$$^I\boldsymbol{V}_E(k) = {}^I\boldsymbol{J}_L^*\left(\boldsymbol{\phi}_B(k), \boldsymbol{q}(k)\right)\dot{\boldsymbol{q}}(k), \tag{1}$$
$$^I\boldsymbol{\Omega}_E(k) = {}^I\boldsymbol{J}_A^*\left(\boldsymbol{\phi}_B(k), \boldsymbol{q}(k)\right)\dot{\boldsymbol{q}}(k) \tag{2}$$

where $^I\boldsymbol{J}_L^*$ and $^I\boldsymbol{J}_A^*$ are called the GJMs of the linear and angular velocities respectively and consist of the following elements:

$$\begin{aligned} {}^I\boldsymbol{J}_L^*(k) &= {}^I\boldsymbol{A}_B(k)\left\{{}^B\boldsymbol{J}_L(k) - {}^B\boldsymbol{J}_C(k)\right. \\ &\quad \left. + {}^B\boldsymbol{H}_{EC}(k)\,{}^B\boldsymbol{H}_B^{-1}(k)\,{}^B\boldsymbol{H}_M(k)\right\}, \end{aligned} \tag{3}$$
$$^I\boldsymbol{J}_A^*(k) = {}^I\boldsymbol{A}_B(k)\left\{{}^B\boldsymbol{J}_A(k) - {}^B\boldsymbol{H}_B^{-1}(k)\,{}^B\boldsymbol{H}_M(k)\right\}. \tag{4}$$

The elements $^B\boldsymbol{J}_L$, $^B\boldsymbol{J}_A$, $^B\boldsymbol{J}_C$, $^B\boldsymbol{H}_{EC}$, $^B\boldsymbol{H}_B$, and $^B\boldsymbol{H}_M$ can be seen in [2].

The difference equation of the position error $\boldsymbol{e}_{PI}$ is given by the following equation [2]:

$$\boldsymbol{e}_{PI}(k) = \boldsymbol{e}_{PI}(k-1) - T\,{}^I\boldsymbol{J}_L^*(k)\dot{\boldsymbol{q}}(k) \tag{5}$$

where

$$\boldsymbol{e}_{PI}(k) := {}^I\boldsymbol{R}_T - {}^I\boldsymbol{R}_E(k). \tag{6}$$

The difference equation of the orientation error $\boldsymbol{E}_{OI}$ can be expressed as the following equation [2]:

$$\boldsymbol{E}_{OI}(k) = \boldsymbol{E}_{OI}(k-1) + T\,\boldsymbol{E}_X(k)\,{}^I\boldsymbol{J}_A^*(k)\dot{\boldsymbol{q}}(k) \tag{7}$$

where

$$\boldsymbol{E}_{OI}(k) := \begin{bmatrix} {}^I\boldsymbol{n}_T - {}^I\boldsymbol{n}_E(k) \\ {}^I\boldsymbol{s}_T - {}^I\boldsymbol{s}_E(k) \\ {}^I\boldsymbol{a}_T - {}^I\boldsymbol{a}_E(k) \end{bmatrix}, \tag{8}$$
$$\boldsymbol{E}_X(k) = \begin{bmatrix} {}^I\tilde{\boldsymbol{n}}_E(k) \\ {}^I\tilde{\boldsymbol{s}}_E(k) \\ {}^I\tilde{\boldsymbol{a}}_E(k) \end{bmatrix},$$
$$^I\boldsymbol{A}_E(\boldsymbol{\phi}_E(k)) = \left[{}^I\boldsymbol{n}_E(k) \quad {}^I\boldsymbol{s}_E(k) \quad {}^I\boldsymbol{a}_E(k)\right],$$
$$^I\boldsymbol{A}_T(\boldsymbol{\phi}_T) = \left[{}^I\boldsymbol{n}_T \quad {}^I\boldsymbol{s}_T \quad {}^I\boldsymbol{a}_T\right].$$

The vectors $^I\boldsymbol{n}_*$, $^I\boldsymbol{s}_*$, and $^I\boldsymbol{a}_*$ are unit vectors along the axes of Σ_* with respect to Σ_I. Since it may be difficult to use the orientation error (8) for the stability analysis as a feedback orientation error for the control law, the orientation error used in the control law is defined as

$$\boldsymbol{e}_{OI}(k) := -\frac{1}{2}\boldsymbol{E}_X^T(k)\boldsymbol{E}_{OI}(k). \tag{9}$$

If the condition [1]

$$^I\boldsymbol{n}_E^T(k)\,{}^I\boldsymbol{n}_T + {}^I\boldsymbol{s}_E^T(k)\,{}^I\boldsymbol{s}_T + {}^I\boldsymbol{a}_E^T(k)\,{}^I\boldsymbol{a}_T > -1$$

holds, the equation that $\boldsymbol{E}_{OI}(k) = \boldsymbol{0}$ is equivalent to the equation that $\boldsymbol{e}_{OI}(k) = \boldsymbol{0}$.

2.3 Linear Parametric Models

The elements $^I\boldsymbol{A}_B$, $^B\boldsymbol{J}_L$, $^B\boldsymbol{J}_A$, $^B\boldsymbol{J}_C$, $^B\boldsymbol{H}_{EC}$, $^B\boldsymbol{H}_B$, and $^B\boldsymbol{H}_M$ of the GJMs in (3) and (4) are linear in the physical parameters. The GJMs $^I\boldsymbol{J}_L^*$ and $^I\boldsymbol{J}_A^*$, however, are nonlinear in the physical parameters because of the inverse of $^B\boldsymbol{H}_B$. In order to introduce on-line parameter estimation in the subsequent section, it is desirable that the physical parameters appear linearly in the GJMs. Taking into account the fact that $^B\boldsymbol{H}_B^{-1}\,{}^B\boldsymbol{H}_M$ varies slowly with time, we assume that $^B\boldsymbol{H}_B^{-1}(k)\,{}^B\boldsymbol{H}_M(k)$ in (3) and (4) is a constant matrix [4]. From this assumption, the GJMs are linearized in the physical parameters as follows:

$$^I\boldsymbol{J}_L^*(k) = \begin{bmatrix} \boldsymbol{\alpha}_{11}^T\boldsymbol{\zeta}_{11}(k) & \cdots & \boldsymbol{\alpha}_{1n}^T\boldsymbol{\zeta}_{1n}(k) \\ \boldsymbol{\alpha}_{21}^T\boldsymbol{\zeta}_{21}(k) & \cdots & \boldsymbol{\alpha}_{2n}^T\boldsymbol{\zeta}_{2n}(k) \\ \boldsymbol{\alpha}_{31}^T\boldsymbol{\zeta}_{31}(k) & \cdots & \boldsymbol{\alpha}_{3n}^T\boldsymbol{\zeta}_{3n}(k) \end{bmatrix}, \tag{10}$$

$$ {}^{I}\boldsymbol{J}_{A}^{*}(k) = \begin{bmatrix} \boldsymbol{\alpha}_{41}^{T}\boldsymbol{\zeta}_{41}(k) & \cdots & \boldsymbol{\alpha}_{4n}^{T}\boldsymbol{\zeta}_{4n}(k) \\ \boldsymbol{\alpha}_{51}^{T}\boldsymbol{\zeta}_{51}(k) & \cdots & \boldsymbol{\alpha}_{5n}^{T}\boldsymbol{\zeta}_{5n}(k) \\ \boldsymbol{\alpha}_{61}^{T}\boldsymbol{\zeta}_{61}(k) & \cdots & \boldsymbol{\alpha}_{6n}^{T}\boldsymbol{\zeta}_{6n}(k) \end{bmatrix} \quad (11) $$

where $\boldsymbol{\alpha}_{ij}$ is a physical parameter vector and $\boldsymbol{\zeta}_{ij}$ is a regressor vector consisting of the trigonometric functions of $\boldsymbol{\phi}_B$ and $\boldsymbol{q}$. Substituting (10) and (11) into (1) and (2) respectively, we obtain the following equations:

$$ {}^{I}\boldsymbol{V}_{E}(k) = \boldsymbol{Y}_{L}(k)\boldsymbol{\alpha}_{L}, \quad (12) $$

$$ {}^{I}\boldsymbol{\Omega}_{E}(k) = \boldsymbol{Y}_{A}(k)\boldsymbol{\alpha}_{A} \quad (13) $$

where

$$ \boldsymbol{Y}_{L}(k) = \begin{bmatrix} \boldsymbol{\xi}_{1}^{T}(k) & & \\ & \boldsymbol{\xi}_{2}^{T}(k) & \\ \boldsymbol{0} & & \boldsymbol{\xi}_{3}^{T}(k) \end{bmatrix}, $$

$$ \boldsymbol{Y}_{A}(k) = \begin{bmatrix} \boldsymbol{\xi}_{4}^{T}(k) & & \\ & \boldsymbol{\xi}_{5}^{T}(k) & \\ \boldsymbol{0} & & \boldsymbol{\xi}_{6}^{T}(k) \end{bmatrix}, $$

$$ \boldsymbol{\alpha}_{L} = [\boldsymbol{\alpha}_{11}^{T}, \cdots, \boldsymbol{\alpha}_{1n}^{T}, \cdots, \boldsymbol{\alpha}_{31}^{T}, \cdots, \boldsymbol{\alpha}_{3n}^{T}]^{T}, $$

$$ \boldsymbol{\alpha}_{A} = [\boldsymbol{\alpha}_{41}^{T}, \cdots, \boldsymbol{\alpha}_{4n}^{T}, \cdots, \boldsymbol{\alpha}_{61}^{T}, \cdots, \boldsymbol{\alpha}_{6n}^{T}]^{T}, $$

$$ \boldsymbol{\xi}_{i}(k) = [\dot{q}_{1}(k)\boldsymbol{\zeta}_{i1}^{T}(k), \cdots, \dot{q}_{n}(k)\boldsymbol{\zeta}_{in}^{T}(k)]^{T}, $$

$$ \dot{\boldsymbol{q}}(k) = [\dot{q}_{1}(k), \cdots, \dot{q}_{n}(k)]^{T}. $$

Furthermore, using the linear parametric models (12) and (13), we can write the difference equations (5) and (7) as

$$ \boldsymbol{e}_{PI}(k) = \boldsymbol{e}_{PI}(k-1) - T\boldsymbol{Y}_{L}(k)\boldsymbol{\alpha}_{L}, \quad (14) $$

$$ \boldsymbol{E}_{OI}(k) = \boldsymbol{E}_{OI}(k-1) + T\boldsymbol{E}_{X}(k)\boldsymbol{Y}_{A}(k)\boldsymbol{\alpha}_{A}. \quad (15) $$

2.4 Dynamic Model

A discrete-time dynamic model is given by the following equation [2]

$$ \dot{\boldsymbol{q}}(k) = \dot{\boldsymbol{q}}(k-1) - T\boldsymbol{H}^{-1}(k)\{\boldsymbol{C}(k)\dot{\boldsymbol{q}}(k) - \boldsymbol{\tau}(k)\} \quad (16) $$

where

$$ \boldsymbol{C}(k) = \frac{1}{2}\dot{\boldsymbol{H}}(k) + \boldsymbol{S}(k). $$

The matrix $\boldsymbol{S}$ is a skew-symmetric matrix, and $\boldsymbol{H}$ is a symmetric and positive definite inertia matrix.

3 Digital Adaptive Control

3.1 Controller Design

Taking (10) and (11) into consideration, we define the estimated GJMs as

$$ {}^{I}\hat{\boldsymbol{J}}_{L}^{*}(k) := \begin{bmatrix} \hat{\boldsymbol{\alpha}}_{11}^{T}(k)\boldsymbol{\zeta}_{11}(k) & \cdots & \hat{\boldsymbol{\alpha}}_{1n}^{T}(k)\boldsymbol{\zeta}_{1n}(k) \\ \hat{\boldsymbol{\alpha}}_{21}^{T}(k)\boldsymbol{\zeta}_{21}(k) & \cdots & \hat{\boldsymbol{\alpha}}_{2n}^{T}(k)\boldsymbol{\zeta}_{2n}(k) \\ \hat{\boldsymbol{\alpha}}_{31}^{T}(k)\boldsymbol{\zeta}_{31}(k) & \cdots & \hat{\boldsymbol{\alpha}}_{3n}^{T}(k)\boldsymbol{\zeta}_{3n}(k) \end{bmatrix}, \quad (17) $$

$$ {}^{I}\hat{\boldsymbol{J}}_{A}^{*}(k) := \begin{bmatrix} \hat{\boldsymbol{\alpha}}_{41}^{T}(k)\boldsymbol{\zeta}_{41}(k) & \cdots & \hat{\boldsymbol{\alpha}}_{4n}^{T}(k)\boldsymbol{\zeta}_{4n}(k) \\ \hat{\boldsymbol{\alpha}}_{51}^{T}(k)\boldsymbol{\zeta}_{51}(k) & \cdots & \hat{\boldsymbol{\alpha}}_{5n}^{T}(k)\boldsymbol{\zeta}_{5n}(k) \\ \hat{\boldsymbol{\alpha}}_{61}^{T}(k)\boldsymbol{\zeta}_{61}(k) & \cdots & \hat{\boldsymbol{\alpha}}_{6n}^{T}(k)\boldsymbol{\zeta}_{6n}(k) \end{bmatrix} \quad (18) $$

where $\hat{\boldsymbol{\alpha}}_{ij}$ is the estimated value of the physical parameter vector $\boldsymbol{\alpha}_{ij}$. From the boundedness of $\boldsymbol{\zeta}_{ij}$, we have

$$ \|{}^{I}\hat{\boldsymbol{J}}_{L}^{*}(k)\| \leq c_{1}\|\hat{\boldsymbol{\alpha}}_{L}(k)\|, \quad (19) $$

$$ \|{}^{I}\hat{\boldsymbol{J}}_{A}^{*}(k)\| \leq c_{2}\|\hat{\boldsymbol{\alpha}}_{A}(k)\| \quad (20) $$

where c_1 and c_2 are positive constants and $\hat{\boldsymbol{\alpha}}_{L}$ and $\hat{\boldsymbol{\alpha}}_{A}$ are the estimated values of the physical parameter vectors $\boldsymbol{\alpha}_{L}$ and $\boldsymbol{\alpha}_{A}$, respectively.

Next, taking (1) and (2) into consideration, we define the estimated values of ${}^{I}\boldsymbol{V}_{E}$ and ${}^{I}\boldsymbol{\Omega}_{E}$ as

$$ {}^{I}\hat{\boldsymbol{V}}_{E}(k) := {}^{I}\hat{\boldsymbol{J}}_{L}^{*}(k)\dot{\boldsymbol{q}}(k), \quad (21) $$

$$ {}^{I}\hat{\boldsymbol{\Omega}}_{E}(k) := {}^{I}\hat{\boldsymbol{J}}_{A}^{*}(t)\dot{\boldsymbol{q}}(k). \quad (22) $$

In addition, substituting (17) and (18) into (21) and (22) respectively, we have

$$ {}^{I}\hat{\boldsymbol{V}}_{E}(k) = \boldsymbol{Y}_{L}(k)\hat{\boldsymbol{\alpha}}_{L}(k), \quad (23) $$

$$ {}^{I}\hat{\boldsymbol{\Omega}}_{E}(k) = \boldsymbol{Y}_{A}(k)\hat{\boldsymbol{\alpha}}_{A}(k). \quad (24) $$

The following discrete-time adaptive laws update the estimates $\hat{\boldsymbol{\alpha}}_{L}$ and $\hat{\boldsymbol{\alpha}}_{A}$ of $\boldsymbol{\alpha}_{L}$ and $\boldsymbol{\alpha}_{A}$ on-line, respectively:

$$ \hat{\boldsymbol{\alpha}}_{L}(k) = \hat{\boldsymbol{\alpha}}_{L}(k-1) - \gamma_{P}T\boldsymbol{Y}_{L}^{T}(k)\boldsymbol{e}_{PI}(k), \quad (25) $$

$$ \hat{\boldsymbol{\alpha}}_{A}(k) = \hat{\boldsymbol{\alpha}}_{A}(k-1) - \gamma_{O}T\boldsymbol{Y}_{A}^{T}(k)\boldsymbol{e}_{OI}(k) \quad (26) $$

where γ_P and γ_O are positive scalar adaptive gains for linear and angular velocities, respectively. It should be emphasized that the unknown parameters are estimated on-line so that the control system is stable; therefore, the estimated parameters $\hat{\boldsymbol{\alpha}}_{L}$ and $\hat{\boldsymbol{\alpha}}_{A}$ don't need to converge to the real values $\boldsymbol{\alpha}_{L}$ and $\boldsymbol{\alpha}_{A}$.

The parameter errors are defined as

$$ \tilde{\boldsymbol{\alpha}}_{L}(k) := \hat{\boldsymbol{\alpha}}_{L}(k) - \boldsymbol{\alpha}_{L}, \quad (27) $$

$$ \tilde{\boldsymbol{\alpha}}_{A}(k) := \hat{\boldsymbol{\alpha}}_{A}(k) - \boldsymbol{\alpha}_{A}. \quad (28) $$

From (25)–(28), the following difference equations of the parameter errors are obtained:

$$ \tilde{\boldsymbol{\alpha}}_{L}(k) = \tilde{\boldsymbol{\alpha}}_{L}(k-1) - \gamma_{P}T\boldsymbol{Y}_{L}^{T}(k)\boldsymbol{e}_{PI}(k), \quad (29) $$

$$ \tilde{\boldsymbol{\alpha}}_{A}(k) = \tilde{\boldsymbol{\alpha}}_{A}(k-1) - \gamma_{O}T\boldsymbol{Y}_{A}^{T}(k)\boldsymbol{e}_{OI}(k). \quad (30) $$

Replacing the physical parameters with their estimates in the control law [2] developed for the known parameters, we obtain the following adaptive control input:

$$ \boldsymbol{\tau}(k) = k_{P}{}^{I}\hat{\boldsymbol{J}}_{L}^{*T}(k)\boldsymbol{e}_{PI}(k) + k_{O}{}^{I}\hat{\boldsymbol{J}}_{A}^{*T}(k)\boldsymbol{e}_{OI}(k) - \boldsymbol{K}_{V}\dot{\boldsymbol{q}}(k). \quad (31) $$

3.2 Stability Analysis

The following theorems establish the stability properties of the proposed digital adaptive control law (25), (26), and (31) :

Theorem 1 The closed-loop system represented by the backward difference equations (14)– (16), (29), and (30) and the digital adaptive control law (25), (26), and (31) has the following properties:

(i) The signals $\boldsymbol{e}_{PI}(k)$, $\boldsymbol{E}_{OI}(k)$, $\dot{\boldsymbol{q}}(k)$, $\boldsymbol{\tau}(k)$, $\hat{\boldsymbol{\alpha}}_L(k)$, and $\hat{\boldsymbol{\alpha}}_A(k)$ are bounded for all k.

(ii) $\lim_{k\to\infty} \dot{\boldsymbol{q}}(k) = \boldsymbol{0}$ and $\lim_{k\to\infty} \boldsymbol{\tau}(k) = \boldsymbol{0}$.

Proof **(i)** We choose the positive function

$$W(k) = \sum_{i=1}^{5} W_i(k), \tag{32}$$

and its first difference $\triangle W_-(k)$ is defined as follows:

$$\triangle W_-(k) := W(k) - W(k-1) = \sum_{i=1}^{5} \triangle W_{i-}(k) \tag{33}$$

where

$$\begin{aligned}
W_1(k) &= k_P \boldsymbol{e}_{PI}^T(k)\boldsymbol{e}_{PI}(k),\\
W_2(k) &= \frac{k_O}{2}\boldsymbol{E}_{OI}^T(k)\boldsymbol{E}_{OI}(k),\\
W_3(k) &= \dot{\boldsymbol{q}}^T(k)\boldsymbol{H}(k)\dot{\boldsymbol{q}}(k),\\
W_4(k) &= \frac{k_P}{\gamma_P}\tilde{\boldsymbol{\alpha}}_L^T(k)\tilde{\boldsymbol{\alpha}}_L(k),\\
W_5(k) &= \frac{k_O}{\gamma_O}\tilde{\boldsymbol{\alpha}}_A^T(k)\tilde{\boldsymbol{\alpha}}_A(k),\\
\triangle W_{i-}(k) &= W_i(k) - W_i(k-1) \quad (i = 1, \cdots, 5).
\end{aligned}$$

From (14), $\triangle W_{1-}(k)$ is given by

$$\begin{aligned}
\triangle W_{1-}(k) &= -2k_P T\boldsymbol{\alpha}_L^T\boldsymbol{Y}_L^T(k)\boldsymbol{e}_{PI}(k)\\
&\quad -k_P T^2\boldsymbol{\alpha}_L^T\boldsymbol{Y}_L^T(k)\boldsymbol{Y}_L(k)\boldsymbol{\alpha}_L\\
&\le 2k_P T\tilde{\boldsymbol{\alpha}}_L^T(k)\boldsymbol{Y}_L^T(k)\boldsymbol{e}_{PI}(k)\\
&\quad -2k_P T\hat{\boldsymbol{\alpha}}_L^T(k)\boldsymbol{Y}_L^T(k)\boldsymbol{e}_{PI}(k).
\end{aligned} \tag{34}$$

Using (9), (15), and the property that $\boldsymbol{E}_X^T(k)\boldsymbol{E}_X(k) = 2\boldsymbol{U}_3$, we can write $\triangle W_{2-}(k)$ as

$$\begin{aligned}
\triangle W_{2-}(k) &= -2k_O T\boldsymbol{\alpha}_A^T\boldsymbol{Y}_A^T(k)\boldsymbol{e}_{OI}(k)\\
&\quad -k_O T^2\boldsymbol{\alpha}_A^T\boldsymbol{Y}_A^T(k)\boldsymbol{Y}_A(k)\boldsymbol{\alpha}_A\\
&\le 2k_O T\tilde{\boldsymbol{\alpha}}_A^T(k)\boldsymbol{Y}_A^T(k)\boldsymbol{e}_{OI}(k)\\
&\quad -2k_O T\hat{\boldsymbol{\alpha}}_A^T(k)\boldsymbol{Y}_A^T(k)\boldsymbol{e}_{OI}(k).
\end{aligned} \tag{35}$$

Assuming that $\boldsymbol{H}(k) \approx \boldsymbol{H}(k-1)$, i.e., $\dot{\boldsymbol{H}}(k) \approx \boldsymbol{0}$ and using (16) and the property

$$\dot{\boldsymbol{q}}^T(k)\boldsymbol{S}(k)\dot{\boldsymbol{q}}(k) = 0, \quad {}^\forall k,$$

we have

$$\triangle W_{3-}(k) = 2T\dot{\boldsymbol{q}}^T(k)\boldsymbol{\tau}(k) - T^2\boldsymbol{d}^T(k)\boldsymbol{H}^{-1}(k)\boldsymbol{d}(k) \tag{36}$$

where

$$\boldsymbol{d}(k) = \boldsymbol{S}(k)\dot{\boldsymbol{q}}(k) - \boldsymbol{\tau}(k).$$

Furthermore, substituting (31) into (36) and using (21)–(24), we obtain

$$\begin{aligned}
\triangle W_{3-}(k) &= 2k_P T\hat{\boldsymbol{\alpha}}_L^T(k)\boldsymbol{Y}_L^T(k)\boldsymbol{e}_{PI}(k)\\
&\quad +2k_O T\hat{\boldsymbol{\alpha}}_A^T(k)\boldsymbol{Y}_A^T(k)\boldsymbol{e}_{OI}(k)\\
&\quad -2T\dot{\boldsymbol{q}}^T(k)\boldsymbol{K}_V\dot{\boldsymbol{q}}(k)\\
&\quad -T^2\boldsymbol{d}^T(k)\boldsymbol{H}^{-1}(k)\boldsymbol{d}(k).
\end{aligned} \tag{37}$$

From (29) and (30), $\triangle W_{4-}(k)$ and $\triangle W_{5-}(k)$ are given by the following equations, respectively:

$$\begin{aligned}
\triangle W_{4-}(k) &= -2k_P T\tilde{\boldsymbol{\alpha}}_L^T(k)\boldsymbol{Y}_L^T(k)\boldsymbol{e}_{PI}(k)\\
&\quad -k_P\gamma_P T^2\boldsymbol{e}_{PI}^T(k)\boldsymbol{Y}_L(k)\boldsymbol{Y}_L^T(k)\boldsymbol{e}_{PI}(k)\\
&\le -2k_P T\tilde{\boldsymbol{\alpha}}_L^T(k)\boldsymbol{Y}_L^T(k)\boldsymbol{e}_{PI}(k),
\end{aligned} \tag{38}$$

$$\begin{aligned}
\triangle W_{5-}(k) &= -2k_O T\tilde{\boldsymbol{\alpha}}_A^T(k)\boldsymbol{Y}_A^T(k)\boldsymbol{e}_{OI}(k)\\
&\quad -k_O\gamma_O T^2\boldsymbol{e}_{OI}^T(k)\boldsymbol{Y}_A(k)\boldsymbol{Y}_A^T(k)\boldsymbol{e}_{OI}(k)\\
&\le -2k_O T\tilde{\boldsymbol{\alpha}}_A^T(k)\boldsymbol{Y}_A^T(k)\boldsymbol{e}_{OI}(k).
\end{aligned} \tag{39}$$

Substituting (34), (35), and (37)–(39) into (33), we have

$$\begin{aligned}
\triangle W_-(k) &\le -2T\dot{\boldsymbol{q}}^T(k)\boldsymbol{K}_V\dot{\boldsymbol{q}}(k)\\
&\quad -T^2\boldsymbol{d}^T(k)\boldsymbol{H}^{-1}(k)\boldsymbol{d}(k)\\
&\le -2\lambda_{min}\{\boldsymbol{K}_V\}T\,\|\dot{\boldsymbol{q}}(k)\|^2\\
&\quad -\lambda_{min}\{\boldsymbol{H}^{-1}(k)\}T^2\,\|\boldsymbol{d}(k)\|^2
\end{aligned} \tag{40}$$

where $\lambda_{min}\{\cdot\}$ is a minimum eigenvalue. Because $\boldsymbol{K}_V$ and $\boldsymbol{H}^{-1}$ are bounded positive definite matrices, we obtain that $0 < \lambda_{min}\{\boldsymbol{H}^{-1}\}, \lambda_{min}\{\boldsymbol{K}_V\} < +\infty$; therefore, we can rewrite (40) as

$$\triangle W_-(k) \le -\bar{c}_1\,\|\dot{\boldsymbol{q}}(k)\|^2 - \bar{c}_2\,\|\boldsymbol{d}(k)\|^2 \le 0 \tag{41}$$

where $\bar{c}_1,\ \bar{c}_2 > 0$.

Because $W(k) \ge 0$, $\triangle W_-(k) = W(k) - W(k-1) \le 0$, and $0 \le W(0) < +\infty$ $(k = 1, 2, \cdots)$, we have

$$0 \le \bar{W}_\infty \le W(k) \le W(k-1) \le \bar{W}_0 < +\infty, \quad {}^\forall k \tag{42}$$

where $\bar{W}_\infty = \lim_{k\to\infty} W(k)$ and $\bar{W}_0 = W(0)$. Hence, it follows that W, $\boldsymbol{e}_{PI}$, $\boldsymbol{E}_{OI}$, $\dot{\boldsymbol{q}}$, $\tilde{\boldsymbol{\alpha}}_L$, $\tilde{\boldsymbol{\alpha}}_A < \infty$. From (9), (27), and (28), the boundedness of $\boldsymbol{E}_{OI}$, $\tilde{\boldsymbol{\alpha}}_L$, and $\tilde{\boldsymbol{\alpha}}_A$ implies that $\boldsymbol{e}_{OI}$, $\hat{\boldsymbol{\alpha}}_L$, $\hat{\boldsymbol{\alpha}}_A < \infty$. Furthermore, using (19), (20) and (31), we obtain the following inequality of the control input:

$$\begin{aligned}
\|\boldsymbol{\tau}(k)\| &\le k_P c_1\|\hat{\boldsymbol{\alpha}}_L(k)\|\|\boldsymbol{e}_{PI}(k)\|\\
&\quad +k_O c_2\|\hat{\boldsymbol{\alpha}}_A(k)\|\|\boldsymbol{e}_{OI}(k)\| + \|\boldsymbol{K}_V\|\|\dot{\boldsymbol{q}}(k)\|.
\end{aligned}$$

Because $\boldsymbol{e}_{PI}$, $\boldsymbol{e}_{OI}$, $\dot{\boldsymbol{q}}$, $\hat{\boldsymbol{\alpha}}_L$, $\hat{\boldsymbol{\alpha}}_A < \infty$, it follows that $\boldsymbol{\tau} < \infty$.

(ii) It follows from (41) that $\triangle W_-(k) \leq -\bar{c}_1 \|\dot{\boldsymbol{q}}(k)\|^2$ and $\triangle W_-(k) \leq -\bar{c}_2 \|\boldsymbol{d}(k)\|^2$; therefore, defining the partial sum S_q of the sequence $\{\|\dot{\boldsymbol{q}}\|^2\}$ as

$$S_q(k) := \sum_{h=1}^{k} \|\dot{\boldsymbol{q}}(h)\|^2,$$

we have

$$0 \leq S_q(k) \leq \frac{1}{\bar{c}_1}\{\bar{W}_0 - W(k)\} < +\infty, \quad {}^\forall k.$$

Because $S_q(k) < \infty$ and $S_q(k-1) \leq S_q(k)$ for all k, the sum S_q has a limit as $k \to \infty$, i.e., the infinite series of the sequence $\{\|\dot{\boldsymbol{q}}\|^2\}$ converges; therefore, $\lim_{k\to\infty} \|\dot{\boldsymbol{q}}(k)\|^2 = 0$ [5], i.e., $\lim_{k\to\infty} \dot{\boldsymbol{q}}(k) = \boldsymbol{0}$. It is similarly shown that $\lim_{k\to\infty} \boldsymbol{d}(k) = \lim_{k\to\infty}\{\boldsymbol{S}(k)\dot{\boldsymbol{q}}(k) - \boldsymbol{\tau}(k)\} = \boldsymbol{0}$. Furthermore, using the property

$$\|\boldsymbol{S}(k)\| \leq c_3\|\dot{\boldsymbol{q}}(k)\|, \quad {}^\forall k$$

where $c_3 > 0$ and the boundedness of $\dot{\boldsymbol{q}}$, we have that $\boldsymbol{S} < \infty$. Because $\boldsymbol{S} < \infty$ and $\lim_{k\to\infty} \dot{\boldsymbol{q}}(k) = \boldsymbol{0}$, $\lim_{k\to\infty} \boldsymbol{S}(k)\dot{\boldsymbol{q}}(k) = \boldsymbol{0}$. Hence, we obtain that $\lim_{k\to\infty} \boldsymbol{\tau}(k) = \boldsymbol{0}$. □

Theorem 2 In addition to Theorem 1 (i) and (ii), the closed-loop system represented by the backward difference equations (14)–(16), (29), and (30) and the digital adaptive control law (25), (26), and (31) has the following property:

If the conditions

$$\text{rank } {}^I\hat{\boldsymbol{J}}^*(k) = 6, \text{ (full rank)} \tag{43}$$

$${}^I\boldsymbol{n}_E^T(k)\,{}^I\boldsymbol{n}_T + {}^I\boldsymbol{s}_E^T(k)\,{}^I\boldsymbol{s}_T + {}^I\boldsymbol{a}_E^T(k)\,{}^I\boldsymbol{a}_T > -1 \tag{44}$$

hold, then we have

$$\lim_{k\to\infty} \boldsymbol{e}_{PI}(k) = \boldsymbol{0}, \quad \lim_{k\to\infty} \boldsymbol{E}_{OI}(k) = \boldsymbol{0}$$

where

$${}^I\hat{\boldsymbol{J}}^*(k) = \begin{bmatrix} {}^I\hat{\boldsymbol{J}}_L^*(k) \\ {}^I\hat{\boldsymbol{J}}_A^*(k) \end{bmatrix}.$$

Proof We can rewrite (31) as

$$\boldsymbol{\tau}(k) + \boldsymbol{K}_V\dot{\boldsymbol{q}}(k) = {}^I\hat{\boldsymbol{J}}^{*T}(k)\boldsymbol{K}\boldsymbol{e}_I(k) \tag{45}$$

where

$$\boldsymbol{K} = \begin{bmatrix} k_P\boldsymbol{U}_3 & \boldsymbol{0} \\ \boldsymbol{0} & k_O\boldsymbol{U}_3 \end{bmatrix}, \quad \boldsymbol{e}_I(k) = \begin{bmatrix} \boldsymbol{e}_{PI}(k) \\ \boldsymbol{e}_{OI}(k) \end{bmatrix}.$$

Using (45), we have

$$\|\boldsymbol{\tau}(k) + \boldsymbol{K}_V\dot{\boldsymbol{q}}(k)\|^2 = \boldsymbol{e}_I^T(k)\boldsymbol{Q}(k)\boldsymbol{e}_I(k) \tag{46}$$

where

$$\boldsymbol{Q}(k) = \boldsymbol{K}\,{}^I\hat{\boldsymbol{J}}^*(k)\,{}^I\hat{\boldsymbol{J}}^{*T}(k)\boldsymbol{K}.$$

Because $\boldsymbol{K}$ is a symmetric and positive definite matrix and the condition (43) holds, $\boldsymbol{Q}(k)$ is a symmetric and positive definite matrix; therefore, (46) is written as

$$\|\boldsymbol{\tau}(k) + \boldsymbol{K}_V\dot{\boldsymbol{q}}(k)\|^2 \geq \lambda_{Qmin}\|\boldsymbol{e}_I(k)\|^2 \geq 0 \tag{47}$$

where

$$0 < \lambda_{Qmin} \leq \lambda_{min}\{\boldsymbol{Q}(k)\}, \quad {}^\forall k.$$

Because $\lim_{k\to\infty} \dot{\boldsymbol{q}}(k) = \boldsymbol{0}$ and $\lim_{k\to\infty} \boldsymbol{\tau}(k) = \boldsymbol{0}$, i.e., $\lim_{k\to\infty} \|\boldsymbol{\tau}(k) + \boldsymbol{K}_V\dot{\boldsymbol{q}}(k)\|^2 = 0$, it follows from (47) that $\lim_{k\to\infty} \|\boldsymbol{e}_I(k)\|^2 = 0$, i.e., $\lim_{k\to\infty} \boldsymbol{e}_{PI}(k) = \boldsymbol{0}$ and $\lim_{k\to\infty} \boldsymbol{e}_{OI}(k) = \boldsymbol{0}$. Furthermore, because $\lim_{k\to\infty} \boldsymbol{e}_{OI}(k) = \boldsymbol{0}$, we have from the condition (44) that $\lim_{k\to\infty} \boldsymbol{E}_{OI}(k) = \boldsymbol{0}$. □

4 Conclusions

This paper presented a digital adaptive control method of space robot manipulators using the transpose of the Generalized Jacobian Matrix. It was shown that the adaptive control system developed for unknown parameters has the same stability property that the control system [2] developed for known parameters has.

References

[1] Y. Masutani, F. Miyazaki, and S. Arimoto, "Modeling and Sensory Feedback Control for Space Manipulators," *Proc. 1989 NASA Conf. on Space Telerobotics*, pp.287–296, 1989.

[2] Y. Taira, S. Sagara, and R. Katoh, "Digital Control of Space Robot Using Transpose of Generalized Jacobian Matrix," *Trans. of the JSME*, Ser.C, **67**(654), pp.436–442, 2001 (in Japanese).

[3] Y. Taira, S. Sagara, and R. Katoh, "Digital Adaptive Control of Space Robot Manipulators Using Transpose of Generalized Jacobian Matrix," *Proc. of IROS 2000* (CD-ROM), 2000.

[4] T. Yamamoto, J. Kobayashi, R. Katoh, and F. Ohkawa, "Digital Adaptive Control of a Manipulator Mounted on Free-Flying Robot in Space," *Proc. Ninth World Congress on the Theory of Machines and Mechanism*, pp.2151–2155, 1995.

[5] R. G. Bartle and D. R. Sherbert, Introduction to Real Analysis, Third Edition, John Wiley & Sons, p.91, 2000.

Proc. of The Ninth Int. Symp. on Artificial Life and Robotics (AROB 9th '04)
Beppu, Oita, Japan, 28-30 January, 2004

Application of Neural Network to Generation of Robot Arm Trajectory

Shuya Imajo, Masami Konishi, Tatsushi Nishi, and Jun Imai
Department of Electrical and Electronic Engineering
Okayama University
3-1-1 Tsushimanaka, Okayama, 700-8530, Japan
konishi@elec.okayama-u.ac.jp

Abstract

In this paper, a neural network model representing robot arm trajectory is proposed. The developed neural network model is based on the recurrent type neural network (RNN) model which calculates the proper trajectory based on data acquired by human as the training data. Furthermore, a self-learning function has been added to the RNN model. The proposed method is applied to 2-DOF robot arm and laboratory experiments were carried out. From the experimental results, it was verified that the trajectory by human could be reproduced by the proposed model. Modification of moving trajectory can be made by learning to escape obstacles or collision.

Keywords : neural network, trajectory generator, robot arm, learning

1 Introduction

Recently, robot system has been applied in a wide variety of fields. The problem in the application is how to install the intelligence on these robots. For example, in case of load handling, it is necessary to train the robot arms to follow up the appropriate trajectory. In this paper, topics are focused on the generation of trajectory for robot hand with two links[1] [2].

Traditionally, trajectory of a robot arm was generated by teaching-play back method. However, there was not clarified how human experts trained in such a way that they moved. To develop the intelligence for robots, it is necessary to estimate movement of robots. That is, some kinds of intelligence are to be developed to determine automatically the appropriate robot trajectory through training. In this paper, automatic generation of robot trajectory by RNN (Recurrent Neural Network) model[3] is studied.

The inputs to RNN are plural evaluated values of robot movement and past locus values of joint angles of the robot arm. The outputs from RNN are desired values for joint angles of robot arm in the next instance. Also the RNN model has been added a self-learning function. Using the function, weights of RNN model are updated so as to realize the desired value of evaluation functions for robot movement determined from the analysis of human operation.

Using the developed RNN model, numerical experiment to check the effectiveness of the model was carried out by using the robot simulator.

Finally, operational experiments in the laboratory using 2-DOF robot arm were carried out to check the practicability of RNN model.

2 Trajectory Generator by RNN

2.1 Generation of Training Data

In order to build the RNN model, it is necessary to generate teaching data. Human grasped robot arm and moved it to target position from initial position on several occasions. Then time series data sets of joint angles are gathered. Using the data, RNN model are identified to cover the wide variety of human operations. As the result, two RNN models are constructed corresponding to two joints by the data sets.

2.2 RNN Model

The structure of RNN model developed in this paper is shown in Fig. 1. These networks are identified for two robot links.

As shown in the figure, the networks have three layers. The first layer is the input layer, which consists of two parts. The one is the plan layer consisting four evaluation functions I_1, I_2, I_3 and I_4 for robot arm movements. The differential between these evaluation value I_i and desired evaluation value I_i^o are input to RNN model. Where these evaluation functions are given as the following normalized functions.

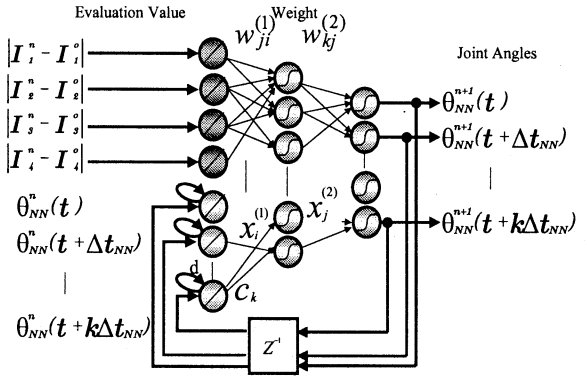


Fig. 1 RNN Model

First, the evaluation function of joint angle variation is expressed by

$$I_1 = \frac{1}{t_f}\int_0^{t_f} |\tilde{\theta}_i| dt \quad (i = 1 \ \ or \ \ 2) \tag{1}$$

where t_f is working time, and $\tilde{\theta}_i$ is given by

$$\tilde{\theta}_i = \frac{\theta_{fi} - \theta_{i(t)}}{\theta_{fi} - \theta_{oi}} \quad (i = 1 \ \ or \ \ 2) \tag{2}$$

Second, the evaluation function of angular velocity is given by

$$I_2 = \int_0^{t_f} |\dot{\tilde{\theta}}_i| dt \quad (i = 1 \ \ or \ \ 2) \tag{3}$$

Third, the evaluation function of normalized distance between target position and end position of robot arm is given by

$$I_3 = \frac{1}{t_f}\int_0^{t_f} \sqrt{\frac{(x_f - x_{(t)})^2 + (y_f - y_{(t)})^2}{(x_f - x_o)^2 + (y_f - y_o)^2}} dt \tag{4}$$

where (x_o, y_o), (x_f, y_f) are the coordinates of initial position and target position respectively.

Finally, the evaluation function of deviation of end effector trajectory from straight trajectory between start position and goal position is expressed as follows.

$$I_4 = \frac{1}{t_f}\int_0^{t_f} \frac{|bx_{(t)} + ay_{(t)} + c|}{\sqrt{a^2 + b^2}} dt \tag{5}$$
$$a = x_f - x_o; \quad b = y_o - y_f; \quad c = x_o y_f - x_f y_o$$

While, the other part of input layer is the context layer of the previous trajectory which is weighted sum of past output data of RNN model expressed as follows.

$$c_k = \sum_{m=1}^{n} d^{n-m} \theta^m_{NN[t+(k-1)\Delta t_{NN}]} \tag{6}$$

where k is number of neuron in output layer, d is a positive constant, which represents forgetting factor.

A linear function is used as the input layer of the neuron. And the sigmoid function is used in neuron of the hidden layer and the output layer.

When the model is used as trajectory generator, the joint angle data output from RNN every Δt_{NN} is interpolated by spline interpolation function.

3 Numerical Experiments

Furthermore, in order to check the effectiveness of the proposed RNN model, the control system for trajectory is developed as shown in Fig. 2.

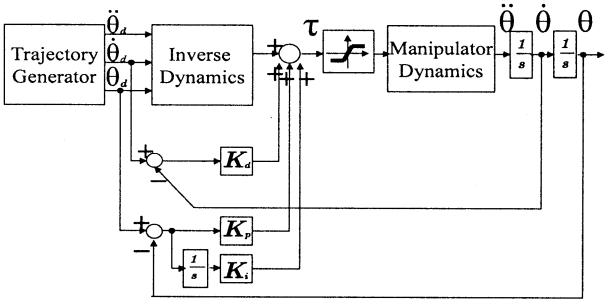


Fig. 2 Block Diagram for Trajectory Control

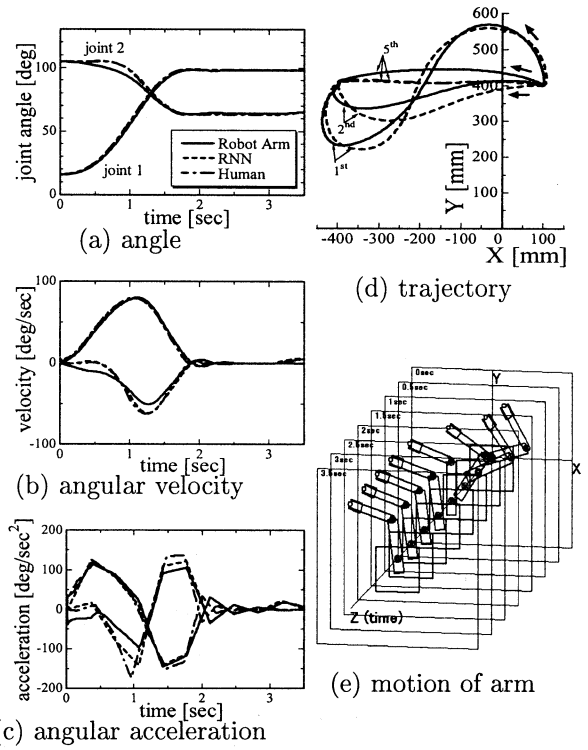


Fig. 3 Simulation Results

Mathematical model for robot movement was developed based on Lagrangian equations for robot dynamics. In the figure, trajectory generator is generated by RNN, and inverse dynamics[4] and manipulator dynamics are determined by Lagrangian equations.

Simulation results for single target point same as training data are shown in Fig. 3. Here, (a),(b),(c) represent joint angle, angular velocity, and angular acceleration at 5 times respectively. As shown here, RNN output and manipulator movement are compared with training data created by human. (d) shows trajectory of end effector from 1^{st} to 5^{th}. We compared the data between robot movement and training data. (e) shows 5^{th} motion of robot arm in every 0.5 sec. As shown here, robot arm trajectory is converged in straight forward manner to human trajectory.

4 Laboratory Experiments

To check the effectiveness of numerical experiments, the robot system using trajectory generator by RNN is built. The appearance is shown in Fig. 4. The experimental result of trajectory for the robot arm is shown in Fig. 5. The results show similar trajectory as shown in Fig. 3.

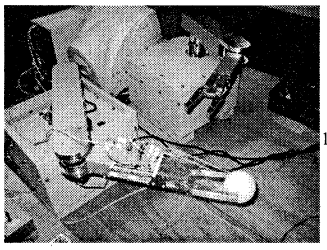


Fig. 4 Overview of Robot Arm

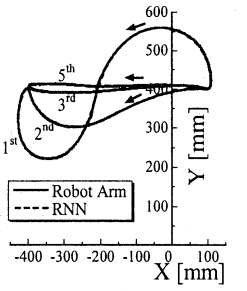


Fig. 5 Experimental Result

5 Learning

The RNN model should be modified according to the current environment, for example, the different target position, purpose of obstacle avoidance, and change of robot arm dynamics and control system. That is, desired evaluation functions I_i^o's according to the change in environment may be modified. There is no training data for trajectory in the unknown environment. In the following, update algorithm for RNN model by back propagation(BP) using evaluation value for trajectory will be described.

First, the error estimation function $E_{[l]}$ is defined as

$$E_{[l]} = \sum_{i=1}^{6} \frac{1}{2} \rho_{ki} (I_{i[l]} - I_i^o)^2 \tag{7}$$

where ρ_{ki} is weight coefficient, and I_i^o is the evaluation value for ideal trajectory. As defined above, the error estimation function contains the evaluation function I_i which is input to RNN model. Here new evaluation function I_5 and I_6 are added which evaluates overshoot for target angle is defined by

$$I_5 = \frac{\theta_{os}}{|\theta_f - \theta_o|}, \qquad I_6 = \frac{\theta_{us}}{|\theta_f - \theta_o|} \tag{8}$$

where θ_{os} is overshoot for target angle, and θ_{us} is undershoot for initial angle.

The objective of the learning is to minimize E as shown in Fig.6.

First the update value $\Delta w_{kj}^{(2)}$ for weight $w_{kj}^{(2)}$ between j^{th} neuron in the hidden layer and k^{th} neuron in the output layer is derived by

$$\Delta w_{kj}^{(2)} = \epsilon_{k[l]} \delta_k^{(2)} x_{j[l]}^{(2)} \tag{9}$$

where

$$\delta_k^{(2)} = -\left\{ \sum_{i=1}^{6} \rho_{ki} (I_{i[l]} - I_i^o) \frac{I_{i[l]} - I_{i[l-1]}}{\theta_{NN}^{l} - \theta_{NN}^{l-1}} \right\} \times \theta_{NN}^{l}(1 - \theta_{NN}^{l}) \tag{10}$$

where $x_{j[l]}^{(2)}$ is output of j^{th} neuron in the hidden layer at l^{th} iteration. $\epsilon_{k[l]}$ is the learning rate at l^{th} iteration for k^{th} neuron in the output layer. The learning rate is given by

$$\epsilon_{k[l]} = \epsilon_{k0} \left(1 - \frac{l}{T_L} \right) \tag{11}$$

where, ϵ_{k0} is initial value for learning rate, and T_L is a learning times which are set in advance.

Next the update value $\Delta w_{kj}^{(2)}$ for weight between i^{th} neuron in the input layer and j^{th} neuron in the hidden layer is expressed as

$$\Delta w_{ji}^{(1)} = \epsilon_{[l]} \left(\sum_k \delta_k^{(2)} w_{kj}^{(2)} \right) x_{j[l]}^{(2)} (1 - x_{j[l]}^{(2)}) x_{i[l]}^{(1)} \tag{12}$$

where $x_{i[l]}^{(1)}$ is output of i^{th} neuron in the input layer at l^{th} iteration. $\epsilon_{[l]}$ is the learning rate which decrease in steps as well as Eq.(11).

After every operation is over, the weights of RNN are updated using past two data of trajectories in the

learning term T_L. For the duration of learning term T_L, the weight of RNN model is updated one iteration using past two times trajectory results at each time when robot finishes one task. Then next trajectory is generated based on updated RNN model.

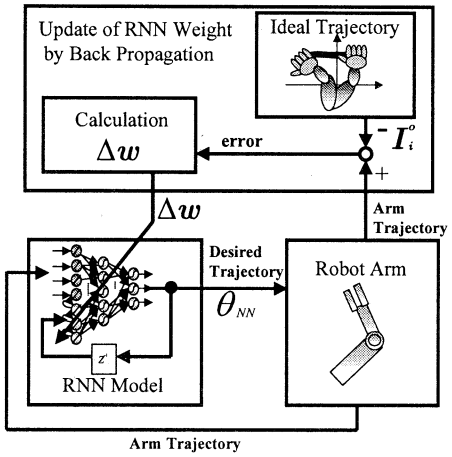


Fig. 6 Update of RNN weight by BP

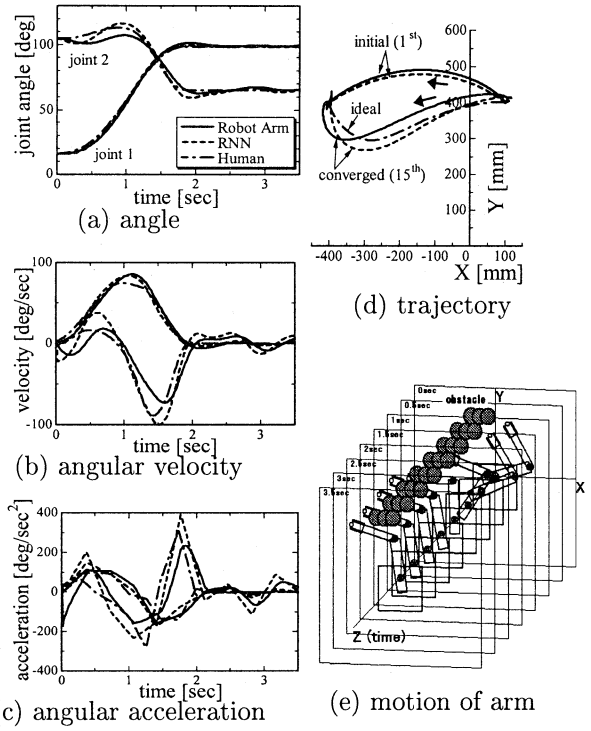


Fig. 7 Simulation Results for Learning

To check the effectiveness of proposed method, learning of trajectory is demonstrated by numerical experiments. Collisions must be avoided in environment that obstacle exists. Since the proposed RNN model generates only one trajectory teached by human, it is expected to generate proper and smooth trajectory according to environment by self-learning.

Fig. 7 shows the results when update of RNN weight by BP is executed at 15 times, where learning term $T_L = 10$ and initial trajectory is generated by cubic polynomials. The ideal trajectory is shown in Fig. 7(d). As shown in Fig. 7, trajectory converged another one, which is different from Fig. 3. The results are useful in avoiding obstacle.

6 Conclusion

In this paper, generation of robot arm trajectory by neural networks is proposed. Using the trajectory data by human operation, RNN model is identified to reproduce the robot trajectory of human operation. In the RNN model, inputs are chosen as evaluation functions showing the characteristics of robot movement. This enables generation of generalized robot trajectory with smooth manipulation. Introduction of learning in evaluation function enables the robot to move avoiding obstacle. Through numerical and laboratory experiments, appropriate robot trajectory was realized.

Acknowledgements

The authors gratefully acknowledge the funding provided by Okayama prefecture.

References

[1] Nojima Y, Kojima F, Kubota N (2003), "Trajectory Generation for Human-Friendly Behavior of Partner Robot using Fuzzy Evaluating Interactive Genetic Algorithm," Proc. IEEE Int. Symp. CIRA, pp.306-311

[2] Y.K. Yiu, Z.X.Li (2003), "Trajectory Generation for a 2-dof Over-actuated Parallel Manipulator with Actuator Speed and Torque Limits Consideration," Proc. IEEE Int. Symp. CIRA, pp.1058-1063

[3] Imajo S, Konishi M, Imai J et al (2002), "Human Model for Gain Tuning of Looper Control in Hot Strip Rolling," CAMP-ISIJ, Vol.15, p931

[4] Isobe D, Imaizumi D, Chikugo Y et al (2003), "A Parallel Solution Scheme for Inverse Dynamics and its Application in Feed-forward Control of Link Mechanisms," Journal of Robotics and Mechatronics, Vol.15, No.1 pp.1-7

Proc. of The Ninth Int. Symp. on Artificial Life and Robotics (AROB 9th '04)
Beppu, Oita, Japan, 28-30 January, 2004

Formation of Agent Behavior by Adaptive Pickup of Ambient Information with Speculative Action

H. Yamagishi, T. Shiose, H. Kawakami, O. Katai
Graduate School of Informatics, Kyoto University
Yoshidahon-machi, Sakyo-ku, Kyoto, 606-8501

Abstract

We propose a new framework of a perception-action system based on reinforcement learning and ecological psychology. In our framework, an agent perceives ambient information, a kind of environmental property related to the agent by speculative action, and behaves adaptively in the environment. In this paper, we explain the difference between Q-learning with only sensory inputs and Q-learning with the adaptive pickup of ambient information by applying each to a boat controlling problem where wind pushes the boat in various directions. As a result, we conclude that the pickup of ambient information by speculative action enables an agent to behave adaptively in a dynamic environment.

1 Introduction

The number of robots and computer agents in our daily life is increasing. Since robots and computer agents are mainly designed to accomplish their static goals in an environment, they are programed to act or learn to act according to the static optimal goals. However, the environment we live in is so complicated and dynamic that we cannot predict optimal goals and all the sensors that are required. Therefore, robots and computer agents enable to interact with humans or to act in a non-predefined dynamic environment, a learning algorithm that is adaptable and robust to the environment by searching the ambient information through speculative action must be developed. In order to develop adaptive learning algorithms, we introduce the notion of ecological psychology into reinforcement learning.

In the field of ecological psychology, it is said that animals, including human beings, behave adaptively to their environment by picking up proper "affordances" [6]. The term "affordance" is defined in various ways, but, in this paper, it means the environmental properties evaluated by animals that "afford" the animals to do something. To pick up proper "affordances", animal have to perceive ambient information[5]. Ambient information is a kind of environmental information related to the animal that is perceived only when the animal is in the middle of an action. Several affordances are picked up from ambient information.

In this paper, we propose a framework of adaptive pickup of "affordances" from ambient information through speculative actions. In our framework of reinforcement learning, an agent can pick up ambient information to behave adaptively in a non-predefined dynamic environment. In this framework, an agent learns to perceive environmental properties by using the information on its last action and subsequent environmental response. Then, the agent decides the next action depending on its states and environmental properties.

In this paper, we examine our framework with a "boat controlling problem," where the wind direction changes depending on time. The wind pushes the boat not only in one direction but also in various directions. This problem is categorized as a non-Markov Decision Process (non-M.D.P.), which is different from the famous reinforcement learning problem "windy gridworld", where the wind direction is constant.

2 Ambient information

2.1 Affordance

"Affordances", coined by J. J. Gibson, are possibilities for action that inform animals whether or not they are allowed to do something. An affordance represents the relation between a relevant environmental property and a property linked to their own body or actions [6]. In affordance theory, animals do not construct perceptual images of the world based on stimulation of their sensory organs, but perceive environmental properties that show them affordances.

For example, walking is not achieved by merely leg contact to the ground and leg-motion but also by

perception of the stiffness of the ground through leg-contact. When the ground is muddy, the walking action has to be changed adaptively according to the environmental response. Therefore, animals and environment co-create the animals' behavior based on that information.

Furthermore, two animals perceive different information from the same environment if their bodies differ. For instance, humans are heavy enough to feel that mud is not stiff, where ants are light enough to feel that the stiffness of mud is almost the same as that of concrete. Therefore, animals may sense sensory inputs via receptors, and at the same time, directly sense the ambient information without guessing. Thus, animals are able to behave more adaptively by the pickup of ambient information.

2.2 Examples of affordances

We must recognize that we do not perceive environmental properties by units such as meters. Gibson explains examples of affordances as follows[6]:

> If a terrestrial surface is nearly horizontal, nearly flat, and sufficiently extended (relative to the size of the animal) and if its surface is rigid (relative to the weight of the animal), then the surface *affords support.* It is a surface of support, and we call it a substratum, ground, or floor. It is stand-on-able, permitting an upright posture for quadrupeds and bipeds. .... Note that the four properties listed — horizontal, flat, extended, and rigid — would be *physical* properties of a surface if they were measured with the scales and standard units used in physics. As an affordance of support for a species of animal, however, they have to be measured *relative to the animal.* They are unique for that animal. They are not just abstract physical properties. They have unity relative to the posture and behavior of the animal being considered.

Therefore, environmental properties are called "affordances" if and only if they are measured relative to the animal. An affordance leads an animal to act in a certain way.

3 Pickup of ambient information

Animals, through the pickup of ambient information, are able to behave more adaptively than robots, which can sense only sensory inputs. Thus, in a complicated dynamic environment, robots have to search information within an environment by speculative action. If robots can distinguish possible actions from impossible actions with the help of the ambient information, the robots can act more adaptively.

Therefore, copying animals, we propose a framework of a perception-action system for agents that can sense ambient information. In the framework shown in figure 1, an agent measures ambient information relative to the agent by speculative actions. As seen in

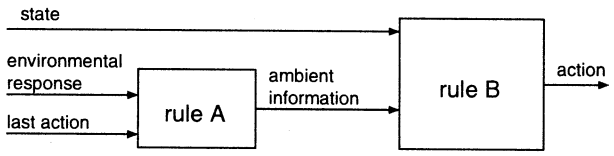


Figure 1: Proposed framework

this figure, "rule A" calculates the ambient information based on both the agent's last action and the environmental response. "Rule B" calculates the agent's next action based on the output of rule A and the state of the agent. Rule A and rule B are learned by a Q-learning method, which is one of reinforcement learning(R.L.).

In this framework, an agent perceives ambient information thanks to the coupling of the agent's action and the environmental response, and acts adaptively. In this way, agent adaptive behaviors are formed.

4 Experiment and result

In this section, we explain and examine the difference between our method and Q-learning with only sensory inputs.

4.1 Experimental environment

In this paper, we examine our framework with a "boat controlling problem", shown in figure 2, where the wind direction changes depending on time. The wind pushes the boat in various directions. If the boat deviates more than distance L away from course, the task is considered a "failure" and finishes one trial.

In our boat problem, an agent controls a boat without a wind sensor, so the agent cannot perceive the wind directly.

In this problem, variables A and T are introduced to represent the wind amplitude and its cycle, respectively.

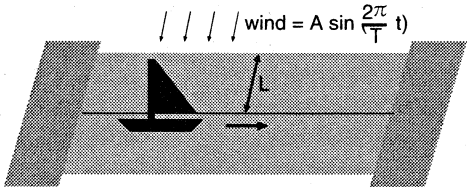


Figure 2: Boat controlling problem

4.2 Q-learning with only sensory inputs

If Q-learning (Q.L.) with only sensory inputs is applied to this problem, we assume that amplitude A and cycle T are constant. First, we measure the two constants, because the Q.L. can only deal with M.D.P. since it constructs the environmental model in its rules.

Therefore, the framework of a perception-action system based on Q.L. with only sensory inputs is shown in figure 3. In this framework, an agent cannot act, and stops after a few steps because the agent action causes noise for measuring A and T. After the measuring process, the agent begins to act and learns how to act. If the wind changes its amplitude or cycle depending on time, we must measure the wind amplitude or cycle again in this framework.

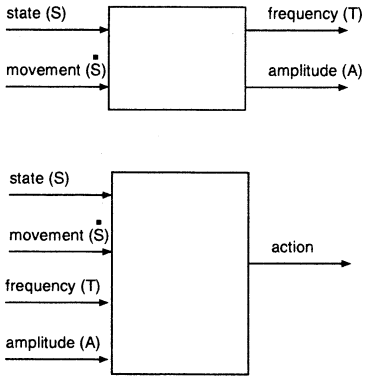


Figure 3: Q-learning with only sensory inputs

4.3 Q-learning with adaptive pickup of ambient information

The framework of the perception-action system based on Q.L. with the adaptive pickup of ambient information is shown in figure 4. In our framework, the perception-action system, which achieve adaptive behaviors in a dynamic environment, has two parts. One is a closed part within the agent that learns the relationship between states and actions. The other is an opened part to its environment that detects the ambient information through speculative actions. Therefore, the agent can perceive the ambient information and can decide the next adaptive action based on that information. Thus, the agent can behave adaptively to its environment, whether or not the environmental properties (wind amplitude and cycle) change.

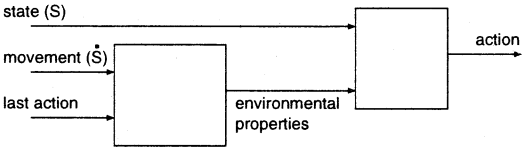


Figure 4: Q-learning with pickup of ambient information

4.4 Experimental result

We show an experimental result in figure 5, where the wind changes its amplitude according to the following equation.

$$A(t+1) = \cos(A(t) + action(t)) \qquad (1)$$

This equation indicates that the wind force and direction is not predictable for the agent. The cycle T is constant. In figure 5, the vertical axis indicates the number of steps divided by T that control the boat within the sailing zone. The horizontal axis indicates the number of trials.

From this figure, we can see that Q.L. with pickup of ambient information controls the boat at around 60 trials. On the other hand, Q.L. with only sensory inputs cannot control the boat during only one controlling time. Therefore, our method enables an agent to form its behavior by the adaptive pickup of ambient information with speculative action and to succeed in controlling in a dynamic environment. In contrast, Q.L. with only sensory inputs cannot enable an agent to adapt to its environment.

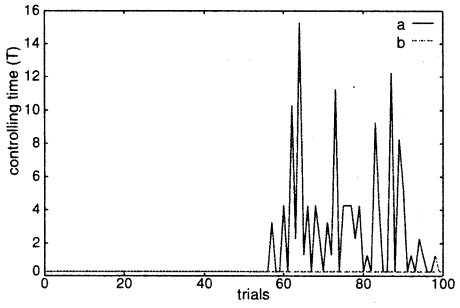


Figure 5: proposed method and only sensory inputs
a: Q.L. with pickup of ambient information
b: Q.L. with only sensory inputs

4.5 Comparison

By Q-learning with only sensory inputs, an agent cannot behave adaptively if the environmental properties such as amplitude and cycle change. On the other hand, the agent with our method perceives the coupling of its speculative action and its environmental response, and, from it, indirectly senses the force and direction of the wind that pushes the boat. Thus, our method enables an agent to perceive the wind without a wind sensor as ambient information and to behave adaptively even in an environment where its properties change.

Hence, the ability to perceive from the coupling of speculative action and its environmental response is very important for an agent to adapt in a dynamic environment where all the necessary sensors cannot be predicted beforehand. By comparing to Q-learning with only sensory inputs, we conclude that the agent can behave adaptively by using our framework.

Therefore, the perception-action system, which constructs an environmental model, has difficulties enabling the agent to behave adaptively in an environment where its properties are different from the constructed one.

5 Conclusion

In this paper, we focused on agent speculative action to search ambient information, introduced an ecological psychological idea to reinforcement learning, and proposed a new framework of reinforcement learning with adaptive pickup of ambient information.

Moreover, we defined "affordance" as environmental properties measured by the agent's body or agent's action, and we assumed that affordances are detected within the ambient information perceived through speculative action. Therefore, we modeled "affordance" as the coupling of agent speculative action and the subsequent environmental response.

By applying the boat controlling experiment, we showed that reinforcement learning with only sensory inputs has difficulty achieving adaptive behavior in a dynamic environment where its properties change. Furthermore, we showed that reinforcement learning with the pickup of ambient information through speculative action enables an agent to

- behave adaptively, and
- indirectly sense environmental change without a direct sensor.

References

[1] Horiuchi, T., Fujino, A., Katai, O., and Sawaragi, T., "Fuzzy Interpolation-Based Q-Learning with Continuous Inputs and Outputs,"(in Japanese), *Trans. of the Society of Instrument and Control Engineers*, Vol. 35, No. 2, pp. 217-279, 1999.

[2] Yamagishi, H., Horiuchi, T., Kawakami, H. and Katai, O., "Q-learning with Condition Reduced Fuzzy Rules and Its Applications,"(in Japanese), *Trans. of the Society of Instrument and Control Engineers*, Vol. 37, No. 12, pp. 1178-1185, 2001.

[3] Sutton, R. S. and Barto, A. G., *Reinforcement Learning: An Introduction*, The MIT Press, 1998.

[4] Watkins, C. and Dayan, P., "Technical Note: Q-learning," *Machine Learning*, Vol. 8, No. 3-4, pp. 279-292,1992.

[5] Gibson, J. J., *The Senses Considered as Perceptual Systems*, Boston: Houghton Mifflin Company, 1966.

[6] Gibson, J. J., *The Ecological Approach to Visual Perception*, Lawrence Erlbaum Associates, 1979.

Proc. of The Ninth Int. Symp. on Artificial Life and Robotics (AROB 9th '04)
Beppu, Oita, Japan, 28-30 January, 2004

Construction and verification of DNA hairpin-based RAM

Naoto Takahashi[1], Atsushi Kameda[2], Masahito Yamamoto[1,2], and Azuma Ohuchi[1,2]

[1] Graduate School of Engineering, Hokkaido University
North 13, West 8, Kita-ku, Sapporo, Hokkaido 060-8628, Japan
Tel : +81-11-716-2111 (ext. 6498), Fax : +81-11-706-7834

[2] CREST, Japan Science and Technology Cooperation (JST)
Honmachi 4-1-8, Kawaguchi, Saitama 332-0012, Japan
Tel : +81-48-226-5601, Fax : +81-48-226-5651

E-Mail : {naoto, kameda, masahito, ohuchi}@dna-comp.org
URL : http://ses3.complex.eng.hokudai.ac.jp/

Abstract

DNA computing is computation utilizing the behavior of DNA. The greatest advantage of DNA computing is the massively parallel nature of processing. Many scientists designed various computation methods and applications utilizing DNA, and DNA memory is one of these. In conventional method, DNA sequences are designed every time we try to solve a different problem, but a RAM utilizing DNA may reduce this overhead. There have been several earlier methods of achieving RAM utilizing DNA. As we thought that there might be a more efficient method of achieving RAM, we designed one utilizing the hairpin structure DNA. We have called it DNA Hairpin-based RAM (DNA-HRAM). Hairpin is the structure of a single-strand DNA that has bonded to itself, and this state is called closed. If one single-strand DNA, that is called opener, is mixed into closed hairpin solution, the hairpin is separated from itself, and this state is called open. By viewing these two states as 1 and 0, we can represent a bit. We explain how to achieve multi-bit DNA-HRAM. In this paper, we constructed the 4-bit DNA-HRAM actually, and verified the behavior. In the future, We would like to apply this DNA-HRAM to aqueous computing.

key words - *DNA computing, aqueous computing, DNA memory, hairpin structure DNA*

1 Introduction

There are some problems belonging classes that have been considered too difficult to solve within a realistic period of time using our present electronic computers, such as the combinatorial optimization problem. In a large scale problem, we have to calculate the enormous numbers of combination, and they increase exponentially. However, our general electronic computers can only process serially. Their processing speed is so fast, nevertheless there is a limit to it.

That trouble may be resolved by biological molecules such as the proteins, RNA, and DNA. In a test tube, chemical reactions of biological molecules occur in parallel. Therefore, if we view these reactions as operations, the test tube can be considered as a very large scale massively parallel computer.

Computation utilizing the behavior of biological molecules is called "molecular computing". As mentioned, the greatest advantage of molecular computing is the massively parallel nature of processing. Molecular computing that utilizes DNA is particularly called "DNA computing". Many scientists from various fields have recently participated in studies of DNA computing because DNA is very easy to handle.

In 1994, Adleman solved an instance of the directed Hamiltonian Path Problem with 7 vertices by utilizing DNA and experimental techniques of molecular biology [1]. This seminal work demonstrated the feasibility of DNA computing and instigated studies of this field.

Many scientists designed various computation methods and applications utilizing DNA after Adleman, and "DNA memory" is one of these. Because DNA molecules are extremely minute, it is possible to achieve a very large scale memory in limited spaces with them. In Adleman's method, DNA sequences were designed every time we tried to solve a different problem. This overhead, however, may be reduced by using Random Access Memory (RAM), because we can widely use same RAM to various problems once we make it. Therefore, we focused on the "DNA RAM".

In this paper, we introduce an application of DNA RAM and propose a method to achieve RAM utilizing the hairpin structure DNA, which we have called DNA Hairpin-based RAM (DNA-HRAM), and then discuss the results of our laboratory experiments.

2 Aqueous computing

Since a DNA RAM exists in a solution, it is easy to split into several processes and is easy to mix them, too. This nature is called "aqueous", and an approach to improve this aqueous nature by computing is "aqueous computing". Aqueous computing is one of the applications that a DNA RAM can be applied to, and the framework of this was suggested by Head [2]. This makes us possible to solve various problems that belong to the class of NP-complete in linear chemical steps. Fig. 1 has an outline of the algorithm for aqueous computing. It is repeated to split the solution, change the bits, and mix them.

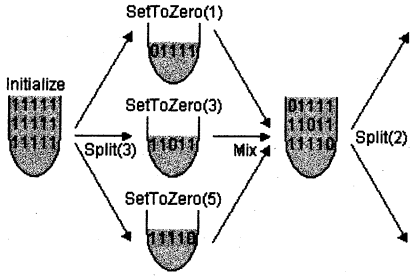


Figure 1: Aqueous algorithm

Aqueous computing is a different approach to Adleman's method that needed to make up the complete set of DNA sequences to search for solutions beforehand, while aqueous computing starts with RAM where all components represent the same bit pattern. This makes it possible to find many solutions during the process of computation, by changing the bit pattern in the RAM. Therefore, aqueous computing does not require optimal DNA sequences to be designed for each given problem. Because designing the sequence can be more difficult than solving the given problem, this is a great advantage.

3 Earlier methods

To achieve DNA RAM, there have been three earlier methods.

The first was the "Cut, Elongate, and Ligate (CEL)" method developed by Head et al. [3]. This method uses several restriction enzymes, polymerase, ligase, and circular double-strand DNA. A restriction enzyme recognizes and cuts DNA only at a particular partial sequence that called "restriction site". Circular double-strand DNA is designed to include several kinds of restriction sites. If we apply a restriction enzyme, circular DNA becomes linear and its both ends become single-strand that called "sticky end". In the next step, polymerase extends DNA and that makes sticky end double-strand. Ligase splices DNA, that called "ligation", and it is used to recircularize the linear strands at last. After recircularizing, this circular DNA does not have an original restriction site. The state that has an restriction site is counted as 1, and the other state that does not is counted as 0. Thus it becomes possible to represent a bit.

The second was the "Cut, Delete, and Ligate (CDL)" method also developed by Head et al. [4]. This method also uses several restriction enzymes, ligase, and circular double-strand DNA, but needs pair of same kind of restriction site to represent a bit. With this, it is possible to use restriction enzymes that make double-strand end, that called "blunt end".

The third was the "Peptide Nucleic Acid (PNA)" method developed by Yamamura et al. [5], which uses single-strand PNA and DNA. PNA is an artificial analogue of DNA, and it can hybridize nucleic acids more strongly than DNA. A reaction, where two single-strand DNA bond to each other and form one double-strand DNA, called "hybridization". The state that PNA has hybridized in a specific segment of a DNA strand is counted as 1, and the other state it has not is counted as 0.

In the first and second methods, to regulate the solution temperature is definitely necessary, because these use enzymes such as restriction enzymes and ligase. In the third method, we can only synthesize short PNA strands, and it is too expensive. As we thought that there might be a more efficient method to achieve RAM, we designed one utilizing the hairpin structure DNA.

4 Hairpin-based methods

"Hairpin" is the structure of a single-strand DNA that has bonded to itself (Fig. 2), and we call this state "closed". Interestingly, the hairpin's bonded stem can be separated by mixing one single-strand. We call this strand "opener", and it is complementary to the hairpin's lead and stem. The opener bonds to the lead

sequence of the hairpin first and then to the stem sequence of the hairpin, as Fig. 3 shows, and we call this state "open". The closed state is counted as 1, and the open state is counted as 0. In this way, we can represent a bit. We can open the hairpin only by mixing the opener. We do not have to regulate the solution temperature because the hairpin reactions occur at room temperature. Additionally, the only materials required for this method are DNA strands.

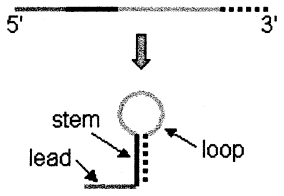


Figure 2: The state of "closed"

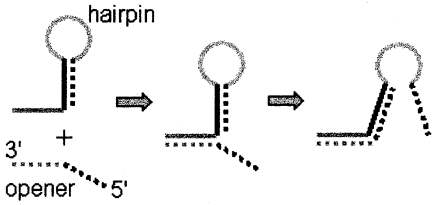


Figure 3: The state of "open"

We explain how to achieve multi-bit DNA-HRAM. In this paper, we constructed the 4-bit DNA-HRAM shown in Fig. 4.

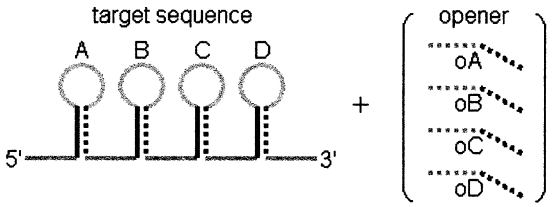


Figure 4: Target sequence

In sequence design step, it is a point to notice that each hairpin is necessary to be opened by its own opener alone. We referred to the recent research by Uejima and Hagiya [6] to resolve this sequence-design problem.

5 Construction

In construction step, because it is very difficult to directly synthesize a long sequence of DNA, we had to decompose the target sequence into several short parts, and then compose the parts by hybridization and ligation. We need to perform "kination" before ligation in fact. Kination is a reaction to phosphorylate the 5'-end of DNA. We tested various ways to decompose the target sequence, and derived that in Fig. 5. These parts hybridize each other at specific stem segments, and are then spliced at the joint, that called the "nick", by ligation.

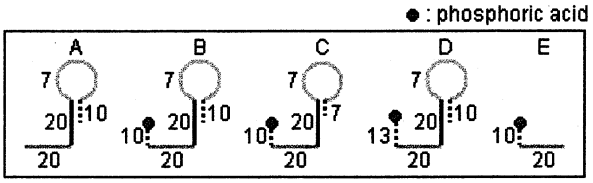


Figure 5: Decomposed parts

To examine whether the target sequence was actually formed, we used PolyAcrylamide Gel Electrophoresis (PAGE). Since DNA becomes negatively charged, it is carried toward the positive electrode. Long sequences are hard to get through the mesh of polyacrylamide gel, while short ones are easy. Thus generally, the distance that a short sequence is carried is longer than that of a long sequence, within a certain period of time. However, this mobility of electrophoresis is changed by not only the length of the sequence, but also the form of it, in fact.

After PAGE, DNA, that stained with chemicals such as Ethidium Bromide and SYBR Gold, visibly appears as a band in the gel.

A+B, the sequence where part A is spliced to part B, has a different length from A and B. Accordingly, the distance A+B is carried is different from that of A and that of B. By the same token, if a new band that is not made up of its parts or its intermediate products appears when several parts are mixed, it can be considered to be a product where all parts are combined. Finally, A+B+C+D+E should have a different band from all the others, and it can be considered to be the product in Fig. 4. The results of this experiment are in Fig. 6, and the completion of the target sequence is indicated by the arrow.

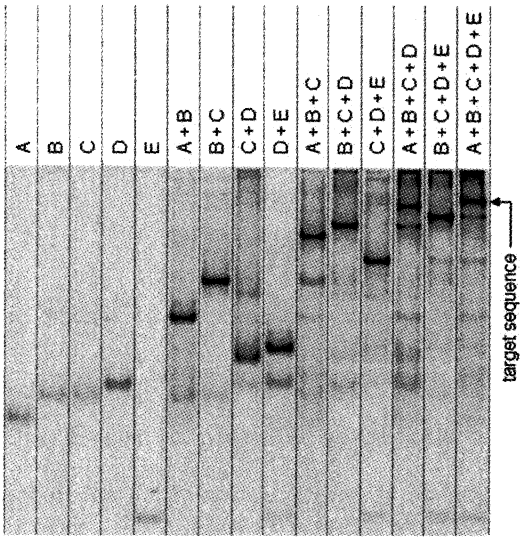


Figure 6: Construction of 4-bit DNA-HRAM

6 Verification

In verification step, we checked whether each bit of this 4-bit DNA-HRAM could be opened independently, and the results are in Fig. 7. Here, we used PAGE again. As remarked above, sequences of different form are carried different distances, even if they have the same length. For example, a state where no openers are mixed, T in Fig. 7, is carried a different distance from a state where opener oA is mixed, T+oA, because each has a different form. By the same token, all 16 states will be carried to different positions. T+oB, T+oC, and T+oD definitely have different band positions. This means that all these four hairpins are able to be opened by their own openers independently. However, the differences between some states are obtuse. To be obvious these differences, we should check with another approach in future experiments.

7 Conclusion

In this paper, we proposed and designed a way to derive a RAM utilizing the hairpin structure DNA, and actually constructed a 4-bit DNA-HRAM. We then checked whether each bit of this 4-bit DNA-HRAM could be opened independently, and verified that all these bits work normally.

In the next step, we will examine whether this

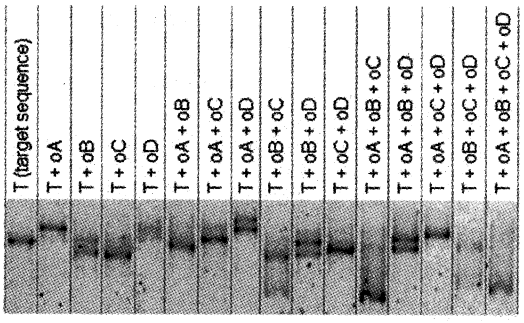


Figure 7: Differentiation of all 16 states

DNA-HRAM works sequentially, because aqueous computing requires the sequential performance of write operation. And then, we plan to apply this DNA-HRAM to aqueous computing. In the future, we would like to try constructing a large-bit DNA-HRAM. We consider that the problem is how to detect the solution of a solved problem and the states of bits. One of our future goals is to contrive a better detection method.

References

[1] L. M. Adleman, "Molecular Computation of Solutions to Combinatorial Problems", *Science*, Vol. 266, pp. 1021-1024, 1994.

[2] T. Head, "Circular Suggestions for DNA Computing", submitted to World Scientific, 1999.

[3] T. Head, M. Yamamura, S. Gal, "Aqueous Computing: Writing on Molecules", *Proceedings of the Congress on Evolutionary Computation*, pp. 1006-1010, 1999.

[4] T. Head, G. Rozenberg, R. S. Bladergroen et al., "Computing with DNA by operating on plasmids", *BioSystems*, Vol. 57, pp. 87-93, 2000.

[5] M. Yamamura, Y. Hiroto, T. Matoba, "Another Realization of Aqueous Computing with Peptide Nucleic Acid", *Proceedings of 7th International Workshop on DNA-Based Computers (DNA7)*, LNCS 2340, pp. 213-222, 2002.

[6] H. Uejima, M. Hagiya, "Secondary Structure Design of Multi-state DNA Machine Based on Sequential Structure Transitions", *Preliminary Proceedings of Ninth International Meeting on DNA Based Computers (DNA9)*, pp. 80-91, 2003.

Proc. of The Ninth Int. Symp. on Artificial Life and Robotics (AROB 9th '04)
Beppu, Oita, Japan, 28-30 January, 2004

The artificial muscle and its application in robot

Masanori Sugisaka, Huailin Zhao, Norrima Mokhtar

Department of Electrical and Electronic Engineering

Oita University, 700 Dannoharu, Oita 870-1192, Japan

Email: msgi@cc.oita-u.ac.jp, zhl@cc.oita-u.ac.jp, norrima@miosh.net

Abstract

The traditional robot uses motors, gears, hydraulics and other expensive, heavy, power-hungry parts to produce motion, which is often too bulky and heavy for smaller-scale applications. After decades some new kinds of artificial equivalent of muscle-artificial muscles-have been sought. The robot made of artificial muscles is quite different from the traditional one. The artificial muscle can give the robot animal-like flexibility and manipulation ability. In this paper a few kinds of artificial muscles are introduced. Some applications of the artificial muscle are given. The use in robot is emphasized.

1. Introduction

For decades, people have been dreaming and developing human-like robots. The robot made of artificial muscle and artificial skin looks more like human, while the traditional robot looks more like a machine. By now artificial muscles have made it possible. After a long time seeking, scientists and engineers who build actuators, or motion-generating devices, have sought an artificial equivalent of muscle, which grows or shrinks significantly in length or volume when subjected to some stimulation. Such substances could serve as the drivers for novel motion-generating devices-possible replacements for the ubiquitous electric motor, which is often too bulky and heavy for some applications.

Simply by changing their length in response to nerve stimulation, muscles can exert controlled amounts of force sufficient to blink an eyelid or hoist a barbell. Muscles also exhibit the property of scale invariance: their mechanism works equally efficiently at all sizes, which is why fundamentally the same muscle tissue powers both insects and elephants[1]. The artificial muscle might therefore be useful in driving devices to produce motion. The robot made of artificial muscles will give robots some new important advantages such as animal-like flexibility and manipulation ability and so on.

2. Artificial muscle

There are different kinds of artificial muscles that have been developing in the world. Their functions and strength are more and more close to human' s.

One of them, which made of inflatable rubber and flexible metal mesh, can behave somewhat like real muscle when gas pressure is applied to it.

This artificial muscle consists of an inflatable rubber tube surrounded by a flexible metal mesh connected at each end of the tube. When the tube inflates, the mesh bulges, which in turn pulls each end in and shortens the artificial muscle.

For instance, a suit made of the artificial muscle could be used to help a frail person. Because the suit covered in pairs of inflatable "muscles" could assist the wearer's real muscles. When they inflate, they help the wearer to move their limbs with greater strength and stability. A pair of these tubes connected between the elbow and shoulder joints of the suit would boost tire power of a frail person's biceps and triceps. The power comes from compressed air, stored in a series of small canisters distributed in the suit, or, if the user is strong enough, in a single tank carried on their back. Pressure sensors all over the suit would tell the artificial muscles when to kick in. Now the suit called Lycra suit is being developed at Science University of Tokyo[2][3]. It is expected to take the place of the Zimmer frame to help patients or weak people.

Another kind of artificial muscle is made of electroactive polymers, which can contracts or extends or bends when electrical voltage is applied to it[4][5].

American Jet Propulsion Laboratory has made two different types of artificial muscle[4].

The first works as the muscle in a robotic hand. The muscle is a flexible polymer ribbon constructed from chains of carbon, fluorine, and oxygen molecules. When an electric charge is applied to one side of the ribbon, charged particles in the polymer get pushed to the far side. The side with more particles lengthens, while the other side shortens. The net result: the ribbon bends. By using four such ribbons, a gripper has been fashioned into what can pick up a rock.

The other type of polymer muscle consists of thin sheets wrapped into a cigarlike cylinder. These polymers stretch when one side of a sheet is given a positive charge and the other a negative. These charges cause each wrapped sheet to contract toward the center of the cylinder, and this constriction forces the cylinder to expand lengthwise. When the power supply is off, the rope relaxes. These polymers can push, pull, and lift loads.

The third kind of artificial muscle is made of shape memory materials, such as shape memory alloy and shape memory resin and so on,

which can behave somewhat like human muscles. Some of them have been tried to put into applications[6]. Shape memory alloys are metals used for jobs that need smooth, even motion, rather than brute strength. They are slow changing but rugged. Some of them have been used to make robot arms[7] or micromanipulators[8].

Because the artificial muscle usually uses the materials such as polymers, interior-empty rubber tubes, and so on, the actuator made of it will has special advantages over the traditional one:

It is softness about the same as muscles.

It is much lighter.

Sound is not generated at the time of a drive.

Small and light drive devices are available.

A motion like a living thing is possible.

Power consumption is expected to be less.

3. Applications in robot

On whole the artificial muscle is in research and development at present. There haven't been many practical applications. But the future is very promising. People have imagined that an artificial muscle arm would be able to win a real human's one. Artificial muscles may someday upstage the world heavyweights of wrestling in a championship arm-wrestling match. Look at the photo 1.

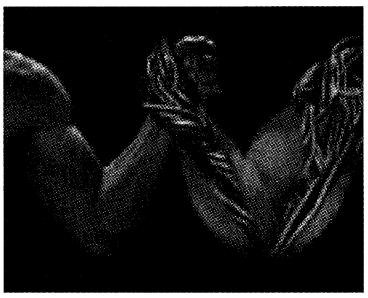


photo 1[9]

One of the applications is the artificial muscle hand made of electroactive polymers. It is being developed at Jet Propulsion Laboratory, America. Look at the photo 2. The electroactive polymer materials can potentially provide actuation with animal-like response and more flexible configurations. With this technology developing, new mechanisms that are biologically inspired are expected to emerge.

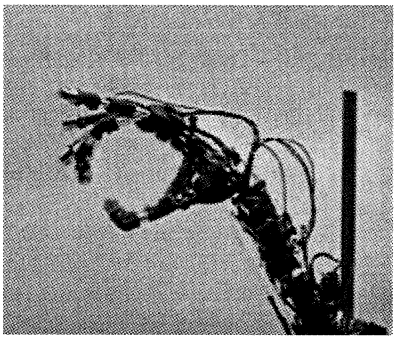


photo 2[10]

Another recent development is the first commercial product-the artificial fish. It is a fish robot which's fin is drove by the polymer actuator. Look at photo 3. It was produced by EAMEX corporation, Japan[11]. This progress is said as an important milestone for the field of

electroactive polymers.

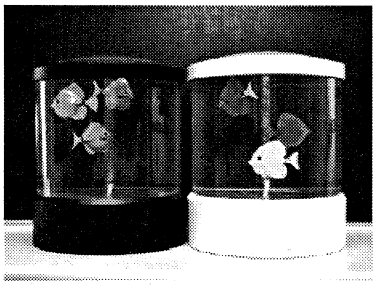


Photo 3[12]

4. Conclusion

Based on the special advantages with the artificial muscle, its technology will has great chance to revolutionize the field of mechanical actuation. It is sure that the artificial muscle will be used in applications relating to industrial, medical, and domestic problems.

The robot made of artificial muscles will have animal-like flexibility and manipulation ability. It will feel more like an animal or human. And it will be much lighter and can save more energy. Someday it may become the real "superman" imagined in fictions. Of course the artificial muscle robot can be used in different fields such as industry, safe guard, social welfare, household assisting, and so on. The time of artificial muscle robots is coming.

Reference

[1] Ashley, Steven, "Artificial Muscles", Scientific American, Oct.2003, Vol. 289, Issue 4

[2] Graham-Rowe, Duncan, "Power Dressing", New Scientist, 5/25/2002, Vol. 174, Issue 2344

[3] http://www.accessibility.com.au/news/health/muscles.htm

[4] "Bendbots", Discover, Aug98, Vol. 19, Issue 8

[5] Graham-Rowe, Duncan, "Minibeast Muscles in on Robot Limbs", New Scientist, 7/6/2002, Vol. 175, Issue 2350

[6] Saunders, Fenella, "Building a better muscle", Discover, Feb2002, Vol. 23 Issue 2, p15

[7] Laurentis, Kathryn J.De; Mavroidis, Constantinos, "Mechanical design of a shape memory alloy actuated prosthetic hand", Technology & Health Care, 2002, Vol. 10 Issue 2, p91, 16p

[8] Johnson, Dan, "bridges with brains, airplanes with feelings", Futurist, Sep/Oct97, Vol. 31 Issue 5, p6

[9] http://www.jpl.nasa.gov/technology/features/images/artificialmuscle_browse.jpg

[10] http://www.jpl.nasa.gov/events/lectures/feb02.html

[11] http://www.eamex.co.jp/index_e.html

[12] http://ndeaa.jpl.nasa.gov/nasa-nde/lommas/eap/EAP-web.htm

Proc. of The Ninth Int. Symp. on Artificial Life and Robotics (AROB 9th '04)
Beppu, Oita, Japan, 28-30 January, 2004

Application of Uncertain Variables to Learning Process in Knowledge-Based Decision Systems*

Z.Bubnicki
Institute of Control and Systems Engineering, Wroclaw University of Technology
Wyb. Wyspianskiego 27, 50-370 Wroclaw, POLAND
e-mail: zdzislaw.bubnicki@pwr.wroc.pl

Abstract

The paper is concerned with a class of intelligent decision systems described by a relational knowledge representation with unknown parameters. The main idea consists in the combination of two approaches: application of uncertain variables and a learning process with *step by step* knowledge updating. The recursive decision algorithm with a modification of a current expert's knowledge at each step is presented. An example and a result of simulations illustrate the presented approach.

Keywords: uncertain variables, uncertain systems, learning systems, knowledge-based systems, decision making, intelligent systems

1 Introduction

The paper is concerned with a class of intelligent uncertain systems described by a relational knowledge representation with unknown parameters. For decision making in such systems two different approaches have been proposed and developed:
1. The application of uncertain variables described by certainty distributions given by an expert [1, 2, 3].
2. The application of a learning process consisting in *step by step* knowledge validation and updating [4, 5, 6, 7].

The purpose of this paper is to present a new idea based on the combination of these two approaches. At each step of the learning process an expert's knowledge is modified according to the current result of the learning. The uncertain variable is described by a certainty distribution given by an expert and characterizing his/her opinion on approximate values of the variable. A short description of the uncertain variables and a basic decision problem are presented in Sec. 2. The details may be found in [2, 3, 7]. Section 3 presents an idea of the learning process without the additional expert's knowledge. The details are described in [5, 7]. Sections 4 and 5 present the main concept of the paper.

2 Uncertain variables and decision problem

In the definition of the uncertain variable $\bar{x}$ we consider two soft properties (i.e. such properties $\varphi(x)$ that for the fixed x the logic value $v[\varphi(x)] \in [0,1]$): "$\bar{x} \cong x$" which means "$\bar{x}$ is approximately equal to x" or "x is the approximate value of $\bar{x}$", and "$\bar{x} \,\tilde{\in}\, D_x$" which means "$\bar{x}$ approximately belongs to the set D_x" or "the approximate value of $\bar{x}$ belongs to D_x". The *uncertain variable* $\bar{x}$ is defined by a set of values X (real number vector space), the function $h(x) = v(\bar{x} \cong x)$ (i.e. the certainty index that $\bar{x} \cong x$, given by an expert) and the following definitions for $D_x, D_1, D_2 \subseteq X$:

$$v(\bar{x} \,\tilde{\in}\, D_x) = \max_{x \in D_x} h(x),$$

$$v(\bar{x} \,\tilde{\notin}\, D_x) = 1 - v(\bar{x} \,\tilde{\in}\, D_x),$$

$$v(\bar{x} \,\tilde{\in}\, D_1 \vee \bar{x} \,\tilde{\in}\, D_2) = \max\{v(\bar{x} \,\tilde{\in}\, D_1), v(\bar{x} \,\tilde{\in}\, D_2)\},$$

$$v(\bar{x} \,\tilde{\in}\, D_1 \wedge \bar{x} \,\tilde{\in}\, D_2) = \min\{v(\bar{x} \,\tilde{\in}\, D_1),\ v(\bar{x} \,\tilde{\in}\, D_2)\}.$$

The function $h(x)$ is called a *certainty distribution.*

C-uncertain variable $\bar{x}$ is defined by the set of values X, the function $h(x) = v(\bar{x} \cong x)$ given by an expert, and the following definition:

$$v_c(\bar{x} \,\tilde{\in}\, D_x) = \frac{1}{2}[v(\bar{x} \,\tilde{\in}\, D_x) + 1 - v(\bar{x} \,\tilde{\in}\, X - D_x)]. \quad (1)$$

Let us consider a static plant with the input vector $u \in U$ and the output vector $y \in Y$, described by a relation $R(u, y; x) \subset U \times Y$ where the vector of unknown parameters $x \in X$ is assumed to be a value of an uncertain variable described by the certainty distribution $h(x)$ given by an expert. If the relation R is not a function then the value u determines a set of possible outputs

$$D_y(u; x) = \{y \in Y : (u, y) \in R(u, y; x)\}. \quad (2)$$

For the requirement $y \in D_y \subset Y$ given by a user, we can formulate the following **decision problem**: For the given $R(u, y; x)$, $h(x)$ and D_y one should find the decision

* This work was supported by the Polish State Committee for Scientific Research under Grant No. 4 T11C 001 22

u^* maximizing the certainty index that the set of possible outputs (2) approximately belongs to D_y (i.e. belongs to D_y for an approximate value of $\bar{x}$). Then

$$u^* = \arg\max_{u\in U} v[D_y(u;\bar{x}) \tilde{\subseteq} D_y] = \arg \max_{u\in U} \max_{x\in D_x(u)} h(x) \tag{3}$$

where $D_x(u) = \{x \in X : D_y(u;x) \subseteq D_y\}$.

3 Learning process

Assume now that the parameter x in the relation R has the value $x = a$ and a is unknown. Then, for the fixed value u it is not known if u is a correct decision, i.e. if $u \in D_u(a)$ and consequently $y \in D_y$. Our problem may be considered as a classification problem with two classes. The point u should be classified to class $j = 1$ if $u \in D_u(a)$ and to class $j = 2$ if $u \notin D_u(a)$. Assume that we can use the learning sequence $(u_1, j_1), (u_2, j_2), \ldots, (u_n, j_n) \stackrel{\Delta}{=} S_n$ where $j_i \in \{1, 2\}$ are the results of the correct classification given by an external trainer.

Let us denote by $\bar{u}_i$ the subsequence for which $j_i = 1$, i.e. $\bar{u}_i \in D_u(a)$ and by $\hat{u}_i$ the subsequence for which $j_i = 2$, and introduce the following sets in X:

$$\bar{D}_x(n) = \{x \in X : \bar{u}_i \in D_u(x) \text{ for every } \bar{u}_i \text{ in } S_n\}, \tag{4}$$

$$\hat{D}_x(n) = \{x \in X : \hat{u}_i \in U - D_u(x) \text{ for every } \hat{u}_i \text{ in } S_n\}. \tag{5}$$

The set

$$\bar{D}_x(n) \cap \hat{D}_x(n) \stackrel{\Delta}{=} \Delta_x(n)$$

may be proposed as the estimation of a. For example, if $D_u(a)$ is described by the inequality $u^{\mathrm{T}}u \le a$ then

$$\bar{D}_x(n) = [x_{\min,n}, \infty), \qquad \hat{D}_x(n) = [0, x_{\max,n}),$$

$$\Delta_x(n) = [x_{\min,n}, x_{\max,n})$$

where

$$x_{\min,n} = \max_i \bar{u}_i^{\mathrm{T}}\bar{u}_i, \qquad x_{\max,n} = \min_i \hat{u}_i^{\mathrm{T}}\hat{u}_i.$$

The determination of $\Delta_x(n)$ may be presented in the form of the following recursive algorithm:

If $j_n = 1$ ($u_n = \bar{u}_n$).

1. **Knowledge validation** for $\bar{u}_n$. Prove if

$$\bigwedge_{x\in\bar{D}_x(n-1)} [u_n \in D_u(x)].$$

If yes then $\bar{D}_x(n) = \bar{D}_x(n-1)$. If not then one should determine the new $\bar{D}_x(n)$, i.e. update the knowledge.

2. **Knowledge updating** for $\bar{u}_n$

$$\bar{D}_x(n) = \{x \in \bar{D}_x(n-1) : u_n \in D_u(x)\}.$$

Put $\hat{D}_x(n) = \hat{D}_x(n-1)$.

If $j_n = 2$ ($u_n = \hat{u}_n$).

3. **Knowledge validation** for $\hat{u}_n$. Prove if

$$\bigwedge_{x\in\hat{D}_x(n-1)} [u_n \in U - D_u(x)].$$

If yes then $\hat{D}_x(n) = \hat{D}_x(n-1)$. If not then one should determine the new $\hat{D}_x(n)$, i.e. update the knowledge.

4. **Knowledge updating** for $\hat{u}_n$

$$\hat{D}_x(n) = \{x \in \hat{D}_x(n-1) : u_n \in U - D_u(x)\}.$$

Put $\bar{D}_x(n) = \bar{D}_x(n-1)$ and $\Delta_x(n) = \bar{D}_x(n) \cap \hat{D}_x(n)$.

The successive estimation of a may be performed in a closed-loop learning system where u_i is the sequence of the decisions. The decision making algorithm is as follows:

1. Put u_n at the input of the plant and introduce y_n.
2. Determine $\Delta_x(n)$ using the estimation algorithm with knowledge validation and updating.
3. Choose randomly x_n from $\Delta_x(n)$, put x_n into $D_u(x)$ and choose randomly u_{n+1} from $D_u(x_n)$.

4 Learning system based on current expert's knowledge

At the n-th step, the result of the learning process in the form of a set $\Delta_x(n)$ may be used to present an expert's knowledge in the form of a certainty distribution $h_n(x)$ such that $h_n(x) = 0$ for every $x \notin \Delta_x(n)$. Thus, the expert formulates his / her current knowledge, using his / her experience and the current result of the learning process based on the knowledge of the external trainer. In particular, $h_n(x) = h(x, b_n)$, i.e. the form of the certainty distribution is fixed, but the parameter b_n (in general, b_n is a vector of parameters) is currently adjusted. For example, if in one-dimensional case $\Delta_x(n) = [x_{\min,n}, x_{\max,n})$ and $h_n(x) = h(x, x_n^*, d_n)$ has a triangular form presented in Fig. 1, then $b_n = (x_n^*, d_n)$ and

$$x_n^* = \frac{x_{\min,n} + x_{\max,n}}{2}, \quad d_n = \frac{x_{\max,n} - x_{\min,n}}{2}. \quad (6)$$

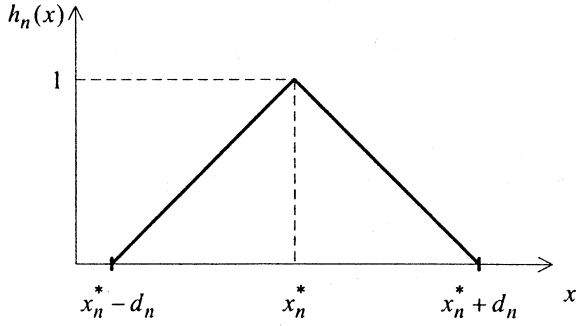


Fig. 1

For $h_n(x)$ the next decision u_{n+1} may be determined in the way presented in Sec. 2, i.e.

$$u_{n+1} = \arg\max_{u \in U} v_n(u) \quad (7)$$

where

$$v_n(u) = v[u \,\tilde{\in}\, D_u(\bar{x})] = v[\bar{x} \,\tilde{\in}\, D_x(u)] = \max_{x \in D_x(u)} h_n(x), \quad (8)$$

and $D_x(u) = \{x \in X : u \in D_u(x)\}$. In general, as a result of the maximization (7) one may obtain a set of decisions $D_{u,n+1}$. For $h(x, b_n)$ we obtain the fixed form of the function $v(u, b_n)$:

$$v_n(u) = \max_{x \in D_x(u)} h(x, b_n) \triangleq v(u, b_n)$$

and consequently, the fixed form of the final result, i.e. one decision $u_{n+1} = u(b_n)$ or the set of decisions $D_{u,n+1} = D_u(b_n)$. The same approach may be presented in the case of C-uncertain variables, with v_c instead of v.

The block scheme of the learning decision making system under consideration is presented in Fig. 2 where G is a generator of random variables for the random choosing of u_{n+1} from $D_{u,n+1}$. The blocks in the figure illustrate parts of the computer decision system or parts of the program which may be used for the computer simulations. The following remark is important for the evaluation of the presented approach: If for every $u_{n+1} \in D_{u,n+1}$ it is not necessary to update the knowledge (i.e. $\Delta_x(n+1) = \Delta_x(n)$), then for $m \geq n+1$ the set $D_u(m) = D_u(n+1) \triangleq D_u = \text{const}$. On the other hand, the set D_u may be much smaller than the set of all correct decisions $D_u(a)$ where $x = a$ is a real but unknown value of x. This property may be considered as a disadvantage of the presented approach.

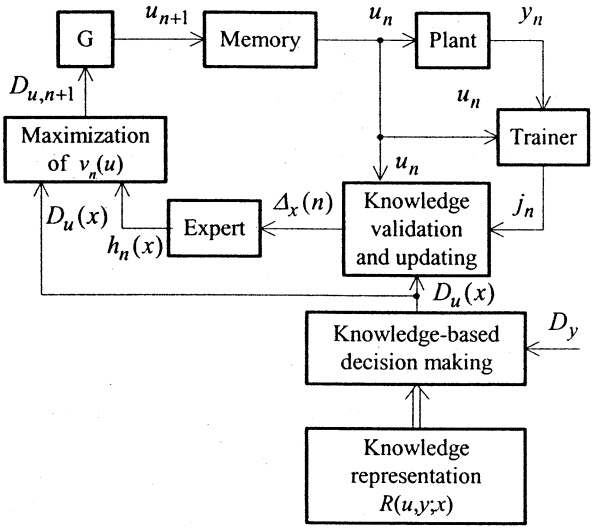


Fig. 2

5 Example

Consider a decision plant with the input vector $\tilde{u}$, one-dimensional output y and one-dimensional unknown parameter x, described by a relation

$$y \leq (\tilde{u}^{\mathrm{T}} \tilde{u}) x^{-1}, \quad x > 0.$$

The components $u^{(l)}$ of u may denote some features of a raw material in a manufacturing process, which may be chosen as decisions, and y may denote a cost of the process. For the requirement $y \leq \bar{y}^2$ we obtain the set $D_u(x)$ described by inequality

$$u^{\mathrm{T}} u \leq x \quad (9)$$

where $u^{(l)} = \tilde{u}^{(l)} \cdot (\bar{y})^{-1}$. In this case, according to (4) and (5)

$$\bar{D}_x(n) = [x_{\min,n}, \infty), \quad \hat{D}_x(n) = [0, x_{\max,n}),$$

$$\Delta_x(n) = [x_{\min,n}, x_{\max,n})$$

where

$$x_{\min,n} = \max_i \bar{u}_i^{\mathrm{T}} \bar{u}_i, \quad x_{\max,n} = \min_i \hat{u}_i^{\mathrm{T}} \hat{u}_i.$$

The estimation algorithm with the knowledge validation and updating is then as follows:

1. Put u_n at the input and introduce j_n.
2. For $j_n = 1 \quad (u_n = \bar{u}_n)$, prove if

$$u_n^{\mathrm{T}} u_n \leq x_{\min,n-1}.$$

If yes then $x_{\min,n} = x_{\min,n-1}$. If not $x_{\min,n} = u_n^{\mathrm{T}} u_n$.

Put $x_{\max,n} = x_{\max,n-1}$.

3. For $j_n = 2 \quad (u_n = \hat{u}_n)$, prove if

$$u_n^{\mathrm{T}} u_n \geq x_{\max,n-1} .$$

If yes then $x_{\max,n} = x_{\max,n-1}$. If not $x_{\max,n} = u_n^{\mathrm{T}} u_n$.

Put $x_{\min,n} = x_{\min,n-1}$, $\Delta_x(n) = [x_{\min,n}, x_{\max,n})$.

Let us assume that $h_n(x)$ has a triangular form presented in Fig. 1 where x_n^* and d_n are determined by (6). Using (8) it is easy to obtain the certainty index that u "approximately" belongs to the set $D_u(x)$ determined by (9): $\nu_n(\alpha) = 1$ for $\alpha \leq x_n^*$, $\nu_n(\alpha) = -d_n^{-1}(d_n - x_n^*) + 1$ for $x_n^* \leq \alpha \leq x_n^* + d_n$, $\nu_n(\alpha) = 0$ for $\alpha \geq x_n^* + d_n$ where $\alpha = u^{\mathrm{T}} u$. Then

$$D_{u,n+1} = \{u_{n+1} \in U : u_{n+1}^{\mathrm{T}} u_{n+1} \leq x_n^*\} \qquad (10)$$

and for every u_{n+1} from this set $\nu_n(u_{n+1}) = 1$. Consequently, the decision making algorithm in the learning system is the following:

1. Put u_n at the input and introduce j_n.
2. Determine $x_{\min,n}$ and $x_{\max,n}$ using the estimation algorithm with the knowledge validation and updating.
3. Choose randomly u_{n+1} from the set (10).

Assume that in (9) $x = a$, i.e. a is the unknown value of x. From (10) it is easy to note that x_n^* may be considered as an estimation of a. Under some conditions, in the same way as that in [5], it may be proved that x_n^* converges to a with probability 1. Figure 3 presents the result of simulations for the following data: $a = 5$, $\alpha_0 = u_0^{\mathrm{T}} u_0 = 20$, $\alpha_{n+1} = u_{n+1}^{\mathrm{T}} u_{n+1}$ is chosen randomly from the interval $[0, x_n^*]$ with the rectangular probability density.

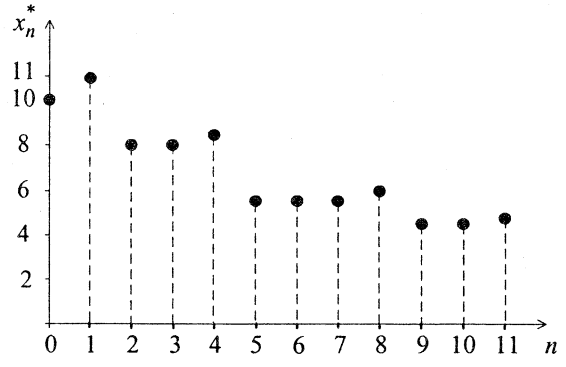


Fig. 3

6 Conclusions

For a class of systems under consideration, at each step of the learning process it is possible to use the current expert's knowledge based on uncertain variables. Numerical examples and simulations show that the using of the expert's knowledge during the learning process may improve the quality of the decisions. The presented approach may be extended to other cases of uncertain systems, for which the application of uncertain variables and the learning algorithms were elaborated separately, especially for complex systems with a distributed knowledge, complexes of operations and for the control of a load distribution in computer systems (see [6, 8, 9, 7, 10]).

References

[1] Bubnicki Z (2001), Uncertain variables and their applications for a class of uncertain systems. International Journal of Systems Science, 32:651–659

[2] Bubnicki Z (2002), Uncertain variables and their application to decision making. IEEE Trans. on SMC, Part A: Systems and Humans, 31:587–596

[3] Bubnicki Z (2002), Uncertain Logics, Variables and Systems. Springer-Verlag, Berlin, London

[4] Bubnicki Z (1999), Uncertain variables and learning algorithms in knowledge-based control systems. Artificial Life and Robotics, 3:155–159

[5] Bubnicki Z (2000), Learning processes in a class of knowledge-based systems. Kybernetes, 29:1016–1028

[6] Bubnicki Z (2000), Knowledge validation and updating in a class of uncertain distributed knowledge systems. In: Proc. of 16th IFIP World Computer Congress. Intelligent Information Processing. Publishing House of Electronics Industry, Beijing, pp 516–523

[7] Bubnicki Z (2004), Analysis and Decision Making in Uncertain Systems, London, Berlin, N. York, Springer-Verlag

[8] Bubnicki Z (2002), Application of uncertain variables to decision making in a class of distributed computer systems. In: Proc. of 17th IFIP World Computer Congress. Intelligent Information Processing, Kluwer Academic Publishers, Montreal, pp. 261–264

[9] Bubnicki Z (2003), Application of uncertain variables and learning algorithm to task allocation in multiprocessor systems. In: Proc. of the 8th International Symposium on Artificial Life and Robotics, Vol. 1, Oita, Japan, pp. I–19 – I–22

[10] Bubnicki Z (2003), Application of uncertain variables to task and resource distribution in complex computer systems. In: Computer Aided Systems Theory - EUROCAST 2003. Lecture Notes in Computer Science. Springer-Verlag, Berlin-Heidelberg, pp. 38-49

Proc. of The Ninth Int. Symp. on Artificial Life and Robotics (AROB 9th '04)
Beppu, Oita, Japan, 28-30 January, 2004

Artificial Knowledge System consisted of impulse response to change for timing representation

Yoshihiro Amemiya and Yasuo Yonezawa*
Complex Adaptive system Laboratory, Division of System Engineering
Graduate school of Science and Engineering, Ibaraki University
4-12-1, Nakanarusawa, Hitachi, Ibaraki, 316-8511, Japan.

Keywords: Reversible connection network, Timing representation, Pattern recognition, Artificial brain

Abstract

At previous research work, we are already reported about interconnectional network with reversible potential of neuron by impulse responses [1]. In this paper, the artificial brain [2] [3] model based on interconnectional network with variable impulse responses by connection of neuron-synapse is described. The presented model is referred the structure and function of natural brain, we designed neuron network model depending mutually that consists of nonlinear oscillators obtaining different frequencies and that can produce stable activation patterns by timing propagating an impulse and learning with channels of synapse at the time of impulse propagation. Also, our presented model is tested with pattern recognition of several symbols and words. Both potentiality of function of associate memory and memory recall at similar and modified symbols and words is indicated by a result of simulation of this model (2D). These tests are carried out the pattern matching by comparing between the matching of activation pattern in case of learning and judgment. The learning of model is given to produce distinctive activation pattern of network pathway that correspond to each symbols and words. Memory recall tests are performed with comparison of activation pattern generated by unknown data, learning modified data and learning data [4].

1 introduction

Neural networks by the computer scientist [5], control engineer or systems engineer is constituted by ignition frequency representation (rate coding), McCulloch-Pitts neuron and the others. As a premise, information releases depend on propagation of spike to obey a law of "All or Nothing". Moreover, spikes frequency of a sensory nerve increases according to strength of physical stimulation. In ignition frequency, frequency of nervous system [6] spikes focuses their attention on the cost that they averaged by arbitrary range in time and space. Then, they do not discuss by a problem of timing of milli-second order of each propagating spikes. However, when we thought about natural brain, from it not being thought that transmission of information between neuron is done by constant speed, we are very interested about a hypothesis that abundant information is expressed in a subtle timing caused by ignition of impulse in natural brain [7]. For example, as a research on the basis of a hypothesis that a timing of impulse expresses information in a brain, there is a report that ignition of the spike with the sufficient accuracy of the time correlation below mill-second at the interval of several hundred mill-second [8].

Real neurons have a cell body, to which are attached dendrites with received input from the terminals of other neurons. From the cell body projects the axon, which is very long in some cases, and, at the end of the axon, the cell branches out to a number of terminals, which then established contact with, and send impulses on to, the dendrites of other neurons. When we thought about a timing of spikes in natural brain, time for the impulse that is brain information to propagate between neuron is important. As for the speed that information propagates between neuron, it is known that it is decided by sensitivity of receptors of reception side and quantity of release of a neurotransmitter of transmission side in synaptic connected site. The information that arrived as an electric signal on the end of an axon in the neuron inside is discharged as a chemical neurotransmitter from the end of synapse chain, it is combined with receptors of postsynaptic

*To whom correspondence should be address;
FAX: 81-294-38-5208, E-mail: yonezawa@mx.ibaraki.ac.jp

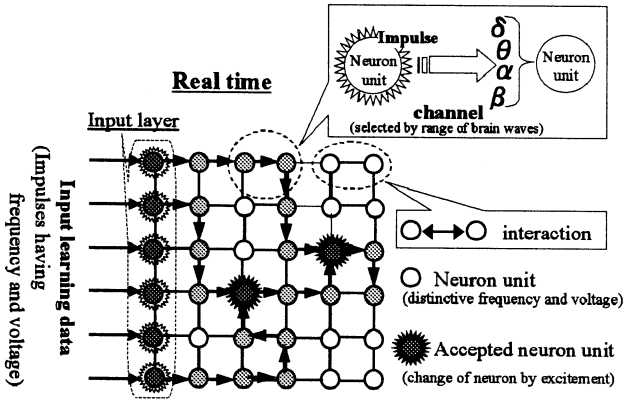


Figure 1: Outline of neuron network. Each neuron is connected by the model of synapse channel. The impulse carries out dynamic change by the synapse channel.

cell, and ion channels produces difference depolarization, and information as electricity signal reaches to the next neuron [9]. In other words, when we thought about information in a brain as timing of transmission, we think that simulation of timing representation (temporal coding) to intend for the entire neuron network by turning a system of the synapse channel into a model becomes possible. Moreover, synapse channel is related to learning to be essential to information processing of a brain high function. Recently, plasticity of the synapse that depended on a change of time gap in a milli-second level of spikes is suggested, timing is watched with interest at learning [10] [11].
In this research, we proposed the construction of artificial brain similar at action of natural brain information's for purpose of timing representation.

2 Materials and methods

2.1 Neuron network model for timing representation

An interdependence type neuron network to produce activated pattern corresponding to the input is a basis a neuron network of this research (Fig.1). A neuron unit in the network consists of a non-linear oscillator obtaining different frequency. A neuron unit has property of oscillator; an excited unit transmits impulse near a unit whose frequency is selected to frequency of the impulse.

In case of some impulses are simultaneously transmitted to one neuron, the properties of unit and impulse are changed by range of brain waves lenght (Table.1).

Table 1: Range of output voltages of impulse depended on exeited unit's frequency

excited neuron unit's frequency	decoded voltage of impulse
15.0 ~ 24.0	5.0 ~ 20.0
7.0 ~ 15.0	20.0 ~ 50.0
4.0 ~ 7.0	50.0 ~ 70.0
0.3 ~ 4.0	35.0 ~ 65.0



Figure 2: chemical propagation process in a synapse.

This neuron network expresses information in a brain by propagation of impulse between neurons. Therefore we design the model of synapse channel, which had plasticity to change by a characteristic of impulse in case of impulse propagation, and it generates an impulse to dynamical behavior into by setting impulse propagation speed. In this model, impulse transmitted speed is a chemical propagation process in a synapse. The concentration of a neurotransmitter depends on the voltage of impulse. Ion channel opens because the receptors receive a neurotransmitter, and ion is transported so that there is an ion concentration difference in a nerve cell When an ion concentration difference reaches a specified cost, the impulse reaches by depolarization. The neurotransmitter is modified by several varieties enzyme.

The model of synapse propagation process that simplified the above leads the next equation (Fig.2).

$$I(t) = \frac{k_{+1}k_{+2}RA_o}{k_{-1}+k_{+2}}\{t + \frac{1}{k_{-1}k_{+2}}(e^{-(k_{-1}+k_{+2})t} - 1)\}$$

In this model, since an impulse with early arrival is chosen when impulses collide, propagation time of impulse to change is important. The synapse channel is selected by range of brain waves length, and threshold for depolarization is set to each channel. Threshold of a channel is divided into short-term memory to decrease or memory elimination to increase of reversible by frequency of propagation. Additionally, when propagation was done by high frequency continuously, structure of a channel changes as long-term

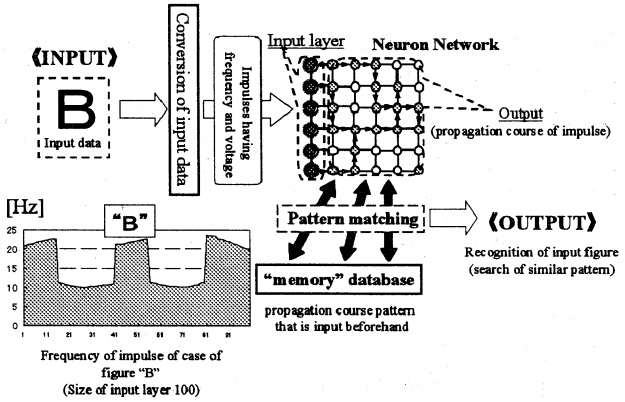


Figure 3: Outline of Artificial Knowledge system. The system consists of "Conversion of input", "Neuron network", "Memory database", and "Remembrance process".

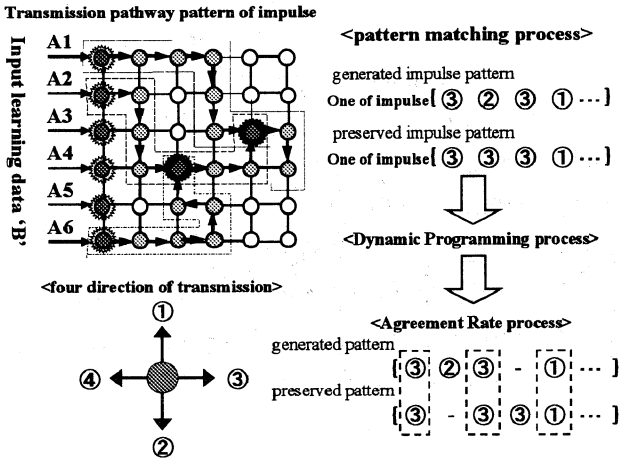


Figure 4: Pattern of transmission pathway of impulse as an output, example of comparison of activation pattern generated by input data 'B'

memory of irreversibility. In this case, long-term memory influences a selection of propagation direction of impulse. Structure of the neuron network which depended on input information is formed by memory and learning in plasticity of a synapse.

2.2 Artificial Knowledge system

Using the model of the neuron network set up describable above, we constructed an artificial knowledge system (Fig.3). First, input information of all the system is converted into an impulse to consist of frequency and voltage for the input of neuron network. These units are arranged such as that shown in Fig., each unit have interconnections with near (4 neighborhood in matrix square) units and the network have one input layer. The network structure of natural brain is observed as heterogeneous network preparing by bifurcation of synapse linkage with neuron growth. Impulse information input into a network makes a revitalization pattern of four directions by interacting with a synapse channel and neuron. The impulse propagation pathway pattern that was formed as internal information by interacting of a neuron network coincides with outside information.

Thus, we obtain the pattern of transmission pathway of each impulses, described the combination of four vectors in time series, as an output (Fig.4). Therefore we constructed the pattern matching system that recognized input information by comparing the revitalization pattern that was formed anew with the basic revitalization pattern that was stored away beforehand by a memory database. We used pattern-matching method to recognize it in total of a propagation pathway so that information is expressed by the entire of an impulse propagation pathway of the output. This method is effective to analyze similarity of character data of biology with a computer. This method looks for a maximum agreement numerical equal thing of character string of the same impulse input position by sliding the most suitable place. We calculate similarity of each revitalization pattern by a cost with the method mentioned above. Thus the pattern recognition seems to compare distinctions of activation patterns; we consider the comparison (pattern matching process) to be the basis of intelligence information processing.

2.3 Simulation procedure for the model

We set basic functional unit of neuron on 100X100 Lattice Square and gave distinctive frequency to each unit of neuron network at random (1.0-24.0). We used alphabets exchanged at bit map ('0' and '1' pattern) on 100X100lattice square as an input data. Because an input data is propagated to the neuron network as impulses pattern, the pattern of input data is altered to impulses. In order to give impulses to features of input data, we transform a row of the bit map pattern of input data into one impulse having frequency and voltage according to number of '1' and the each position. We used alphabets and some words as input data and took out the global pattern of transmission pathway of impulses as output. Moreover, in order to confirm that our model can recognize the difference in

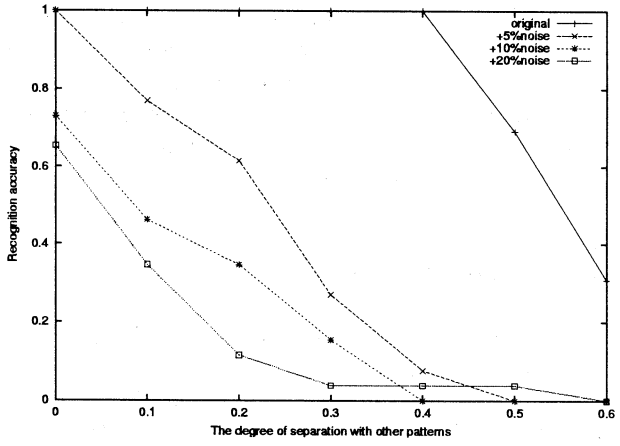


Figure 5: Accuracy of alphabets recognition. "The degree of separation with other patterns" is the difference in the degree of similar with other patterns. "Recognition accuracy" is the rate recognized in other patterns.

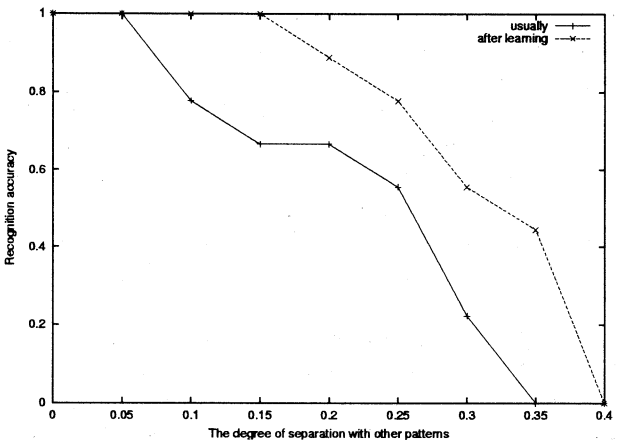


Figure 6: Accuracy of words recognition.

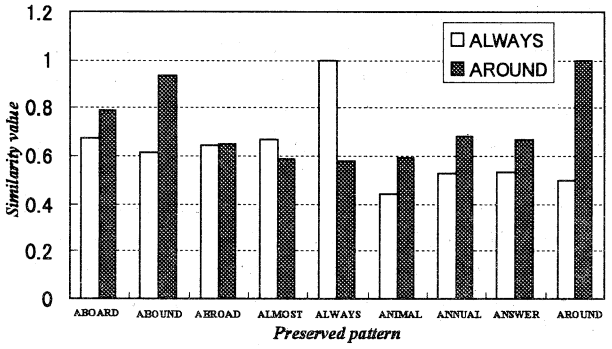


Figure 7: Word recognition (No learning); input data is "ALWAYS" and "AROUND".

clear input data, we used all alphabets including noise as input data. At first we propagate each original input data to the neuron network and each basic generated pattern is preserved. Next, some input data is propagated to the network, the learning can be classified into some categories to compute pattern matched of similarity with pattern matching between preserved patterns and generated pathway pattern. In the words recognition, each alphabet of the word is successively propagated to the network at fixed intervals.

3 Simulation result

In these simulation results, we observed that the input data was roughly classified into correct category. The values of similarity tend to be higher among similar input data. We used alphabets, some words and alphabets including noise as an image data. In order to examine a ratio of pattern recognition, we changed a classified rate of similarity each input data. The results are shown in Fig. 5 and Fig. 6.

In these results, our model could properly recognize with input data. However, in the pattern recognition of alphabets including much noise, our model could not achieve good results so that the features of alphabet were turned off by noise.

Additionally, when a synapse channel is learned by classification, improvement of some recognition precision was found in pattern recognition of word. However separation with word to recognize and other words is not generally high.

For example, similarity rate of "ABOUND" and "AROUND" that image resembles is higher than other words (Fig.7). We think that a classification of learning data is possible by coordinating learning and a cost of classification standard.

4 Discussion and Conclusion

At past research, Neural network model based on the hierarchic structure, each unit of neuron network transmits input information altered by connection weights to other units, and the information are communicated to only decided directions and the output is limited by network size. Thus a capacity of the network fundamentally depends on the network size.

However, in order to generate the propagation pathway that depended on the input as the output by real-time, our model can obtain the memory capacity that does not depend on size of network by having decided on arbitrary propagation time and method based on the individuality of a neuron. From these properties, the model can preserve many memories without disturbing encoding memories, because it is possible to represent a good deal various transmission pathways in the network [12] [13].
In our model, transmission direction of the impulse that depended on the input is decided by neighboring units' frequencies, and all the networks influence the propagation pathway of time series. Moreover, the action of all the impulses hangs down a complicated action not to converge in a specified category by setting propagation time corresponding to neuron of propagation direction in propagation. By complexity of the propagation pathway of impulse in network, Naturally recall of memory information in artificial brain becomes difficult. However, the recall that is stability of network output information is possible by the dynamic control of impulse that used a synapse channel model to convert into a channel corresponding to impulse information and learning from impulse propagation frequency. So that the self-organization of the network structure depending on the input is carried out, it is possible with the methodology how a save of huge information is simple.
From these properties of our model, we consider that our model carries out self-organization, that is to say the model has the dynamic condition of network derived from variable neuron property and control property of synapse channel, with the result that the model generates characteristic activation pattern which reflects features of input data.

5 Summary

It this paper, In order to elucidate possible about the generative intelligence from timing representation of information observed in natural brain. Then for we presented the artificial knowledge system constructed neuron network based on the properties of structure and dynamic action as natural brain. The result own computer experiments show that our model obtained an output pattern and the channel structure that depended on input information by timing representation of information in brain and the dynamic control of channel. Much theoretical and experimental result's suggests that this is the level of neural networks; it means potentiality of the neural network that used a timing of information transmission in a brain. Moreover, key behavioral properties are emergent properties to show by three dimensions structure of this model. Currently, we let this model develop moreover by extending own research to three-dimensional structure in the artificial brain system, and are simulating it.

Acknowledgements

The authors would like to thank Naoki Nishinomiya of Fujitsu co. Ltd, for fruitful discussion. Also, One of author (Yasuo Yonezawa) thank for Dr. Sinobu Nagano of Tokyo International Medical Institute for various discussion. And we thanks research stuffs for paper preparation in our laboratory.

References

[1] N.Nishinomiya and Y.Yonezawa, "Artificial Knowledge system constructed Interconnectional Network modeled on the natural Brain" *AROB.5th*, pp. 651-656,2000.

[2] Stephen Grossberg, *Neural Networks and Natural Intelligence*, A Bradford Book The MIT Press, 1988.

[3] Patricia, S.Churchland and Terrence, J.Sejnowski, *The Computational Brain*, A Bradford Book The MIT Press London, 1993.

[4] Siino, M. and Fulcui, T., "Self-consistent signal to noise analysis of the statistical behavior of analog neural networks and enhancement of storage capacity", *Physical Rev. E.*, Vol. 48, pp.687-697,1993.

[5] Kandel, E. R., Schewartz, J. H. and Jessell, T. M., *Principalls of Neural Science*, Elsevior. M. Y, 1991.

[6] Ken, Mogi, "Multiple-valued energy function in neural network with asymmetric connections", *Phy. Rev.5.49*, pp4616-4626, 1994.

[7] Fujii H. et al., "Dynamical Cell Assembly Hypothesis-Theoretical Possibility of Spatio-Temporal Coding in the Cortex, *Neural Networks*, Vol.9, pp1303-1350, 1996,

[8] Abeles, M., *Corticonics-Neural circuits of the cerebral cortex*, Cambridge University Press, 1991.

[9] M. Tanvir Islam and Yoichi Okabe, "Pattern Learning by Multilayer Neural Networks Trained by a Moderatism-Based New Algorithm", *ICONIP2002*, 2002.

[10] Bi, G-q and Poo, M-m, "Synaptic modifications in cultured hippocampal neurons: Dependence on spike timing, synaptic strength, and postsynaptic cell type", *J. Neurosci. 18*, pp.10464-10472, 1998.

[11] Markram, H., Lübke, J., Frotscher, M. and Sakmann, B., "Regulation of synaptic efficacy by coincidence of postsynaptic APs and EPSPs", *Science*, pp.213-215, 1977.

[12] Damasio, A., "Time-locked multiregional retroactivation: A system level proposal for the neural substrate recall and recognition", *Cognition*, Vol.33, pp.25-62, 1986.

[13] Damasio, A. and Damasio, H., "Brain and language", *Scientific American*, Vol.267, pp.88-95, 1992.

Proc. of The Ninth Int. Symp. on Artificial Life and Robotics (AROB 9th '04)
Beppu, Oita, Japan, 28-30 January, 2004

State Estimation of Nonlinear Stochastic Systems by Evolution Strategies Based Particle Filter*

Katsuji Uosaki Yuuya Kimura Toshiharu Hatanaka
Department of Information and Physical Sciences
Graduate School of Information Science and Technology, Osaka University
Suita, Osaka 565-0871, Japan

Abstract

Recently, particle filters have attracted attentions for nonlinear state estimation. They evaluate a posterior probability distribution of the state variable based on observations in simulation using so-called importance sampling. However, degeneracy phenomena in the importance weights deteriorate the filter performance. A new filter, Evolution Strategies Based Particle Filter, is proposed to circumvent this difficulty and to improve the performance. Illustrating numerical simulation results are presented.

1 Introduction

State estimation of dynamic systems using a sequence of their noisy observations is ubiquitous in control system science. This problem can be solved by a Bayesian approach, that is, inference on the unknown state can be performed according to the posterior probability distribution (pdf), which is obtained by combining a prior pdf for the unknown state with a likelihood function relating them to the observations. When observations come sequentially in time, recursive state estimation, which evaluates the evolving posterior pdf recursively in time, is often interested. However, the posterior pdf only admits an analytical expression for a very restricted cases, including linear Gaussiian state space models where well-known Kalman filter [1], [10] can be applied. In many realistic problems, state space models include nonlinear and non-Gaussian elements that preclude a closed form of expression for the optimal state estimate and that many approximations have been proposed such as the extended Kalman filter (EKF) and Gaussian sum filter [7], [5]. By the recent progress of computing ability, "particle filtering," a simulation-based method for Bayesian sequential analysis attracts much attentions. In this approach, the integrals in Bayes' rule is approximated by a weighted sum based on the discrete grid sequentially chosen by the importance sampling and the estimates are obtained based on corresponding importance weights [3], [2]. A common problem in the particle filter is the degeneracy phenomenon, where almost all importance weights tend to zero after some iteration. It implies a large computational effort is devoted to updating the particles with negligible weights. Some modifications such as resampling particle filter have been proposed to resolve this difficulty. We propose here a novel particle filter, Evolution Strategies Based Particle Filter, by recognizing the similarities and differences of the operations in particle filters and evolution strategies [9], one of the evolutionary computation approaches. Numerical simulation studies have been conducted to exemplify the applicability of this approach to nonlinear filtering.

*This work is partially supported by the Grant-in-Aid for Scientific Research from the Japan Society for the Promotion of Science (C)(2)14550447.

2 Particle Filters

Consider the following nonlinear state space model.

$$x_{k+1} = f(x_k, u_k, v_k) \quad (1)$$
$$y_k = g(x_k, w_k) \quad (2)$$

where x_k, u_k, y_k are the state variable, input and observation, respectively, f, g are known possibly nonlinear functions, v_k, w_k are i.i.d. system noise and observation noise sequences, respectively. We assume v_k and w_k are mutually independent. Problem to be considered here is to find the best estimate of the state variable x_k in some sense based on the all available data of observations $y_{1:k} = \{y_1, y_2, \ldots, y_k\}$. We can solve the problem by calculating the posteriori probability density function (pdf) of the state variable x_k of time instant k based on all the available data of observation sequence $y_{1:k}$.

The posteriori pdf $p(x_k|y_{1:k})$ of x_k based on the observation sequence $y_{1:k}$ is evaluated recursively from a priori pdf $p(x_0|y_0) \equiv p(x_0)$ of the initial state variable x_0 as follows.

Time evolution (Chapman-Kolmogorov equation)

$$p(x_k|y_{1:k-1}) = \int p(x_k|x_{k-1}) p(x_{k-1}|y_{1:k-1}) dx_{k-1} \quad (3)$$

Observation update (Bayes' rule)

$$p(x_k|y_{1:k}) = \frac{p(y_k|x_k)p(x_k|y_{1:k-1})}{p(y_k|y_{1:k-1})} \quad (4)$$

where normalizing constant

$$p(y_k|y_{1:k-1}) = \int p(y_k|x_k)p(x_k|y_{1:k-1})dx_k$$

depends on the likelihood $p(y_k|x_k)$, which is determined by the observation equation (2).
The recursive propagation of the pdf based on the recurrence relations (3) and (4) cannot be determined analytically except a restrictive set of cases, including the Kalman filter [1], [10].. When the analytic solutions are intractable, some approximations should be introduced. The most popular approach is the extended Kalman filter (EKF) [7], [5], which is applicable to nonlinear models with additive Gaussian noise and uses a linearization technique based on a first order Taylor expansions of the nonlinear system and observation equations about the current estimate. However, it approximates the posterior pdf to be Gaussian. If the true density is non-Gaussian, then a Gaussian can never described it well. In such cases, approximate grid-based filters and particle filters will yield an improvement in performance. They approximate the integrals with the following weighted sum on the discrete grids.

$$p(x_k|y_{1:k}) \approx \sum_{i=1}^{n} w_k^i \delta(x_k - x_k^i) \quad (5)$$

where $\delta(\cdot)$ is Dirac's delta function and w_k^i is the weight for the discrete grid x_k^i with $w_k^i \geq 0$, $\sum_{i=1}^n w_k^i = 1$. The weights are chosen using the principle of "importance sampling" [3]:
Suppose $p(x) \propto \pi(x)$ is a pdf from which it is difficult to samples, but for which $\pi(x)$ can be evaluated. Let x^i $(i = 1, \ldots, n)$ be samples that are easily generated from a pdf $q(x)$, called an importance density. Then a weighted approximation to the density $p(x)$ is given by

$$p(x) \approx \sum_{i=1}^{n} w^i \delta(x - x^i) \quad (6)$$

with the normalized weight of the i-th particle

$$w^i \propto \frac{\pi(x^i)}{q(x^i)} \quad (7)$$

So, if the samples x_k^i were drawn from an importance density $q(x_k^i|y_{1:k})$ then the weights in (5) are defined by (7) to be

$$w_k^i = \frac{p(x_k^i|y_{1:k})}{q(x_k^i|y_{1:k})} \quad (8)$$

If the importance density $q(x_k|y_{1:k-1})$ is chosen to factorize such that

$$q(x_k|y_{1:k}) = q(x_k|x_{k-1}, y_{1:k})q(x_{k-1}|y_{1:k-1}) \quad (9)$$

Then we can obtain samples x_k^i by augmenting each of the existing samples x_{k-1}^i sampled from the importance density $q(x_{k-1}|y_{1:k-1})$ with the new state sampled from $q(x_k|x_{k-1}, y_{1:k})$.
Noting that

$$\begin{aligned} p(x_k|y_{1:k}) &= \frac{p(y_k|x_k, y_{1:k-1})p(x_k|y_{1:k-1})}{p(y_k|y_{1:k-1})} \\ &= \frac{p(y_k|x_k, y_{1:k-1})p(x_k|x_{k-1}, y_{1:k-1})p(x_{k-1}|y_{1:k-1})}{p(y_k|y_{1:k-1})} \\ &= \frac{p(y_k|x_k)p(x_k|x_{k-1})}{p(y_k|y_{1:k-1})}p(x_{k-1}|y_{1:k-1}) \\ &\propto p(y_k|x_k)p(x_k|x_{k-1})p(x_{k-1}|y_{1:k-1}) \end{aligned} \quad (10)$$

we have

$$w_k^i \propto \frac{p(y_k|x_k^i)p(x_k^i|x_{k-1}^i)p(x_{k-1}^i|y_{1:k-1})}{q(x_k^i|x_{k-1}^i, y_{1:k})q(x_{k-1}^i|y_{1:k-1})} \quad (11)$$

$$= w_{k-1}^i \frac{p(y_k|x_k^i)p(x_k^i|x_{k-1}^i)}{q(x_k^i|x_{k-1}^i, y_{1:k})} \quad (12)$$

2.1 Sampling Importance Resampling Filter

A common problem in SIS filter is the degeneracy phenomenon, where almost all particles will be almost zero after a few iterations. By this degeneracy, a large computational effort is devoted to updating particles whose contribution to the approximation of the posterior pdf $p(x_k|y_{1:k})$ is negligible. In order to prevent this phenomenon, we can introduce resampling process, where particles with smaller weights are eliminated and particles with relatively larger weights are resampled. The resampling process involves generating new grid points x_k^{*i} $(i = 1, \ldots, n)$ by resampling from the grid approximation (5) randomly with probability

$$\Pr(x_k^{*i} = x_k^j) = \tilde{w}_k^j \quad (13)$$

The weights are reset to

$$w_k^{*i} = 1/n \quad (14)$$

The effective sample size defined by

$$\hat{N}_{eff} = \frac{1}{\sum_{i=1}^n (\tilde{w}_k^i)^2} \quad (15)$$

is used as a measure of degeneracy, where $\tilde{w}_k^i$ is a normalized weight. Note that $1 \leq \hat{N}_{eff} \leq n$ and that smaller N_{eff} implies severe degeneracy. Hence if $\hat{N}_{eff} < N_{thres}$ for some predetermined N_{thres}, resampling should be desirable. Particle filter with this resampling process is called "Sampling Importance Resampling Particle Filter" (SIR).

2.2 Evolutionary Computation

Evolutionary computation approaches such as 'Evolutionary Programming' (EP) [4], 'Evolution Strategies' (ES) [9], 'Genetic Algorithm' (GA) [6], and 'Genetic Programming' (GP) [8] are computational models of natural evolutionary processes as key elements in the design and implementation of computer-based problem solving systems. The common conceptual base is simulating the evolution of individual structures via processes of selection and perturbation such as recombination and mutation. These processes depend on the perceived performance (fitness) of the individual structures as defined by the environments.
Here we only explain ES briefly, which will be used hereinafter. It was developed by Rechenberg and Schwefel [9] to solve hydrodynamic problems. It is applied to continuous function optimization in real-valued n-dimensional space. The simplest method can be implemented as follows: Let $\boldsymbol{x}^{(k)} = (x_1^{(k)}, \cdots x_n^{(k)}) \in \boldsymbol{R}^n$, $(k = 1, \cdots, \mu)$ be each individual in the population.

2.2.1 Generation of initial population

We generate an initial population of parent vectors $\{\boldsymbol{x}^{(k)}, (k = 1, \cdots, \mu)\}$ randomly from a feasible range in each dimension.

2.2.2 Evolution operations

1. Crossover

   This process allows for mixing of parental information while passing it to their descendants. A typical crossover rule is

   $$x'_j = x_{S,j} + \chi \cdot (x_{T,j} - x_{S,j}) \tag{16}$$

   where S and T denote two parent individuals selected at random from the population and $\chi \in [0, 1]$ is a uniform random or deterministic variable. The index j in x'_j indicates j-th component of new individuals.

2. Mutation

   This process introduces innovation into the population. It is realized by following additive process,

   $$\begin{aligned} \sigma'_j &= \sigma_j \exp(\tau' N(0,1) + \tau N_j(0,1) \\ x''_j &= x'_j + \sigma'_j N_j(0,1) \end{aligned} \tag{17}$$

   Here, $N(0,1)$ denotes a realization of normal random variable with mean and unit variance, $N_j(0,1)$ denotes random variable sampled anew for counter j of normal random variable with mean and unit variance and σ_j denote the mean step size. The factors τ and τ' are chosen dependent on the size of population μ. In this approach, small variations are much more frequent than larger variations, expressing the state of affairs on the phenotypic level in nature.

3. Selection

   This is the completely deterministic process choosing the individuals of higher fitness out of the union of parents and offspring or offspring only to form the next generation in order to evolve towards better search region. There are two main selection processes, $(\mu + \lambda)$-selection and (μ, λ)-selection. In $(\mu + \lambda)$-selection, λ offspring are created from μ parents and the μ best individuals are selected out of the union of parents and offspring. While, in (μ, λ)-selection, λ offspring are created from μ parents and the μ best individuals are selected out of offspring $(\lambda \geq \mu)$.

2.3 Evolution Strategies Based Filter

Recognizing the fact the importance sampling and resampling processes in SIR filter are corresponding to mutation and selection processes in ES, we will develop a novel particle filter, Evolution Strategies Based particle filter. In SIR filter, the importance sampling process samples x_k^i according to the importance density $q(x_k^i | x_{k-1}^i, y_{1:k})$, and this corresponds to mutation process in ES from the viewpoint of generating offspring x_k^i from the parents x_{k-1}^i with extrapolation by $f(x_{k-1})$ and perturbation by v_k. On the other hands, resampling process in SIR filter selects offspring with probability given by (11) and this corresponds to selection process in ES with fitness function w_k^i. The main difference is resampling in SIR is carried out randomly and the weights are reset as $1/n$, while the selection in ES is deterministic and the fitness function is never reset. Hence, by replacing the resampling process in SIR by the deterministic selection process in ES, we can derive a new particle filter as follows.
Based on the particles x_{k-1}^i, $(i = 1, \ldots, n)$ sampled from the importance density $q(x_{k-1} | y_{1:k-1})$, we generates t $x_k^{i(j)}$, $(j = 1, \ldots, \ell)$ sampled from the importance density function $q(x_k | x_{k-1}^i, y_{1:k})$. Corresponding weights $w_k^{i(j)}$ are evaluated by

$$\begin{aligned} w_k^{i(j)} = w_{k-1}^i \frac{p(y_k | x_k^{i(j)}) p(x_{k-1}^{i(j)} | x_{k-1}^i)}{q(x_k^{i(j)} | x_{k-1}^i, y_{1:k})} \\ i = 1, \ldots, n, \; j = 1, \ldots, \ell \end{aligned} \tag{18}$$

From the set of $n\ell$ particles and weights $\{x_k^{i(j)}, w_k^{i(j)}, (i = 1, \ldots, n, \; j = 1, \ldots, \ell)\}$, we choose n sets with the larger weights, and set as $x_k^i, w_k^i (i = 1, \ldots, n)$. This process corresponds to $(n, n\ell)$-selection in ES.

We call this particle filter as the Evolution Strategies Based Particle Filter (SIE).

3 Numerical Example

Consider the following nonlinear state space model.

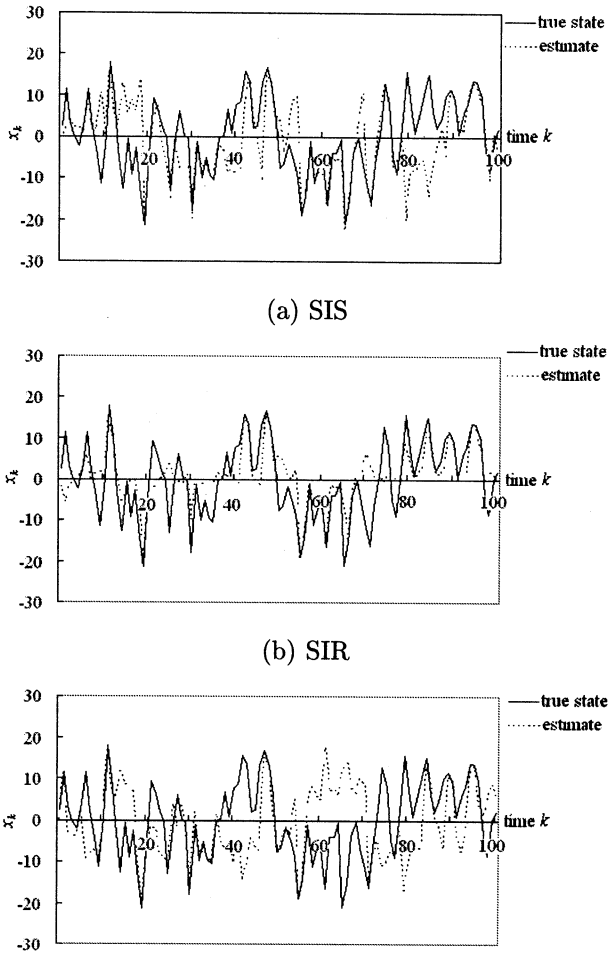
$$p(x_k|x_{k-1}) = \mathcal{N}(x_k; f_k(x_{k-1}, k), Q_{k-1}) \quad (19)$$

$$p(y_k|x_k) = \mathcal{N}\left(y_k; \frac{x_k^2}{20}, R_k\right) \quad (20)$$

where

$$f_k(x_{k-1}, k) = \frac{x_{k-1}}{2} + \frac{25x_{k-1}}{1+x_{k-1}^2} + 8\cos(1.2k)$$

and v_k and w_k are i.i.d. zero-mean normal random variates with variance $Q_k = 10$ and $R_k = 1$, respectively. The sample behaviors of the estimates by SIS ($n = 400$), SIR ($n = 200, N_{eff} = 200$) and proposed SIE ($n = 20, p = 20$) filters are given in Fig.1. Mean squared errors at time instant $k = 100$ for 10 simulations are 133.44 for SIS, 48.87 for SIR and 61.21 for SIE, respectively. Though SIE filter shows the intermediate performance between SIS and SIR filters, it can be carried out routinely since evaluation of the effective number and comparison with the threshold value as in SIR are not necessary. The performance of course depends on the choice of design parameters n, N_{eff} and p and better choice will be pursued.



(a) SIS

(b) SIR

(c) SIE

Figure 1: Sample paths of state estimation

4 Conclusions

Recognizing the similarity and the difference between the importance sampling and resampling processes in SIR filter and mutation and selection processes in ES, have derived a novel particle filter, SIE filter, by substituting (μ, λ)-selection in ES into resampling process in SIR. Application of other evolution operations such as crossover and modification of mutation will have the potential to create high performance particle filters.

References

[1] B. D. O. Anderson and J. B. Moore: *Optimal Filtering*, Prentice-Hall (1979)

[2] S. Arulampalam, S. Maskell, N. Gordon and T. Clapp: "A tutorial on particle filters for on-line non-linear/non-Gaussian Bayesian tracking," *IEEE Trans. on Signal Processing*, Vol. SP-50, No.2, 174/188 (2002)

[3] A. Doucet: "On sequential simulation-based methods for Bayesian filtering," Technical Report CUED/F-INFENG/TR 310, Department of Engineering, Cambridge University (1998)

[4] L. J. Fogel, A. J. Owens and M. J. Walsh: "Artificial intelligence through a simulation of evolution," *Proc. of the 2nd Cybernetics Science Symp.*, pp.131–155 (1965) reprinted in D. B. Fogel (eds.), *Evolutionary Computation, The Fossil Record*, pp.230–254, IEEE Press (1995)

[5] G. C. Goodwin and J. C. Agüero: "State and parameter estimation for linear and nonlinear systems," *Proc. of the 7th International Conf. on Control, Automation, Robotics and Vision* (2002)

[6] J. H. Holland: *Adaptation in Natural and Artificial Systems*, MIT Press (1992)

[7] A. H. Jazwinski: *Stochastic Process and Filtering Theory*, Academic Press (1970)

[8] J. R. Koza: *Genetic Programming: On the Programming of Computers by Means of Natural Selection*, MIT Press (1992)

[9] H.-P. Schwefel: *Evolution and Optimum Seeking*, J. Wiley (1995)

[10] H. Sorenson: *Kalman Filtering: Theory and Application*, IEEE Press (1985)

Proc. of The Ninth Int. Symp. on Artificial Life and Robotics (AROB 9th '04)
Beppu, Oita, Japan, 28-30 January, 2004

Linear Feature Prediction for Confidence Estimation of Sonar Readings in Map Building

Shane O'Sullivan
IBM Software Group
Santry
Dublin 9, Ireland.
Email:osushane@ie.ibm.com

J.J. Collins, Mark Mansfield, David Haskett, and Malachy Eaton
Dept. of Computer Science and Information Systems
University of Limerick, Limerick
Limerick, Ireland.
Email:[j.j.collins/mark.mansfield/david.haskett/malachy.eaton]@ul.ie

Abstract

This paper presents a method for detecting specular sonar readings called Feature Prediction. The position and orientation of features in the robot's local space are predicted from reliable sonar readings, and confidence measures are assigned to each sonar reading to indicate the probability that it is reliable. The confidence values are used by map building algorithms to weaken the effect of specular sonar readings on the global map, or to discard the reading completely if the confidence value is sufficiently low. The Feature Prediction algorithm is shown to significantly improve the quality of maps using a suite of benchmarks.

1. Introduction

One of the greatest challenges in using sonar sensors for map building with mobile robots is that of compensating for *specular reflection* of the sonar beam. Sonar sensors detect obstacles by emitting a sound wave, which would ideally strike the obstacle and reflect diffusely, meaning that it scatters in all directions, returning a correct range reading to the sensor. The distance of the object from the sensor is calculated using a simple time-of-flight equation, and this information is integrated some form of internal representation of the environment, e.g. a map. When the sound wave strikes a smooth flat object at an angle sufficiently distant from perpendicular however, it is often reflected away from the sonar, resulting in an incorrect noisy range reading, as in Fig 1. The mapping algorithm incorporating the sonar range information into a map will then either interpret all the space in the sonar beam as freespace if no range reading was returned, or place an obstacle further from the sensor than is correct if the sonar wave struck multiple obstacles before returning to the sensor.

This paper details a method called *Feature Prediction*, which is used to identify specular readings by predicting the state of the world and assigning confidence values to each sonar range reading. Feature Prediction identifies reliable sonar readings in each scan, and from these extrapolates the position and orientation of the features in the environment that caused the sound wave to reflect back to the sensor. These features are used to calculate confidence values for each sonar range reading, which are then used to alter how the sonar range data is incorporated into the global map.

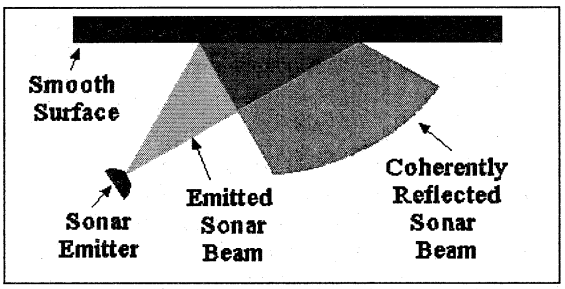


Fig. 1 Specular sonar reflection giving a noisy reading - when a sonar beam strikes a smooth surface at an angle far from 90° it does not return directly to the emitter.

2. A Trio Of Environment Models

Three models of the environment are maintained:

- A sonar map *S*.
- A local map *L*.
- A global map *G*.

The sonar map *S* is a stateless model which contains features extrapolated from the current set of sonar readings. These features take the form of straight line segments. The local map *L* maintains a set of features estimated from previous scans, but only within the area immediately surrounding the robot. The global map *G* can take any form desired, but the results presented in this paper used a grid based metric map, similar to the occupancy grids proposed by Moravec and Elfes.

3. The Feature Prediction Algorithm

There are seven steps involved in calculating a confidence measure for each sonar based on all past and current readings and using it to update a global map.

1. **Create a feature hypothesis for each sonar that claims to have detected an obstacle and place it in the sonar map *S***

   FOR EACH range reading < max range
   Create line segment feature s_i at centre of beam, at 90° to direction of beam, and place in *S*

2. **Compare each feature in *S*, s_i, with all the other features in *S*, s_j, to determine if they represent the same object in the environment.**

   FOR EACH s_i in *S*
   FOR EACH s_j in *S* NOT EQUAL TO s_i
   IF similar(s_i , s_j) THEN
   Create new feature s_k between s_i and s_j and place it in *S*
   Remove s_i and s_j from *S*

3. **Remove any feature in *S* caused by incorrect readings. Confidence values derived from the sonar view are denominated by c_x^s , where the *s* signifies that this confidence value was derived from the sonar view, and *x* indicates the formula used to calculate it. An ^{L} superscript signifies that the confidence value was derived from the local map *L*. θ is the difference in angle between the sonar and the feature, and ω is the beam aperture.**

   FOR EACH son_j in *SONARS*
   $c_a^s = c_d^s = c_a^L = c_d^L = 0.5$
   FOR EACH s_i in *S*
   IF inconsistent(s_i , son_j) THEN
   IF son_j should detect s_i THEN
   $$c_a^s = 0.5 - \left(\frac{(\theta - (90 - \omega))}{\omega} \right) * 0.25$$
   ELSE IF son_j should not detect s_i
   $$c_d^s = (\delta / R)^2 / 2$$
   $$c_{da}^s = combine(c_a^s, c_a^s)$$
   FOR EACH l_i in *L*
   IF inconsistent(l_i , son_j) THEN
   IF son_j should detect l_i THEN
   $$c_a^L = 0.5 - \left(\frac{(\theta - (90 - \omega))}{\omega} \right) * 0.25$$
   ELSE IF son_j should not detect l_i
   $$c_d^L = (\delta / R)^2 / 2$$
   $$c_{da}^L = combine(c_a^L, c_a^L)$$
   FOR EACH s_i in *S*
   IF s_i detected by only 1 sonar AND
   ($c_{da}^s < T_s$ OR $c_{da}^L < T_s$) THEN
   Remove s_i from *S*

4. **Compare all remaining features in *S* with all lines in *L*, refining the hypothesis of the angle and position of the features in *L***

   FOR EACH s_i in *S*
   FOR EACH l_j in *L*
   IF similar(s_i , l_j) THEN
   Create new feature between s_i and l_j and place it in *L*
   Remove s_i from *S* and remove l_j from *L*
   FOR EACH s_i in *S*
   Place s_i in *L* as a new segment
   Remove s_i from *S*

5. **Features in *L* too far from the robot are removed**

   FOR EACH l_i in *L*
   IF dist(robot_position, last_position_detected(l_i)) > T_d THEN
   Remove l_i from *L*

6. **Generate final sonar confidence values, c_{da}^L. For any segment in *L* that should have been detected but was not, split in two and shorten it. Confidence values derived from the local model *L* are denoted with a superscript *L*, with the formula used to calculate the confidence value referred to with a subscript, as in c_x^L.**

   FOR EACH son_i in *SONARS*
   $c_a^L = c_d^L = 0.5$
   FOR EACH l_j in *L*
   IF inconsistent(s_i , son_j) THEN
   IF son_i should sense l_j if it exists THEN
   $$c_a^L = 0.5 - \left(\frac{(\theta - (90 - \omega))}{\omega} \right) * 0.25$$
   Divide l_j at point of intersection with son_j, creating l_k and l_l
   Remove l_j from *L* and insert l_k and l_l into *L*
   Reduce length of l_k and l_l
   IF length(l_k) < T_L
   Remove l_k from *L*
   IF length(l_l) < T_L
   Remove l_l from *L*
   IF son_i should not sense l_j if it exists THEN
   $$c_d^L = (\delta / R)^2 / 2$$
   $$c_{da}^L = combine(c_a^L, c_a^L)$$

7. **Use sonar confidence values to alter how the sonar information is integrated into the global map. The implementation of this step is specific to the method being used to generate the global map.**

4. Calculating Confidence Values

A sonar beam is represented as three lines, as in Fig 4. If none of the three lines intersect with a feature, then that

sonar is given a confidence value $c_{da}^{X} = 0.5$, where X is either s or L. The value 0.5 is used due to the fact that when it is used in a Bayesian update formula, it has no effect. If any of the three lines intersects with a feature either in S or L then the sonar is inconsistent with that feature. At this point, either c_d^X or c_a^X must be calculated. If the difference in orientation between the sonar and the feature is less than 25° (given a beam aperture ω of 25°), then the sonar *should* detect the feature if the feature were at the predicted position and orientation. In this case, the closer to perpendicular the sonar is to the feature, the more likely it is to detect it. Therefore the confidence, c_a^X with regard to angle is:

$$c_a^X = 0.5 - \left(\frac{(\theta - (90 - \omega))}{\omega} \right) * 0.25$$

This maps the confidence value into the range [0.25, 0.5], meaning that a feature which should have been detected by the sonar can, at worst, halve the confidence in the sonar. If the difference in orientation between the sonar beam and the feature it is inconsistent with is more than 25° from perpendicular, then the sonar would not be expected to detect the feature, assuming that it is a smooth obstacle. In this case the confidence in the sonar, c_d^X is directly proportional to the distance from the sonar to the feature.

$$c_d^X = (\delta / R)^2 / 2$$

When a range reading is inconsistent with a feature, only the are behind the feature is updated incorrectly as being freespace. The closer the feature is to the sonar, the lower the confidence value must be to prevent the cells behind the feature being effected by the map building algorithm, as can be seen in Fig 2 and Fig 3.

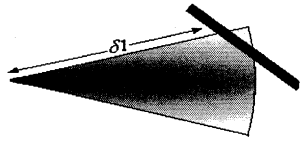


Fig. 2. Sonar beam with an undetected feature at distance δ1 from the emitter. The darker the area, the more strongly it is believed to be unoccupied.

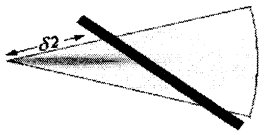


Fig. 3. Sonar beam with undetected obstacle δ2 from the emitter. The strength of the freespace update has been reduced.

5. Combining Confidence Values

Once c_d^s and c_a^s have been computed, they are combined to give a single confidence value for the sonar, c_{da}^s. The confidence combination formulae are derived from techniques for parallel combination of rules in expert [1].

$$c_{da}^s = \begin{cases} 2\, c_d^s\, c_a^s & \text{when } c_d^s < 0.5 \text{ and } c_a^s < 0.5 \\ c_d^s + c_a^s - 0.5 & \text{when } c_d^s = 0.5 \text{ or } c_a^s = 0.5 \end{cases}$$

As stated earlier, the initial confidence value of each sonar is 0.5.

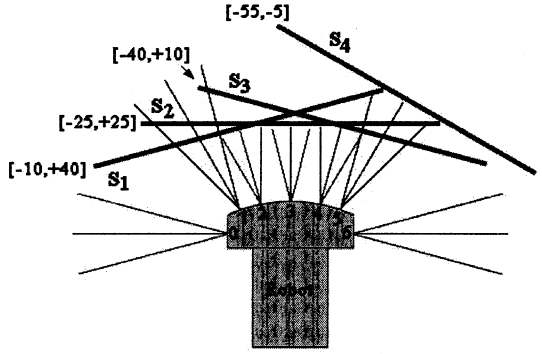


Fig. 4. The predicted features in the sonar model S after Step 1. The robot is facing straight into a wall with sonars 2, 3, 4 and 5 returning a reading that is less than the maximum range. Sonars 0, 1 and 6 return no reading, and sonar 5's reading, while less than the maximum, is incorrect.

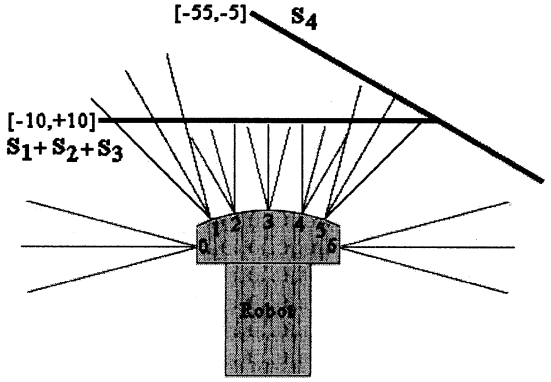


Fig. 5. Predicted features after Step 2 is applied to the sonar view from Fig 4. The three line segments S_1 S_2 and S_3 have been merged to create one segment.

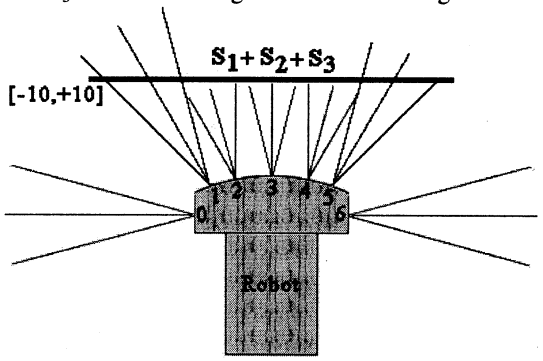


Fig. 6. State of the sonar model S after Step 3 has been applied. Sonar 5 is inconsistent with the line created by sonars 2, 3 and 4, and its confidence is low enough so that the line predicted by it has been removed.

6. Experimentation Results

A suite of benchmarking techniques published in [3] have been applied to 128 maps generated with and without feature prediction, both in simulation and in real world experiments on a Pioneer 1 robot from ActivMedia robots. Each of the maps generated in the course of experimentation are compared against hand drawn ideal maps of the environment the robot traversed. A complete description of all environments, benchmarks, and procedures followed can be obtained from [2].
The four tests are as follows:

1. Correlation. A technique from the image recognition field that tests the similarity of two maps using the average and standard deviation the cells, as well as comparing the maps on a cell-to-cell basis. A higher percentage indicates a greater degree of similarity between the maps.[4]
2. Map Score. A technique developed by Martin and Moravec [5] which calculates the difference between two maps by summing the squared difference of corresponding cells in each map. The lower the percentage difference, the greater the similarity between the two maps.
3. Map Score of Occupied Cells. Similar to the previous benchmark, but only tests those cells that are occupied, i.e. >0.5 in one or both of the maps being tested.
4. Path Comparison For False Positive Paths. Examines the freespace areas of a map by calculating the percentage of paths in the map which would cause a robot to collide with an obstacle. The lower the percentage, the fewer paths would cause a collision, and therefore the better the map.

Table 1.

	Correlation	Map Score	Map Score Occupied Cells	Path Comparison False Positives
Without Feature Prediction	59.77%	13.80%	11.05%	59.60%
With Feature Prediction	71.56%	9.18%	7.80%	40.20%

6.1 Analysis of Results

All four benchmarks show considerable improvement in map quality when Feature Prediction is applied.

- The correlation benchmark shows the map quality increasing by 120%.
- The Map Score benchmark shows the map quality increasing by 150%.
- The Map Score of Occupied Cells shows an increase in map quality of 142%.
- The Path Comparison for False Positive Paths benchmark shows an increase of 148%.

7. Discussion

This paper presented a method of detecting specular sonar reflections and assigning confidence values to the sonar range readings in order to enable more accurate map building. Experiments which employed the Feature Prediction algorithm with a simple two-dimensional gaussian sonar model from [6] showed an average increase of map quality of 140% over four different benchmarks. Performing Feature Prediction requires a negligible amount of computational resources, with a standard desktop workstation capable of performing mapping for ten or more robots simultaneously. However it vastly increases the quality of a map, resulting in more effective navigation routines.

References

[1] Heckerman, D. (1986). Probabilistic interpretation for MYCIN's uncertainty factors. Uncertainty in Artificial Intelligence. L. N. L. Kanal, J.F. North-Holland: 197-196.

[2] O'Sullivan, S. (2003). An Empirical Evaluation Of Map Building Methodologies in Mobile Robotics Using The Feature Prediction Sonar Noise Filter And Metric Grid Map Benchmarking Suite. MSc Thesis, University of Limerick, Ireland.

[3] Collins, J. J., O'Sullivan, S., Mansfield, M., Eaton, M., Haskett, D. (2004). Developing a benchmarking framework for map building paradigms. In Proceedings Ninth International Symposium on Artificial Life and Robots, Oita, Japan, January 2004.

[4] Baron, R. J. (1981). Mechanisms of human facial recognition." International Journal of Man Machine Studies 15: 137-178.

[5] Martin, M. C., Moravec, H.P. (1996). Robot Evidence Grids. Technical Report, Robotics Institute, Carnegie Mellon University, Pittsburgh, Pennsylvania, USA.

[6] Moravec, H. P., Elfes, A. (1985). High Resolution Maps from Wide Angle Sonar. In Proceedings of the 1985 IEEE International Conference on Robotics and Automation.

Proc. of The Ninth Int. Symp. on Artificial Life and Robotics (AROB 9th '04)
Beppu, Oita, Japan, 28-30 January, 2004

A Quantitive Evaluation of Sonar Models and Mathematical Update Methods for Map Building with Mobile Robots

Shane O'Sullivan
IBM Software Group
Santry
Dublin 9, Ireland.
Email:osushane@ie.ibm.com

J.J. Collins, Mark Mansfield, David Haskett, and Malachy Eaton
Dept. of Computer Science and Information Systems
University of Limerick, Limerick
Limerick, Ireland.
Email:[j.j.collins/mark.mansfield/david.haskett/malachy.eaton]@ul.ie

Abstract

A wide range of sonar models and map update methods have been developed by researchers to create a map of an environment using a mobile robot. However these are generally developed in isolation from each other, and are rarely compared directly with other map building methods. When they are, either qualitative methods are applied, or the comparisons are based on different test data, making it problematic to correctly assess the merits of the various map building approaches. This paper presents a qualitative comparison of two sonar models and three mathematical update methods. The sonar models are based on models proposed by Moravec and Elfes, as well as Konolige. The mathematical map update formulae evaluated include methods based on Bayesian probability theory in addition to more simplistic methods. All evaluations are performed using identical data in identical environments, both in simulation and in real world experiments.

1. Introduction

Though robotic map building is a relatively new field, a wide variety of solutions to the world-modelling problem have been proposed in the literature. One of the most popular sensors used is sonar, due to its low cost and the resulting widespread inclusion in many robotic systems, its ability to sense a volume, and the speed at which sonar information can be incorporated into a world model. One of the most common types of world model built with sonars is the occupancy grid, in which an environment is discretised into regular shaped areas, usually squares, which are arranged in grid formation.

Although a great deal of research is taking place in robotic map building, correctly evaluating the strengths or weaknesses of any particular approach is difficult. This is due to the fact that work by different researchers is rarely directly evaluated with identical data from identical environments, which is the only way to reliably compare contrasting algorithms. This paper empirically evaluates a variety of mapping paradigms from a number of researchers. These paradigms are comprised of two of the primary issues which must be addressed when building an occupancy grid with sonar sensors.

1. Which sonar model to use.
2. Which mathematical formula to use to incorporate the information from the sonar model with the world map.

1.1 Sonar Models

A sonar model determines how to interpret the range reading of a sonar. Unlike a laser, which has a very small aperture and therefore detects a very small area, a sonar sound wave spreads outwards from the emitter in a cone-like fashion. An obstacle anywhere in the sonar cone can cause a the wave to reflect back to the sensor, giving a range reading. While there is no way to determine exactly where in the cone the obstacle that caused the reflection is, studies have shown that a sonar cone's energy is stronger nearer to the emitter and directly in the direction the emitter is facing. The places in the cone where the energy is stronger are more likely to reflect a signal back to the emitter, and therefore a sonar model can be developed to estimate the behaviour of the sonic beam by assigning a value to each part of the sonar cone which represents the probability that the obstacle located there. This paper presents a direct comparison of Konolige's sonar model and the sonar model of Moravec and Elfes, using identical data and benchmarks.

1.2 Mathematical Map Update Formulae

The mathematical formulae used to integrate new information into a map have been the area of much study. Whereas earlier methods used less mathematically robust formulae [1,2], the map building community quickly came to the general conclusion that formulae based on Bayesian probability theory led to more accurate maps being created [3]. A number of different theories based upon Bayesian theory have been proposed [4, 5], but as with the sonar models the various approaches have never been directly compared using identical data. This paper contrasts three different

mathematical update methods. The first is the *ad hoc* method based upon the formulae proposed in [2], the second uses the Bayesian update formula as presented in [3], and the third is the modified Bayesian update formulae using log odds presented in [4].

2. Sonar Models

Two sonar models are quantitively contrasted in this paper. The first is the two dimensional gaussian sonar model proposed by Moravec and Elfes [2]. The second is the sonar model designed by Konolige [4], the multiple target model, which is based on the normal distribution. This paper is not intended to be an in depth discussion of these sonar models, for that see the source papers. However, an overview of the models is given below. Each of these models translates a sonar range reading into a set of values which must applied to a set of cells in a map. The mathematical formulae used to perform this cell update procedure are discussed in section three.

2.1 Two Dimensional Gaussian Sonar Model

A sonar beam contains information which pertains to an area, rather than a point, regardless of whether it strikes an obstacle or not. The two dimensional gaussian (2DG) model represents a sonar range reading as a segment, as in Fig 1. The beam is divided into two parts, the freespace area and the surface (obstacle) area. The freespace area is the part of the beam between the sensor and the range the obstacle was detected at, i.e. the unshaded area in Fig 1. There is always some uncertainty as to the exact distance an obstacle was measured at, which lead to the introduction of the value ε. It is also unknown where on the arc the obstacle is. For these two reasons, the occupied part of the beam is represented by the shaded area in Fig 1, covering the full arc of the beam, and wide to represent the range uncertainty.

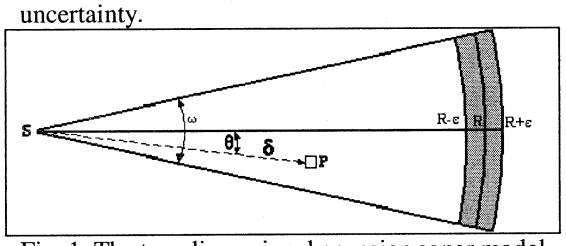


Fig. 1. The two dimensional gaussian sonar model

Fig 1 illustrates Moravec and Elfes' 1985 model of the sonar beam. In this model,

- S is the sonar sensor
- P is the cell being updated
- ε is the mean sonar deviation error
- ω is the beam aperture, the angle at which the beam spreads from the sensor S
- δ is the distance from P to S
- θ is the angle between the main axis of the beam and the line SP.
- R is the range reading – the distance the sonar beam travelled before it bounced off an object

2.1.1 Freespace Updates with the 2D Gaussian Sonar Model

A cell which is inside the freespace area of the beam has its freespace probability increased with the value $P_E(X,Y)$, using the formula: $P_E(X,Y) = E_r(\delta) * E_a(\theta)$

$E_r(\delta)$ is the estimation of the cell's freespace based on its range from the sensor. The closer it is to the sensor, the more likely that it is not occupied.

$$E_r(\delta) = \begin{cases} 1-((\delta - R_{min})/(R-\varepsilon-R_{min}))^2 & \text{for } R_{min} \le \delta \le R-\varepsilon \\ 0 & \text{otherwise} \end{cases}$$

$E_a(\theta)$ is the estimation that a cell is unoccupied based on the difference in angle between it and the central beam of the sonar, θ. Cells closer to the central beam of the sonar are more strongly updated as freespace than cells near the extrmeties of the beam.

$$E_a(\theta) = 1-(2\theta/\omega)^2 \text{ for } (-\omega/2) \le \theta \le (\omega/2)$$

2.1.2 Surface Updates with the 2D gaussian sonar model

A cell in the surface area of the beam, the shaded area in Fig 1, is updated in a similar manner. The update value $P_O(X,Y)$, the probability that a cell is occupied is calculated using the following formulae:

$$P_O(X,Y) = O_r(\delta) * O_a(\theta)$$

$O_r(\delta)$ is the probability that the cell is occupied based on its range from the sensor. The closer it is to the range reading received, the higher the probability that the cell is occupied.

$$O_r(\delta) = 1-((\delta - R)/\varepsilon)^2 \text{ for } (R-\varepsilon) \le \delta \le (R+\varepsilon)$$

where $O_a(\theta)$ is the probability that the cell is occupied based on the difference in angle between the obstacle and the central beam of the sonar. The closer the cell is to the centre of the beam, the more likely it is that the cell is occupied.

$$O_a(\theta) = 1-(2\theta/\omega)^2 \text{ for } (-\omega/2) \le \theta \le (\omega/2)$$

2.2 Multiple Target Sonar Model

The multiple target model, similar to the 2DG model, separates the sonar model into two sections. Therefore both $P_E(X,Y)$ and $P_O(X,Y)$ must be calculated. However in the Multiple Target Model, both freespace and surface

readings are calculated using an identical formula. As with the 2DG sonar model, cells closer to the sonar sensor are more likely to be unoccupied and cells closer to the range reading are more likely to be occupied. Also, cells closer to the central beam of the sonar are updated more strongly than cells near the extremities of the beam, whether it be a freespace or surface update.

On receipt of a sonar range reading, all cells in the beam are updated with the value $P(X,Y)$, using the formula:

$$P(X,Y)=\frac{p(r=D|C_i)*p(r\not<D|C_i)}{(1-(F*r_i))*F}$$

In the above formula, D is the range reading received by the sonar, and C_i states that the cell C_i is occupied. $p(r=D|C_i)$ is the probability of receiving the range reading D given that the cell C_i is occupied. r_i is the distance from the sonar to the cell being updated, and F is a small constant representing the probability that an obstacle could exist at point in the beam other than at the range measured, hence the name *Multiple Target Model*.

$$p(r=D|C_i)=$$

$$\alpha(r_i)\left(\frac{1}{\sqrt{2\pi}\delta(r_i)}e^{-(D-r_i)^2/2\delta(r_i)^2}\right)\left(\frac{1}{\sqrt{2\pi}\sigma}e^{-(\theta_i-0)^2/2\omega^2}\right)+F$$

$\alpha(r_i)$ is the attenuation of detection with distance, meaning that the farther away an obstacle is, the less likely it is to be detected. For the experiments, $\alpha(r)=0.6(1-\min(1,0.4r))$, giving a maximum sonar range of 2.5 metres. $\delta(r_i)$ is the range variance, meaning that the farther the obstacle is from the sonar, the more the range measured will fluctuate. In experiments this was set to $\delta(r)=.01+0.015r$, which means that there is a fixed error of 1cm, plus 1.5% of the range. For experiments, this was set to 0.05. As in the 2DG sonar model, θ is the difference in angle between the cell and the central axis of the sonar beam, and ω is half the aperture of the beam.

The above equation is a modified version of the normal distribution, $\frac{1}{\sqrt{2\pi}\sigma}e^{-(x-\mu)^2/(2\sigma^2)}$, meaning that the majority of the calculations required for this formula are already tabulated, making it quick and simple to calculate.

The value $p(r\not<D|C_i)$ is the probability that no range reading less than the one measured D would be received if the cell C_i were occupied. This is calculated by integrating the probability of all ranges less than D.

$$p(r\not<D|C_i)=1-\int_0^D\int_{-\pi}^{\pi}p(r=x|C_i)d\theta dx$$

Due to the fact that $p(r=D|C_i)$ is based on the normal distribution, the integration of it is tabulated, and can be stored for lookup, making it quick to calculate.

3. Mathematical Map Update Methods

Three mathematical methods of integrating the value $P(X,Y)$ from the sonar model with an occupancy grid are examined. The first is a slightly modified version of Moravec and Elfes [2] map update rules, from now on referred to as *Simple Update Formula*. The second is based upon the Bayesian update formula as described in [3], from now on referred to as *Bayesian Update Formula*. The third method is based on the use of log odds as proposed by Konolige in [4], referred to as *Log Update Formula*.

3.1 Simple Update Formula

If the cell at the Cartesian coordinates (x, y) being updated is in the freespace area of the sonar beam, the value $P_E(x, y)$ is generated, which is integrated with the prior probability that the cell is unoccupied, $Emp(x,y)$, using the formula.

$$Emp(x,y)'=Emp(x,y)+P_E(x,y)-Emp(x,y)*P_E(x,y)$$

If the cell is in the occupied area of the sonar beam, the value $P_O(x,y)$ is generated, which is integrated with the prior probability that the cell is occupied. Before that can happen however, the update values of all the cells in the occupied area of the sonar beam are normalised to one. This accounts for the fact that it is assumed that only a single cell on the arc of the beam caused the sound wave to reflect, therefore one cell should have its probability of occupancy set to one. However, as it is not possible to determine which cell caused the reflection, the probability of one is divided amongst all the cells in a weighted distribution.

$$P_O(x,y)=P_O(x,y)/\sum P_O(x,y)$$

The second step integrates $P_O(x,y)$ with the prior probability that the cell is occupied, $Occ(x,y)$ to give a posterior probability that the cell is occupied, $Occ(x,y)'$.

$$Occ(x,y)'=Occ(x,y)+P_O(x,y)-Occ(x,y)*P_O(x,y)$$

Finally, the value stored in the cell is decided based on which value is greater, $Emp(x,y)$ or $Occ(x,y)$.

$$Map(x,y) = \begin{cases} 1 - Emp(x,y) & if\ Emp(x,y) > Occ(x,y) \\ Occ(x,y) & if\ Occ(x,y) > Emp(x,y) \end{cases}$$

3.2 Bayesian Update Formula

This Bayesian Update Formula makes the assumption that the probability of a cell being occupied is one minus the probability of it being empty, and vice-versa, therefore $Occ(x,y) = 1 - Emp(x,y) = Map(x,y)$. If the cell is in the freespace area of the sonar beam, the value $P_E(x,y)$ is generated.

The first step is to translate $P_E(x,y)$ so that rather than representing the probability that a cell is unoccupied using number is the range [0..1], the range of numbers [0..0.5] is used, where zero means that the cell is definitely empty, and 0.5 means there is no information about the cell.

$$P_E(x,y)' = (1 - P_E(x,y))/2$$

$P_E(x,y)$ is then integrated with the prior value of the cell using the equation below, the Bayesian probabilistic update formula.

$$Map(x,y) = \frac{P_E(x,y) * Map(x,y)}{P_E(x,y) * Map(x,y) + (1 - P_E(x,y)) * (1 - Map(x,y))}$$

A similar procedure is performed on an update on a cell in the occupied area of the beam. First $P_O(x,y)$ is translated from the range [0..1] to [0.5..1], where 0.5 represents a lack of knowledge about the cell, and 1 means the cell is definitely occupied.

$$P_O(x,y)' = 0.5 + P_O(x,y)/2$$

Finally the map is updated with the new value.

$$Map(x,y) = \frac{P_O(x,y) * Map(x,y)}{P_O(x,y) * Map(x,y) + (1 - P_o(x,y)) * (1 - Map(x,y))}$$

3.3 Log Update Method

The Log Update Method uses a multiplication to integrate new values from the sonar model with *a priori* information, and then combines the probabilities of the cell being occupied and empty using logarithms and addition. Because of the use of multiplication, it is required for $P_O(x,y)$ to be translated to a number greater than one, and for $P_E(x,y)$ to be translated in a similar manner to a number less than one. This ensures that a surface reading causes the overall value to rise, while a freespace reading causes it to fall.

$$P_E(x,y) = 1 - P_E(x,y)$$
$$P_O(x,y) = 1 + P_O(x,y)$$

$P_E(x,y)$ and $P_O(x,y)$ are then integrated with the prior information using multiplication.

$$Emp(x,y)' = Emp(x,y) * P_E(x,y)$$
$$Occ(x,y)' = Occ(x,y) * P_O(x,y)$$

Finally, the freespace and surface values are combined to form the map using logarithms and addition.

$$Map(x,y) = \log_{10}(Emp(x,y)) * \log_{10}(Occ(x,y))$$

Unlike the previous two mathematical update methods, the Log Update Method does not map values into a range [0..1]. For this reason a cut off value must be set at which it can be said that a cell is definitely occupied, and another value at which the cell is definitely unoccupied. In the experimental results presented in section six, a range of [-2..+2] was used.

4. Benchmarking Techniques Used

A suite of benchmarking techniques published in [6,7] have been applied to 126 maps generated with all sonar models and mathematical update methods. Both simulated and in real world environments were utilised. Each of the maps generated in the course of experimentation are compared against hand drawn ideal maps of the environment the robot traversed. A complete listing of all environments, benchmarks, and procedures followed can be obtained from [7]. All sonar models and mathematical methods were tested using identical sensor and motor data to facilitate an accurate comparison.

The four tests are as follows:

1. Correlation. A higher percentage indicates a greater degree of similarity between the maps.
2. Map Score. A technique proposed in [5] which calculates the difference between two maps. The lower the percentage difference, the greater the similarity between the two maps.
3. Map Score of Occupied Cells. Similar to the previous benchmark, but only tests those cells that are occupied, i.e. >0.5 in one or both of the maps being tested
4. Path Comparison For False Positive Paths. Calculates the percentage of paths in the map which would cause a robot to collide with an obstacle. The lower the percentage, the fewer paths would cause a collision, and therefore the better the map.

5. Experimental Results

Table 1: Sonar model experimentation results

	Correlation	Map Score	Map Score Occupied Cells	Path Comparison False Positives
2DG Model	53.11%	16.50%	11.65%	64.20%
Multiple Target Model	63.33%	13.50%	10.48%	42.70%

Table 2. Mathematical map update formulae Results

	Correlation	Map Score	Map Score Occupied Cells	Path Comparison False Positives
Simple Update	56.70%	16.57%	11.11%	62.54%
Bayesian Update	55.34%	16.44 %	12.19%	65.85%
Log Update	63.33%	13.50%	10.48%	42.69%

6. Discussion

When comparing the results of the two sonar models, the Multiple Target Model consistently performed better than the Two Dimensional Gaussian Model. The Correlation and Path Comparison benchmarks showed the most improvement. The Correlation benchmark shows the maps built more than a 10% increase in similarity with the ideal hand-drawn map. The Path Comparison benchmark shows the most dramatic improvement, with 22% fewer paths leading to collision with an obstacle. These results clearly demonstrate that the Multiple Target Model performs significantly better than the Two Dimensional Gaussian Model. This is largely due to the fact that it updates the map in much smaller increments than the 2DG model. Whereas the 2DG model can cause a cell to go from a freespace probability of zero to a probability of one with just two or three range readings, the Multiple Target Model updates the map much more gradually, usually requiring twenty or thirty freespace readings at a cell before its freespace probability converges to its maximum value. This more gradual update approach means the map is less affected by erroneous sonar readings, as a single noisy reading does not affect the map to a large degree, and can be corrected later by accurate range readings.

The results for the mathematical map update methods are not quite as clear as those of the sonar models. The Simple Update and Bayesian Update methods perform more or less identically in the benchmarks, despite the fact that they use considerably different mathematics to update the map. While the Bayesian Update method is more mathematically robust than the Simple Update, it offers no advantage over the Simple Update other than mathematical elegance. The Log Update performs considerably better than both other update methods, with an 8% increase in Correlation, and a huge improvement of 20% in the Path Comparison benchmark. This result is highly dependant on the Min/Max threshold values chosen for the map however. If a higher maximum value is chosen then obstacles will not be recognised as quickly, whereas if a lower maximum value is used, then surface areas may be given over generous updates. The same holds true for the minimum threshold. It is possible that a Min/Max threshold that results in acceptable performance in one environment may not perform as well is another environment with different levels of noise. That being said however, if a method exists to estimate the noisiness of an environment, the Multiple Target Model can then be tuned for that environment, making it a highly adaptable sonar model.

7. References

[1] Crowley, J. L. (1985). Navigation for an Intelligent Mobile Robot. IEEE Journal of Robotics and Automation 1:31-41

[2] Moravec, H. P., Elfes, A. (1985). High Resolution Maps from Wide Angle Sonar. In Procs. of the 1985 IEEE Int. Conf. on Robotics and Automation.

[3] Matthies, L., Elfes, A. (1988). Integration of Sonar and Stereo Range Data Using a Grid-Based Representation. In Procs. of the 1988 IEEE Int. Conf. on Robotics and Automation.

[4] Konolige, K. (1997). Improved Occupancy Grids for Map Building. Autonomous Robots 4(4): 351-367.

[5] Martin, M. C., Moravec, H.P. (1996). Robot Evidence Grids. CMU Technical Report CMU-RI-TR-96-06, Robotics Institute, Carnegie Mellon University, Pittsburgh, Pennsylvania.

[6] Collins, J. J., O'Sullivan, S., Mansfield, M., Eaton, M., Haskett, D. (2004). Developing an extensible benchmarking framework for map building paradigms. In Procs. Of the 9th Int. Symp. on Artificial Life and Robots, Japan, 2004.

[7] O'Sullivan, S. 2003. An Empirical Evaluation Of Map Building Methodologies in Mobile Robotics Using The Feature Prediction Sonar Noise Filter And Metric Grid Map Benchmarking Suite. MSc Thesis, University of Limerick, Ireland.

Proc. of The Ninth Int. Symp. on Artificial Life and Robotics (AROB 9th '04)
Beppu, Oita, Japan, 28-30 January, 2004

Obstacle avoidance strategy for a mobile robot in the guideline navigation

Jiwu Wang[1] Hidenori Kimura[2,3] Masanori Sugisaka[1,2]

Department of Electrical and Electronics Engineering, Oita University, Oita 870-1192, Japan[1]
The Institute of Physical and Chemical Research (RIKEN), Bio-Mimetric Control Research Center,
Shimoshidami, Moriyama-ku Nagoya, 463-0003, Japan[2]
Department of Complexity Science and Engineering Graduate School of Frontier Science,
The University of Tokyo, Tokyo 113-8656, Japan[3]
Email: wangjiwu@cc.oita-u.ac.jp, kimura@crux.t.u-tokyo.ac.jp, msugi@cc.oita-u.ac.jp

Abstract: Obstacle avoidance is a basic skill to make a mobile robot move effectively and safely even in any arbitrarily given environment. Because of the difficulty of self-location caused by unavoidable slip and drift errors of sensors and determination of the three dimensions of an encountered obstacle, only finite and simple obstacle avoidance strategies can be carried out. In this paper we mainly explored how to make a robot perform effectively obstacle avoidance in the guideline navigation with one CCD video camera and some supersonic sensors. Making use of the specially designed guideline, the detection and determination of the geometric dimensions of the encountered obstacle became simpler. And possible avoidance strategies appropriate to our navigation were studied and the simulations results were given.

Key Words: Obstacle avoidance, Mobile robot, Image processing, Guideline navigation

1. Introduction

In the navigation research of a mobile robot, obstacle avoidance is a basic skill that can make the robot move purposely and safely in an environment even with some known or unknown obstacles. Although that function seems easy to a human being, many problems have to be solved before a mobile robot can move freely in such environment. These problems mainly include: the unavoidable slip; the drift errors of sensors; the three dimensional geometry of an obstacle appeared suddenly and its relative position or speed to the robot[1, 3 5]. In a word, they are the robot's self-location and the geometric information of that obstacle. At present stage, for simplification, only static obstacle avoidance was studied.

At first, the robot must have the functions to detect that obstacle and get its geometric information before avoidance. More researchers have explored such problems in this field. One general solution is the sensors based motion planning method, in which information about obstacles is assumed to be obtained from on-line sensors without previous detailed given plan. It is helpful for the navigation in unstructured environments and avoidance of unexpected obstacles, and its navigation strategies are simple. But it will be easily to often make robot miss its original goal and reach its target uneffeciently. Especially, it will make a long distance navigation unefficient or even fail.

The second problem is the mobile robot's self-location. Because of the unavoidable slip and drift errors of sensors, it is difficult to realize accurately self-location especially after a long distance navigation. The perceptual landmark is an effective solution to that problem. But it was generally used as self-location adjustment in some local areas. Because the obstacles will appear any spot along its moving trace, it makes self-location more difficult[2,3,4].

On the other hand, all control strategies were designed based on the robot's physical structure and behavior abilities. Their output actions were planned from the mapping information of sensor's feedback. Till now it is nearly impossible to consider all practical environment settings. That means we can not design a robot with enough sensors to get all necessary information. Furthermore, the sensor's error can not be avoided and some

information processing algorithms of sensors are still be explored. Therefore, the only sensors based motion planning strategies are not comprehensive. It is necessary to build a flexible system for some special applications.

In view of above problems, we explored the mobile robot's navigation with obstacle avoidance in this paper. Our robot has two CCD video cameras, but only one was used in our research. It has six supersonic sensors for obstacle detection which can detect objects less than 0.5 meter in its vertical direction. On the front side, two supersonic sensors were set on each end respectively. The same arrangement was done on the left and right sides. In order to realize reliable self-location in its navigation, we design a continuous visual landmark and put it on the floor as the robot's moving trace. Thus the obstacle avoidance becomes how to avoid obstacles on the guideline.

With the continuous guideline, the robot can adjust its relative position gradually and make the navigation more efficiently even if there is obstacle avoidance. At the same time it is helpful for obstacle detection. This is because parts of the guideline will disappear if there are something on the guideline. And if the obstacle is near to the guideline, the relative position can be determined by the supersonic sensor and CCD video camera together. Most of important, compared with other sersors based obstacle avoidance, the robot will not miss its navigation direction after the obstacle avoidance because of the guideline setting. Because the guideline will occupy some fixed areas in the navigation space, the obstacle avoidance has to be carried out in the residual areas. This makes some bigger obstacle avoidance impossible.

In this paper, by using gradient runs based guideline detection technique, we can find guideline effeciently even under poor lighting conditions. Thus we can indirectly detect obstacles on or near the guideline. Cooperated with the detection results of the supersonic sensors, the robot will know the approximate dimensions of that obstacle. At last, the robot will whether to carry out the obstacle avoidance or not based on the obstacle avoidance strategies. And some simulation results were given.

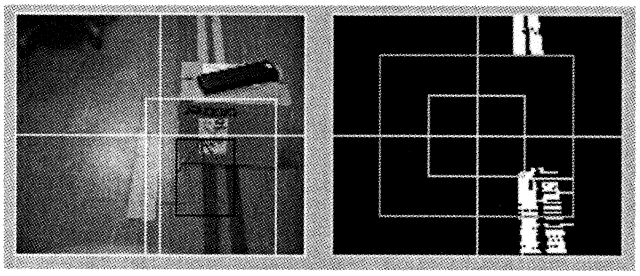
2. Obstacle detection

In order to carry out obstacle avoidance effectively, the robot must detect that obstacle firstly. The best way is to obtain the three dimensional geometric information of that obstacle. Till now, it is possible to get such data by special hardware settings. But it is still more difficult to directly apply that technique in practical long distance navigation at higher speed. This is mainly because its efficiency and accuracy sometimes are not satisfied.

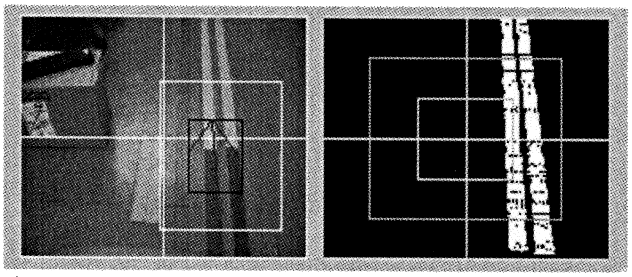
In this paper, we detect the obstacle and determine its necessary dimensions for avoidance by the cooperation of a CCD video camera and six supersonic sensors. Here with a CCD video camera we indirectly detect the obstacle and then determine its necessary dimensions by corresponding supersonic sensors.

In order to make obstacle detection more robust, the guideline must be extracted effectively under various lighting conditions. Thus the obstacle will be judged indirectly when some parts of the guideline disappeared or the guideline became discontinuous. Because the robot will gradually adjust its position relative to the guideline, some low level image processing technique was used for perceptual landmarks extraction. It can effectively save the time for image processing, but sometimes detection was not so robust under different lighting conditions.

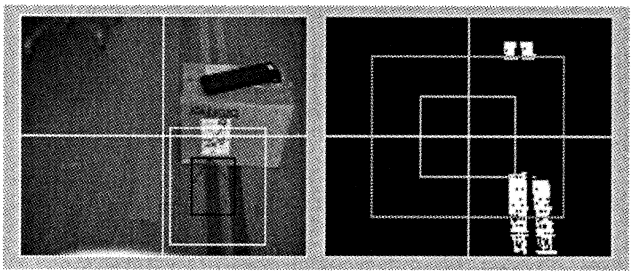
In this paper gradient runs based target detection technique was used for guideline extraction. As we know, there are the gradients everywhere in an image. If we use the guideline with strong color contrast with the floor, it is easy to extract it even under poor lighting conditions. The experiments under different lighting also gave the same results in figure 1. In the figure 1, we can find some parts of the extracted guideline missed when there is a box on the guideline no mater that it is under the normal or poor lighting condition. On the other hand, it is important to have a robust image processing for guideline extraction. Otherwise, it is difficult to make obstacle detection reliabile.



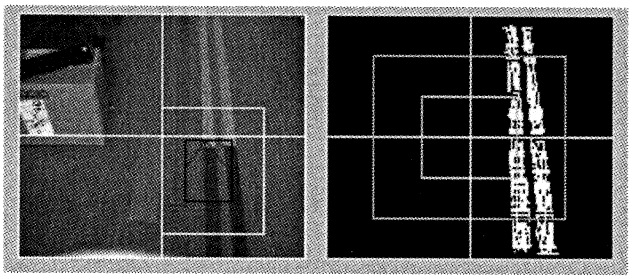
1) Obstacle detection under the normal lighting condition



2) Guideline extraction under the normal lighting condition



3) Obstacle detection under the poor lighting condition



4) Guideline extraction under the poor lighting condition

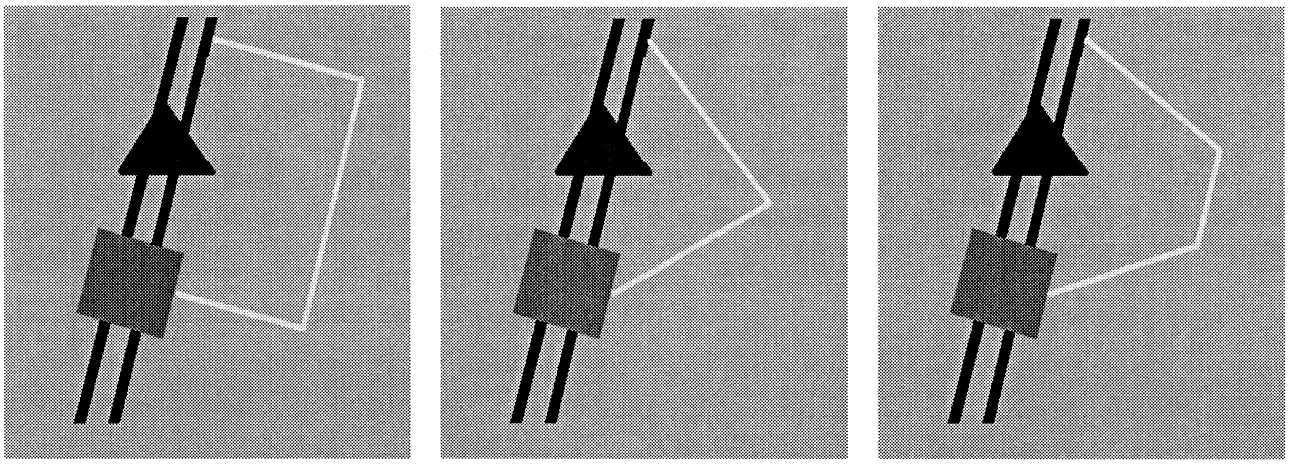
Figure 1 Illustration on the comparision of the obstacle detection under different lighting conditions

Till now, it is not possible to develop the direct and effective image processing for various obstacle detection. That means we can not calculate the necessary geometric dimensions of the encountered obstacles. Here the supersonic sensors were used for detection the width and length of the obstacles. In the front side of the robot, the distance between the two supersonic sensors is nearly the same as the width of the robot. If both of the two supersonic sensors detect obstacle, the width of that obstacle will be larger than the width of the robot. Because the residual space is smaller for avoidance, the robot can not avoid that obstacle. Therefore, now the robot is only possible to avoid some obstacle when only one of the frontal supersonic sensors detected obstacle. The distance between two supersonic sensors on the left or right side is equal to the length of the robot. Thus when the robot passes the obstacle, it will start when the first sensor detected the obstacle and end when two sensors can not detect the obstacle. Those data now are enough for our obstacle avoidance strategies.

3. Obstacle avoidance strategy

Because the robot will move along the guideline put on the floor, it can not avoid all encountered obstacles. The possibility of obstacle avoidance is determined by the maximum width of the residual free space for obstacle avoidance and the width of the robot. If the residual maximum width is larger than the width of the robot, the robot will generally perform three categories of obstacle avoidance in figure 2. In figure 2, the two blue lines represent the guideline, the yellow line is the obstacle avoidance moving trace, the red triangle represents one obstacle and the green rectangle represents the mobile robot.

The three types of obstacle avoidance was determined by the moving efficiency and considering the errors of the sensors. If the obstacle is small in length, the triangle avoidance moving trace is better. If the length of the obstacle is large, the trapezoid moving trace is better. And the rectangle moving trace is easier for the control system. In fact, because of the errors of sensors, it is nearly impossible to make robot move accurately along the given trace. Compared with other two moving trace, although the rectangle is not efficient in theory, it is more effective in practical applications. This is because it is more flexible so that it can reduce the influence of the errors of sensors.

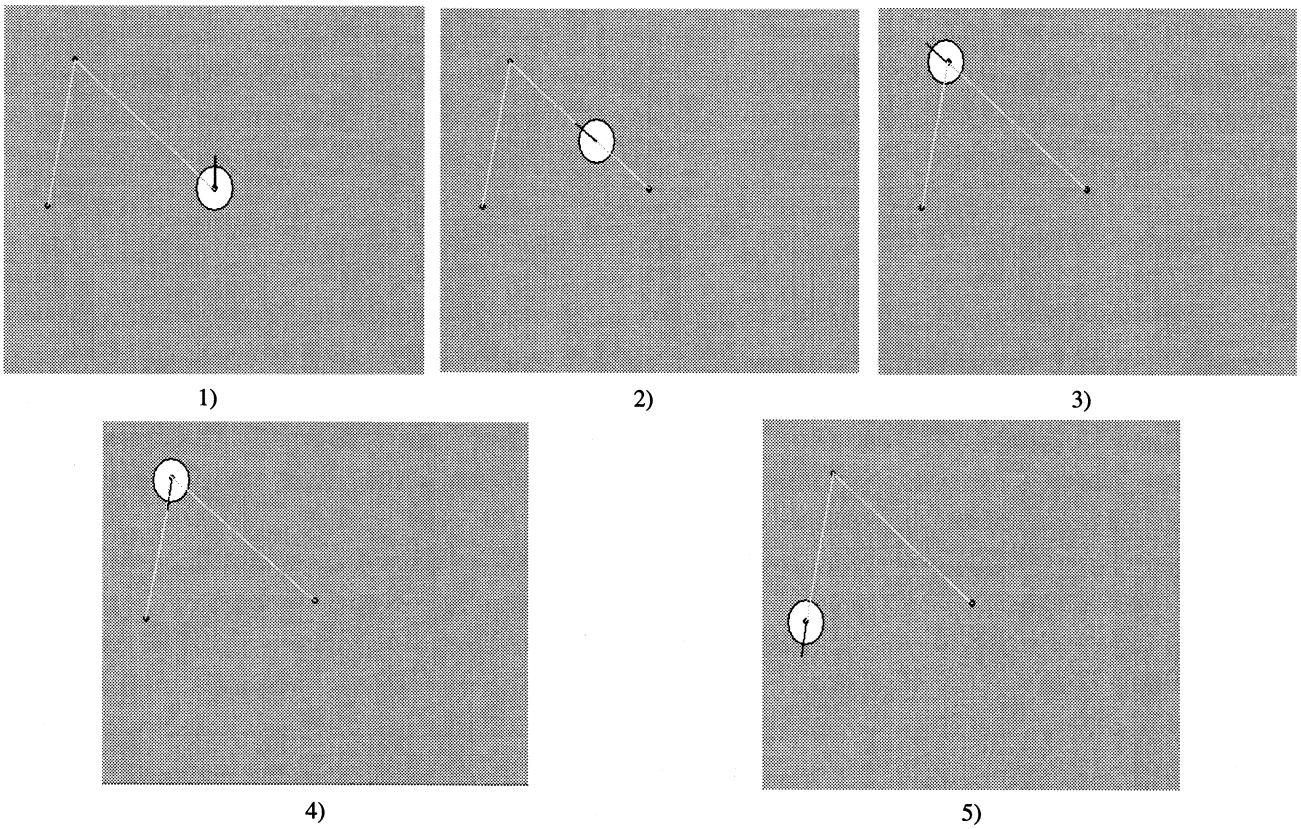


1) Rectangle 2) Triangle 3) Trapezoid

Figure 2 An illustration of the strategies of the obstacle avoidance

4. Simulation

When we developed the navigation system for our mobile robot, we also developed a simulation system with the same control theory. Although it is impossible to consider all factors of practical applications in the simulation system, some developed algorithms can be tested before practical experiments and give some necessary simulation results and optimization parameters for some specified working conditions. In the following figure 3, we give some simulation results for normal navigation without obstacle on its navigation trace. The yellow line is the specified navigation trace, the red point represents target point, the blue circle represtns the robot and its blue line is robot's frontal side. The moving sequence was the same as the marked number.



1) 2) 3)

4) 5)

Figure 3 Simulation on the curve navigation without obstacle

In figure 4, it is an illustration for obstacle avoidance. The black point represents the obstacle, the green line is the obstacle avoidance trace, others are the same as the meaning as those in figure 3. When the robot performs the obstacle avoidance, it try to find the short trace for obstacle avoidance. In figure 4, we only gave the case for triangle obstacle avoidance trace. The other two are similar to the triangle trace.

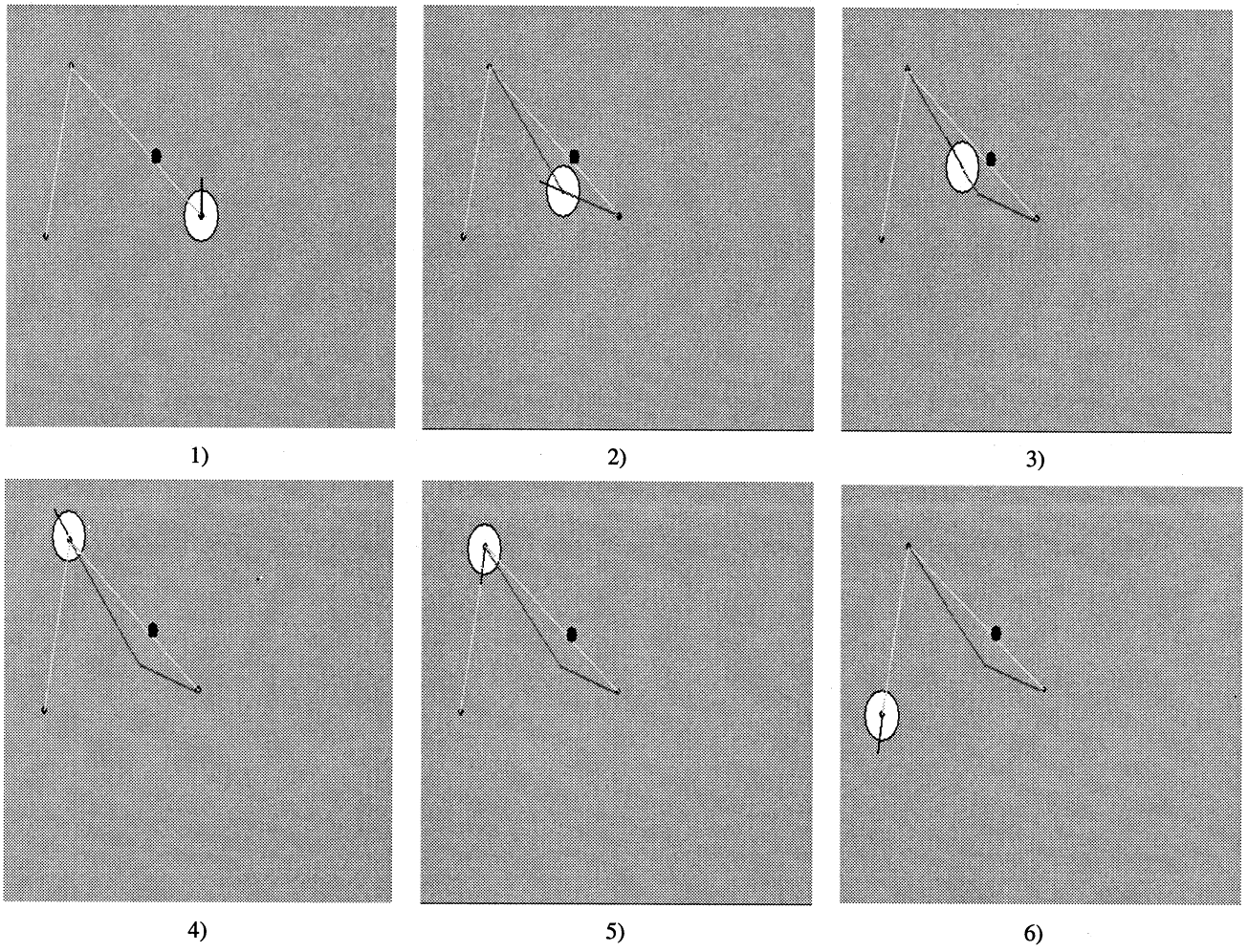


Figure 4 Simulation on the cruve navigation with obstacle avoidance

5. Conclusions

The real time obstacle detection and avoidance was carried out for our mobile robot in the guideline navigation by using a CCD video camera and six supersonic sensors. By making use of the guideline to adjust robot's self-location, the obstacle detection became more reliable and simpler if the guideline can be extracted robustly under various lighting conditions. Considering the errors of sensors and the difficulty of the determination of three dimensional geometric information of the encountered obstacle, it is more appropriate to build a flexible obstalce avoidance strategy in the practical application. The experiment results showed the reliability of the obstacle detection method even under the poor lighting condition. And the simulation of the navigation with obstacle avoidance showed how the robot avoided an encountered obstacle.

Reference

[1] Masanori Sugisaka, Xin Wang, Ju-Jung Lee, Intelligent control with new image processing strategy for a mobile vehicle, Artificial life robotics, 1998: 113-118.

[2] J. Wang, M. Sugisaka, Study on a color based target detection technique", Proceedings of 7-th international symposium in artificial life and robotics (AROB 7-th'02), B-Con Plaza, Beppu, Oita, Japan, Jan. 16-18 : 532-536

[3] J. Wang, M. Sugisaka, Study on visual-based indoor navigation for an alife mobile robot, ICSEng2002, Las Vegas, USA, 2002, August 6-8 : 390-396.

[4] J. Wang, M. Sugisaka, Improvement on the image processing for an automous mobile robot with an intelligent control system, International conference on control, automation and system (ICCAS2001), 2001: 437-440

[5] Seydou Soumare, Akihisa Ohya, etc. Real-time obstacle avoidance by an autonomous mobile robot using an active vision sensor and a vertically emitted laser slit, http://www.roboken.esys.tsukuba.ac.jp/ ~ohya/pdf/IAS2002-SUM.pdf

[6] J. Borenstein, Real-time obstacle avoidance for fast mobile robots, IEEE Trans. Syst. Man Cybern., 1989, vol. 19: 1179-1187

[7] A. Ohya, A. Kosaka and A.Kak, Vision-based navigation by a mobile robot with obstacle avoidance using single-camera vision and ultrasonic sensing, IEEE Trans. Robot. Automat., 1998, vol.14: 969-978

[8] K. Yoshida, S.Yokota and I. Watabe, A real-time motion stereo vision based on brightness difference, Proc. IEEE/RSJ IROS 99, 1999, vol1: 77-82

Proc. of The Ninth Int. Symp. on Artificial Life and Robotics (AROB 9th '04)
Beppu, Oita, Japan, 28-30 January, 2004

Fuzzy Obstacle Avoidance and Navigation for Mobile Robot

Masanori SUGISAKA and Renping CHEN
msugi@cc.oita-u.ac.jp, chenrp@cc.oita-u.ac.jp
Department of Electrical & Electronic Engineering, Oita University
700 Dannohara, Oita, 870-1192, Japan

Abstract: The control problem is a well-known problem in the field of robotics. This paper describes an intelligent navigation system for mobile robot based on fuzzy logic. Owing to its simplicity and hence its short response time, the fuzzy navigator is especially suitable for on-line applications with strong real-time requirements. The fuzzy rule-base of the proposed system combines the repelling influence, which is related to the distance and the angle between the robot and nearby obstacles. It can be considered as an on-line local navigation method for mobile robots for the generation of instantaneous collision-free motions. The functioning of the fuzzy navigator with respect to mobile robots and results of simulated experiments are presented.

Keywords: obstacle avoidance, mobile robot, fuzzy logic, local navigation

Introduction

The goal of mobile robotics is to build physical systems that can move purposefully and without human intervention in unmodified environments that is, in real-world environments that have not been specifically engineered for the robot. The development of techniques for autonomous robot navigation constitutes one of the major trends in the current research in robotics. This trend is motivated by the current gap between the available technology and the new application demands. On the one hand, current industrial robots have low flexibility and autonomy: typical, these robots perform pre-programmed sequences of operations in highly constrained environments, and are not able to operate in new environments or to face unexpected situations. On the other hand, there is a clear emerging market for truly autonomous robots. Possible applications include intelligent service robots for offices, hospitals, and factory floors; maintenance robots operating in hazardous or hardly accessible areas; domestic robots for cleaning or entertainment and semi-autonomous vehicles for help to disabled people.

Despite the impressive advances in the field of autonomous robotics in recent years, a number of problems remain. Most of the difficulties originate in the nature of real-world, unstructured environments, and in the large uncertainties that are inherent to these environments. First, prior knowledge about the environment is, in general, incomplete, uncertain, and approximate. For example, maps typically omit some details and temporary features, spatial relations between objects may have changed since the map was built, and the metric information may be imprecise and inaccurate. Second, perceptually acquired information is usually unreliable. The limited range, combined with the effect of environmental features (e.g., occlusion) and of adverse observation conditions (e.g., poor lighting), lead to noisy and imprecise data; and errors in the measurement interpretation process may lead to incorrect beliefs. Third, real-world environments typically have complex and unpredictable dynamics: objects can move, other agents can modify the environment, and relatively stable features may change with time. Finally, the effect of control actions is not completely reliable, e.g. the wheels of a mobile robot may slip resulting in accumulated odometric errors.

Obstacle Avoidance and Navigation Strategy

In developing our strategy we were influenced by Khatib's obstacle avoidance method. The technique is based on a fuzzy-based obstacle

avoidance unit which controls the mobile robot. This unit has three principal inputs:

1) the distance between the robot and the nearest obstacle d_j,
2) the angle between the robot and the nearest obstacle γ_j, and
3) the angle between the robot's direction and the straight line connecting the current position of the robot and the goal configuration $\theta_j = \alpha_j - \beta_j$, where β_j is the angular difference between the straight line connecting the robot's current position and the goal configuration, and α_j is the current direction of the robot (see Figure 1).

The output variable of the unit is the motor command τ_j.

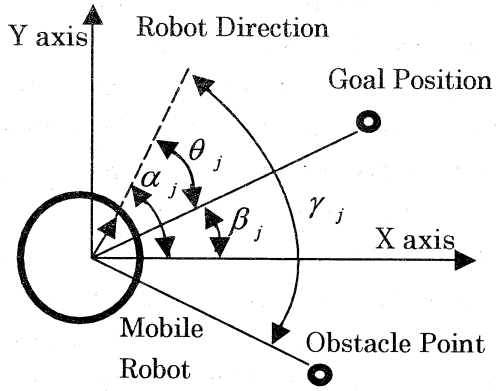


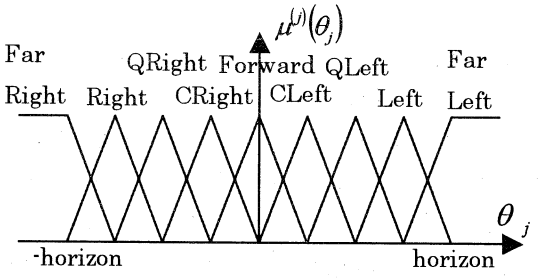
Figure 1 The environment configuration of the mobile robot

For the calculation of the distance, the only obstacles considered are those which fall into a bounded area surrounding the robot and moving along with it. In this implementation, this area is chosen to be a cylindrical volume around the mobile. This area can be seen as a simplified model for the CCD camera. Mobile robots are usually equipped with a pan/tilt platform where a camera is mounted. If no obstacle is detected inside the scan area, the fuzzy unit is informed of an obstacle in the far distance.

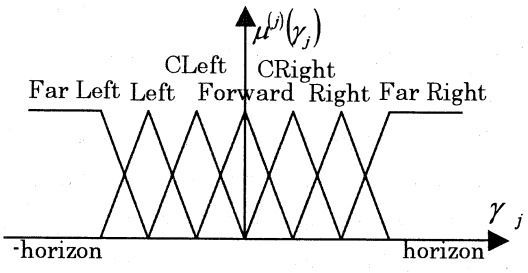
The task of the fuzzy unit is to provide a control function, which produces an appropriate motor command from the given inputs. In broad lines, the control function can be described as follows: on the one hand the function has to lead the mobile robot to its attracting goal-position; on the other hand it has to force the robot to back up when approaching an obstacle which conveys a repelling influence. The fuzzy-rule-base (which represents the control function in the fuzzy unit) is built up by using common sense rules.

The Proposed Fuzzy-algorithm

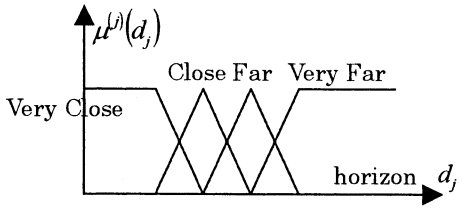
The fuzzy controller in our approach is based on the fuzzy control principles developed. Each input space is partitioned by fuzzy sets as shown in Figure 2. In the literature, a variety of functions can be found which are employed to represent fuzzy sets. Here, asymmetrical triangular and trapezoidal functions which allow a fast computation, essential under real-time conditions, are utilized to describe each fuzzy set. The fuzzy sets of the three inputs *d* are depicted in Figure 2. To calculate the fuzzy intersection, the product operator is employed. The final output of the unit is given by a weighted average over all rules.



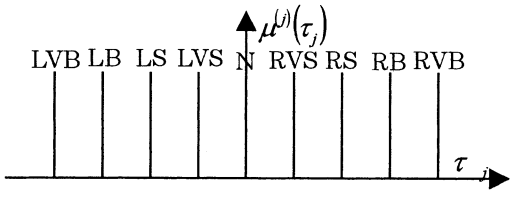
(a) angle between robot and goal position



(b) angle between robot and obstacle



(c) distance to obstacle



(d) motor command

Figure 2 : fuzzy sets for the mobile robot

Intuitively, the rules for obstacle-avoiding navigation can be written as sentences with three antecedents and one conclusion. This structure lends itself to a tabular representation such as the one shown in Table 1. This table represents the prior knowledge of the problem domain. The tools of fuzzy logic allow us to translate this intuitive knowledge into a control system.

ν_j \ μ_j	Very close	Close	Far	Very far
Far right	RB	RS	LVB	LVB
Right	RB	RS	LB	LB
Quite right	RB	RS	LS	LS
Close right	RB	RS	LVS	LVS
Forward	NULL	NULL	NULL	NULL
Close left	RVB	RVS	RVS	RVS
Quite left	RS	RS	RS	RS
Left	RB	RB	RB	RB
Far left	RVB	RVB	RVB	RVB

Table 1: A rule-base for the mobile robot

In fuzzy logic terms, the range of a variable is called the universe of discourse. To translate Table 1 into fuzzy logic, the universe of discourse D_j which describes the distance $d_j \in D_j$ to the obstacle is partitioned by fuzzy sets $\mu_1^{(j)},...,\mu_{p_j}^{j}$, where p_j is the number of fuzzy sets. Since d_j is a measure of distance, it may be considered as a particular fuzzy value of the variable distance and each d_j is assigned a number : $\mu(d_j) \in [0,1]$ which indicates the extent to which this particular d_j is considered to be "*very close*". Similarly, fuzzy sets $\nu_1^{(j)},...,\nu_{q_j}^{(j)}$ can be defined over the universe of discourse Θ_j which represents the distance to the goal: $\theta_j \in \Theta_j$. Finally, fuzzy sets can be defined over the universe of discourse Γ_j that represents the angle to the nearest obstacle $\gamma_j \in \Gamma_j$. Thus, the rule conclusions merely consist of scalars τ_{γ_j}.

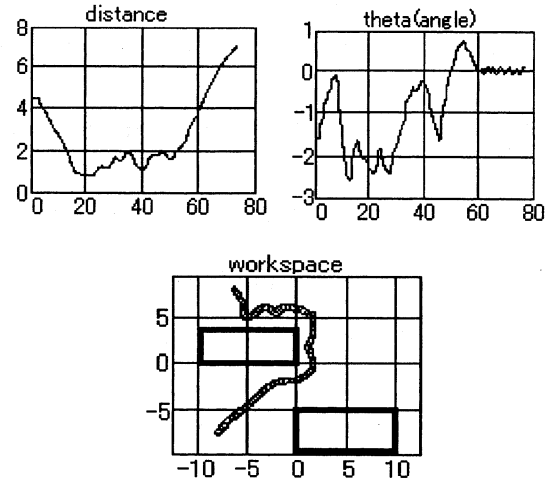
As an example, the control rules for the particular mobile robot are shown in Table 1. In this application, the number of fuzzy sets which fuzzy the obstacle distance d_j, the angle to the goal θ_j and the angle to the nearest obstacle γ_j are chosen to be four, nine and seven, respectively. All the other parameters were refined by trial and error.

Experimental Results

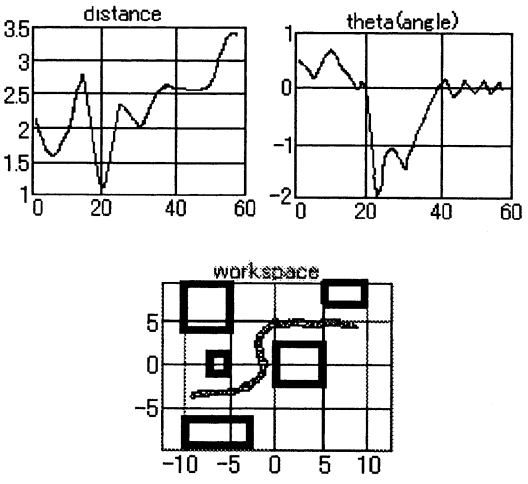
To test the functionality of the basic algorithm, the fuzzy navigator was applied to a simulated our mobile robot. All experiments were carried out on a Personal Computer.

The performance of the fuzzy navigator for the mobile robot was tested in a variety of environments, with different obstacle constellations and working scenarios. In all cases, the fuzzy navigator provided the system with a collision free motion. Simulation results obtained in

two different working scenarios (with different obstacle constellations) are presented in Figure 3.



(a)



(b)

Figure 3: Simulation results using the mobile robot.

The proposed fuzzy navigator was successfully tested for the navigation/ obstacle avoidance problem in two working scenarios with different obstacle constellations (a) and (b), each time providing the mobile robot with a collision-free trajectory.

Conclusions

In this paper, a fuzzy-based navigator has been proposed for the obstacle avoidance and navigation problem in mobile robots. It has been tested in a variety of working scenarios with different obstacle constellations, both static and dynamic, providing each time a collision-free trajectory for the robotic platform. This method has shown a robust and stable performance and the experimental results were very satisfactory.

The difference between our approach and the existing obstacle avoidance techniques is that the proposed navigator considers only the nearest obstacle to decide upon the manipulator's next move. Clearly, this clearly leads to a large reduction in the required remote sensing and computations. A drawback is that, this reduction in information about the robot's environment, leads to an increased possibility of getting trapped to local minima. There may be routes leading to the goal that avoid the obstacles, which our navigator will not be able to find.

The proposed fuzzy navigator is a fast local method that can perform in real time, providing the system with a collision-free trajectory. However, the problem of local minima cannot be ignored. Future work will aim to the design of a hierarchical structure with higher planning levels (e.g. global path planning modules), which will be able to detect these obstacle constellations that lead to local minima and provide the system with an escaping manoeuvre. Also future research should consider the application of neural learning mechanisms to the fuzzy navigator providing an adaptive (neurofuzzy) planner

REFERENCES

Althoefer, K., 1996, Neuro-Fuzzy Path Planning for Robotic Manipulators, PhD Thesis, King's College, London,U.K.

Bison, P.; Chenello, G.; Sossai, C.; Trainito, G., 1997, A Syntactical Approach to Data Fusion, European Conference on Symbolic and Quantitative Approaches to Reasoning and Uncertainty, pp. 58 œ 70.

Brooks, R. A., 1986, A robust Layered Control System for a Mobile Robot, IEEE Journal of Robotics and Automation, RA-2(1), pp. 14 œ 23.

Erdmann, M.; Lozano-Perez, T., 1987, On Multiple Moving Obstacles, Algorithmica 2(4), pp. 477 œ 521.

Proc. of The Ninth Int. Symp. on Artificial Life and Robotics (AROB 9th '04)
Beppu, Oita, Japan, 28-30 January, 2004

Driving Control of Autonomous Vehicle with Vision System using Cell Mediated Immune Algorithm(CMIA) Controller

Young Jin Lee
Department of Electrical Instrument and Control
Korea Aviation Polytechnic College
438, Sachoni, Kyongnam, Korea
airlee@kopo.or.kr

Sang Ki Kim
Department of Electrical Engineering
Dong-A University
840-1, Hadan-dong, Saha-gu, Busan, Korea
smiledu@donga.ac.kr

Jin Ho Suh
Department of Electrical Engineering
Dong-A University
840-1, Hadan-dong, Saha-gu, Busan, Korea
suhgang@hanmai.net

Kwon Soon Lee
Division of Electrical, Electronics & Computer Eng.
Dong-A University
840-1, Hadan-dong, Saha-gu, Busan, Korea
kslee@daunet.donga.ac.kr

Abstract

In this paper, CMIA(Cell Mediated Immune Algorithm) controller based on PID scheme was proposed to control the autonomous guided vehicle(AGV) more effectively. The proposed controller was based on specific immune response of the biological immune system which is the cell mediated immunity. Moreover, we designed an AGV system using in the port and some experiments are shown to verify the performance of the proposed controller. The tracking error of the AGV driving was mainly investigated for this purpose. As a result, the capability of realization and reliability were proved by comparing the response characteristics of the proposed CMIA controllers with those of the conventional PID and NNPID(Neural Network PID) controller.

1. Introduction

AGVs are characterized by highly nonlinear and complex dynamics[1]. So, it is too difficult to control by linear control techniques like conventional PID scheme. However, we can use the PID control technique when it was tuned precisely its parameter which are proportional, integral, and derivative gains. Recently, biological information processing systems such as NN, GA, and ES have been applied engineering fields to design more powerful controller.

In this paper, we wishes to develop new control system that can correspond as being strong in external environment by introducing immunity system to solve difficulty of such PID controller parameter design as accommodative. Cell-mediated immune response is applied using cellular reaction model, but it is real condition that is not so many[2,3]. Therefore, we used neural network identification techniques to model the AGV system to overcome nonlinearity and complexity. The tracking error of the AGV driving was mainly investigated for this purpose. As a result, the capability of realization and reliability were proved by comparing the response characteristics of the proposed CMIA controllers with those of the conventional PID and NNPID(Neural Network PID) controller.

2. Autonomous guided vehicle with vision system

We construct an AGV experimantal system used in the port and some experiments are shown to verify the performance of the proposed controller. The AGV is consist of 4 parts which is control department, drive department, communications department and sensor department greatly. First, control department is composed two parts which are personal computer(PC) and 80C196 microprocessor to control AGV system again. PC is composed Pentium 586Ⅲ, and run main monitoring program that can process image information sensing the driving line form vision sensor. Also, information about traveling by driving displacement error that get from reflex acquired in PC composed to be transmitted by 80C196 through RS232 communication and exchanges necessary information in controller drive.

In the 80C196 microprocessor, each control algorithm is proceeded, it can get the speed data and steering data form each sensor, and generate drive signaling for each motor. Figure 1 displays AGV's whole system that has composition such as above structure.

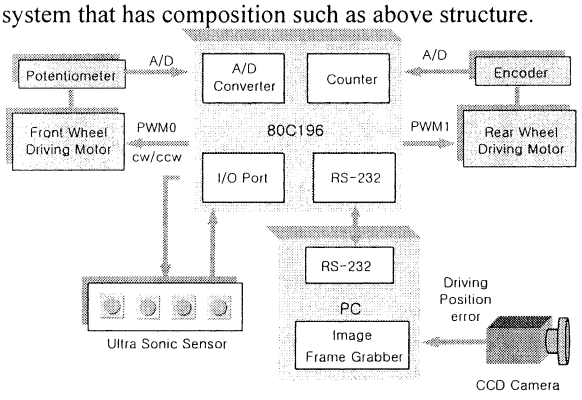


Fig. 1 The AGV system scheme

Generally various sensors(magnetic, ultrasonic and infrared sensor etc.) are used to detect the path trajectory or recognize the obstacle. The steering angle of AGV can be calculated using measured values from the data of sensors. Here, we used the vision sensor to recognize the guideline of AGV's location information of traveling by driving path. That is, we utilized sensor to get error about guideline and relative location with AGV and angle that is guide.

Figure 2 shows process to get relative displacement error e_d and angle error α to decide Reference steering angle δ in image information. To get δ, we feedback the displacement error and we feed forward the angle error of guide line with estimate element.

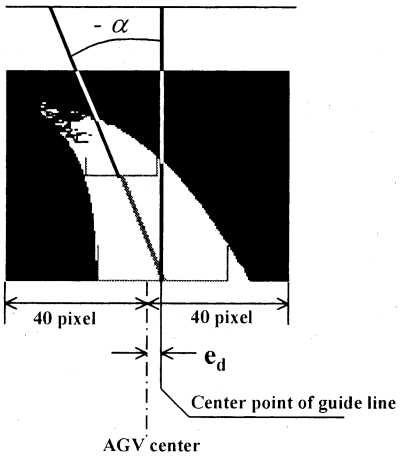


Fig. 2 The relative errors of distance and angle between the AGV and guideline

Being the setting speed regulates R_{speed}, if AGV's speed increases, ration that angle error occupies increases more than displacement error, and did so that put and calculate weight in displacement error relatively if the speed decreases. Also, we did get δ from scaling of whole value of part that become feed forward and feedback by gains K. Through these process, standard steering angle δ can be shown follow equation (1).

$$\delta = K\left\{\left(\frac{e_d}{R_{speed}}\right) + (R_{speed} \cdot \alpha\right\} \tag{1}$$

3. Design of CMIA Controller

3.1. Cell-mediated immune response

The relation of cell-mediated immunity(CMI) is deep with main meals cell and T cell. T cell is consisted of three parts(T_s, T_h, T_c) greatly, and T_s controls immune response, and T_h helps, and T_k acts role that destroy pathogenic bacteria directly. Analogously, Macrophages stimulates humoral immunity cooperating with T cell, and Macrophages activated does strong Phagocytosis. Except complement great Phagocyte, T cell and antibody role that destroy province and pathogenic bacteria directly do. Specially, main reaction mechanism can appear as follow figure 3. As show in figure 3, if antigen(Ag) is invaded from outside, antigen presenting cell(APC) that act role that inform truth tainted from these secretes interleukin-1(IL-1) and pass the information to T_h. This time, T_h is being activated and then stimulate B cell, T_k cell and Ts by secreting interleukin-2(IL-2). Also, Ts acts the role of control mechanism that secrete TSF(T-Suppressor Factor) and control T_h, B cell, T_k's excitement. Through above control process, immunity system has function that recover state that stabilize and protect own from stuff and material simultaneously invaded from outside[4].

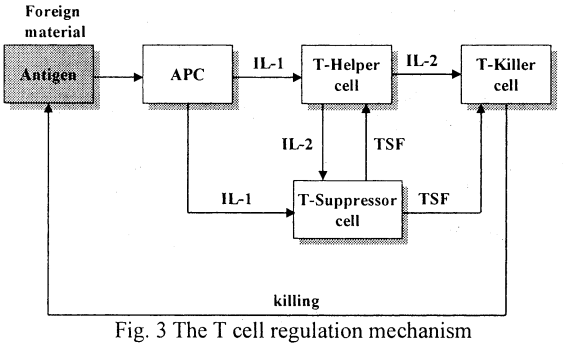


Fig. 3 The T cell regulation mechanism

Therefore, we wishes to design intelligence control construction with more adaptability and flexibility in dynamic environment using modeling mathematically self-adjustment process of this immunity system.

3.2. Design of the CMIA controller

Cellular Molecular Kinetics model becomes basis of all immune response as being based to conservation law or mass action principle of chemistry[5,6]. Recently, mathematical model of cancer-immunity is reported based on this cellular molecular kinetics. Immune response process with antigen and T cell can be modeled from cellular molecular kinetics equation. That is, we can get model such as equation (2) if consider reaction mechanism for only T cell from that kinetics[7,5].

$$\begin{aligned}
\frac{dx_1}{dt} &= p_1 x_1 - \frac{x_1}{\tau_1} - p_{31} x_1 \\
\frac{dx_2}{dt} &= p_2 x_2 - \frac{x_2}{\tau_2} - p_{31} x_2 \\
\frac{dx_3}{dt} &= p_3 x_3 - \frac{x_3}{\tau_3} - p_{31} x_3 \\
\frac{dx_4}{dt} &= p_4 x_4 - \frac{x_4}{\tau_4} - p_{31} x_4
\end{aligned} \tag{2}$$

Here, x_1, x_2 and x_3 displays T_h, T_k and T_s cell respectively, and x_4 displays antigen. Also, p_i is each cell and growth coefficient of antigen, and p_{23} and p_{24} are cell activation coefficient that express degree of reaction which T_s' control element and T_k for each other cell remove antigen. All these act role that control military expedition of immune response.

In this paper, we designed CMIA controller through some assumption from equation (2). First, T_k can suppose antigen that do destruction by fire and part that remove and remainder T_h and Ts help this or acts role that control acting directly in antigen in actuality immune system. Therefore, if antigen $\varepsilon(t)$ that is invasion material from outside on t times time is happened, occurrence of external material is informed by APC in immunocyte in living body. From this T_h and T_s according to proliferating function by equation (3) and

(4) stimulus and control and immune response consists [2].

$$P(\varepsilon) = H_{\max} + \frac{H_{\min} - H_{\max}}{1 + \left(\frac{\varepsilon(t)}{C_h}\right)^{g_k}} \quad (3)$$

$$TSF(\Delta T_k) = S_{\max} + \frac{S_{\min} - S_{\max}}{1 + \left(\frac{\Delta T_k}{C_S}\right)^{g_k}} \quad (4)$$

Here, $P(\varepsilon)$ and $TSF(\Delta T_k)$ display cell activation function and cell control function respectively.

ε (t) display the antigen and H_{max}, H_{min}, S_{max} and S_{min} that is external invasion material expresses the necessary maximum smallest reaction amount in cell growth. They can fluctuate by ratio according to the external invasion amount and ΔT_k as that antigen. Also, C_h, g_h, C_s, and g_s are parameters about cellular growth speed. Each cell(T_h, T_s, T_k) can consist immune response by these two equations (3) and (4). Also, if focus to truth that it is T_k that act opposing directly in antigen in immunity reaction, T_k can display equation (5) because T_k is regulated by $P(\varepsilon)$ and $TSF(\Delta T_k)$.

$$T_k(t) = K_k\{P(\varepsilon) - TSF(\Delta T_k)\} \quad (5)$$

Here, T_k depends on $\varepsilon(t)$ change amount and T_h and T_s' regulation amount as antigen delete cell, and K_k displays T_k's growth element. Figure 4 displays control mechanism of T cells.

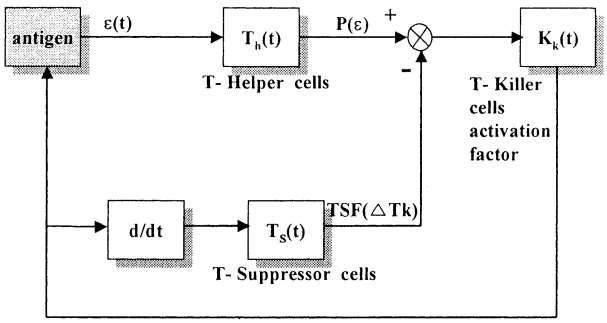


Fig. 4 The T-cells regulation mechanisms based on the CMI

Therefore, this immune response can act role that control antigen that invade from outside being regulated spontaneously in the body interior and is kept the body in stable state. Also, cell activation function and control function of equation (3) and (4) can be considered as design parameter that decide performance of controller. Equation (4) of $T_k(t)$ can be considered by control amount $U(t)$ that control system in engineering field because $T_k(t)$ acts role that remove this fighting directly with antigen. This time, ΔT_k can be thought as $\Delta U(t)$ that is control amount change of controller and ε(t) can appear by $e(t)$ that is system output error and K_k that is T_k's growth element can be considered to scale factor of controller. From these results, we can design of the controller using cell-mediated immunity as equation (6) from similarity with cell-mediated immune response and PID controller.

$$\begin{aligned} U_{CMIA}(t) &= K_1\{P_P(e) - TSF_P(\Delta u)\}e(t) \\ &+ K_2\left\{P_I\left(\int e\right) - TSF_I(\Delta u)\right\}\int e(t) \\ &+ K_3\{P_D(\Delta e) - TSF_D(\Delta u)\}\frac{de(t)}{dt} \end{aligned} \quad (6)$$

Here, K_1, K_2, K_3 are scale element of control gains, and , $P(\cdot)$ is considered proliferating factor of the control amount, $TSF(\cdot)$ is considered suppression factor compared with proportional, derivative, and integral terms in the controller parts. Also, that must satisfy next conditions to act within area that controller is robust, K_1, K_2, $K_3 > 0$ and $P(\cdot)>0$, and satisfy $TSF(\cdot) \geq 0$'s condition H_{max} and $S_{max} > 0$, H_{min}, S_{min} are 0 and C_h, $C_s > 0$ become must. Our designed control system can be guaranteed in the convergency and stability under these conditions.

3.3. Optimal Design of the CMIA controller using NN

In this paper, we used neural network identification techniques to model at AGV system with nonlinearity. This technique has function that can forecast future output from learning past information. We can get more approximation modeling of the AGV system without complicated classical mathematical modeling process. We used the structure of neural network with parallel modeling structure[6].

Neural network of the AGV is embodied steering system and speed system respectively. For input data, we used the PWM signal about input voltage 12[V]s. For output data, we used A/D and counter value. The structure of neural network for learning is used multi layer neural network. Also, identity function is used for activation function to decide Neuron's reaction degree when learning. 700 Pattern number, and 5 input layers and 7 hidden layers are used for neural network identifier of the AGV. The learning rate is 0.9 and momentum value is 0.3. Averages of whole percent error for neural network identification were about 15 [%]. However, case of thing outside that modeling error is big in maximum value can know that error is not happened almost. Averages of percent error are 6.9 [%].

For CMIA controller that propose in this research, controller parameter include the nonlinear element should be considered when designing. So, regulation of most suitable is required in reply. To tune the controller parameter automatically using HIA(Humoral Immune Algorithm)[7,8]. For CMIA controller design, g_s and g_h put by 1 all to reduce nonlinear element so far as possible. To steering and speed parts including K_1, K_2, K_3 and H_{max} of each function and C_h and S_{max} of $TSF(\Delta u)$ function and C_s necessary everybody 14 parameters adjusting most suitable controller plan. Figure 5 shows auto tuning structure of CMIA controller.

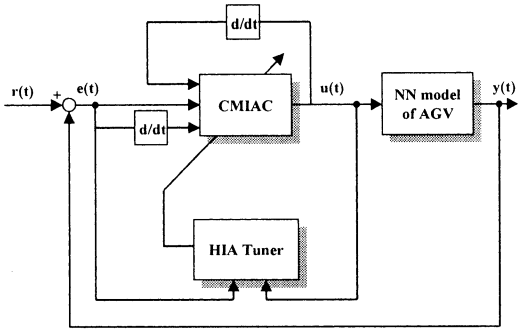


Fig. 5 The HIA tuned CMIA control system using NN

4. Experimental Results

For AGV's travelling by driving experiment, sine wave path is used actually. Figure 6 shows the path and travelling by driving place used in an actuality travelling by driving experiment. Amplitude of travelling by driving path did 1[m] and the line is white with 1[cm] width.

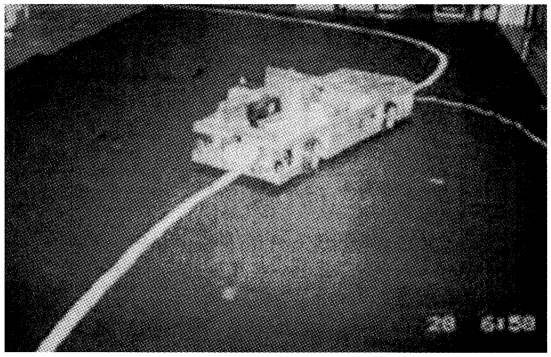
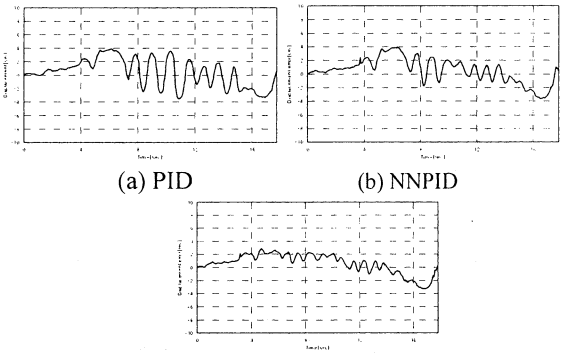

Fig. 6 The photograph of the AGV driving experiments

Figure 7 shows traveling by driving displacement error about PID, NNPID, CMIA control of when driving speed is 0.5[m/sec] with load of 25[kg]s.


(a) PID (b) NNPID

(c) CMIA

Fig. 7 Experiment results (constant load)

As result that achieve an experiment in state that fixed load is applied, proposed CMIA control was improved 17[%]s and 16[%] than PID and NNPID control for the maximum displacement error proposes. Also, displacement error happened averagely in traveling by driving, our CMIA controller was improved 27[%]s and 20[%]s than PID and NNPID control respectively. In the case of the driving speed, we did not appear by picture, but whereas overshoot of about 5.5[%]s of PID control happens, but CMIA controller is improved more than about 60[%] as about 2.5[%] others.

5. Conclusions

In this paper, we designed an experimental AGV systme for using in the port and CMIA(Cell- Mediated Immune Algorithm) controller were proposed to control the AGV more effectively. The proposed controllers were based on specific immune response of the biological immune system that is the cell-mediated immunity.

However, AGV system is highly recommended to enhance the productivity by ensuring the stable and speedy transportation in the ports. On this case, each controller must be designed to have the adaptiveness for the load fluctuation or environmental change. From the experimental result, we can get verification and some improvement for designed AGV and controller. Moreover, because of its adaptiveness of the immune system, proposed CMIA controller performed more effectively than PID and NNPID.

Acknowledgement

This work was supported by the National Research Laboratory Program of the Korean Ministry of Science & Technology (MOST).

References

[1] D. Wang and G. Xu, "Full State Tracking and Internal Dynamics of Nonholonomic Wheeled Mobile Robots," in Proc. Amer. Contro. Conf., pp. 3274-3278, 2000.

[2] K. Takahashi and T. Tamada, "Application of an Immune Feedback Mechanism to Control Systems," *Int. Journal of JSME, Series C*, Vol 41. No. 2, pp. 184-191, 1998.

[3] Y. J. Lee, J. H. Shon, J. W. Lee, H. C. Cho, K. S. Lee, "A desing of IRC using Immune Response Algorithm," ICMT, pp. 389-398, 1999.

[4] I. Roitt, *Essential Immunology*, Blackwell Scientific Publications, 1980.

[5] K. S. Lee, *Mathematical Modeling and the Control of Immune Processes with Application to Cancer*, Ph. D. Dissertation, Oregon State University, 1990.

[6] C. T. Lin and C. S. George Lee, *Neural Fuzzy Systems*, Prentice Hall, 1996.

[7] S. Endoh, N. Toma, and K. Yamada, "Immune Algorithm for n-TSP," *Proc. of the IEEE Int. Conf. on Systems, Man, and Cybernetics*, Vol. 4, pp. 3844-3849, 1998.

[8] J. H. Jun, D. W. Lee, K . B. Sim, "Realization of Cooperative Strategies and Swarm Behavior in Distributed Autonomous Robotic systems using Artificial Immune System," *SMC Proc.*, pp. 614-619, 1999.

Proc. of The Ninth Int. Symp. on Artificial Life and Robotics (AROB 9th '04)
Beppu, Oita, Japan, 28-30 January, 2004

Decentralized Control of Cooperative 3-Wheeled Mobile Robots using Passive Velocity Field Control

- *Adaptive generation method of desired velocity field* -

Jin Ho Suh*, Sang Ki Kim*, Young Jin Lee**, and Kwon Soon Lee†

* Department of Electrical Engineering, Dong-A Univ, Korea, 604-714
** Department of Elec. Instrument and Control, KAPC, Korea, 664-180
† Division of Elecrtical, Electronics, and Computer Eng., Dong-A Univ., Korea, 604-714

Abstract

This paper presents the decentralized control and adaptive generation method of desired velocity field for cooperative mobile robots with passive velocity field control handling a common object in coordination. The proposed control method is constructed by the extended passive velocity field control(PVFC), and a common desired velocity is generated by an initial states. In the design, the stability and boundedness in the resultant system is also guaranteed, moreover, the proposed algorithm is examined by numerical simulations for cooperative tasks. The simulation results illustrate the validity of the proposed control algorithm in this paper.

1 Introduction

Multiple robot systems can execute various tasks which could not be done by a single robot system such as handling of a heavy object. In order to solve these problems, many control algorithms for the coordinated motion of multiple robot systems have been proposed by using *centralized control* and *decentralized control*. The centralized control system may be effective in case of the coordinated motion control of robot systems handling as an object, however, in this case, a single controller is supposed to control all of the robot systems in a centralized way although it is difficult for a single controller to control many robot systems in coordination because of its computational burden. Therefore, a centralized controller is no more realistic to control such number of robot systems. The overcome these problems, several decentralized control algorithm have also been proposed for the manipulation of an object and many research have proposed a decentralized control algorithm for multiple robot systems handling an object in coordination [2].

Moreover, in our previous research [5], we proposed *decentralized PVFC(passive velocity field control) algorithm* for cooperative mobile robot system conveying a common object. This research had proposed how to realize the decentralized PVFC for 3-wheeled cooperative mobile robots using an original PVFC introduced by *Li* [3], that is, we described the realization of specification by a decentralized PVFC controller though a centralized PVFC was applied for the same system. Especially, in this research, we assumed that a desired motion or task was specified as a common desired velocity field in advance and there exists some drawbacks [4]-[5].

In order to overcome some weaknesses for previous researches, we propose an adaptive generation method of desired velocity field for cooperative robot systems. As the motivation of this research, the behavior of the group can be easily specified by the introduction of *leader-follower* robot system with an appropriate initial state. In the decentralized control algorithm, a leader-follower type is one of a control method among decentralized control algorithms. The motion command of an object is given to one of the robots, referred to as a leader, and the other robots, referred to as followers, estimate the motion of the object and control themselves by their own controllers.

In this paper, we will focus on how to realize an adaptive generation of desired velocity field for leader-follower type cooperative robot systems using decentralized PVFC algorithm. The proposed method can guarantee to give a common desired velocity since the desired velocity of a leader and followers converge to an initial velocity field of a leader. Moreover this method can be applied in spite of unknowing the explicit relationship between the magnitude of a common desired velocity and the total energy of the system.

2 Decentralized Passive Velocity Field Control

In the previous research [5], we proposed a method to apply decentralized PVFC with some modifications to cooperative mobile robots and the applied robot systems consisted of two planar mobile robots which convey a common rigid object attached to the robots with passive rotational joints in a horizontal plain as shown in Fig.1. Each mobile robot is a 3-wheeled mobile robot and is the well-known systems with nonholonomic constraints.

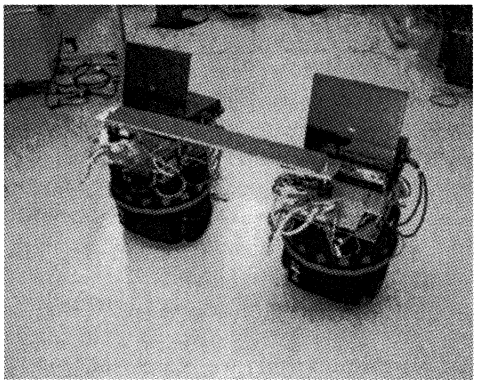


Figure 1: Constructed experimental system

In this research, we assumed that a desired motion and task was specified as a common desired velocity field in advance. In case of some assumption in this research, there exist some drawbacks and it is simply described as follows:

1. Even if we assume that there is a common desired velocity field and the desired velocity field is given by a central controller, we must broadcast all informations to robot systems about desired velocity field before the start motion.

2. We should estimate the desired motion as desired velocity field since each robot system is controlled by decentralized PVFC.

In this paper, we will focus on how to realized the specifications above, it is a decentralized PVFC controller though a centralized PVFC was applied for the same system. Therefore we address an adaptive generation method of desired velocity field for cooperative mobile robots with decentralized PVFC. Moreover a common desired velocity is generated by an initial state of the system and interactions, and the behavior of the system can be specified by an appropriate initial state. That is, we propose an adaptive method which generates a desired velocity field using decentralized PVFC algorithm. Furthermore, the behavior of group for robot systems can be easily specified by the introduction of leader-follower system.

3 Adaptive Generation Algorithm

This section describes the considered dynamic model for leader-follower type cooperative mobile robot systems.

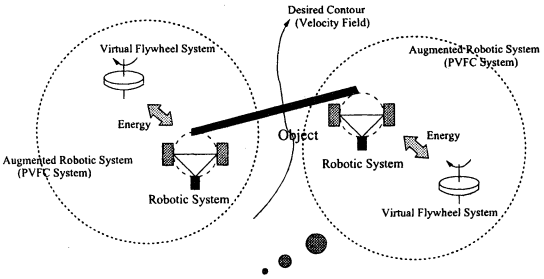


Figure 2: The Considered System Modeling

The considered robot systems is shown in Fig.2 and we assume the following conditions:

1. The coordinated system consists of $n+1$ mobile robots and each mobile robot has m DOF.

2. Each subsystem has own PVFC controller and tip of the moboil robots are kinematically constrainted to an object.

Besides the assumptions we assume that parameters required for the control are all known, however, signals in other subsystems can not be accessed.

We assume that the dynamic equation of a leader and each follower robot system is locally compensated all complex terms including gravity and damping terms. Therefore we can simply represent the dynamic equations of $n+1$ mobile robots with respect to the coordinate of mass center of the object after minor loop compensation as follows:

$$\mu_i M_i \ddot{x} = T_i - F_i, \quad (i = 0, 1, \cdots, n) \tag{1}$$

where x is the coordinate of the mass center of the single object, μ_i is a constant scalar and $\sum_{i=0}^{n} F_i = 0$. Note that M_i, T_i and F_i may be different for each subsystem i, however, x is common [1].

3.1 The desired velocity field

If we consider trajectories which have cross paths, we have to introduce a time-varying desired velocity field. In such a case, a self-pacing to be a virtual time is introduced [3] [4]. The augmented dynamic system of $n+1$ robotic systems can be represented as follows:

$$\begin{bmatrix} \mu_i M_i & 0 & 0 \\ 0 & 1 & 0 \\ 0 & 0 & I_f \end{bmatrix} \begin{bmatrix} \ddot{x} \\ \ddot{s}_i \\ \ddot{\theta}_i \end{bmatrix} = \begin{bmatrix} T_i \\ \tau_{si} \\ \tau_{fi} \end{bmatrix} - \begin{bmatrix} F_i \\ 0 \\ 0 \end{bmatrix} \quad (2)$$

i.e.,

$$M_i^a \ddot{x}_{ai} = T_i^a - F_i^a \quad (3)$$

where T_i^a is a control input of the augmented subsystem and F_i^a is the augmented equivalent constraint force.

Let's assume that the desired velocity field $V_i(x, s_i)$ for the motion of the tip of a leader and ith follower robotic system is given by:

$$V_i(x, s_i) = \sum_{j=1}^{N} w_i^j(s_i)\phi_j(x) = \Phi(x)W_i(s_i) \quad (4)$$

Therefore we can assume the augmented desired velocity fields for a leader and n followers as follows:

$$V_{ai}(x, s_i) = \begin{bmatrix} V_i^T(x, s_i) & 1 & \Omega_i(x, s_i) \end{bmatrix}^T \quad (5)$$

Then, Δ_{ai} of a leader and each n follower can be represented as follows:

$$\begin{aligned} \Delta_{ai} &= M_i^a \frac{\partial V_{ai}}{\partial x_{ai}} \dot{x}_{ai} \\ &= \begin{bmatrix} \mu_i M_i[(\sum_{j=1}^{N} w_i^j \nabla\phi_j)\dot{x} + \Phi\nabla W_i \dot{s}_i] \\ 0 \\ I_f \nabla\Omega_i[(\sum_{j=1}^{N} w_i^j \nabla\phi_j)\dot{x} + \Phi\nabla W_i \dot{s}_i] \end{bmatrix} \end{aligned} \quad (6)$$

The coupling control law of the augmented dynamic system for $n+1$ robotic systems ($i = 0, 1, \cdots, n$) is determined by the following equation:

$$T_i^a = (G_i + \gamma_i R_i)\dot{x}_{ai} \quad (7)$$

where γ_i is the gain, not necessarily positive. When the kinetic energy of the augmented system $H_a(t)$ is defined by $H_a(t) = \frac{1}{2}\sum_{i=0}^{n} \dot{x}_{ai}^T M_i^a \dot{x}_{ai}$, it can be easily shown that the whole dynamic system becomes passive between the external force F_e and $\dot{x}$ in the following sense :

$$\begin{aligned} \int_0^t F_e^T \dot{x} dt &= \int_0^t < F_e, \dot{x} > dt \\ &= H_a(t) - H_a(0) \geq -H_a(0) \end{aligned} \quad (8)$$

where $H_a(t)$ is a storage function.

3.2 Coupling control law for adaptive generation of desired velocity field

To design the adaptive desired velocity field tracking controller, firstly, we consider the following *Lyapunov function candidate*:

$$\begin{aligned} & J(t, e, V_{ai}) \\ &= \frac{1}{4(n+1)} \sum_{i=0}^{n}\sum_{j=0}^{n} (V_{ai} - V_{aj})^T M^{ai} (V_{ai} - V_{aj}) \\ &+ \frac{1}{2}\sum_{i=0}^{n} e_{\alpha i}^T M_i^a e_{\alpha i} + \frac{1}{2}\tilde{W}_0^T \tilde{W}_0 \end{aligned} \quad (9)$$

where $\tilde{W}_0 = W_0 - W_0^0$, W_0 and W_0^0 are a weight function of a leader and a constant weight of a leader, respectively. Moreover, we should note that the inertia matrices, M^{ai} and M_i^a, are different, respectively.

In coupling control law for the augmented dynamic system, we can represent the time derivative of Lyapunov function candidate as follows :

$$\begin{aligned} & \frac{d}{dt} J(t, e, V_{ai}) = \tilde{W}_0^T \dot{W}_0 \\ & + \frac{1}{n+1}\sum_{i=0}^{n} V_{ai}^T \left[\sum_{j=0, j\neq i}^{n} (\Delta_i - \Delta_j) + \alpha(n+1)F_i^a \right] \\ & - \sum_{i=0}^{n} \gamma_i \alpha (4H_{ai}\bar{E}_i - << V_{ai}, \dot{x}_{ai} >>_{ai}^2) \end{aligned} \quad (10)$$

Therefore the best possible way to keep the derivative negative. In this case, we can obtain the solution to satisfy the best possible way as follows:

$$\Delta_i = -\alpha F_i^a, \quad (i = 0, 1, \cdots, n) \quad (11)$$

Theorem 1 *[6] If we use the proposed adaptive generation method with leader-follower type given by projection algorithm, then a common bounded desired velocity of each follower robot is generated and the velocities of the mobile robots asymptotically convergence to a common bounded desired velocity.*

We can simply summarize this result as Theorem 1 implied that all desired velocities of each follower robot converge to a common desired velocity, that is, the adaptation mechanism adjusts the desired velocity field so that all followers $V_i(x, s_i)$ eventually converge to V^* which is a common desired velocity.

4 Simulation Results

The coordinated dynamic system of mobile robots for simulation is shown in Fig.3 based on the constructed experimental system for two Nomad Scouts

and an object which is a wooden plate in [5]. A con-

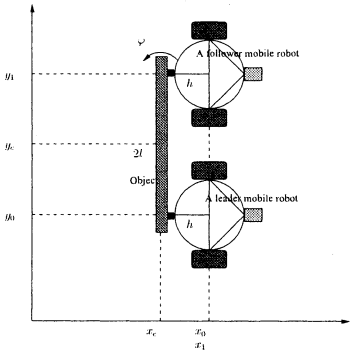


Figure 3: Coordinated Mobile Robots

trol period is assumed $4[msec]$ in order to realize the experimentation and the constraint force is measured through a filter whose transfer function is $\frac{1}{s+10}$. Moreover, since we assume that the whole system is controlled by point-to-point(PTP) command, the basis function for the desired velocity field is given by a gradient of *a Gaussian distribution type function* as :

$$\Phi_i(x) = \sigma^2 \nabla (e^{\frac{\|x-\delta_i\|^2}{2\sigma^2}}) \qquad (12)$$

The center of object follows the desired trajectory as shown in Fig.4 and the tracking performance of the angles for desired signals is shown in Fig.5. It shows good tracking performance for desired angle of object, φ_d. These results show that the desired velocity field of a follower generated by adaptation is exactly tracking the initial desired velocity field of a leader.

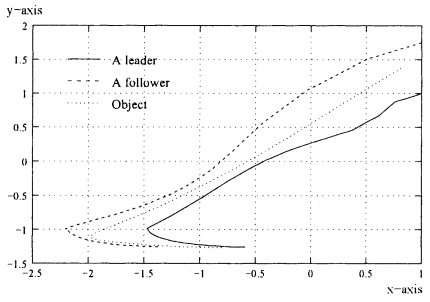


Figure 4: Trajectories of robotic systems and an object

5 Conclusions

In this paper, we proposed an adaptive generation method of desired velocity field of cooperative mobile robots using leader-follower type with decentralized

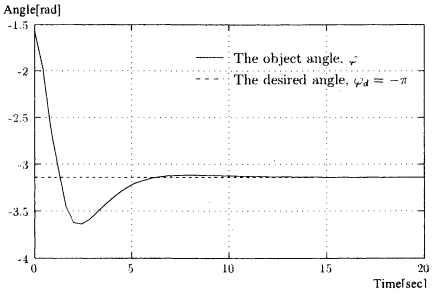


Figure 5: Tracking of the angle of an object φ

passive velocity field control. A common desired velocity field is generated by the initial states of the robotic system and the interactions. Moreover, the stability and boundedness of the resultant system with the proposed control algorithm is also guaranteed.

Acknowledgements

This work was supported by the National Research Laboratory Program of the Korean Ministry of Science and Technology (MOST).

References

[1] P. Hsu, "Adaptive Coordination of Multiple Manipulator System", *Proceedings of IEEE ICRA*, pp.259-264, 1993.

[2] K. Kosuge, et. al., "Decentralized Control of Multiple Manipulators Handling an Object in Coordination Based on Impedance Control of Each Arm", *Proceedings of IEEE IROS*, pp.17-22, 1997.

[3] Perry Y. Li, Roberto Horowitz, "Passive Velocity Field Control of Mechanical Manipulators", *IEEE Trans. on Robotics and Automation*, Vol.15, No.4, pp.751-763, 1999.

[4] M. Yamakita, J. H. Suh, "Adaptive Generation of Desired Velocity Field for Cooperative Mobile Robots with Decentralized PVFC", *Proceedings of IEEE IROS*, 2000.

[5] M. Yamakita, J. H. Suh, and K. Hashiba, "Decentralized PVFC for Cooperative Mobile Robots", *Trans. on IEE Japan*, Vol.120-C, No.7, pp.1485-1491, 2000.

[6] J. H. Suh, M. Yamakita, "A Study on Adaptive Desired Velocity Field Generation for Leader-Follower Type Cooperative 3-Wheeled Mobile Robots with Decentralized PVFC", *Trans. on System, Control, and Information Engineers*, Vol.15, No.9, pp.9-18, 2002.

Proc. of The Ninth Int. Symp. on Artificial Life and Robotics (AROB 9th '04)
Beppu, Oita, Japan, 28-30 January, 2004

Diversity and evolutionary implication of Archaea, the third domain of life

Takashi Itoh
Japan Collection of Microorganisms
RIKEN (The Institute of Physical and Chemical Research)
Wako-shi, Saitama 351-0198, Japan
E-mail: ito@jcm.riken.jp

Abstract

Archaea are prokaryotic microorganisms representing one of the three domains of life. Well-studied, culturable Archaea are represented by methanogens, halophiles and thermophiles, which grow under rather confined growth conditions such as anoxic state, high salinity and high temperature. Their unique phenotypic and genetic properties would be testifying their adaptability to the inhospitable habitats as well as their separate evolutionary status. Besides, recent detection of new groups of Archaea from a variety of terrestrial, freshwater and marine habitats are giving us new insights into the diversity and distribution of Archaea in natural environments. As Archaea have kept antiquated cellular properties and group together on short and deep branches of the universal phylogenetic tree, they may provide good models for understanding of early life forms on Earth.
KEY WORDS: Archaea, methanogens, halophiles, thermophiles, evolution

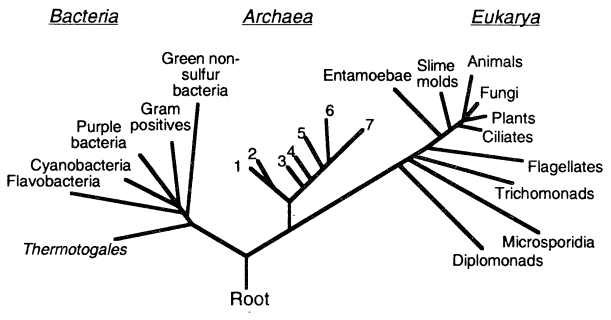


Fig. 1 Rooted universal phylogenetic tree derived from the small subunit rRNA sequences. The domain Archaea comprises two phyla, Crenarchaeota and Euryarchaeota: the former includes *Pyrodictium* (1) and *Thermoproteus* (2), and the latter includes *Thermococcus celer* (3), *Methanococcus* (4), *Methanobacterium* (5), *Methanosarcina* (6) and Halophiles (7). (modified from Wheelis et al.[9])

1 Introduction

In the late 1970's, Woese and colleagues first showed the tripartite division of the living organisms on Earth by analyzing small subunit rRNA[1], leading to the proposal of the three domains of life, Archaea, Bacteria and Eukarya[2]. Archaea and Bacteria are prokaryotic microorganisms, however, Archaea are no more closely related to Bacteria than they are to Eukarya by comparing the rRNA sequences (see Fig. 1). In line with the fact, some genetic features of Archaea (e.g., initiator tRNA, and composition of the DNA-dependent RNA polymerases) seem to be closer to eukaryotic patterns than to bacterial ones. Uniqueness of Archaea is also recognized in their cellular constituents such as membrane lipids composed of isoprenoids ether-liked to the glycerol moiety, and cell envelopes devoid of peptidoglycan. These facts should justify Archaea as organisms evolutionary distinct from Bacteria and Eukarya.

Well-studied lifestyles of Archaea are represented by methanogenic, halophilic and thermophilic Archaea[3,4]. These culturable Archaea inhabit rather confined habitats: however, recent culture-independent molecular ecological studies illustrate that Archaea exist ubiquitously in terrestrial, freshwater, and marine habitats. In this paper, Archaea representing the third domain of life are reviewed from systematic, ecological and evolutionary viewpoints.

1.1 Methanogens

Methanogenic Archaea are extremely oxygen-sensitive, and yield methane via complex methane-synthetic pathways as part of their energy metabolism. They occur widely in anaerobic habitats including marine and lake sediments, intestinal tracts of animals, anaerobic waste digesters, and hydrothermal vent systems.

Methanogenic Archaea usually use a limited number of substrates, like CO_2+H_2, acetate, formate, methanol and methylamines, to reduce to methane. In environments where anoxic decomposition of organic substrates occur, however, methanogenic Archaea serve as the final step of the anoxic carbon cycle, by coupling with other anaerobic bacteria, including the substrate-hydrolytic bacteria, fermentative bacteria, acetogens, and H_2-producing fatty acids oxidizing bacteria.

To date, methanogenic Archaea comprise 27 genera and nearly 100 species. Phylogenetically, all methanogenic Archaea belong to the phylum Euryarchaeota, although, they are heterogeneous being distributed into five different orders. They are also divergent in morphological, physiological and biochemical properties. Interestingly, certain species are extremely halophilic, and some are hyperthermophilic growing optimally more than 80-85 °C.

1.2 Halophiles

Halophilic Archaea thrive in hypersaline environments where NaCl is almost saturated, such as salted fishes, salterns, salt lakes and salted mines. Besides, haloalkalophilic Archaea are encountered in alkaline saline environments such as soda lakes. Halophilic Archaea, except for halophilic methanogens, are aerobic or facultatively anaerobic chemoorganotrophs requiring at least 1.5 M NaCl for growth (3-4 M NaCl for optimal growth). In such a highly osmotic environment, cells of *Halobacterium* accumulate a large amount of K^+ from the environment into the cells to maintain the structural integrity. They contain cartenoids which give their reddish pigments. Under light with low partial pressure of oxygen, certain species synthesize a purple pigment, known as bacteriorhodopsin, which is involved in a light-mediated synthesis of ATP.

Halophilic Archaea are phylogenetically coherent, belonging to a single family Halobacteriaceae in the phylum Euryarchaeota. Owing to the 16S rRNA gene sequences and the polar lipid composition, they are divided into 19 genera. Although alkalophilic members are phenotypically similar to each other, they are phylogenetically diverse, and certain alkalophilic species are closely related to non-alkalophilic species.

1.3 Thermophiles

Thermophiles could be generally characterized as organisms growing optimally at more than 50-60 °C. In Archaea, however, most of them are hyperthermophiles (i.e., grow best at > 80-85 °C). Certain hyperthermophilic Archaea grow even above 100 °C, whereas bacterial species growing at such high temperatures have yet to be discovered. So far, the highest growth temperature of hyperthermophilic Archaea is as high as 120 °C. As a rule, thermophilic Archaea have been isolated from terrestrial and submarine high-temperature environments where geothermal energy is available. Terrestrial habitats include hot springs, mud holes, solfataras and several anthropogenic environments like the wastewater of geothermal plants, whereas submarine habitats include shallow and abyssal hydrothermal vents and geothermally heated sediments. Recently, subterrestrial hot environments, such as geothermally heated deep oil reservoirs, are also recognized as their habitats. Thermophilic Archaea tend to be anaerobic, acidophilic, and/or sulfur-metabolizing in accordance with their growing environments.

Thermophilic Archaea, including 33 non-methanogenic genera and 5 methanogenic genera, are quite diverse phylogenetically, occurring in both phyla, Crenarchaeota and Euryarchaeota. All cultivated Crenarchaeota, represented by three orders, are exclusively thermophilic. Hyperthermophilic Euryarchaeota are located at deep branches on the phylogenetic tree. Two methanogenic orders, i.e., Methanobacteriales and Methanococcales, contain both hyperthermophilic and mesophilic members. The order Thermoplasmatales contains thermoacidophilic members, except for *Ferroplasma*, optimally growing at 60 °C. Notably, an obligately symbiotic hyperthermophilic Archaea representing a new lineage of Archaea, Nanoarchaeota, was discovered recently.

1.4 Ubiquity of Archaea

Currently, a number of the archaeal signatures (or phylotypes), which are revealed by PCR-based, ribosomal RNA-gene surveys from environmental samples, have been detected from not only the confined habitats described above but a variety of terrestrial, freshwater and

marine habitats[5,6]. Many of the archaeal signatures were assigned to new lineages, although, Archaea that correspond to the signatures have not been successfully isolated or cultivated yet. Some archaeal signatures from hot springs represent entirely new lineage, Korarchaeota. Besides, the Marine Group I that is abundantly detected from cold or temperate marine habitats forms a new lineage in the phylum Crenarchaeota. These facts suggest that the culturable Archaea represent only a part of the archaeal diversity, and Archaea could spread and adapt in the diverse environments in nature.

1.5 Evolution of Archaea

Until recently, phylogenetic analyses of the three domains (i.e., Archaea, Bacteria and Eukarya) have been heavily relied on the rRNA sequence comparison. However, recent progress of the genome sequences projects allows to discuss the evolutionary relationships among the three domains from different viewpoints[7,8]. For example, it has become evident that archaeal genome share bacterial and eukaryotic features: in general, genes involved in informational activities affiliate to the eukaryotic homologs, while genes in operational activities to the bacterial homologs. Informational genes are less subject to lateral gene transfer, therefore, Archaea must have played important roles in emergence of proto-eukaryotic cells. On the other hand, a genome-content analysis or phylogenetic analysis of combined orthrogous proteins over the three domains was congruent with the universal tree depicted by the rRNA sequence analysis. In the domain Archaea, the distinction of two major phyla, Crenarchaeota and Euryarchaeota, is supported by the fusion of the sequences of ribosomal proteins.

On the universal phylogenetic tree, Archaea tend to branch off shortly at a point closest to the root, indicating Archaea might have evolved more slowly than Bacteria and Eukarya. It is particularly true for hyperthermophilic Archaea. In addition, hyperthermophilic Bacteria also represent most deeply rooted lineages. These facts lead to a hypothesis that the universal ancestor of all living organisms was hyperthermophiles. Thus, the phenotypic properties of the current hyperthermophiles, such as thermophily, anaerobicity, sulfur-metabolism, may be reminiscent of the early Earth geochemical conditions. This hypothesis has been challenged over the last few years and still open questions, nonetheless, they should provide us clues for an inference about the origin and history of early life on Earth.

References

[1] Woese CR, Fox GE (1977). Phylogenetic structure of the prokaryotic domain: the primary kingdoms. Proc. Natl. Acad. Sci. USA 74: 5088-5090.

[2] Woese CR, Kander O, Wheelis ML (1990). Towards a natural system of organisms: proposal for the domains Archaea, Bacteria, and Eucarya. Proc. Natl. Acad. Sci. USA 87: 4576-4579.

[3] Garrity GM, Holt JG. (2001). Phylum AI. Crenarchaeota phy. nov. In: Boone DR, Castenholz RW. (ed.) Bergey's Manual of Systematic Bacteriology, 2nd ed. vol. 1, pp. 169-210. Springer, New York.

[4] Garrity GM, Holt JG. (2001). Phylum AII. Euryarchaeota phy. nov. In: Boone DR, Castenholz RW. (ed.) Bergey's Manual of Systematic Bacteriology, 2nd ed. vol. 1, pp. 211-355. Springer, New York.

[5] Pace NR (1997). A molecular view of microbial diversity and biosphere. Science 276: 734-740.

[6] DeLong EF (2003). Oceans of Archaea. ASM News 69: 503-511.

[7] Eisen JA (2000). Accessing evolutionary relationships among microbes from whole-genome analysis. Cur. Opin. Microbiol. 3: 475-480.

[8] Campbell AM, Karlin S (2002). Evolution of genome structures (overview). Theor. Pop. Biol. 61: 365-366.

[9] Wheelis ML, Kandler O, Woese CR (1992). On the nature of global classification. Proc. Natl. Acad. Sci. USA. 89: 2930-2934.

Proc. of The Ninth Int. Symp. on Artificial Life and Robotics (AROB 9th '04)
Beppu, Oita, Japan, 28-30 January, 2004

Self-organizing mechanism of biosystems

- Purine and pyrimidine density ratios in tRNA and rRNA -

Ken NAITOH

Yamagata University, 4-3-16 Jyonan, Yonezawa-shi, Yamagata, 992-8510 Japan
Email: k-naito@yz.yamagata-u.ac.jp

Key Words: Density ratio of bases, tRNA, rRNA

Abstract

The sequence data in the world-wide databases on codons and ribosome RNA (rRNA) shows that the averaged density ratio of purine and pyrimidine for a lot of species is around 1.3, while the average density ratio in transfer RNA (tRNA) is around 1.1. The reason of why this difference between tRNA, codons, and rRNA causes is clarified in the present report.

Introduction

First, we had proposed the hypothesis on the origin of nitrogenous bases, that is, on why the size ratio of purine and pyrimidine is around silver and golden ratios [1, 2, 3]. Then, it was shown that the size asymmetry brings mainly two types of purines and three types of pyrimidines [2, 3]. Moreover, we found qualitatively that the density asymmetry of purine and pyrimidine promotes the generation of clover structure such as tRNA [3, 4, 5].

However, the hypothesis and analysis were conceptual, because sugar and phosphoric acids were not considered.

Thus, in the present report, we propose the quantitative analysis by considering the molecules connecting between bases. Then, we will examine the density ratio of purine and pyrimidine in tRNA, codons, and ribosome RNA (rRNA).

Density ratios of purine and pyrimidine in tRNA, codons, and rRNA

The ratio of molecular weights for purine and pyrimidine, which connect with sugar and phosphoric acids, is around 1.1.

We examined the database [6] in detail. The averaged density ratio of purines and pyrimidines in over five-thousand types of tRNA sequences is about 1.1, while the averaged density ratio of purines and pyrimidines in each species is also around 1.1. (See Table 1.)

The asymmetry of molecular weights of purine and pyrimidine is apparently related to the asymmetric density ratio. This fact supports the hypothesis shown previously [1, 2, 3, 4, 5].

The codon usage database [7, 8, 9] and the database on rRNA [10, 11] show that the averaged density ratios for purines and pyrimidines in codons and rRNA is around 1.3. (See Tables 2 and 3.)

Table 1 Density ratio of purine and pyrimidine calculated from the database of tRNA.

Species	Density ratio of purine and pyrimidine in tRNA
Pyrococcus furiosus	1.06
Pyrobaculum aerophilum	1.11
Sulfolobus solfataricus	1.10
Escherichia coli	1.05
Aeropyrum pernix	1.07
Pseudomonau aeruginosa	1.06
Average	**1.08**

Dynamics for explaining the purine-pyrimidine density ratios in tRNA, codons, and rRNA

The simple mathematical consideration is introduced in order to examine the above differences between the density ratios of bases in tRNA, codons, and rRNA.

In DNA, purines and pyrimidines have the same density, because purine and pyrimidine at each locus become a base pair due to hydrogen bonding (Fig. 1a). On the other hand, the fact that tRNA has the loops in clover makes it possible for asymmetric density ratios of purines and pyrimidines to exist, because the loci inside the loops are free from hydrogen-bonded connections (Fig. 1b). Moreover, it should be stressed that, when the density ratio is infinite or zero, that is, if neither purine nor pyrimidine is in the sequence, stems of RNA can not be generated. This is because stems must be with pairs of purine and pyrimidine. The production of RNA shapes can be for density ratios between 1.0 and a finite value greater than 1.0.

Inevitability of the difference between tRNA and codons

The "symmetric" density ratio of purine and pyrimidine in stems brings us the fact that the density ratio of purine and pyrimidine in codons and loops must be larger than the averaged density ratio of tRNA. The averaged density ratio around 1.1 for tRNA is possible, because of the density ratios around 1.0 in stems and that around 1.3 in loops. (Loop implies leaf in the clover structure of tRNA.)

Asymmetric density ratio in codons around 1.3 leads to asymmetric density ratio of polar and nonpolar amino acids. This brings the asymmetric density ratio of rRNA.

Table 2 Density ratio of purine and pyrimidine calculated from codon usage database.

Species	Density ratio of purine and pyrimidine in codon usage database
Acidianus ambivalens	1.27
Pyrococcus abyssi	1.35
Pyrococcus endeavori	1.44
Pyrococcus furiosus	1.35
Pyrococcus horikoshii	1.27
Pyrococcus woesei	1.34
Pyrobaculum aerophilum	1.21
Pyrobaculum islandicum	1.36
Pyrobaculum oguniense	1.35
Pyrodictium abyssi	1.08
Pyrodictium occultum	1.32
Sulfolobus acidocaldarius	1.36
Sulfolobus metallicus	1.49
Sulfolobus solfataricus	1.29
Escherichia coli	1.08
Aeropyrum pernix	1.11
Thermoproteus tenax	1.24
Methanopyrus kandleri AV19	1.20
Methanopyrus kandleri	1.23
Pseudomonas alcaligenes	1.06
Pseudomonas fluorescens	1.01
Average	**1.26**

Conclusion

The dynamical relation between bases, tRNA, codons, and rRNA are clarified by examining the density ratio of purine and pyrimidine.

This research was partially supported by the Ministry of Education, Science, Sports and Culture, Grant-in-Aid for Scientific Research (B), 14550140, (2002).

Table 3 Density ratio of purine and pyrimidine calculated from the database of rRNA.

Species	Density ratio of purine and pyrimidine in rRNA
Acidianus ambivalens	1.32
Pyrococcus abyssi	1.31
Pyrobaculum aerophilum	1.32
Pyrodictium occultum	1.30
Sulfolobus solfataricus	1.25
Aeropyrum pernix	1.28
Thermoproteus tenax	1.34
Pseudomonas alcaligenes	1.31
Thermococcus fumicolans	1.33
Average	**1.31**

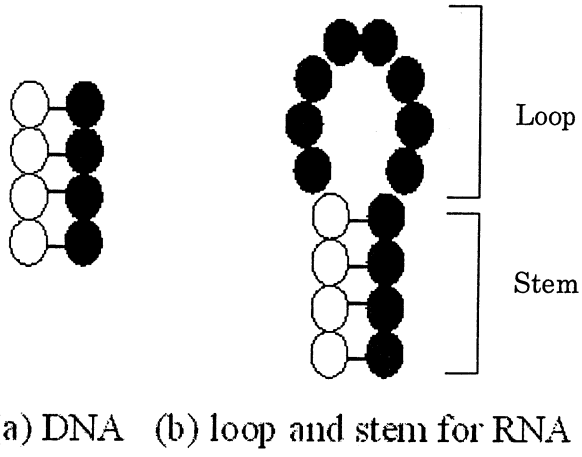


Fig. 1 Schematic diagram of DNA and RNA. (Black and white circles imply pyrine and pyrimidine, while the straight lines between bases are hydrogen bond connections.)

References

[1] Naitoh, K. (1999). Cyto-fluid Dynamic Theory for Atomization Processes, *Oil&Gas Science and Technology*, Vol. 54, No.2 205-210. (Also in *Proc. of COMODIA*, 1998)

[2] Naitoh, K. (2000). Mesoscopic Kinetic Theory for Fluid Phenomena and Biochemical Reaction Processes. *J. of Advanced Science*, 12-3, 223 (2000). (Also in *Proc. of the Design & System Conference '99, Osaka University*. 1999 and *Proc.*

of 3rd Japan-France Seminar of Intelligent Materials, 2000)

[3] Naitoh, K. (2001). Cyto-fluid Dynamic Theory, *Japan Journal of Industrial and Applied Mathematics*, Vol.18, No.1.

[4] Naitoh, K. (2002). Cyto-fluid Dynamic Theory of the Origin of Base, Information, and Function. *Artificial Life and Robotics,* **6-1 & 2,** 82.

[5] Naitoh, K. (2000). Cyto-fluid Dynamic Theory of the Origin of Base, Information, and Function. *Proc. of the 6th Int. symp. on Artificial life and Robotics 6th.*

[6] Lowe, T.M., Eddy, S.R., (1997). *Nucleic Acids Res.*, **25**, 955. (available at http://rna.wustl.edu/tRNAdb/.)

[7] Benson, D.A., Boguski,M.S., Lipman, D.J., and Ostell, J., Ouellette, B. F. F., (1998). *Nucl. Acids Res.*, **26**, 1.

[8] Benson, D. A., Karsch-Mizrachi, I., Lipman, D. J., Ostell, J., Wheeler, D. L., (2003). *Nucleic Acids Res.*, **31**, 23.

[9] Nakamura, Y., Gojobori, T., Ikemura, T., (2000). *Nucl. Acids Res.*, **28**, 292. (available at http://www.kazusa.or.jp/codon/.)

[10] DNA Data Bank of Japan, http://www.ddbj.nig.ac.jp/.

[11] JCM On-line catalogue, Japan Collection of Microorganisms, RIKEN (The Institute of Physical and Chemical Research), http://www.jcm.riken.go.jp/.

Proc. of The Ninth Int. Symp. on Artificial Life and Robotics (AROB 9th '04)
Beppu, Oita, Japan, 28-30 January, 2004

Repulsive Delayed Random Walk

T. Ohira
Fundamental Research Lab

Sony CSL
Tokyo, Japan 141-0022

T. Hosaka
Department of Computational Intelligence
and Systems Science
Tokyo Institute of Technology
Yokohama, Japan 226-8502

Abstract

We study here a random walk with delayed feedback around an unstable fixed point. It is found that the random walker can be kept to be around the fixed point with longer delay. This is in contrast to the normal role of delay, which is generally thought to be a source of instability. We discuss a possibility of our model to stick balancing experiments.

1 introduction

For many biological and artificial feedback control system, feedback control delay and noise pose a challenging problem. They together give rise to undesirable behavior for the control objectives, and how to deal with these undesirable two factors of noise and delay is an important issue.

With this background, we have studied "delayed stochastic systems" with noise and delay by proposing "delayed random walks" [1, 2]. Previous works concentrated on delayed random walk around a stable fixed point. These random walks have found applications to systems such as human postural controls.

In this paper, we would like to propose another type of delayed random walks, whose fixed point is unstable or repulsive. One of the motivations to consider such delayed random walks is the control systems in the unstable situation. A typical example is the stick balancing control at a fingertip [3]. Experiments have shown that even thought the human control delay is order of 0.1 seconds, the typical motion of the stick is shorter than that time scale. How can one control the unstable system whose time constant is much shorter than the control time delay? The clear answer is not yet obtained, but it appears necessary to understand the role of noise and delay in such systems.

The model we propose in this paper is not a direct model of the stick balance as described above. Yet, it gives rise to a peculiar behavior of the slower diffusion with the longer delay. The model is designed such that delay, which normally makes systems unstable, helps the stability of the system.

2 Model

We consider random walk with a unit discrete step pre unit discrete time on one dimension. Let the position of the random walker at time step t is given by $X(t)$ and the fixed pint is set at the origin, $X(t) = 0$. The delayed random walk is defined by the following conditional probabilities.

$$P(X(t+1) = X(t) + 1 | X(t-\tau) > 0) = p \quad (1)$$

$$P(X(t+1) = X(t) + 1 | X(t-\tau) = 0) = \frac{1}{2} \quad (2)$$

$$P(X(t+1) = X(t) - 1 | X(t-\tau) < 0) = 1 - p \quad (3)$$

Where $0 < p < 1$ and τ is the delay. We dealt with the case of $p < 0.5$, where the origin becomes attractive with no delay, $\tau = 0$. In this paper, we investigate the case of the "repulsive origin" where $p > 0.5$. By symmetry with respect to the origin the average position is $< X(t) >= 0$. In contrast to the attractive case, the walker escapes away from the origin and we do not have a stationary probability distribution. Hence, it is more difficult to analyze this model.

3 Simulations

In order to capture the effect of delay, we have performed computer simulations of the model. We have found that longer delay τ helps to keep the walker closer to the origin. To see this, we have studied two aspects. The simulation is taken for an ensemble of 10000 walkers, all starting from the origin at $t = 0$.

The first is the probability distribution of time for the walker to reach a certain point. In other words,

first passage time to cross a specified cite. Typical result is shown in the Fgure 1. We see that longer delay causes more time steps to reach a specified point. This means that the walker is around the origin for longer period of time when the feedback delay is longer.

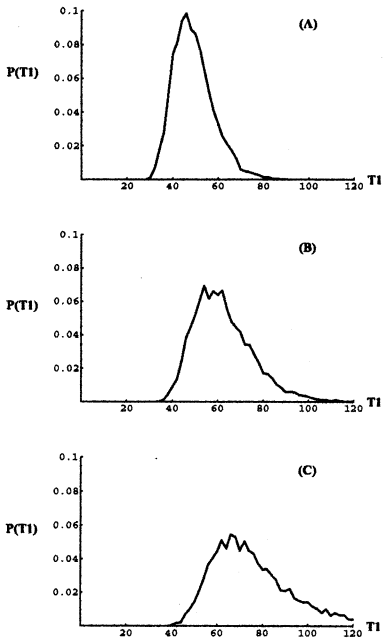


Figure 1: Probability distribution $P(T1)$ of time $T1$ for the walker to reach to the fixed point $X = 30$ for the first time. The parameters are $p = 0.8$ and (A) $\tau = 0$, (B) $\tau = 10$, (C) $\tau = 10$, respectively.

The second quantity is the return time distribution to the origin: distribution of time interval for the walker to return to the origin. Some examples are shown in Figure 2. We see that longer delay allows longer return time for the walker. The delay keeps the walker to come back to the origin for longer time.

4 Summary

Our repulsive delayed random walk model has shown a property of "delay stabilization". This is in contrast to normal role of delay in the feedback system. It requires further investigation to see if this type of behavior is actually useful in biological and artificial feedback control system.

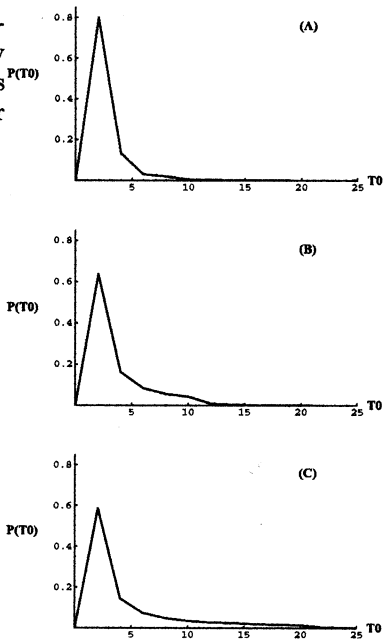


Figure 2: Probability distribution $P(T0)$ of time interval $T0$ for the walker to return to the origin. The parameters are $p = 0.8$ and (A) $\tau = 0$, (B) $\tau = 10$, (C) $\tau = 10$, respectively.

Acknowledgements

T. Ohira thanks Dr. Juan Luis Cabrera for his insightful comments.

References

[1] T. Ohira and J. G. Milton, "Delayed Random Walks", *Phys.Rev.E* Vol. 52, pp. 3277-3280, 1995.

[2] T. Ohira and T. Yamane, "Delayed Stochastic Systems", *Phys.Rev.E* Vol. 61, pp. 1247-1257, 2000.

[3] J. L. Cabrera and J. G. Milton, "On-Off Intermittency in a Human Balancing", *Phys.Rev.Lett.* Vol. 89, p.. 158702, 2002.

Proc. of The Ninth Int. Symp. on Artificial Life and Robotics (AROB 9th '04)
Beppu, Oita, Japan, 28-30 January, 2004

Data Reduction for 3D Visualized data distribution

Hideo MIYACHI
Visualization Division
KGT Inc.
Shinjuku2-8-8 Shinjuku-ku Tokyo, Japan
160-002

Naohisa SAKAMOTO
Center for the Promotion of Excellence in
Higher Education
Kyoto University
Yoshida-Honmachi Sakyo-ku Kyoto, Japan
606-8501

Abstract

We propose an application of apply Image-based Modeling and Rendering technique for data reduction of visualized model. So far, this technique has been used for reconstruction 3D graphic models from real objects. By using this technique, we can separate the process of reduction control between image and geometry. This is important feature for visualized model especially to the scientific area. We obtained a reduction ratio of 85.4% of original file size without image quality degradation. We expected that this approach can contribute for more lightweight 3D graphic models distribution on the Internet.

1. Introduction

This paper presents a new approach for data reduction of visualized model to the scientific area, by using IBMR (Image-based Modeling and Rendering technique) [1][2][3][4].

IBMR is generally used for reconstruction of 3D graphical models from real objects. However, we propose an approach in which IBMR is used for data reduction of visualized graphic models.

Our goal is to develop an efficient modeling method for distribution of 3D graphical model throughout the Internet. We believe that this approach can bring two benefits for this distribution purpose.

First, we can control the model accuracy proportionately to the resolution of final image in which the objects will be displayed.

Second, we can control the reduction ratio of image compression and geometric simplification separately. This is an important feature as bellow.

Fig.1 shows an example of visualized data which represent an electric density distribution of a hydrogen (H_2) molecule inside a cube. The cube surfaces consist of 64x64x6 nodes and 63x63x6 squares. A color value composed of red, green and blue value is defined at each node. By using only geometric simplification, the cube can be transformed into a cube consists of 6 squares as a maximum level of simplification. As a result, color information disappear according vertex removal. Therefore, Long et al, propose to separate the physics information, as texture, from the geometric model [5]. (Fig.2)

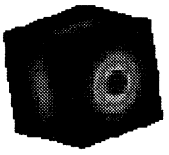


Fig.1 Scientific visualization example

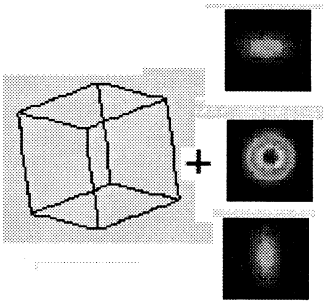


Fig.2 Separation between geometry and texture

We will introduce the IBMR concept, then, explain about Silhouette and Voxel method for geometric reconstruction in Section 2. We

describe our software environment in Section 3. Sample model is demonstrated in Section 4. Finally, conclusion is summarized in Section 5.

2. Related Works

2.1 Image-based Modeling and Rendering

IBMR is the technique to reconstruction of 3D graphical models from real objects.

First, Multiple photographs, i.e. images, are captured by a camera from multiple directions. Then, we have to get the matrix to determine the relative position between the camera and the object. Then we have to do camera calibration precisely [6][7]. A typical system of IMRB has a table which can be rotated and a camera fixed on a floor. The system automatically captures images while rotating the table synchronously (Fig.3).

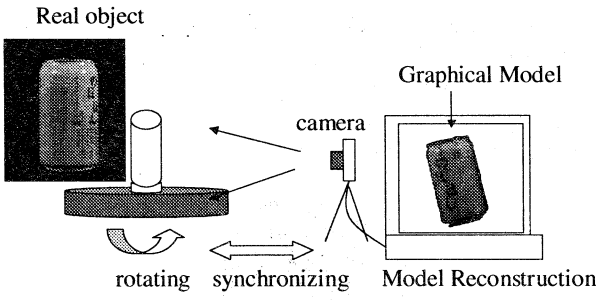


Fig.3 Typical IBMR system concept chart

2.2 Silhouette and Voxel method [8]

Amount of works preexist in model reconstruction area. We chose Silhouette and Voxel method to reconstruct 3D model.

After capturing images, images are converted in binary, i.e. white and black like Fig.4.

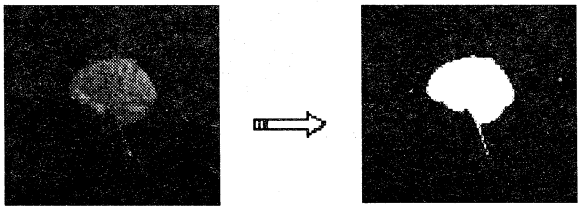


Fig.4 Silhouette Extraction

Next, volume data to explain the object is generated from a series of binary image.

1) The voxel region (cube) is generated from the extent of the captured object.
2) The M x M x M number of voxel data in empty (voxel value=0 at all) is generated. Here, the resolution is controllable. The number of voxel is 2^N x 2^N x 2^N, when setting the number of resolution in N.
3) Voxel value is set in 1 if the voxel locates in inside of the object.

Fig.5 illustrates the evaluation method. Projecting the generated voxel onto a silhouette image by the matrix calculated when capturing image, if the shadow of voxel is inside the area, the voxel value is set in 1. We evaluated only a point, which is the gravity point of the voxel, for quick evaluation.

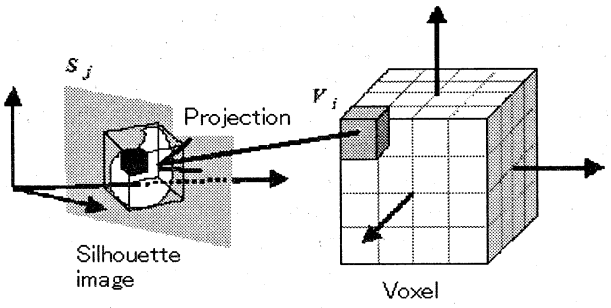


Fig.5 Voxel value evaluation

A voxel is evaluated to all silhouette images. Then, voxel value is accumulated.

Hence, the voxel value takes from 0 to N_{image}. (N_{image}: the number of captured photograph.) After evaluating all voxel, the volume includes object as a voxel value.

2.3 Triangulation and geometric simplification

Volume data is transformed to a triangular data by iso-surface algorithm.

After the process, the triangular data is simplified by geometric simplification algorithm. Fig.6 demonstrates these two steps.

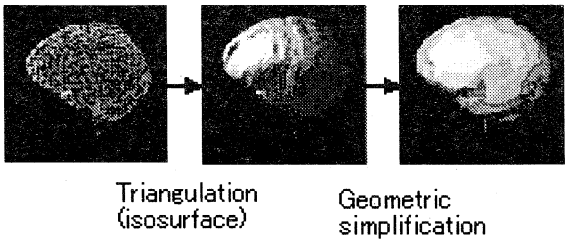


Fig.6 Triangulation and simplification

2.4 Texture Mapping

Finally, texture is mapped on each triangle. Projecting the triangle onto the most frontal image among captured one, the image on the shadow area is mapped on the triangle as texture.

3. Modeling Environment

3.1 Real Object or Graphical Object

Our approach is to apply IBMR to computer graphics model.

Hence, the modeling procedure is the same as description from Section 2. We, however, replaced the image capturing by camera to rendering by software. This replacement makes the modeling easier. We can get the camera position easily and precisely and also we can set the camera in any place, even under the object. Although it is difficult to capture a real object from the bottom, because it should be on something.

3.2 Experiment environment

We used Windows PC for experiments. The program we developed was embedded into AVS/Express, an application package for visualization by AVS Inc., because it has much functions such as 3D rendering, iso-surface, data reduction and output VRML for our experiments in defaults.

For image capturing step, we developed the macro program of AVS/Express to automatically capture multiple images from surround position. The matrix calculation program and Silhouette and Voxel method were written in C as completely new program. For triangulation and geometric simplification, we used the standard functions named "isosurface" and "data reduction" modules respectively. The isoruface uses is Marching cubes algorithm [9]. The data reduction uses error control method [10].

Image data is stored in jpeg file. Geometric data is stored in VRML (Ver.1) file.

4. Sample Modeling

4.1 Test data

We used 3D medical data for experiment shown in Fig.6. This was VRML triangular data that includes 74,176 vertexes and 148,460 triangles. The surface data was generated by iso-surface of AVS/Express from CT data with 127x127x108 resolution.

VRML file size exported from AVS/Express was about 29MB.

4.2 Image capturing (rendering)

We captured images by CG camera while rotating the object twice around X axis and Y axis. The picture was captured every 10 degree, hence the number of images was 74.

The resolution of the image was 500 x 500.

4.3 Voxel generation

We tested the Voxel resolution N=3-9 levels. (N=4, 5 and 6 shown in Fig.7)

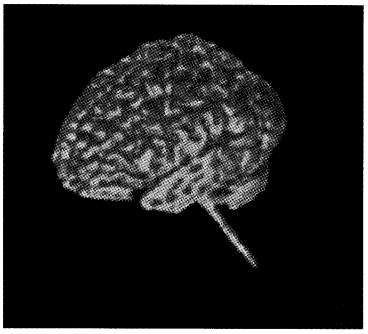


Fig.6 Sample Model (Brain)

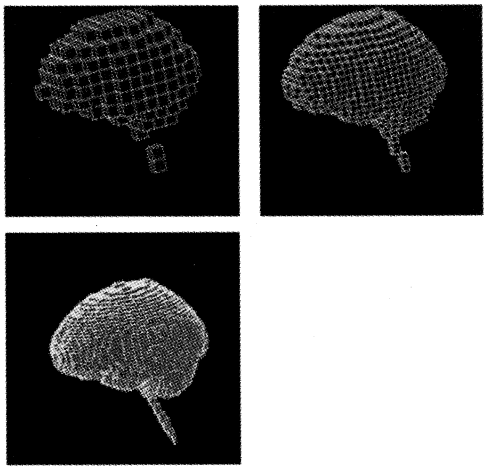


Fig.7 Voxel models (Level 4,5 and 6)

We decided that the level 6 was minimum resolution to be shown properly appearence as a brain. The model had 265,093 voxel.

4.4 Triangulation and geometric simplification

Fig.8 demonstrates the change by triangulation and simplification.

As a result, the final geometric data includes 818 vertexes and 4,422 triangles.

The simplification ratio was 93.5% for vertex number and 97.0% for triangle number.

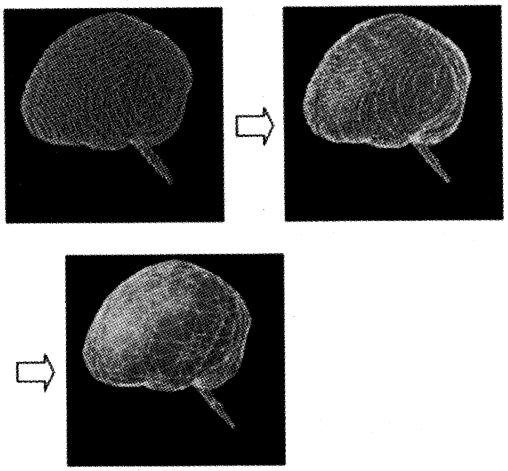


Fig.8 Triangulation and Simplification

VRML file exported was 2.42MB. The reduction ratio was 91.6% of original VRML file..

4.5 Texture Mapping

Fig.9 shows the final result.

Texture size was 1.82MB. Therefore, the total data size for this picture was 4.24MB (= 2.42+1.82). The reduction ratio was 85.4%.

Comparing the image quality between Fig.6 to Fig.9, we did not observe significant error, although some fine structures in Fig.6 were smoothed in Fig.9. Fig.9 messaged us that the picture obviously presented a brain well, comparing to Fig.8, which has no texture.

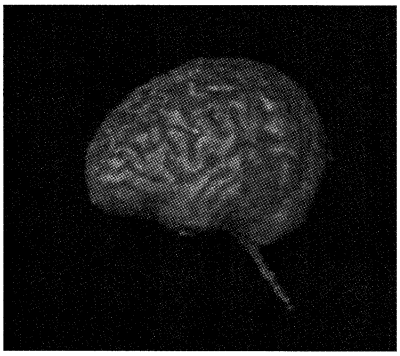


Fig.9 Final image

5. Conclusion

We obtained a reduction ratio of 85.4% of original file size without image quality degradation as an example result.

This approach gave us two benefits. The first, we controlled the resolution of reconstructed model without relation to the original data resolution. The second, we reduced the data size of the texture and the geometry independently. However, it is enable to apply complex model like torus.

We think it will be suitable for the data distribution of scientific research result through Internet. And also we expect it contribute 3D data archive. We would like to enhance this system along quantitative evaluation in future.

References

[1] R. Szeliski,(1993) "Rapid Octree Construction from Image Sequences", Graphical Models and Image Understanding, Vol. 58, No. 1, pp.23-32.

[2] W. Niem and J. Wingbermuhle (1997), "Automatic Reconstruction 3D Objects Using a Mobile Monoscopic Camera", In Int. Conf. on Recent Advances in 3D Imaging and Modeling.

[3] K. Kutulakos and S. Seitz(1999), "A theory of shape by space carving", In IEEE Int. Conf. on Computer Vision, pp.307-314.

[4] T. Wada, X. Wu, S.Tokai and T. Matsuyama (2000), "Homography Based Parallel Volume Intersection: Toward Real-Time Reconstruction Using Active Camera", Proc. of Int. Workshop on Computer Architectures for Machine Perception, pp.183-189.

[5] Paul E. D., Camilo J.T., Jitendra M.(1996), "Modeling and Rendering Architecture from Photographs: A hybrid geometry-and image-based approach", Technical Report UCB//CSD-96-893.

[6] R. Tsai(1986), "An Efficient and Accurate Camera Calibration Technique for 3D Machine Vision", In IEEE Conf. CVPR86, pp.364-374.

[7] Z. Zhang(2000), "A flexible new technique for camera calibration", IEEE Trans. on PAMI, Vol. 22, No. 11, pp.1330-1334.

[8] A. Y. Mulayim, U. Yylmaz and V. Atalay(2003), "Silhouette-based 3D model reconstruction from multiple images", IEEE Trans. on Systems, Man and Cybernetics,Part B, Vol. 33, No. 4, pp.582-591.

[9] M. Nakajima, I. Fujishiro(2000), Computer Visualization (in Japanese), Kyoritu ISBN4-320-01643-2, pp.38-39.

[10] Ian Curington(1999),"Visualization Methods and Application for Industry", Proc. of The 5th Visualization Conference, pp.5-12.

Proc. of The Ninth Int. Symp. on Artificial Life and Robotics (AROB 9th '04)
Beppu, Oita, Japan, 28-30 January, 2004

Symbiotic fusion of life and artifact

- A new possibility of biomass -

Ken NAITOH

Yamagata University, 4-3-16 Jyonan, Yonezawa-shi, Yamagata, 992-8510 Japan
Email: k-naito@yz.yamagata-u.ac.jp

Key Words: Desulfurobus, biomass, cellulose

Abstract

Cultivation of Desulfurobus Ambivalens in cellulose tube without normal nutrients brings increase of the species. This fact brings the possibility that this species can decompose cellulose and also leads to a new type of biomass technology.

Introduction

Fossil fuels come from ancient living systems. In this sense, industrial products made from fossil fuels, many artifacts, have a deep relation with living beings.

Today, our activities using these fuels may lead us to a dilemma, the global environmental problem such as increasing carbon dioxide and methane. Even a small increase of carbon dioxide may bring the evolution of pathogenic bacteria, although the increase does not influence human beings directly.

A new paradim of recyclic chemical reaction routes in artifact and life is necessary to face up to this dilemma.

Regeneration of alcohol from carbon dioxide and water has been tried by using phototrophs belonging to Eucarya [1]. However, this system is inefficient, since the cell cycle of Eucarya is long. The use of cyanobacteria may be possible, but the green color of Chlorela disturbs to get light efficiently for the cells, which are relatively far from the light.

Here we examine whether Desulfurobus Ambivalens [2] belonging to Archaea [3] decompose cellulose about at 100 C° without photosynthesis. This is because decomposition of cellulose brings us a new possibility of biomass.

Desulfurobus Ambivalens

Desulfurobus Ambivalens is one of Archaea, which was found by W. Zillig at 1986. At the temperature around 70 - 85 C° and around pH 2.5, Desulfurobus Ambivalens grows, although Desulfurobus in conventional vial cannot increase well in comparison with E.coli.

Traditional cultivation of Desulfurobus

The normal medium with rich nutrients [2] is used, which consist of eighteen components with yeast extract, sulfur, $Na_2S \cdot 9H_2O$, and Resazurin, and salt base solution.

Then, the vials including a small amount of the species, the medium, hydrogen, and carbon dioxide are cultivated under anaerobic condition without repeated shaking, at 75 C° and at pH 2.5.

We took the photomicrographs of Desulfurobus cultivated during six days in the vial (see Fig. 1). The density of Desulfurobus in the vial with the normal liquid culture is 1.2×10^5 cell / cm^2.

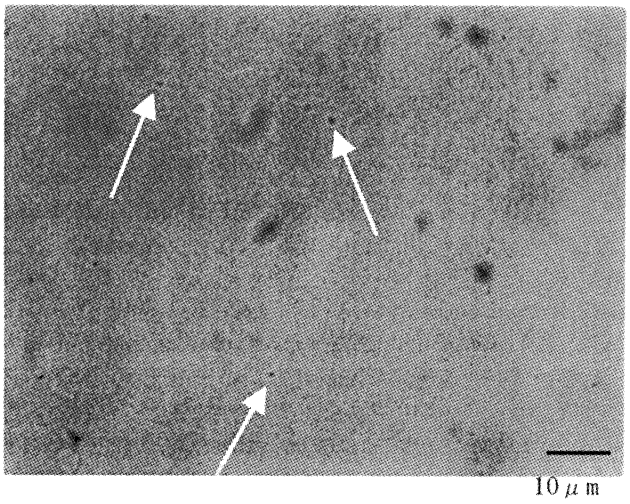


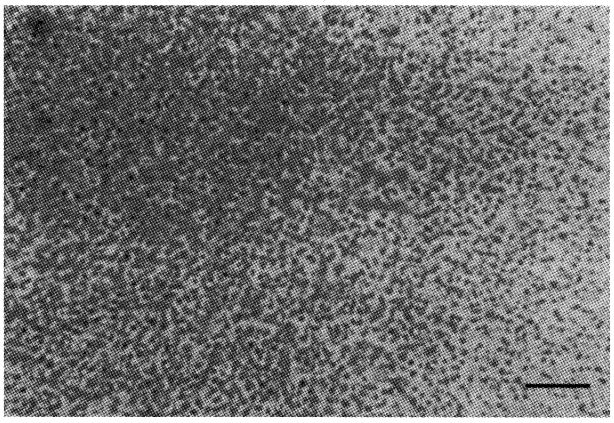
Fig. 1 Desulfurobus cultivated during six days in vial by the traditional way.

High-density cultivation of Desulfurobus by using cellulose tube and normal medium with rich nutrients

Cellulose tubes were cut into pieces of about 30 mm in length. The tubes were dried in an oven for thirty minutes at 120 C°.

The cuellulose tubes are used by the way close to that of Ref. 4. We put 1 ml of the normal medium in 30 ml of vials. Then, the tubes including a small amount of the species, hydrogen, and carbon dioxide are added into the vial with the medium. The vials are cultivated under anaerobic condition without repeated shaking, at 75 C° and at pH 2.5.. (The tubes are closed at both ends firmly, after the species was put.)

We took the photomicrographs of Desulfurobus cultivated during six days in the tubes (see Fig. 2). We found that Desulfurobus in the tubes reached high cell densities. (The density of Desulfurobus in the tube is 1.2×10^7 cell / cm^2, while the density in the normal liquid culture without tubes is 1.2×10^5 cell / cm^2.) This is about 100 times higher than cell densities in the normal liquid cultures.



10 μm

Fig. 2 Desulfurobus cultivated in cellulose tube with the normal medium having sufficient nutrients.

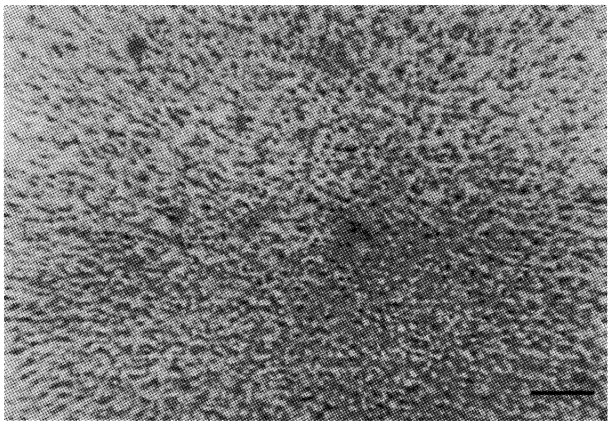
Cultivation of Desulfurobus in cellulose tube without normal nutrients

Here, cultivation in cellulose tube is tested with the medium, in which the nutrients are reduced. Only two components of $Na_2S\cdot9H_2O$ and Resazurin are employed. Carbon dioxide, yeast extract, and salt base solution are not included.

Figure 3 shows the photomicrographs of Desulfurobus cultivated during six days in the tubes with the few components of nutrients, at 75 C° and at pH 2.5. We can see again that Desulfurobus in the tubes reaches high cell densities (1.2×10^7 cell/cm^2).

The present result brings us the possibility that Desulfurobus can decompose hard cellulose. (Cellulose tubes are closed certainly also after cultivation, because high density of Desulfurobus is seen. Cellulose decomposition will occur only at the surface, if it occurs.)

High density cultivation technique is essential in order to find this possibility, because traditional cultivation in vial is insufficient to obtain certain and stable results.



10 μm

Fig. 3 Desulfurobus cultivated in cellulose tube with the medium having less components of nutrients.

Conclusion

Carbon sources are only cellulose tube and Resazurin in Fig. 3.

If Desulfurobus decomposes cellulose, we get a new possibility of biomass. If Resazurin is decomposed, we will get a new insight for decomposing aromatic compound.

It is well-known that chemical reactions in living beings basically become faster according to increasing temperature. In this sense, thermophile is advantageous for engineering applications.

Acknowledgement

Ken Naitoh expresses sincere thanks to Profs. Koki Horikoshi and Akira Inoue of Toyo University and Japan Marine Science and Technology Center, Japan for their advice concerning this paper.

References

[1] RITE project reports (1996) Research Institute of Innovative Technology for the Earth (RITE)

[2] W. Zillig, S Yeasts, I. Holz. A. Bock, M. Rettenberger, F. Gropp, and G. Simon, (1986). Desulfurobus ambivalens, gen. nov. sp. Nov, an Autotrophic Archaebacterium Facultatively Oxidizing or Reducing Sulfur, *System Appl. Microbiol.* 8. 197-203.

[3] Stetter K O, (1995). Microbial life in hyperthermal environments, *Am. Soc. for Microbiol. News* 61: 285-290.

[4] Rieger G, Muller K, Hermann R, Stetter K O, Rachel R, (1997). Cultivation of hyperthermophilic archaea in capillary tubes resulting in improved preservation of fine structures. *Arch. Microbiol.* 168: 373-379.

[5] Tsuji, D. (2003), Master thesis (of the research directed by K. Naitoh), Yamagata University.

Proc. of The Ninth Int. Symp. on Artificial Life and Robotics (AROB 9th '04)
Beppu, Oita, Japan, 28-30 January, 2004

Evaluation of Vibration on many positions by SOM

Nobuaki Kamimoto, Matsushita Electric Works Ltd. Technical management staff Kadoma, Osaka 571-8686
Yutaka Yamada, Matsushita Electric Works Ltd. Power-tool division Hikone, Shiga 522-8520
Masami Kitamura, Matsushita Electric Works Ltd. Power-tool division Hikone, Shiga 522-8520
Kiyoshi Nishikawa, Kanazawa University Computer and System Sciences Kanazawa, Ishikawa 920-8667

Abstract

In this paper, an evaluating method of Motor Operated Electric Tools (MOETs) using the self-organizing Feature map (SOM) based on the spectrum of vibration. We collect eighteen data from different positions on three kinds of MOETs. We compute the spectra of those vibrate data and input them to a SOM network. After classification, the quantitative differences of all vibrate spectra are able to obtained by computing the distance between each other, and therefore the position on which vibrate stress concentrated can be specified for each designed MOETs.

1. Introduction

Machines using motors and gears have vibration and acoustic noise. The reason of acoustic noise is vibration in most case. We must reduce vibration. MOETs have not spaces of the reducing vibration. According to, the vibration of MOET is large. We have two methods for the evaluation of vibration. One is the evaluation by human. This evaluation is not accuracy. Another is evaluation by vibrate spectrum. But the MOET has many data. So, we used SOM for classify spectra. Many spectra have various patterns. The problem is that spectra of MOET are different unusually for spectra of another positions.

The upper problem cause next trouble.

(1) The exhaustion of material breaks out in structure of MOET by stress of vibration.
(2) If every position has various spectra, the user has trouble for works.

In this purpose, we used the SOM. The reasons are next.

(1) We do not know featured quantity of every cluster for learning.
(2) SOM have not arbitrary for the classification of cluster. Because SOM is automatic classification from given data.

We propose next points in this paper.

- We can have quantitative diagnosis of design for vibration.
- We can make the standard of evaluation for work.
- We can know unevenness of vibrate spectra on each position and we can evaluate to design MOET for vibration.

2. The measurement and management of Vibration data

2.1 The measurement of Vibration

We show the measurement system of vibration in Fig. 1. We measured vibrating data by the sensor of vibrating acceleration. We managed vibration data by A/D Transformation to power spectrum. We gave vibrate power spectrum by Fast Fourier Transform, and we classified fixed patterns by SOM.

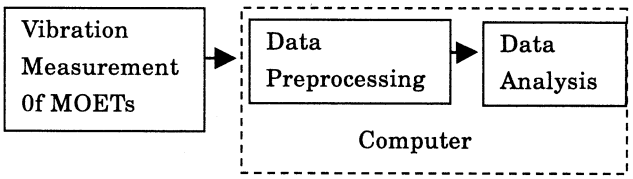


Fig.1 Block diagram of the measurement and processing system.

We show appearance of measurement machine and method of Vibration in the Fig.2

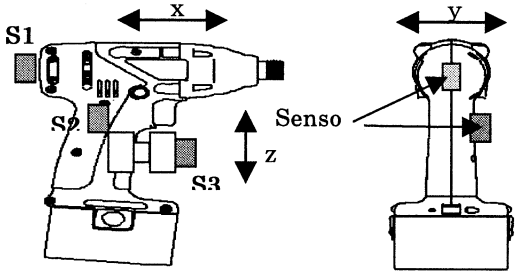


Fig.2 The MOET appearance, the method of measuring vibration and vibration direction.

. S1 is the position of motor-back, S2 is the position of grip, S3 is the position of wrist. Each position have three sensors in x,y,z directions. We show three directions in Fig.2. The front and rear Vibration is the x direction. The side Vibration is y direction. The top and bottom Vibration is z direction.

2.2 The management condition of Vibration data and Example of Vibration spectrum

In this paper, we gave spectrum until 400Hz. This reason is that we know the frequency to give impact for wrist suggested by International Organization for Standardization (ISO).

The sampling frequency is 1,024Hz. This frequency is 2.56 times for frequency range. The measuring time is one second. We show the example of spectrum in Fig.3. The spectrum has big peaks at 150Hz and 200Hz in Fig.3.

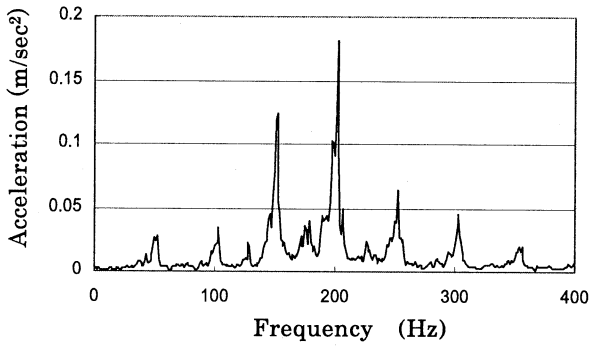


Fig.3 The example of vibration spectrum.

3. Statistics

If measured data are independent, we have statistics. We show the Average with formula (1), the Dispersion with formula (2), the Standard deviation with formula (3), Alteration coefficient (4).

Average: $$\tilde{x} = \frac{x_1 + x_2 + \cdots + x_n}{n} \quad (1)$$

Dispersion: $$V = \frac{1}{n-1}\left[\sum x_i^2 - \frac{(\sum x_i)^2}{n}\right] \quad (2)$$

Standard deviation: $$s = \sqrt{V} \quad (3)$$

Alteration coefficient: $$CV = \frac{s}{\tilde{x}} \quad (4)$$

4. SOM

This network have input layer and out layer. The SOM classify input data. Another feature of SOM is next.

(1) If dimension increase, the SOM treat only the Euclid distance.

(2) The SOM show many dimension to two dimensions.

(3) The SOM have feature to clear between data.

According to, we used SOM.

We show the learning algorithm of SOM in next.

The formula (5) select winner unit to be minimizes the Euclid distance.

$$\| X - V_c \|^2 = \min_j \| X - V_j \|^2 = \min_j \left\{ \sum_i^n (x_i - v_{ji})^2 \right\} \quad (5)$$

$$X^T = [x_1, x_2, \cdots x_n]$$

$$V_c^T = [v_{c1}, v_{c2}, \cdots, v_{cn}] \ , \ V_j^T = [v_{j1}, v_{j2}, \cdots, v_{jn}]$$

The v_{ji} show weight from the unit of input layer i to the unit of competitive layer j, a^T show convergent of a, V_c show the weight vector, X show the input vector. The renewal formula of weight show (6).

$$V_j(n+1) = V_j(n) + \Delta V_j(n) \quad (6)$$

$$\Delta V_j(n+1) = \begin{cases} \eta(n)(X - V_j(n)) & if \ j \in N_c(n) \\ 0 & if \ j \notin N_c(n) \end{cases}$$

$$\eta(n) = \eta_0 (1 - \frac{n}{N})$$

N is all times of learning, n is learning times. We renew weight vector include node c neighbor $N_c(n)$.

The distance $d_c(n)$ neighboring N_c show next in n times learning.

$$d_c(n) = \left[d_o (1 - \frac{n}{N}) \right] \quad (7)$$

d_o is distance of initial neighbor N_0, Usually, That distance institute larger than half of scale of output layer.

5. The classification by 3 × 3 SOM and Statistics

We have adopted the SOM for evaluation of eighteen spectra of vibration data on a MOET. If we evaluate vibration spectra of MOETs, we can check the trouble of structure of MOETs for the vibration.

And we can check good or bad to use. Example, we know that tools have many troubles, if spectrums are different on each place of Tools. The SOM has characteristic to represent the mutual relationship. So we used SOM to analysis of spectrum's statistics.

5.1 Data using SOM

Vibration data are next.

(1) MOETs are three types, measuring positions are three positions (S1,S2,S3), and each position have three directions (x,y,z). Loads are universal screw (cs) and coach screw (cs). According to each sample have eighteen spectra.

(2) The scale of SOM is 3 × 3. Because we thought that the SOM is as small as possible. Usually, the scale of SOM decide that if number of patterns are N, we select a natural number "m" of $m^2 \geq N$. In this paper, data of each sample are eighteen. So we selected scale 3 × 3.

(3) Constants show next using SOM. Learning-rate factor is 0.4. Learning-time factor is 100,000.

(4) We set average spectrum of each sample to center unit (1,1) of each SOM. Average spectrum is next. "A ave.", "B ave." , "C ave.".

5.2 The classification by SOM

We checked the classification of each sample by SOM. We show sample A in Table 1, sample B in Table 2, and sample C in Table 3. We arranged the average power spectrum of each sample in the each central unit (1,1) of SOM. "A,B,C" show samples, "x,y,z" show directions, "us" show universal screw, "cs" show coach screw. For example, "gCxus" show sample C, x direction, universal screw, and grip data. The average spectrum of each samples show "Aave", "Bave", "Cave". We have nineteen spectra in SOM.

Table 1. The classified A sample by 3x3 SOM.

	0	1	2
0	gxAcs (1.02) gyAcs (0.78) gzAcs (1.24)	gxAus (0.46) gzAus (0.54)	gyAus (0.01)
1	hyAcs (0. 71) hzAcs (0.69)	Aave (0.00) byAcs (1.50)	hyAus (0.78) hzAus (0.98)
2	hxAus (1.09) hxAcs (1.70) byAus (1.16)	bxAus (1.13) bzAus (0.95)	bxAcs (1.34) bzAcs (1.23)

1.48, 1.50, 2.33, 1.18, 1.47, 1.71, 1.47, 2.25

The result and consideration of Table 1. In Table 1, we could classify spectra of grip to unit (0,0) , (0,1) and (0,2) and spectra of hand-arm to unit (1,0) , (1,2) and (2,0) and spectra of back to unit (2,0) , (2,1) and (2,2). Data of each position made separately cluster. The distance is short from center to each cluster.

Table 2. The classified B sample by 3x3 SOM.

	0	1	2
0	bxBcs (0.51) bzBcs (0.50) gyBus (0.27) gyBcs (0.36) gzBus (0.35)		bxBus (0.87) byBcs (0.67)
1	gxBcs (0.03)	Bave (0.00) bzBus (0.62) hyBcs (0.97) hzBcs (0.95)	gzBcs (0.01)
2	byBus (0.83) gxBus (0.84) hyBus (0.61) hzBus (0.87)	hxBus (0.01)	hxBcs (0.01)

0.81, 0.87, 0.61, 1.88, 1.32, 1.15, 2.83

The result and consideration of Table 2. In Table 2, we could classify many spectra to unit (0,0) , (2,0) and (1,1). The distance is short from center to each cluster.

Table 3. The classified C sample by 3x3 SOM.

	0	1	2
0	bxCus (1.82) bxCcs (1.85)		hxCcs (1.54) hyCcs (0.52) hzCcs (1.63)
1	byCcs (0.00)	Cave (0.00) byCus (2.21)	gxCcs (0.01)
2	bzCus (0.51) bzCcs (0.53)	gyCus (0.73) gyCcs (1.18) gzCus (0.83) hxCus (1.24) hyCus (0.76) hzCus (1.36)	gxCus (0.85) gzCcs (0.78)

5.12, 2.17, 1.36, 1.29, 2.64, 3.52, 2.17

The result and consideration of Table 3. In Table 3, Spectra of back made cluster in unit (0,0) , (1,0) and (2,0). We could classify spectra of grip to unit (2,2) , (1,2) and (2,1). The distances of each unit are far from unit (1,1). We show statistics of upper data of each sample in Table 4.

Table 4. Statistics of sample A,B,C

Sample	A	B	C
Number	18	18	18
Average	2.564	1.674	3.438
Standard deviation	0.710	0.905	2.048
Alteration coefficient	0.277	0.541	0.596
Maximum	3.81	3.42	7.78
Minimum	1.50	0.62	0.95

The order of sum of the average spectra is next.

Sample B < Sample A < Sample C

(3.438) (2.564) (1.674)

According to, spectra of sample C are various patterns. We could know that sample C is impossible structure.

6. Compare of average spectra

We could evaluate each sample by SOM. But we must check absolute vibrate acceleration. We can compare good or bad for vibration by vibrate acceleration. We show the average spectrum of each sample in Fig.4.

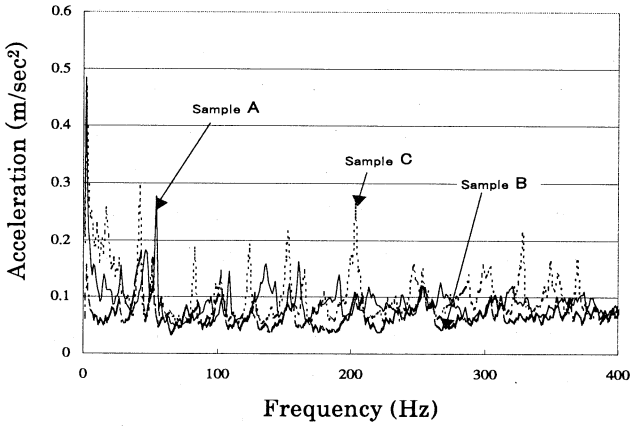


Fig.4 Comparison of average spectra.

Average of sample	Sum	Square sum
A ave.	36.91	3.90
B ave.	26.60	1.96
C ave.	40.46	5.02

In this paper, we could have quantitative analysis of vibrating stress to the structure of MOET by SOM. We could know that the design of sample C is worst.

(1) The structure of MOET have large vibrate stress.

(2) User has trouble for works.

7. Summary

In this paper, we could have quantitative analysis of vibrating stress to the structure of MOET by SOM. This method could change to quantitative analysis from evaluation of human on vibration. The characteristic of this method is next.

(1) We analyzed the distance of each spectrum from weight vector of combination.

(2) We analyzed statistics of that distance from average spectrum.

We can evaluate good or bad design of structure of vibrating machine using this method.

After this, we will analyze another vibrating machine to improve quality.

References

(1) J. Dayhoff: "Neural Network Architectures : An Introduction", International Thomson Computer Press, Boston, USA (1996)

(2) Nobuaki Kamimoto, Toshiro Abe, Lin Ken, Sogeru Omatu : "Quality Recognition of Interphones by the LVQ Method" Trans. IEE of Japan, Vol. 122-C, No. 4, pp. 648-654 (2002-4)

(3) Shigeaki Fukuda, Toshihisa Kosaka, Sigeru Omatu : "Bill Money Classification of Japanese Yen Using Time Series Data" Trans. IEE of Japan, Vol. 115-C, No. 3, pp. 354-360 (1995-3)

(4) Hideki Asou: "Information Processing by Neural Network"

(5) T. Kohonen: " Self-Organizing Maps", Springer, Berlin, Germany (1995)

(6) Toshihisa Kosaka, Norikazu Taketani, Sigeru Omatu, Kunihiro Ryo: "US Dollar Classification by the LVQ Method Based on Reliability Criterion " Trans. IEE of Japan, vol. 119-No. 11 pp1359-1364(1999-11)

(7) Takashi Soeda, Mituo Ota, Sigeru Omatu: "Introduction to Mathematical Statistics" Nisshin Publishing Company

(8) Nobuaki Kamimoto, Bingchen Wang, Sigeru Omatu : "Quality Test of Interphones Using Two kinds of Neural Networks" Trans. IEE of Japan, vol. 122-C, No. 10, 2002

Proc. of The Ninth Int. Symp. on Artificial Life and Robotics (AROB 9th '04)
Beppu, Oita, Japan, 28-30 January, 2004

Separation of Acoustic Signals of Transmission Machines by ICA

Nobuaki Kamimoto*, Yutaka Yamada*, Masami Kitamura*, and Kiyoshi Nishikawa**
* Matsushita Electric Works Ltd., **Kanazawa University

Abstract

In this paper, we propose a method of separating the acoustic signals of motors and gears of transmission machines by using independent component analysis (ICA). The frequency distribution of a recorded acoustic signal of a operating transmission machine can be divided into three regions, the low-frequency field, which corresponds to the frequency characteristics of gear, the medium-frequency field, which is mixed with the frequency characteristics of gear and motor, and the high-frequency field, which corresponds to the frequency characteristics of motor. Since only the medium-frequency components are the mixture of acoustic signals of gears and motors, we input the medium-frequency components to the ICA. Then we recover the acoustic signals of gears and motors by adding the low-frequency and high-frequency components to the separation results of the ICA, respectively. The experimental results show that our proposed method can separate the acoustic signals of motors and gears of transmission machines successfully.

1. Introduction

In quality evaluation of transmission machines, it is important to separate the sounds of a motor and a gear in order to identify the causes of failures. The ICA method, which is developed to solve the cocktail-party problem, can separate two original acoustic signals from their mixtures by using the information measure of statistically independent properties [1]-[3]. However, many applications in practice denote that the ICA does not perform well in separation by using the observed acoustic signals directly [4]-[5]. To separate the original acoustic signals correctly, additional data processing is necessary before applying the ICA.

By applying the fast fourier transform (FFT) to a recorded acoustic signal of a operating transmission machine, we observe that its frequency distribution can be divided into three regions, the low-frequency field, which corresponds to the frequency characteristics of gear, the medium-frequency field, which is mixed with the frequency characteristics of gear and motor, and the high-frequency field, which corresponds to the frequency characteristics of motor. Thus, we design two signals to simulate the separation process of acoustic signals of a gear and a motor. The simulation results show that we can obtain the better separation results by only using the medium-frequency field. It seems that those low-frequency and high-frequency components, which are not mixed in the frequency field of observed acoustic signals, affect the separation accuracy.

In this paper, we first record the acoustic signals of operating transmission machines. By applying the band-pass filters, we obtain the respective components of low-frequency, medium-frequency and high-frequency. Then we input the medium-frequency components to the ICA. Finally, we recover the acoustic signals of gears and motors by adding the low-frequency and high-frequency components to the separation results of the ICA, respectively. The experimental results show that our proposed method can separate the acoustic signals of motors and gears of transmission machines successfully.

2. Simulation Results

Suppose we have two original signals s_1 and s_2, their frequency characteristics are illustrated in Figs. 1 and 2, respectively where f_1, f_2 and f_4 are constant and f_3 is variable. If we use two microphones to record the acoustic signals, we have two observed

signals $x_1(t) = a_{11}s_1 + a_{12}s_2$, $x_2(t) = a_{21}s_1 + a_{22}s_2$. We use the ICA to separate the original signals s_1 and s_2 from the observed signals.

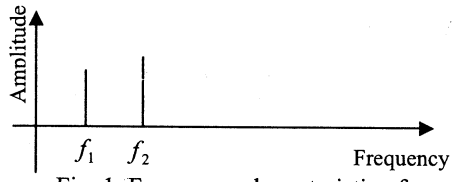


Fig. 1. Frequency characteristic of s_1.

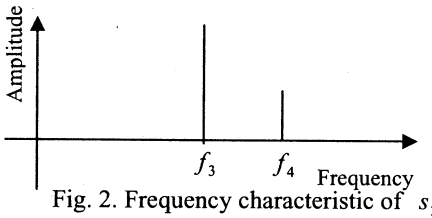


Fig. 2. Frequency characteristic of s_2.

Table1 shows the separation results of observed signals x_1 and x_2 by using the ICA where "Y" denotes that the original signals s_1 and s_2 can be separated correctly and "N" denotes that the original signals cannot be separated correctly. From Table 1, it can be seen that sometimes we fail to separate the acoustic signals s_1 and s_2 by using the observed signals x_1 and x_2 directly.

Table 1. Separation results of observed signals (unit: Hz)

f_3	30	40	50	60	70	80	90	100	110
Y/N	Y	Y	Y	N	Y	Y	Y	N	Y
f_3	120	130	150	160	170	180	190	200	210
Y/N	N	Y	Y	Y	Y	N	Y	Y	Y
f_3	220	230	$f_1 = 20$, $f_2 = 140$, $f_4 = 240$						
Y/N	Y	Y							

Figures 3 and 4 show the frequency characteristics of observed acoustic signals x_1 and x_2 while $f_3 = 100$ Hz. Figures 5 and 6 show the separated signals s_1' and s_2' by using the ICA. From these figures, it can be seen that the original signals s_1 and s_2 are not separated correctly. However, we can separate the frequency components f_2 and f_3 successfully by using the ICA after filtering the frequency components f_1 and f_4 with a band-pass filter. Thus, we can obtain the original acoustic signals s_1 and s_2 by adding the frequency components f_1 and f_4 to the separation results of the ICA, respectively.

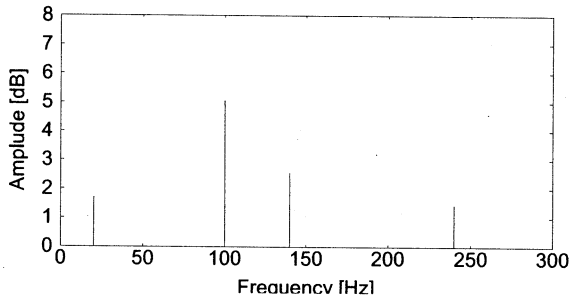


Fig. 3. Frequency characteristic of observed signal x_1.

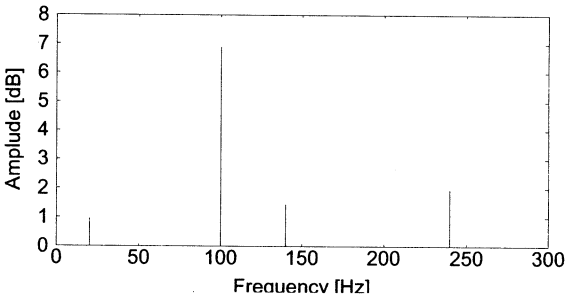


Fig. 4. Frequency characteristic of observed signal x_2.

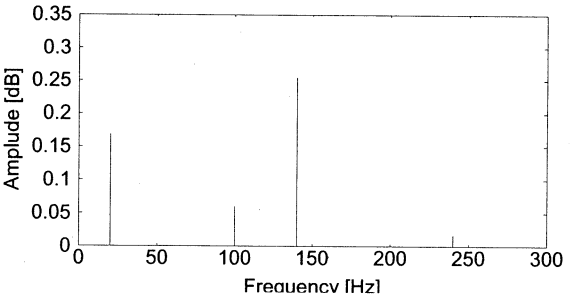


Fig. 5. Frequency characteristic of separated signal s_1'.

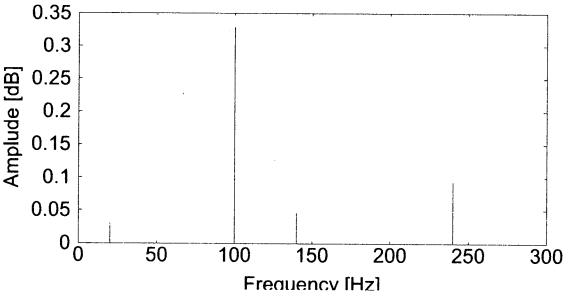


Fig. 6. Frequency characteristic of separated signal s_2'.

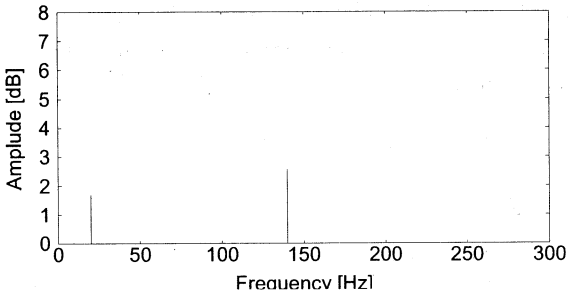


Fig. 7. Frequency characteristic of separated signal s_1' with band-pass filter.

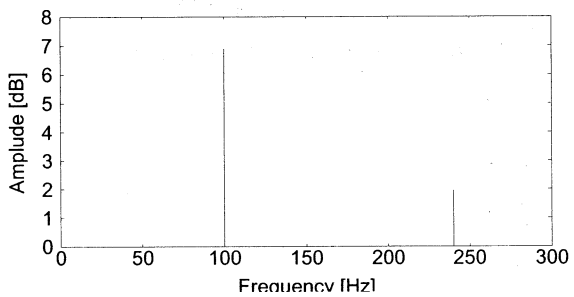


Fig. 8. Frequency characteristic of separated signal s_2' with band-pass filter.

Figures 7 and 8 show the frequency characteristics of separated signals s_1' and s_2' with band-pass filter, respectively where the amplitudes of frequencies f_2 and f_3 are amplified according to the relationships between f_1 and f_2, f_3 and f_4 in Figs. 3 and 4. From these figures, it can be seen that the original acoustic signals of s_1 and s_2 are separated correctly.

3. Experiment Results

According to the above simulation results, we separate the acoustic signals of motors and gears of transmission machines by using the ICA. We show the system of measuring acoustic signals in Fig.9. We first use two microphones, which are held in different locations, to record the acoustic signals of operating transmission machines. By applying the band-pass filters, we obtain the respective components of low-frequency, medium-frequency and high-frequency. Since only the medium-frequency components are the mixture of acoustic signals of gears and motors, we input the medium-frequency components to the ICA. Then we recover the acoustic signals of gears and motors by adding the low-frequency and high-frequency components to the separation results of the ICA, respectively. To verify the effectiveness of our proposed method, we also give the separation results by applying the recorded acoustic signals of transmission machines to the ICA directly.

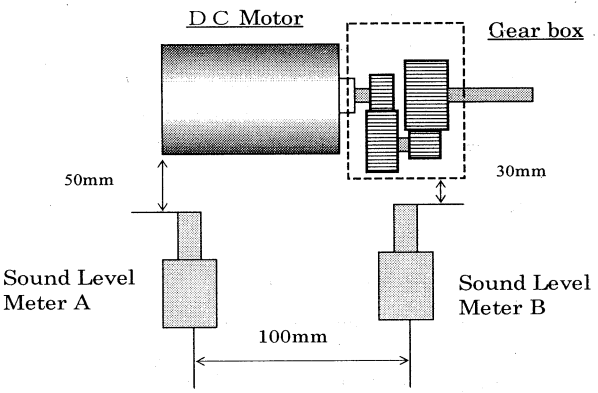


Fig. 9. System of measuring acoustic signals.

We show acoustic signal and spectra of two sound level meters (SLMs) and result of ICA in next. Fig.10 (a) is acoustic signal of sound level meter A. Fig.10 (b) is acoustic signal of sound level meter B. The rotational speed ratio of motor (3200rpm) and gear output is 30:1. According to, frequency band of both spectra are different. The fundamental frequency of motor rotation is in medium-frequency band. The fundamental frequency of gear rotation is in low-frequency band. But, high-frequency band has higher harmonic frequency of motor rotation. Medium-frequency band has rotational speed of motor and harmonic frequency of gear. If motor has trouble, the sign of abnormality appear at high-frequency band. If gear has trouble, the sign of abnormality appear at medium-frequency band.

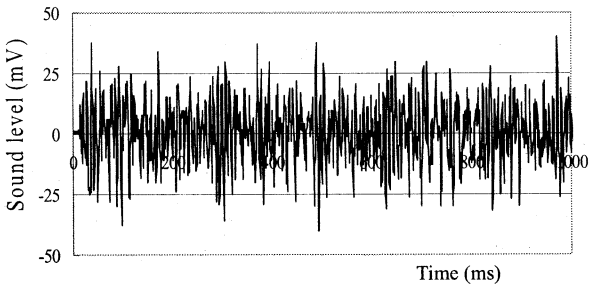


Fig. 10 (a). Acoustic signal of the left SLM.

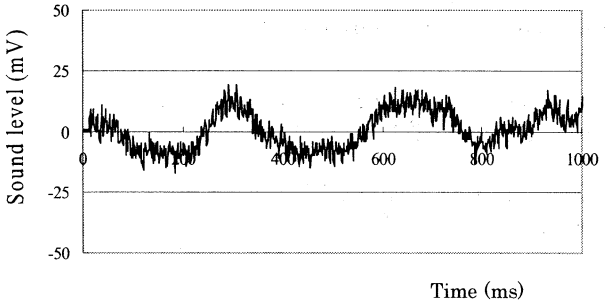


Fig. 10 (b). Acoustic signal of the right SLM.

Fig.11 (a) is spectrum of Fig.10 (a). Fig.11 (a) is spectrum of Fig.10 (b).

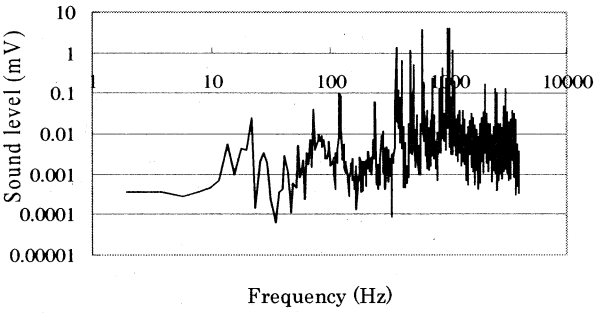


Fig. 11 (a). Spectrum of signal (a).

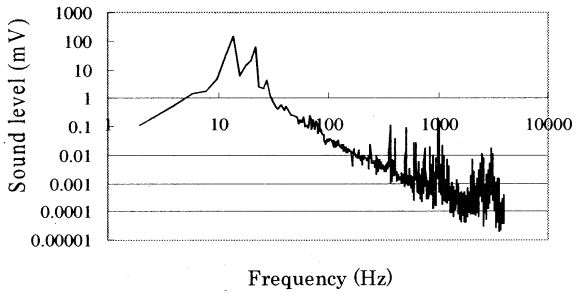


Fig. 11 (b). Spectrum of signal (b).

We decided low-frequency band is below 300Hz, high-frequency band is more than 2 kHz and medium-frequency band is from 300Hz to 2 kHz.

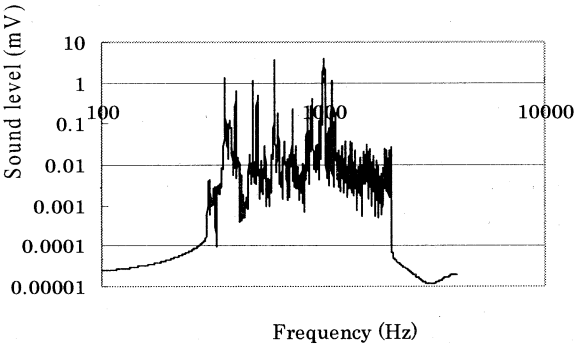


Fig. 12 (a). medium-frequency spectrum of signal (a).

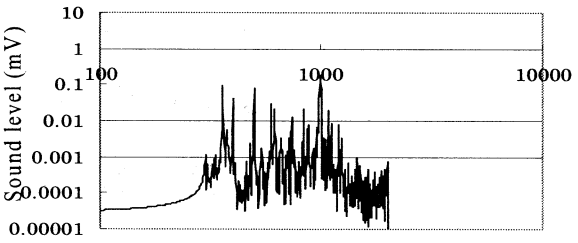


Fig. 12 (b). medium-frequency spectrum of signal (b).

Fig. 12 (a) is medium-frequency of Fig.11 (a). Fig. 12 (b) is medium-frequency of Fig.11 (b).

We applied ICA to medium- frequency spectrum of signal (a) and (b).

Fig. 13 (a) is medium- frequency spectrum of signal (a) after ICA. Fig. 13 (b) is medium- frequency spectrum of signal (b) after ICA.

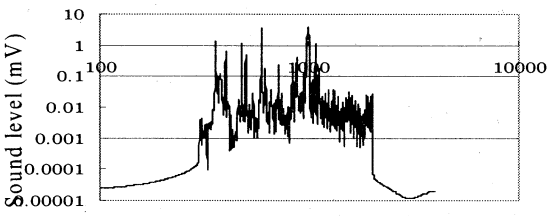


Fig. 13 (a). medium-frequency spectrum of signal (a) after ICA.

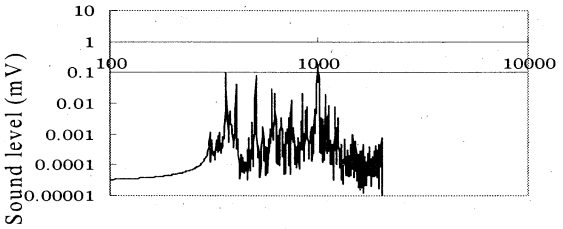


Fig. 13 (b). medium-frequency spectrum of signal (b) after ICA.

4. Conclusion

Until, the separate acoustic noise of motor and gear was difficult. But we used this method; we could separate two acoustic noises.

5. Reference

1. T.W./Lee, Independent Component analysis: Theory and Applications, Kluwer Academic Publishers, 1998.
2. A.Cichocki, and S.amari, Adaptive Blind Signal and Image Processing, John Wiley, 2002.

Proc. of The Ninth Int. Symp. on Artificial Life and Robotics (AROB 9th '04)
Beppu, Oita, Japan, 28-30 January, 2004

Intelligent Classification of Bill Money

Sigeru Omatu[+], Masaru Teranisi[++], and Toshihisa Kosaka[+++]
[+]Osaka Prefecture University, Sakai, Osaka 599-8531, Japan
: omatu@cs.osakafu-u.ac.jp
[++]NaraUniversity of Education, Takahata-cho, Nara 630-8528
[+++]Glory TD Himeji, Hyougo 670-8567 Japan

Abstract

For the pattern classification problems the neuro-pattern recognition which is the pattern recognition based on the neural network approach has been paid an attention since it can classify various patterns like human beings. In this paper, we adopt the learning vector quantization(LVQ) method to classify the various money. The reasons to use the LVQ are that it can process the unsupervised classification and treat many input data with small computational burdens. We will construct the LVQ network to classify the Italian Liras. Compared with a conventional pattern matching technique, which has been adopted as a classification method, the proposed method has shown excellent classification results.

1. Introduction

Bill money classification by transaction machines has been important to make progress the office automation[1]. Since sizes of bills are different according to kinds of bills, the measurement data of bills include various variations. Human being can classify the bills correctly even if they are suffered from those variations such as rotation and shift. But usual pattern recognition using a conventional transaction machine cannot give us the correct classification result under such cases since the basic method is a pattern matching principle. Furthermore, the conventional pattern matching method requires many template patterns for many kinds of bills, which takes much time and needs much experience[1].

Recently, neural networks which are based on the biological mechanism of human brain have been focussed since they have intelligent pattern recognition ability[2]. In this paper, we will apply the neural network approach to classify the bill money under various conditions by using transaction machines. The learning vector quatization(LVQ) has been used to classify the bills since it can treat high dimensional input and has simple learning structure[3]. The LVQ network adopted here has 64x15 units in the input layer and many units at the output layer. The bills are Italian Liras of of 8 kinds, 1,000, 2,000, 5,000, 10,000, 50,000 (new), 50,000 (old), 100,000 (new), 100,000 (old) Liras with four directions A,B,C, and D where A and B mean the normal direction and the upside down direction and C and D mean the reverse version of A and B. The simulation results show that the proposed method can produce the excellent classification results compared with the conventional method..

2. Competitive Neural Networks

We will explain the competitive neural networks that are used to classify the bill money. The structure of a LVQ competitive network is shown in Fig. 1. The input for the LVQ is bill money data where an original image consists of 128x64 pixels and the input data to the network is compressed as 64x15 pixels to decrease the computational load. The output of the network consists of the Italian Liras of 8 kinds, 1,000, 2,000, 5,000, 10,000, 50,000 (new), 50,000 (old), 100,000 (new), 100,000 (old) Liras with four directions A,B,C, and D where A and B mean the normal direction and the upside down direction and C and D mean the reverse version of A and B.

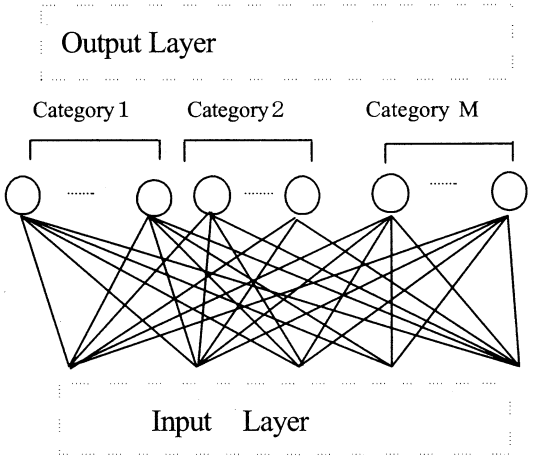


Fig. 1. Structure of the LVQ networks.

In the input layer the original bill money data are applied and all the units at the input layer are connected to all the neurons at the output layer with connection weight W_{ij}. W_{ij} denotes the connection weight from the unit j in the input layer to unit i in the output layer. The output layer will output only one neuron which is called winner neuron. The winner neuron is selected as the neuron with the minimum distance between an input vector and its connection weight vector. The connection weights W_{ij} are set by the random number at the beginning. Here, we set the mean vector of the cluster plus small random number. Then the following learning algorithm of the connection weight vector is used.

LVQ algorithm

Step 1. Find the unit c at the output layer which has the minimum distance from the input data **x** (t)

$$\|\mathbf{x}(t)-\mathbf{W}_c\| = \min_i \|\mathbf{x}(t)-\mathbf{W}_i\|$$

where $\|\ \|$ denotes the Euclidean norm and t denotes the iteration time.

Step 2. If the input **x** (t) belongs to Category c, then

$$\mathbf{w}_c(t+1) = \mathbf{w}_c(t) + \alpha(t)(\mathbf{x}(t) - \mathbf{w}_c(t))$$

$$\mathbf{w}_i(t+1) = \mathbf{w}_i(t),\ i \neq c$$

and if the input **x** (t) belongs to the other Category j ($j \neq c$), then

$$\mathbf{w}_c(t+1) = \mathbf{w}_c(t) - \alpha(t)(\mathbf{x}(t) - \mathbf{w}_c(t))$$

$$\mathbf{w}_i(t+1) = \mathbf{w}_i(t),\ i \neq c$$

where $\alpha(t)$ is a positive function and denotes learning rate.

In the usual LVQ $\alpha(t)$ is given by $\alpha(t) = \alpha_0(1-\frac{t}{T})$

where ($0<\alpha_0<1$) is a positive and T is a total number of learning iterations.

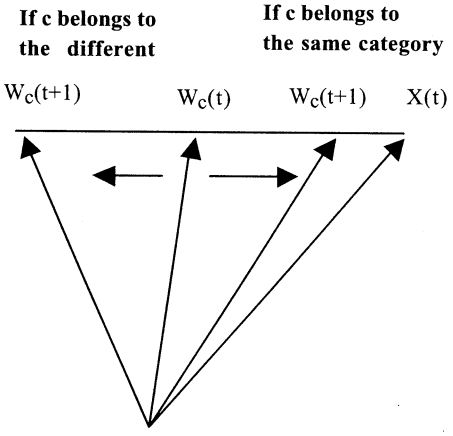


Fig.2. Principle of the LVQ algorithm where the right hand side shows the same category case of **x**(t) and Category c and the left hand side denotes the different category case.

The above algorithm for selection of new weight vector $W_c(t+1)$ can be explained graphically as Fig. 2 .

In the above LVQ algorithm, the learning rate $\alpha(t)$ plays an important role for convergence. To adjust the parameter, Kohonen has proposed an optimization method without proof as follows:

$$\alpha_c(t) = \frac{\alpha_c(t-1)}{1+s(t-1)\alpha_c(t-1)}$$

where s(t) =1 if **x**(t) belongs to the same Category c and s(t)=-1 if **x**(t) does not belong to the same Category c. Here, $\alpha_c(t)$ denotes the learning rate for the pattern of Category C. In what follows, we will prove the above relation. From the learning rule of the LVQ, we have

$$\mathbf{w}_c(t+1) = \mathbf{w}_c(t) + s(t)\alpha_c(t)(\mathbf{x}(t) - \mathbf{w}_c(t))$$
$$= (1-s(t))\alpha_c(t)\mathbf{w}_c(t) + s(t)\alpha_c(t)\mathbf{x}(t)$$

and

$$\mathbf{w}_c(t) = \mathbf{w}_c(t-1) + s(t-1)\alpha_c(t-1)$$
$$(\mathbf{x}(t-1) - \mathbf{w}_c(t-1))$$
$$= (1-s(t-1))\alpha_c(t-1)\mathbf{w}_c(t-1)$$
$$+ s(t-1)\alpha_c(t-1)\mathbf{x}(t-1)$$

Substituting the latter equation the former one, we have

$$\mathbf{w}_c(t+1) = (1-s(t)\alpha_c(t))(1-s(t-1)\alpha_c(t-1))\mathbf{w}_c(t-1)$$
$$+ s(t)\alpha_c(t)\mathbf{x}(t) + s(t-1)\alpha_c(t-1)(1-s(t)\alpha_c(t))\mathbf{x}(t-1).$$

We assume that the optimal rate adjusts the effect of x(t) and x(t-1) equally within the absolute value, that is,

$$\alpha_c(t) = (1-s(t)\alpha_c(t))\alpha_c(t-1).$$

Then we have

$$\alpha_c(t) = \frac{\alpha_c(t-1)}{1+s(t-1)\alpha_c(t-1)}.$$

From the above equation, we can see that the value of $\alpha_c(t)$ become larger than 1 when s(t-1)= - 1, which may make the learning algorithm unstable. Thus, we must fix the $\alpha_c(t)$ to a boundary value α_0 when it becomes larger than 1.

$$\alpha_c(t+1) = \alpha_0 \quad \text{if} \quad \alpha_c(t+1) > 1.$$

Using the above OLVQ1 algorithm, we will classify the Italian bills in the following section.

3. Preprocessing Algorithms

The images obtained by transaction machine, there are variations such as rotation or shift. Therefore, we must adjust the images such that the variations may be reduced as much as possible by using the preprocessing. The flow char of the preprocessing procedure is illustrated in Figure 3. In this figure, the original image with 128x64 pixels are observed at the transaction machine in which rotation and shit are included. After correction of these effects, we select a suitable aria which show the bill image and compressed as the image with 64x15 pixels to the neural networks. Although the neural network of the LVQ type could process any order of the dimension of the input data, the small size is better to achieve the fast convergence result. Thus, we have selected the above size of the image.

4. Italian Lira Classification

The bills used here are Italian liras, which have 8 kinds such as 1,000 Liras, 2,000 Liras, 5,000 Liras, 10,000 Liras, new 50,000 Liras, old 50,000 Liras, new 100,000 Liras, and old 100,000 liras. Those Lira bills are used at the input of the transaction machine where four directions such as A, B, C, and D appear since normal direction, reverse direction, and their upside down directions occur at the input as shown in Fig.4.The typical images of 1,000 Lira for four directions are shown in Fig.5. Thus, thirty-two bill images are one set of the classification pattern of the experiment. Total number of data sets is 30 and 10 data sets are used for training of the network

and the remaining 20 data sets are used to test the network. In order to reduce the misclassification, we have set the threshold value d_θ such that if $d_c > d_\theta$, unit c is not fired. This means that
if the minimum distance is not less than d_θ, the input data is not classified. The parameters of the neural network used here are as follows:

Number of units in the input layer=960.

Number of units in the output layer in the initial state=32 where every 50 iterations the number has been adjusted.

Total learning timeT=150.

$\alpha_i(0) = 0.5$, $i = 1, \cdots M$.

Initial values of the weight vectors=mean vectors for training patterns.

$d_\theta = \min_c (m_c + 4.5\sigma_c)$.

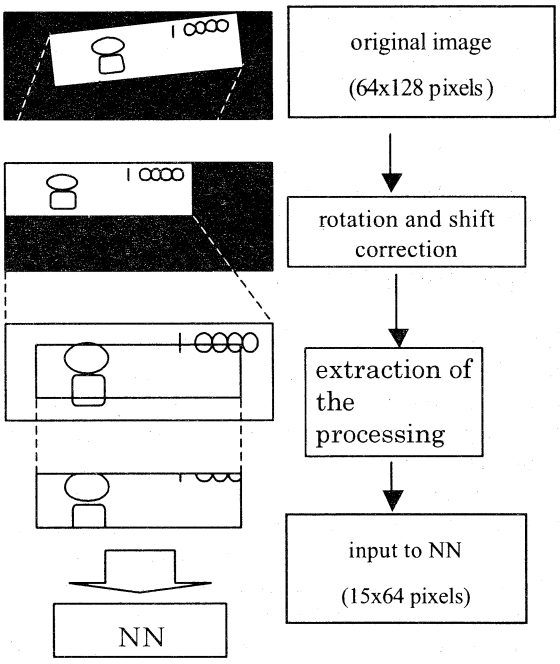


Fig. 3. Preprocessing algorithm.

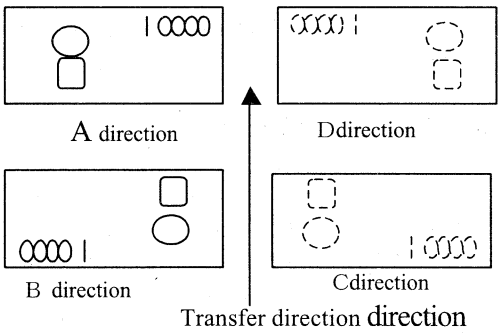
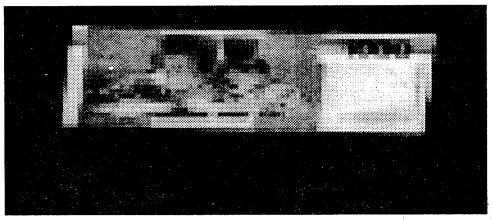


Fig. 4. Four directions of bill money.

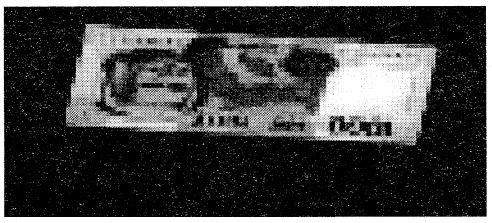
From the original image data we can see that the difference between 50,000 Lira old and new is slight and the difference between old and new100,000. Therefore, it is rather difficult to recognize them so perfectly. but in this case the misclassification like old and new bills within the same values is not serious. Thus, we have regarded these misclassification as the correct one. Furthermore, we have introduced the threshold value to prevent from occurring the misclassification. Thus, even if the minimum distance criterion results in the correct classification, we have decided these bells are unknown. Without these threshold constraint, we could obtain 100% recognition rate in any case.



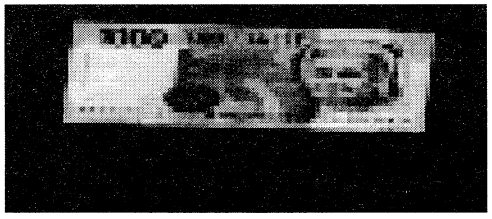
(a) A direction of 1,000Lira



(b) B direction of 1,000 Lira



(c) C direction of 1,000 Lira



(d) D direction of 1,000 Lira

Fig.5. Image of four directions of 1,000 Lira.

5. Conclusions

We have proposed a new classification method of Italian Liras by using the OLVQ1 algorithm. The experimental results show the effectiveness of the proposed algorithm compared with the conventional pattern matching method.

References

[1] S. Fukuda, T. Kosaka, and S. Omatu: Bill Money

Classification of Japanese Yen Using Time Series Data, Trans. Of IEE of Japan, Vol.115-C, No.3, pp.354-360, 9995(in Japanese).
[2] J. Dayhoff: Neural Network Architectures: An Introduction, International Thompson Computer Press, New York, 1990.
[3] T. Kohonen: Self-Organizing Maps, Springer, Berlin, 1995.

Table 1. Recognition rate(%) at t=0.

		Directions			
		A	B	C	D
Italian Liras	1,000	100	100	100	100
	2,000	100	100	100	100
	5,000	100	100	100	100
	10,000	100	100	100	100
	50,000(new)	100	100	100	100
	50,000(old)	85	100	80	95
	100,000(new)	100	100	90	100
	100,000(old)	100	100	95	90

Table 2. Not fired rate(%) at t=0.

		Directions			
		A	B	C	D
Italian Liras	1,000	20	15	15	10
	2,000	5	10	25	25
	5,000	15	20	5	0
	10,000	10	10	10	5
	50,000(new)	5	0	20	5
	50,000(old)	0	0	0	0
	100,000(new)	0	0	0	0
	100,000(old)	0	5	0	0

Table 3. Recognition rate(%) at t=160.

		Directions			
		A	B	C	D
Italian Liras	1,000	100	100	100	100
	2,000	100	100	100	100
	5,000	100	100	100	100
	10,000	100	100	100	100
	50,000(new)	100	100	100	100
	50,000(old)	100	100	95	95
	100,000(new)	100	100	90	100
	100,000(old)	100	100	95	90

Table 4. Not fired rate(%) at t=160.

		Directions			
		A	B	C	D
Italian Liras	1,000	5	0	5	0
	2,000	0	10	25	25
	5,000	15	20	5	0
	10,000	10	0	0	5
	50,000(new)	5	0	0	0
	50,000(old)	0	5	0	0
	100,000(new)	0	0	0	0
	100,000(old)	0	5	0	0

Table 5. Number of units after learning.

		Directions			
		A	B	C	D
Italian Liras	1,000	2	2	2	2
	2,000	2	1	1	1
	5,000	1	1	1	1
	10,000	1	2	2	1
	50,000(new)	2	1	1	1
	50,000(old)	2	1	3	1
	100,000(new)	1	1	1	1
	100,000(old)	1	1	1	1

Proc. of The Ninth Int. Symp. on Artificial Life and Robotics (AROB 9th '04)
Beppu, Oita, Japan, 28-30 January, 2004

Removal of Environmental Noise with Adaptive Filter

Yuji Kogeichi
Computer and Systems Science
Osaka Prefecture University
1-1 Gakuencho Sakiai-City Osaka
599-8531

Sigeru Omatu
Computer and Systems Science
Osaka Prefecture University
1-1 Gakuencho Sakiai-City Osaka
599-8531

Abstract

Based on independent component analysis (ICA) and an adaptive filter, we propose audio-signal separation under a periodical noise. In real circumstances, there are some time delays from sound sources to microphones since the microphones are located at the different points with different distances. The time delays affect the accuracy of the signal separation. In this paper, we formulate the observation system as the convolution summation by consideration of the time delays and the microphone dynamics. Then we apply the ICA in the frequency domain to the audio-signal separation. The simulation results are compared with those of the time domain method. Furthermore, to improve the separation results in which some pseudo-periodic noisy sounds have remained, we adopt the adaptive filter. The simulation result shows effectiveness of audio-signal separation under pseudo-periodical noisy.

Keywords: ICA, Adaptive filter, Signal processing

1 Introduction

Human auditory sense is one of the outstanding abilities of human. We can specify number of sources and classify them when we listen to sounds in environmental noise. At nondestructive inspection, inspectors often use audio data for classifying defective and non-defective items. In specific, they hit objects with tool and listen to the sound. Then they judge defective or non-defective. But the judge is too difficult for an amateur and a specialist is in need.

We are setting a goal at building a human assistant system of audio recognition which specifies number of sources and classify them in an environment noise like a specialist. In this paper, we propose audio-signal separation under a periodical noise. We use the ICA for separating an audio-signal from a noise and adaptive filter to remove an removing environmental noise from the audio-signal. ICA is an approach which estimates original signals using only information of mixed signals which were observed by microphones. The adaptive filter is an approach which adjusts their own filter weights to approximate optimal ones automatically. Using this filter, we only decide a step size and filter length of two parameters. For amateurs, this filter seems to be the best filter to use because of these characteristics. Our purpose is to recognize sounds and denoise. But it is too difficult to separate them. So in this paper, we assume that the number of source signals is two and our recording environment is in a factory which holds only periodical noise. We use two of one channel sound data which were recorded by microphones which were located at different points at the same time. One microphone is pointed to object sound source to record the source signal with an environmental noise. The other is pointed to other direction to record only the environmental noise.

2 Temporal structure of ICA

When microphones are located at the same distance from source signals, no time delay occurs among observed signals. It is called temporal structure. The M vector of observed signals is indicated by $\mathbf{x}(t)$ and N vector of source signals is indicated by $\mathbf{s}(t)$.

$$\mathbf{x}(t) = [x_1(t), \cdots, x_M(t)]^T \quad (1)$$

$$\mathbf{s}(t) = [s_1(t), \cdots, s_N(t)]^T. \quad (2)$$

The source signals $s_1, \cdots, s_N$ are assumed mutually statistically independent, and zero-mean. It is assumed that $\mathbf{x}(t)$ can be written as

$$\mathbf{x}(t) = \mathbf{A}\mathbf{s}(t). \quad (3)$$

where $\mathbf{A}$ is an unknown full rank $M \times N$ mixing matrix. An ICA problem is to find separating matrix W which

makes output signals $y_1, \cdots, y_N$ mutually statistically independent as much as possible. $\mathbf{y}(t)$ is written as

$$\mathbf{y}(t) = \mathbf{W}\mathbf{x}(t). \tag{4}$$

As we assume, source signals are statistically independent mutually. The probability density distribution is written as

$$\begin{aligned} P(\mathbf{s}) &= P(s_1, s_2, \cdots, s_n) \\ &= P(s_1)P(s_2)\cdots P(s_n). \end{aligned} \tag{5}$$

When we change W optimally to make $\mathbf{y}$ as independent as possible, we can obtain next equation.

$$\begin{aligned} P(\mathbf{y}) &= P(y_1, y_2, \cdots, y_n) \\ &= P(y_1)P(y_2)\cdots P(y_n). \end{aligned} \tag{6}$$

As we see those equations, we can obtain the same probability density distribution when we shuffle elements of the vector. So we can not determine which element of $\mathbf{y}(t)$ corresponds to the element of $\mathbf{s}(t)$.

We can not obtain a real probability density distribution from observed signal because what we observed is a part of infinite data. But what we want to know is independency of the output signal $\mathbf{y}$. So we use mutual information as a scale of independency in stead of probability density distribution. Mutual information I is defined as

$$\begin{aligned} I(\mathbf{y}) &= \int p(\mathbf{y}) \log \frac{p(\mathbf{y})}{\prod_{i=1}^{n} p(y_i)} d\mathbf{y} \\ &= \sum_{i=1}^{n} H(y_i) - H(\mathbf{y}). \end{aligned} \tag{7}$$

where we indicate an entropy of information theory by $H(\cdot)$. Using $\mathbf{x}$ and $\mathbf{W}$, we can rewrite $H(\mathbf{y})$ as

$$H(\mathbf{y}) = H(\mathbf{x}) + \log|\mathbf{W}|. \tag{8}$$

Then we obtain the next equation.

$$I(\mathbf{y}) = \sum_{i=1}^{n} H(y_i) - H(\mathbf{x}) - \log|\mathbf{W}|. \tag{9}$$

A lot of approaches have been proposed to minimize the mutual information [1].

3 Convolutive structure of ICA

Time delay is occurred if microphones are located at different distance from source signals. When signals contain a time delay, it is called a convolutive structure. The convolutive structure is formulated as

$$\mathbf{x}(t) = \sum_{\tau} \mathbf{A}(\tau)\mathbf{s}(t-\tau). \tag{10}$$

In frequency domain, Equation (10) is rewriten as

$$\mathbf{X}(\omega, t_s) = \mathbf{A}(\omega)\mathbf{S}(\omega, t_s). \tag{11}$$

where t_s is frame number of short time Fourier transformation.

Now, we apply the temporal structure of ICA on each frequency bin. But we have to be careful to recompose the ICA result to time data. Because we can not tell which element of $\mathbf{y}$ corresponds to the same element of $\mathbf{s}$ on each frequency bin. Several approaches are proposed on this permutation problem [2] [3].

We use Murata and Ikeda's method for this analysis. Before explain it, we need to define several things. Operator ε is defined as

$$\varepsilon\hat{\mathbf{v}}_\omega(t_s; i) = \frac{1}{2M} \sum_{t'_s=t_s-M}^{t_s+M} \sum_{j=1}^{n} \cdot \parallel \mathbf{v}_{j,\omega}(t'_s; i) \parallel \tag{12}$$

where M is a positive constant and suffix j is the jth element of $v_{j,\omega}(t_s; i)$.

An inner product and norm are defined as

$$\varepsilon\hat{\mathbf{v}}_\omega(t) \cdot \varepsilon\hat{\mathbf{v}}_{\omega'}(j) = \sum_{t_s} \varepsilon\hat{\mathbf{v}}_\omega(t_s; i)\varepsilon\hat{\mathbf{v}}_{\omega'}(t_s; j) \tag{13}$$

$$\parallel \varepsilon\mathbf{v}_\omega(i) \parallel = \sqrt{\varepsilon\hat{\mathbf{v}}_\omega(i) \cdot \varepsilon\hat{\mathbf{v}}_\omega(i)}. \tag{14}$$

Now, using the defined inner product and norm, similarity is defined as

$$\mathrm{sim}(\omega) = \sum_{i \neq j} \frac{\varepsilon\hat{\mathbf{v}}_\omega(i) \cdot \varepsilon\hat{\mathbf{v}}_\omega(j)}{\parallel \varepsilon\hat{\mathbf{v}}_\omega(i) \parallel \parallel \varepsilon\hat{\mathbf{v}}_\omega(j) \parallel}. \tag{15}$$

Then the ICA problem can be solved in the following way. Step1. Sort ω in order of weakness correlation.

$$\hat{\mathbf{y}}_{\omega_1}(t_s; i) = \hat{\mathbf{v}}_{\omega_1}(t_s; i) \qquad i = 1, \cdots, n. \tag{16}$$

Step2. Figure correlation between envelope of ω_k and aggregated envelope from ω_1 through ω_{k-1}

$$\sum_{i=1}^{n} \varepsilon\hat{\mathbf{v}}_{\omega_k}(\sigma(i)) \cdot \left(\sum_{j=1}^{k-1} \varepsilon\hat{\mathbf{y}}_{\omega_j}(i) \right). \tag{17}$$

where σ is a permutation operator.

Step3. Substitute higher similarity one to $\hat{\mathbf{y}}_{\omega_k}(t_s; i)$

$$\hat{\mathbf{y}}_{\omega_k}(t_s; i) = \hat{\mathbf{v}}_{\omega_k}(t_s, \sigma(i)). \tag{18}$$

Step4. Until all frequency elements finish sorting, back to Step2

4 Adaptive filter

Adaptive filter is a filter which adjusts their own parameters automatically [3]. The filter requires little or no prior knowledge of the signal or noise characteristics. So it is well-suited to our purpose. In our recording environment, we want to remove periodical noise. But we don't have knowledge about the noise.

If desired output and filter output signal are indicated by d_i and y_i, the filter error e_i is written as

$$e_i = d_i - y_i \tag{19}$$

$$y_i = \sum_{k=0}^{N-1} w_{ki} x_i - k$$

$$= \mathbf{W}_i^T \mathbf{X}_i \tag{20}$$

where x_i is filter input signal, and w_{ki} is a filter weight $(k = 0, 1, \cdots, N)$, suffix i is a sample number of discrete time.

Vectors $\mathbf{W}_i$ and $\mathbf{X}_i$ are defined as

$$\mathbf{W}_i = [w_{0i}, w_{1i}, \cdots, w_{N-1i}]^T \tag{21}$$

$$\mathbf{X}_i = [x_i, x_{i-1}, \cdots, x_{i-N+1}]^T \tag{22}$$

Then filter changes their own weight to minimize J given by

$$J = e_i^2. \tag{23}$$

Several approaches have been proposed to minimize J. We use the simplest LMS algorithm. An update rule of the LMS algorithm is

$$\Delta \mathbf{W}_i = \mathbf{W}_{i+1} - \mathbf{W}_i \tag{24}$$

$$= -\mu \frac{\partial J}{\partial \mathbf{W}_i} \tag{25}$$

where μ is a step size of update.

5 Removal of noise

Our proposed method is shown as Fig. 1. First, we separate observed data by the convolutive ICA. If priodical noise exists on recorded data, the noise is distributed on separated data. Then we need more microphones to separate them. But in real situation, we don't know how much noises exist.

Next, we remove noise on separated data by the adaptive filter. As we explain, we need no knowledge to use this filter. The setting parameters are step size and filter length.

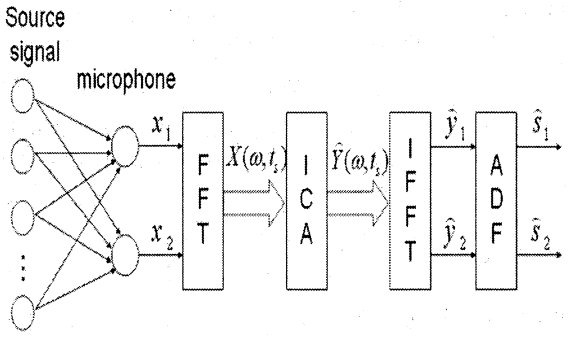


Figure 1: Proposal method

6 Simulations

As we simulate our proposed method, we recorded human voices by microphones. Sound data format is as below.

Format	PCM
Sampling rate	16kHz
Average data rate	32KB/sec
Block size	16bit
Number of channel	1 channel

We make mixing data using $A(z)$ on computer where $A(z)$ is

$$\mathbf{A}(z^{-1}) = \begin{pmatrix} a(z^{-1}) & b(z^{-1}) \\ c(z^{-1}) & d(z^{-1}) \end{pmatrix}$$

$$a(z^{-1}) = 0.7810 + 0.1704z^{-1} + 0.0531z^{-2}$$

$$b(z^{-1}) = 0.4342z^{-1} + 0.2170z^{-2}$$

$$c(z^{-1}) = 0.2641z^{-1} + 0.0724z^{-2}$$

$$d(z^{-1}) = 0.4342 + 0.1824z^{-1} + 0.0412z^{-2}.$$

Figures 2 and 3 are waveforms of human voices. Then we mixed those sounds using $A(z)$ and added 160Hz of periodical noise. Observed data are shown in Figs. 4 and 5. We applied the ICA to those data. We obtained separate a result in Figs. 6 and 7. As we can see, periodical noise is still on separated result in Fig. 6. But in Fig. 7, we see a little effect of the periodical noise. This is from characteristic of the convolutive structure of ICA. Convolutive structure of the ICA separate signals in each frequency bin. Similar data are chosen when reconstruction of separating results. Then we applied adaptive filter in Fig. 6. Figure 8 is an adaptive filter output. Now we can see that the periodical noise is suppressed.

7 Conclusion

Based on ICA and an adaptive filter, we have proposed audio-signal separation method under a periodical noise. We have suppressed the periodical noise by the proposed method. For the future study, we will investigate the case of multichannel signals, and new separation methods.

References

[1] Andrzej Cichocki, Shun-ichi Amari, "Adaptive Blind Signal and Image Processing", *WILEY*, 2002.

[2] Noboru Murata, Shiro Ikeda, Andreas Ziehe, "An Approach to Blind Source Separation Based on Temporal Structure of Speech Signals", *Neurocomputing*, Vol.41, pp.1-24,October 2001.

[3] Hiroshi Sawada,Ryo Mukai,Shoko Araki,Shoji Makino, "A robust and precise method for solving the permutation problem of frequency-domain blind source separation", *ICA2003*,2003.

[4] Bernard Widrow, Samuel D. Stearns, "Adaptive Signal Processing", *Prentice-Hall*, 1985.

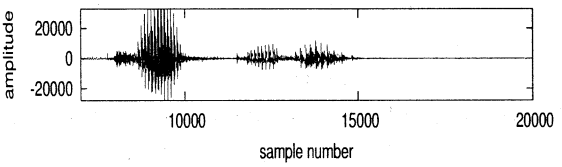


Figure 2: human voice zakuro

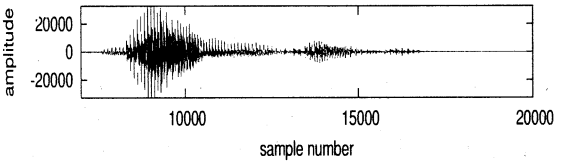


Figure 3: human voice mango

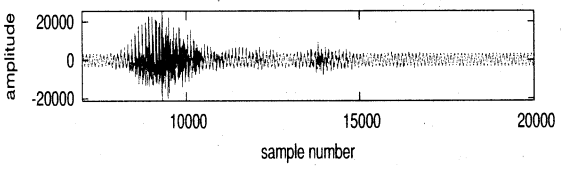


Figure 4: Observed signal 1

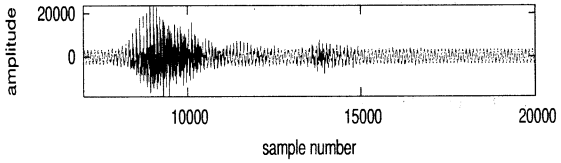


Figure 5: Observed signal 2

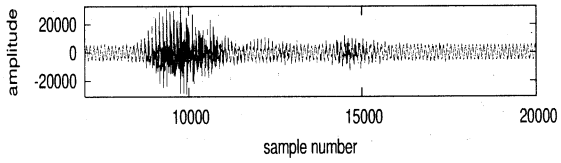


Figure 6: Separate signal 1

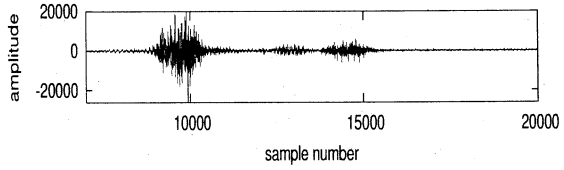


Figure 7: Separate signal 2

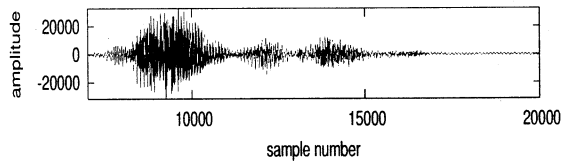


Figure 8: adaptive filter output

Proc. of The Ninth Int. Symp. on Artificial Life and Robotics (AROB 9th '04)
Beppu, Oita, Japan, 28-30 January, 2004

Quadruped Robot Positioning Control of Leg by Linear Visual Servoing

Yukinari Inoue
Graduate School of Systems Engineering
Wakayama University
Sakaedani 930, Wakayama, JAPAN, 640-8510

Noriaki Maru
Faculty of Systems Engineering
Wakayama University
Sakaedani 930, Wakayama, JAPAN, 640-8510

Abstract

We propose the quadruped robot positioning control of the leg by linear visual servoing (indicated as LVS in the following lines). LVS is a visual servoing using binocular visual space, and based on linear approximation of the inverse kinematics. The advantages of this method are robust to calibration errors, and easy to get feedback signals by using only image data. In the past, the effectiveness of LVS had been shown only in humanoid hand-eye system. In this paper, we show that we have a linear relationship between joint space and binocular visual space even for a quadruped robot and LVS is realizable. Additionally we present some experimental results which show the performance and the effectiveness of this method.

1 Introduction

The quadruped walking robot chooses between all dispersed point a stable one to walk on, in order to provide a right shifting also on irregular terrain. Moreover, the four legs expand the movements ability of the robot which is expected to operate on irregular, steep and inclined ground. In such environment, there are many level differences, holes, buried and dangerous objects that is the reason why the accurate positioning control of leg to safe landing point is required. Under these circumstances, the swing legs to a landing point may generate errors because of exterior disturbance or internal robot disturbance that is why the positioning control of leg by vision is needed.

Various kinds of mechanisms of visual servoing have been proposed [1]. But the conventional visual servoing method have many problems. For example, it requires the exact joint angles and camera angles which is very hard to obtain and needs large amounts of calculation.

Mitsuda et al. proposed LVS using binocular visual space in order to solve problems mentioned before[2][3].

When we use a hand-eye system which has a similar structure as a human being, we can approximate the transformation from a binocular visual space (defined as the vergence angle and the horizontal and vertical viewing directions) to a joint space of the arm as a linear function. LVS is a visual servoing based on linear approximation of the inverse kinematics. This method is robust to calibration errors, because it uses neither camera angles nor joint angles. Another advantage of this method is that we can get feedback signals by using only image data.

In the past, the advantages of LVS had been shown only in humanoid hand-eye system. In this paper, we show that we have a linear relationship between joint space and binocular visual space even for a quadruped robot. Furthermore, we propose a positioning control method of the leg of the quadruped robot by LVS. In addition to that, we present some experimental results which shows the performance and the effectiveness of this method.

2 LVS

2.1 Model of the Quadruped Robot

Fig.1 shows the leg-eye coordination of the quadruped robot which has two active cameras mounted on a head which pan and tilt. Robot coordinate system $\sum_r(X_r, Y_r, Z_r)$ is located at the center of the quadruped robot as shown in **Fig.1**. The origin of the Camera coordinate system $\sum_c(X_c, Y_c, Z_c)$ is located at $(0, -(N_H + N_L), G + Z_{off})$ in the robot coordinate system when the neck angle $\zeta = \xi = 0$. Let N_H and N_L be the link length of robot head.

The leg consists of three links and three joints. The elbow joint has 1 d.o.f. We call this joint j_{10}. and the shoulder joint has 2 d.o.f. We call these joints j_{11}, j_{12} respectively. Let L_0 be the link length between first joint and second joint and L_1 be the link length between second joint and third joint and L_2 be the

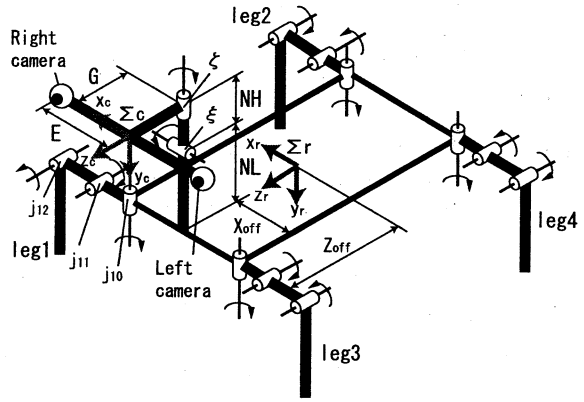


Fig. 1: Model of the quadruped robot

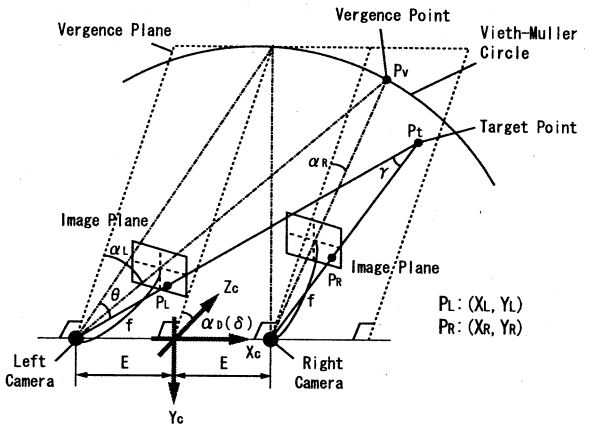


Fig. 2: Model of the active stereo camera

link length between third joint and end tip of the leg. We call the right forward leg as Leg1. The shoulder joint of the Leg1 is located at (X_{off}, Z_{off}) in the robot coordinate system. The focal point of the left and right cameras which pan and tilt independently are located at $(-E, 0, 0)$ and $(E, 0, 0)$ in the Camera coordinate system respectively. We show the parameters of the leg-eye coordination of the quadruped robot in **Table1**

Table 1: Parameters of the model (unit:mm)

Link Length	$L_0 = 45, L_1 = 155, L_2 = 243$
Camera Position	$G = 135, N_H = 30, N_L = 255$
Neck Position	$X_{off} = 101, Y_{off} = 201$
Baseline Length/2	E=50
Focal Length	f=4.5

2.2 Binocular Visual Space

The binocular visual space is defined as the vergence angle γ and the viewing directions θ, δ. This space has been employed by psychologists and physiologists as a model of binocularly-perceived space. The binocular visual space has a close relation to the camera image. We show the stereo camera geometry in **Fig.2.**

The coordinates of a feature point projected on the camera image planes are transformed into binocular visual coordinates by

$$\mathbf{V} = \begin{bmatrix} \alpha_L - \alpha_R \\ (\alpha_L + \alpha_R)/2 \\ \alpha_D \end{bmatrix} + \begin{bmatrix} (X^L - X^R)/f \\ (X^L + X^R)/2f \\ (Y^L + Y^R)/2f \end{bmatrix} \quad (1)$$

where (X^L, Y^L) and (X^R, Y^R) are the coordinates of a feature in the left and right image respectively, and α_L, α_R and α_D are the camera angles. Note that we use the approximation such as $\tan^{-1}(X^{L,R}/f) \simeq X^{L,R}/f$. This approximation is available around the fixation point. Camera angles and image data are transformed into binocular visual coordinates.

2.3 Linear Approximation

Fig.3 show the joint space of the leg1 projected onto camera coordinate system when the neck angles are $\zeta = 60°, \xi = 30°$. This figure shows mapping after neck angle rotated to be able to look the leg1 well. We can find that this mapping is not so linear.

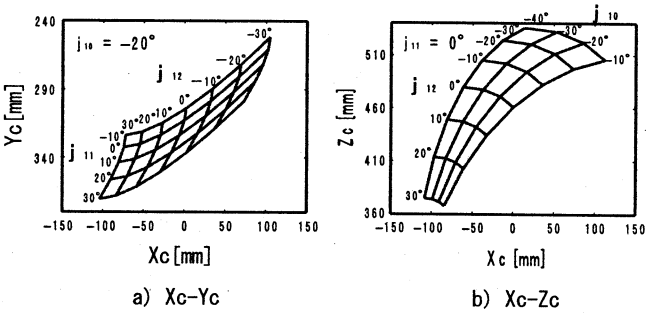


Fig. 3: Joint space projected onto camera coordinate system ($\zeta = 60°, \xi = 30°$)

Fig.4 show the joint space of the leg1 projected onto binocular visual space. This figure indicates that

the joint space projected onto binocular visual space is more linear than that onto camera coordinate system.

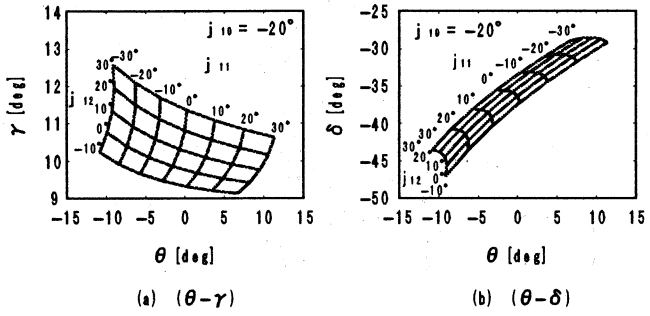


Fig. 4: Joint space projected onto binocular visual space ($\zeta = 60°, \xi = 30°$)

We linearize the transformation between binocular visual space and joint space using the least-squares approximation in the space defined as $-40[deg] \leq j_{10} \leq -10[deg], -10[deg] \leq j_{11} \leq 30[deg], -30[deg] \leq j_{10} \leq -30[deg]$. Then the transformation from binocular visual space to joint space is given by

$$\mathbf{j} = \mathbf{RV} + \mathbf{C} \tag{2}$$

where $\mathbf{V} = (\gamma, \theta, \delta)^T$ and $\mathbf{j} = (j_{10}, j_{11}, j_{12})^T$, **R**:matrix$(3 \times 3)$,**C** :vector$(3 \times 1)$.

The least-squares approximation using binocular visual space result in

$$\mathbf{R} = \begin{bmatrix} -3.115 & 1.944 & -1.728 \\ 20.454 & 0.489 & 0.182 \\ 1.329 & -1.802 & -1.644 \end{bmatrix}, \tag{3}$$

$$\mathbf{C} = \begin{bmatrix} -24.784 \\ -175.641 \\ -94.024 \end{bmatrix}. \tag{4}$$

Fig.5 show the joint space of the leg1 projected onto binocular visual space. In this figure, solid-line indicates linear approximated joint space projected onto binocular visual space, and dotted-line indicates former joint space projected onto binocular visual space.

2.4 LVS

LVS is given by

$$\begin{aligned} \mathbf{u} &= -\lambda \mathbf{R}(\mathbf{V} - \mathbf{V_d}) \\ &= -\lambda \mathbf{R} \begin{bmatrix} (X^L - X^R) - (X_d^L - X_d^R)/f \\ (X^L + X^R) - (X_d^L + X_d^R)/2f \\ (Y^L + Y^R) - (Y_d^L - Y_d^R)/2f \end{bmatrix} \\ &= -\lambda \mathbf{RT}(\mathbf{I} - \mathbf{I_d}), \end{aligned} \tag{5}$$

$$\mathbf{T} = \begin{pmatrix} 1/f & -1/f & 0 & 0 \\ 1/2f & 1/2f & 0 & 0 \\ 0 & 0 & 1/2f & 1/2f \end{pmatrix}$$

$$\mathbf{I} = (X^L, X^R, Y^L, Y^R)^T$$

$$\mathbf{I_d} = (X_d^L, X_d^R, Y_d^L, Y_d^R)^T$$

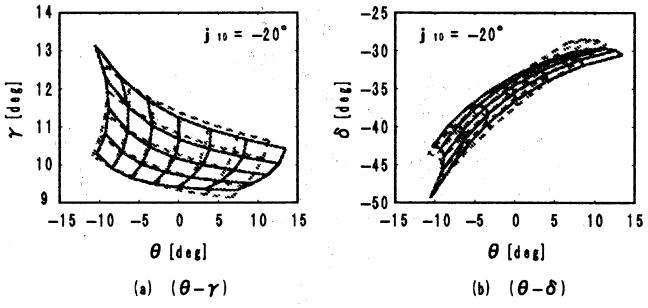


Fig. 5: Comparison of mapping before and after approximation ($\zeta = 60°, \xi = 30°$)

where **u** are control signals to joint velocity controllers, **V** is the binocular visual coordinates of the leg point, $\mathbf{V_d}$ is the binocular visual coordinates of a target and λ is a scalar gain, **R** is the linear approximation matrix of the inverse kinematics obtained in the previous section.

LVS is very robust to calibration error, especially to camera angle errors and joint angles, because the control law includes neither camera angles nor joint angles. Furthermore, the amount of the calculation is very small compared to the conventional visual servoing schemes.

3 Experiment

3.1 System Construction

Fig.6 shows the experimental system. We used quadruped robot TITAN-Ⅷ (TOKYO SEIKI Co.Ltd.). The leg has 3 link and 3 d.o.f. as 2 shoulder joints and 1 elbow joint. We used two cameras(ELMO UN411)which has pan and tilt independently, and image processing board (HITACHI IP5000). We attached a yellow marker at the leg point and used a red object to simplify image processing. The stereo

images are converted in an image using a picture separator (Video Device Co. Ltd.) and input to IP5000. The stereo images are binarized by each color and the gravity centers are calculated to obtain the image coordinates of both the leg point and the target. Then the feedback commands are calculated and sent to the motor driver of TITAN-Ⅷ using DA converter.

In experiment, we used λ=0.15,and the sampling time is 66[msec]. The start and goal are set as **Table2**.

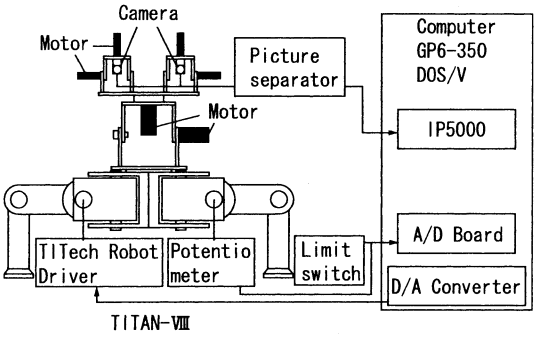


Fig. 6: Experimental system

Table 2: Experimental condition

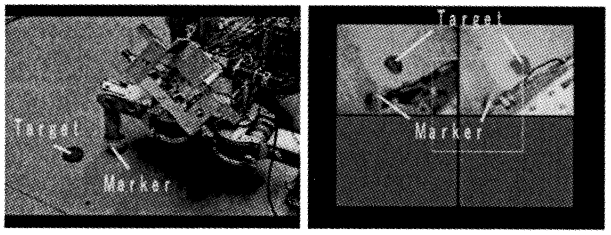
Initial point	$(X_r, Y_r, Z_r) = (269, 165, 263)[mm]$
Target point	$(X_r, Y_r, Z_r) = (400, 243, 320)[mm]$

3.2 Experimental Results

Fig.7 shows overview of experiment and camera image, and **Fig.8** shows 3-D trajectories of the leg1 by LVS. In **Fig.8**, the circle shows the location of the leg point in each sampling time. This figure indicates that LVS is also effective in 3-D positioning control of the leg of the quadruped robot.

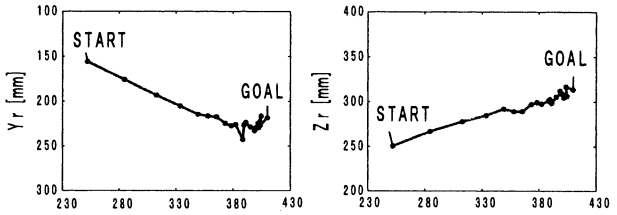
4 Conclusion

We have proposed the quadruped robot positioning control of the leg by LVS. LVS is a visual servoing using binocular visual space, and based on linear approximation of the inverse kinematics. In this paper, we have shown that we have a linear relationship between joint space and binocular visual space even for a quadruped robot and LVS is realizable. Additionally we have presented some experimental results



(a) Overview of experiment (Initial state) (b) Camera image (Initial state)

Fig. 7: Overview of experiment and camera image



(a) X–Y plane (b) X–Z plane

Fig. 8: 3-D Trajectory of the leg1 by LVS

which shows the performance and the effectiveness of this method.

A future research is adaptation to the gait of quadruped robot.

References

[1] K.Hasimoto, T.Ebine and H.Kimura, "Visual servoing with Hand-Eyemanipulator - Optical Control Approach", *IEEE Trans. Robotics and Automation*,Vol.12, No.5, pp. 766-774,1996.

[2] T.Mitsuda, N.Maru, K.Fujikawa and F.Miyazaki, "Linear Approximation of the Inverse Kinematics by using a Binocular Visual space", *Journal of the Robotics Society of Japan*, Vol.14, No.8, pp. 1145-1151,1996.(In Japanese)

[3] T.Mitsuda, N.Maru, and F.Miyazaki, "Binocular visual servoing based on linear time-invariant mapping", *Advanced Robotics*, Vol.11, No.5, pp. 429-443,1997.

Proc. of The Ninth Int. Symp. on Artificial Life and Robotics (AROB 9th '04)
Beppu, Oita, Japan, 28-30 January, 2004

Evolution of Sidewinding Locomotion of Simulated Limbless, Wheelless Robots

Ivan Tanev[1], Thomas Ray[1) 2)]

[1)] ATR Human Information Science Laboratories, 2-2-2 Hikaridai, "Keihanna Science City", Kyoto 619-0288, Japan

[2)] Department of Zoology, 730 Van Vleet Oval, Room 314, University of Oklahoma Norman, Oklahoma 73019, USA

e-mail: {i_tanev, ray}@atr.co.jp

Abstract

Inspired by the efficient method of locomotion of the rattlesnake *Crotalus cerastes*, the objective of this work is automatic design through genetic programming, of the fastest possible (sidewinding) locomotion of simulated limbless, wheelless artifacts. The realism of the simulation is ensured by employing the Open Dynamics Engine (ODE), which facilitates implementation of all the physical forces, resulting from the actuators (muscles), frictions, gravity, collisions and joints constrains. The empirically obtained results demonstrate that the complex sidewinding locomotion emerges from relatively simple motion patterns of morphological segments (vertebrae). The robustness of automatically evolved locomotion is verified by (i) minimal performance degradation when partial damage to the artifact is inflicted and (ii) the ability to tackle obstacles. Contributing to the better understanding of sidewinding locomotion, this work could be considered as a step towards building real limbless, wheelless robots, which feature unique engineering characteristics and are able to perform robustly in difficult environments.

Keywords: genetic programming, locomotion, open dynamics engine, sidewinding, snake robot

1 Introduction

1.1 Advantages and Drawbacks of Snake Robots

Wheelless, limbless snake robots feature potential robustness characteristics beyond the capabilities of most wheeled and legged vehicles – ability to traverse terrain that would pose problems for traditional wheeled or legged robots, and insignificant performance degradation when partial damage is inflicted. Moreover, due to their modular design, snake robots may be cheaper to build, maintain and repair. Some useful features of snake robots include smaller size of the cross sectional areas, stability, ability to operate in difficult terrain, good traction, high redundancy, and complete sealing of the internal mechanisms [1,2]. Robots with these properties open up several critical applications in exploration, reconnaissance, medicine and inspection. However, compared to the wheeled and legged vehicles, snake robots feature (i) smaller payload, (ii) more difficult thermal control, (iii) more difficult control of locomotion gaits and (iv) relatively inferior speed characteristics. Considering the first two drawbacks as beyond the scope of our work, and focusing on the drawbacks of control and speed, we intend to address the following challenge: how to control such a snake robot in order to achieve fastest possible speed of locomotion.

1.2 Automated Design of Locomotion of Snake Robot

Although for many tasks, handcrafting the robot locomotion control code can be seen as a natural approach, it might not be feasible for developing the control code of the snake robot due to its morphological complexity. While the overall locomotion gait of the snake robot might emerge from relatively simply defined motion patterns of morphological segments of the robot, neither the degree of optimality of the developed code nor the way to incrementally improve the code is evident to the human designer [3]. Thus, an automated mechanism for solution evaluation and corresponding rules for incremental optimization of the intermediate solution(s) are needed. The proposed approach of employing genetic programming (GP) implies that the code, which governs the locomotion of the snake robot is automatically designed by a computer system via simulated evolution through selection and survival of the fittest in a way similar to the evolution of species in the nature. The use of an automated process to design the control code opens the possibility of creating a solution that would be better than one designed by a human.

1.3 Evolving Realistically Simulated Snake Robot

Evolving a snake robot's locomotion (and in general, behavior of any robot) is often performed as a first step in the sequence of simulated off-line evolution (phylogenetic learning) of the robot's software model, followed by on-line adaptation (ontogenetic learning) of evolved code on a physical robot situated in a real environment [4]. Off-line software simulation can facilitate the process of robot controller design because the verification of robot behavior on physical robots is extremely time consuming, costly and often dangerous for the robot and surrounding environment. Moreover, in some cases it is appropriate to initially model not only the locomotion, but also to co-evolve the most appropriate morphology of the artifact (i.e. number of phenotypic segments; types and parameters of joints which link segments; actuators' power; type, amount and location of sensors; etc.) [5,6] and only then (if appropriate) to physically implement it as hardware. The software model, used to simulate the robot should fulfill the basic requirements of being quickly developed, adequate, and fast running [7]. The

typically slow development time of GP stems from the highly specific semantics of the main attributes of GP, such as representation, genetic operations and fitness evaluation. Development time of GP can be significantly reduced through incorporating off-the-shelf software components and open standards in software engineering. To address this issue, we developed an XML-based GP framework, which, employing the open XML standard, contributes to significant reduction of development time of GP by utilizing (i) the off-the-shelf document object model (DOM) parsers for representing simulated individuals in GP and (ii) built-in API of DOM parsers for implementing genetic operations (crossover and mutation). To address the issues of adequacy and runtime efficiency of snake robot simulation, we applied the Open Dynamic Engine (ODE) freeware software library for simulation of rigid body dynamics.

1.4 Objective

The objective of our work is to investigate the feasibility of applying GP for automatic design of the fastest possible locomotion of realistically simulated snake robot. Inspired by the fast sidewinding locomotion of the rattlesnake *Crotalus cerastes*, this work is motivated by our desires to (i) better understand the mechanisms underlying sidewinding locomotion of natural snakes, (ii) explore the phenomenon of emergence of locomotion of complex bodies from simply defined motion patterns of the morphological segments comprising these bodies, (iii) verify the feasibility of employing ODE for realistic software simulation of a snake robot, and (iv) investigate the practicality of building real snake robots.

The remainder of this document is organized as follows. Section 2 emphasizes the key features of the GP proposed for evolution of locomotion of simulated snake robot. Section 3 presents empirical results of evolving locomotion patterns of snake robots and discusses the emergence of sidewinding locomotion. Finally, Section 4 draws a conclusion and discusses directions for future research.

2 Approach

2.1 Representation of Snake Robot

The snake robot is simulated as a set of identical spherical morphological segments ("vertebrae"), linked together via universal joints. All joints feature identical (finite) angle limits and have two groups of actuators ("muscles") that perform the rotation of the joint in the horizontal and vertical planes (Figure 1). Considering the representation of the snake robot, the task of designing the fastest locomotion can be rephrased as discovering temporal patterns of desired turning angles of horizontal and vertical actuators of each segment, that result in fastest overall locomotion of the snake.

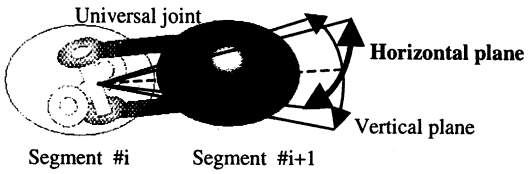


Figure 1. Morphological segments linked via universal joint. Actuators of the joint perform the rotation of the segment `#i+1` in horizontal and vertical plane.

In order to realistically simulate the overall locomotion of a snake robot for a given pattern of desired turning angles of actuators, accounting for all the forces which result not only from actuators, but also from gravity, mass of morphological segments, friction with the surface (the major driving force of wheelless, limbless locomotion), collisions and joint constrains, we implemented the snake robot model in the Open Dynamics Engine ODE environment [8]. ODE is a free, industrial quality library for simulating articulated rigid body dynamics. It is fast, flexible and robust, and it has built-in collision detection.

2.2 GP

Genetic programming (GP) [9] is a domain-independent problem-solving approach in which a population of computer programs (individuals' genotypes) is evolved to solve problems. The simulated evolution in GP is based on the Darwinian principle of reproduction and survival of the fittest. The fitness of each individual is based on the quality with which the phenotype of the simulated individual is performing in a given environment. In applying GP to evolution of the snake robot, the genotype of the snake is associated with two arithmetical expressions, which represent the temporal patterns of desired turning angles of both the horizontal and vertical actuators of each morphological segment. Since locomotion gaits are periodical, we include the `sin` and `cos` in the GP function set in addition to the arithmetical functions. Terminal symbols include the variables `time`, `index` of the current morphological segment of the snake, and two constants: `Pi`, and `random` constant within the range [0, 2]. The main parameters of the GP are shown in Table 1. As depicted in the table, the fitness function measures the velocity of snake, which is estimated from the distance, which the center of the mass of the snake travels during the trial. The fitness evaluation routine is shown in Figure 2.

Inspired by its flexibility, and the recently emerged widespread adoption of document object model (DOM) and extensible markup language (XML), we represent evolved genotypes of simulated snake robots (expressions `GenH` and `GenV` in Figure 2) as DOM-parse trees represented as flat XML text. Our approach implies that both evaluation of the desired turning angles during fitness evaluation (functions `EvalHorisontalAngle` and `EvalVerticalAngle`, shown in Figure 2) and genetic operations are performed on DOM-parse trees using off-the shelf, platform- and language neutral DOM-parsers. The corresponding XML-text representation (rather than S-expression) is used as a flat file format, feasible for migration of genetic programs among the computational nodes in an eventual distributed implementation of the GP. The benefits of using DOM/XML-based representations of genetic programs, as documented in

[10] can be briefly summarized as follows: (i) W3C-standard XML schema offers a generic way for representing the grammar of STGPE; (ii) using the standard built-in API of DOM-parsers for maintaining and manipulating genetic programs; (iii) OS neutrality of parsers; (iv) algorithmic language neutrality of DOM-parsers, and (vi) inherent Web-compliance of eventual parallel distributed implementation of the GP.

Table 1. Main parameters of GP

Category	Designation
Function set	{sin, cos, +, -, *, /}
Terminal set	{time, segment_ID, Pi, random constant}
Population size	200 individuals
Selection	Binary tournament, ratio 0.1
Elitism	Best 4 individuals
Mutation	Random subtree mutation, ratio 0.01
Fitness	Velocity of the snake during the trial
Trial interval	600 time steps
Termination criteria	(Fitness >100) or (Generations>30)

```
function Evaluate(GenH, GenV: TGenotype): real;
// GenH and GenV is the pair of arithmetical
// expressions, which represent the genotype of snake
var
   AngleH, AngleV :real;          //desired angles
   CurrAngleH, CurrAngleV:real;   //current angles
   InitialPos,FinalPos: 3Dvector; //(X,Y,Z)
begin
 InitialPos:=GetPosOfCenterOfMassOfSnake;
 for each time step of the trial t do begin
   for each segment s do begin
     AngleH     := EvalHorisontalAngle(GenH,s,t);
     AngleV     := EvalVerticalAngle(GenV,s,t);
     CurrAngleH := GetCurrentAngleH(s);
     CurrAngleV := GetCurrentAngleV(s);
     SetDesiredVelocityH(CurrAngleH-AngleH,s);
     SetDesiredVelocityH(CurrAngleV-AngleV,s);
   end;
   Obtain the new properties (position, orientation,
   velocity vectors, etc.) of morphological segments
   of snake as a result of applying all forces.
 end;
 FinalPos := GetPosOfCenterOfMassOfSnake;
 return GetDistance(InitialPos, FinalPos)/(TimeSteps);
end;
```

Figure 2. Fitness evaluation routine. Fitness is evaluated as the distance that the center-of-mass of the snake travels during the trial.

3 Results

Sidewinding is defined as motion predominantly perpendicular to the long axis of the snake. Figure 3 shows sample snapshots of evolved best-of-generation locomotion gaits. As the figure illustrates, in the intermediate stages of evolution a non-sidewinding forward direction of locomotion emerges (Figure 3b). However, despite the fact that fitness is measured as velocity in *any* direction, the *sidewinding* locomotion emerged in all independent runs of GP, suggesting that it provides superior speed characteristics for the morphology of the robot. In order to verify the superiority of sidewinding locomotion we compared the fitness convergence characteristics for the following two cases: (i) fitness is measured in any direction, and (ii) fitness is measured in forward (non-sidewinding) direction only. The corresponding diagrams are shown in Figure 4. Although unconstrained, all runs of Figure 4a produced sidewinding, while those constrained to non-sidewinding motion (Figure 4b) feature much inferior speed characteristics (a factor of nearly 7).

The evolved horizontal and vertical velocities of actuators of each morphological segment of the snake are shown in Figure 5. These velocities result in characteristic circular motion pattern of segments around the center of the mass (Figure 6) suggesting that during sidewinding the shape of the snake takes the form of a rolling helix. Figure 6 demonstrates that the artificial evolution of locomotion via GP is able to invent the improvised "wheel" of the sidewinding snake as a necessary attribute of efficient locomotion.

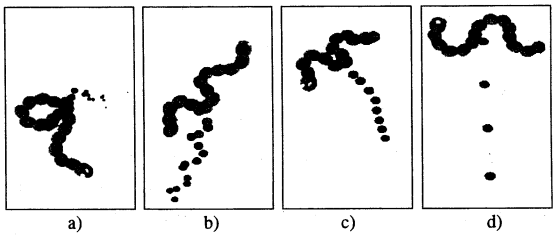


Figure 3. Snapshots of evolved best-of-generation locomotion gaits: initial (a), intermediate (b) and final stages of evolution (c). The best-of-run locomotion gait is shown in (d). The trailing circles depict the trajectory of the center of the mass of the snake. Since the timestamp interval between each of these circles is fixed and it is the same (10 time steps) for all four snapshots, the distance between circles comparatively illustrates the achieved velocity of locomotion.

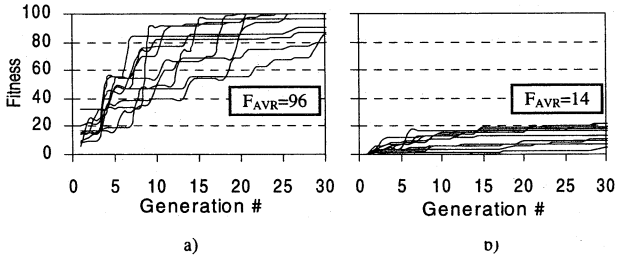


Figure 4. Fitness convergence characteristics of 10 independent runs of GP for cases when fitness is measured as velocity in any direction (a) and in forward direction only (b). The average of the fitness F_{AVR} of all independent runs is estimated at the generation #30.

The robustness characteristics are illustrated by the ability of the snake robot to retain its functionality when partial damage is inflicted. Table 2 shows the degradation of velocity for various amounts of damaged actuators in an evolved sample best-of-run locomotion. The damage is evenly distributed along the snake. As Table 2 illustrates, even when more than 50% (8 out of 15) of actuators are damaged, the snake retains 39% of its original performance. Additional increase of damage yields a sharp decrease in performance of the snake due to the unfavorable effect of the chain of three consecutively connected "dead" actuators on the locomotion gait. Another aspect of robustness – the ability of the snake to overcome obstacles – is illustrated in Figure 7, which illustrates the snake passing over a pile of blocks.

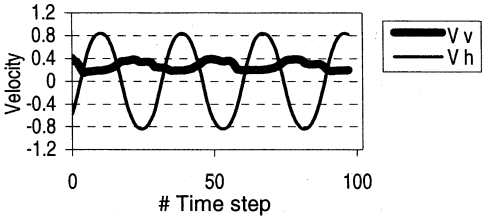


Figure 5. Horizontal (Vh) and vertical (Vv) velocities of actuators of a sample evolved best-of-run sidewinding locomotion.

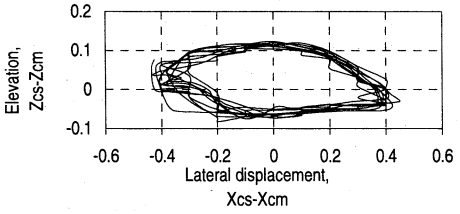


Figure 6. Trajectory of the central segment (cs) around the center of the mass (cm) of the snake for a sample evolved best-of-run sidewinding locomotion.

Table 2. Performance degradation of snake on partial damage

	Amount of damaged actuators (out of 15)									
	0	1	2	3	4	6	8	10	12	14
Fitness	102	70	46	51	36	51	39	19	4	4



Figure 7. Ability of snake with evolved sample best-of-run locomotion to tackle obstacles. Obstacles are represented as random boxes. Both the density (mass per unit volume) of boxes and the coefficient of the friction with the surface are identical to the analogous values of simulated snake.

4 Conclusion

We presented an approach to automatic design through genetic programming, of sidewinding locomotion of simulated limbless, wheelless artifacts. The software model used to simulate the robot should fulfill the basic requirements of being quickly developed, adequate, and fast running. To address the first of these issues, we employed an XML-based GP framework. To address the issues of adequacy and runtime efficiency of snake robot simulation we applied the Open Dynamic Engine (ODE) – a freeware software library for simulation of rigid body dynamics. The empirically obtained results demonstrate that the complex locomotion of sidewinding emerges from relatively simple motion patterns of phenotypic segments (vertebrae). The evolved locomotion pattern of each segment is such that the segment is rotating in a circle-like trajectory around the center of the mass of the simulated robot. This suggests that evolved sidewinding locomotion can be viewed as a process of rolling of the body of the simulated robot in a helix shape, effectively inventing a kind of improvised wheel. The efficiency of sidewinding locomotion is much superior to locomotion in the forward direction, suggesting that sidewinding is the fastest possible locomotion for the simulated limbless wheelless robots with the characteristics used in this study (morphology, limits of actuator forces, joint type, joint movement limits, etc.). The robustness of automatically evolved locomotion is verified by (i) the reasonable performance degradation when partial damage to the artifact is inflicted and by (ii) the ability to pass over obstacles. Contributing to the better understanding of sidewinding locomotion, this work could be considered as a step towards building real limbless, wheelless robots, which featuring unique engineering characteristics are able to perform robustly in difficult environments.

Better adaptation (through epigenetic development employing histone code modifications) to unpredictable, changeable environments and/or partial damage; and co-evolution of locomotion patterns and relevant morphological traits (power and angular limits of actuators, amount of segments in the snake, etc.) are planned for the near future.

Acknowledgements

This research was conducted as part of "Research on Human Communication" with funding from the telecommunications Advancement Organization of Japan.

References

[1] K.Dowling, Limbless Locomotion: Learning to Crawl with a Snake Robot, doctoral dissertation, tech. report CMU-RI-TR-97-48, Robotics Institute, Carnegie Mellon University, December, 1997

[2] S.Mahdavi and P.J.Bentley, Evolving Motion of Robots with Muscles. In Proc. of EvoROB2003, the 2nd European Workshop on Evolutionary Robotics, EuroGP 2003: 655-664, 2003

[3] H.J.Morowitz, The Emergence of Everything: How the World Became Complex, Oxford University Press, New York, 2002

[4] L.Meeden and D.Kumar, Trends in Evolutionary Robotics, Soft Computing for Intelligent Robotic Systems, edited by L.C. Jain and T. Fukuda, Physica-Verlag, New York, NY, pp.215-233, 1998

[5] K.Sims, Evolving 3D Morphology and Behavior by Competition, Artificial Life IV Proceedings, MIT Press, pp.28-39, 1994

[6] T.Ray, Aesthetically Evolved Virtual Pets, Leaonardo, Vol.34, No.4: 313 – 316, 2001

[7] N.Jacobi, Minimal Simulations for Evolutionary Robotics. Ph.D. thesis, School of Cognitive and Computing Sciences, Sussex University, 1998

[8] R.Smith, Open Dynamics Engine, 2001-2003, http://q12.org/ode/.

[9] J.R.Koza, Genetic Programming: On the Programming of Computers by Means of Natural Selection, Cambridge, MA: MIT Press, 1992

[10] I.Tanev, DOM/XML-Based Portable Genetic Representation of Morphology, Behavior and Communication Abilities of Evolvable Agents, Artificial Life and Robotics, an International Journal, Vol 8. (accepted)

Proc. of The Ninth Int. Symp. on Artificial Life and Robotics (AROB 9th '04)
Beppu, Oita, Japan, 28-30 January, 2004

Design of a Real Time Adaptive Controller of Robot Manipulator with Eight Joint Based on DSPs

Sung Hyun Han
Division of Mechanical and Automation Eng.,
Kyungnam University,
Masan, Korea, 631-701.

Hong Rae Kim, Dong Yean Jung
Dept. of Mechanical Design,
Kyungnam University,
Masan, Korea, 631-701.

Abstract

We describe a new approach to the design and real-time implementation of an adaptive controller for robotic manipulator based on digital signal processors in this paper. The Texas Instruments DSPs(TMS320C80) chips are used in implementing real-time adaptive control algorithms to provide enhanced motion control performance for dual-arm robotic manipulators. In the proposed scheme, adaptation laws are derived from model reference adaptive control principle based on the improved direct Lyapunov method. The proposed adaptive controller consists of an adaptive feed-forward and feedback controller and time-varying auxiliary controller elements. The proposed control scheme is simple in structure, fast in computation, and suitable for real-time control. Moreover, this scheme does not require any accurate dynamic modeling, nor values of manipulator parameters and payload. Performance of the proposed adaptive controller is illustrated by simulation and experimental results for a dual arm robot consisting of two SCARA four degree of freedom robots at the joint space and cartesian space.

Keywords : Adaptive Control, DSP(TMS320C80), Dual-Arm Robot, Real Time Control, Real-Time Implementation

1. Introduction

At recent there are mach advanced techniques that are suitable for servo control of a large class of nonlinear systems including robotic manipulators (P.C.V. Parks, 1966; Y.K.Choi et al., 1986; Y.M.Yoshhiko, 1995). Since the pioneering work of Dubowsky and DesForges (1979), the interest in adaptive control of robot manipulators has been growing steadily (T. C. Hasi, 1986; D. Koditschck, 1983; A. Koivo et al., 1983; S. Nicosia et al., 1984). This growth is largely due to the fact that adaptive control theory is particularly well-suited to robotic manipulators whose dynamic model is highly complex and may contain unknown parameters. However, implementation of these algorithms generally involves intensive numerical computations (J. J. Craig, 1988; H. Berghuis et al., 1993).

Current industrial approaches to the design of robot arm control systems treat each joint of the robot arm as a simple servomechanism. This approach models the time varying dynamics of a manipulator inadequately because it neglects the motion and configuration of the whole arm mechanism. The changes in the parameters of the controlled system are significant enough to render conventional feedback control strategies ineffective. This basic control system enables a manipulator to perform simple positioning tasks such as in the pick-and-place operation. However, joint controllers are severely limited in precise tracking of fast trajectories and sustaining desirable dynamic performance for variations of payload and parameter uncertainties (R. Ortega et al., 1989; P. Tomei, 1991). In many servo control applications the linear control scheme proves unsatisfactory, therefore, a need for nonlinear techniques is increasing.

Digital signal processors (DSP's) are special purpose microprocessors that are particularly suitable for intensive numerical computations involving sums and products of variables. Digital versions of most advanced control algorithms can be defined as sums and products of measured variables, thus can naturally be implemented by DSP's. DSPs allow straightforward implementation of advanced control algorithms that result in improved system control. Single and/or multiple axis control systems can be controlled by a single DSP. Adaptive and optimal multivariable control methods can track system parameter variations. Dual control, learning, neural networks, genetic algorithms and Fuzzy Logic control methodologies are all among the digital controllers implementable by a DSP (N. Sadegh et al., 1990; Z. Ma et al., 1995). In addition, DSP's are as fast in computation as most 32-bit microprocessors and yet at a fraction of their prices. These features make them a viable computational tool for digital implementation of advanced controllers. High performance DSPs with increased levels of integration for functional modules have become the dominant solution for digital control systems. Today's DSPs with performance levels ranging from 5 to 5400 MIPS are on the market with price tags as low as $3 (P. Bhatti et al., 1997; T. H. Akkermans et al., 2001). In order to develop a digital servo controller one must carefully consider the effect of the sample-and-hold operation, the sampling frequency, the computational delay, and that of the quantization error on the stability of a closed-loop system (S. A. Bortoff, 1994). Moreover, one must also consider the effect of disturbances on the transient variation of the tracking error as well as its steady-state value (F. Mehdian et al., 1995; S. H. Han et al., 1996).

This paper describes a new approach to the design of adaptive control system and real-time implementation using digital signal processors for robotic manipulators to achieve the improvement of speedness, repeating precision, and tracking performance at the joint and cartesian space. This paper is organized as follows : In Section Ⅱ, the dynamic model of the robotic manipulator is derived. Section Ⅲ derives adaptive control laws based on the model reference adaptive control theory using the improved Lyapunov second method. Section Ⅳ presents simulation and experimental results obtained for a dual-arm robot. Finally, Section Ⅴ discusses the findings and draws some conclusions.

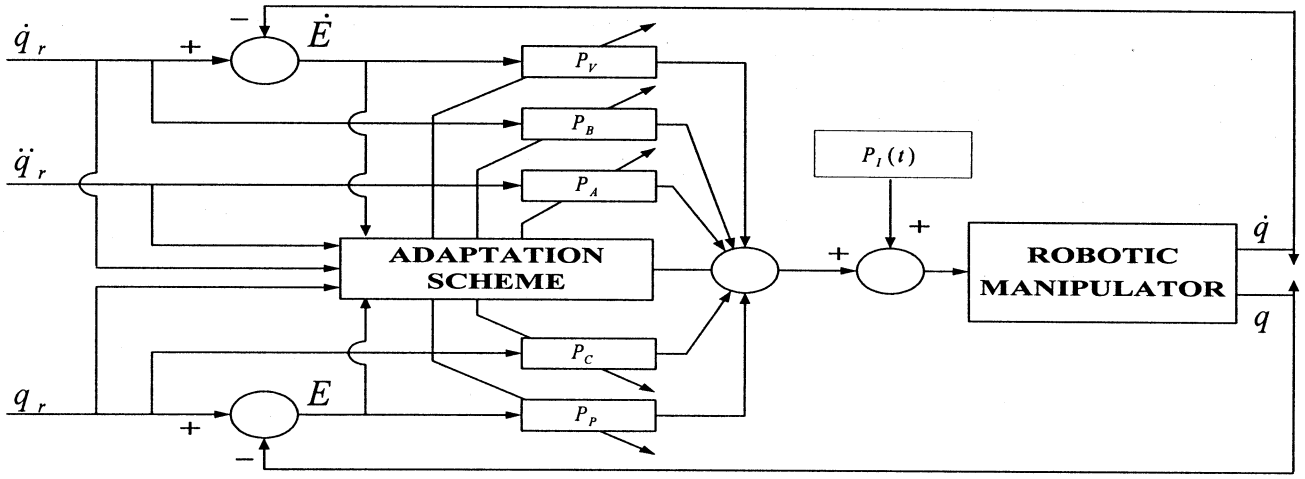


Fig. 1. Adaptive control scheme of Robotic Manipulator with eight joint

2. System Modeling

The dynamic model of a manipulator-plus-payload is derived and the tracking control problem is stated in this section.

Let us consider a nonredundant joint robotic manipulator in which the n×1 generalized joint torque vector τ (t) is related to the n×1 generalized joint coordinate vector q(t) by the following nonlinear dynamic equation of motion

$$D(q)\,\ddot{q} + N(q,\dot{q}) + G(q) = \tau(t) \tag{1}$$

where $D(q)$ is the n×n symmetric positive-definite inertia matrix, $N(q,\dot{q})$ is the n×1 coriolis and centrifugal torque vector, and $G(q)$ is the n×1 gravitational loading vector.

Equation (1) describes the manipulator dynamics without any payload. Now, let the n×1 vector X represent the end-effector position and orientation coordinates in a fixed task-related cartesian frame of reference. The cartesian position, velocity, and acceleration vectors of the end-effector are related to the joint variables by

$$\begin{aligned} X(t) &= \Phi(q) \\ X(t) &= J(q)\,\dot{q}(t) \\ X(t) &= \dot{J}(q,\dot{q})\,\dot{q}(t) + J(q)\,\ddot{q}(t) \end{aligned} \tag{2}$$

where Φ(q) is the n×1 vector representing the forward kinematics and J(q) = [∂ Φ(q)/ ∂ q] is the n×n Jacobian matrix of the manipulator.

Let us now consider payload in the manipulator dynamics. Suppose that the manipulator end-effector is firmly grasping a payload represented by the point mass ΔM_p. For the payload to move with acceleration $\ddot{X}(t)$ in the gravity field, the end-effector must apply the n×1 force vector $T(t)$ given by

$$T(t) = \Delta M_p\,[\,\ddot{X}(t) + g\,] \tag{3}$$

where g is the n×1 gravitational acceleration vector.

The end-effector requires the additional joint torque

$$\tau_f(t) = J(q)^T\,T(t) \tag{4}$$

where superscript T denotes transposition. Hence, the total joint torque vector can be obtained by combining equations (1) and (4) as

$$J(q)^T\,T(t) + D(q)\,\ddot{q} + N(q,\dot{q}) + G(q) = \tau(t) \tag{5}$$

Substituting equations (2) and (3) into equation (5) yields

$$\begin{aligned} &\Delta M_p\,J(q)^T[J(q)\,\ddot{q} + \dot{J}(q,\dot{q})\,\dot{q} + g\,] \\ &+ D(q)\ddot{q} + N(q,\dot{q}) + G(q) = \tau(t) \end{aligned} \tag{6}$$

Equation (6) shows explicity the effect of payload mass ΔM_p on the manipulator dynamics. This equation can be written as

$$\begin{aligned} &[D(q)+\Delta M_p J(q)^T J(q)]\,\ddot{q} + [N(q,\dot{q}) \\ &+ \Delta M_p J(q)^T \dot{J}(q,\dot{q})\,\dot{q}] + [G(q) + \Delta M_p J(q)^T g] = \tau(t) \end{aligned} \tag{7}$$

where the modified inertia matrix $[D(q)+\Delta M_p J(q)^T J(q)]$ is symmetric and positive-definite. Equation (7) constitutes a nonlinear mathematical model of the manipulator-plus-payload dynamics.

3. Adaptive Controller

The manipulator control problem is to develop a control scheme which ensures that the joint angle vector $q(t)$ tracks any desired reference trajectory $q_r(t)$, where $q_r(t)$ is an n×1 vector of arbitrary time functions. It is reasonable to assume that these functions are twice differentiable, that is, desired angular velocity $\dot{q}_r(t)$ and angular acceleration $\ddot{q}_r(t)$ exist and are directly available without requiring further differentiation of $q_r(t)$. It is desirable for the manipulator control system to achieve trajectory tracking irrespective of payload mass ΔM_p.

The controllers designed by the classical linear control scheme are effective in fine motion control of the manipulator in the

neighborhood of a nominal operating point P_o. During the gross motion of the manipulator, operating point P_o and consequently the linearized model parameters vary substantially with time. Thus it is essential to adapt the gains of the feedforward, feedback, and PI controllers to varying operating points and payloads so as to ensure stability and trajectory tracking by the total control laws. The required adaptation laws are developed in this section. Fig. 1 represents the block diagram of adaptive control scheme for robotic manipulator.

Nonlinear dynamic equation (7) can be written as

$$\tau(t) = D^*(\Delta M_p, q, \dot{q})\,\ddot{q}(t) + N^*(\Delta M_p, q, \dot{q})\,\dot{q}(t) + G^*(\Delta M_p, q, \dot{q})\,q(t) \tag{8}$$

where D^*, N^*, and G^* are n×n matrices whose elements are highly nonlinear functions of ΔM_p, q, and $\dot{q}$.

In order to cope with changes in operating point, the controller gains are varied with the change of external working condition.

This yields the adaptive control law

$$\tau(t) = [P_A(t)\,\ddot{q}_r(t) + P_B(t)\,\dot{q}_r(t) + P_C(t)\,q_r(t)] + [P_V(t)\,\dot{E}(t) + P_P(t)\,E(t) + P_I(t)] \tag{9}$$

where $P_A(t)$, $P_B(t)$, $P_C(t)$ are feedforward time-varying adaptive gains, and $P_P(t)$ and $P_V(t)$ are the feedback adaptive gains, and $P_I(t)$ is a time-varying control signal corresponding to the nominal operating point term, generated by a feedback controller driven by position tracking error $E(t)$ defined as $q_r(t) - q(t)$.

The gains of adaptive control low in equation (9) are defined as follows:

$$P_A(t) = a_1[p_{a1}E + p_{a2}\dot{E}][\ddot{q}_r]^T + a_2\int_0^t[p_{a1}E + p_{a2}\dot{E}][\ddot{q}_r]^T dt + p_a(0) \tag{10}$$

$$P_B(t) = b_1[p_{b1}E + p_{b2}\dot{E}][\dot{q}_r]^T + b_2\int_0^t[p_{b1}E + p_{b2}\dot{E}][\dot{q}_r]^T dt + p_b(0) \tag{11}$$

$$P_C(t) = c_1[p_{c1}E + p_{c2}\dot{E}][q_r]^T + c_2\int_0^t[p_{c1}E + p_{c2}\dot{E}][q_r]^T dt + p_c(0) \tag{12}$$

$$P_I(t) = \lambda_2[p_{i2}E] + \lambda_1\int_0^t[p_{i1}E]^T dt + p_i(0) \tag{13}$$

$$P_P(t) = p_1[p_{p1}E + p_{p2}\dot{E}][E]^T + p_2\int_0^t[p_{p1}E + p_{p2}\dot{E}][E]^T dt + p_p(0) \tag{14}$$

$$P_V(t) = v_1[p_{v1}E + p_{v2}\dot{E}][\dot{E}]^T + v_2\int_0^t[p_{v1}E + p_{v2}\dot{E}][\dot{E}]^T dt + p_v(0) \tag{15}$$

where $[p_{p1}, p_{v1}, p_{c1}, p_{b1}, p_{a1}]$ and $[p_{p2}, p_{v2}, p_{c2}, p_{b2}, p_{a2}]$ are positive and zero/positive scalar adaptation gains, which are chosen by the designer to reflect the relative significance of position and velocity errors E and $\dot{E}$.

4. Simulation And Experiment

A. Simulation

This section represents the simulation results of the position and velocity control of a four-link robotic manipulator by the proposed adaptive control algorithm, as shown in Fig.2, and discusses the advantages of using joint controller based-on DSPs for motion control of a dual-arm robot. The adaptive scheme developed in this paper will be applied to the control of a dual-arm robot with eighth axes. Fig.2 represents link coordinates of the dual-arm robot.

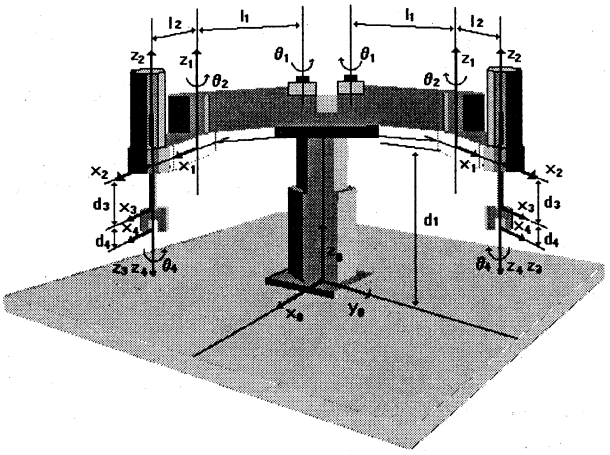


Fig.2. Link coordinates of dual-arm robot

Table I Link parameters of robot.

Mass of link(kg)		Length of link(kg)		Inertia of link(kg)		Gear ratio of link	
m1	15.0067	l1	0.35	I1	0.1538	r1	1/100
m2	8.994	l2	0.3	I2	0.0674	r2	1/80
m3	3.0	l3	0.175	I3	0.045	r3	1/200
m4	1.0	l4	0.007	I4	0.0016	r4	1/75
m5	15.067	l5	0.35	I5	0.1538	r5	1/100
m6	8.994	l6	0.3	I6	0.0674	r6	1/80
m7	3.0	l7	0.175	I7	0.045	r7	1/200
m8	1.0	l8	0.007	I8	0.0016	r8	1/75

Table II Motor parameters of robot

Rotor inertia (kg · m²)		Torque constant (K m/a)		Back emf constant (V s/rad)		Amaturewinding resistance(ohms)	
Jm1	5.0381×10^{-5}	Ka1	21.4839×10^{-2}	Kb1	2.148592×10^{-3}	Ra1	15
Jm2	1.3734×10^{-5}	Ka2	20.0124×10^{-2}	Kb2	2.005352×10^{-3}	Ra2	42
Jm3	0.8829×10^{-5}	Ka3	20.0124×10^{-2}	Kb3	2.005352×10^{-3}	Ra3	9
Jm4	0.2256×10^{-5}	Ka4	17.6580×10^{-2}	Kb4	1.766520×10^{-3}	Ra4	20
Jm5	5.0381×10^{-5}	Ka5	21.4839×10^{-2}	Kb5	2.148592×10^{-3}	Ra5	15
Jm6	1.3734×10^{-5}	Ka6	20.0124×10^{-2}	Kb6	2.005352×10^{-3}	Ra6	42
Jm7	0.8829×10^{-5}	Ka7	20.0124×10^{-2}	Kb7	2.005352×10^{-3}	Ra7	9
Jm8	0.2256×10^{-5}	Ka8	17.6580×10^{-2}	Kb8	1.766520×10^{-3}	Ra8	20

B. Experiment

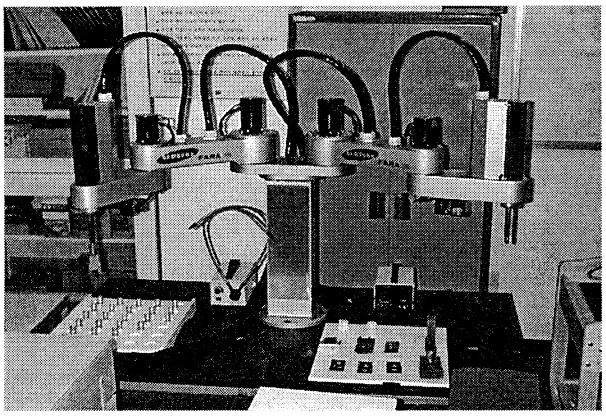


Fig. 3. Experimental set-up

The performance test of the proposed adaptive controller has been performed for the dual-arm robot at the joint space and cartesian space. At the cartesian space, it has been tested for the peg-in-hole tasks, repeating precision tasks, and trajectory tracking for B-shaped reference trajector. At the joint space, it has been tested for the trajectory tracking of angular position and velocity for a dual-arm robot made in Samsung Electronics Company in Korea. Fig. 3 represents the experimental set-up equipment. To implement the proposed adaptive controller, we used our own developed TMS320C80 assembler software. Also, the TMS320C80 emulator has been used in experimental set-up. At each joint of a dual-arm robot, a harmonic drive (with gear reduction ratio of 100 : 1 for joint 1 and 80 : 1 for joint 2) has been used to transfer power from the motor, which has a resolver attached to its shaft for sensing angular velocity with a resolution of 8096 (pulses/rev). Fig. 4 represents the schematic diagram of control system of dual-arm robot. And Fig. 5 represents the block diagram of the interface between the PC, DSP, and dual-arm robot.

The performance test in the joint space is performed to evaluate the position and velocity control performance of the four joints under the condition of payload variation, inertia parameter uncertainty, and change of reference trajectory.

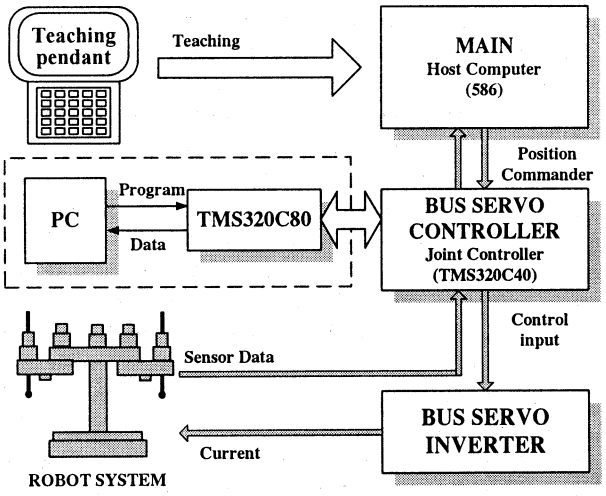


Fig. 4. The block diagram of the interface between the PC. DSP, and dual-arm robot.

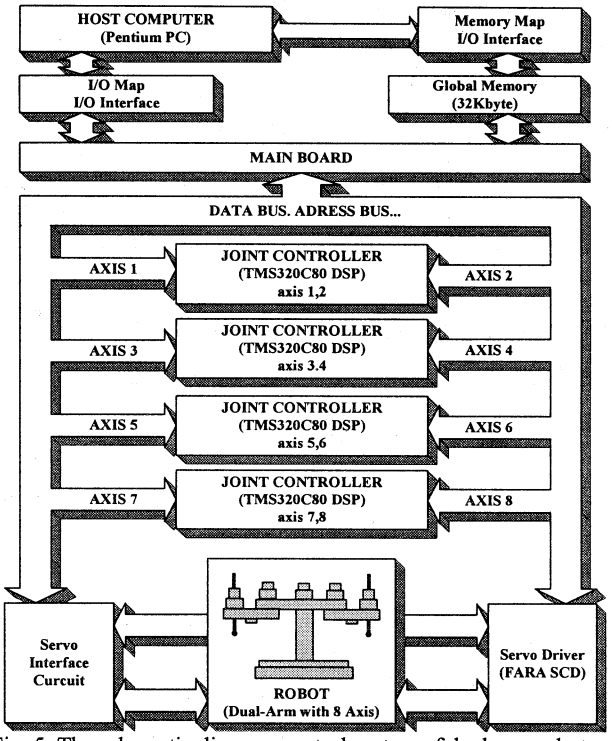


Fig. 5. The schematic diagram control system of dual-arm robot.

Fig.6 represents the B-shaped reference trajectory in the cartesian space. Fig. 7 shows the experimental results of the position and velocity control at the first joint with payload 4 kg and the change of reference trajectory. Fig. 8 shows the experimental results for the position and velocity control at the second joint with 4 kg payload. Fig.'s 9 and 10 show the experimental results for the position and velocity control of the PID controller with 4 kg payload. As can be seen from these results, the DSP-based adaptive controller shows extremely good control performance with some external disturbances. It is illustrated that this control scheme shows better control performance than the exiting PID controller, due to small tracking error and fast adaptation for disturbance.

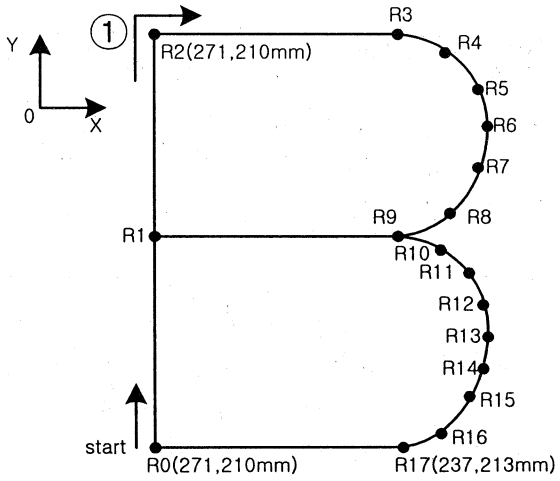


Fig. 6. The B shaped reference trajectory in the cartesian space.

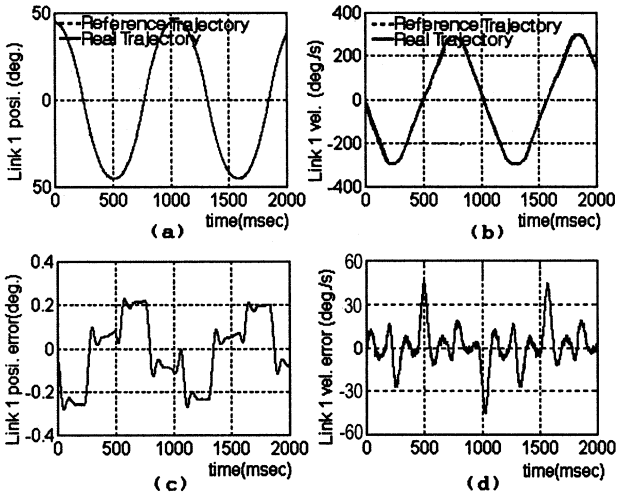


Fig. 7. (a)-(d) Experimental results for the position and velocity tracking of adaptive controller at the first joint with 4kg payload.

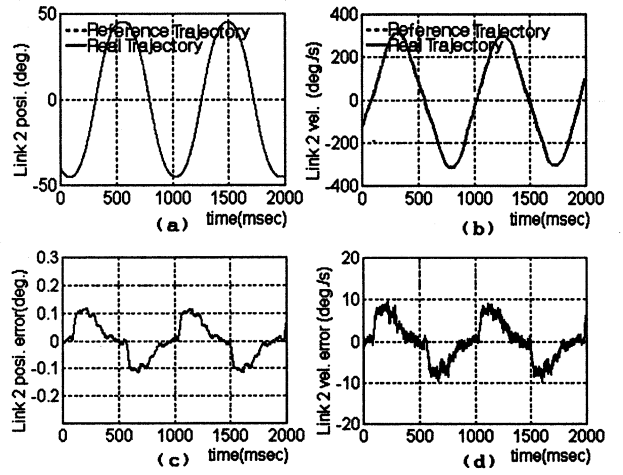


Fig. 8. (a)-(d) Experimental results for the position and velocity tracking of adaptive controller at the second joint with 4kg payload.

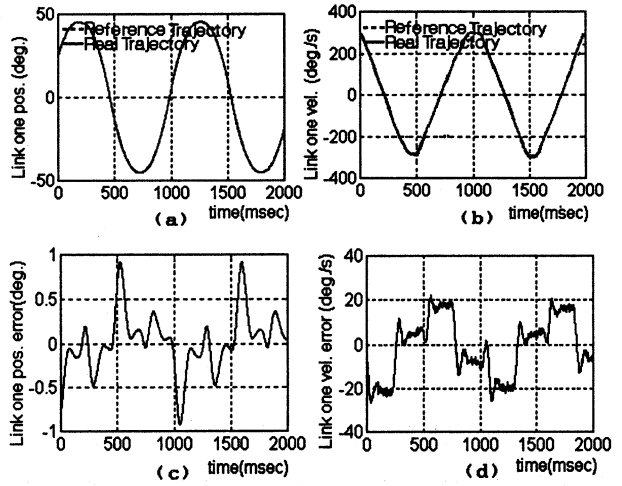


Fig. 9. (a)-(d) Experimental results of PID controller for the position and velocity tracking at the first joint with 4kg payload.

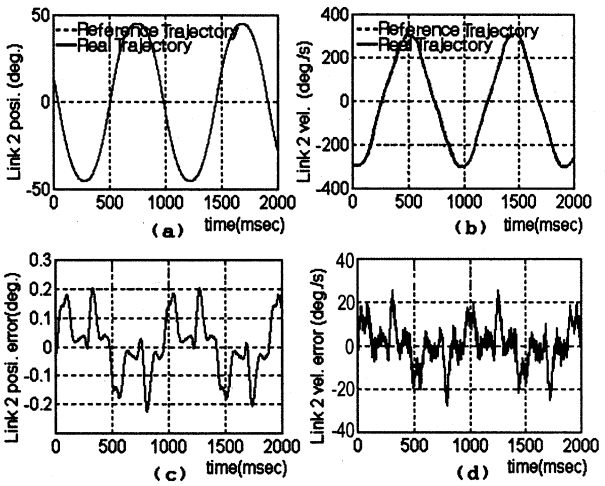


Fig. 10. (a)-(d) Experimental results of PID controller for the position and velocity tracking at the second joint with 4kg payload.

5. Discussion and Conclusions

A new adaptive digital control scheme is described in this paper using DSP(TMS320C80) for robotic manipulators. The adaptation laws are derived from the direct adaptive technique using the improved Lyapunov second method. The simulation and experimental results show that the proposed DSP-adaptive controller is robust to the payload variation, inertia parameter uncertainty, and change of reference trajectory. This adaptive controller has been found to be suitable to the real-time control of robot system. A novel feature of the proposed scheme is the utilization of an adaptive feedforward controller, an adaptive feedback controller, and a PI type time-varying control signal to the nominal operating point which result in improved tracking performance. Another attractive feature of this control scheme is that, to generate the control action, it neither requires a complex mathematical model of the manipulator dynamics nor any knowledge of the manipulator parameters and payload. The control scheme uses only the information contained in the actual and reference trajectories which are directly available. Futhermore, the adaptation laws generate the controller gains by means of simple arithmetic operations. Hence, the calculation control action is extremely simple and fast. These features are suitable for implementation of on-line real-time control for robotic manipulators with a high sampling rate, particularly when all physical parameters of the manipulator cannot be measured accurately and the mass of the payload can vary substantially. The proposed DSP-based adaptive controllers have several advantages over the analog control and the micro-computer based control. This allows instructions and data to be simultaneously fetched for processing. Moreover, most of the DSP instructions, including multiplications, are performed in one instruction cycle. The DSP tremendously increase speed of the controller and reduce computational delay, which allows for faster sampling operation. It is illustrated that DSPs can be used for the implementation of complex digital control algorithms, such as our adaptive control for robot systems.

References

[1] P.C.V. Parks, "*Lyapunov Redesign of Model Reference Adaptive Control System*," IEEE Trans. Auto. Contr., Vol. AC-11, No. 3, pp. 362-267, July 1966,

[2] Y.K. Choi, M.J. Chang, and Z. Bien, "*An Adaptive Control Scheme for Robot Manipulators*." IEEE Trans. Auto. Contr., Vol. 44, No. 4, pp. 1185-1191, 1986.

[3] Y.M. Yoshhiko, "*Model Reference Adaptive Control for Nonlinear System with unknown Degrees*, "In the proceeding of American Control Conference, pp.2505-2514, Seatle., June 1995.

[4] S. Dubowsky, and D.T. DesForges, "*The Application of Model Reference Adaptation Control to Robot Manipulators*," ASME J. Dyn. Syst., Meas., Contr., Vol. 101, pp. 193-200, 1979.

[5] T.C. Hasi, "*Adaptive Control Scheme for Robot Manipulators-A Review*." In Proceeding of the 1987 IEEE Conference on Robotics and Automation, San Fransisco, CA., 1986.

[6] D. Koditschek, "*Quadratic Lyapunov Functions for Mecanical Systems*," Technical Report No. 8703, Yale University, New Haven, CT. Koivo and T. H. Guo, 1983, "*Adaptive Linear Controller for Robot Manipulators.*" IEEE Transactions and Automatic Control, Vol. AC-28, pp. 162-171, 1983.

[7] S. Nicosia and P. Tomee, "*Model Reference Adaptive Control Algorithm for Imdustrial Robots*," Automatica, Vol. 20, No. 5, pp. 635-644, 1984.

[8] J. J. Craig, "*Adaptive Control of Meduanical Manipulator*," Addison-wesley., 1988.

[9] H. Berghuis, R.Orbega, and H.Nijmeijer, "*A Robust Adaptive Robot controller*," IEEE Trans., Robotics and Automation, Vol. 9, No. 6, pp. 825-830, 1993.

[10] R. Ortega and M.W. Spong, "*Adaptive Motion Control of Rigid Robots: A Tutorial*," Automatica, Vol. 25, pp. 877-888, 1989.

[11] P. Tomei, "*Adaptive PD Controller for Robot Manipulators,*" IEEE Trans. Robotics and Automation, Vol.7, No.4, Aug. 1991.

[12] N. Sadegh and R. Horowitz, "*An Exponentially Stable Adaptive Control Law for Robot Manipulators*," IEEE Trans. Robotics and Automation, Vol. 9, No. 4, Aug. 1990.

[13] Z. Ma, J. shen, A. Hug, and K. Nakayama, "*Automatic optimum Order Assignment in Adaptive Filters*," international conference on signal Processing Applications & Technology, Boston pp. 629-633, October 1995.

[14] T. A. Lasky and T. C. Hsia, "*Application of a Digital Signal Processor in Compliant Control of an Industrial Manipulator*," Proceedings of American Control Conference, July 1994.

[15] K. Michael and P. Issa, "*Digital Signal Processor : A Control Element*," In Proceedings of American Control Conference, Seatle, pp. 470-474, June 1995.

[16] S. A. Bortoff, "*Advanced Nonlinear Robotic Control Using Digital Signal Processing*," IEEE Trans. Indust. Elect., Vol. 41, No. 1., Feb. 1994.

[17] F. Mehdian and M. Wirth, "*Adaptive Control of Robotic Manipulators Using DSPs*," In Proceedings of American Control Conference, Seatle, pp.480-481, June 1995.

[18] S. H. Han, J. Lee, D. Ahn, M. Lee, and K. Son, "*Implementation of Robust Adaptive Controller of Robotic Manipulator using DSPs*, "In Proceedings of Eleventh International Conference on System engineering, Lasvegas, pp. 668-673, July 1996.

[19] T. H. Akkermans and S. G. Stan, "*Digital servo IC for optical disc drives*", *Contr. Eng. Pract.*, vol. 9, no. 11, pp. 1245-1253, 2001.

[20] P. Bhatti and B. Hannaford, "*Single-chip velocity measurement system for incremental optical encoders*", IEEE Trans. Contr. Syst. Techn., vol. 5, no. 6, pp. 654-661, 1997.

Proc. of The Ninth Int. Symp. on Artificial Life and Robotics (AROB 9th '04)
Beppu, Oita, Japan, 28-30 January, 2004

Induction of Prototypes in a Robotic Setting using Local Search MDL

Gregory M. Kobele* Jason Riggle* Richard Brooks†
David Friedlander‡ Charles Taylor§ Edward Stabler*

Abstract

Categorizing objects sets the stage for more advanced interactions with the environment. Minimum Description Length learning provides a framework in which to investigate processes by which concept learning might take place. Importantly, the concepts so acquired can be viewed as having a prototype structure - the concepts may apply to one object better than to another. We ground our discussion in a real-world setting - objects to categorize are sensor readings of the behaviours of two mobile robots.

1 Introduction

Natural and artificial agents are confronted with the problem of constructing models of their environments, thereby imposing order on an otherwise chaotic stream of sensory data. An important step in this direction is to recognize when a novel sense datum is sufficiently similar to a previously seen one to make a similar response adaptive. This is the problem of categorization - how does one decide which properties of sense data are relevant, and which are accidental. Obviously, treating all properties as relevant leads to no generalization at all, and treating all properties as accidental leads to maladaptive behaviour (unless the environment is perverse). This problem has been explored in various settings using Minimal Description Length (MDL) concept learning, where the notions of concise encoding of the hypothesis and of efficient encoding of the observed data impose competing pressures (generalizing by minimizing theory size while still being informative about the data), where the measures of theory size and empirical informativeness can be adjusted to fit the domain. We have previously applied this framework both to the classification of simple robotic behaviour [1], as well as to language evolution [4, 5]. In these previous studies concepts (or languages) were represented as deterministic finite state automata, and percepts were finite strings over a fixed finite alphabet. Our current study extends the previous ones in two ways. First, we enrich the hypothesis space of our agents to include non-deterministic automata. Although deterministic and non-deterministic machines are equivalent in expressive power, enriching the agent's hypothesis space in this manner has repercussions for the results of the learning process. Second, we exploit a particular property of the MDL setup, yielding a cognitively interesting prototype structure of concepts which allows for degrees of membership in a category. One novel aspect of the prototype structure presented here is that the degrees of category membership are a holistic and emergent property of the conceptual space. That is, whether a perception is a "good example" of a particular category depends on what other categories are available. In our setting, concepts are represented as finite automata, and perceptions as strings over a fixed finite alphabet. Given a space of concepts $\mathcal{C}$, a perception p is a good example of a category $C \in \mathcal{C}$ just in case $p \in L(C)$ and for any other $C' \in \mathcal{C}$ with $p \in L(C')$, the cost of encoding p in C is less than or equal to the cost of encoding p in C' ($enc(p, C) \leq enc(p, C')$).

We present a simple example in which a learner is faced with the task of categorizing the behaviour of two robots, given by means of sensors in the robots' environment. In the learning stage each set of sensor data is labeled as an instance of a concept (e.g. 'random walking', 'wall following', 'chasing', ...). Our robot learner then extracts the salient structure from each training set, possibly generalizing its theory of the training sets to include as yet unseen sensor inputs.

2 Minimum Description Length

The basic idea of the MDL framework is that the best hypothesis to adopt when confronted with a set of data is the one that best navigates between the charyb-

*Department of Linguistics, UCLA. Los Angeles, CA 90095
†Distributed Systems Department, The Pennsylvania State University, State College, PA 16804
‡Informatics Department, The Pennsylvania State University, State College, PA 16804
§Department of Organismic Biology, Evolution and Ecology, UCLA. Los Angeles, CA 90095

dis of theory complexity and the scylla of faithfullness to the data set. In other words, we want the simplest theory with the greatest predictive power. Here we adopt the length of the binary encoding of a machine as our measure of theory complexity, and the cost of specifying a parse of the input (an accepting path though the machine) as our measue of faithfulness to the data. The intuition is that the cost of encoding a string is the amount of information one needs to exactly reconstruct it. This intuition motivates the following definition: as there might be more than one parse of a string through a given machine, we define the cost of encoding a string in a machine as the cost of the *least* path through the machine reading the string.

Formally, we define the cost of the binary encoding of a machine $M = \langle Q, \Sigma, S, F, \delta \rangle$, where Q is a finite set of states, Σ is a finite vocabulary, $S, F \subseteq Q$ are the start and final states, respectively, and $\delta \subseteq Q \times \Sigma_\epsilon \rightarrow 2^Q$ is the transition function, to be

$$size(M) = size(\delta) + size(S) + size(F)$$

where

$$size(\delta) = |\delta| \left(2log_2 |Q| + log_2(|\Sigma| + 1)\right)$$

and for $Q_0 \subseteq Q$,

$$size(Q_0) = |Q_0| \left(log_2 |Q|\right)$$

Identifying a parse with a sequence of arcs $\pi = a_1 a_2 \ldots a_n$ in M, we define the cost of a parse $cost(\pi)$ to be the sum of the number of bits needed to specify the path through the machine. Setting z_i to be the number of arcs with the same source as a_i,

$$cost(\pi, M) = \Sigma_{i=1}^{n} z_i$$

and the cost of encoding a string σ in M is the amount of information needed to recover σ given M; for Π_σ the set of parses of σ in M,

$$enc(\sigma, M) = min(\{cost(\pi) | \pi \in \Pi_\sigma\})$$

Given a set of training data T, we first construct the prefix-tree acceptor $P(T)$ for T. Next, we construct the set of machines formed by merging two states in $P(T)$, greedily keeping only those machines M which minimize $size(M) + \Sigma_{\sigma \in T} enc(\sigma, M)$. We continue this process of merging states and discarding machines which are suboptimal until we reach a fixed point.

3 Behavior Recognition with Two Robots

The floor was divided into four rectangular sections and each section was assigned a letter. At any instant, the positions of the two robots can be represented by a pair of letters. The position of the robots in a section was determined by two sensors placed in the room. The sensor setup is shown in figure 1.

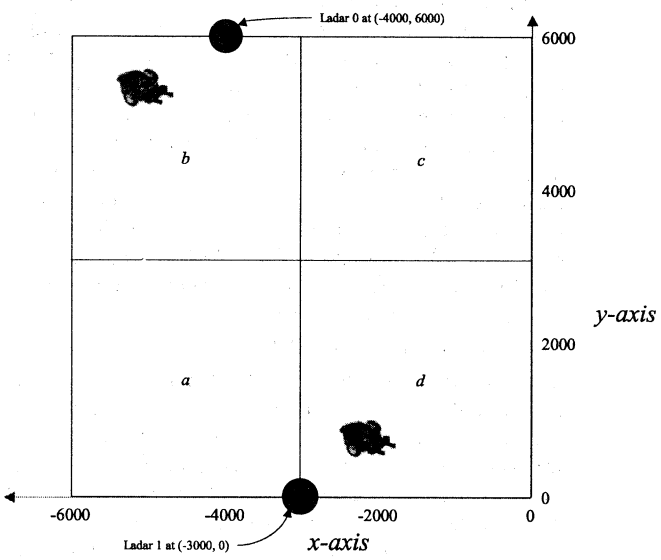


Figure 1: Experimental Setup

Each robotic configuration (i.e. pair of letters indicating the positions of the first and second robots) is taken as a primitive symbol in a larger alphabet (of 16 symbols), into which the sensor readings are ultimately translated. Sensor readings were taken every .2 seconds. As the machines induced by our algorithm for even a five minute time slice were too large to fit readably in the space allotted, we give simplified examples in the next sections.

4 Prototypes

Prototype theory [3] is a theory of concepts which is intended to account for behavioural asymmetries in identifying objects as falling under particular concepts, as well as regularities in 'prototypicality judgements' across individuals. A model of this type of

data, should minimally provide an ordering relation across entities participating in the concept. Osherson and Smith [2] challenged the sufficiency of this minimal criterion of adequacy. They argued that fuzzy set theory [6] does not provide an adequate model of the data, even though fuzzy set membership does provide just such an ordering over individuals. They point out that the theory of concepts should be able to account for the compositional nature of concepts - that is, that some concepts are formed from others. They claim that concept compositionality is not faithfully reflected in Zadeh's fuzzy set operators. As a simple example they chose the concept *striped apple*, which they took to be composed of the (more) atomic concepts of *striped* and *apple* via concept conjunction. On the assumption that a prototypical striped apple is neither a prototypical striped thing nor a prototypical apple, this fact is not well-modeled using Zadeh's fuzzy set intersection operator, which identifies the degree of membership of an object in the conjunction of two fuzzy sets with the least degree of membership of that object in the conjuncts.

In the model presented herein, the cost of encoding a percept into a machine yields an ordering across participants of a concept, with p being a more prototypical M than p' iff $enc(p, M) < enc(p', M)$. If we take the standard operations of machine intersection (cross-product of machines followed by removal of dead states and arcs) and machine union (creation of a new start state, and empty transitions to the start states of each concept) to model the binary conceptual connectives 'and' and 'or', we see that in the 'or' case our model and the fuzzy set model (in which an element is in the union of two sets to the greater of the degrees in which it is in each of the individual sets) coincide (recall that in the fuzzy set model, the higher the degree of membership, the more prototypical, and in our model, the lower the cost of the encoding, the more prototypical). As shown below (in figures 2, 3 and 4), the removal of dead states (and, more importantly, of the arcs to them) after machine intersection can increase the goodness of fit of the conjoined concept to the instance. This allows for a prototypical striped apple to be a better example of the concept *striped apple* than of either *striped* or *apple*.

Using the floor layout described in figure 1, figure 2 represents the concept of a single robot remaining arbitrarily long in section a, then moving to b for two sensor readings, and finally possibly going to c and staying there.

Figure 3 represents the concept of a single robot remaining in a for two sensor readings, then possibly moving to b and remaining there arbitrarily long, and finally possibly going to c and staying there.

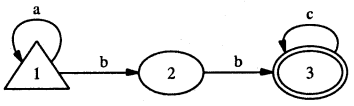


Figure 2: machine M_1 recognizes $L_1 = a^*bbc^*$. The strings with the cheapest encoding (and highest prototypicality) are those in bbc^*.

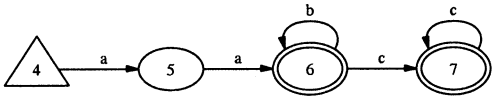


Figure 3: machine M_2 recognizes $L_2 = aab^*c^*$. The most prototypical strings are in aac^*.

Finally, figure 4 represents the concept which is the conjunction of the two previous ones; namely, that of a single robot remaining in a for two sensor readings, then moving to b and staying there a like amount of time, and then possibly moving to c and staying there indefinitely. The observation $aabb$, which is of the robot staying in a for two turns before moving to b and staying there for two turns, participates in all three concepts, although it is cheapest to describe (and thus most prototypical) in M_3 (see figure 5) as desired.

5 Summary

We have presented a model of categorization which results in a natural ordering between instances of a concept, as well as a way to determine which concept best fits a new instance. This latter point might be extremely valuable in practice, especially as having a way to discriminate between concepts which apply to the given instance may allow for a more adaptive response. The model also seems able to surmount some intuitive difficulties previous models of concepts had in regard to the compositional nature of conceptual structure.

Acknowledgements

This work was supported by the UCLA Center for Embedded Network Sensors, the Defense Advance Research Projects Agency (DARPA), administered by

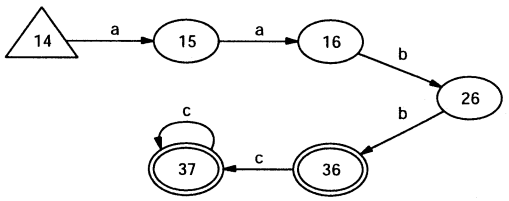


Figure 4: machine $M_3 = M_1 \times M_2$ recognizes $L_3 = L_1 \cap L_2 = aabbc^*$. The most prototypical strings are those in $aabbc^*$.

	Encoding
M_1	2
M_2	2
M_3	0

Figure 5: A comparison between the costs of encoding the string $aabb$ in each machine.

the Army Research Office under Emergent Surveillance Plexus MURI Award No. DAAD19-01-1-0504, and DARPA MURI award administered by the US Airforce No. F49620-01-1-0361. Any opinions, findings, and conclusions or recommendations expressed in this publication are those of the authors and do not necessarily reflect the views of the sponsoring agencies.

References

[1] Yoosook Lee, Jason Riggle, Travis C. Collier, Edward Stabler, and Charles E. Taylor. Adaptive communication among collaborative agents: Preliminary results from symbol grounding. In Masanori Sugisaka and Hiroshi Tanaka, editors, *Proceedings of the Eighth International Symposium on Artificial Life and Robotics*, pages 149–155, 2003.

[2] D. N. Osherson and E. E. Smith. On the adequacy of prototype theory as a theory of concepts. *Cognition*, 11:237–262, 1981.

[3] E. Rosch. On the internal structure of perceptual and semantic categories. In T. E. Moore, editor, *Cognitive development and the acquisition of language*. Academic Press, New York, 1973.

[4] Tracy Teal, Daniel Albro, Edward Stabler, and Charles E. Taylor. Compression and adaptation. In J. Nicoud D. Floreano and F. Mondada, editors, *ECAL99*, pages 709–719, Berlin, 1999. Springer-Verlag.

[5] Tracy K. Teal and Charles E. Taylor. Effects of acquisition on language evolution. *Artificial Life*, 6(2):129–143, Spring 2000.

[6] L. Zadeh. Fuzzy sets. *Information and Control*, 8:338–353, 1965.

Proc. of The Ninth Int. Symp. on Artificial Life and Robotics (AROB 9th '04)
Beppu, Oita, Japan, 28-30 January, 2004

Learning of Reaching a Colored Object Based on Direct-Vision-Based Reinforcement Learning and Acquired Internal Representation

Kazuyoshi Yuki Masanori Sugisaka Katsunari Shibata
Dept. of Electrical and Electronic Engineering,Oita University.
700 Dannoharu Oita 870-1192 Japan. shibata@cc.oita-u.ac.jp

Abstract

In this paper, it is shown that a mobile robot with a color line sensor could learn to reach a colored target object for which a reward was given, based on Direct-Vision-based Reinforcement Learning. In the learning, non-processed color sensor signals were the input of the neural network. On the hidden layer of the network, global information of the target location was represented by integrating the local sensor signals. The representation was almost the same between the colors of the rewarded target objects, even though the input signals differ completely by color even when the target location is the same.

1. Introduction

In recent years, reinforcement learning (RL) has been focused on as an autonomous learning for autonomous robots. By using a neural network in RL, continuous state and continuous action can be handled. The method has been applied to some control problems [1] [2].

On the other hand, the authors have proposed Direct-Vision-Based RL (D-V-B RL)[3][4] in which non-processed visual sensor signals are the input of a neural network and the network is trained based on RL when a robot learns its actions autonomously. Through the learning, continuous state space is formed in the hidden layers, and not only planning the actions but also the whole process from sensors to motors can be learned in harmony.

Then, a task in which a real mobile robot with a monochrome visual sensor reached and pushed a black box made of paper was employed, and visual sensor signals were inputted to a neural network directly. It was confirmed that the robot could learn to approach and push the box without giving any knowledge about the task and image processing in advance[4]. It was also shown that even if each input signal represents only local information, global spatial information of the object position is represented in the hidden layer of the neural network by integrating the signals.

In this paper, color visual sensor signals are used as input. At first, it is verified whether the robot can learn to reach the object as well as the case of monochrome sensor or not. Moreover, it is observed how the object position information and the color information are represented in the hidden layer.

It has been said that color information and position information are processed separately in the brain[5]. The possibility that the acquisition of the separate processing can be accounted for based on the combination of RL and neural network is also considered.

2. Direct-Vision-Based Reinforcement Learning (D-V-B RL)[3][4]

Fig.1 shows the concept of D-V-B RL. Here, actor-critic architecture is employed, and the actor and critic are composed of one layered neural network. Visual sensor signals are inputted to the neural network directly. The motor commands are generated from the actor output of the neural network. The training signal is generated based on RL, and the network is trained by the signal.

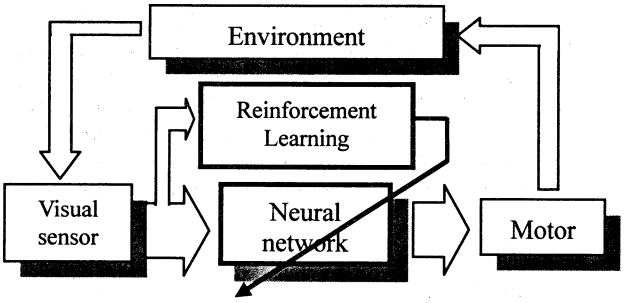


Fig.1 Direct-Vision-Based Reinforcement Learning.

TD (Temporal Difference) learning is applied for the critic learning. TD error is defined as

$$\hat{r}_t = r_t + \gamma P(\mathbf{x}_t) - P(\mathbf{x}_{t-1}) \quad (1)$$

where γ: a discount factor, r_t: a reward, P: the critic output and $\mathbf{x}_t$: observation vector. TD error is calculated from the present state value and the previous one. The previous critic output $P(\mathbf{x}_{t-1})$ is trained by the training signal as

$$P_{s,t-1} = P(\mathbf{x}_{t-1}) + \hat{r}_t = r_t + \gamma P(\mathbf{x}_t). \quad (2)$$

On the other hand, the motor command vector of the robot is the sum of the actor output vector $\mathbf{a}(\mathbf{x}_t)$ and a random number vector $\mathbf{rnd}_t$ as trial and error factors. The actor output vector $\mathbf{a}(\mathbf{x}_{t-1})$ is trained by the training signal as

$$\mathbf{a}_{s,t-1} = \mathbf{a}(\mathbf{x}_{t-1}) + \hat{r}_t \mathbf{rnd}_{t-1}. \quad (3)$$

The neural network is trained by Back Propagation (BP) method according to Eq. (2) and (3). In this way, when $\hat{r}_t$ is positive, $\mathbf{a}(\mathbf{x}_{t-1})$ is reinforced in the direction of $\mathbf{rnd}_{t-1}$.

3. Simulations

3.1 Task and environment

In this paper, a task is employed in which a mobile robot with a color line sensor reaches a colored target object. Fig.2 shows the simulation environment. Three colored objects, red (R), green (G), and blue (B) one, are prepared. At each trial, one of them is chosen randomly and is located randomly in front of the robot. Fig.3 shows the robot and the color line sensor that is mounted on the robot.

The robot height is 4.0, and the distance between left and right wheels are 3.8. The motor command for each wheel is continuous value from –0.3 to 0.3, and is used as the forward speed of the wheel. The color line sensor has 64 pixels, and the view angle is 180 degree. The sensor is installed a little backward from the robot center.The image is determined depending on the object color and the relative object position from the robot. The number of input signals is 192, since each of 64 pixels contains the information of the three colors, R, G and B. Each signal is continuous and ranges from 0 to 1. The background of the image is always black that means that the pixel values for the three colors are all 0.0. Therefore, when the color that a sensor cell detects is different from the object color, the pixel value is always 0 not depending on the object position. For simple analysis, only the primary colors are used as the object color.

Here, 4-layer neural network with 192 input units, 30 and 10 hidden units, and 3 output units was used. One of the outputs was for critic, and the other two were for actor. The output function of each neuron was a sigmoid function that ranges from –0.5 to 0.5. Since the critic ranges from 0 to 1 here, 0.5 was added to the critic output of the neural network. Each element of the random vector **rnd** was a cubed uniform random number that ranges from -1.0 to 1.0. Since the range of each motor command is from –0.3 to 0.3, the actor output was multiplied by 0.6. All the initial connection weights between the upper hidden layer and the output layer were 0. The other initial weights were small random numbers whose range was from –0.5 to 0.5. The discount factor γ was 0.99.

The goal of the robot is that the robot center passes through the object whose diameter is 2.0. When the robot reached the blue and green object, a reward is given. The training signal of the critic $P_{s,t}$ is 0.9 as a reward according to Eq. (2) with r_t=0.9 and P_t= 0.0. When the robot reached the red object, the critic is not trained. Moreover, when the object goes to the back of the robot without passing through the robot, the training signal of the critic $P_{s,t}$ is 0.1 as a penalty. Otherwise, the critic is trained according to Eq. (2) with r_t=0.

At every trial, the robot was returned to a starting position initially, and the object color and position are determined randomly. At the early phase of learning, the object position range is set near from and in front of the robot. As learning progresses, the range is gradually extended to the area far from the robot and the area at the side of the robot. The maximum distance from the robot to the object is 30 and the maximum angle from the front of the robot to the object is 90 degree.

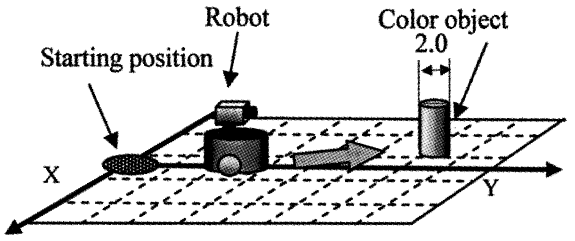


Fig.2 Simulation environment

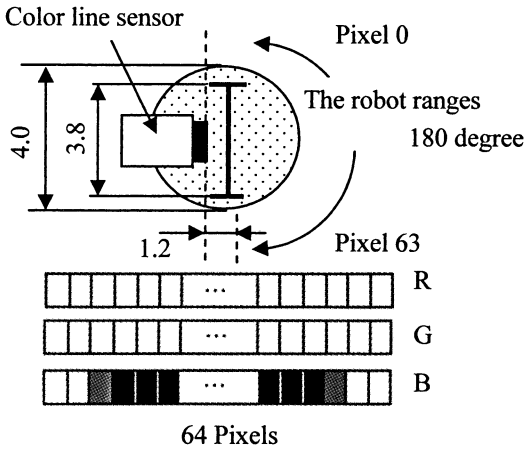


Fig.3 The robot and color line sensor

3.2 Results

Fig.4 shows the loci of the robot for some object locations for each object color after 30000 trials of learning. Fig.5 shows the distribution of the state value (critic output) as a function of the object position after learning. The robot is fixed at the position (0, 0) in this figure. The figure is drawn from the values for 1474 object positions on a lattice with a constant interval of 1. In case of the green or the blue object, the state value became larger gradually as the object was closer to the robot. It can be seen that the robot could reach the object not depending on the object position. It can be also seen that the loci and the state value were similar between the green and blue objects.

On the other hand, in case of the red object, though the robot was sometimes punished, it never got a reward. Therefore, the state value of the red object was small not depending on the object position. The action to reach the red object was not learned.

3.3 The analysis of the hidden representation

It was observed how the color information and the position information were represented in the hidden layer through learning. Using the weight after 30000 trials of learning, the output distribution of each neuron in the hidden layer that is closer to the output layer was observed.

An agreement index between two colors for each hidden neuron is defined to know how much the output of the neuron agrees between two colors. The agreement index is defined as

$$M_{color1,color2} = \sqrt{\sum_{p \in P} (h_{color1,p} - h_{color2,p})^2 / N_P} \,/\, \sigma_{color1,color2} \quad (3)$$

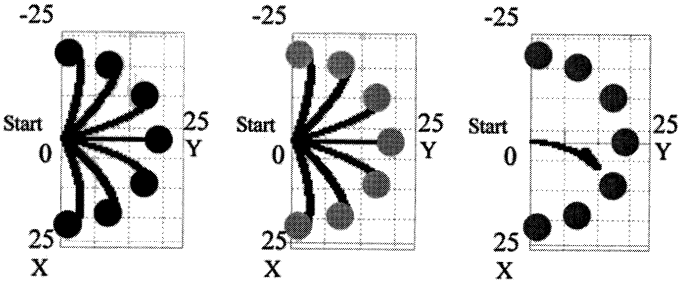
where $h_{color,p}$ is the output of the hidden neuron when the object color is *color* and the object position is p. P is the sample set of the object positions. N_P is the number of elements of P. Here, N_P is 1474. $\sigma_{color1,color2}$ is the standard deviation of the hidden neuron's output for both *color*1 and *color*2 objects. It should be noticed that when the hidden output agrees more between two colors, the agreement index becomes smaller.

Table 1 shows the agreement indices between red and blue and that between green and blue for each hidden neuron. The connection weight to each output neuron is also shown. Before learning, it can be seen that all the agreement indices are more than 1. However, after learning, some agreement indices between green and blue are less than 1. The underlined weight values indicate that the absolute weight value is the maximum for one of the output neurons, in other words, the hidden neuron contributes the most to the output neuron.

Fig.6 shows the output distribution of the four hidden neurons. In the first three neurons, the output distribution is very similar between the green and blue objects. On the other hand, the distribution for the red object is different from that for the other colors. The neuron 3 that contributes to the critic output represents the distance to the object when the object color is blue or green. The neuron 4 and 5 that contribute to the actor outputs classify the object location into right or left for the object colors. The distance and "right or left" are both global information that are calculated by integrating local sensor signals. On the other hand, in case of red object, the distribution is influenced by the locality of the receptive field of the sensor cells.

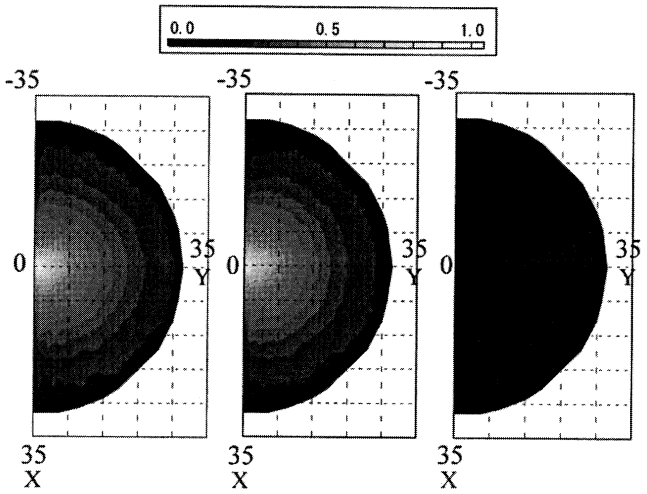
The contribution of the hidden neuron 9 to the actor1 is also large, but the agreement index between the green and blue object is not small. When the object color is green or blue, the output is almost 0.5 for all the object positions as shown in Fig.6 (d). The representation is not different actually between the blue and green objects.

From this result, it can be said that if the reward



(a) Blue object (b) Green object (c) Red object

Fig.4 The tracks of the robot after 30000 trials



(a) Blue object (b) Green object (c) Red object

Fig.5 Distribution of the state value (critic output) as a function of the relative target location.

Table1 Agreement index and connection weight to each output neuron for each hidden neuron.

Neuron	Agreement index				Connection weight to each output neuron of each hidden neuron		
	Before learning		After learning				
	R-B	G-B	R-B	G-B	Critic1	Actor1	Actor2
1	1.37	1.41	1.14	0.59	1.02	-0.004	0.01
2	1.45	1.43	1.75	1.42	-0.93	-0.07	-0.1
3	1.49	1.49	1.88	**0.149**	**-1.67**	-0.01	0.03
4	1.44	1.48	1.67	**0.253**	0.04	0.005	**-4.4**
5	1.61	1.13	1.36	**0.274**	0.03	**4.42**	0.01
6	1.35	1.22	1.79	1.67	0.05	-0.07	-0.01
7	1.42	1.40	1.3	0.78	0.35	0.03	0.03
8	1.59	1.55	1.69	1.59	0.2	-0.05	0.01
9	1.43	1.42	1.77	1.32	0.02	**4.36**	0.07
10	1.36	1.52	1.59	0.85	0.09	-0.02	-0.01

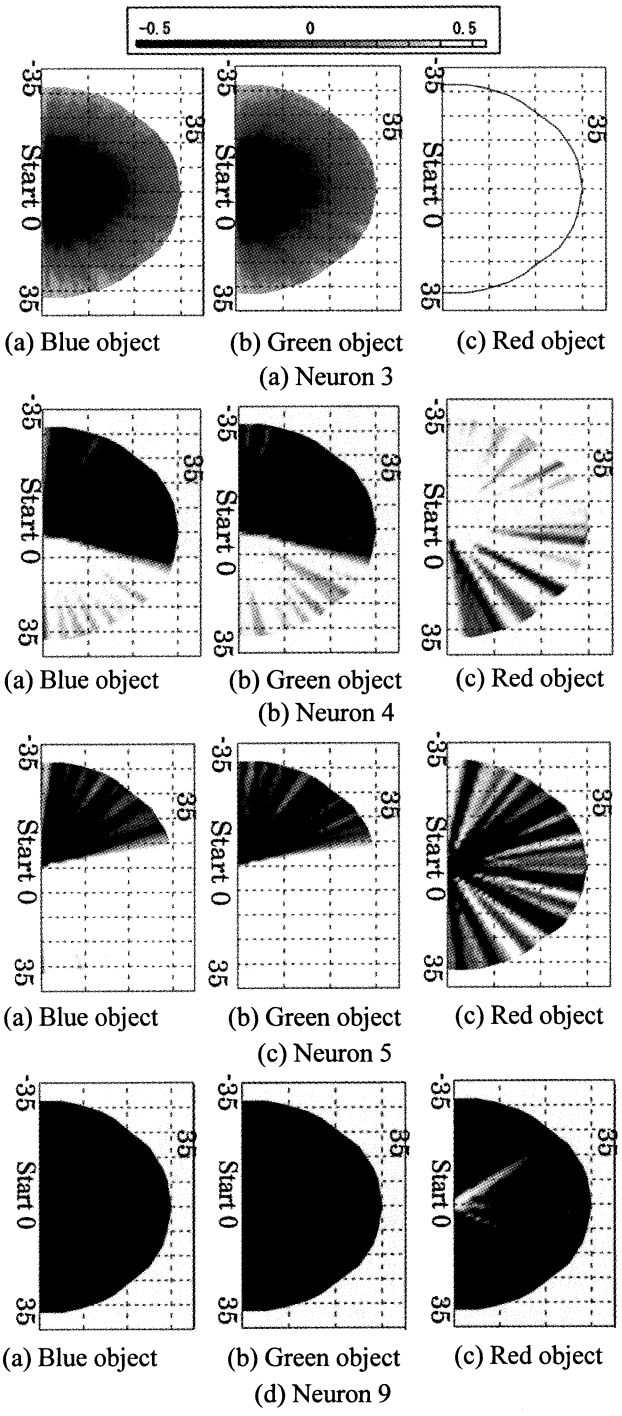


Fig.6 The output distribution of the hidden neurons that have large connection weights to one of the output neurons.

condition is the same between two colored objects, the hidden neuron that has a strong connection weight to one of the output neurons represents the same information about object position. It has been shown that even if the input patterns are not close, the hidden representation tends to be closer if the training signals are close[6]. It is thought that the nature of the neural network causes the result in this paper.

It has been said that color information and position information are processed separately in the brain of our living things[5]. In the result of this paper, in the hidden layer, the position information not depending on the color is extracted when the reward condition is the same. In the real world, there are many situations in which the position information not depending on the object color is important. For example, the range of the object location to which a person can reach its hand does not depend on the object color. We think that the possibility that reinforcement learning contributes to process the color information and the position information separately could be suggested from this result.

4. Conclusion

The learning of the task in which a reward is given depending on the object color when a mobile robot reaches a target object was simulated. The robot learned to reach the rewarded colored object by Direct-Vision--Based Reinforcement Learning.

Moreover, it was verified in the hidden neurons that the global information of the object position not depending on the object color is represented for the rewarded colors.

Acknowledgements

This research was partially supported by the Ministry of Education, Culture, Sports, Science and Technology of Japan or the Japan Society for the Promotion of Science, Grants-in-Aid for Scientific Research, #13780295, #14350227 and #15300064.

References

[1] Anderson, C.W: Learning to Control an Inverted Pendulum Using Neural Networks IEEE Control System Magazine, Vol.9 pp 31-37 (1989)

[2] Morimoto, J. and Doya, K.: Acquisition of Stand-up Behavior by a Real Robot using Hierarchical Reinforcement learning, Robotics and Autonomous Systems, Vol.36,pp.37-51 (2001)

[3] K.Shibata, K.Ito and Y.Okabe Direct-Vision-Based Reinforcement Learning Using a Layered Neural Network -For the Whole Process from Sensor to Motors- ,Trans. of SICE,Vol.37, No2, p168-177 (2001) (in Japanese)

[4] K.Shibata and M.Iida: Acquisition of Box Pushing by Direct-Vision-Based Reinforcement Learning Proc.of SICE Annual Conf. 2003, 0324.Pdf, pp.1378-1383 (2003)

[5] S.Amari and K.Toyama Editor: Brain Science Encylopedia, 1.1Visual Recognition, Asakura Shoten, pp102-142 (2002) (in Japanese)

[6] K.Shibata and K.Ito: Adaptive Space Reconstruction on Hidden Layer and Hidden-level Generalization in Layered Neural Networks with Local Signal Inputs, Technical Report of IEICE NC2001-152, pp.151-158 (2002) (in Japanese)

Proc. of The Ninth Int. Symp. on Artificial Life and Robotics (AROB 9th '04)
Beppu, Oita, Japan, 28-30 January, 2004

Optical flow as a tool for optical speed sensor

Tomasz Kubik† Masanori Sugisaka*

† Institute of Cybernetics Engineering, Wroclaw University of Technology,
Janiszewskiego 11/17, Wroclaw 50-372, Poland
E-mail: tkubik@ict.pwr.wroc.pl
* Department of Electrical and Electronic Engineering, Oita University, 700 Dannoharu, Oita 870-1124, Japan
E-mail: msugi@cc.oita-u.ac.jp

Keywords: image processing, optical flow

Abstract

Modern autonomous flying objects are equipped with a standard set of navigation devices. In common practice these devices are duplicated in order to replace mal functioning device with a spare one on fly. In a remotely controlled, unmanned helicopters one of the crucial on board devices is a speedometer. Nowadays GPS plays this role. But there are some conditions in which GPS cannot work properly (magnetic storms, vanishing signal, etc.) At that time there is a need for another device ready to provide data reliably. In the paper we present a system which can measure ground speed based on the real time video signal processing. The system is based on optical flow calculation.

1 Introduction

One of the most important points in the autonomous system design is an invention of an efficient sensory system. Such a system should provide all necessary data for autonomous locomotion and navigation implementation. In general, three-dimensional perception of the world is required.

Three-dimensional perception of the world is common to many biological vision systems. Amazing examples are humans with their ability to perceive depth, surface orientation and spatial relationships with remarkably accuracy under most circumstances. The primary mechanism used by human's vision system is stereopsis, i.e. the lateral displacement of objects in two retinal images. Another one is motion parallax, i.e. the differential motion of points relative to the fixation point. Since years these two mechanisms were basis for the artificial vision systems development.

In artificial (computer) vision community stereopsis and motion parallax were analyzed and several algorithms were proposed. In most cases these algorithms are based on stereopsis since the underling geometry is well understood. In this paper we focus on the development of the method based on optical flow calculation (a method that inherits from stereopsis). More exactly, we concern only one of possible optical flow application, namely: its use for camera motion (speed) estimation.

Optical flow, in general, can be used to compute motion detection, time to collision, structure, focus of expansion, object segmentation, etc. In our paper we plan to use an optical flow to estimate ground speed of the flying object. Thus optical flow is defined as a representation of the apparent motion of the world projected on the image plane of a moving camera. We assume that observed world is static, so optical flow is the 2D velocity field resulting from the camera motion (excluding a motion resulting from independently moving objects in the scene).

2 Problem statement and solution

The optical speed sensor based on optical flow calculation can solve a problem stated as follows (Fig. 1): *Given two images P and C taken (within a period tp) from a video camera mounted on a helicopter flying at a given height h find an unknown helicopter's ground linear speed V (and angular speed Ω)*

One can notice that the motion of the helicopter gives rise the optical flow field that can be observed on two consecutive images captured. Since that the idea of an optical speed sensor implementation can be expressed by a simple sentence:
If the parameters of transformation from one captured image to the second image are known (i.e. translation - T, and rotation angle - Θ) then the local speed $V = [v_x, v_y]^T$ and angular speed Ω can be cal-

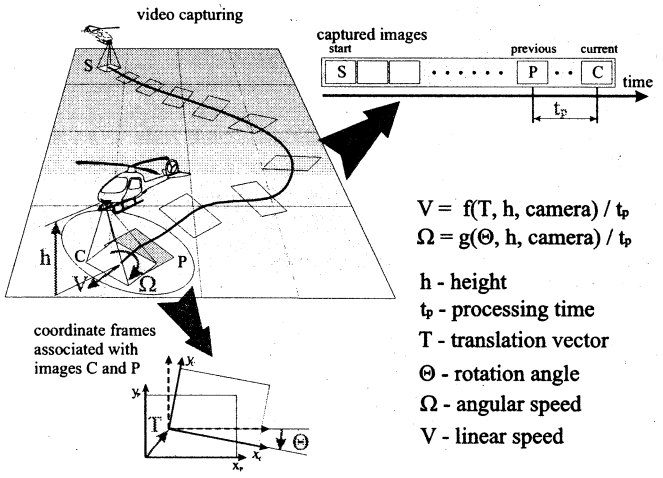


Figure 1: Problem statement: given P, C, t_p, h find V and Ω

culated from functions: $V = f(T, h, camera)/t_p$, $\Omega = (\Theta, h, camera)/t_p$, *where* t_p *- time interval in which two images were captured, h and camera - height and camera parameters that have influence on the image scale (relation between distances on image and distances on the ground).*

This sentence comes true when: - both images are projections of the same area (or they share a part of it); - pixel-to-pixel distances on both images represent the same distances on the ground (geometry is preserved). Of course problem definition does not assure that both mentioned condition are true. Before any further proceeding we assume that camera used on helicopter has been calibrated.

3 Implementation of the sensor

The key point in the implementation of this system was calculation of T and Θ. The calculation were performed according to the following scheme.

At first original color images P and C were processed by applying two operations: grey level requintizing (to receive gray images), and then Sobel filtering. Next optical flow based on Lucas-Kanade method was calculated. More exactly: in this step for the selected points in the image P corresponding points were found in image C. To enhance obtained results coordinates of points found in image C were filtered with Kalman filter (in this part we used coordinates of points memorized from a previous step of calculation). Finally, having two sets of points (selected in image P and enhanced in C) T and Θ were calculated. This part was based on the least-square approach. In this approach the actual rotation angle (i.e. rotation matrix which transforms coordinate frame associated with image P to the coordinate frame associated with image C) is computed through a minimization of a certain criterion. To evaluate how much we can trust in the obtained results we introduced a "goodness" parameter. This parameter is defined with the help of the sample variance. Sample variance measures the difference between points in C (received after Kalman filtering) and another points in C (which was obtained from points in image P transformed by the use of obtained T and *Theta*).

The preliminary optical speed sensor implementation we have tested consisted of the following components (see Fig. 2):

- image preprocessing (captured images were converted to the gray level images, then they were filtered with Sobel filter for independency from lighting condition, Fig. 2a)
- image processing (an optical flow was calculated, Fig. 2b) and c)
- data filtering (the results of optical flow were filtered with Kalman filter, Fig. 2d)
- T and Θ calculation (by the least-square approach Fig. 2e)
- goodness calculation (Fig. 2f)

There are a number of ways to compute the optical flow. The basic classification of methods is into gradient-based, correlation-based, and energy-based methods. For our needs in a preliminary research we have chosen Lucas-Kanade method [1]. This method served us as a tool for calculation such points in image C that corresponded to the selected points in image P. Because points received not always matched expected points, its coordinates were filtered with Kalman filter [2]. Such a filtering allowed us to reduce noise and increase robustness of the method. Final step (transformation parameters calculation) was a matter of solving planar movements problem by the means of the least-square approach [3]. In this problem transformation parameters are calculated trough the certain criterion minimization. The quality of obtained results are measured by goodness parameter.

Let us explain the final step in details. When a rigid object rotates from position 1 to position 2 around a point by the angle φ (see Fig. 3), the following holds:

$$p_{2i} - p_c = R(\varphi)\,(p_{1i} - p_c) \qquad (1)$$

where $p_{ji} = [x_{ji}, y_{ji}]^T$, $R(\varphi)$ is a rotation matrix, and

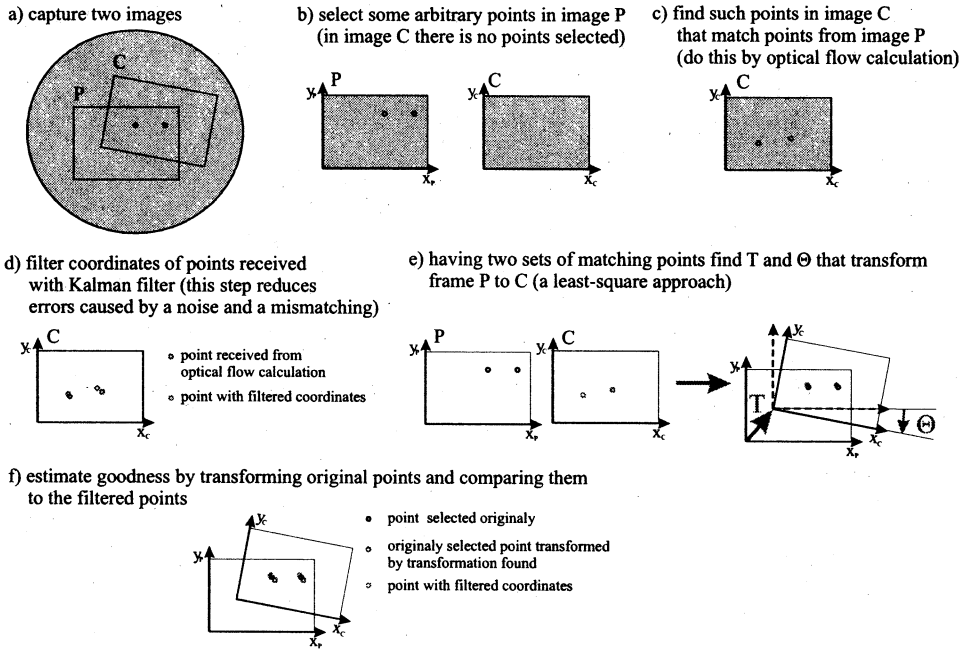


Figure 2: Scheme of two consecutive frames processing

$p_c = [x_c, y_c]^T$ is the center of rotation in x_0y_0 coordinate frame. Let p_{10} and p_{20} are two consecutive

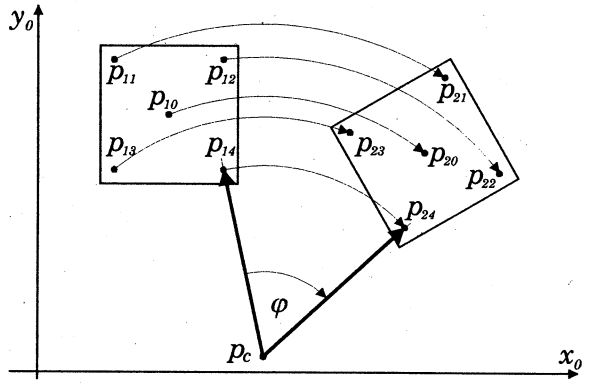


Figure 3: Rotation of a rigid object around point p_c

position of an arbitrary point of the object (local reference point) measured in the inertial reference frame. Then the following also holds:

$$p_{2i} - p_{20} = R(\varphi)\,(p_{1i} - p_{10}) \tag{2}$$

Although local reference point can be choosen arbitrarly, let it be the center of all distinguished points i on the object. The coordinates of $p_{j0} = [x_{j0}, y_{j0}]^T$, $j = 1, 2$, correspond to the coordinates of a local reference point at two consequtive position. They can be calculated as follows:

$$x_{j0} = \frac{\sum_{i=1}^{N} x_{ji}}{N} \text{ and } y_{j0} = \frac{\sum_{i=1}^{N} y_{ji}}{N} \tag{3}$$

Let $\bar{p}_{ji} = p_{ji} - p_{j0} = [x_{ji} - x_{j0}, y_{ji} - y_{j0}]^T$ be a vector connecting p_{j0} with p_{ji}. Then the following holds:

$$\bar{p}_{2i} = R(\varphi)\bar{p}_{1i} \tag{4}$$

This leads to the equation that can be used to find the unknown angle of rotation φ:

$$\bar{p}_{2i} - R(\varphi)\bar{p}_{1i} = 0 \tag{5}$$

The equation involves four unknown variables – elements of matrix $R(\varphi)$. But because

$$R(\varphi) = \begin{bmatrix} r_{11} & r_{12} \\ r_{21} & r_{22} \end{bmatrix} = \begin{bmatrix} \cos\varphi & -\sin\varphi \\ \sin\varphi & \cos\varphi \end{bmatrix} \tag{6}$$

φ is the only unknown variable. Calculation of this angle requires one pair of vectors $\bar{p}_{1i}$, $\bar{p}_{2i}$. But when the position of points is not exact (is measured with some noise) the rotation angle must be calculated in

a different way. One option is to follow a least-square approach In this approach the actual rotation matrix (and angle of rotation) is computed trough the minimization:

$$min\frac{1}{N}\sum_{i=1}^{N}(\bar{p}_{2i}-R\bar{p}_{1i})^T(\bar{p}_{2i}-R\bar{p}_{1i}) \quad (7)$$

where R substituted $R(\varphi)$ for simplicity. The solution to this problem is given by the following equation:

$$\varphi=\text{atan2}\left(\sum_{i=1}^{N}(\bar{x}_{1i}\bar{y}_{2i}-\bar{y}_{1i}\bar{x}_{2i}),\sum_{i=1}^{N}(\bar{x}_{1i}\bar{x}_{2i}+\bar{y}_{1i}\bar{y}_{2i})\right) \quad (8)$$

Let p^e_{2i} be a point given by:

$$p^e_{2i}=p_{20}+R\bar{p}_{1i} \quad (9)$$

The coordinates of p^e_{2i} might differ from the coordinates of p_{2i} (see Fig. 4). This difference will serve as a base for goodness estimation. Let

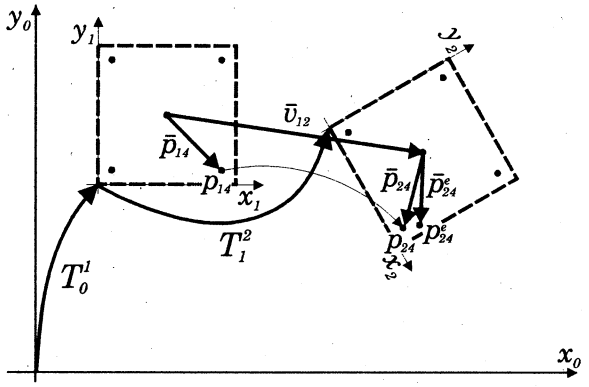


Figure 4: Rotation of a rigid object with erroneous measurements

$$e_i=p_{2i}-p^e_{21}=p_{2i}-(p_{20}+R\bar{p}_{1i})=\bar{p}_{2i}-R\bar{p}_{1i} \quad (10)$$

defines the error. Then the sample variance $\sigma_s^2=[x_s,y_s]^T$ can be calculated as follows:

$$\sigma_s^2=\sqrt{\frac{\sum_{i=1}^{N}(e-\bar{e})^2}{N}} \quad (11)$$

where

$$\bar{e}=\frac{1}{N}\sum_{i=1}^{N}e_i \quad (12)$$

The "goodnes" g can be defined as:

$$g=\begin{cases} M-k, & \text{if } \left(k\frac{|\bar{v}_{12}|}{M}<=x_s<(k+1)\frac{|\bar{v}_{12}|}{M} \text{ or } k\frac{|\bar{v}_{12}|}{M}<=y_s<(k+1)\frac{|\bar{v}_{12}|}{M}\right) \\ 1, & \text{otherwise} \end{cases} \quad (13)$$

where $k=0,\ldots,M-1$, and $\bar{v}_{12}=p_{20}-p_{10}$, and M is an arbitrary precision step. The equation (13) can be interpreted in the following way: the goodness is inversely proportional to the fraction of sample variance in the total movement.

4 Conclusions

Despite rich mathematical foundations and steady progress in optical flow study and computing, there are only a few practical implementation based on it. Since that our proposal appears to have an innovative and promising character. As it was documented by preliminary experiments, our optical speed sensor have a chance to be robust and efficient and most of all, practically usable.

References

[1] Lucas B., Kanade T. (1981), An Iterative Image Registration Technique with an Application to Stereo Vision. In *Proc. of 7th International Joint Conference on Artificial Intelligence (IJCAI)*, pp. 674–679

[2] Welch G., Bishop G. (1995), Technical Report TR95-041. Technical report, University of North Carolina at Chapel Hill

[3] Challis J.H. (1995), A procedure for determining rigid body transformation parameters. *J. Biomechanics*, 28:733–737

Proc. of The Ninth Int. Symp. on Artificial Life and Robotics (AROB 9th '04)
Beppu, Oita, Japan, 28-30 January, 2004

An Assymetric 2-D Passive Dynamic Walker

N. Mayer*, J. M. Herrmann†, A. A. Forough-Nassiraei*, M. Browne*, T. Christaller*‡
* GMD - Japan Research Laboratory Collaboration Center, 2-1 Hibikino, Wakamatsu-ku, Kitakyushu 808-0135, Japan
† Institut für Nichtlineare Dynamik, Universität Göttingen, Bunsenstr. 10, D-37073 Göttingen, Germany
‡ Fraunhofer Institut für Autonome Intelligente Systeme, Schloss Birlinghoven, D-53754 St. Augustin, Germany

Abstract

The dynamic behavior of a passive walker is difficult to predict in advance, and extremely sensitive to the parameters of the hardware design. Within a simplified setting experimental, numerical, and theoretical methods are combined in order to benefit both from the efficiency brought about by passive dynamics and the flexibility provided by adaptive control. A walker optimized for downhill motion at given slope is controlled such that walking at a range of slopes is stable and the walking speed can be modified within certain limits. For numerical simulations we used a genetic algorithm for parameter optimization.

1 Introduction

The goal of passive dynamic walking is to exploit the natural dynamics of pendulum-like legs in order to achieve fast walking in bipedal robots. This approach is increasingly interesting as an alternative to the conventional method of trajectory planning. A large number of publications have addressed properties of bipedal walking in machines and living beings. However, practical applications suffer from narrow stability intervals, complexities involving nonlinear control, and tight restrictions in achievable gait properties.

Two-dimensional walkers are an intermediate step in the development of passive-dynamic biped walking systems. Walkers such as those studied by McGeer and colleagues [1] show a moderately stable gait at downhill slopes without using any control whatsoever. With respect to speed these walkers can compete with state-of-the art humanoid robots, provided the slope is sufficiently steep. The speed is, however, determined by the slope and payload cannot be changed for a given design. Walking machines without knees show particularly simple dynamics, but are impractical because they are unable to raise the swing leg above ground. This basic problem can be avoided while keeping the system as simple as possible by using a one-kneed walker with legs of slightly different sizes. Two-dimensional walkers use actually two pairs of tightly coupled legs in order to avoid instabilities orthogonal to the walking plane. Such a machine has been tested and analyzed in the present project. In the present contribution numerical and theoretical studies on this walking machine are presented and experiments with a hardware walker are described. Finally, possibilities for control are discussed and first results are reported.

2 Numerical results

In order to understand its dynamics we investigated computer models of two-dimensional one- and two-kneed walkers. We assumed point masses and point contacts instead of feet. The simulation was based on the Lagrange formalism, where two different Lagrangians for the bended-knee condition and the knee-stretched condition were used alternatingly. The parameters of the walker, such as mass distributions and initial conditions, were optimized by a simple genetic algorithm. Random mutation and crossover were employed, and a combination of walking speed, step length, and conservation of the initial energy was used as a fitness function. The evolved walkers were able to walk stably at any (fixed) slope below 45 degrees. However, sliding motion was not considered and at small slopes the achieved step size decayed rapidly, although the overall speed improved.

For an parameter set that was optimized for a slope of 11.5 degrees the number of steps that could be performed in a given time interval was found to dependent in an irregular fashion on the slope. This indicates chaotic walking behavior of the simplified model, in accordance to findings in passive dynamic walkers without knees [3], where the the basin of attraction of regular motion was investigated. Equal step lengths are practically impossible due to vanishing basins of at-

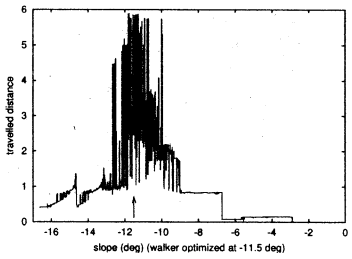


Figure 1: Dependence of the distance in a given time interval on slope.

traction for slopeslarger than a critical value of about 1.25 degrees. In the hardware walkers with knees the critical slope is apparently higher (3 - 5 degrees, M. Wisse, personal communication). Above this critical value the motion becomes irregular by a period doubling of the step sizes. The irregular motion increases the chance of falling over and presents a challenge to control mechanisms.

3 Experiments with a real walker

A walker has been constructed according to the precise descriptions in [2]. However, since the walking properties depend on the exact weight distribution, a few modifications for this individual were necessary. The walkers were equipped with four legs where pairs of legs move synchronously and stabilize in this way the dynamics in the direction orthogonal to the walking plane. Thus only the dynamics within the walking plane is to be considered. Yet, this attempt failed, tended to fall forward and was hardly able to walk more than a few steps. Two main problems seemed to prevent the walker from a stable gait:

- The walking pattern was not optimized. Thus, the movement of the upper leg against the lower leg did not fit together. In humans during walking the lower leg has to move much faster than the upper leg, because the moving leg has to be stretched in the moment it hits the ground.
- The walker was not well balanced. A successful walker has due to the shape of its legs an optimal angle against the ground. In dependence of the slope the weight distribution has to be optimized in order to result in an stable gait.

The aim was to improve the balance and the gait pattern in order to allow for a stable downhill gait.

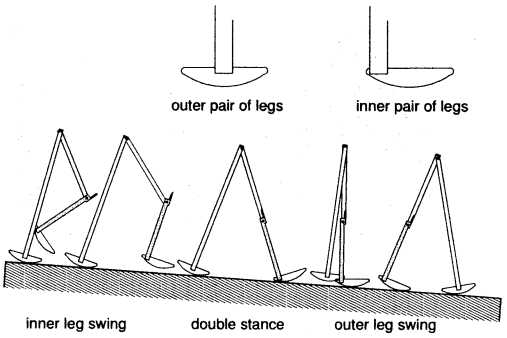


Figure 2: Scheme of the changes on the feet of the 2D-walker with one knee. In order to prevent the walker stumbling over its stiff leg the foot must be modified. Left: The attached point is shifted towards its middle. Right: Swinging is possible for both the kneed leg and the stiff leg.

The balancing can be done by adding weight either in front or in the back of the walker. The same is true for improving the gait, however additional changes were necessary. Thus, we proceeded to:

- stiffen the outer pair of knees and modified the position of the feet. The walker tended to fall because the second pair of legs bend to early resembling a human using crutches
- shift position of the feed in the inner pair of legs in order to prevent the swinging leg from hitting the ground (cf. fig. 2 for illustration)
- allowed a maximum stretching of the knee of more than 180 degrees. Thus the knee maximum stretching of the knee is around 185 degrees. This increases the stability of the stretched knee and prevents the standing leg from bending.
- increased the weight of the upper leg. In this way the pendulum constant of the upper leg was elongated, whereas the pendulum constant of the lower leg remained unchanged.

After the changes the walker showed a stable gait over the whole tested distance (about 15 steps) for a slope of around 3-5 degrees. The motion resembles now the motion of a person walking with crutches. Still also the motion of our one-kneed walker appears to include two different step sizes which is due to the construction of the knee in the middle pair of legs and the stiffening of the outer legs.

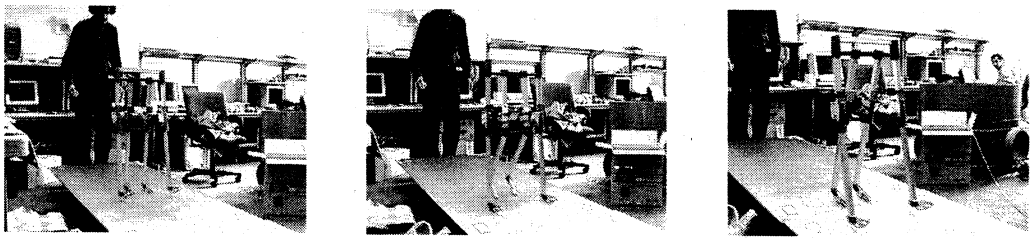


Figure 3: 2-D Walker:
Images are ordered from left to right and top to bottom, taken from test run of the walker (Movie can also be downloaded from [8]).

A robot could only walk down a slope from a narrow range of angles which strongly limits the applicability of passive dynamic walkers. There are two ways to overcome this problem. Either the robots internal configuration adapts to the slope, e.g. by variable mass configurations of spring constants or the passive dynamics are supplemented by actuated control. Clearly for uphill walking and in order to reach reasonable speed at low slopes, energy has to be fed in the system.

At present the walker is brought by hand in the right set of initial conditions. With respect to theoretical considerations in [3] it would be interesting to find out the size of the basin of attraction. We see indications from our experiments that the stability of the walking is increased by stiffening one knee. However, it is not clear if this remains true for the final walker. The speed of the walker was around 0.5 m/s. The total weight of the walker is about 5 kg. This results in an energy consumption of roughly 1 W. The walker seems to be able to walk by a slope from around 8 degrees to 3 degrees, however this depends of course strongly on the initial conditions, that at present are set by hand.

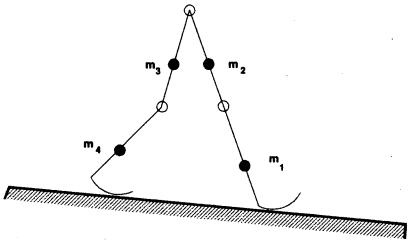


Figure 4: Sketch of the simulated walker: Point masses and feet without any weight were assumed for the simulation

4 Control

A simple method to enable the walker to walk at arbitrary slopes with arbitrary speed is to raise the back leg by an certain amount during the stance of this leg. This corresponds to a virtual slope given by the difference between the raised back leg and front leg at the moment when the front leg hits the ground. The virtual slope should be equal to the slope the walker is designed for but may also serve to reach a certain target speed provided the range of stability is large enough. Moreover, variations of the virtual slope can be used to enhance the stability of the walking cycle.

In the simulation a control method was realized in the simulation of the above mentioned simplified walking model. In order to overcome the strong dependence of the slope in the simplified walker for big slopes the control was that the leg behind was elongated in the moment it left the ground. In this way the performance of the walker could be significantly improved. However, appropriate control to control systems and to exploit the natural dynamics of a robot is still a challenging problem, not only with regard to walking systems, but also for control of other limbs like the arms [4]. For the design of such systems two problems appear. First the programming of the control algorithm and second the design of appropriate actuators that can switch from active to passive dynamics. For the techniques like hierarchical reinforcement learning [5] or such methods as Homeokinetics [6] seem to be appropriate. Here we see our main subjects for investigations in future. Regarding actuators we expect the use of mechanisms with springs - as presented in [7] - and clutches to be useful.

5 Discussion

The real walker is able to walk with one leg kneed and one without knee. Since the swing leg has to be shorter than the standing leg this is virtually the minimal possible configuration for a biped walking robot. The main points for investigations in future will be to investigate the dynamic properties and to implement an appropriate control mechanism. So far, the control method was only realized in that simulation of the above involved a simplified walking model. In order to overcome the strong dependence of the slope in the simplified walker for big slopes, the control was that the leg behind was elongated in the moment it left the ground. In this way the performance of the walker could be significantly improved.

Whereas above a push with the back foot was used to reach a virtual slope, it is also possible to operate the walker in a more realistic regime by exploiting one the following possibilities

- active straightening of the stance leg during its stance phase. Here the front leg is (as in real human walking) not straightened before the heel-strike, i.e. knee strike and heel strike occur in reversed order as in McGeer's kneed walkers. In order to obtain a stable walking, however, the knee must be actively straightened in the stance leg approximately when the stance leg is directly under the hip. For increasing upward slopes the moment of straightening is to be appropriately advanced. For downhill movement this procedure can include a passive component, i.e. a spring which stores energy at the heel strike and which during the stance phase returns the energy to the walking system.
- An actuator at the hip which actively pushes the swing leg forward which allows for larger steps and (thus) walking speeds.
- Specific movements of the trunk and the arms may as well enhance stability and efficiency.

Passive-dynamic biped walkers show in many respects interesting properties. Robotics, nonlinear dynamics and control play a role, here. One important initial idea of this project was to use experiences from the simulation in the real walking model. The work on the real passive dynamic walker revealed that still after finishing the optimization in the simulation program a lot of practical experiments are necessary in order to get the walker walking. One big open point for further investigations will be to close this remaining gap between simulation and practical application.

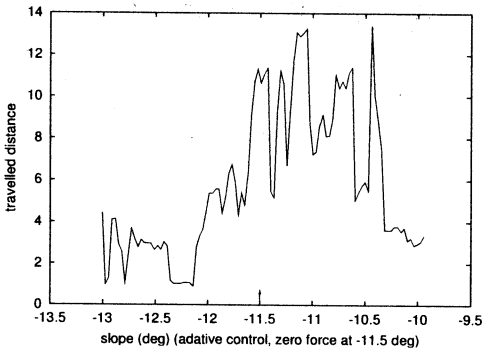


Figure 5: Dependence of the distance in a given time interval on slope for a controlled walker

Acknowledgment

We thank M. Wisse, F. Pasemann, S. Ghidary, K. Koganezawa, for helpful hints and discussions, K. Ishi and his students for their help. J.M.H. thanks the GMD-JRL for the kind hospitality that he experienced during a stay in Kitakyushu in February 2003 and the members of GMD-JRL for very stimulating discussions. The work was supported by the Foundation for the Advancement of Industry and Science, Kitakyushu.

References

[1] T. McGeer. Passive Dynamic Walking. International Journal of Robotics Research 9:2 (1993) 62-82.

[2] M. Garcia (1999) PhD Thesis. Cornell University.

[3] A.L. Schwab, M. Wisse, Basin of Attraction of the simplest walking model, Proceedings of the DETC'01, DETC2001/VIB-21363.

[4] M. M. Williamson, Oscillators and Crank-Turning: Exploiting Natural Dynamics with a Humanoid Robot Arm Hewlett-Packard Labs Tech. Rep., HPL-2002-132, 20020611 (2002).

[5] J. Morimoto, K. Doya, Acquisition of stand-up behavior by a real robot using hierarchical reinforcement learning, Robotics and Autonomous Systems 36 (2001) 37-51.

[6] R. Der, J. M. Herrmann, R. Liebscher, Homeokinetic approach to autonomous learning in mobile robots. In: R. Dillmann, R. D. Schraft, H. Woern: Robotik (2002) VDI-Berichte 1679, 301-306.

[7] K. Koganezawa, O. Matsumoto, Active/Passive Hybrid Walking by the Biped Robot Tokai Robo Habilis 1, Paper Number 541, IROS 2002.

[8] Movie of the passive dynamic biped walker of GMD-JRL *http://www.gmd.gr.jp:16080/html/movies/Walker.avi*

Proc. of The Ninth Int. Symp. on Artificial Life and Robotics (AROB 9th '04)
Beppu, Oita, Japan, 28-30 January, 2004

Robot Manipulator Control Using Topology Representing Network According to Initial Posture

Takeshi Yamakawa, Keiichi Horio, Keisuke Ueno
Graduate School of Life Science and System Engineering
Kyushu Institute of Technology
Hibikino2-4, Wakamatsu, Kitakyushu, Fukuoka, 808-0196, Japan
e-mail:yamakawa@brain.kyutech.ac.jp

Abstract

Since it is difficult to calculate the inverse kinematics in robotics, it is effective to solve it by using learning algorithm. Robot manipulator control using Self-Organizing Map (SOM) can lead the end effector to any target positions precisely. However, it is not always able to do in small joint angle displacement, because this algorithm learns one to one relationships between the end effector positions and the sets of joint angles. In this paper, we propose a new algorithm to solve the inverse kinematics in small joint angle displacement by using Topology Representing Network.

1 Introduction

For robot manipulator control in the robotics, inverse kinematics is to calculate the set of joint angles which leads the end effector to target position. It is not simply calculated an unique set of joint angles from the end effector position because there are some sets of joint angles which lead end effector to a same position. Also, parameters of robot manipulator must be known in order to calculate the kinematics and the inverse kinematics. In this paper, we propose robot manipulator control according to the initial posture without the parameters by using learning system.

Robot manipulator control using Self-Organizing Maps (SOM)[1][2] has been proposed in order to solve the inverse kinematics without the parameters by using learning algorithm. This algorithm learns input-output relationships. The input is target position of the end effector, and the output is a set of joint angles which leads the end effector to the target position. It can lead the end effector to target positions precisely after learning, but it is no consideration of motion planning because of learning one end effector position to one set of joints angles. Therefore, it is not always able to lead end effector in small joint angle displacement. Motion planning of robot manipulators is generally defined in joint angle space. Motion planning using Topology Representing Network (TRN)[3][4], inspired from SOM, has been proposed in order to lead the end effector in efficiently joint angle displacement. In the learning, it configures neighborhood relationships by connecting close distance units with links. In the execution, it applies the links for motion planning.

In this paper, fundamentally we combine both of two ideas which are robot manipulator control using SOM and motion planning using TRN in order to lead the end effector to any target position precisely in small joint angle displacement.

2 Robot Manipulator control Using SOM

Robot manipulator control using SOM learns input-output relationships without the parameters, *e.g.* the lengths of robot manipulator segments. The structure of the SOM is shown in Fig.1. In the SOM, each unit has weight vectors $\boldsymbol{w}_i$, $\boldsymbol{u}_i$, and a weight matrix $\boldsymbol{A}_i$. The weight vector $\boldsymbol{w}_i$ corresponds to target positions. The weight vector $\boldsymbol{u}_i$ and the weight matrix $\boldsymbol{A}_i$ generate desirable output $\vec{\theta}_i$ which is the set of joint angles after learning. When $\boldsymbol{u}_i$ has learnt desired values, the set of joint angles $\boldsymbol{u}_i$ leads the end effector to the position of $\boldsymbol{w}_i$. The weight matrix $\boldsymbol{A}_i$ is a Jacobian matrix to be able to lead the end effector to the target positions precisely, which are input vectors $\boldsymbol{X}$, even if the target positions do not coincide with $\boldsymbol{w}_i$. In the execution, the winner unit c, which has the closest weight vector to an input vector $\boldsymbol{X}$, is determined. The set of joint angles $\vec{\theta}_c$ is given by

$$\vec{\theta}_c = \boldsymbol{u}_c + \boldsymbol{A}_c(\boldsymbol{X} - \boldsymbol{w}_c). \quad (1)$$

This algorithm is not always able to lead the end effector in small joint angle displacement, because of no consideration of motion planning from any initial posture. This algorithm learns the one to one relationships which are the sets of one end effector position to one set of joints angles.

3 Motion Planning Using TRN

The TRN is inspired from SOM. The essential difference between the SOM and the TRN is the defi-

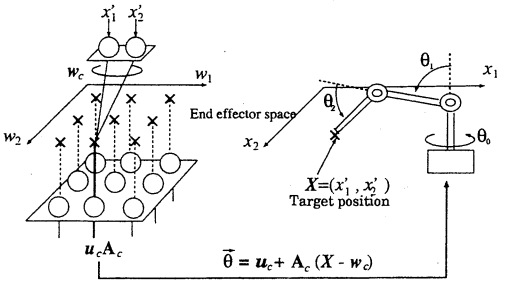


Figure 1: Structure of the SOM

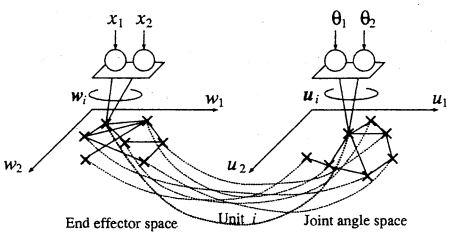


Figure 2: Structure of the TRN

nition of neighborhood. The TRN algorithm determines, in each learning step, neighborhood relationships which are given by unit's ranking which is determined by distance between input vectors $\boldsymbol{X}$ and weight vectors $\boldsymbol{w}_i$ as follows:

$$\|\boldsymbol{X} - \boldsymbol{w}_{i_0}\| \leq \|\boldsymbol{X} - \boldsymbol{w}_{i_1}\| \leq \cdots \leq \|\boldsymbol{X} - \boldsymbol{w}_{i_{N-1}}\|. \quad (2)$$

While adapting the weight vectors, the TRN configures neighborhood relationships by connecting close distance units with links or removing the links.

Motion planning using TRN learns a combined space which are end effector space and joint angle space. Thefore, this algorithm can lead the end effector in efficient joint angle displacement after learning. The input vector $\boldsymbol{I} = [\boldsymbol{X}, \boldsymbol{Y}]$, which is the combination of the end effector position $\boldsymbol{X}$ and the set of joint angles $\boldsymbol{Y}$, is applied for learning. The structure of the TRN is shown in Fig.2. In the TRN, each unit has the weight vector $\boldsymbol{W}_i = [\boldsymbol{w}_i, \boldsymbol{u}_i]$. The weight vector $\boldsymbol{w}_i$ corresponds to the target position $\boldsymbol{X}$. The weight vector $\boldsymbol{u}_i$ corresponds to the set of joint angles $\boldsymbol{Y}$. In the learning, the unit's ranking is determined by

$$\|\boldsymbol{I} - \boldsymbol{W}_{i_0}\| \leq \|\boldsymbol{I} - \boldsymbol{W}_{i_1}\| \leq \cdots \leq \|\boldsymbol{I} - \boldsymbol{W}_{i_{N-1}}\|. \quad (3)$$

After learning, the set of joint angles $\boldsymbol{u}_i$ leads to end effector to the position of $\boldsymbol{w}_i$. In the execution, this algorithm generates a path from any initial position to a target position to guide an end effector in the presence of obstacles within the workspace. This algorithm is not able to lead the end effector to target positions precisely. It is because this algorithm's purpose is just motion planning. This algorithm just leads the end effector to the goal unit which is obtained as the unit of the closest distance in end effector space. Therefore, this algorithm is not always able to lead from the initial end effector position to the target position in efficient joint angle displacement.

4 Proposed Algorithm

We propose a new algorithm to lead the end effector to any target position precisely in small joint displacement by using TRN. The fundamental idea is based on the combination of robot manipulator control using NGN and motion planning using TRN. The proposed algorithm uses the TRN, and each unit has the weight vectors $\boldsymbol{w}_i$, $\boldsymbol{u}_i$ and the weight matrix $\boldsymbol{A}_i$. The improvement points are two ideas. One is the way to calculate distances between the input vector $\boldsymbol{I} = [\boldsymbol{X}, \boldsymbol{Y}]$ and the weight vectors $\boldsymbol{W}_i = [\boldsymbol{w}_i, \boldsymbol{u}_i]$ in the learning algorithm. The other one is to consider subwinner units in order to determine an optimal winner unit in the execution algorithm.

4.1 Learning Algorithm

In the motion planning using TRN, dead-link might be created. If the end effector is led along a dead-link, the robot manipulator comes up against obstructions. Dead-link creation depends on the structures of the robot manipulator, the work space and obstructions. In order to avoid the dead-link creation, a new distance d_i between the input vector $\boldsymbol{I}$ and the weight vector $\boldsymbol{W}_i = [\boldsymbol{w}_i, \boldsymbol{u}_i]$ is proposed. It is calculated by

$$d_i = \mu\|\boldsymbol{X} - \boldsymbol{w}_i\| + (1 - \mu)\|\boldsymbol{Y} - \boldsymbol{u}_i\|, \quad (4)$$

where, μ is a constant ($0 \leq \mu \leq 1$) to determine the relative importance of the distances in end effector space and joint angle space. $\mu = 0$ causes the dead-link creation. It is because there are units which are not close in end effector space, even if the units are close in joint angle space to each other (Fig.3). On the other hand, during learning with $\mu = 1$, the dead-link creation can be constrained. However, there are some sets of joint angles which lead a same end effector position (Fig.4). Therefore, the weight vector $\boldsymbol{u}_i$ and the weight matrix $\boldsymbol{A}_i$ can not learn precisely. The value of the optimal parameter μ is determined to constrain dead-link creation and to lead end effector precisely.

The learning of the proposed algorithm can be illustrated as follows:

0. Follow initialization of the weight vectors $\boldsymbol{w}_i$ and $\boldsymbol{u}_i$, the weight matrices $\boldsymbol{A}_i$, and reset all links to unconnected $C_{ij} = 0$. C_{ij} is a link connection between unit i and unit j. $C_{ij} = 0$ means no link connection between the units.

1. Read in an input vector $\boldsymbol{I} = [\boldsymbol{X}, \boldsymbol{Y}]$.
2. Calculate the distances d_i for all units $i = 1...N$. The distances d_i are given by
$$d_i = \mu\|\boldsymbol{X} - \boldsymbol{w}_i\| + (1-\mu)\|\boldsymbol{Y} - \boldsymbol{u}_i\|. \quad (5)$$
μ is $0 \leq \mu \leq 1$.
3. Determine the orders of units according to
$$d_{i_0} \leq d_{i_1} \leq \cdots \leq d_{i_{N-1}}. \quad (6)$$
4. Update the weight vectors w_i for all units, $i = 1...N$.
$$\boldsymbol{w}_i^{\text{new}} = \boldsymbol{w}_i^{\text{old}} + \varepsilon(t)g(k_i)(\boldsymbol{X} - \boldsymbol{w}_i^{\text{old}}) \quad (7)$$
$\varepsilon(t)$ is the learning parameter, $g(k_i)$ is the ranking parameter, and t is current number of learning step. The values of the parameters $\varepsilon(t)$, $g(k_i)$ decrease with the number of performed learning iteration. Also, the value of the parameter $g(k_i)$ decreases to 0 from 1 as k_i which is ranking of unit i increases.
5. Update weight vectors $\boldsymbol{u}_i$ and the weight matrices $\boldsymbol{A}_i$ for all units, $i = 1...N$. The updating method of the weight matrix $\boldsymbol{A}_i$ is determined by the Widrow-Hoff method. The Widrow-Hoff method leads to decrease of the error $E(\boldsymbol{A}_i^{old}) = \frac{1}{2}(\boldsymbol{Y} - \boldsymbol{u}_i^{new} - \boldsymbol{A}_i^{old}(\boldsymbol{X} - \boldsymbol{w}_i^{new}))^2$.
$$\boldsymbol{u}_i^{\text{new}} = \boldsymbol{u}_i^{\text{old}} + \varepsilon(t)g(k_i)(\boldsymbol{Y} - \boldsymbol{u}_i^{\text{old}}) \quad (8)$$
$$\boldsymbol{A}_i^{\text{new}} = \boldsymbol{A}_i^{\text{old}} - \varepsilon(t)g(k_i)\frac{1}{\|\boldsymbol{X} - \boldsymbol{w}_i^{new}\|^2}\frac{\partial E}{\partial \boldsymbol{A}_i^{old}} \quad (9)$$
6. Update the link connection $C_{i_0 i_1}$ between units currently ranked at 0 and 1. Set $C_{i_0 i_1} = \|\boldsymbol{u}_{i_0} - \boldsymbol{u}_{i_1}\|$ which is a distance between the units in joint angle space, and set $l_{i_0 i_1} = 0$. The l_{ij} is the age of the link connection between the units i and j.
7. Increase the age $l_{i_0 j}$ of all link connections $C_{i_0 j}$ by setting $l_{i_0 j} = l_{i_0 j} + 1$ for all units j with $C_{i_0 j} > 0$.
8. Remove link connections $C_{i_0 j}$ which exceed a given lifetime $L(t)$ by setting $C_{i_0 j} = 0$ for all j with $C_{i_0 j} < 0$ and $l_{i_0 j} > L(t)$.
9. continue with step 1.

4.2 Execution Algorithm

It is not always proper to determine a winner unit just in end effector space. Therefore, our algorithm considers some sub-winner units which are close to target position in end effector space. Then, our algorithm determines the optimal winner which is the closet sub-winner unit to the initial position in joint angle space. The image of our algorithm is shown in Fig5. The execution of the proposed algorithm is able to be formulated as follows:

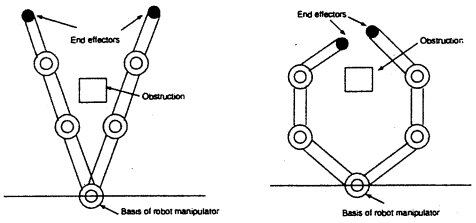


Figure 3: small joint angle displacement

Figure 4: end effectors

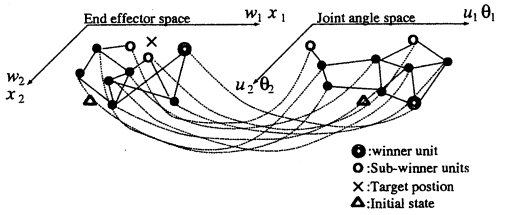


Figure 5: Execution algorithm

0. Determine a start unit r_0 according to the initial posture $\boldsymbol{Y}_p$.
$$\|\boldsymbol{Y}_p - \boldsymbol{u}_{r_0}\| \leq \|\boldsymbol{Y}_p - \boldsymbol{u}_i\| \quad (10)$$
1. Input a target $\boldsymbol{X}$.
2. Determine some units for sub-winner units from a unit which has close distance $\|\boldsymbol{X} - \boldsymbol{w}_i\|$.
3. Determine the shortest route from the start unit to the each sub-winner units using C_{ij} which means determine them in the joint angle space. In this paper, we apply the Dijkstra's shortest path algorithm.
4. Determine the winner unit r_{max} which is the shortest route of the sub-winners.
5. Output sets of joint angles $\vec{\theta}_r$ along units on the route $r = (r_0, r_1, \cdots, r_{max})$. The sets of joint angles $\vec{\theta}_r$ are given by
$$\vec{\theta}_r = \boldsymbol{u}_r + \boldsymbol{A}_r(\boldsymbol{X}'_r - \boldsymbol{w}_r). \quad (11)$$
$$\boldsymbol{X}'_r = \begin{cases} (\boldsymbol{X}_p + \boldsymbol{w}_r + \boldsymbol{w}_{r+1})/3 & , r = r_0 \\ (\boldsymbol{w}_{r-1} + \boldsymbol{w}_r + \boldsymbol{w}_{r+1})/3 & \\ & , r = r_1, \cdots, r_{max-1} \\ (\boldsymbol{w}_{r-1} + \boldsymbol{w}_r + \boldsymbol{X})/3 & , r = r_{max} \end{cases}$$
where, $\boldsymbol{X}_p$ is the initial end effector position.
6. Output a set of joint angles $\vec{\theta}$.
$$\vec{\theta} = \boldsymbol{u}_{r_{max}} + \boldsymbol{A}_{r_{max}}(\boldsymbol{X} - \boldsymbol{w}_{r_{max}}) \quad (12)$$

5 Simulation and Result

We present the result of a simulation involving the proposed algorithm. The number of units are $N = 300$. The maximum learning step is $T_{max} = 50000$. The parameters $\varepsilon(t)$, $g(k_i)$, and $L(t)$ are determined by $\varepsilon(t) = \varepsilon_i(\varepsilon_f/\varepsilon_i)^{t/T_{max}}$, $g(k_i) = exp(-k_i/\lambda(t))$, and

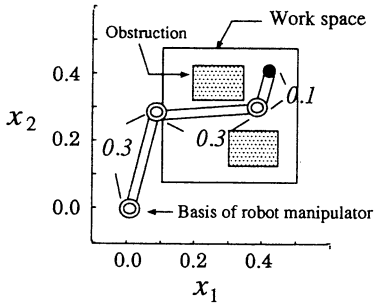


Figure 6: Robot manipulator and work space

$L(t) = L_i(L_f/L_i)^{t/T_{max}}$. The parameter $\lambda(t)$ is determined by $\lambda(t) = \lambda_i(\lambda_f/\lambda_i)^{t/T_{max}}$. The values are chosen as $\varepsilon_i = 1.0$, $\varepsilon_f = 0.05$, $\lambda_i = 270$, $\lambda_f = 1$, and $L_i = 5$, $L_f = 10$. We determine 6 sub-winner units in the execution. Obstructions are in the work space. The input spaces are two dimensions. The robot manipulator of the simulation has 3 degrees of freedom(DOF). During learning, the input vectors $\boldsymbol{I}$ are determined by random moving as follows:

1. Input a set of random value to the joint angles.
2. Apply the end effector position $\boldsymbol{X}_i$ and the set of joint angles $\boldsymbol{Y}_i$ to input vector $\boldsymbol{I}$, if the end effector is in workspace, and the robot manipulator does not touch the obstruction and itself.

During learning, 300 test input vectors are input every 100 learning iteration. The robot manipulator and the work space are shown in Fig.6. In this time we choose $\mu = 0.6$ because the result of learning is not created any dead-link and the position error is small.

The simulation results are shown in Fig.7. First, we input a target position as shown in Fig.7(a). Next, we input the target position which is the same position as the end effector of the initial state of Fig.7(a) as shown in Fig.7(j). This simulation shows that the proposed algorithm leads the end effector in small joint angle displacement avoiding the obstructions.

6 Conclusion

In this paper, we proposed the new algorithm to lead the end effector in small joint displacement by using TRN. The fundamental idea is based on the combination of robot manipulator control using SOM and motion planning using TRN. The novel features of the algorithm are the way to calculate the distances d_i and the sub-winner units.

References

[1] T. Kohonen, *Self-Organizing Maps*, Springer-Verlag, 1995.

[2] Helge Ritter, Thomas Martinetz, and Klaus Schulten, "Topology-Conserving Maps for Motor Control," *Neural Networks from Models to Applications N'EURO*,pp579-591,1989

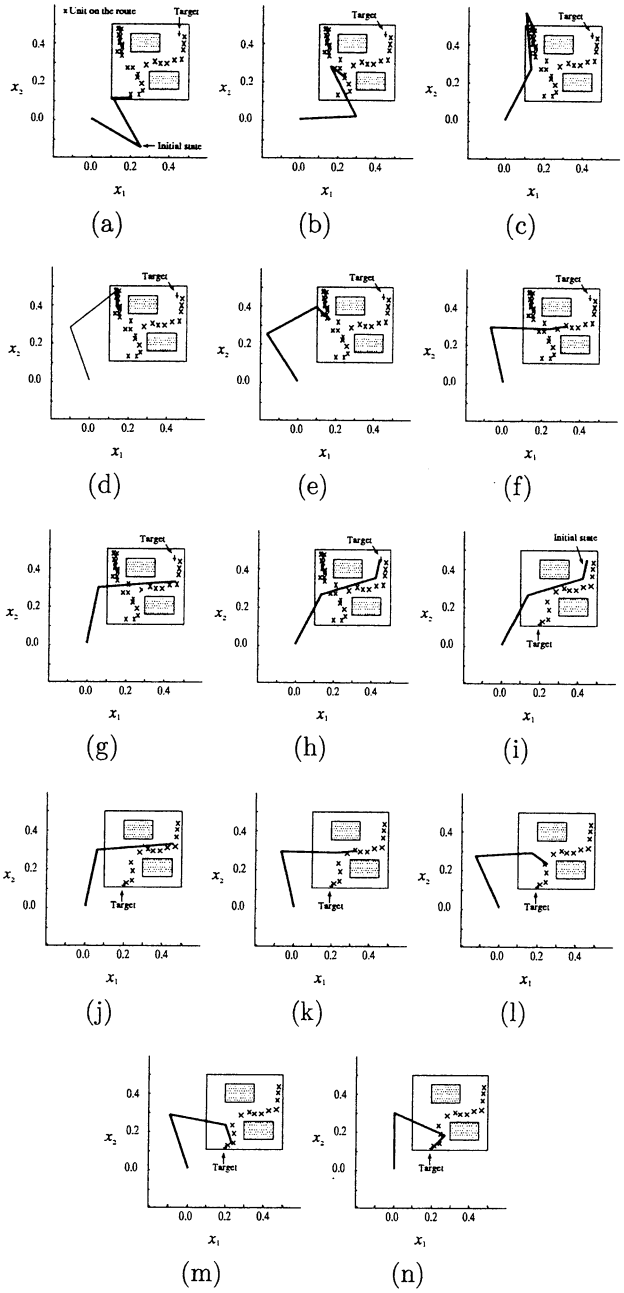


Figure 7: Result of simulation

[3] M. Zeller, K. Schulten, and R. Sharma, "Visuo-Based Robot Motion Planning Using A Topology Representing Network", *Proceeding of the IEEE Int. Symposium on Intelligent Control*, pp7-12, 1996.

[4] T. Martinetz and K. Schulten, "Topology Representing Network," *Neural Network*, vol.7, no.3, pp507-522, 1994.

Proc. of The Ninth Int. Symp. on Artificial Life and Robotics (AROB 9th '04)
Beppu, Oita, Japan, 28-30 January, 2004

Study on Computer Simulation System of Biological Modeling for Move-in-Mud Robot

Ren Fujun[1] Wang Dianjun[2] Zhang Lan[2] Meng Qingxin[2]

(1. Mechanical & Dynamic Engineering College
Harbin University of Science & Technology, Harbin,150080,China)
(2. Harbin Engineering University, Harbin, 150001,China)
E-MAIL:renfujun@tsinghua.org.cn; renfj@public.jm.hl.cn

Abstract: Under the guidance of using computer simulation to study the law of motion in biological modeling move-in-mud robot, some key problems appeared in the motion of biological modeling by means of OpenGL are studied based on the background of computer simulation. Taking general mathematical models, which are established by the authors for biological modeling robot, as simulation model, the authors have studied the motion process of move-in-mud robot when it works with computer simulation. A large number of graphically simulating programs with which the simulation of motion of robot cab be realized have been compiled and the results obtained are relatively ideal. This work can provide the foundation to the studies of dynamic simulation and the virtual model machine of biological modeling move-in-mud robot. Moreover, it can be beneficial to the design improvement of both the model machine and the practical machine of biological modeling move-in-mud robot based on creeping motion, to the application analysis of the robot, and to the study of other kinds of biological modeling robots as well.

Key Words: biological modeling move-in-mud robot; motion process; computer simulation; OpenGL

0 Introduction

The computer simulation system plays an important role during the development of modern robot technique. It is also an effective tool for the design and research of robot in computer simulation system. For example, computer simulation system of robot can provide reference material for the design of the real robot; it can help the researchers finding out the shape and limit of the area where the robot works; it can be used to analyze the validity and rationality of the track's and work's planning; and it can be used as an effective measure for offline programming technique [1~12].

Move-in-mud robot based on creeping motion is a new concept in biological modeling robot [9]. The main purpose is to use this kind of robot to do some serous underwater work such as refloating sunk ships, laying checking oil pipelines and communication optic cable and so on. This kind of biological modeling move-in-mud robot not only can substitute divers for drilling holes in refloating sunk ships in shallow waters but can do some work in deep waters where human beings can not stand. Therefore, the problems that divers must have drilled the holes for several decades in China can be solved thoroughly. Moreover, this kind of robot is of wide use in many fields such as military affairs, offshore mineral exploitation, scientific exploitation, and terrestrial holing and measuring without digging. In order to produce commercial robot as soon as possible, the authors put forward the subject to study the computer simulation system for move-in-mud robot based on creeping principle [9,12]. The combination of VC++6.0 and OpenGL1.2 in the simulation is discussed and the development of simulation system is demonstrated through a practical design of robot with OpenGL1.2 [12~16].

A new area of combining digital production with biological modeling robot is explored in this study. Some new manufacturing thoughts and concepts are promoted in the subject. The results obtained in the study are of significant importance and substantial application prospect [12].

1 A Brief Review on the Components of Biological Modeling Move-in-mud Robot and the Tools Used in the Development of Simulation System

1.1 Components of Biological Modeling Move-in-mud Robot

The principle model machine of biological modeling robot is composed of mechanical structure, compressed air drive device, sensor checking system and computer control system. The mechanical structure is composed of compact heads and creeping components. Some ripple pipes are placed outside each joint in the creeping components to prevent the mud from entering the robot. The component of biological modeling move-in-mud robot is shown in fig.1 [9,12].

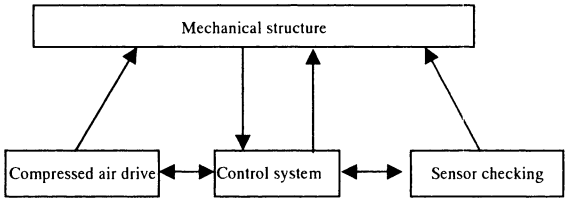


Fig.1 The frame of component of

1.2 The Tools Used in the Development of Simulation System

The OOP programming languages of and are selected as the developing tools in development of simulation system for biological modeling move-in-mud robot [12, 16].

Because of its advantages such as OOA, OOD and OOP, Visual C++ 6.0, which is one of the most popular 32-bit programming languages used in Windows 95, Windows 98and Windows NT operating systems, provides more effective method than traditional languages do in developing complex application programs.

The former version of OpenGL was IRIS GL developed by SGI Company for its graphic workstation, which was a industrial standard for the interface of three-dimensional graphic software. When drawing a picture, the OpenGL takes the following steps. First, it locates the coordinates of each acnode of an object through modeling and viewing transformation. Then, it treats all of the acnodes with projective transform. Finally, it maps these acnodes into view area. The flow chart of graphic treatment is shown in Fig. 2.

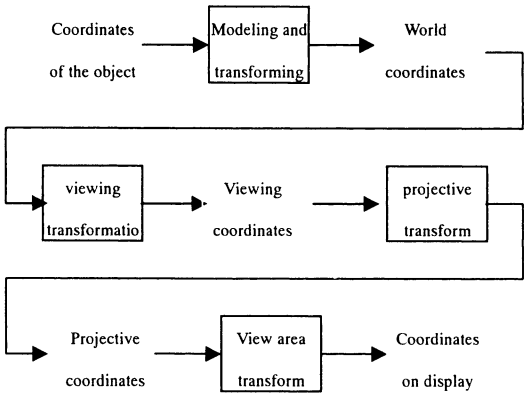


Fig.2 The flow chart of graphic treatment of OpenGL

2 The Realization of Computer Simulation for Biological modeling move-in-mud robot

The simulation system for biological modeling move-in-mud robot is mainly to carry out the simulation of working environment, real time motion, and so on.

This system is chiefly composed of modeling of three-dimension contour, mutual interface design of simulation system, moving track programming of the robot, romance of working environment and the realization of animation simulating. Fig.3 is the logical scheme of simulation system [12, 16].

2.1 Mutual interface design

The parameters of structure contour and motion of the robot must be input into the computer in order to study and produce the computer simulation system of biological modeling move-in-mud robot. And the parameters of motion speed, display proportion and working environment must be determined as well. Therefore, the computer simulation software has to be a graphic application program with mutual function [12~16].

The separate window in the simulation program is created with the class CsplitterWnd() in the MFC lib of VC++. The separated static window is separated vertically into two working areas (see Fig.4). The left window is a dialog box whose function is to display and receive input and output parameters, and to provide interfaces for input parameters and output real time data. The right window is a drawing window which responses the input messages and uses these messages to carry out computer simulation. Meanwhile, the data to describe the posture of biological modeling move-in-mud robot are

collected and returned into the documentary class. These real time data reflecting the posture of the robot provides the necessary materials for controlling the robot [12, 16]

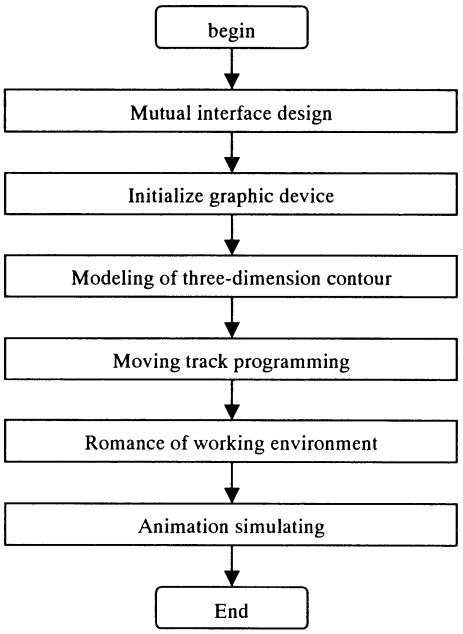


Fig.3. Logical scheme of simulation system

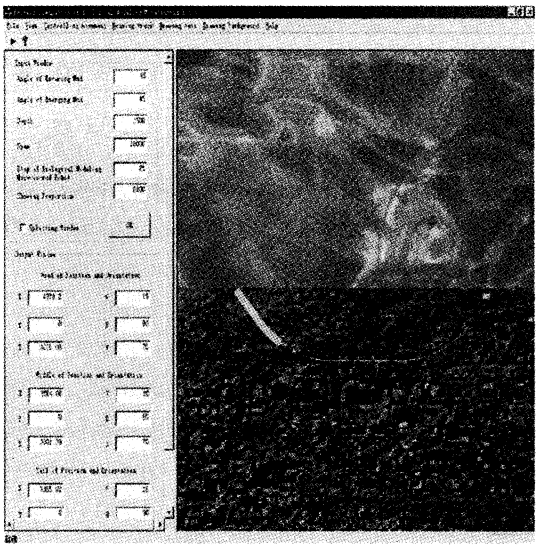


Fig.4. Display window of the simulation system

2.2 The Modeling of Three-dimensional Contour of Biological modeling move-in-mud robot

All geometric structures of complex object are composed of basic graphic elements such as point, lines and polygons. The Basic Lib and Practical Lib of OpenGL provide a large number of methods to draw various graphic elements and functions to describe complex three-dimension pictures. For example, they provide the methods of extension of graphic elements, calculation of normal direction, creation of curves, construction of curves and so on. These methods are very helpful in programming [12, 16].

The robot is composed of compact heads and creeping components. The modeling of three-dimensional contour of biological modeling move-in-mud robot can be completed by calling functions of OpenGL.

2.3 Moving Track Planning of Biological modeling move-in-mud robot

In practical application, the robot is required to move exactly on a series of given points. Thus, the motion track must be controlled for the robot. Because the forces acting on the robot are not concerned in the control of motion track, the control of motion track belongs to kinematics. The control of motion track can be divided into two types, offline and online. Offline control is that the motion track was calculated before the motion of the robot. Online control, however, is that the motion track is calculated during the moving process at real time [12].

The principle block diagram of offline control is shown in Fig.5. A table of motion track is calculated according to the ideal position and posture and current position and posture. And the kinematics transform is carried out according to the table.

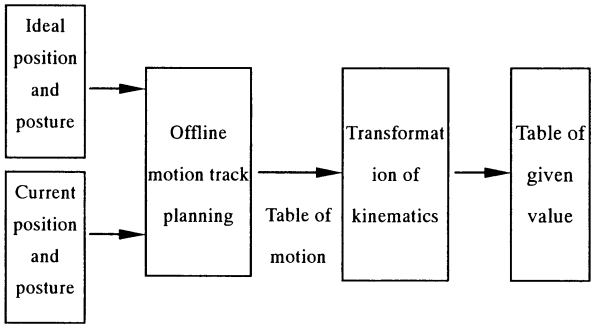


Fig.5 Principle block diagram of offline control

Based on the above concept, the ideal track for biological modeling move-in-mud robot is divided into three parts, which are entering the mud, moving along straight line and getting out of the mud respectively. If we input the entering angle, digging depth, digging length and getting out angle of the biological modeling move-in-mud robot in the input window, the ideal track can be calculated (see the white line in the drawing window in Fig. 4).

2.4 Romance of Working Environment of Biological modeling move-in-mud robot

In order to carried out the romance of biological

modeling move-in-mud robot's moving in mud, it is necessary to add the real background in the simulation. However, if we use OpenGL to simulate the real background, the work of programming will be extremely heavy and we cannot get the ideal results. To solve this problem, we can paste the image of a bitmap file (*.bmp) directly into the simulation graph of biological modeling move-in-mud robot. Because the bitmap files are very abundant and they can be pre-treated with software like Photoshop to get the optimal effect, selecting bitmap images as the background of biological modeling move-in-mud robot is an ideal resolution. We can select a bitmap file of mud and white its image message into the frame buffer of OpenGL. Then, through the graphic operation processes such as reading, zooming and writing, the screen romance effect of working environment can be realized. The romance speed is very high. The romance effect of the simulation system is shown in Fig.4 (see the right drawing window)

2.5 The Realization of Simulating Animation of Biological modeling move-in-mud robot

Double-buffering display, also called real time animation or page changing animation, is an ideal method to realize animation. In this method, the key technique is to reduce the drawing time on the drawing pages as much as possible in order to promote the animation effect. OpenGL provides a series of functions to realize double-buffering. The animation produced with this technique can be as smooth as normal movies. Double-buffering includes foreground buffer and backstage buffer. Only foreground buffer can be displayed at any time and the drawing routine can only renew the backstage buffer. To achieve an animation with smooth effect, a picture in the foreground buffer is usually displayed a certain time interval (say one thirtieth second), at the same time the drawing routine draws the next picture in the backstage buffer, and then the function is called to exchange the images in the two buffers and display the new picture on the screen. With this method, an animation effect is realized [12~16].

Some OpenGL classes are built and sealed to be used in the programming process. And the ideal moving track is scattered into coordinates of points. The three-dimensional geometric model of biological modeling move-in-mud robot is slipped and rotated from one point to the adjacent point to obtain the position and posture of the next time. An ideal animation effect can be obtained with the double-buffering method [12].

Fig.6 is the outline of simulation chart of biological modeling move-in-mud robot.

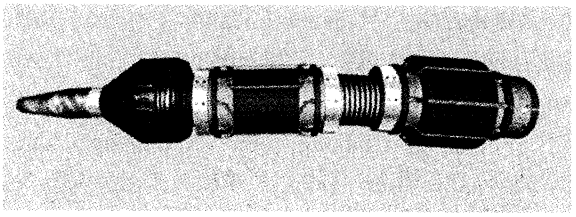


Fig.6 The outline of simulation chart of biological modeling move-in-mud robot

3 Conclusions

Currently, products of three-dimensional graphic software based on OpenGL, including shooting games running on windows, browsing of virtual scenery, simulation of motion, visualization of scientific calculation and CAD/CAM, are booming rapidly. OpenGL is a practical tool develop a high efficiency and low cost computer simulation system with high efficiency and low cost for biological modeling move-in-mud robot rapidly. By means of computer simulation for biological modeling move-in-mud robot, we can observe the moving state of the robot on the screen without its moving in practical environment. This can provide the foundation to the studies of dynamic simulation and the virtual model machine of biological modeling move-in-mud robot. Moreover, it can be beneficial to the design improvement of both the model machine and the practical machine of biological modeling move-in-mud robot based on creeping motion, to the application analysis of the robot, and to the study of other kinds of biological modeling robots as well.

Acknowledgements

The research was supported by China Nature Science Foundation. The authors would like to thank its supporting .

References

[1]Research on Experimentation of Model AUA Automatic Follow Pipeline under Water [J]. Robot

Technology and It's Application.2000(1):2 ～ 4(in Chinese)

[2]Yuan Youling. Do Best for Developing Chinese Robot Undertaking[J]. Robot Technology and It's Application.2000(1):5～10(in Chinese)

[3]Li Chengdong. Thinking about Chinese Robot Industry[J]. Robot Technology and It's Application.2000(4):2～6(in Chinese)

[4]Chen Jianping. Thinking about Developing Chinese Devices under Deep Water [J]. Robot Technology and It's Application.2001(2):33～36(in Chinese)

[5] Xin Jiancheng.The under Water Robots of American Navy In the Future[J]. Robot Technology and It's Application. 2000(3): 19～21(in Chinese)

[6] Yu Xong,Chen Jianping. Contrast and Analyses of Capability Some Robots under Water[J]. Robot Technology and It's Application.1997(1):18～20(in Chinese)

[7]Chen Jianping. Thinking about Problems of Chinese Devices under Water [J]. Robot Technology and It's Application..1999 (2):7～9

[8]Liu Junkao,Chen Zaili,Chen Weishan,Wang Ligang. New Model Thruster of Simulating Ship Fim under Water.ROBOT.2000(5):427～432

[9]Meng Qingxin,Wang Liquan.Study on Principle Projects of Move-In-Mud Robot Based Creeping Principle[J].CHINA SHIP BUILDING.2001(1)(in Chinese)

[10]Felipe M.G.Franca, Zhijun Yang, "Building Artificial CPGs with Asymmetric Hopfield Networks". Neural Networks,IEEE Conf. 2000(4): 290～295

[11]T.Sasaki,Y.hasegawa,K.Ozawa.Application of Self-propelled Devices to In-piping Inspection Technology[J].Robot.1998,51:98~103

[12]Ren Fujun.A Study on Computer Simulation of Move-in-Mud Robot Moving & Machining Non-sphere by Rotary Electrode EDM.The Work Report of Past Doctor of Harbin Engineering University.2001,9(in Chinese)

[13]Wang Xiaotong. Summarizing of Simulation And It's Application[J].Computer Engineering.1998（8）: 2022

[14]Peter C.Bell,Robert M.O'keefe.Visual Interactive Simulation-History,recent development,and major issues[J].Simulation.1987,49(3):109-112

[15]Wang Min. Design of Moving Painting Programs for Games[M].Beijing: XUEYUAN PRESS.1994

[16] OpenGL ARB.OpenGL Programming Guide:Version 1.2[M].Prentice Hall.1999

Proc. of The Ninth Int. Symp. on Artificial Life and Robotics (AROB 9th '04)
Beppu, Oita, Japan, 28-30 January, 2004

Autonomous Navigation Towards Intelligently Behaving Robots

Maki K. Habib
School of Engineering and Science, Monash University
Bandar Sunway, Selangor, Malaysia
maki@ieee.org

Abstract

Autonomous navigation of a mobile robot requires efficiently perceiving its local environment and links that to properly selected actions. To have intelligently behaving robot, an autonomous mobile robot must be able to learn and maintain models of their environments. Occupancy grids techniques provide a robust description of the local environment to support robot motion. There are several techniques used to build occupancy grids of an unknown environment using sensory information provided by a ring of ultrasonic range finders. Also, there are several sensor models are presented to handle uncertainty according to the selected building procedure. This paper is presenting a grid based navigation system that includes grid based mapping and obstacle avoidance approach using Histogram based techniques. The system has been implemented and demonstrated.

Keywords: Mobile Robot, Autonomous Navigation, Obstacle Avoidance, Geometrical, Topological, and Occupancy Grid

1 Introduction

The aims of research on mobile robots are to develop a control architecture that enables a mobile robot to move safely, function autonomously, intelligently, purposefully, and robustly through unstructured and dynamic world represents a fundamental milestone towards intelligently behaving robots. These features allow mobile robot to be used in a wide range of applications that are not possible with a high level of control by human interaction.

The most common and important problem for mobile robot localization and navigation is the creation or building of a map. Map building in an unknown dynamic environment has been under study for a long time and many different approaches have been evaluated [1-3, 10, 13, 14]. Other important issues related to navigation of an autonomous mobile robot are moving obstacles and the use of multiple sensors. Each of these leads to lack of knowledge of the environment, unpredictability and uncertainties that stems from sensory information, reliability and real time response. These issues usually cannot be resolved through the use of conventional navigation techniques. However, by modularizing the task of navigation and treating it as three different subtasks (robot localization, goal recognition, and path planning), some of the techniques in combination can be used to build a mobile robot system that can work in a dynamic indoor and outdoor environment.

Ultrasonic range finders are common in mobile robot navigation due to their simplicity of operation and high working speed. These sensors provide relative distances between them and surrounding obstacles located within their radiation cone. However, these devices are prone to several measuring errors due to various phenomena, such as, multiple reflections, wide radiation cone, and low angular resolution.

Toward intelligently behaving robot and to carry out efficiently a complex task, autonomous mobile robots must be able to acquire and maintain models of their environments. The task of acquiring models is difficult and far from being solved [1, 6, 8, 10]. There are many factors impose practical limitations on a robot's ability to learn and use accurate models, some of there are:

a. Available sensors often are not capable of directly measuring the quantity of interest,
b. The perceptual range of most sensors is limited to a small range around the robot that makes acquiring global information a difficult task,
c. Sensor measurements are typically corrupted by noise and often, the distribution of this noise is unknown,
d. Robot motion is inaccurate due to drift and slippage,
e. Complexity and dynamics of robot environment, and
f. Real time requirements demands to have a model that is easy to access and maintain.

2 Maps for Indoor Mobile Robot Navigation

While it is possible for a robot to be mobile and not do mapping for navigational purpose, sophisticated tasks require that a mobile robot build maps dynamically or having proper knowledge representation about robot's environment along with efficient way to integrate and use them to move around without any priori knowledge about the environment.

Map building and learning is a crucial issue in autonomous mobile robot navigation, where robots must

acquire appropriate models of their environment from their actual sensory perceptions and interaction with the real world. Generally there are two main approaches to generate such purposeful maps. These are the geometrical and topological approaches. The Topological approach is a qualitative one and less sensitive to sensor errors. The topological model consists of a graph where nodes in such graphs represent perceptually distinct situations, places or landmarks. They are connected by arcs to indicate the spatial relations between them, i.e. the existence of a direct path between them. Such models involve more compact representations and allow fast planning. However, it relies heavily on the existence of recognizable landmarks [7-9]. Topological maps can be used much more efficiently, yet accurate and consistent topological maps are considerably difficult to learn in large-scale environments. Since sensory input depends strongly on the viewpoint of the robot, topological approaches may fail to recognize geometrically nearby places. The key advantage of topological representation is their compactness. The resolution of topological maps corresponds directly to the complexity of the environment. The compactness of topological representations gives them three key advantages over grid-based approaches: they permit fast planning; they facilitate interfacing to symbolic planners and problem-solvers; and they provide natural interfaces for human instructions. Since topological approaches usually do not require the exact determination of the geometric position of the robot, they often recover better from drift and slippage that must constantly be monitored and compensated in grid-based approaches.

In the geometrical approach, the map quantitatively reproduces the metric a spatial features of the environment. The metric map is a grid based with each cell of the grid representing some amount of space in the real world. Sensors are then used to detect obstacles. The acquired sensory data are used to determine the occupancy value of each grid space so that a map can be generated. While grid-based methods produce accurate metric maps, their complexity often prohibits efficient planning and problem solving in large-scale indoor environments. The advantage of metric maps is its high resolution. On the downside, it is slow, not expressive and also the local minima problem. On the other hand, grid-based approaches suffer from their enormous space and time complexity. This is because the resolution of a grid must be fine enough to capture every important detail of the world [7-10].

There are different uncertainty calculi techniques to build occupancy grids of an unknown environment using sensory information provided by a ring of ultrasonic range finders. These techniques are based on Bayesian theory, Dempster–Shafer theory of evidence, fuzzy set theory, and the Histogrammic In-Motion Mapping (HIMM) method [1, 11]. Each of these methods has its own approach in transforming sensor readings into the representation of uncertainty and the update rule for combining the uncertainty for a pair of observation. It has been recognized that De mpster-Shafer method provides an accurate map compared to HIMM. However, the computational time required by HIMM method is significantly less than that required by Bayesian and Depmpster-Shafer methods.

A representation used for modeling the physical attributes of the environment and the entities present in it must possess certain qualities. It must be powerful enough to express all the entities that need to be represented. At the same time, it must be adaptive in those only entities that affect the navigation algorithm at any given stage need to be represented during that stage. Also, the characteristics of any representation must be able to quickly update its knowledge about the current state of the environment without too much computation effort [14].

3 The Generation of the Grid Map

The traditional paradigm to recover spatial information is based on the use of a two-dimensional tessellation called occupancy grids or certainty grids that were first introduced by Moravec and Elfes [5, 12] as a way to construct an internal representation of static environments by evenly spaced grids based on ultrasonic range measurements. The grids allow the efficient accumulation of small amounts of information from individual sensor readings for increasingly accurate maps of the robot's surroundings. The incoming sensor range data is interpreted using probabilistic sensor models. This method is basically a data structure to store data acquired from different sources and takes into account the uncertainty of sensory data by working with probabilities or certainty values. The resulting probabilistic spatial models obtained from these sensor models serve as maps of the robot's environment, and can be used directly for robot navigation tasks such as path planning and obstacle avoidance, position estimation, and also to incorporate the motion uncertainty into the mapping process. It provides a way of representing data to be later extracted as useful and informative maps that can be used directly in robotic planning and navigation [5]. The data structure represents, for each point in the environment, the probability that some object occupies the point. In principle, uncertainty grip store qualitative information about which areas of the robot's surroundings are (completely) empty, and which areas are (even partially) occupied by obstacles. Besides, no other characterization of the environment is of interest.

The occupancy grids considered in this paper is a discrete state stochastic process defined over a set of continuous spatial coordinates. An Occupancy grid is a multi-dimensional typically 2D or 3D tessellation of space into cells, where each cell in a map stores a probabilistic estimate of its state. This state is determined based on sensor readings. In the Occupancy grid, the state variable associated with a cell is defined as a discrete random variable with two states: occupied and empty. More specifically, it contains the belief whether or not the center of the robot can be moved to the center of that cell. These two states are mutually exclusive and exhaustive. The map of robot's environment has been constricted using the Histogrammic In-Motion Mapping (HIMM) approach [3] in which the environment is represented by 2D histogram grid. The size of each cell is 10x10 cm and each cell has its own coordinate and holds a certainty value with range from 0 to 15 to represent the confidence of the algorithm in the existence of an obstacle.

The work has been implemented and integrated with simulated environment and a cylindrical mobile robot simulator (15 cm in radius) equipped with 24 ultrasonic sensors equally spaced and arranged in a ring around the robot circumferences. Sensor position is determined relative to robot position and orientation. Sensor readings are mapped to occupancy values. The update rule for HIMM method consists two steps. It starts by having the certainty values of all cells assigned to zero. Then, sensor readings are mapped to occupancy values. The only cells that have to be updates are that lies along the sonar acoustic axis and at the radial distance within the view of the sensor. The certainty values of the cells that lie on the radial distance are update by adding 3 to it and the other cells that lie along the acoustic axis and don't correspond to the range reading its certainty values is decremented by 1. To achieve a fast construction of the map a 3x3 mask is summation of the used. The center of the mask is fitted directly over the incremented cell that corresponds to the range reading. The update of the cell will equal to the summation of the multiplication between each cell of the mask and its corresponding grid cell. Any certainty values exceeding 15 is ceil back to 15. Multiple sensor interpretations are integrated over time, to yield a combined estimate of occupancy value. Also, constantly track and update of position and orientation of the robot using odometry and map information and errors are corrected accordingly

4 Real Time Obstacle Avoidance and Grid Map Representation

The Vector Field Histogram approach [2] that is based on occupancy grid concept has been further developed for real time mobile robot obstacle avoidance [3]. The extended approach offers smoother robot trajectories and better reliability. The approach has been implemented with the obstacle avoidance algorithm. It uses the 2D histogram grid representing robot's environment. It employs a four-stage data reduction process to compute the new direction of motion. In the first three stages, the two-dimensional map grid is reduced to one-dimensional polar histograms that are constructed around the robot's momentary location. In the fourth stage, the algorithm selects the most suitable direction based on the masked polar histogram and a cost function.

The first data reduction stage maps the active region of the map grid onto the primary polar histogram. The active region is a circular window of a certain diameter that moves with the robot. The active region is divided into 72 sectors of 5 degree and every cell within each sector is treated as obstacle vector. The histogram is built around the current robot position independent of its orientation. The result of this process is a polar histogram that takes into account the width of the robot. Then, a binary polar histogram is built based on the previous stage. Two thresholds are used to identify sectors of the binary polar histograms whether it is free or blocked and if it is free whether it is with wide opening or narrow opening. The threshold values are determined experimentally. After all possible candidate direction is determined a cost function is used to select the most appropriate candidate as new direction for the robot. Then, the final stage is done through a masked polar histogram to enable the robot to achieve a desired target through simultaneous translation and rotation. The navigation system continuously reads sensory input and writing motor commands at regular intervals. The sensory input comprises the readings of the ultrasonic and odometry sensors. The motor commands govern information about the environment that is stored in the internal map.

Histogram grids suffer from stability problems due to their discrete nature [2]. When a robot changes cell, quantities tied to its position such as, discretised distances and speeds change abruptly and this demand for the necessity for high resolution, i.e., small cell size. Also, it will require filtering techniques. The grid discreteness also raises the critical need for efficient geometric transforms in terms of rotation and translation. A local grid is usually centered on the robot and must move with it. This involves expensive interpolation methods or advanced mathematical analysis. This is computationally heavy and is a well-known shortcoming of grid techniques [7]. These shortcomings disappear when two usual assumptions are removed. The first is that the robot should be perfectly centered on the grid. The second assumption second is that the grid should be seen as a discretisation of the space.

Due to the limitations associated with Grid and Topological based mapping, it is necessary to find way to efficiently integrate both paradigms, On top of the grid representation, more compact topological maps can be generated by splitting the metric map into coherent regions, separated through critical lines. Critical lines correspond to narrow passages such as doorways. By partitioning the metric map into a small number of regions, the number of topological entities is several orders of magnitude smaller than the number of cells in the grid representation. Therefore, the integration of both representations has unique advantages that cannot be found for either approach in isolation [10].

5 Conclusion

The paper presented a grid based navigation techniques that utilize HIMM and the extended Vector Field Histogram (VFH+). Through the integrated implementation the modeled robot was able to map the environment, avoid obstacles and move towards its target. As for future expansion, it is important to consider a technique that will help to deal with dynamic size of robot's environment map without imposing size or shape constraints on the grid map. The area of the environment may not be rectangular in structure and it can be grown, as the robot is moving through its surrounding environment.

References

[1] R.R. Murphy, " Introduction to AI Robotics", The MIT Press, Massachusetts Institute of Technology, MA-USA, 2000.

[2] J. Borenstien and Y. Koren, "Histogrammic In-Motion Mapping for Mobile Robot Obstacle Avoidance", IEEE Transaction on Robotics and Automation, Vol. 7, No. 4, pp. 535-539, 1991.

[3] J. Borenstien and I. Ulrich, "VFH+: Reliable Obstacle Avoidance for Fast Mobile Robots", IEEE International Conference on Robotics and Automation (ICRA'98), Leuven-Belgium, pp. 1572-1577, 1998.

[4] A. Elfes, "Using Occupancy Grids for Mobile Robot Perception and Navigation", Computer Magazine, pp. 46-57, June 1989.

[5] H. P. Moravec, "Sensor Fusion in Certainty Grids for Mobile Robots", AI Magazine, 9, pp. 61-74, Summer, 1988.

[6] H. R. Evertt, "Sensors for Mobile Robots: Theory and Application", AK Peters Ltd, 1995.

[7] E. Dedieu and J. dR Millan, "Efficient Occupancy Grids for Variable Resolutions Map Building",

[8] B. J. Kuipers and Y. T. Byun, "A Robot Exploration and Mapping Strategy Based on a Semantic Hierarchy of Spatial Representations, Robotics and Autonomous Systems, 8, pp. 47-63, 1991.

[9] S. P. Engelson and D. V. McDermott, "Error Correction in Mobile Robot Map Learning", IEEE International Conference on Robotics and Automation (ICRA'92), pp. 2555-2560, 1992.

[10] S. Thrun and A. Bucken. "Learning maps for indoor mobile robot navigation", Technical Report CMU-CS-96-121, Carnegie Mellon University, School of Computer Science, Pittsburgh, PA 15213, 1996.

[11] M. Ribo and A. Pinz, "A comparison of three uncertainty calculi for building sonar-based occupancy grids", The Journal of Robotics and Autonomous Systems 35, pp. 201-209, 2001.

[12] J. Moravec and A. Elfes, "High resolution maps from wide angle sonar", IEEE International Conference On Robotics and Automation, 116-121, 1985.

[13] B. K. Ellore, "Dynamically Expanding Occupancy Grids", M. Sc. Thesis, Computer Science, Texas Technical University, 2002.

[14] A. Singhal, "Issues in Autonomous Mobile Robot Navigation", Report, Computer Science Department, University of Rochester, 1997.

Proc. of The Ninth Int. Symp. on Artificial Life and Robotics (AROB 9th '04)
Beppu, Oita, Japan, 28-30 January, 2004

Speed Control of a Stepping Motor of the Electric Vehicle Based on Speed Parameters Estimation via PWM Inverter

Masanori SUGISAKA, MBAITIGA- Zacharie
Dept. of Electrical & Electronic Engineering, faculty
of Engineering,700 Dannoharu, 870-1192 ,Oita University

Abstract

Electric vehicles may be one of the main future transportation for the next generation due to their low-pollution and high efficiency. Reviewing the papers in the literature we can see that the best engine equipment is stepping motor. Its design results in lower rotor inertias; higher rotor speed and higher motor supply voltage compared to conventional dc motors. Its high reliability and robust make it suitable for EV applications. Many papers have discussed the control strategy of stepping motor in the open literature. This paper proposed a novel speed control of stepping motor of the electric vehicle based on speed parameters estimation (SPE) and investigate its variation with pwm. The basic concept is first to estimate and set the four SPE by monitoring computer to the motor through motor controller PCI-7208 card, the speed control system which acts like a bridge between the motor and PC. The second steps consist of increasing gradually the number of the acceleration pulse each time by 10 to know how many steps to make from current position. The main objective is to obtain the acceleration pedal position that gives a medium speed in a reasonable time for future automatic driving of the EV. A Comprehensive analysis of the motor design and control algorithm as well as the result is described.

Key words: electric vehicle, acceleration pedal, speed parameters estimation, stepping motor.

1. Introduction

As environment problems have become an increasing global concern due to pollution, automobile manufacturers are now actively studying possibilities of electric vehicles for widespread for future generation transportation [1]. This includes the type of the motor to be used. For driving motors, induction motors are being studied which have a solid structure and can be small sized when designed as high-speed motors [2]]. But this cause a new problem; the cores easily saturated when primary currents flowing in the winding are increased, because the primary and secondary iron core size for motor must be smaller. This leads to difficulties in accurate and stable torque control of the motor [3]. The conventional dc motors, which are very popular due to their reasonable price and easy to control, are also being studied. The main drawback is the mechanical collector, which has only a limited lifespan. In addition brush sparking can destroy the rotor coil, generate EMC problems, and reduce the insulation to an unacceptable limit. That why stepping motors are now widely used in constant speed drives at line frequency as well as in variable speed drives with inverter-fed frequency supplies [4]. The main advantages as compared with conventional dc motors are the absence of rotor slip power loss and the natural ability to supply reactive current. Its high reliability, higher rotor speed, and robust make it suitable for EV as well as in industry. Reviewing the previous research and papers many control method have been proposed [5, 6]. In [5] the paper presents the speed and position sensorless control of permanent magnet (PM) brushless dc motor, with a sinusoidal flux distribution. Two approaches were proposed and compared with each other; one is based on the voltage model of the motor and other is based on the current model. In spite of the comparison, the starting procedure is very difficult problem under sensorless drive, because the sensorless drives uses both voltage and current for estimation of the rotor position and no information is available before starting. This paper presents the speed control of a stepping motor based on speed parameters estimation (SPE) of the EV via pwm-inverter. Two different steps of approaching the control are presented. The fist step is to estimate and set the SPE; the second step is to increase gradually the number of acceleration pulse each time by 10 to know how many steps to make from current position. A Comprehensive analysis of the motor design and control algorithm as well as the results is described.

2. Stepper Motor Design

The Stepper motor consider here is a variable speed polyphase permanent magnet synchronous with sinusoidal flux distribution fed from current source inverter. This flux distribution excites the three windings so the motor drive can start from standstill. The permanent magnet creates the rotor flux and the stator windings create electromagnetic poles. The rotor is attracted by the energized stators phase generating a

rotation. By using an appropriate sequence to supply the stator phases, a rotating field on the stator is creates and rotor rotates. Due to the construction of the steeper dc motor, the motor power losses are almost entirely in the stationary stator hence, heat can be easily transferred to the atmosphere. This is becoming increasingly in variable speed and constant speed applications since it can produce a torque speed characteristic similar to PM dc motor, while avoiding the problems of failure of brush and mechanical commutation. Basic voltage current relations according to [3] and [4] can be given as follows:

$$\begin{bmatrix} V_a \\ V_b \\ V_c \end{bmatrix} = \begin{bmatrix} R_s & 0 & 0 \\ 0 & R_s & 0 \\ 0 & 0 & R_s \end{bmatrix} \begin{bmatrix} i_a \\ i_b \\ i_c \end{bmatrix} + s \begin{bmatrix} L & M & M \\ M & L & M \\ M & M & L \end{bmatrix} \begin{bmatrix} i_a \\ i_b \\ i_c \end{bmatrix} \quad (1)$$

Where

R_s is the winding resistance per phase
L is the self induction per phase
L_s is the equivalent self-induction per phase
M is the mutual induction between phases
e is the EMF per phase
V is voltage per phase
ω_r is the rotor electrical speed
ω_m is the rotor mechanical speed
p is the number of poles of the motor

Due to symmetry in isolate neutral configuration of the motor windings of the motor,

$$i_a + i_b + i_c = 0 \quad (2)$$

Hence

$$M_{ib} + M_{ic} = - M_{ia} \quad (3)$$

Using equation (2) and (3) in (1), the model equation can be reduce to the following state form.

$$\begin{bmatrix} \frac{di_a}{dt} \\ \frac{di_b}{dt} \\ \frac{di_c}{dt} \end{bmatrix} = \begin{bmatrix} -\frac{R_s}{L_s} & 0 & 0 \\ 0 & -\frac{R_s}{L_s} & 0 \\ 0 & 0 & -\frac{R_s}{I} \end{bmatrix} \begin{bmatrix} i_a \\ i_b \\ i_c \end{bmatrix} + \begin{bmatrix} \frac{1}{L_s} & 0 & 0 \\ 0 & \frac{1}{L_s} & 0 \\ 0 & 0 & \frac{1}{I} \end{bmatrix} \begin{bmatrix} V_a \\ V_b \\ V_c \end{bmatrix} \quad (4)$$

Where

$$L_S = L - M \quad (5)$$

3. Inverter fed frequency supply

There are two types of inverter, the voltage-source inverter (VSI) and the current-source inverter (CSI). In the voltage source inverter, the DC input appears as a DC voltage source ideally to the inverter. Whereas for the current-source inverter, the DC input appears as a DC current source ideally to the inverter. The VSI has a fast response, power-conditioning ability, and superior variable speed performance than CSI. The Fig.1 shows the closed loop speed control system of the stepper motor fed by the VS Inverter. As in many phase motor applications, the inverter here too acts like an electronic commutator. It receives PWM switching signals from the drive circuit behind, based on the converted current feedbacks of Hall sensors and the position of the encoder. In the torque mode operation, current reference signal (I_{ref}) is the external input to the closed loop system formed by the decoder, PWM generator and hysteresis comparator which is used generally to impose a dead-band from the reference current There are three Hall sensors placed on the startor of the stepper motor that give $120°$ phase shifted square waves in phase with respective phase voltages. These waves represent the rotor position

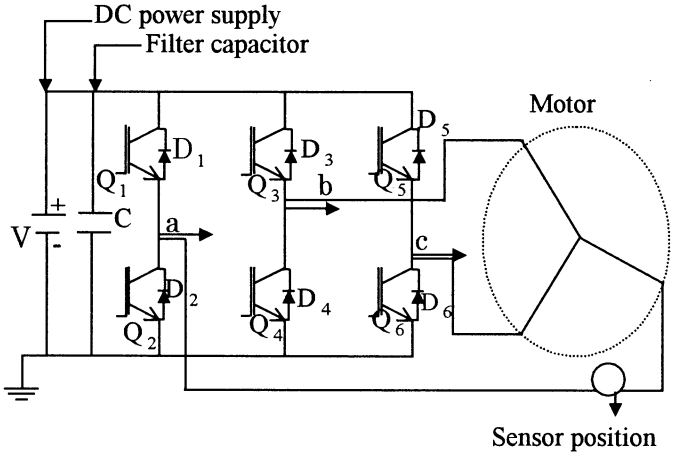


Fig.1 Inverter fed stepping motor

4. Experimental system

The considered Stepper motor with a rotary encoder E6C2-WZ6C for position feedback has a mechanical power of 5.2kw at a rated speed of 6000 rpm the maximum permissible revolution and it can be synchronized at high frequency. The CPU Pentium Celeron II 466 MHz performs the control process of the stepping motor connected to the controller PCI-7208 without having direct access to the Stepper motor. Fig.2 shows the control block diagram. A 24 V DC battery is used as a power supply for to the motor, whose DC/AC converter is connected to computer and battery in order

to convert a 24V DC to 100V AC for running the computer. The vehicle operation consists of four main segments. The initial acceleration (starting form low speed), which force takes the vehicle from the standstill to its rated velocity v_e in some specified time tf seconds, cruising at vehicle rated speed, where the motor provides the necessary propulsion force at rated vehicle speed, cruising at maximum speed and deceleration as shown is Fig.3. Where $V_{\min}$, V_{Acc}, $V_{\max}$, V_{Dec} denotes the four segments define above respectively. A drivetrain capable of meeting these constraints will function adequately in the other regimes but this is beyond the scope of this paper. The objective here is to meet these constraints for self-control of the EV. To this end, the position and speed parameters presented in Table.1 are estimated in the range of the PWM frequency operating performance.

Table.1 Speed Parameter Estimation

dwLowSpeed	100 Hz
dwSpeed	1000 Hz
dwAcc	500 msec
DwDec	500 msec
dwSSpeed	300 Hz
Base Clock	50 Hz
tmp	60 Hz
iPos	Initial position
nStep	tmp-iPos

Where, dwLowspeed is the starting pulse speed, dwSpeed is the maximum pulse speed; dwAcc and dwDec are the number of milliseconds over which the acceleration and deceleration take place respectively.
tmp is where we want the acceleration pedal to be, iPos is where the acceleration pedal is. As the motor is driven by the sine function acceleration profile MTR_ACC_SIN, the break speed for sinusoidal acceleration profile dwSSpeed along with a base clock frequency of 50Hz, for getting the current base clock tick interval of the pulse speed is used to support the estimated speed parameters in order to avoid the failure of the motion. The use of sinusoidal acceleration profile can be explained by two reasons. First it sets the acceleration (speed step) to be used for the motion profile. And second it allow the calculation for new speed = current speed +(speed step*time step). If it is not set the default value is 0 and the new speed will not produce a change from initial speed of 0. With reference to equation (3) and equation (3) the back EMF is directly proportional to the motor speed, and the developed torque is almost directly proportional to the phase current. So to kwon how many steps to make from the current position, the

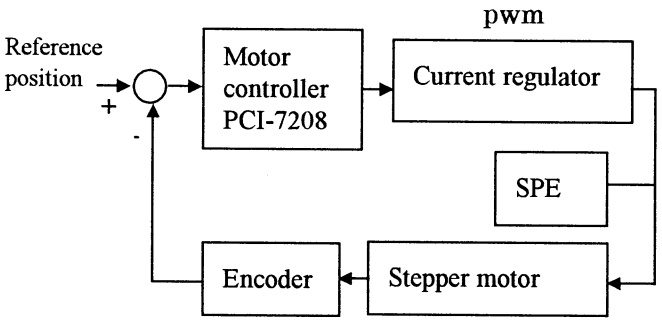


Fig.2 Control block diagram of the speed

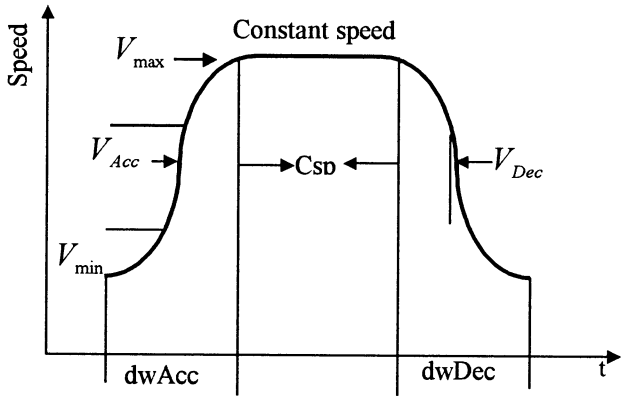


Fig.3 Expected speed form

expected acceleration pedal position (tmp) is subtracted from the initial acceleration pedal position (iPos) as the speed of the vehicle depends on the position of the acceleration. The speed specified in the MTRMOTION (motor motion) refers to the speed at which the motor that is controlling the acceleration will move. The specification of the motion profile that the motor have to follow after the current position have been made was done by using the preset position function (MTR_TPT (0x02)). This is to give a positional move to the direction and distance. The current position is detected by the current sensor of a stepper motor and the voltage are obtained by using the information on the PWM but not by calculation [2]. The phase current is produced by voltage quasi-static state. In order to keep smooth rotation and the constant developed torque the condition of V/f = constant have been verified and satisfied. The control software is code in MFC/C++ language.

5. Experimental results.

The proposed speed parameter estimation was carried out using a stepping motor CSK543AP-T20. Fig.4 shows the speed variation under that control algorithm. During the running test, the motor starts and quickly reaches 350

rpm and gains its maximum speed of approximately 430 rpm at around 40 seconds, then stabilized for a while before decelerating toward zero.

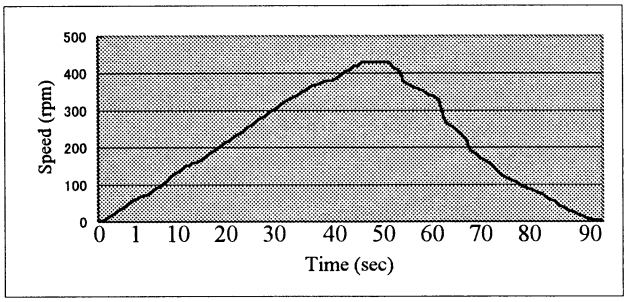


Fig.4 Speed variation versus time

This motor speed responds to the expected speed illustrated earlier in Fig.3 and agrees with the four constraints of vehicle operation on that Figure.

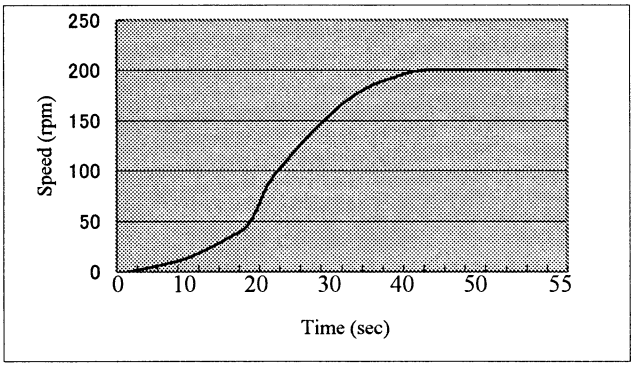


Fig.5 Speed with accelaration pedal position 50 pulse steps

Fig.5 and Fig.6 show two different types speed response for two acceleration pedal position tmp (see Table.1).

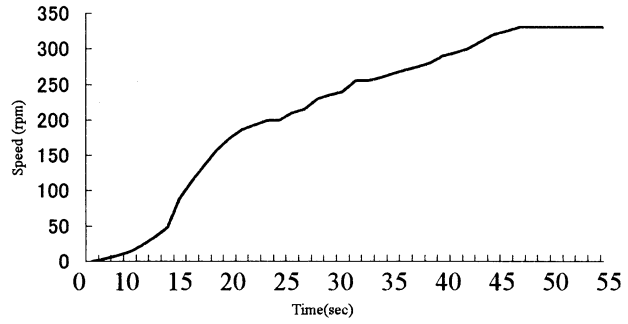


Fig.6 Speed with accelaration pedal position 60 pulse

It explain how the motor speed depends on the position of the acceleration pedal. , and the state of the road. This pedal is controlled by the position of the stepper motor. in Fig.5 tmp was set to 50 pulse and in Fig.6 it was set to 60 pulses.

6. Conclusion

In this paper, the speed control of the electric vehicle based on speed parameter estimation have been proposed. This control algorithm shows , the the speed of the motor depends on on the acceleration pedal position, which is controlled by the position of the stepper motor. this position is controlled by the program, with tapezoidal/sinusoidal motion profile. The control operation is done via mouse and a satisfactory results have been found.

References

[1] H. Yamamura, R. Masaki, o.Koizumi ,K Noi and S.naito,"Developpment of power system for Nissan Fev" in 11th electric-vehicle symposium, Florence, Italy 1992 vol.2 n.1303

[2] S Naito, N.Mutoh, T.Takagi, and Y.Kouchi," AC drive system for electric vehicle Hitachi hyoron, vol.77 n.2 pp 33-38 (1995)

[3] Y.Kimura, T.Sekimori, and N.Takagi" Development of the practical electric vehicle in 93 Symposium Environmental Eng. Japan society mechanical.

[4] Nobuyoshi Matsui, Satoru Keneko, Taizou Miyazaki Ryosu masaki and sanshi obara," A torque control suitable for electric vehicle," IEEE Transaction on Industrial Electronics vol.44 n.1 pp 54-63 april 97

[5] Nobuyoshi Matsui, "sensorless PM brush less dc motor drives, "IEEE Transaction on Industrial Electronics vol. 43 n.2 pp 300-308 (1996)

[6] CC. Chan, K.T chan, J.Z Jiang, W.Xia, Meiling Zhu, and Ruoji Zhang," Novel permenet magnet motor drives for electric vehicles," IEEE, Transaction Transaction on Industrial Electronics vol. 43 n.2 pp 331-338 (1996)

[7] Masanori Sugisaka and Xin Wang, Ju-Jung Lee, " In-telligent control strategies for mobile vehicle", Applied mathematics and computation 91/98 (1998)

[8] G.Fathala and M. Farsi. "Modeling and control of a brushlessDC motor using RBF neural network ", proceedings of the International Conference on Intelligent, Robot and Systems, IEEE/RSJ, 248/251(1999)

[9] Ch. S Kim and H Lee "Fuzzy logic control of robot manipulation on visual servoing." Proceedings of the 2000 International Sympotium on Mechatronics and Intelligent Mechanical System for 21century", ISIM 396/395 (2000)

[10] Bouzouia, M. Kadri "experimental neural decomposed dynamic adaptive control of robot manipulator", Proceedings of the International Conference on Intelligent Robots and System, IEEE/RSJ volume.1

Proc. of The Ninth Int. Symp. on Artificial Life and Robotics (AROB 9th '04)
Beppu, Oita, Japan, 28-30 January, 2004

A ROBUST ADAPTIVE DIRECT CONTROLLER FOR NON-LINEAR FIRST ORDER SYSTEMS

Manh-Minh NGUYEN, *Hoang Minh JSC, Hanoi*
Van-Long NGUYEN, Thi-Tam NGUYEN,
Van-Cuong PHAM, Thi-Thu-Huong DO,
Thi-Hien NGUYEN, *Hoa Ban Co., Ltd, Hanoi*

Hong-Bich NGUYEN, Thi-Kim-Hoa NGUYEN,
The-Vu LE, Quoc-Sinh NGUYEN
Phu Bao, Co., Ltd., Hanoi, Vietnam
nguyenmanhminh2003@yahoo.com

Abstract

This paper presents new results on designing a robust adaptive direct controller for a class of non-linear first order systems. The designing method based on the use of dead zone in the parameters' update law. It is shown that the size of the dead zone does not depend on the upper bounds of the disturbances. That means that even if the bounds are large, the tracking error will always converge to a set of the dead zone size. However, in the ideal case, when the exogenous signal functions and the function represents un-modeled dynamics of the systems equal to zero, the proposed controller does not mean the convergence to zero of the tracking error.

Computer simulation results show the effectiveness of the controller in dealing with the stated problems.

Keywords: Adaptive Control, Dead zone, Robustness, Nonlinear System

1 Introduction

Concerning nonlinear systems, several results dealing with robust adaptive control of robot manipulators are now available in the literature (see [1], [2], [3], [4]). For the general case, however, few results have been obtained ([5], [6], [7], [8]), and robustness of those schemes has not been studied.

In this paper, the problem of controlling a first order nonlinear system subject to bounded input and output exogenous disturbances and un-modeled dynamics which are smooth enough is studied. The proposed scheme has been inspired from previous works (see [9], [5]), but the scheme in this paper allows us to considerably reduce the size of the dead zone, i.e. the size of the tracking error residual set. Furthermore, the a *priori* upper bounds knowledge on the system uncertainties and disturbances is significantly reduced, and is eliminated when the functions in the system equations are Lepschitz.

The paper is organized as follows: in the next section, the class of nonlinear plants to be studied and the structure of the controller are presented. In section 3, we propose three different robust adaptive control laws and we discuss their properties. In section 4, a numerical example simulated is presented. Finally, some conclusions are given in the last section.

2 Problem statement and robust controller structure design

Consider the class of nonlinear systems

$$x' = -D^T f(x) - bu + w_1(t) + g(x) \tag{1}$$

$$\bar{x} = x + w_2(t) \tag{2}$$

where u, x and R denote the input, state and measured state, respectively; $D \in R^p$ and $b \in R$ are unknown parameters; $f(x) \in R^p$ is a known vector function and g(x) is an unknown scalar function which represents un-modeled dynamics.

Assume that the exogenous signal $w_1(t)$, $w_2(t)$ as well as f(x) and g(x) have standard smoothness and boundedness properties so that the existence of solutions for the ordinary differential equations involved in the remaining of the paper is guaranteed [10].

The aim of the control is to make plant (1) - (2) asymptotically match a linear first order reference model of the form:

$$x_m' = a_m x_m + r \tag{3}$$

where $r \in R$ is the reference signal and $a_m < 0$. From (1) and (2) we have:

$$\bar{x}' = x' + w_2'(t) = -D^T f(\bar{x}) + D^T \Delta f(x, w_2) - bu + w_2' + w_1 + g(x) \tag{4}$$

where $\Delta f(x, w_2) = f(\bar{x}) - f(x)$ (5)

is a measure of the sensitivity of the nominal model ($g(x)=w_1=w_2=0$) with respect to the output noise $w_2(t)$.

Now, from (3) and (4) the error equation can be derived:

$$e' = \bar{x}' - x_m' = a_m e + b[-\bar{D}^T f - u + \frac{w_2}{b} + \frac{w_1}{b} + \frac{1}{b} D^T \Delta f(x, w_2)] \tag{6}$$

$$\bar{D}^T = \left[\frac{a_m}{b}, \frac{D^T}{b}, \frac{1}{b}\right] \tag{7}$$

where

$$\bar{f}' = [\bar{x}, f^T(\bar{x}), r] \tag{8}$$

Assumption 1: b is unknown but its sign is known. We will consider b>0 in the fest of the paper without loss of generality.

Assumption 2: Suppose that for a suitable unknown parameter w_M and a known continuous-time function $h(\bar{x})$ we have

$$\frac{1}{b}|(w_2' + w_1 + D^T \Delta f(x, w_2) + g(x))| \leq w_M h(\bar{x}) \quad (9)$$

where w_M, $h(\bar{x}) > 0$.

Note that e and $\bar{f}$ are measurable and therefore available for control purpose. Now, the following control law is proposed:

$$u = -\hat{D}^T f(\bar{x}) + \frac{e|e|h(\bar{x})}{\varepsilon_0(e)} \hat{w}_M \quad (10)$$

where:

$\hat{D} \in R^{P+2}$ denotes an estimate for the unknown parameter vector in (7).

$\varepsilon_0(e)$ is a suitable function of the tracking error and $\hat{w}_M$ is an auxiliary parameter estimate. Both will be specified later.

To show the stability of the closed loop system (1), (10) we choose the following Lyapunov positive definite function:

$$V(t) = \frac{1}{2}e^2 + \frac{1}{2}b(\tilde{D}^T \tilde{D} + \tilde{w}_M^2 \quad (11)$$

where:

$\tilde{D} = \hat{D} - \bar{D}$ and $\tilde{w}_M = \tilde{w}_M - w_M$ are parameter errors.

Taking derivative of V along the trajectory of the closed loop system combined with (6) and (10) then in conjunction with (9) we have:

$$V'(t) \leq a_m e^2 + b\{-\frac{e^2|e|}{\varepsilon_0(e)} h(\bar{x}) \hat{W}_M + |e| w_M h(\bar{x})\} + b\tilde{D}^T(e\bar{f} + \bar{D}') + b\tilde{w}_M \tilde{w}'_M \quad (12)$$

Since $\bar{D}$ and w_M are unknown but constant parameters we have $\tilde{D}' = \hat{D}'$ and $\tilde{w}' = \hat{w}'_M$ Now let us choose:

$$\hat{w}'_M = \begin{cases} |e| \frac{e^2}{\varepsilon_0(e)} h(\bar{x}) & if\ |e| \geq \varepsilon_1 \\ 0 & if\ |e| \leq \varepsilon_1 \end{cases} \quad (13)$$

$$\hat{D}' = \begin{cases} -e\bar{f} & if\ |e| \geq \varepsilon_1 \\ 0 & if\ |e| \leq \varepsilon_1 \end{cases} \quad (14)$$

where ε_1 specifies the dead zone size. From (13), (14), (12) we get:

$$V' \leq a_m e^2 + b|e| w_M [1 - \frac{e^2}{\varepsilon_0(e)}] h(\bar{x}) \quad for\ |e| \geq \varepsilon_1 \quad (15)$$

if furthermore $\varepsilon_0(e)$ is chosen such that:

$$|e| \geq [\varepsilon_0(e)]^{1/2} \quad \forall |e| \geq \varepsilon_1 \quad (16)$$

we obtain:

$$V' \leq a_m e^2 \leq a_m \varepsilon^2 \quad for\ |e| \geq \varepsilon_1 \quad (17)$$

So V(t) decreases until $|e|$ reaches the bound of the dead zone, i. e $|e| = \varepsilon_1$ while assuming bounded initial conditions on e, D and $\hat{w}_M$.

To conclude boundedness of e, D and $\tilde{w}_M$ we follow the ideas in [5] and [9].

Let $\Omega_1 = (t/|e| \leq \varepsilon_1)$ and $\Omega_2 = (t/|e| > \varepsilon_1)$. For $\tau \in \Omega_1$, $\hat{D}$ and $\tilde{w}_M$ are constant. Assume that for $t=t_0 \in \Omega_1, |e(t_0)| = \varepsilon_1$, i. e the trajectory lies on the boundary of Ω_1.

Assume also that $|e|$ leans Ω_1 at t_1, that there exists $t_2 > t_1$ such that $t_2 \in \Omega_2$. First note that the length of the interval (t_2, t_1) must be finite, see equation (17). Therefore, there exists a time $t_3 > t_2$ such that $|e(t_3)| = \varepsilon_1$. Since $e^2(t_3) = e^2(t_1)$, and V(t)is strictly decreasing for $t \in \Omega_2$ it follows that:

$$\| \tilde{D}(t_3) \|^2 + \tilde{w}^2{}_M(t_3) < \| \tilde{D}(t_1)^2 + \tilde{w}_M^2(t_1) \quad (18)$$

Remark:

Note that inequality (9) in assumption (2) is satisfied if the following three inequalities hold:

$$\frac{1}{b}|w_2' + w_1| \leq w_{M1} \quad (19a)$$

$$\frac{1}{b}|w_2' + w_1| \leq w_{M1} \quad (19b)$$

$$\frac{1}{b}|g(x)| \leq w_{M3} h_3(\bar{x}) \quad (19c)$$

where w_{Mi} (i = 1, 2, 3) are unknown positive constant and $h_i(\bar{x})$ (i = 2,3) are known positive functions. The interest of the above inequalities is that the exogenous disturbances, the sensitivity term Δf and the un-modeled dynamics can be treated separately. Moreover, if f and g are globally Lepschitz, we can set $h_2(\frac{1}{b}|g(x)| \leq w_{M3} h_3(\bar{x}))=1$ and $h_3(\bar{x}) = \bar{x}$. In this case, one sees that no a priori upper bounds knowledge is required neither in the above equation nor in (9).

3 Choice of the dead zone size

In the previous section we have shown that the system (1), (2) is globally stable with the control law (10), (13)

and (14) provided that the function $\varepsilon_0(e)$ is chosen such that (16) holds. In this section, we present three different choices for $\varepsilon_0(e)$:

$\varepsilon_0(e) = e^2$ and $\varepsilon_1 = 0$. In this case, we obtain:

$$\hat{w}'_M = |e|\, h(\bar{x}) \tag{20}$$

$$\hat{D}' = e\bar{f} \tag{21}$$

$$\hat{D}^T f + \mathrm{sgn}(e)\hat{w}'_M h(\bar{x}) \tag{22}$$

where sgn denotes the sign function.

From (20), (21) it follows that the parameters are frozen when the sliding surface e=0 is reached. This condition can not met in practice because actual switchers only provide an approximation of the sign function. If a numerical implementation is used, round off errors in the tracking errors in the tracking error may destroy the information of its sign in the neighborhood of e=0.

$\varepsilon_0(e) = \{e^2 \ \ if |e| \geq \varepsilon_1$ where >0 and small enough

The stability (16) is verified and in this case we have:

$$\hat{w}'_M = \begin{cases} |e|\, h(\bar{x}) & if\ |e| \geq \varepsilon_1 \\ 0 & if\ |e| < \varepsilon_1 \end{cases} \tag{23}$$

$$\hat{D}' = \begin{cases} -e\bar{f} & if\ |e| \geq \varepsilon_1 \\ 0 & if\ |e| < \varepsilon_1 \end{cases} \tag{24}$$

$$u = -\hat{D}\bar{f} + sat(e/\varepsilon_1)\hat{w}h(\bar{x}) \tag{25}$$

where sat denotes the saturate function [11] (see Figure 1).

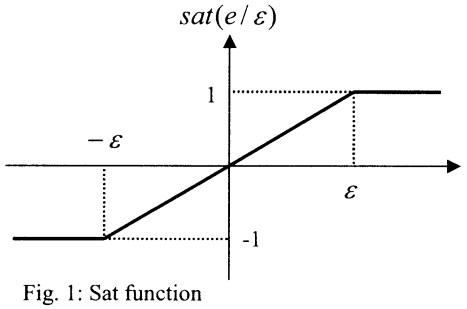


Fig. 1: Sat function

This function has been used by several authors for robustness purposes (see [12]). As long as e is outside the dead zone, the controllers in 3.1, 3.2 are ideal. If e is inside the dead zone, the parameters in (23), (24) are frozen and the input in (25) is linear continuous function of the tracking error. Thus the problems encountered in 3.1 are avoided, provided that ε_1 designs a "sufficiently large "neighborhood of the origin e = 0.

$\varepsilon_0(e) = \varepsilon_1^{\ 2} + \alpha(e^2 - \varepsilon_1^{\ 2})$ where $\alpha \in [0, e]$ and $\varepsilon_1 > 0$. Then the stability condition in (16) is verified and (13), (14) yield:

$$\hat{w}'_M = \begin{cases} \dfrac{|e|\, e}{\varepsilon_1^{\ 2} + \alpha(e^2 - \varepsilon_1^{\ 2})} & if\ |e| \geq \varepsilon_1 \\ 0 & if\ |e| < \varepsilon_1 \end{cases} \tag{26}$$

$$\hat{D}' = \begin{cases} -e\bar{f} & if\ |e| \geq \varepsilon_1 \\ 0 & if\ |e| < \varepsilon_1 \end{cases} \tag{27}$$

$$u = \hat{D}^T \bar{f} + \frac{|e|\, e}{\varepsilon_1^2 + \alpha(e^2 - \varepsilon_1^2)} \hat{w}_M h(\bar{x}) \tag{28}$$

For a fixed value of ε_1 if, one sees that it approaches 1, then (e) approaches e^2. Hence u in (28) to the discontinuous input defined in (22). But now, I e is inside the dead zone, the parameters are frozen and the control input is a nonlinear continuous time function. Thus the problem in-countered in section 3.1 are again avoided.

4 Simulation example

The simulation results presented in this section were obtained by using MATLAB with nonlinear control tool box (NCD) added.

Let us consider the following nonlinear system:

$$x' = \sum_{n=0}^{100} \frac{1}{(n+1)^2} \sin(nx) + u + w_1 \tag{29}$$
$$\bar{x} = x + w_2$$

The reference model is $x'_M = -a_M x_M + r$, where r is depicted shown in Figure 2.

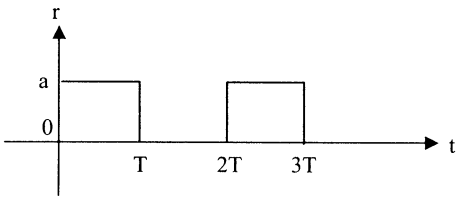


Fig. 2: Reference signal r

For a = 1, T = 8 sec, $\varepsilon_1 = 10^{-3}$, h($\bar{x}$) =1, g(x)=0 we have got the simulation results in Figure 3.

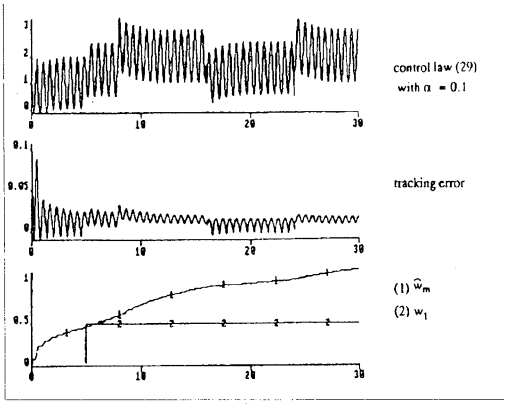


Fig. 3: Simulation result

5 Conclusions

In this work, we have presented a robust adaptive direct controller applied to a class of nonlinear first order systems. It is based on the use of a dead zone in the parameters update law. The size of the dead zone in (13) and (14) does not depend on the upper bounds of the disturbances. It follows that even If the bounds are large, the tracking error convergence to a set of size defined ε_1. In spite of this convergence, in the ideal case when $w_1=w_2=g(x) = 0$, the proposed scheme does not allow one to conclude convergence to zero of the tracking error. The extension of the results presented in this paper to systems of dimension greater than one is under currently research.

References

[1] Reed, J. S., "Instability analysis and robust control of robotic manipulator", *IEEEj. Of Robot and Automation,* 15, 1984.

[2] Ioannou, P.A and K.S. Tsakalis, "A robust direct adaptive controller. *IEEE Trans. OnAut. Control,* AC - 31, 1033-1043, 1986.

[3] Lim, K.Y., "Robust adaptive controller design for robot rigid manipulator systems", *IEEEJ. Of robot and Automation,* AC-33, 50-58, 1987.

[4] Kang, H.D.M Dawson, F.L Leves and G.J. Vachtsevano, "A robust adaptive controller for rigid robots", *12th IEEE Conf. On Decision and Control,* Tampa, FL, 1989.

[5] Satry, S.S,. . . "Model reference adaptive control", IMA J of Mathematical Control *and Information,* 1, 27-66, 1989.

[6] Knellakopoulos, I.,P.V. Kokotovic and A.S. Morse, "Adaptive output-feedback control of systems with output nonlineaeities", Technical report DC-126, University of Illinois at Urbana-Champaing, 28 September-1 October, 1990.

[7] Knellakopoulos, I.,P.V. Kokotovic and A.S. Morse, "Systematic design of adaptive controllers for feedback linearizable systems", *IEEE Trans. On Aut. Control,* 36, 1241-1253, 1991.

[8] Campion, G. and G. Bastin, "Indirect adaptive state feedback control of linearly paramiterized nonlinear systems", *Int.J of Adaptive control and Signal processing,* 4, 345-358, 1990.

[9] Peterson, B. B., "Bounded error adaptive control. *Trans", On IEEE Automatic Control,* AC-27, 1982.

[10] Coddington , E.A and N, levison, "Theory of ordinary differential equations", McGraw hill, New York, 1955.

[11] Astrom K. J. and Wittenmark B., "Computer control systems - theory and design", Prentice Hall, 1997.

[12] Shoureshi, R., "Robust control for manipulators with uncertain dynamics", *Automatica,* 26,353-359, 1990.

Proc. of The Ninth Int. Symp. on Artificial Life and Robotics (AROB 9th '04)
Beppu, Oita, Japan, 28-30 January, 2004

SHIPS' OPTIMAL AUTOPILOT USING A MULTIVARIATE AUTO-REGRESSIVE EXOGENOUS MODE

Thanh_Ha NGUYEN, *Hoang Minh JSC*
Thi-Tu HA, Van-Vinh VO,
Viet-Them NGUYEN, Cu NGUYEN,
Bac Ninh Consultant and Investment, Co., Ltd

Dinh-Ky NGUYEN, Thi-Quy PHAM,
Minh-Chuan NGUYEN, Thi-Minh NGUYEN
Tan Viet Hoang, Co., Ltd., Hanoi, Vietnam
thanhha_hoangminh2003@yahoo.com

Abstract

Linear quadratic Gaussian (LQG) control algorithm linked to Recursive Least Squares (RLS) algorithm has been applied to a multivariate auto-regressive exogenous (MARX) model of ships to construct a ship autopilot. It has been found from computer simulation and full-scale experiments aboard a training ship that the autopilot is robust and has good features in both course keeping and course changing maneuvers.
Keywords: modeling, estimation and identification, quadratic optimal control, control design, ship steering dynamics

1 Introduction

A ship operating in sea water is usually influenced strongly by unpredictable environmental disturbances such as wind, waves and current. Therefore, the ship must have a robust autopilot system with good maneuvering characteristics. To design such a robust computer-based autopilot system that is well adapted to the changes of the environment a designer should construct a good mathematical representation of ship steering dynamics and find a suitable estimation method for a chosen model [1], [2], [3].

In modern control theory, an identification algorithm is often combined with an appropriate control law to construct an automatic control system. Many authors have introduced the stochastic approach to the analysis and control of ship motion [1], [4], [5], [6]. In the self-tuning control theory, Wellstead et al [7] proposed self-tuning control algorithms which are linked to the estimation methods, one of which known as Recursive Least Squares Algorithm. Self-tuning control algorithms were applied to design automatic control systems for many machines. Among these algorithms, the minimum variance control algorithm with an SISO model of ship was applied to design an autopilot for tankers [8]. The another one often referred to as the self-tuning pole assignment control algorithm was applied to design route tracking controller in the PID form for ships [9] and then to design autopilots for ship's course-keeping and course-changing [1], [11]. The RLS algorithm was also combined with an optimal control law to design an adaptive dynamic positioning system for vessels [12].

In this paper, a new method for designing ship autopilot system is presented. An ocean-going vessel is assumed an MARX model with unknown parameters. The RLS algorithm treated as an online estimator is applied to estimate unknown parameters of the assumed model. The parameters identified by the RLS algorithm are used to calculate control gain by the LQG optimal control law. The design method is verified by computer simulation and by full-scale experiments. Computer simulation is performed for a Japanese small training ship. Full-scale experiments were implemented aboard the training ship.

The authors have got a goal to design an optimal route tracking controller with a multivariable ARX model for ships by combining the RLS algorithm with the LQG optimal control algorithm. As the first step on the way to realize such a route tracking system, the authors have done a primary feasibility study on this type of autopilot. Purposes of the work are as follows:

- To formulate the optimal control algorithm by combination of the RLS algorithm with the linear quadratic Gaussian optimal control algorithm
- To perform a simulation study for the training ship with a nonlinear model to verify the design method.
- To actually test the performance of the designed optimal autopilot for course-keeping and course-changing by full-scale experiments.

2 Control Algorithm

In this section, the control algorithm including the RLS algorithm linking to the LQG optimal control law to construct the optimal autopilot is described in more details.

2.1 Recursive Least Squares Algorithm Applied to Estimate Parameters of an MARX Model

Assuming that a vessel is a dynamic system expressed by a linear discrete-time MARX model as follows.

$$\mathbf{A}(z^{-1})y(t) = \mathbf{B}(z^{-1})u(t-k) + \varepsilon(t) \quad (1)$$

where k is time delay, $\varepsilon(t)$ is the Gaussian white noise with zero mean, y(t) and u(t-k) are vectors of measured outputs and inputs, respectively, and $\mathbf{A}(z^{-1})$ and $\mathbf{B}(z^{-1})$ are matrix polynomials of z^{-1} known as the unit backward shift operator $z^{-i}y(t) = y(t-i)$ and defined by

$$\mathbf{A}(z^{-1}) = I + a_1z^{-1} + a_2z^{-2} + \ldots + a_mz^{-m} \quad (2)$$

$$\mathbf{B}(z^{-1}) = b_0 + b_1z^{-1} + b_2z^{-2} + \ldots + b_nz^{-n} \quad (3)$$

The system (1) can be expressed in the following matrix form:

$$\mathbf{y}(t) = \theta\varphi + \varepsilon(t) \tag{4}$$

where $\theta = [\mathbf{A}\ \mathbf{B}] = [a_1, a_2,\ldots, a_m, b_0, b_1,\ldots, b_n]$ is the matrix of unknown parameters and $\varphi = [-y^T(t-1), -y^T(t-2),\ldots, -y^T(t-m), u^T(t-k), u^T(t-k-1),\ldots, u^T(t-k-n)]^T$ is the matrix of input and output measurements.

The RLSA applied to the MARX model is to minimize the following cost function:

$$J = \sum_{i=1}^{t} \varepsilon^T(t)\lambda^{t-1}\varepsilon(t) \tag{5}$$

The forgetting factor (FF) λ is a number between 0.95 to 0.998 and used to progressively reduce the emphasis placed on past information [1),6)]. The RLSA is summarized as follows. At time step t + 1:

(i) Step 1: Form $\varphi(t+1)$ using new data

(ii) Step 2: Form the prediction error using

$$\varepsilon(t+1) = y(t+1) - \theta(t)\varphi(t+1) \tag{6}$$

(iii) Step 3: Form the covariance matrix using

$$P(t+1) = \lambda^{-1}P(t)\left[I_M - \frac{\varphi^T(t)\varphi(t)P(t)}{\lambda + \varphi(t)P(t)\varphi^T(t)}\right] \tag{7}$$

(iv) Step 4: Update the parameter matrix by

$$\theta(t+1) = \theta(t) + P(t+1)\varphi^T(t+1)\varepsilon(t+1) \tag{8}$$

(v) Step 5: Wait for the next step to elapse and loop back to step (i).

It should be noted that M = n + m + 1 is the number of unknown parameters and the initial covariance matrix is chosen as $P(0) = \alpha I_M$ in which α is a large number, for example 10^3 or 10^4 [7], [10], [11], [13].

2.2 LQG Optimal Control Algorithm

For designing the optimal autopilot, using the estimated parameters (θ) the system (1) is expressed by a discrete-time state-space model as follows.

$$\begin{aligned} x(t+1) &= F(\theta)x(t) + G(\theta)u(t) \\ y(t) &= C(\theta)x(t) \end{aligned} \tag{9}$$

where $F(\theta)$, $G(\theta)$ and $C(\theta)$ are matrices formed by estimated parameters (matrix θ). The linear optimal control law is to minimize the cost function (J_O)

$$J_O = \sum_{t=0}^{M-1}\left[x^T(t)Qx(t) + u(t)^T Ru(t)\right] \tag{10}$$

where Q and R are weighting matrices (symmetric and positive definite matrices). The state feedback control gain can be obtained from the solution of the following discrete-time Riccati equation:

$$F^TSF - S - F^TSG(R + G^TSG)^{-1}G^TSF + Q = 0 \tag{11}$$

The state feedback control gain is resulted as

$$K = [R + G^TSG]^{-1}G^{-1}SF \tag{12}$$

Finally, the command rudder angle is calculated by

$$u(t) = -Kx(t) \tag{13}$$

In practical aspect of designing and implementing such the autopilot, the main task is to choose design parameters such as proper weightings (Q and R) in the cost function, sampling time and initial parameters during implementing computer simulations and full-scale experiments. This task will be discussed in further details in the next section.

3 Simulation study

Simulations were performed for the training ship *Shioji Maru* of Tokyo University of Mercantile Marine by using its nonlinear model known as MMG model. In this section, computer simulations are described.

3.1 Simulation for the SISO ARX model

Simulation was performed for the 3rd-order ARX model in the matrix form as follows.

$$\mathbf{y}(t) = \theta\varphi + \varepsilon(t) \tag{14}$$

where

$$\theta = [a_1, a_2, a_3, b_0] \tag{15}$$

$$\varphi = [-y(t-1), -y(t-2), -y(t-3), u(t-1)]^T \tag{16}$$

The state space model for the optimal control is:

$$\begin{aligned} x(t+1) &= F(\theta)x(t) + G(\theta)u(t) \\ y(t) &= C(\theta)x(t) \end{aligned} \tag{17}$$

where x(t) is the state vector of deviation between the set course and true course, u(t) is rudder angle, and $F(\theta)$, $G(\theta)$ and $C(\theta)$ are formed by estimated parameters as follows.

$$x(t) = \begin{bmatrix} y(t-3) \\ y(t-2) \\ y(t-1) \end{bmatrix},\ F(\theta) = \begin{bmatrix} 0 & 1 & 0 \\ 0 & 0 & 1 \\ -a_3 & -a_2 & -a_1 \end{bmatrix},$$

$$G(\theta) = \begin{bmatrix} 0 \\ 0 \\ b_0 \end{bmatrix} \text{ and } C(\theta) = [0\ \ 0\ \ 1] \tag{18}$$

In this case, the number of parameters is 4. Designing parameters were chosen as $Q = 2.5I_3$, $R = 1.0$ and sampling time = 0.5 seconds, with I_3 is the unique matrix. Simulation was performed for a 90-0-50 maneuvering. Rudder was limited in the range of -10 to +10 degrees.

Figure 1 shows time series of ship's responses and state feedback control gains. Figure 2 shows time series of estimated parameters. Random noise was added into the model to verify the robustness of the autopilot.

Looking at Fig. 1, it is seen that the ship course is controlled as desired. When changing the course, the course oscillates lightly before getting stable. However,

overshoot is a little bit large. Estimated parameters

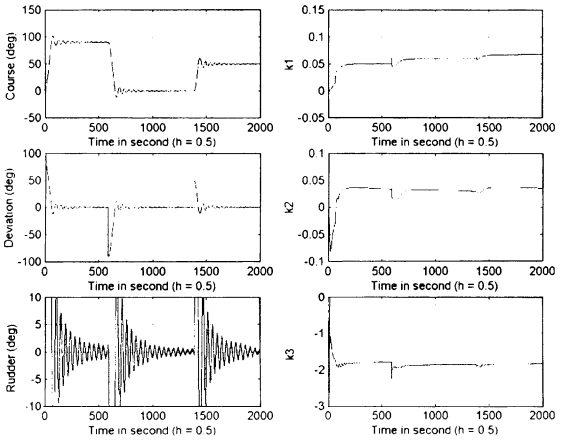


Fig. 1: Time series of ship responses (left) and state feedback gains (right) (SISO model)

converge well as shown in the same figure.

3.2 Simulation for the Optimal Autopilot with a Multivariate ARX model

When implementing simulation for the MARX model, for computational convenience, the MARX model is written in the discrete-time state space model as follows.

$$x(t+1) = F(\theta)x(t) + G(\theta)u(t)$$
$$y(t) = C(\theta)x(t) \qquad (19)$$

where

$$x = \begin{bmatrix} v \\ r \\ \Delta\psi \end{bmatrix}, \quad F = \begin{bmatrix} a_{11} & a_{12} & a_{13} \\ a_{21} & a_{22} & a_{23} \\ a_{31} & a_{32} & a_{33} \end{bmatrix}$$

$$G = \begin{bmatrix} b_{11} \\ b_{21} \\ b_{31} \end{bmatrix} \text{ and } C = \begin{bmatrix} 1 & 0 & 0 \\ 0 & 1 & 0 \\ 0 & 0 & 1 \end{bmatrix} \qquad (20)$$

It should be noted that v is sway velocity; r is yaw rate and $\Delta\psi$ is the deviation between set course and true course. In this case, the number of parameters is 12 and designing parameters were chosen as $Q = 0.25I_3$, $R = 1.0$ and sampling time = 0.5 seconds. Random noise was added to the model to verify the robustness of the autopilot.

Simulation was performed for a 90-0-90 maneuvering. Rudder was limited in the range of -10 to +10 deg. Figure 2 shows time series of ship responses and state feedback control gains. Looking at the Fig. 2, it can be seen that the ship course is controlled as well as desired. Generally speaking, overshoot in this case is zero.

In comparison of the autopilot with a multivariate ARX model with the autopilot with an SISO ARX model as mentioned in the previous section, the autopilot with a multivariate ARX model would have better steering characteristics and robustness than those of the autopilot with an SISO ARX model. Table 1 shows some statistical values of estimated parameters. Generally speaking, overshoot in this case is zero.

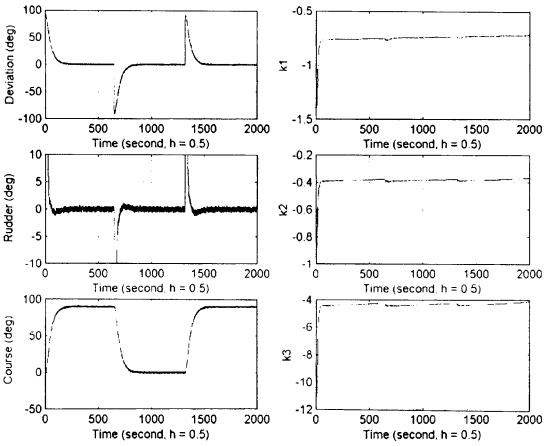


Fig. 2: Time series of ship responses (left) and state feedback control gains (right) (MARX model)

Table 1: Statistical values of estimated parameters

Para.	Mean	Max	Min	Final
a_{11}	-0.9009	-0.8998	-0.9030	-0.9009
a_{12}	1.9673	2.0179	1.9509	1.9670
a_{13}	0.0018	0.0020	0.0013	0.0018
b_{11}	-0.0923	-0.0891	-0.0935	-0.0923
a_{21}	0.0325	0.0331	0.0322	0.0325
a_{22}	-0.1228	-0.1153	-0.1372	-0.1229
a_{23}	-1.8e-4	-1.5e-4	-2.0e-4	-1.8e-4
b_{21}	0.0229	0.0234	0.0214	0.0230
a_{31}	-0.5649	-0.5600	-0.5741	-0.5646
a_{32}	-13.762	-13.552	-13.890	-13.762
a_{33}	-0.9947	-0.9943	-0.9951	-0.9947
b_{31}	-0.2520	-0.2262	-0.2616	-0.2539

4 Full Scale Experiments and Results

Table 2: Particular dimension of *Shioji Maru*

Length	46.00m	**Breath**	10.00m
Depth	2.08m	**Displacement**	717.52t
GRT	425.00t	**Propeller**	CPP
B. Thruster	2.4t	**S. Thruster**	1.8t

The ship's autopilot designed based on the above-mentioned algorithm was verified by full-scale experiments aboard the training ship *Shioji Maru* of Tokyo University of Mercantile Marine. Table 2 shows the particular dimensions of the *Shioji Maru*. Three

real-time control systems were installed in the training ship for full-scale experiments. The control program for experiments was coded in a Simulink model.

Many full-scale experiments for the optimal autopilot with SISO ARX model were implemented aboard the *Shioji Maru*. The model for the full-scale experiments is the same with model expressed by the equations (14)-(18). Designing parameters were chosen as Q = $2.5I_3$, R = 1.0 and sampling time = 0.5 seconds. Set course was set at 180 degrees. Total time for experiment was 500 seconds. Figure 3 shows time series of ship responses and state feedback control gains. Looking at Fig. 3, it could be seen that the ship course was kept as stable as desired.

Unfortunately, by the time of preparing this paper full-scale experiments for MARX models have not yet been carried out because of financial problem and of difficulty in getting correct measurement of sway velocity by REALoop aboard the *Shioji Maru*.

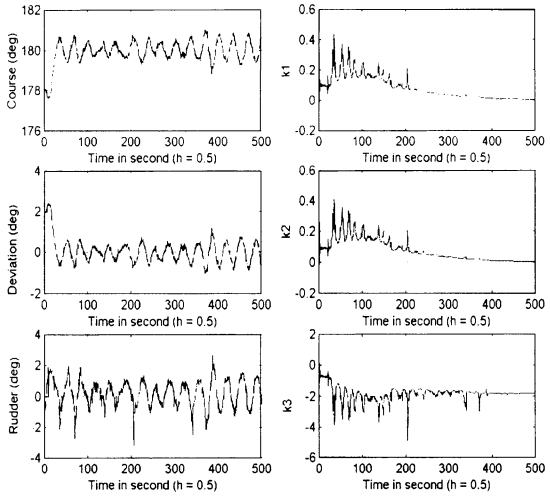


Fig. 3: Time series of ship responses (left) and estimated parameters (right)

5 Conclusions and Future Research

In this study, Linear Quadratic Gaussian (LQG) control algorithm linked to Recursive Least Squares (RLS) algorithm has been applied to a multivariate auto-regressive exogenous (MARX) model of ships to construct a ship autopilot. It has been found by computer simulations and full-scale experiments that the designed optimal autopilot has very good performance to keep and change the ship's course as desired. It could also be found that the autopilot with the MARX model is more robust in course-changing control than the autopilot with an SISO ARX model.

More full-scale experiments for the autopilot with the MARX model should be implemented to investigate the steering characteristics and robustness in real conditions. The control algorithm will further be developed to design an optimal route-tracking controller for ships.

References

[1] Fossen, T. I., "Guidance and Control of Ocean Vehicles", John Wiley and Sons Ltd., UK. 1994.

[2] Ohtsu, K., H. Oda and T. Iida, "Challenge to Advanced Optimal Ocean Navigation System" (in Japanese), the 13th Dynamic Symposium: Ship Motion and Its Control at Seas, **2**, 45-91, the Society of Naval Architecture of Japan, Tokyo, Japan, 1997.

[3] Nguyen, D. H. and M. D. Le, "A Challenge to Advanced Autopilot Systems for Ships" Proc. of the 4th Vietnam Conference on Automation, 226-232, Hanoi, Vietnam, 2000.

[4] Astrom, K .J. and C. G. Kallstrom, "Identification of Ship Steering Dynamics", Automatica, **12**, 9-22, Pergamon Press, UK., 1976.

[5] Ohtsu, K, M. Horigome and G. Kitagawa, "A New Ship's Autopilot Design through a Stochastic Model", Automatica, **15**, 255-268, Pergamon, UK., 1979.

[6] Holzhuter, T., "A High Precision Track Controller for Ships", IFAC 11th Triennial World Congress, 425-430, Talinn, Estonia, Russia, 1990.

[7] Wellstead, P.E. and M. B. Zarrop, "Self-tuning Systems: Control and Signal Processing", John Wiley and Sons Ltd., UK, 1991.

[8] Kallstrom, C. G., K. J. Astrom, N.E. Thorell, J. Eriksson and L. Sten, "Adaptive Autopilots for Tankers", Automatica, 15, 241-254, Pergamon Press, UK., 1979.

[9] Mizuno, H., T. Okawa, I. Komine, N. Mizuno and K. Ohtsu , "Route Tracking System by Adaptive Autopilot", Proc. of CAMS'89, 77-82, Copenhagen, Denmark, 1989.

[10] Nguyen, D. H., J. S. Park and K. Ohtsu, "Designs of Self-tuning Control Systems for Ships", The Journal of Japan Institute of Navigation, 99, 235-245, Japan, 1998.

[11] Nguyen, D. H., N. Mizuno and K. Ohtsu, "A Modified Pole Assignment Typed Autopilot for Ships", The Journal of Japan Institute of Navigation, 102, 327-337, Japan, 2000.

[12] Iida, T., "On an Adaptive Dynamic Positioning System for Vessels" (in Japanese), Journal of Western Japan Society of Naval Architects, 213, 89-96, Japan, 1990.

[13] Tokumaru, H. et al., "A Handbook for Statistical Engineering" (in Japanese), Chapter 6 System Identification, 283-328, Baifukan Publisher, Japan, 1987.

Proc. of The Ninth Int. Symp. on Artificial Life and Robotics (AROB 9th '04)
Beppu, Oita, Japan, 28-30 January, 2004

Enhancing Awareness in Cooperative Robots Through Perceptual Anchoring

Sherwin A. Guirnaldo*,[1], Keigo Watanabe** and Kiyotaka Izumi**
*Department of Engineering Systems and Technology,
**Department of Advanced Systems Control Engineering,
Graduate School of Science and Engineering,
Saga University, 1-Honjomachi, Saga 840-8502, Japan
†E-mail: sheronell@msn.com, {watanabe, izumi}@me.saga-u.ac.jp

Abstract

In this paper, we propose a system for controlling the perceptual processes of two cooperative robots that addresses the issue of enhancing "awareness". The proposed system benefits from a formalism called perceptual anchoring. Here, perceptual anchoring will enhance the awareness of the system by employing an anchor-based active gaze control strategy to control the perceptual effort according to what is important at a given time. We demonstrate the proposed system through a simulation of two nonholonomic mobile robots performing a cooperative transportation by carrying a cargo to a target location where there are other robots moving around. The system is able to efficiently focus the perceptual effort and to safely carry the cargo to the target position.

1 Introduction

Vision is believed to be the most valuable sensor that a robot can be equipped with, but as we give robots more human-like capabilities robots are also experiencing more and more human-like problems. Consider Fig. 1, which shows two robots cooperatively transporting an object to a certain destination. The robots are equipped with panned camera system. In actual implementation of this system one can easily identify the problems to be solved, i.e., recognition; each robot must be able to recognize landmarks to estimate its position and to aid its navigation system; it must be able to recognize other moving robots or objects in order to avoid collision. But if the vision system is plagued with limitations, how should we perform it?

Inherent problems of a typical camera include limited field of view and range, and occlusion, in which a vision system cannot see through walls or through its partner or its cargo as in the case of Fig. 1. In this sense, tracking all important details in the environment is trivial if we would like for the controller or behaviors to include them in decision making — more information will result to a more reliable system. Therefore, it is required for a cooperative robot to create and maintain models of the features and objects in the environment that are relevant to its task.

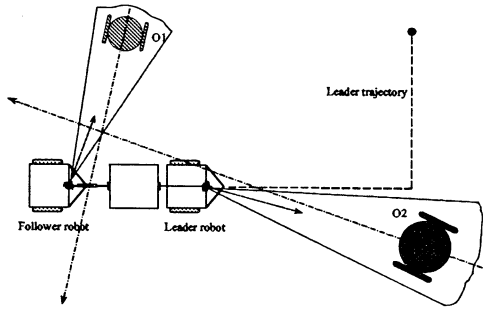


Figure 1: Cooperation in a dynamic environment.

Here, we develop a decentralize control system for a cooperative transportation of objects using two mobile robots. The control system employs an active perceptual anchoring system [1]. The goal of employing the active perceptual anchoring system is to enhance the awareness of the system. Anchoring is the process of creating and maintaining the correspondence between symbols and sensor data that refers to the same physical objects [2]. The anchors here will be used as models of the relevant features and objects in the environment.

2 Active Perceptual Anchoring

The main idea of active perceptual anchoring is that, the perceptual controller can use the information inside the anchors to narrow down the search space; for example if the controller wants to monitor a moving object, the active perceptual control can simply search within the anchors, find one among the anchors that matches the description of the object and use the estimated values of properties stored in that an-

[1]Permanent address: Dept. of Mechanical Engineering, Mindanao State University, Marawi, Philippines

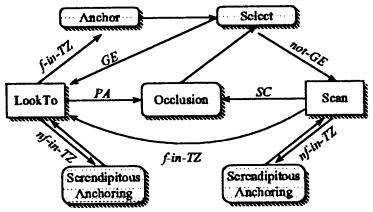


Figure 2: Active perceptual anchoring system.

chor making the perceptual effort more efficient. As with [1], an anchor will include an *anchored* value on a [0,1] scale, which measures how recently the anchor was actually anchored to the real object in the environment. Shown in Fig. 2 is a finite state machine, in which we employed it here to control the perception system to generate a sensor control command that will change the fixation of the camera. Moreover, the robot main controller will pass to the perception controller a *needed* measure. The needed measure will tell the perception system how necessary is a certain object or anchor to the current state of the main controller. To select an anchor, the perception control module will compute the important measure base on the needed and anchored values. If the controller module is not on obstacle avoidance mode, the perception module will select the most important anchor to be the focus of attention. For a given anchor a in S, where S is a set of anchors, we measure the importance of a as

$$important(a) = needed(a) * (1 - anchored(a)). \quad (1)$$

On the other hand, if the controller is on obstacle avoidance mode, the perception module will use only the *needed* measure to select the next focus of attention. The main control module must be supplied with fresh and accurate information of the most threatening object in the environment. In our simulation study, the *needed* values for non threatening object is set to 0.5 and 1 if it is so closed. Moreover, the *anchored* values for newly updated anchor is set to 1; otherwise it is reduced by 1 percent every time step. The details of each processes are given below.

1. Select: choose an anchor x on which to focus the attention of the panned camera using the *important* measure. Set the fixation (or desired orientation) of the camera to the expected orientation of x. If the *anchored* level is above a given threshold, exit via GE (good estimate); otherwise, exit via the not-GE transition.
2. Scan: perform a visual scan to explore the part of the space where x could be located. Here, scan is performed by moving the camera to the fixation and searching areas near to it. Exit when one of the following occurs:

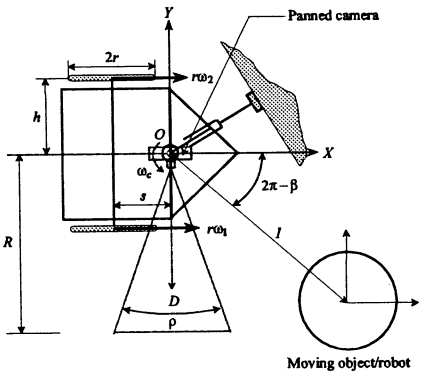


Figure 3: Kinematic model of the mobile robot.

   (a) If an object is detected along the TZ (tracking zone) that matches x, set the fixation of the camera to the object relative orientation and exit via f-in-TZ (found in TZ);
   (b) If an object that matches an anchor other than x is detected along the TZ, exit via nf-in-TZ;
   (c) If the physical scan is completed, exit via the S.C (scan complete).
3. LookTo: turn the camera to the current fixation, when:
   (a) If an object that matches x appears within the TZ, exit via f-in-TZ;
   (b) If an object that matches an anchor other than x appears within TZ, exit via nf-in-TZ;
   (c) If the desired orientation of the camera has been achieved and no object is detected that matches x, exit via P.A (position achieved).
4. Anchor: measure the (relative) orientation and distance of the object and update the x anchor associated to the object; select a new focus.
5. Serendipitous anchor: if an object other than the one represented by x is in TZ, measure its (relative) orientation and distance and update the corresponding anchor; continue to search x.
6. Lost: if either Scan or LookTo has been completed without finding the object that x represents, mark x as lost and go and select a new focus of attention.

In our simulation study, we considered two nonholonomic mobile robots that cooperatively deliver a cargo by carrying it to a desired destination (Fig. 1 will give a good illustration). Moreover, the working environment is cluttered with two other moving robots, O1 and O2.

3 Simulation Study

To demonstrate the new concept of enhancing awareness through active perceptual anchoring in cooperative robots, we used the robotic system developed

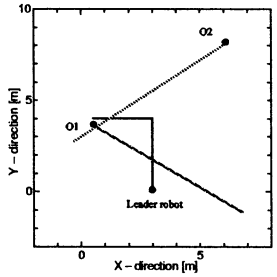


Figure 4: Desired trajectory for the leader robot and the trajectories for the two other robots working in the environment. Starting positions are marked with a circle.

by [3]. The kiematic model of the system is shown in Fig. 3. To model the sensor, we used a triangle. The height R represents the range of the sensor, and angle ρ defines how wide the field of view of the camera is. To detect a moving robot, the reference point of that robot must be within the area of the triangle. Here, we assumed that once an object is detected the sensor will be able to return the color, the relative orientation, and its relative distance to the observer robot. Moreover, occlusion is declared if one of the cooperative robots appears inside the area of the triangle. In our simulation study, the range of the sensor was assumed to be long enough to detect every robot moving in the simulated environment. And thus, the possible causes of problems are reduced to limited field of view and occlusion. Other parameters worth to mention are β, the orientation of the moving object relative to the observing robot, I, the distance of the moving robot relative to the observing robot, and ω_c, the angular velocity of panning the camera.

The main task of the two cooperative robots is for them to carry and transport the cargo to the desired location via a predefined trajectory. The trajectories for the leader and the two robots are shown in Fig. 4. The leader robot task is to follow the trajectory and avoid colliding its body with others. We assumed here that the two other robots are blind such that they don't have any ability to avoid collision, they will just go straight and follow their trajectories. On the other hand, the follower robot is designed to have the ability for self and cargo preservation, i.e., it is capable of doing collision avoidance not just for its own body but also for the cargo as well. Moreover, the follower robot is designed to carry the cargo safely by maintaining a safe length of its passive hand. Unlike with the leader robot's hand, the hand of the follower robot are capable of increasing and decreasing its length.

The schematic diagram of the decentralized con-

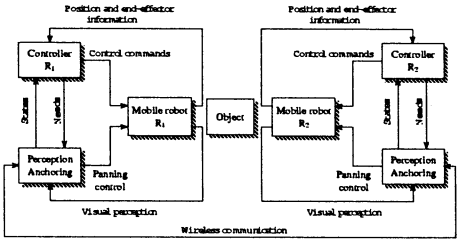


Figure 5: Decentralized control strategy.

troller for the cooperative robots is shown in Fig. 5. Here, a decentralized controller is essential to magnify the sensory limitation of each agent, otherwise we will consider the whole system as one with two sensory systems. The controller also proposes a sharing of information between cooperative robots through a communication channel. Active gaze control and information sharing will further enhance the awareness of each robot.

The control module of the leader is composed of two components, a trajectory following module and a fuzzy logic based obstacle avoidance. The former is made of a radial basis function neural network (RBFNN) trained to follow a given trajectory using genetic algorithm (GA). The leader robot control will switch to one of these modules depending on the situation at hand. If the distance of an object is within less than the safe distance, the leader control module will switch to obstacle avoidance mode. On the other hand, the follower robot controller is similar of that proposed by [3] for a follower robot. The difference is that in our case we did not employ the posture control module, leaving us only the avoidance module and hand length control module. Moreover, both modules used fuzzy logic type controller, and a fuzzy based panning control was used to control the LookTo and scan processes.

4 Results and Discussions

The simulation results can be shown in two views, with respect to leader robot's eye view and the follower robot's eye view. With respect to the leader robot's eye view, the results are shown in Fig. 6. Here, A and B show the anchored relative distance and orientation for O1 and O2. On the other hand, C and D show the anchored (measure) values for robot O1 and O2 respectively for the entire simulation time. The results show that before hitting the 9 seconds mark, the the perception system evenly anchored both O1 and O2. The camera swings back and forth from O1 to O2. Soon, after O1 became so close the avoidance module of the leader robot was activated. The activation resulted to assignment of higher *needed* value for the anchor O1. This in turn resulted to a full tracking attention for

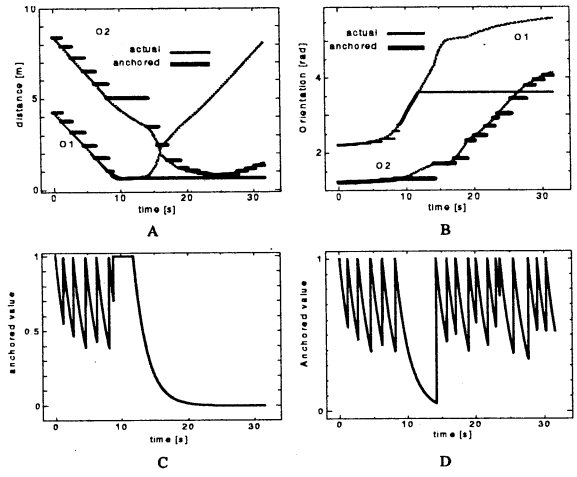


Figure 6: At the leader's view. A and B show the anchored and actual values of distance and orientation. C and D on the other hand show the plot of the anchored measure for O1 and O2 respectively.

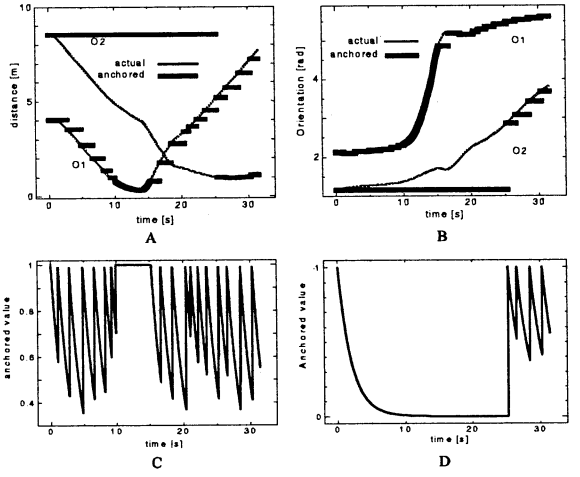


Figure 7: At the follower's view. A and B show the anchored and actual values of distance and orientation. C and D on the other hand show the plot of the anchored measure for O1 and O2 respectively.

O1, its anchor contents were updated every time step and O2 is left unattended for approximately 3 seconds. When the leader robot and O1 parted ways, O1 swings to the south of the leader robot that later resulted to occluded view due to the presence of the cargo and the follower robot in that direction. The anchor for O2 was updated again after the close encounter with O1.

In the follower robot's eye view, result is shown in Fig. 7. A and B show the content of the anchor for O1 and O2 respectively for the entire simulation time. C and D show the *anchored* values for O1 and O2 respectively. The result tells us a different story with what the leader robot saw. The plots show that, for almost the entire simulation time O2 is not visible for the follower robot. It starts appearing only near the end of the simulation time. This is what happens since O2 started up north relative to where the follower robot started (see Fig. 4) and since it follows the leader robot, it cannot see up north due to occlusion with the leader robot. On the other hand, O1 is visible all throughout the simulation time.

Here, the two cooperative robots broadcast to each other their position and the anchors. Specifically, every time O1 or O2 is lost (or occluded), a cooperative robot will use the information available from the anchor of the other cooperative robot, and transform it according to its own local coordinates. This technique resulted to a more efficient perception control.

5 Conclusions

In this paper, we have presented a formalizing approach of controlling the perceptual effort to enhance the awareness of two mobile robots designed for cooperative transportation of a cargo object. We demonstrated the approach through a simulation of two mobile robots platform that cooperatively transports an object to a certain destination through a predefined trajectory. Both cooperative robots are equipped with a panned camera as the main sensor. The inherent limitations for the sensor system such as limited field of view and occlusion will make the task more complicated than normal. To cope up with these limitations is important if we want our system to work in a dynamic environment such as what we have in our simulation. Although the anchoring process was not fully implemented such as the initial pattern recognition process, our simulation results showed that our approach can work and potentially feasible.

References

[1] A. Saffiotti and K. LeBlanc, "Active perceptual anchoring of robot behavior in a dynamic environment," In *Proc. of the IEEE Int. Conf. on Robotics and Automation*, San Francisco, CA, April 2000, pp. 3796–3802.

[2] S. Coradeschi and A. Saffiotti, "Perceptual anchoring: A key concept for plan execution in embedded systems," In *Advances in Plan-Based Control of Robotic Agents*, 2002, pp. 89–105.

[3] X. Yang, K. Watanabe, K. Kiguchi, K. Izumi, "Coordinated transportation of a single object by two nonholonomic mobile robots," In *Proc. of The Seventh Int. Symp. on Artificial Life and Robotics*, vol. 2, 2002, pp. 417–420.

Proc. of The Ninth Int. Symp. on Artificial Life and Robotics (AROB 9th '04)
Beppu, Oita, Japan, 28-30 January, 2004

A Study on Constructing a Neuro-interface Using the Concept of Virtual Master-Slave System

Rafiuddin Syam, Keigo Watanabe, and Kiyotaka Izumi
Department of Advanced Systems Control Engineering,
Graduate School of Science and Engineering, Saga University
E-mail: 02td74@edu.cc.saga-u.ac.jp; {watanabe,izumi}@me.saga-u.ac.jp

Abstract

To ease the control of a nonholonomic robot by non-expert, a neuro-interface is proposed by using a concept of virtual master-slave system. The design procedure of the interface is elaborated for the control of nonholonomic two-wheeled robots; in particular, it is shown that if the coordinate transformation from the slave to the master is assumed to be known, the resultant inverse mapping of the master robot can be simply realized by a neural network (NN) with all linear units. Two construction examples are given to explain the present method.

1 Introduction

Since an expert has special knowledge (or abundant experience) to deal with a master robot successfully, he can easily operate the master robot to control the slave robot in a conventional master-slave framework. However, if a beginner wants to do the same operation, then it is not easy for him to operate the master robot to obtain a desired motion of the slave robot, due to a lack of experience.

Recently, Widrow and Lamego [1] proposed a concept of neuro-interface to ease the control of a nonholonomic system by non-expert. In their method, they explained a mapping the inverse system [2] for the closed-loop of a final controlled objective (or robot) by using a specialized learning mechanism, as a guideline of the neuro-interface construction. It should be noted, however, that a stable and reliable inverse system cannot be trained by directly using an NN, if the controlled objective has an unstable zero dynamics. In such a situation, a natural question is arisen that how to determine a suitable NN structure, even if an approximate mapping is constructed by NN techniques [3].

In this paper, we consider a master robot that plays the similar role to the neuro-interface studied by Widrow and Lamego, in which we regard it as a virtual robot that can simply generate the manipulated variables based on a user reference command to control a slave robot. However, it is assumed that both robots have the same dimensions for an actual reference trajectory (through any transformation) and the manipulated variables, respectively, while allowing the existence of differences in structure. Thus, introducing the concept of virtual master-slave would give us a high degree of freedom in the selectivity of the approach for controlling the virtual master robot as a neuro-interface, so that a designer can easily obtain various guidelines for constructing a model-based or NN-based mapping.

For example, if the data for controlling a virtual master robot can be directly utilized from an expert, it is possible to implement an NN mapping by the generalization learning architecture. If a simplified model of the virtual master robot, which has no unstable zero dynamics and is stable, can be utilized, then a model-based interface can be easily developed by applying the inverse model and a neuro-interface can be also easily constructed by mapping the input-output data of the inverse system.

2 Construction of Virtual Master Robots Using a Steering Model

Consider the dynamical model for a general nonholonomic two-wheeled robot [4] given by

$$\ddot{\boldsymbol{q}}(t) = \boldsymbol{f}_M(\dot{\boldsymbol{q}}(t), \boldsymbol{q}(t), \boldsymbol{\tau}(t)) \tag{1}$$

where $\boldsymbol{q}(t) \triangleq [x(t) \quad y(t) \quad \theta(t)]^T$ denotes the generalized coordinate vector, in which let the center of gravity of the robot be (x, y) and the azimuth of the robot be θ. Moreover, $\boldsymbol{f}_M \in \Re^3$ and $\boldsymbol{\tau} \triangleq [\tau_r(t) \quad \tau_l(t)]^T \in \Re^2$, where τ_r and τ_l are the driving torques of the right and left wheels, respectively. It is well-known that this inverse dynamical system cannot be solved uniquely, so that we further consider the so-called steering model, which is given by

$$\dot{\boldsymbol{v}}(t) = \boldsymbol{f}_S(\boldsymbol{\tau}(t)) \tag{2}$$

where $\boldsymbol{v}(t) \triangleq [v(t) \quad \dot{\theta}(t)]^T$ and $\boldsymbol{f}_S \in \Re^2$, where $v(t)$ is the translational velocity of the robot. The inverse of this model is known to be solved uniquely.

In what follows, assume that the model (1) represents the slave robot to be controlled, whereas it is assumed that

the model (2) represents a master robot to control the slave robot in Eq. (1).

2.1 Torque generation by an inverse model of master robot based on a backward difference equation

In general, we can solve the inverse model of the above equation such as

$$\tau(t) = g_M(\dot{v}(t)) \tag{3}$$

where $g_M \in \Re^2$ is a unique vector-valued inverse function of f_M. In order to discretely give $v(t)$ at any time t, we consider a backward difference model approximation for $\dot{v}(t)$. As a result, the above equation can be reduced as

$$\tau(t) = g_M([v(t) - v(t-1)]/\Delta t) \tag{4}$$

where Δt is the sampling width. Given the master's reference velocity vectors $v_r(t)$ and $v_r(t-1)$ at times t and $t-1$, we can obtain the desired input torque vector $\tau_r(t)$ at time t using the above relation.

On the other hand, we have to be aware of the kinematic relation given by

$$\dot{q}(t) = J(\theta(t))v(t),\ J(\theta(t)) = \begin{bmatrix} \cos(\theta) & -d\sin(\theta) \\ \sin(\theta) & d\cos(\theta) \\ 0 & 1 \end{bmatrix} \tag{5}$$

because the slave robot has its desired reference as $q_r(t)$. Therefore, the master's references $v_r(t)$ and $v_r(t-1)$ can be generated by

$$v_r(t) = J^+(\theta_r(t)) \left[\frac{q_r(t) - q_r(t-1)}{\Delta t} \right] \tag{6}$$

$$v_r(t-1) = J^+(\theta_r(t-1)) \left[\frac{q_r(t-1) - q_r(t-2)}{\Delta t} \right] \tag{7}$$

Thus, given the desired references $q_r(t), q_r(t-1), q_r(t-2)$, we can discretely generate $\tau(t)$ by using Eqs. (4) to (7).

2.2 Consideration to torque compensation due to friction term

As can be seen from Eq. (4), if $v_r(t)$ is constant, then the desired torque $\tau_r(t)$ will be zero in the sequel. However, in practice, there exist some disturbances such as floor frictions etc. Therefore, we include a small disturbance torque $\tau_d(t)$ to avoid a zero input torque such as

$$\tau_r(t) = g_M([v_r(t) - v_r(t-1)]/\Delta t, \tau_d) \tag{8}$$

Figure 1 depicts the computational block diagram for the inverse system of a virtual master robot with backward difference, which is here called a "model-based interface with backward difference" to control a slave robot as the final controlled objective.

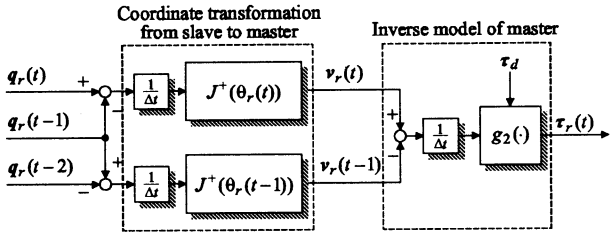


Figure 1: Inverse system of virtual master robot with backward difference

3 Mapping of Virtual Master Robot by Neural Network

According to the concept discussed above, we can easily obtain the robot operation by a virtual master-slave method with NN, regarding the master robot as a virtual robot with NN. We here simply give the following two-types of NN mapping.

3.1 Inverse system of virtual master robot with coordinate transformation and NN

In the first inverse system of virtual master robot, the associated with the coordinate transformation from slave to master is constructed by using the conventional kinematic relations, so that the inverse function of Eq. (2) is simply replaced by an NN, as shown in Fig. 2.

3.2 Inverse system of virtual master robot with only NN

In the second one of virtual master robot, the associated with the coordinate transformation from slave to master is included in the total NN as shown in Fig. 3, so that the NN has $q_r(t), q_r(t-1), q_r(t-2)$ as the direct inputs.

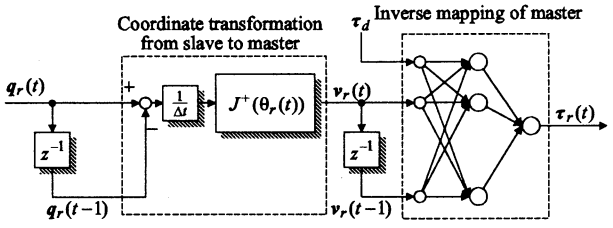


Figure 2: Inverse system of virtual master robot with coordinate transformation and NN

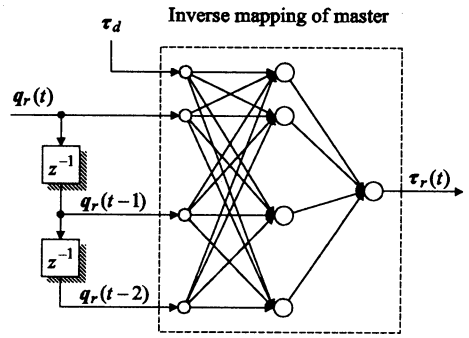


Figure 3: Inverse system of virtual master robot with NN

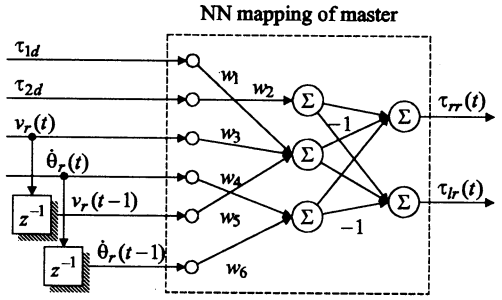


Figure 4: NN-based inverse mapping of virtual master robot with its dynamical structure, where all the physical parameters are assumed to be unknown except for d

4 Construction Example of Neuro-Interface

In this section, we concretely explain the neuro-interface by following the contents of Section 3.1. In this case, further assumptions will be required to derive the detail structure of NN. That is, we consider two cases: one is for the case (named as Case I) where all physical parameters are unknown except for the offset distance d; the other case (named as Case II) where the physical parameters m and I are unknown.

4.1 Slave and master models

The dynamical model [5] as a slave robot, is now transformed into a more appropriate representation for controlling a master robot. That is, the concrete model of Eq. (2) as a master robot can now be reduced as follows:

$$\begin{bmatrix} m & 0 \\ 0 & I - md^2 \end{bmatrix} \begin{bmatrix} \dot{v} \\ \ddot{\theta} \end{bmatrix} + \boldsymbol{\tau}_d = \frac{1}{r} \begin{bmatrix} 1 & 1 \\ R & -R \end{bmatrix} \begin{bmatrix} \tau_r \\ \tau_l \end{bmatrix} \quad (9)$$

where m denotes the mass of the robot, d is an offset distance of steering axis, I is the inertia moment of the robot, $2R$ denotes the tread of the robot, and r denotes the radius of wheel.

4.2 Case I

From Eqs. (3) and (9), we have the following model-based interface given by

$$\begin{aligned} &\boldsymbol{\tau}(t) \\ &= r \begin{bmatrix} 1 & 1 \\ R & -R \end{bmatrix}^{-1} \left\{ \begin{bmatrix} m & 0 \\ 0 & I - md^2 \end{bmatrix} \dot{\boldsymbol{v}}(t) + \boldsymbol{\tau}_d \right\} \\ &= \begin{bmatrix} \frac{1}{2} mr\dot{v}(t) + \frac{1}{2} r\tau_{1d} + \frac{r}{2R}(I - md^2)\ddot{\theta}(t) + \frac{r}{2R}\tau_{2d} \\ \frac{1}{2} mr\dot{v}(t) + \frac{1}{2} r\tau_{1d} - \frac{r}{2R}(I - md^2)\ddot{\theta}(t) - \frac{r}{2R}\tau_{2d} \end{bmatrix} \end{aligned} \quad (10)$$

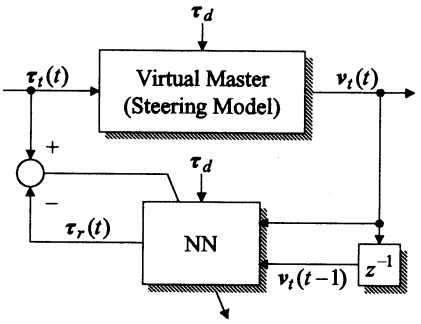


Figure 5: Training for an NN-based inverse mapping of virtual master robot using generalized learning architecture

Replacing the coordinate vector $\dot{\boldsymbol{v}}(t) = [v(t) \quad \dot{\theta}(t)]^T$ in the above equation by its reference vector $\dot{\boldsymbol{v}}_r(t)$ and applying a backward difference model approximation for the reference vector $\dot{\boldsymbol{v}}_r(t)$, we can obtain the desired torque vector $\boldsymbol{\tau}_r = [\tau_{rr} \quad \tau_{lr}]^T$ through an NN structure depicted in Fig. 4.

Note here that $w_i, i = 1, \ldots, 6$ are weightings between the input and hidden units, and to be learned, where their ideal values are as follows: $w_1 = 0.5r, w_2 = 0.5r/R$, $w_3 = 0.5mr/\Delta t, w_4 = 0.5r(I - md^2)/(R\Delta t)$, $w_5 = w_3$, and $w_6 = w_4$. Here, weightings between the first and third hidden units and the second output unit are should be -1; others are all to be 1.

This NN with all linear units can be trained to obtain an inverse mapping of virtual master robot using generalized learning architecture, as shown in Fig. 5, in which the training data set of $\{\boldsymbol{\tau}_t(t), \boldsymbol{v}_t(t)\}$ are assumed to be collected in advance from an expert operation of the master robot, and the disturbance torque $\boldsymbol{\tau}_d$ is regarded as a known, small deviation torque to operate the robot in a real floor with frictions. The detail training algorithm for each weighting can be readily derived by conventional backpropagation algorithm [6] with all linear units [7].

For example, under the physical parameter settings as

Table 1: Physical parameters for the robot

m [kg]	I [kgm^2]	R [m]	r [m]	d [m]
10	5	0.5	0.05	0.2

shown in Table 1, if we regard the desired operational data by an expert as those from the inverse for the steering model in Eq. (9), using the reference given by

$$\begin{aligned} x_r &= 2.5\sqrt{2} + 0.5at^2\cos\theta_r \ /4 \\ y_r &= 2.5\sqrt{2} + 0.5at^2\sin\theta_r \\ \theta_r &= -3\pi \end{aligned}$$

for $0 \leq t < 2$ and

$$\begin{aligned} x_r &= 2.5\sqrt{2} + 0.5t\cos\theta_r \\ y_r &= 2.5\sqrt{2} + 0.5t\sin\theta_r \\ \theta_r &= -3\pi/4 \end{aligned}$$

for $2 \leq t \leq 10$, where $a = 0.25$, we should obtain the weightings close to $w_1 = 0.025, w_2 = 0.05$, $w_3 = 12.5, w_4 = 11.5$, where the sampling width is $\Delta t = 0.02$ [s], after many iterations.

4.3 Case II

From the first equality of Eq. (10), we can also realize an NN-based inverse mapping of virtual master robot with its dynamical structure, as shown in Fig. 6, where only the physical parameters m and I are assumed to be unknown.

Note here that $w_i, i = 1, \ldots, 4$ are weightings between the input and hidden units, and to be learned, where their ideal values are as follows: $w_1 = m/\Delta t, w_2 = (I - md^2)/\Delta t$, $w_3 = w_1$, and $w_4 = w_2$. Here, other weightings are should be fixed as suggested in the figure.

This NN can also be trained to obtain an inverse mapping of virtual master robot using generalized learning architecture in Fig. 5. If the same conditions as used above will be applied for this case, then the resultant weighting should have to be $w_1 = 500, w_2 = 230$, because this NN structure has fixed, relatively small weights between the hidden and output layers.

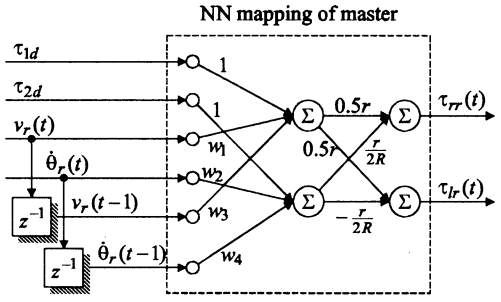


Figure 6: NN-based inverse mapping of virtual master robot with its dynamical structure, where only the physical parameters m and I are assumed to be unknown

5 Conclusions

We have described a design procedure for constructing a neuro-interface to control nonholonomic robots by applying the concept of a virtual master-slave system, in which the master robot was assumed to be regarded as a virtual robot that can simply generate the manipulated variables based on a user reference command to control a slave robot. For controlling a nonholonomic two-wheeled mobile robot, we concretely showed the construction method of neuro-interface for the case where all physical parameters are unknown or for the case where inertia related parameters are unknown, in which the coordinate transformation from the slave to the master was assumed to be known.

For a case where there exits a relatively large initial error between the robot initial coordinate and the initial reference, we have to add a feedback mechanism to cancel the effect of initial disturbance, as suggested by [5].

References

[1] W. Widrow and M. L. Lamego, Neurointerfaces, *IEEE Trans. on Control System Technology*, vol. 10, no. 2, pp. 221–228, March 2002.

[2] B. Widrow and G. L. Plett, Nonlinear adaptive inverse control, in *Proc. of the 36th Conf. on Decision and Control*, San Diego, California USA, December 1997.

[3] C. Kambhampati, R. J. Craddok, M. Tham, and K. Warwick, Inverse model control using recurrent networks, *Mathematics and Computers in Simulation*, vol. 51, pp. 181–199, 2002.

[4] R. Fierro and F. L. Lewis, Control of nonholonomic mobile robot using neural networks, *IEEE Trans. on Neural Networks*, vol. 9, no. 4, pp. 589–600, 1998.

[5] K. Izumi, R. Syam, and K. Watanabe, Neural network based disturbance canceler with feedback error learning for nonholonomic mobile robots, in *Proc. of the 4th Int. Symposium on AI System (ISIS 2003)*, Sept. 25–28, 2003, Jeju, Korea, pp. 443–446

[6] M. Teshnehlab and K. Watanabe, Intelligent Control Based on Flexible Neural Networks, Dordrecht, The Netherlands: Kluwer Academic Publishers, 1999, pp. 47–49

[7] K. Watanabe, T. Fukuda, and S. G. Tzafestas, An adaptive control for CARMA systems using linear neural networks, *Int. J. Control*, vol. 56, no. 2, pp. 483–497, 1992

Proc. of The Ninth Int. Symp. on Artificial Life and Robotics (AROB 9th '04)
Beppu, Oita, Japan, 28-30 January, 2004

Neural Network Approach to Acquire the Free-Gait Motion of Quadruped Robots in Obstacle Avoidance

Tomohiro Yamaguchi, Keigo Watanabe and Kiyotaka Izumi
Dept. of Advanced Systems Control Engineering,
Graduate School of Science and Engineering,
Saga University, 1-Honjomachi, Saga 840-8502, Japan.
E-mail: 01td72@edu.cc.saga-u.ac.jp; {watanabe,izumi}@me.saga-u.ac.jp

Abstract

In this paper, a neural network (NN) is used to determine the action of a quadruped robot in the obstacle avoiding path by using information on the destination, the obstacle configuration, and the robot's self-state. To acquire a free-gait in static walking, the order of swing leg is realized using an alternative NN whose inputs are the amount of movements and the robot's self-state. The design parameters of the former NN are adjusted by genetic algorithm (GA) offline.

1 Introduction

Although legged mobile robots are inferior to wheeled or crawler types in mobility efficiency on the flat ground, they can demonstrate high motion performance and adaptation capability to the ground by utilizing their high degrees-of-freedom. Since such robots choose stable leg-placement, stable movements can be performed on irregular terrains. From this fact, legged robots are not necessary to avoid all the obstacles by altering their path, unlike wheeled or crawler types. Because, they can avoid an obstacle by crawling-over or striding, according to the obstacle's nature and the current state of the robot. Thus, it can be found that the mobility efficiency to reach a destination is improved by such an action. Moreover, when robots have many legs like 4-legged or 6-legged types, the movement range is affected by the order of swing leg.

Quadruped robots can realize both static walk and dynamic walk. Static walk is suitable for action acquisition of quadruped robots in the geographical feature in which obstacles, such as a level difference, exist. Free-gait is realizable changing the order of swing leg in static walk of quadruped robots. A free-gait planning in the static walk was already formulated as an optimization problem with constraints and the solution method by the Monte Carlo method was proposed by Nakamura et al. [1]. However, a dedicated environment limits the result obtained from this method; it has no flexibility against the deviation of search environment.

When avoiding an obstacle by quadruped robot, there are many combinatorial solutions, such as combinations of turn and forward movements, combinations of sideway and forward movements, etc. We proposed a method for determining the action of a quadruped robot using the neural network (NN) from the position of the destination, the obstacle configuration, and the robot's self-state [2]. However, free-gait motion was not taken into consideration.

The present paper examines the obstacle avoidance action of quadruped robots with consideration to free-gait. About free-gait, the order of swing leg is determined from a amount of movements and robot's self-condition using an NN [3]. An NN for determining the robot action is acquired by re-learning the NN that was built in the case when the order of swing leg was fixed. To reach a destination with a minimum number of walking cycles, NN design parameters are optimized by a GA, using data from several environments, in which each environment has different destinations and obstacle dimensions.

2 Determination of the Action of Quadruped Robot

Robot actions, i.e., the amount of forward and sideway movements and the turning angle, are determined by a three-layered NN shown in Fig. 1.

Inputs to the NN are assumed to be the position of each sole $\{x_{f1}(k),\ y_{f1}(k)\},\ldots,\ \{x_{f4}(k),\ y_{f4}(k)\}$, the robot's body height $Z_r(k)$, x-directional maximum and minimum distances to an obstacle at right $\{x_{or\,\max}(k),\ x_{or\,\min}(k)\}$, the y-directional maximum and minimum distances to the obstacle at right

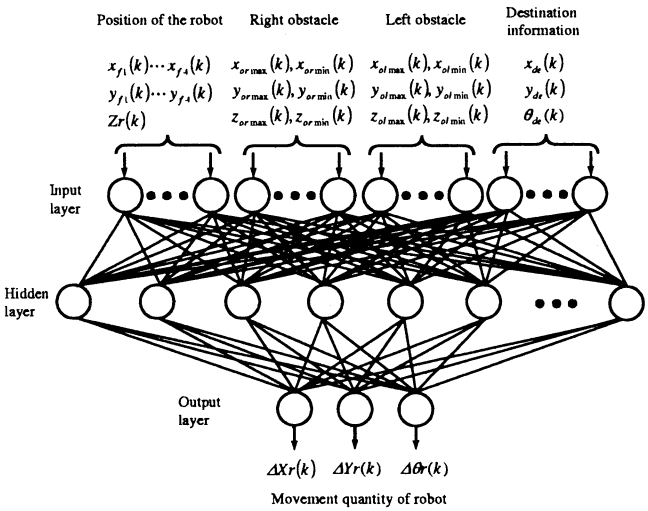


Figure 1: Neural network for avoiding an obstacle

$\{y_{or\,\max}(k),\ y_{or\,\min}(k)\}$, and the height of the obstacle at right $\{z_{or\,\max}(k),\ z_{or\,\min}(k)\}$, the x-directional maximum and minimum distances to the obstacle at left $\{x_{ol\,\max}(k),\ x_{ol\,\min}(k)\}$, the y-directional maximum and minimum distances to the obstacle at left $\{y_{ol\,\max}(k),\ y_{ol\,\min}(k)\}$, and the height of the obstacle at left $\{z_{ol\,\max}(k),\ z_{ol\,\min}(k)\}$; x-directional distance error, i.e., distance between the c.g. of the robot and destination $x_{de}(k)$, y-directional distance error $y_{de}(k)$, and direction error, i.e., the direction between the destination and forward direction of the robot $\theta_{de}(k)$. Positions of each sole and obstacles are defined in the frame whose origin is fixed to the body center. Outputs of the NN are the amount of x- and y-directional movements of the robot $\{\Delta Xr(k), \Delta Yr(k)\}$ and the turning angle of the robot $\Delta\theta r(k)$.

A radial basis function neural network (RBFNN) [4], known as an NN that realizes various approximation functions, is used in the control system. Here, the number of units at the hidden layer is to set 100.

3 Acquisition of Avoidance Action

A block diagram of obstacle avoidance control system is shown in Fig. 2. When there are any obstacles, in order to avoid them not only by turning but also by getting-over or striding, the avoidance action of the robot may be limited unless the height of the body is changeable. From this fact, the height of the body is adjusted and changed to that of an obstacle, after recognizing the obstacle. The avoidance action

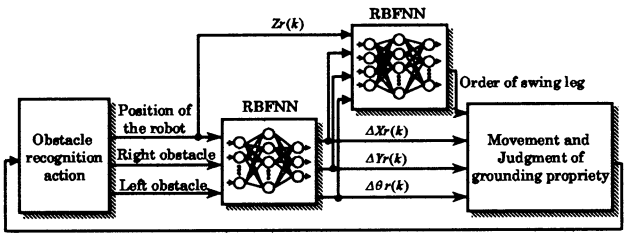


Figure 2: Obstacle avoidance control system

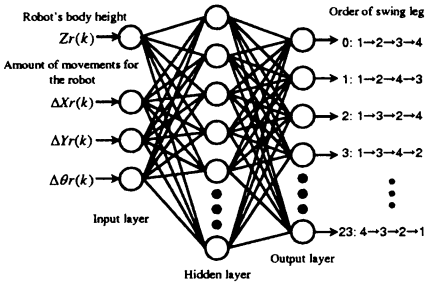


Figure 3: Neural network for determining the order of swing leg

of quadruped robot is determined by the lower NN. Furthermore, the order of swing leg is determined by the upper NN from the amount of movements of the robot.

In this research, the order of swing leg is acquired by a three-layered NN shown in Fig. 3. Inputs to the NN are assumed to be the robot's body height $Z_r(k)$, the amount of x- and y-directional movements of the robot $\{\Delta Xr(k), \Delta Yr(k)\}$ and the turning angle of the robot $\Delta\theta r(k)$. Moreover, we prepare 24 units at the output, to represent 24 kinds of the order. The actual order of swing leg fed to the quadruped robot is the order of the unit whose output value is closest to one among output units. RBFNN is also used for the NN, where the number of units at the hidden layer is set to 50.

3.1 Simulation conditions

The simulation environment is shown in Fig. 4. The y-axis is set to the forward direction of the robot. The robot is assumed to start from point (0.0, 0.0, 0.3) [m] and approach the goal, a circle having radius 0.2 [m], centered on the destination point. Simulations were conducted three times by setting distance errors as $(x_{de},\ y_{de})$=(0.0, 1.8), (0.15, 2.2), (−0.15, 2.2) [m]. We assume that one obstacle exists at the robot's right and the other at the left. Coordinates of legs and the obstacle are shown in Fig. 5. Initial posi-

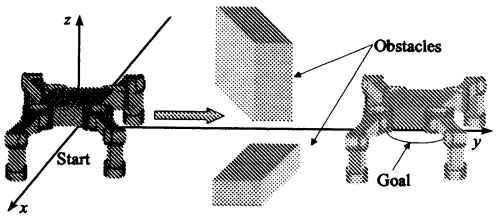


Figure 4: Setup of the environment

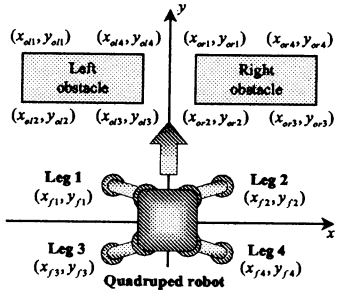


Figure 5: Coordinates of the robot's legs and the obstacle

tions for legs are set to (x_{f1}, y_{f1})=(−0.25, 0.3), (x_{f2}, y_{f2})=(0.25, 0.25), (x_{f3}, y_{f3})=(−0.25, −0.25), and (x_{f4}, y_{f4})=(0.25, −0.3) [m]. Positions of x- and y- coordinates of obstacles are shown in Table 1, where each row represents coordinate data combined to produce coordinates of any two obstacles. Height coordinates z_{or} and z_{ol} of obstacles are set to 0.06, 0.12, 0.3 [m], where data can be combined to produce a combination of heights. Coordinate $z_{or}(z_{ol}) = 0.3$ [m] implies that it is an obstacle the robot cannot get over, so that the combination of z_{or}=0.3 [m] and z_{ol}=0.3 [m] is not considered in simulation. One of the two obstacles is assumed to be the obstacle that the robot cannot get over, so that simulation is conducted for 96 obstacles.

3.2 Setup of fitness function

In simulation, connection weights of the lower NN and parameters (center and standard deviations) of RBFs are optimized by a GA so that the robot avoids obstacles and reaches the destination with a minimum number of walk cycles. The associated fitness function of an individual is defined by

$$fitness = \sum_{i=1}^{ob_n}(fitness_o + fitness_a + fitness_c) \quad (1)$$

whose solution is searched for as a minimization problem. ob_n is the number of environments considered in optimization. $fitness_o$ is an evaluation function associated with penalty for collision with an obstacle:

$$fitness_o = \begin{cases} 0.0, & \text{if there is no collision} \\ [x_{de}^2(k) + y_{de}^2(k)] \times 10, & \text{otherwise} \end{cases} \quad (2)$$

Walking stops if the robot collides with an obstacle. $fitness_a$ is an evaluation function related to joint constraints, i.e., whether each joint angle is in an admissible range or not:

$$fitness_a = \begin{cases} 0.0, & \text{if inside of the range} \\ [x_{de}^2(k) + y_{de}^2(k)] \times 10, & \text{otherwise} \end{cases} \quad (3)$$

Walking stops if the joint exceeds joint constraints. $fitness_c$ is an evaluation function related to walk cycles required to reach the destination, and given by

$$fitness_c = [x_{de}^2(k) + y_{de}^2(k)] \times \frac{T}{50} \quad (4)$$

where T denotes walk cycles required to move from the starting point to the destination while avoiding obstacles by stable walking. The maximum number of walk cycles $T_{\max}$ in one environment is set to 50 and walking stops if the walk cycles exceed $T_{\max}$.

Table 1: x- and y-directional coordinates of obstacles

No	x_{or1}	x_{or2}	x_{or3}	x_{or4}	x_{ol1}	x_{ol2}	x_{ol3}	x_{ol4}
1	0.5	0.1	0.1	0.5	−0.5	−0.1	−0.1	−0.5
2	0.5	0.1	0.1	0.5	−0.5	−0.2	−0.2	−0.5
3	0.5	0.2	0.2	0.5	−0.5	−0.1	−0.1	−0.5
4	0.5	0.2	0.2	0.5	−0.5	−0.2	−0.2	−0.5
No	y_{or1}	y_{or2}	y_{or3}	y_{or4}	y_{ol1}	y_{ol2}	y_{ol3}	y_{ol4}
1	0.85	0.65	0.55	0.75	0.86	0.66	0.65	0.85
2	0.85	0.65	0.66	0.86	0.75	0.55	0.65	0.85

4 Simulation Result

We set the initial distance errors at (x_{de}, y_{de})=(−0.15, 2.2) [m], and x- and y-directional coordinates of two obstacles at (x_{or1}, y_{or1})=(0.1, 0.85), (x_{or2}, y_{or2})=(0.1, 0.65), (x_{or3}, y_{or3})=(0.5, 0.66), (x_{or4}, y_{or4})=(0.5, 0.86), (x_{ol1}, y_{ol1})=(−0.5, 0.75), (x_{ol2}, y_{ol2})=(−0.5, 0.55), (x_{ol3}, y_{ol3})=(−0.2, 0.65), and (x_{ol4}, y_{ol4})=(−0.2, 0.85) [m], together with z-directional coordinates at z_{or}=0.12 and z_{ol}=0.3 [m]. Here, although a robot can get over a right-side obstacle, a left-side obstacle shall not be get over.

4.1 When the order of swing leg is fixed

The simulation result using the RBFNN of action determination without re-learning is shown in Fig. 6, where the order of swing leg was fixed. The number of walk cycles to the goal was 10 times, and the distance from the robot's c.g. to the destination point was $(x_{de}, y_{de}) = (0.068, -0.027)$ [m].

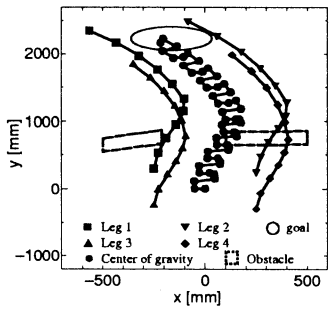


Figure 6: Movement path of the quadruped robot when fixing the order of swing leg

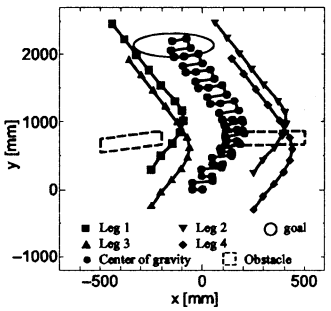


Figure 7: Movement path of the quadruped robot when changing the order of swing leg using RBFNN

4.2 When the order of swing leg is determined by RBFNN

The simulation result using the learned RBFNN of action determination is shown in Fig. 7, where the order of swing leg was determined by the RBFNN in Fig. 3. The number of walk cycles to the goal was 11 times, and the distance from the robot's c.g. to the destination point was $(x_{de}, y_{de}) = (0.018, -0.014)$ [m]. Moreover, the amount of movements of the robot and the order of swing leg are shown in Table 2. Here, the leg number used as swing leg is assigned as the left foreleg to 1, right foreleg to 2, left hind-leg to 3 and right hind-leg to 4. It is found that the order of swing leg changes with the amount of movements of the robot.

Table 2: The amount of movements of the robot when changing the order of swing leg using RBFNN

$\Delta Xr(k)$ [mm]	$\Delta Yr(k)$ [mm]	$\Delta\theta r(k)$ [degree]	$Zr(k)$ [mm]	Order of swing leg
45.379	198.899	−0.298	300.0	4→2→3→1
55.253	181.795	0.837	360.0	4→2→3→1
49.297	172.875	1.419	360.0	4→2→3→1
36.077	165.824	1.896	360.0	2→4→3→1
18.925	159.794	2.220	360.0	2→4→3→1
−0.386	155.208	2.319	360.0	2→4→1→3
−23.440	241.344	0.167	360.0	4→2→3→1
−23.620	239.286	0.087	300.0	4→2→3→1
−24.022	237.751	0.013	300.0	4→2→3→1
−24.397	236.259	−0.060	300.0	4→2→3→1
−24.746	234.816	−0.131	300.0	4→2→3→1

5 Conclusion

In order to acquire the obstacle avoidance action of quadruped robots with consideration to the order of swing leg, the action of a quadruped robot has been determined through an RBFNN, whose inputs were the destination information, the obstacle configurations, and the robot's self-state. Furthermore, the order of swing leg was determined from the amount of movements and the robot's body height by using an alternative NN. The NN for determining the robot's action is acquired by re-learning the NN that was built in the case when the order of swing leg was fixed. Compared to the case where the RBFNN without re-learning is used, the final distance error of the present approach to the destination was small; however the walk cycle was comparable to each other. It is attributed to the fact that a priority was assigned to the error distance in the evaluation of GA. For this reason, in order to make a walk cycle smaller, further fitness function of GA needs to be reexamined.

References

[1] T. Nakamura, M. Seki, Y. Mori and H. Adachi, "Free gait planning using Monte Carlo method for locomotion on rugged terrain," *1999 JSME Conference on Robotics and Mechatronics*, 1A1-42-061 (CD-ROM), 1999.

[2] T. Yamaguchi, K. Watanabe, K. Izumi and K. Kiguchi, "Acquisition of an obstacle avoiding path in quadruped robots," *J. of Advanced Computational Intelligence*, Vol. 7, No. 2, pp. 115–123, 2003.

[3] T. Yamaguchi, K. Watanabe, K. Izumi and K. Kiguchi, "Obstacle avoidance of quadruped robots with consideration to the order of swing leg," *2003 International Conference on Control, Automation and Systems*, TP08-2 (CD-ROM) 2003.

[4] M. Sakawa and M. Tanaka, *Introduction to Neurocomputing*, Tokyo, Morikita Shuppan Co., Ltd, pp. 97–116, 1999.

Proc. of The Ninth Int. Symp. on Artificial Life and Robotics (AROB 9th '04)
Beppu, Oita, Japan, 28-30 January, 2004

Coordination of Voice and Visual Information for Intelligently Cooperating Between Human and Robot

Kiyotaka Izumi, Yuya Tamano, Yoshiharu Nose and Keigo Watanabe
Dept. of Advanced Systems Control Engineering,
Graduate School of Science and Engineering, Saga University,
1-Honjomachi, Saga 840-8502, Japan

Abstract

In this paper, voice commands based on natural spoken language are used so that two or more same colored objects are tracked by a robot manipulator. More precisely, after receiving a voice command regarding the color information, the end-effector of the robot is controlled to approach a desired object out of many objects by visual feedback, in which the visual information is further applied to the human if a more correct motion of the robot will be required. Thus, the present objective is to obtain a smoother cooperative system between human and robot, by coordinating voice and visual information.

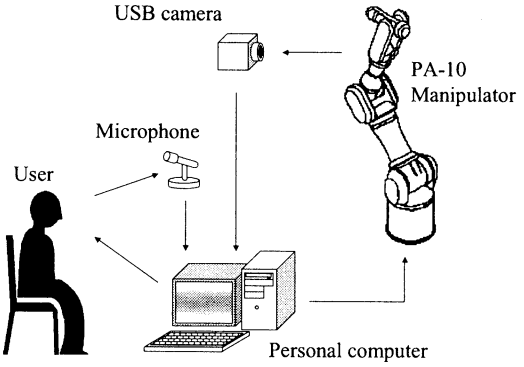


Figure 1: Experimental system setup

1 Introduction

In recent years, voice is used as an interface between human and robot or computer. For example, there are various amusement-type robots including a toy that can react to voice commands and some speech-recognition softwares are also sold. Such products, as an input device with voice to the computer, are now spreading in a general home. In the future, applications of such products are further expected to be enlarged to various fields such as home-appliances, welfare instruments, etc. As for the advantages that one uses voice to an interface, it is easily pointed out that 1) there are few burdens to users because we need not necessarily remember the special knowledge and operations on input devices such as keyboards and mouse; 2) it is an available interface to the man who has a handicap in hand and foot, old people, and the man whose both hands are closed by some manual operation; and 3) since it is a sociable interface ordinarily utilized by human beings, we can have an attached heart to a controlled object.

From the above backgrounds, attention has gathered also in the research of a robot control by voice commands [1]~[4]. However, in the conventional researches of a robot control by voice, it is difficult to apply for an actual task, because a user has to command by voice repeatedly with observing carefully the robot motion. In other words, a user provides many voice commands to the robot to perform an actual task.

In this paper, in order to achieve a cooperating between human and robot, we construct the voice interface with visual information. The effectiveness of the present method is illustrated through some simple experiments.

2 Construction of experimental system

The experimental system is constructed with a manipulator, a microphone, a USB camera and a personal computer, as shown in **Fig. 1**.

2.1 Manipulator

The manipulator is redundant type with 7 degrees-of-freedom which is called PA-10 by Mitsubishi Heavy Industries, Ltd. The control system bases on open architecture in which the operator can change the control input any time. The maximum length of the manipulator is 1345 [mm]. The weight of the manipulator is 35 [kgf]. The maximum operational weight of the manipulator is 10 [kgf]. The number of the type commands for the manipulator is

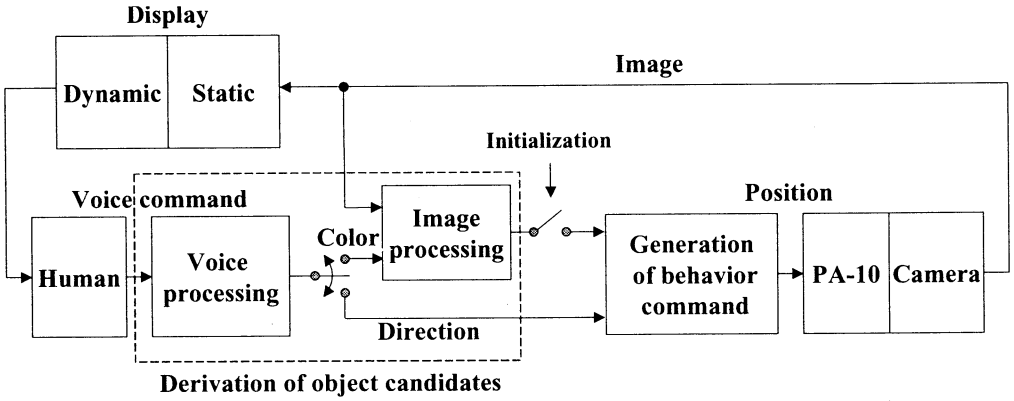


Figure 2: Construction of speech based interface with visual feedback

7, so that we use the position command in order to operate the manipulator in this research.

2.2 Voice recognition tool

The voice command from the user is collected through a microphone. Such voice is transformed to text by a software of speech recognition. The software is the ViaVoice for Windows Pro version 8 (Japanese Version) provided by IBM Co. Ltd. A Software Development Kit (SDK) to the ViaVoice is offered for developers.

2.3 Morphology analysis tool

A Japanese morphological analysis system is introduced to solve unique problems in Japanese. The system is called "ChaSen"[5], which was developed by Computational Linguistics Laboratory, Graduate School of Information Science, Nara Institute of Science and Technology (NAIST). The proposed system integrates the morphological analysis system by the dynamic link library (DLL) of ChaSen.

3 Construction of voice interface

The construction of proposed voice interface with vision is shown in **Fig. 2**. The proposed system is constructed with the derivation part of object candidates and the generation part of behavior command. The process that provides the manipulator a final command is listed as follows:

1. **Initialization of the generation part of behavior command:** A user command by voice is given for object's color at first. The environmental data is initialized with each geometric center of object candidates and the commanded color. The initial object is determined as the object which has minimum distance between the initial position of manipulator's tip and the geometric center of the object.
2. **Voice command:** If a user command is given for direction, then the derivation part of object candidates outputs the commanded direction to the generation part of behavior command. When a user command is given for the color which is different from that of the environmental data, the process returns 1.
3. **Generation of behavior command:** The generation part of behavior command provides the reference point of the manipulator's tip in the world coordinate depending on direction command and the environmental data. If a user doesn't command about direction, the reference point is held.

3.1 Derivation part of object candidates

The derivation part of object candidates is constructed with the voice processing part and the image processing part. The voice processing part is constructed with the voice recognition process, the morphology analysis and the pattern matching. The image processing creates the environmental data for the generation part of behavior command. The image process is carried out at initial stage or at changing the color of the object. The derivation part of object candidates outputs the commanded direction or the environmental data.

3.1.1 Voice processing

The voice processing part is constructed with a voice recognition process, a morphology analysis and a pattern matching.

Table 1: Basic word groups used for keywords

Basic word groups	Examples
Color	Red, Blue, Green, $\cdots$
Direction	Up, Down, Right, Left, *cdots*

Voice recognition process This process outputs the text data of the command by voice. The text data doesn't include a space such as English.

Morphological analysis This system divides a sentence to words in some unit forms, where such words to be divided are determined from the parts of speech by the system.

Pattern matching The pattern matching compares the results obtained from the morphological analysis with the basic word group that represents "color" and "direction", as shown in **Table 1**. The action command is determined from the combination of words that are the results of the pattern matching.

3.1.2 Image processing

Image processing part provides each geometric center of object candidates using an image and the voice command related to the color. The concrete process is as follows:

1. Get a color command from voice recognition part
2. Compare a brightness, a chrome saturation and a hue between the commanded color and the image
3. Calculate each shape of object candidates
4. Calculate each geometric center of object candidates

3.2 Derivation part of behavioral command

This part provides a reference point of the manipulator using all geometric centers of object candidates and the voice command related to the direction. Needless to say, the image coordinate is transferred to the world coordinate. If a user doesn't provide the voice command, then the reference point retains its value.

4 Experiments

Figure 3 shows the image when the system is started. A user observes the working environment by this image in

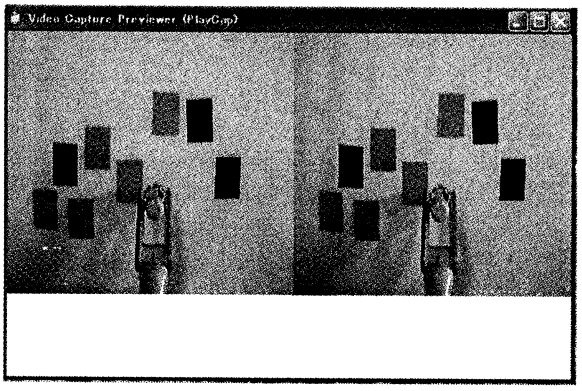


Figure 3: Starting view of the system

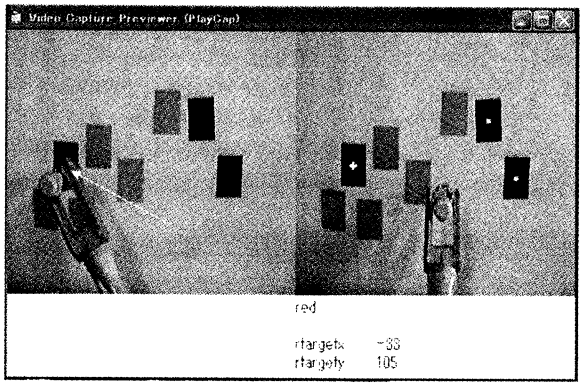


Figure 4: Initial movement

which the left image is a movie in the current working environment and the right image is the static image when the system was started. As shown in **Fig. 4**, when a user commands "red", right image shows + or □ on each geometric center of red colored objects, where + means the target object, whereas □ means the red colored objects except for the target object. A user can observe the command and the position of the target object at the image coordinate through the bottom area of the image. It is found from Fig. 4 that the manipulator moves to the target object. Next, when the user commands "move right", the target object is changed. The user confirms the desired object from + position in the right image and the displayed data at the bottom area as shown in **Fig. 5**. When the user commands "move down", it is found from **Fig. 6** that the user can perform the same fact as stated in Fig. 5. Finally, the user commands "move right" after completing the Fig. 4. The user selects a new target object on the manipulator's way to the former target object. The user can check the change of the target object

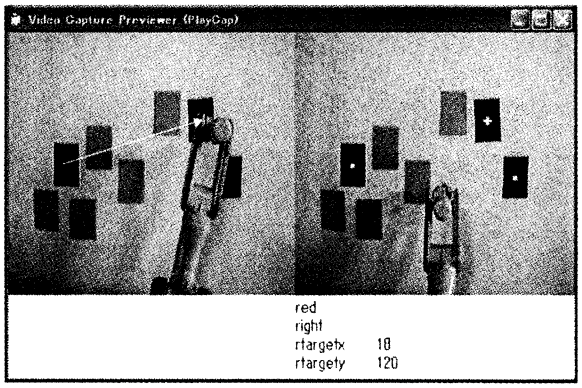


Figure 5: Result of voice command "move right"

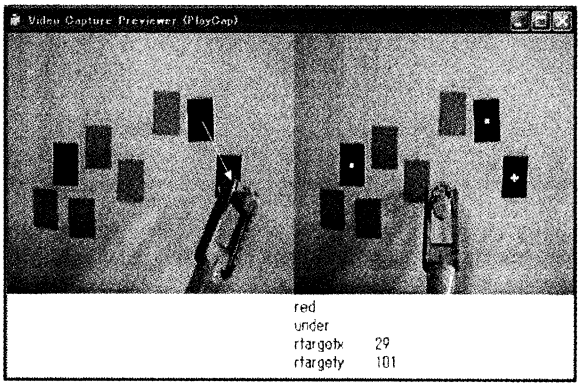


Figure 6: Result of voice command "move down"

in the right image and the movement of the manipulator in the left movie, as shown in **Fig. 7**. Note that, there are two object candidates in this case, but the right object which has minimum distance between the tip of manipulator and the object is selected.

5 Conclusions

The robot interface which can cooperate voice commands and visual information has been discussed in this paper. According to the use of the present system, it was easy to change the robot movement by voice command at any time. Simple experimental results showed that the present method can fuse the sense of hearing and the sense of sight. Additionally, it is easy to expand for teleoperational tasks.

In the future, the present method is applied for more actual tasks such as the object handling, surgery, etc.

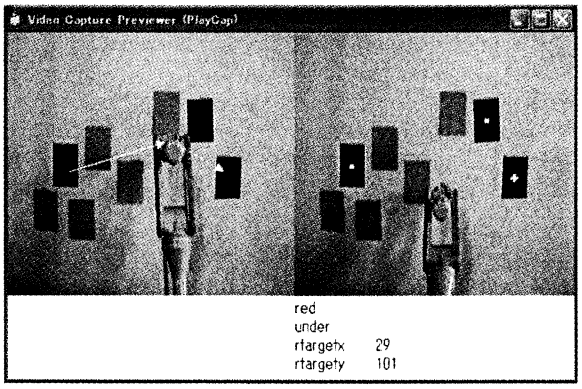


Figure 7: Result of voice command "move right" and "move down"

References

[1] K. Komiya, K. Moita, K. Kakegawa, and K. Kurosu, "Guidance of a Wheelchair by Voice," *Proc. of IECON'2000*, pp. 102–107 (2000)

[2] K. Pulasinghe, K. Watanabe, K. Kiguchi, and K. Izumi, "A Novel Modular Fuzzy Neural Controller Driven by Natural Language Commands," *Proc. of the 40th SICE Annual Conference (SICE2001), Int. Session Papers*, 312C-4, 2001.

[3] K. Pulasinghe, K. Watanabe, K. Kiguchi and K. Izumi, "Modular Fuzzy Neural Controller Driven by Voice Commands," *Proc. of ICCAS2001*, pp. 194–197, 2001.

[4] C.T. Lin and M.C. Kan, "Adaptive Fuzzy Command Acquisition with Reinforcement Learning," *IEEE Trans. on Fuzzy Systems*, Vol. 6, No. 1, pp. 102–121, 1998.

[5] Y. Matsumoto, A. Kitauchi, T. Yamashita, Y. Hirano, H. Matsuda, K. Takaoka, and M. Asahara, "Morphological Analysis System ChaSen version 2.2.9 Manual," http://chasen.aist-nara.ac.jp/chasen/doc/chasen-2.2.9.pdf, 2002.

Proc. of The Ninth Int. Symp. on Artificial Life and Robotics (AROB 9th '04)
Beppu, Oita, Japan, 28-30 January, 2004

Fuzzy Hint Acquisition for the Inverse Kinematic Solution of Redundant Manipulators Using Neural Network -Tracking Unknown Enclosed Trajectory-

Samy F. M. Assal, Keigo Watanabe, and Kiyotaka Izumi
Department of Advanced Systems Control Engineering,
Graduate School of Science and Engineering, Saga University
1-Honjomachi, Saga 840-8502, Japan.
Tel: +81-952-28-8602; Fax: +81-952-28-8587
s_assal2000@yahoo.com, {watanabe,izumi}@me.saga-u.ac.jp

Abstract

A novel sensor-based position control system for redundant manipulator is proposed. A laser transducer at the end effector rotating in a gyroscopic motion to scan the enclosed space for on line planning the trajectory is proposed. A back propagation neural network is presented for the inverse kinematic problem. Since the inverse kinematics has infinite number of joint angle vectors, a fuzzy logic system is designed to generate an approximate value for that vector, which is considered as a hint and fed into the neural network as a second input vector rather than as a training example to limit and guide the searching space. Simulations are implemented on a three-link redundant planar manipulator. The proposed control system is shown to be capable of tracking the planned trajectory while avoiding the collision. This is due to the ability that appeared for the neural network to follow the hint that generated from the fuzzy system. Neither discontinuity nor highly abrupt change is appeared in the joint angle profiles, which verifies good performance of the control system.

1 Introduction

Kinematically redundant manipulators are those that have more degrees of freedom than that required for a given task. Such manipulators offer several advantages over non-redundant ones in many aspects such as singularity and obstacles avoidance, keeping the joints within their limits and torque optimization. Those objectives are used as a second subtasks while the end-effector tracking is the first. Obstacle avoidance is the most important investigating subtask for those manipulators. This problem can be solved either off-line or on-line. Off-line obstacle avoidance is specified as, given the end-effector trajectory, a set of obstacles in space and initial manipulator configuration, then require the joint trajectory for the obstacle avoidance. This approach needs expensive computations for global path planning before the manipulator starts its motion. On the other hand, on-line obstacles avoidance enables those manipulators to move in an unstructured environment including both fixed and moving obstacles without collision depending on local path planning which is based on sensor information.

An adaptive fuzzy logic approach for obstacles avoidance in an environment with a given end-effector trajectory and a set of obstacles is proposed in [1]. A minimum distance from the obstacles, which is taken to be greater than a preplanned threshold distance, is proposed as a criterion for the obstacles avoidance. A neural network approach to solve the inverse kinematics problem in an environment with obstacles is introduced in [2]. Training patterns for both obstacle free and obstacle avoidance cases have been developed. The training algorithm is augmented with a distance penalty function for obstacles avoidance case. On the other hand, several strategies have been developed for on-line problem. Collision avoidance using reflex control is proposed in [3]. It describes enhancements to reflex control through the use of a higher level attractive potential function which helps to guide the reflexes for simultaneous goal attraction and obstacle avoidance. For the real-time collision avoidance proposed in [4], the obstacles avoidance requirement is represented as inequality constraints in the workspace and those inequalities are satisfied while the end-effector tracks the desired trajectory. The scheme is based on the implementation of the configuration control. A new approach based on velocity potential function is proposed in [5] for the repulsive function, which has no local minima even for a cluttered environment. A kinematic control algorithms, which is based on the re-

dundancy resolution at the velocity level is proposed in [6]. The obstacles avoidance strategy is to assign each point on the manipulator, which is close to the obstacle, a velocity component in a direction that is away from the obstacle.

In this paper, a new concept for on-line planning and tracking enclosed unknown trajectory is introduced. The proposed method for planning the trajectory using the exploring sensor is presented in Section 2. The concept of limiting the searching space using the hint generator is presented in Section 3. In Section 4, simulation results are presented. Finally, concluding remarks are given in Section 5.

2 The Proposed Solution

The proposed solution depends on using a laser transducer at the end-effector as shown in Fig. 1. This transducer rotates in a two-axis gyroscopic motion to scan the enclosed space for the maximum distance. First, at the starting point of the enclosed space, the transducer is used to measure the distance in two perpendicular directions in order to adjust the end-effector approximately at the origin of the entrance to the enclosed space. After that, the transducer is used to scan the enclosed space; then record the angle γ_y for the plan that has the maximum distance; and within this plan record the angle γ_z that corresponds to the direction of half the way of the rang of equal maximum distance. Those two angles (γ_y, γ_z) define the orientation of the planned trajectory with respect to the mechanical interface coordinate system throughout the enclosed space.

A unit vector $\boldsymbol{p}_{ti}$ along each segment of the planned trajectory, with respect to the mechanical interface coordinate system can be determined by rotating a unit vector along X_e -axis direction $\boldsymbol{p}_s$, which represents the initial position of the transducer, an angle γ_{yi} around Y_e -axis then an angle γ_{zi} around Z_e -axis such that:

$$\begin{aligned} \boldsymbol{p}_{ti} &= R_z(\gamma_{zi})R_y(\gamma_{yi})\boldsymbol{p}_s \\ &= \begin{bmatrix} \cos\gamma_{zi}\cos\gamma_{yi} \\ \sin\gamma_{zi}\cos\gamma_{yi} \\ -\sin\gamma_{yi} \end{bmatrix} \end{aligned} \tag{1}$$

where i is the index for the segment number.

Definition 1 *The cone angles (ψ_i): they are the angles between each link being inside the enclosed space and the corresponding intersected segment of the line defining the planned trajectory as shown in Fig. 2. They are defined for the measure of the most dexterous configuration before going inside (ψ angle) and for the criterion of the collision avoidance while going inside (ψ_1 and ψ_2 angles). The maximum limit of the cone angles (ψ_i) is*

$$\psi_{i_{max}} = \sin^{-1}\left(\frac{d_r}{2l_i}\right)$$

where d_r is bore diameter of the enclosed space and l_i is the length of link i. At the entrance, the cone angle ψ can be calculated by using the dot product of a two unit vectors: the first is $\boldsymbol{p}_{t1}$ while the second is a unit vector along X_e-axis of the end link $\boldsymbol{p}_e = [1 \quad 0 \quad 0]^T$ such that

$$\begin{aligned} \psi &= \cos^{-1}\frac{\boldsymbol{p}_{t1}\cdot\boldsymbol{p}_e}{\|\boldsymbol{p}_{t1}\|\ \|\boldsymbol{p}_e\|} \\ &= \cos^{-1}(\cos\gamma_{z1}\cos\gamma_{y1}) \end{aligned} \tag{2}$$

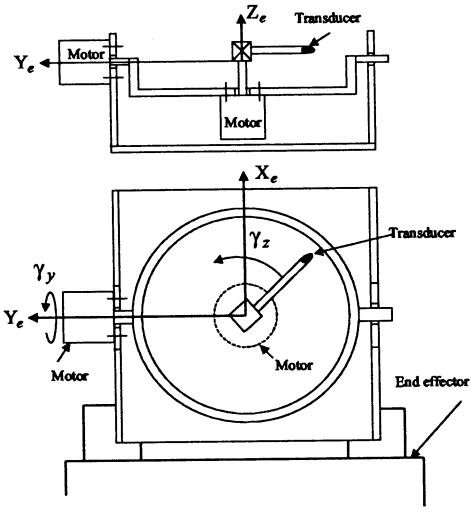


Figure 1: Construction of the exploring sensor

Definition 2 *The ϕ_i angles: they are the angles between each consequent intersected segment of the multi-segment line defining the planned trajectory. They can be calculated by using the dot product of two unit vectors along each segment, considering the first segment of the trajectory as a reference and has $\phi_1 = 0$. Representing $\boldsymbol{p}_{ti}$ with respect to the base coordinate, ϕ_i angles can be calculated as:*

$$\phi_{i+1} = \cos^{-1}\frac{\boldsymbol{p}^b_{ti}\cdot\boldsymbol{p}^b_{t(i+1)}}{\|\boldsymbol{p}^b_{ti}\|\ \left\|\boldsymbol{p}^b_{t(i+1)}\right\|} \tag{3}$$

where

$$\boldsymbol{p}^b_{ti} = R^e_0\boldsymbol{p}_{ti}$$

in which R^e_0 is the rotational matrix.

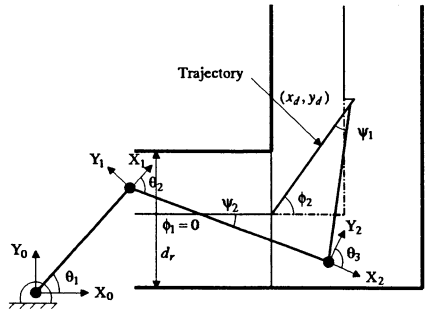


Figure 2: Task and parameters description

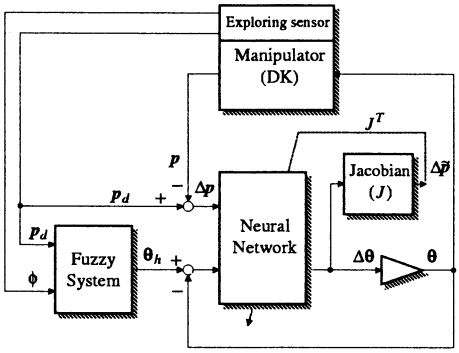


Figure 3: The proposed control system

3 Problem Formulation

The task under consideration is to control the manipulator to track an enclosed unknown trajectory. This problem is a kind of inverse kinematic problem of redundant manipulator; given the Cartesian coordinate values of the end-effector, search the joint angles to avoid the collision with the enclosed space. The proposed control system is shown in Fig. 3, where $\boldsymbol{p_d} = [x_d \quad y_d]^T$ is the desired Cartesian vector of the end-effector position.

The fuzzy system works as a hint generator. A hint is an approximate solution of the inverse kinematic problem. Especially, the fuzzy system generates approximate values of the joint angles of the manipulator. Those values are within the values required to avoid the collision with the enclosed space. They are fed to the neural network, which works as the inverse of the kinematic problem as a second input vector rather than as training examples [7]. The fuzzy system is designed based on considering the cone angle around the planned trajectory as a criterion for the collision avoidance. Since the inverse kinematics of redundant manipulator has infinite number of solutions, the hints generated from the fuzzy system are fed into the neural network to limit the searching space, to accelerate and to improve the quality of the solution. Unfortunately, the fuzzy system can generate values only for each link being inside the enclosed space; therefore, we substitute for the rest of the joint angle values by their previous values and then train the neural network to obtain the correct values.

Concisely, whenever the explorer plans different trajectory, the fuzzy system accordingly on-line generates different hints to the neural network to give the appropriate solution.

Moreover, from the mathematical point of view, the problem can be visualized as a solution of the following nonlinear equation:

$$\boldsymbol{x} = \boldsymbol{f}(\boldsymbol{\theta}) \tag{4}$$

where

$\boldsymbol{x} \in \Re^m$: m dimensional Euclidean space
$\boldsymbol{\theta} \in \Re^n$: n dimensional joint space.

Linearizing this equation by considering small displacement about the current configuration, we obtain

$$\Delta \boldsymbol{x} = J \Delta \boldsymbol{\theta} \tag{5}$$

where $J = \frac{\partial \boldsymbol{f}}{\partial \boldsymbol{\theta}}$: $m \times n$ Jacobian matrix.

For redundant manipulator, $m < n$ and J is of full rank, so that the system has infinite number of solutions.

The general solution of equation (5) is given by

$$\Delta \boldsymbol{\theta} = J^+ \Delta \boldsymbol{x} + (I - J^+ J)\boldsymbol{y} \tag{6}$$

where $\boldsymbol{y}$ is an arbitrary vector and J^+ is the pesudoinverse of the Jacobian matrix.

If the utilization of redundancy will not be considered, the solution can be given by the first term only as in equation (7), which is the least square solution with minimum norm for the joint angle:

$$\Delta \theta = J^+ \Delta \boldsymbol{x} \tag{7}$$

This solution can be replaced by a neural network with $\Delta \boldsymbol{x}$ as input vector and $\Delta \boldsymbol{\theta}$ as output vector.

On the other hand, if the utilization of redundancy will be considered, the solution can be given by equation (6) where the second term represents the set of all vectors in the null space of the Jacobian, i.e., do not produce any change in the end-effector. This equation has two input vectors $\Delta \boldsymbol{x}$ and $\boldsymbol{y}$ for sharing the output vector $\Delta \boldsymbol{\theta}$. Therefore, a neural network with two input vectors and one output vector can replace this equation. The first input vector is the differential change of the Cartesian coordinate values of the

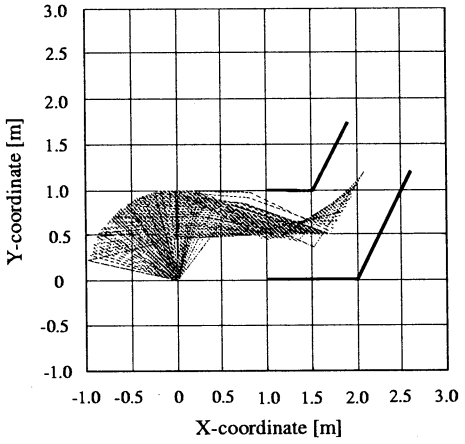
end-effector while the second, the arbitrary one can be chosen to represent the desirable joint angle vector to avoid the collision with the enclosed space; it can also be obtained from the fuzzy system and presented on-line as a hint to the neural network to search for the suitable solution.

4 Simulation Results

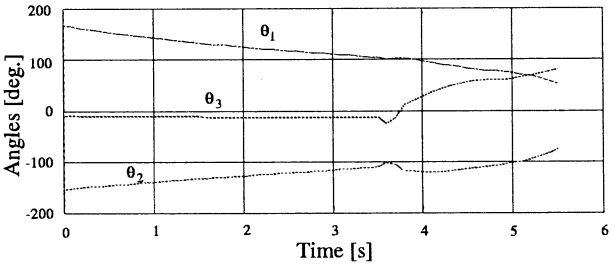
Simulations have been conducted based on three-link planar manipulator with three revolute joints. Each link has a length of 1 [m]. The simulation results are presented to demonstrate the performance of the proposed position control system for redundant manipulator to track unknown enclosed trajectory. The objective is to simulate the redundant manipulator while going inside an enclosed space specified as a bended tube of a bore diameter of 1 [m]. The first portion of the tube is a straight line along X-axis while the second portion is bended with different inclined angles in positive direction as well as negative one. Figure 4 represents the simulation results; the manipulator successive configurations throughout the planned trajectory are represented in Fig. 4(a), while the joint angle profiles are represented in Fig. 4(b). The results demonstrate the efficacy of the proposed control system to track the trajectory while avoiding the collision with the environment. This performance is due to the ability that appeared for the neural network to follow the hint generated from the fuzzy system. Neither discontinuity nor highly abrupt change is appeared in the joint angle profiles, which verifies good performance of the proposed control system.

5 Conclusions

The problem of on-line planning and tracking an enclosed unknown trajectory while avoiding the collision with the environment has been addressed in this paper. A novel sensor-based position control system for redundant manipulator was designed to provide dexterous motion of that manipulator. The results verified good performance of the proposed control system.



(a) Manipulator configurations



(b) Joint angle profiles

Figure 4: Simulation results

References

[1] M. T. H. Beheshti and A. K. Tehranl, "Obstacle avoidance for kinematically redundant robots using an adaptive fuzzy logic algorithm," In *Proc. the American Control Conf.*, San Diego, California, June, 1999, pp. 1371–1375.

[2] M. Ziqiang and T. C. Hsia, "Obstacle avoidance inverse kinematics solution of redundant robots by neural networks," *Robotica*, Vol. 15, Jan–Feb, 1997, pp. 3–10.

[3] T. S. Wikman and W. S. Newman, "A fast, on-line collision avoidance method for a kinematically redundant manipulator based on reflex control," In *Proc. IEEE Int. Conf. Robot. and Automat.*, 1992, pp. 261–266

[4] K. Glass, R.. Colbaugh, D. Lim and H. Seraji, "Real-time collision avoidance for redundant manipulators," *IEEE Trans. on Robot. and Automat.*, Vol. 11, No. 3, June, 1995, pp. 448–257.

[5] W. J. Cho and D. S. Kwon, "A sensor-based obstacle avoidance for a redundant manipulator using a velocity potential function," In *Proc. IEEE Int. workshop on Robot and Human communication,* 1996, pp. 306–310.

[6] L. Zlajpah and B. Nemec, "Kinematic control algorithms for on-line obstacle avoidance for redundant manipulators," In *Proc. IEEE/RSJ Int. Conf. On Intelligent Robots and Systems,* Lausanne, 2002, pp. 1898–1903.

[7] Y. S. Abu-Mostafa, "A method for learning from hints," In *Advances in Neural Information Processing Systems*, Vol. 5, 1993, pp. 73–80.

Proc. of The Ninth Int. Symp. on Artificial Life and Robotics (AROB 9th '04)
Beppu, Oita, Japan, 28-30 January, 2004

Statistical micro mechanical method for dynamic kinetic binary Interaction among biomolecules with moderate density.

Hirohumi, Hirayama.
Department of Health Science, Asahikawa medical college.
hirayama@asahikawa-med.ac.jp

Abstract.
Statistical thermodynamical approach for moderate dense bio molecular particles system have been introduced to calculate local viscosity and thermal flux In the biological reaction system. The present approach will be available for evaluating the biological reaction rate and local movement of biological particles.

1.Introduction.

Biological reactions can be described by statistical thermodynamical approach because of the biological particles can be regarded as assembly of statistical identical molecules. In actual local physical reactions, the concentration of biological species are not uniform not dilute but can be regarded as a moderate to dense system. Thus, there may be thermodynaical gradient and equilibrium equations are not adequate to describe the reaction. The present paper applies statistical method [1,2] to calculate viscosity and thermal flux for moderate dense biological particles system.

2. Mathematical method.

2-1.Modified Boltzmann equation.

We consider the system consisted of $N\alpha$ molecules of species α and $N\beta$ molecules of species β .The system can be expressed by the normalized specific distribution function $f(N)(R(N),p(N),t)$. $R(N)$ and $p(N)$ represent the N position and N momentum vectors $R\alpha 1, R\alpha 2---, R\alpha N\alpha$ $R\beta 1, R\beta 2--, R\beta N\beta$.$p\alpha 1, p\alpha 2--, p\alpha N\alpha$,$p\beta 1, p\beta 2---, p\beta N\beta$. The most important problem is to determine the singlet distribution function

$$f^{(1)}(R\alpha 1, p\alpha 1, t)$$

where the n body reduced distribution function is

$$f^{(n)}(R\alpha^{(n)}, R\beta^{(m)}, p\alpha^{(n)} p\beta^{(m)}; t) = 1/[(N\alpha - m)!(N\beta - s)!]\, f^{(N)}(R^{(N)}p^{(N)};t)\, dR^{(N-n)} dp^{(N-m)} \quad -(1)$$

The Liouville equation is

$$\partial f^{(N)} / \partial t + \Sigma[(pk/mk)\cdot\nabla_{Rk} f^{(N)} + Fk\cdot\nabla_{pk} f^{(N)}] = 0 \quad -(2)$$

where Fk is the force acting on molecule k due to all other molecules in the system. The sums extended over the both species and molecular number. To obtain the differential equation satisfied by the singlet distribution function of species α, the Liouville equation is reduced by (N-2) fold integration and the use of Green theorem. The result of the reduction is

$$\partial f^{(1)} / \partial t + (p\alpha 1/m\alpha 1)\cdot\nabla_{R\alpha 1} f^{(1)}(R\alpha 1, p\alpha 1; t) = -1/(N\alpha - 1)\int \Sigma(N\alpha - \delta_{\alpha\beta}) F1j^{\alpha\beta}\cdot\nabla_{p\alpha} f^{(2)}(R1\alpha, R2\beta, p1\alpha, p2\beta; t)\, dR2\beta\, dp2\beta \quad ----(3)$$

Defining a coarse grained distribution function by

$$Gf^{(N)} = 1/\tau \int f^{(N)}(R^{(N)}p^{(N)};t+s)\, ds \quad ---(4)$$

where τ is the interval of coarse graining. Defining a phase space distribution function

$$f^{(N)}(R^{(N)}p^{(N)};t+s) = \int\int\int K^{(N)}(R^{(N)}p^{(N)} / R'^{(N)}p'^{(N)};s)\, f^{(N)}(R'^{(N)}p'^{(N)};t)\, dR'^{(N)} dp'^{(N)} \quad ---(5)$$

where $K^{(N)}$ satisfies the Liouville equation and (3) becomes

$$Lf^{(1)}(\alpha,1) = -1/((N\alpha - 1)\tau)\int \Sigma(N\alpha - \delta_{\alpha\beta}) F1j^{\alpha\beta}\cdot \nabla_{p\alpha} K^{(2)}(s) f^{(2)}(R'1\alpha, R'2\beta, p'1\alpha, p'2\beta; t)\, ds\, dR2\beta\, dp2\beta\, dR'1\alpha\, dR'2\beta\, dp'1\alpha\, dp'2\beta \quad ----(6)$$

The pair transition probability $K^{(2)}(s)$ is obtained as a solution of the integrated Liouville equation.

$$\Sigma[\partial K^{(2)}(s) / \partial s + p\alpha 1/m\alpha 1\cdot\nabla_{R\alpha 1} K^{(2)}(s) = -\int \Sigma[F1j^{\alpha\beta}\cdot\nabla_{p1j} + F2j^{\alpha\beta}\cdot\nabla_{p2j} K^{(2)}(s)]dR^{(N-2)} dp^{(N-2)} \quad ---(7)$$

We consider only the binary collision. The right side of Eq(7) vanishes and solution is

$$K^{(2)}(R1\alpha, R2\beta, p1\alpha, p2\beta / R'1\alpha, R'2\beta, p'1\alpha, p'2\beta; s) = \Pi\, \delta(Rik - R'1k - \Delta R'1k)\, \delta(pik - p'1k - \Delta p'1k) \quad ---(8)$$

where the increments in momenta and positions are to be evaluated from the dynamics of the two body collision. Because of the use of (8), Eq(7) is only valid in $\tau \to 0$,. The time integral of duration + 0 can not allow the centers of the mass of the colliding particles to move apart so that integrating Eq(6)

$$LCf^{(1)}(\alpha,1) = -1/((N\alpha - 1)\tau) \int \Sigma(N\beta - \delta_{\alpha\beta})(f^{(2)}(R1\alpha, R2\beta, p1\alpha - \Delta p1\alpha, p2\beta - \Delta p2\beta; t) - f^{(2)}(R1\alpha, R2\beta, p1\alpha, p2\beta; t))\, ds\, dR2\beta\, dp2\beta \quad ----(9)$$

with the positions of the colliding molecules the same before and after the collision. The integration over the volume is replaced by an integration over the collision cylinder specified by the impact parameter b, the azimuthal angle epsilon ε and the relative velocity $p1\alpha 2\beta / \mu\alpha\beta$ where $\mu\alpha\beta$ is the reduced mass of the colliding pair. Defining the pair correlation function

$$g^{(2)}(R1, R2, p1, p2; t) = f^{(2)}(R1, R2, p1, p2; t) / [f^{(1)}(R1, p1; t) f^{(1)}(R2, p2; t)] \quad ---(10)$$

is introduced into Equ (9), The modified Boltzmann equation becomes after a second time smoothing

$$LG^{(m)}(\alpha,1)=-1/((N_\alpha-1)\tau)\int p_{12\alpha\beta}/\mu_{\alpha\beta}\Sigma(N_\beta-\delta_{\alpha\beta})$$
$$g_0^{(m)}(\sigma_{\alpha\beta})(G^{(m)}(R_{1\alpha},p_{1\alpha}-\Delta p_{1\alpha})G^{(m)}(R_{2\beta},p_{2\beta}-\Delta p_{2\beta};t)$$
$$-f^{(1)}(R_{1\alpha},p_{1\alpha};t)f^{(m)}(R_{2\beta},p_{2\beta};t))\,b_{\alpha\beta}db_{\alpha\beta}d\varepsilon\,dp_{2\beta}\quad\text{----(11)}$$

2-2. Solution of the modifies Boltzmann equation.

When the gradients of temperature, velocity and concentration are small, the distribution functions are slowly varying function of the position coordinates. Under such conditions, the Taylor's expansion gives,

$$G^{(m)}(R_{2\beta},p_{2\beta};t)=G^{(m)}((R_{1\alpha},p_{2\beta};t)$$
$$+\sigma_{\alpha\beta}k\cdot\nabla_{R1\alpha}G^{(m)}(R_{1\alpha},p_{2\beta};t)\quad-(12)$$

Eq(12) is used to simplify Eq(11). k is a unit vector directed along the line of centers on the contact between two particles. For the perturbation to the equilibrium distribution function,

$$G^{(m)}(R_{1\alpha},p_{1\alpha};t)=G_0^{(m)}(1_\alpha)(1+\Phi_{1\alpha})\quad-(13\text{-}a)$$
$$G^{(m)}(R_{1\alpha},p_{1\alpha}-\Delta p_{1\alpha};t)=G_0^{(m)*}(1_\alpha)(1+\Phi_{1\alpha}{}^*)\quad-(13\text{-}b)$$

where asterisk indicates quantity after the collision. The unperturbed distribution function $f_0^{(m)}$ is chosen to correspond to the local equilibrium in coordinate and momentum space,

$$G_0^{(m)*}(1_\alpha)=(2\pi m_\alpha kT)^{-3/2}/v_\alpha)\exp(-[p_{1\alpha}-m_\alpha u]^2/(2m_\alpha kT)$$
$$\text{--(14)}$$

with u and $1/v_\alpha$ the local hydrodynamic velocity and local concentration. Using equ(12), (13) and (14) in Eq(11) and neglecting the second order terms result in

$$LG^{(m)}(\alpha,1)=\Sigma(N_\beta-\delta_{\alpha\beta})/(N_\alpha-1)\,g_0^{(m)}(\sigma_{\alpha\beta})\int\int$$
$$G_0^{(m)}(1_\alpha)G_0^{(m)}(2_\beta)\,p_{12\alpha\beta}/\mu_{\alpha\beta}([\Phi_{1\alpha}{}^*+\Phi_{2\beta}{}^*-\Phi_{1\alpha}$$
$$+\Phi_{2\beta}]+k\sigma_{\alpha\beta}\cdot[(1/2kT^2)m_\beta[p_{12\alpha\beta}/\mu_{\alpha\beta}\cdot k]^2$$
$$-2[p_{12\alpha\beta}/\mu_{\alpha\beta}\cdot k]k\cdot[p_{2\beta}-m_\beta u]\nabla_{R1\alpha}T+k\sigma_{\alpha\beta}\cdot$$
$$[-m_\beta/kT[p_{12\alpha\beta}/\mu_{\alpha\beta}\cdot k]k\cdot\nabla_{R1\alpha}u]]b_{\alpha\beta}db_{\alpha\beta}d\varepsilon\,dp_{2\beta}$$
$$\text{----(15)}$$

The equation of changes are given by

$$\partial v_\alpha/\partial t=v_\alpha\cdot\nabla_{R1\alpha}u/v_\alpha\quad\text{----(16-a)}$$
$$\partial u/\partial t=-u\cdot\nabla_{R1\alpha}u-1/\rho\,\nabla_{R1\alpha}p\quad\text{----(16-b)}$$
$$\partial T/\partial t=-u\cdot\nabla_{R1\alpha}T-(T/2Cv)\Sigma v_\alpha\,\partial p/\partial t\,\rho\,1:\nabla_{R1\alpha}u$$
$$\text{----(16-c)}$$

These result in

$$LG^{(m)}(\alpha,1)=f_0^{(m)}(1_\alpha)[2b_{1\alpha}$$
$$+(v/Cv(\partial p/\partial T)_\rho 3/2)(3/2-W_{1\alpha}{}^2 1):\nabla_{R1\alpha}u$$
$$+(3/2-W_{1\alpha}{}^2 1)([p_{1\alpha}/m_\alpha-u]\cdot\nabla_{R1\alpha}\mathrm{Log}T$$
$$+\{(1/\rho)(2m_\alpha/kT)^{1/2}\nabla_{R1\alpha}p-(2kT/m_\alpha)^{1/2}\nabla_{R1\alpha}\mathrm{Log}v_\alpha\}\cdot W_{1\alpha}]$$
$$\text{---(17)}$$

where ρ is the density, v is the mean volume velocity

$$v=(v_\alpha+v_\beta)\quad\text{---(18-a)}$$
$$W_{1\alpha}=(m_\alpha/kT)^{1/2})[p_{1\alpha}/m_\alpha-u]\quad\text{--(18-b)}$$
$$b_{1\alpha}=W_{1\alpha}W_{1\alpha}-1/3W_{1\alpha}{}^2 1\quad\text{--(18-c)}$$

To complete the formulation of the linearized transport equation, the integrals in Equ(15) must be evaluated. If a polar coordinate system is chosen with $p_{12\alpha\beta}/\mu_{\alpha\beta}$ along the polar axis. Collecting all the terms, the complete linearized equations are

$$\Sigma(N_\beta-\delta_{\alpha\beta})/(N_\alpha-1)\,g_0^{(m)}(\sigma_{\alpha\beta})\int\int G_0^{(m)}(1_\alpha)G_0^{(m)}(2_\beta)$$
$$p_{12\alpha\beta}/\mu_{\alpha\beta}[\Phi_{1\alpha}{}^*+\Phi_{2\beta}{}^*-\Phi_{1\alpha}+\Phi_{2\beta}]\,b_{\alpha\beta}db_{\alpha\beta}d\varepsilon\,dp_{2\beta}$$
$$=G_0^{(m)}(1_\alpha)[2b_{1\alpha}+(v/Cv(\partial p/\partial T)_\rho 3/2)(3/2-W_{1\alpha}{}^2 1)$$
$$:\nabla_{R1\alpha}u+(3/2-W_{1\alpha}{}^2 1)([p_{1\alpha}/m_\alpha-u]\cdot\nabla_{R1\alpha}\mathrm{Log}T$$
$$+\{(1/\rho)(2m_\alpha/kT)^{1/2}\nabla_{R1\alpha}p-(2kT/m_\alpha)^{1/2}\nabla_{R1\alpha}\mathrm{Log}v_\alpha\}\cdot W_{1\alpha}]$$
$$+\Sigma(N_\beta-\delta_{\alpha\beta})/(N_\alpha-1)g_0^{(m)}(\sigma_{\alpha\beta})[\int m_\alpha/(kT)G_0^{(m)}$$
$$(1_\alpha)G_0^{(m)}(2_\beta)\nabla_{R1\alpha}u:[4\pi\sigma_{\alpha\beta}{}^3/15(p_{12\alpha\beta}/\mu_{\alpha\beta})$$
$$(p_{12\alpha\beta}/\mu_{\alpha\beta})+2\pi\sigma_{\alpha\beta}{}^3/15(p_{12\alpha\beta}/\mu_{\alpha\beta})^2 1]]]dp_{2\beta}-1/(kT^2)$$
$$\int G_0^{(m)}(1_\alpha)G_0^{(m)}(2_\beta)\nabla_{R1\alpha}\mathrm{Log}(T)\cdot[m_\alpha 3\pi\sigma_{\alpha\beta}{}^3$$
$$/15(p_{12\alpha\beta}/\mu_{\alpha\beta})^2(p_{12\alpha\beta}/\mu_{\alpha\beta})-2\pi\sigma_{\alpha\beta}{}^3/15$$
$$[p_{2\beta}-m_\beta u](p_{12\alpha\beta}/\mu_{\alpha\beta})^2 1-4\pi\sigma_{\alpha\beta}{}^3/15$$
$$[p_{2\beta}-m_\beta u](p_{12\alpha\beta}/\mu_{\alpha\beta})(p_{12\alpha\beta}/\mu_{\alpha\beta})]dp_{2\beta}\quad\text{----(19)}$$

The perturbation to the distribution function is

$$\Phi_{1\alpha}=-A_{1\alpha}\cdot\nabla_{R1\alpha}\mathrm{Log}T-B_{1\alpha}:\nabla_{R1\alpha}u+C_{1\alpha}\cdot\gamma_{1\alpha}$$
$$\text{----(20)}$$
$$\gamma_{1\alpha}=1/\rho(2m_\alpha/kT)^{1/2}\nabla_{R1\alpha}p-(2kT/m_\alpha)^{1/2}\nabla_{R1\alpha}\mathrm{Log}v_\alpha$$
$$\text{---(21)}$$

Substituting (20) into (19), we have

$$\Sigma(N_\beta-\delta_{\alpha\beta})/(N_\alpha-1)\,g_0^{(m)}(\sigma_{\alpha\beta})\int\int G_0^{(m)}(1_\alpha)$$
$$G_0^{(m)}(2_\beta)p_{12\alpha\beta}/\mu_{\alpha\beta}[A_{1\alpha}{}^*+A_{2\beta}{}^*-A_{1\alpha}+A_{2\beta}]$$
$$b_{\alpha\beta}db_{\alpha\beta}d\varepsilon\,dp_{2\beta}=K_\alpha\quad\text{---(22)}$$

$$\Sigma(N_\beta-\delta_{\alpha\beta})/(N_\alpha-1)\,g_0^{(m)}(\sigma_{\alpha\beta})\int\int G_0^{(m)}(1_\alpha)$$
$$G_0^{(m)}(2_\beta)p_{12\alpha\beta}/\mu_{\alpha\beta}[B_{1\alpha}{}^*+B_{2\beta}{}^*-B_{1\alpha}+B_{2\beta}]$$
$$b_{\alpha\beta}db_{\alpha\beta}d\varepsilon\,dp_{2\beta}=L_\alpha\quad\text{---(23)}$$

$$\Sigma(N_\beta-\delta_{\alpha\beta})/(N_\alpha-1)\,g_0^{(m)}(\sigma_{\alpha\beta})\int\int G_0^{(m)}(1_\alpha)G_0^{(m)}(2_\beta)$$
$$p_{12\alpha\beta}/\mu_{\alpha\beta}[C_{1\alpha}{}^*+C_{2\beta}{}^*-C_{1\alpha}+C_{2\beta}]$$
$$b_{\alpha\beta}db_{\alpha\beta}d\varepsilon\,dp_{2\beta}=M_\alpha\quad\text{---(24)}$$

To evaluate the coefficients A, B, and C, the right sides of Equ (22) and (23) have to be integrated. Let the mole fraction of component α be $x_\alpha=N_\alpha/N$.

$$K_\alpha=G_0^{(m)}(1_\alpha)[(2kT/m_\alpha)^{1/2}(3/2-W_{1\alpha}{}^2)W_{1\alpha}+g_0^{(m)}(\sigma_{\alpha\alpha})\pi\sigma_{\alpha\alpha}$$
$$^2/(15v_\alpha)(2kT/m_\alpha)^{1/2}(5-6W_{1\alpha}{}^2)W_{1\alpha}+\gamma_{\alpha\beta}$$
$$(1-x_\alpha)/x_\alpha\pi\sigma_{\alpha\beta}{}^2\,g_0^{(m)}(\sigma_{\alpha\beta})/(15v_\beta)(2kT/m_\alpha)^{1/2}$$
$$+Z_{1\alpha}(20-15m_\beta/2(\mu_{\alpha\beta})-6m_\beta/2(\mu_{\alpha\beta})Z_{1\alpha}{}^2)]$$
$$\text{---(25)}$$
$$\gamma_{\alpha\beta}=\mathrm{Log}10(10-9\delta_{\alpha\beta})\quad\text{--(26-a)}$$
$$Z_{1\alpha}=\Sigma(m_\nu/2kT)^{1/2}[p_{1\alpha}/m_\nu-u]\,\gamma_{\alpha\nu}\quad\text{--(26-b)}$$

$$L_\alpha{}^{(m)}=-G_0^{(m)}(1_\alpha)[2b_{1\alpha}-g_0^{(m)}(\sigma_{\alpha\alpha})2\pi\sigma_{\alpha\alpha}{}^2/(15v_\alpha)$$
$$4(W_{1\alpha}W_{1\alpha}-1/3W_{1\alpha}{}^2)-\gamma_{\alpha\beta}(1-x_\alpha)/x_\alpha 2\pi\sigma_{\alpha\beta}{}^2$$
$$g_0^{(m)}(\sigma_{\alpha\beta})/(15v_\beta)m_\alpha{}^2/\mu_{\alpha\beta}{}^2 4(Z_{1\alpha}Z_{1\alpha}-1/3Z_{1\alpha}{}^2 1)]$$
$$\text{----(27)}$$

$$L_\alpha{}^{(m)}=-G_0^{(m)}(1_\alpha)[2b_{1\alpha}$$
$$-g_0^{(m)}(\sigma_{\alpha\alpha})2\pi\sigma_{\alpha\alpha}{}^2/(15v_\alpha)(5+2W_{1\alpha}{}^2+4/3W_{1\alpha}{}^4)$$
$$+\gamma_{\alpha\beta}(1-x_\alpha)/x_\alpha 2\pi\sigma_{\alpha\beta}{}^2/(15v_\beta)g_0^{(m)}(\sigma_{\alpha\beta})m_\beta{}^2$$
$$/(4\mu_{\alpha\beta}{}^2)(5+Z_{1\alpha}{}^2+4/3Z_{1\alpha}{}^4 1)]$$
$$\text{----(28)}$$

We expand each scalar function of $|W_{1\alpha}|$ and $|Z_{1\alpha}|$ in a finite series of Sonine Polynomials.

$$S_n{}^{(m)}(x)=\Sigma_{r0}(-1)(m+n)!/[(n+j)!(m-j)!]\,x^j\quad\text{----(29)}$$

$$C_{1\alpha}(|W_{1\alpha}{}^2|)=\Sigma C_{1\alpha}{}^{(m)}S_{3/2}{}^{(m)}(W_{1\alpha}{}^2)\quad\text{----(30)}$$

Then being integrated over all variables of the relevant variables. The result of this technique is to obtain a set of equations equal in number to the number of unknown expansion coefficients. Substituting the equation (30) into (24)

$$\Sigma\Sigma(N\beta-\delta_{\alpha\beta})/(N_\alpha-1)g_0^{(2)}(\sigma_{\alpha\beta})\int Gf_0^{(1)}(1\alpha)Gf_0^{(1)}(2\beta)$$
$$p_{1\alpha 2\beta}/\mu_{\alpha\beta}[C_{1\alpha}^{(m)}[S_{3/2}^{(m)}(W_{1\alpha}^{*2})W_{1\alpha}'-S_{3/2}^{(m)}(W_{1\alpha}^{*2})W_{1\alpha}']$$
$$+C_{2\beta}^{(m)}[[S_{3/2}^{(m)}(W_{2\beta}^{*2})W_{2\beta}'-S_{3/2}^{(m)}(W_{2\beta}^{*2})W_{2\beta}']]$$
$$b_{\alpha\beta}db_{\alpha\beta}d\varepsilon\,dp_{2\beta}=W_{1\alpha}Gf_0^{(1)}(1\alpha)\quad---(31)$$

When the series expansions is truncated after 2 terms that correspond to the detemtion of $C_{\alpha(0)}$ and $C_{\alpha(1)}$ only, there are 4 unknown coefficients. Multiplying eq(31) by $S_{3/2}^{(m)}(W_{1\alpha}^2)W_{1\alpha}$ and subsequent integration over $dp_{1\alpha}$

$$\Sigma\Sigma(N\beta-\delta_{\alpha\beta})/(N_\alpha-1)\,g_0^{(2)}(\sigma_{\alpha\beta})/(v_\alpha v_\beta)$$
$$[[S_{3/2}^{(m)}(W_{1\alpha}^2)W_{1\alpha};S_{3/2}^{(m)}(W_{1\alpha}^2)W_{1\alpha}]_{1\alpha 2\beta}C_{1\alpha}^{(m)}$$
$$+[S_{3/2}^{(m)}(W_{1\alpha}^2)W_{1\alpha};S_{3/2}^{(m)}(W_{2\beta}^2)W_{2\beta}]_{1\alpha 2\beta}C_{2\beta}^{(m)}$$
$$=\int W_{1\alpha}^2Gf_0^{(1)}(1\alpha)S_{3/2}^{(m)}(W_{1\alpha}^2)\,dp_{1\alpha}\quad---(32)$$

where the bracket Integral of Hirshfleder Is

$$[G;H]_{1\alpha 2\beta}=-v_\alpha v_\beta\int\int Gf_0^{(1)}(1\alpha)Gf_0^{(1)}(2\beta)p_{1\alpha 2\beta}/\mu_{\alpha\beta}$$
$$G(H-H^*)\,b_{\alpha\beta}db_{\alpha\beta}d\varepsilon\,dp_{2\beta}\quad---(33)$$

Thus, we can express

$$A_\alpha=\Sigma[a_{1\alpha}^{(m)}S_{3/2}^{(m)}(W_{1\alpha}^2)+a_{1\alpha}^{(m)'}S_{3/2}^{(m)}(Z_{1\alpha}^2)]\quad---(34)$$

Substituting (34) into (22), we have

$$\Sigma\Sigma(N\beta-\delta_{\alpha\beta})/(N_\alpha-1)\,g_0^{(2)}(\sigma_{\alpha\beta})[[\int\int$$
$$Gf_0^{(1)}(1\alpha)Gf_0^{(1)}(2\beta)p_{1\alpha 2\beta}[a_{1\alpha}^{(m)}(S_{3/2}^{(m)}(W_{1\alpha}^{*2})W_{1\alpha}*$$
$$-S_{3/2}^{(m)}(W_{1\alpha}^2)W_{1\alpha})+a_{2\beta}^{(m)}(S_{3/2}^{(m)}(W_{2\beta}^{*2})W_{2\beta}*$$
$$-S_{3/2}^{(m)}(W_{2\beta}^2)\,W_{2\beta})]\,b_{\alpha\beta}db_{\alpha\beta}d\varepsilon\,dp_{2\beta}$$
$$+\int Gf_0^{(1)}(1\alpha)Gf_0^{(1)}(2\beta)p_{1\alpha 2\beta}[a_{1\alpha}^{(m)'}(S_{3/2}^{(m)}(Z_{1\alpha}^{*2})Z_{1\alpha}*$$
$$-S_{3/2}^{(m)}(Z_{1\alpha}^2)Z_{1\alpha})+a_{2\beta}^{'(m)}(S_{3/2}^{(m)}(Z_{2\beta}^{*2})Z_{2\beta}*$$
$$-S_{3/2}^{(m)}(Z_{2\beta}^2)Z_{2\beta})]\,b_{\alpha\beta}db_{\alpha\beta}d\varepsilon\,dp_{2\beta}=K_\alpha\quad---(35)$$

$$Z_{2\beta}=\Sigma(m_\nu/2kT)^{1/2}[p_{2\beta}/m_\nu-u]\,\gamma_{\beta\nu}\quad---(36)$$

Now, we have to determined the coefficients $a_{1\alpha}^{(m)}$ in(34).Truncation of (34) after the first two terms gives eight unknowns. By multiplying each of the equations by $S_{3/2}^{(m)}(W_{1\alpha}^2)W_{1\alpha}$ and $S_{3/2}^{(m)}(Z_{1\alpha}^2)Z_{1\alpha}$,we have linear algebraic equations. They are give by putting

$$C11=[S_{3/2}^{(m)}(W_{1\alpha}^2)W_{1\alpha};S_{3/2}^{(m)}(W_{1\alpha}^2)W_{1\alpha}]_{1\alpha,2\beta}$$
$$C12=[S_{3/2}^{(m)}(W_{1\alpha}^2)W_{1\alpha};S_{3/2}^{(m)}(W_{2\beta}^2)W_{2\beta}]_{1\alpha,2\beta}$$
$$C13=[S_{3/2}^{(m)}(W_{1\alpha}^2)W_{1\alpha};S_{3/2}^{(m)}(Z_{1\alpha}^2)Z_{1\alpha}]_{1\alpha,2\beta}$$
$$C14=[S_{3/2}^{(m)}(W_{1\alpha}^2)W_{1\alpha};S_{3/2}^{(m)}(Z_{2\beta}2)Z_{2\beta}]_{1\alpha,2\beta}$$

we have

$$a_{1\alpha(r,m)}C_{11}+a_{2\beta(r,m)}C_{12}+a_{1\alpha'(r,m)}C_{13}+a_{2\beta'(r,m)}C_{14}$$
$$=\int S_{3/2}^{(m)}(W_{1\alpha}^2)W_{1\alpha}\cdot K_\alpha dp_{1\alpha}\quad---(37)$$

putting

$$C81=[S_{3/2}^{(m)}(Z_{1\alpha}^2)Z_{1\alpha};S_{3/2}^{(m)}(W_{1\alpha}^2)W_{1\alpha}]_{1\alpha,2\beta}$$
$$C82=[S_{3/2}^{(m)}(Z_{1\alpha}^2)Z_{1\alpha};S_{3/2}^{(m)}(W_{2\beta}^2)W_{2\beta}]_{1\alpha,2\beta}$$
$$C83=[S_{3/2}^{(m)}(Z_{1\alpha}^2)Z_{1\alpha};S_{3/2}^{(m)}(Z_{1\alpha}^2)Z_{1\alpha}]_{1\alpha,2\beta}$$
$$C84=[S_{3/2}^{(m)}(Z_{1\alpha}^2)Z_{1\alpha};S_{3/2}^{(m)}(Z_{2\beta}^2)Z_{2\beta}]_{1\alpha,2\beta}$$

Then, we have

$$a_{1\alpha(r,m)}C_{81}+a_{2\beta(r,m)}C_{82}+a_{1\alpha'(r,m)}C_{83}+a_{2\beta'(r,m)}C_{84}$$
$$=\int S_{3/2}^{(m)}(Z_{1\alpha}^2)Z_{1\alpha}\cdot K_\alpha dp_{1\alpha}\quad---(38)$$

putting

$$C121=[S_{5/2}^{(m)}(W_{1\alpha}^2)(W_{1\alpha}W_{1\alpha}-1/3\,W_{1\alpha}^2\,1)$$
$$;S_{5/2}^{(m)}(W_{1\alpha}^2)(W_{1\alpha}W_{1\alpha}-1/3\,W_{1\alpha}^2\,1)]_{1\alpha,2\beta}$$
$$C122=[S_{5/2}^{(m)}(W_{1\alpha}^2)(W_{1\alpha}W_{1\alpha}-1/3\,W_{1\alpha}^2\,1)$$
$$;S_{5/2}^{(m)}(W_{2\beta}^2)(W_{2\beta}W_{2\beta}-1/3\,W_{2\beta}^2\,1)]_{1\alpha,2\beta}$$
$$C123=[S_{5/2}^{(m)}(W_{1\alpha}^2)(W_{1\alpha}W_{1\alpha}-1/3\,W_{1\alpha}^2\,1)$$
$$;S_{5/2}^{(m)}(Z_{1\alpha}^2)(Z_{1\alpha}Z_{1\alpha}-1/3\,Z_{1\alpha}^2\,1)]_{1\alpha,2\beta}$$
$$C124=[S_{5/2}^{(m)}(W_{1\alpha}^2)(W_{1\alpha}W_{1\alpha}-1/3\,W_{1\alpha}^2\,1)$$
$$;S_{5/2}^{(m)}(Z_{2\beta}^2)(Z_{2\beta}Z_{2\beta}-1/3\,Z_{2\beta}^2\,1)]_{1\alpha,2\beta}$$

Then,

$$b_{1\alpha}^{(m)}(rm)C_{121}+b_{2\beta}^{(m)}(r,m)C_{122}+b_{1\alpha}^{'(m)}(r,m)C_{123}+b_{2\beta}^{'}(1)(r,m)\,C_{124}$$
$$=\int L_\alpha^{(m)}:(W_{1\alpha}W_{1\alpha}-1/3\,W_{1\alpha}^2\,1)S_{5/2}^{(m)}(W_{1\alpha}^2)dp_{1\alpha}$$
$$---(39)$$

and putting

$$C161=[S_{5/2}^{(m)}(Z_{1\alpha}^2)(Z_{1\alpha}Z_{1\alpha}-1/3\,Z_{1\alpha}^2\,1)$$
$$;S_{5/2}^{(m)}(W_{1\alpha}^2)(W_{1\alpha}W_{1\alpha}-1/3\,W_{1\alpha}^2\,1)]_{1\alpha,2\beta}$$
$$C162=[S_{5/2}^{(m)}(Z_{1\alpha}^2)(Z_{1\alpha}Z_{1\alpha}-1/3\,Z_{1\alpha}^2\,1)$$
$$;S_{5/2}^{(m)}(W_{2\beta}^2)(W_{2\beta}W_{2\beta}-1/3\,W_{2\beta}^2\,1)]_{1\alpha,2\beta}$$
$$C163=[S_{5/2}^{(m)}(Z_{1\alpha}^2)(Z_{1\alpha}Z_{1\alpha}-1/3\,Z_{1\alpha}^2\,1)$$
$$;S_{5/2}^{(m)}(Z_{1\alpha}^2)(Z_{1\alpha}Z_{1\alpha}-1/3\,Z_{1\alpha}^2\,1)]_{1\alpha,2\beta}$$
$$C164=[S_{5/2}^{(m)}(Z_{1\alpha}^2)(Z_{1\alpha}Z_{1\alpha}-1/3\,Z_{1\alpha}^2\,1)$$
$$;S_{5/2}^{(m)}(Z_{2\beta}^2)(\;Z_{2\beta}Z_{2\beta}-1/3\,Z_{2\beta}^2\,1)]_{1\alpha,2\beta}$$

Thus, we have

$$b_{1\alpha}^{(m)}(rm)C_{161}+b_{2\beta}^{(m)}(1)(r,m)C_{162}+b_{1\alpha}^{'(m)}(r,m)C_{163}+b_{2\beta}^{'}(1)(r,m)\,C_{164}$$
$$=\int L_\alpha^{(m)}:(Z_{1\alpha}Z_{1\alpha}-1/3\,Z_{1\alpha}^2\,1)S_{5/2}^{(m)}(Z_{1\alpha}^2)dp_{1\alpha}\quad---(40)$$

The integrations in the right sides of these equations are performed about the momentum space in the vector is converted to the real space by

$$dp_{1\alpha}=4\pi p_{1\alpha}^2\,dp_{1\alpha}$$
$$W_{1\alpha}=p_{1\alpha}/(2\,m_\alpha kT)^{1/2}$$
$$f_0(1)(1\alpha)=\exp(-p_{1\alpha 2}/(2\,m_\alpha kT))/[(2\pi m_\alpha kT)^{1/2}v_\alpha]$$

Then,

Right side of (37) $=1/[\pi^{1/2}(2\,m_\alpha kT)^{1/2}v_\alpha]$

$$\int\exp(-p_{1\alpha}^2/(2m_\alpha kT))\,p_{1\alpha}^2/(2m_\alpha kT)$$
$$S_{3/2(r)}(p_{1\alpha}^2/(2m_\alpha kT))4\pi p_{1\alpha}^2\,dp_{1\alpha}$$
$$=2/(\pi^{1/2}v_\alpha)\Gamma(5/2)\quad---(41)$$

By these mathematical procedures, we can have coefficients for mass flux, stress tensor, viscosity and the heat flux.

3. Computed results and discussion.

Fig. 1 shows heat flux as a function of mass of the first particle m1 which has been Increased from m1=1.25 to 2.0 and diameter (Sigma) of that particle from 0.2 to 0.4.As the mass Increased, the heat flux decreased while it increased a little by the increase in diameter. Fig.2 shows kinetic contribution to the heat current as a function of mass and the diameter of the first particle. Fig 3 shows those of the mass current flow as a function of the same parameters. These thermo dynamical properties are sensitive to the changes in mass and diameter of the bio molecular particles.

4. Conclusion.

The present method may be available for evaluating the local thermodynamical activity of the biomolecular particles.

Fig 1

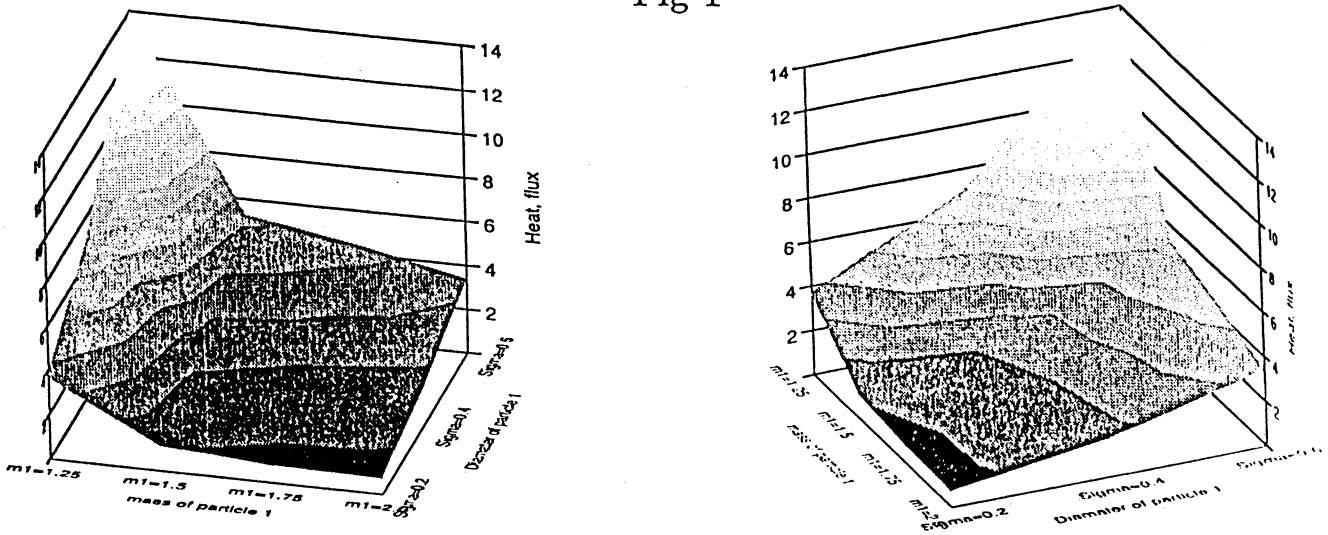


Fig 2

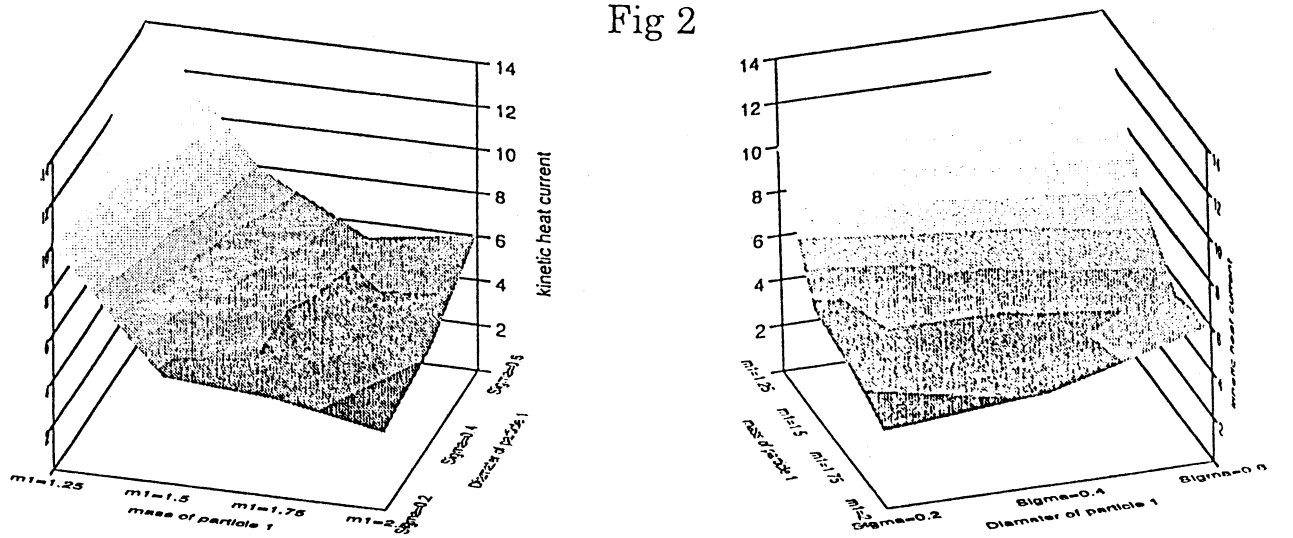
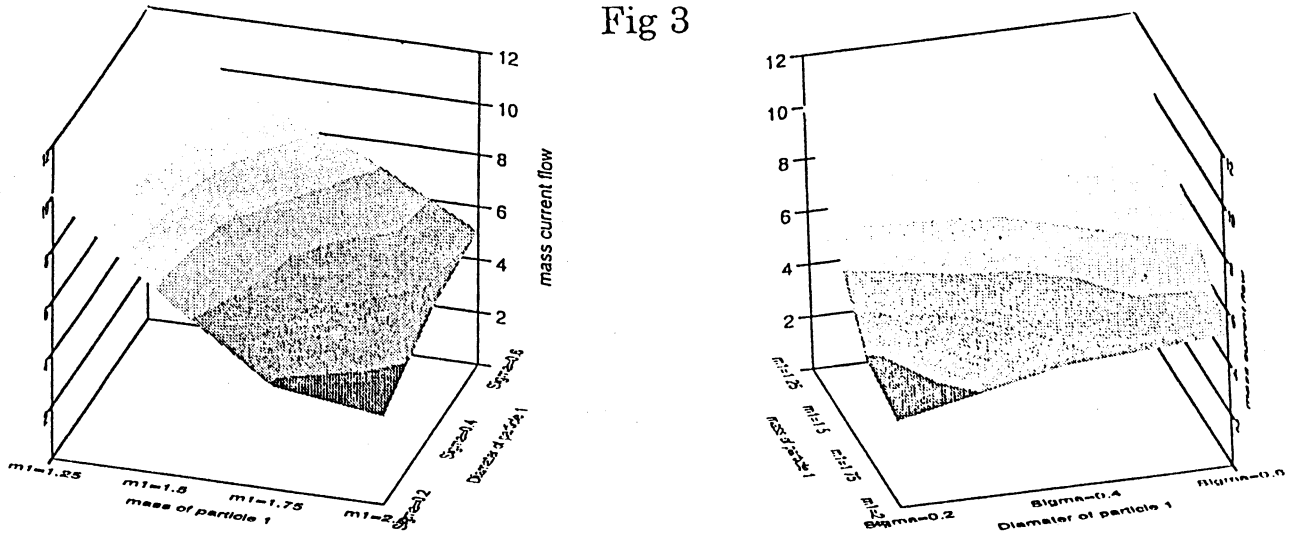


Fig 3



5. References.

1. Harris,R,A and Rice S.A. J. Chem. Physics. vol 32. No 2. pp538-547. 1960.

2. Harris,R,A and Rice S.A. J. Chem. Physics. vol 33. No 4. pp1047-1054. 1960.

Proc. of The Ninth Int. Symp. on Artificial Life and Robotics (AROB 9th '04)
Beppu, Oita, Japan, 28-30 January, 2004

A Cellular Automata Model for HIV Infection and Antigenic Diversity Threshold

Hiroshi UEDA and Yoshiteru ISHIDA
Department of Knowledge-based Information Engineering
Toyohashi University of Technology
Hibarigaoka 1–1, Tempaku, Toyohashi, Aichi 441–8580

Abstract

In this paper, we modeled the interaction between immune system and HIV with cellular automata approach, and consider about the influence of diversity of HIV on the interaction.

Keywords HIV, Immune system, Cellular automata, Antigenic diversity threshold

1 Introduction

Many mathematical models have been proposed [1] to examine the interaction between immune system and HIV. Because it is not clear how HIV undermines immune system, and causes acquired immune deficiency syndrome (AIDS) .

For example, Nowak and May proposed a dynamical model to account for their *antigenic diversity threshold* theory [2, 3]. According to this theory, there is a threshold of number of HIV strains which HIV infection leads to AIDS [4].

In contrast, we proposed a *stochastic–lattice model* based on Nowak–May's model [5, 6]. A threshold that can be expressed by parameters of HIV and T-Cell was observed on our *stochastic–lattice model.* To conclude, the behavior of these two models is similar. Thus, our next interest is different way of modeling for the interaction between immune system and HIV.

2 Why we use Cellular Automata?

It would appear that T-cell and HIV are doing local interaction in vivo. Because immune system make the response from long succession of local responses by network of immune cells and antigens [7].

Cellular automata (CA) approach is based on fundamental rule such like local interaction. CA have been popularly applied to physics, chemistry, traffic, economics because of reproducibility of complicated phenomenon from simple local interaction.

CA approach is also applied to dynamics of immune system as follows:

Pandey's work Each CA site has state bits correspond to HIV, T-cell, etc. Update rule is boolean operation [8, 9, 10].

Santos et al.'s work State of initial infection, latency and onset of AIDS was reproduced by simple 2-dimensional CA [11].

Advantage of CA approach is that can simplify complicated interaction between immune system and HIV into simple local interaction. For this reason, we use CA approach to model the interaction.

3 A model

Our CA model is based on Nowak–May's mathematical model similar to the following [2, 12].

$$\dot{v}_i = v_i(b - px_i), \tag{1}$$

$$\dot{x}_i = kv_i - u\sum_{i=1}^{N} v_i x_i, \quad i = 1, 2, \ldots, N. \tag{2}$$

where v_i and x_i are time dependent variables indicating the population size of HIV type i strain and that of its corresponding clones of T helper lymphocytes stimulated by HIV type i, respectively. N is number of HIV strains. The following parameters are all positive;

- b: the net replicating rate of HIV,
- p: the rate of elimination of HIV by immune response specific to type i,
- k: the rate of stimulation of i-specific T-cells,
- u: the rate of depletion of T-cells by HIV.

We use 2-dimensional and 3-states CA. Each CA site has four parameter (b, p, k, u) corresponds to equation (1) , (2) and following states: (a) HIV infected; (b) activated T-cell; and (c) healthy (deactivated) T-cell.

The initial CA formation is filled of (c) healthy T-cells, with a small fraction, $pHIV$, of (a) HIV infected cells. The next updated state of CA site depends on the states of its Moore neighbors. For each site, we apply following update rules:

Rule 1: *Update of a healthy T-cell:* If it has at least one HIV infected neighbor, it becomes HIV infected or active T-cell by probability $min[(b/8, b/(k+b)], min[k/8, k/(k+b)]$, respectively. If it has no HIV infected neighbor, it still remain a healthy T-cell.

Rule 2: *Active T-cell is attacked by HIV:* If it has at least one HIV infection neighbor, it becomes healthy T-cell by probability $uV/8$, where V is number of HIV infected cells $(0 \leq V \leq 8)$. This rule implies that active T-cell dies from attack of HIV, after that, it begin to supply of healthy T-cell from thymus.

Rule 3: *HIV infected cell is eliminated by active T-cell:* If it has at least one active T-cell neighbor, it becomes healthy T-cell by probability $pX_i/8$, where X_i is number of active type i-specific T-cells $(0 \leq X \leq 8)$. This rule also implies dead of infected cell and supply of healthy T-cell from thymus.

4 Simulations and results

We performed simulations of the model, using periodic boundary conditions, on a 100×100 lattice , $pHIV = 0.05$.

According to Nowak and May's *antigenic diversity threshold* theory, the stability condition for the HIV population size (basically, the condition to decrease number of HIV) can be formulated as follows:

$$\sum_{i=1}^{N} \frac{b_i u_i}{p_i k_i} < 1. \qquad (3)$$

First, we use parameters in table 1 to investigate the existence of threshold like Nowak–May's model under diversity of HIV is $N = 1$. Since $N = 1$, parameters 1–4 corresponds to the case of below the threshold, tight to the threshold, upper for a while from the threshold, above the threshold, respectively.

Table 1: Parameters of simulation 1–4. Simulation 1, 4 corresponds to the case of below threshold. Simulation 2 is the case of threshold value. Simulation 3 is the case of above threshold.

Simulation	b	u	p	k
1	3	2	3	3
2	3	3	3	3
3	3.1	3.1	3	3
4	4	4	3	3

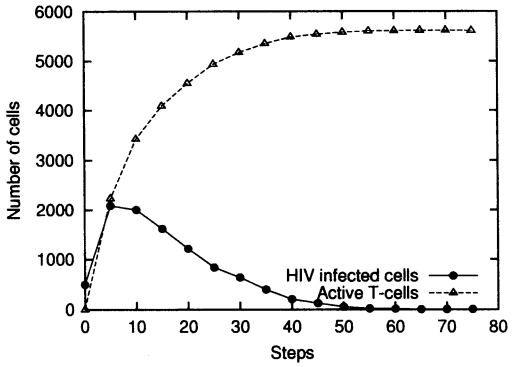


Figure 1: Number of cells versus steps in simulation 1. Initial infection of HIV and control of HIV by T-cell has appeared.

Simulation 1 *In the case of below the threshold:* In figure 1, number of HIV is decreasing. Figure 5 shows snapshot of during simulation 1.

Simulation 2 *In the case of tight to the threshold:* In figure 2, HIV is contained but it takes many time steps compare with simulation 1.

Simulation 3 *In the case of upper for a while from the threshold:* In figure 3, this simulation runs long time more than 25,000 steps. Because in this case, the power of HIV and a T-cell is the about the same, and is competing fiercely.

Simulation 4 *In the case of above the threshold:* In figure 4, although immune response in about 10 step, HIV infected cells fastly increase. Figure 6 shows snapshot of during simulation 4.

These simulations show that 1 is made into a boundary line (=threshold) and behavior of a model is completely reverse. Consequently, there is the threshold like Nowak–May's model.

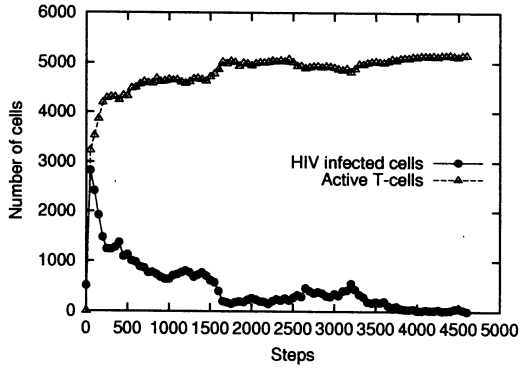


Figure 2: Number of cells versus steps in simulation 2. It takes long time steps to control HIV by T-cell.

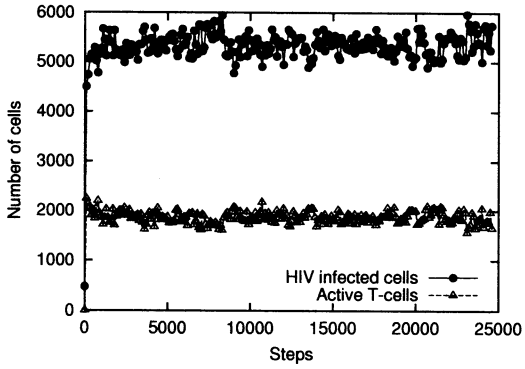


Figure 3: Number of cells versus steps in simulation 3. It runs over 25,000 steps.

Second, we introduce mutation of HIV into this CA model because of a feature of HIV is its enormous genetic diversity resulting from mutation. We define mutation of HIV as follows:

(i) Mutate site is randomly chosen from entire lattice by probability $pMutate$.

(ii) For mutate site, variable i for describing type of HIV is perturbate.

These process makes change of new HIV strain if the CA site is HIV infected state, or new specific T-cell if the CA site is not infected.

If mutation of HIV has occured, we expect sudden increase of HIV infected cells. This anticipation is verified by the simulation. In figure 7, we made mutation artificially at step 50 under same parameters in simulation 2. Apparently, HIV infection grows up after mutation.

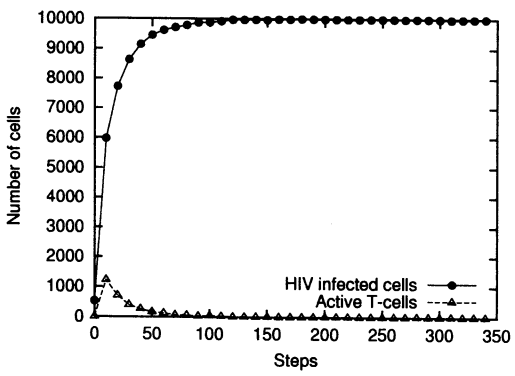


Figure 4: Number of cells versus steps in simulation 4. HIV infected cells fastly increased.

5 Summary and future work

We proposed CA approach model for interaction between immune system and HIV. In our CA approach model, there is threshold describing parameters. Additionary, mutation of HIV is introduced into CA model. For the furture work, expressing the diversity of HIV as a difference in a parameter is mentioned.

Acknowledgements

This work was supported in part by a the 21st century COE (Intelligent human sensing) from the Ministry of Education, Culture, Sports, Science and Technology.

References

[1] Angela R. Mclean. The balance of power between HIV and the immune system. *Trends in Microbiorogy*, Vol. 1, pp. 9–13, 1993.

[2] Martin A. Nowak, Roy M. Anderson, Angela R. McLean, Tom F. W. Wolfs, Jaap Goudsmit, and Robert M. May. Antigenic diversity thresholds and the development of AIDS. *Science*, Vol. 254, pp. 963–969, 1991.

[3] Martin A. Nowak and Robert M. May. Mathematical biology of hiv infections: Antigenic variation and diversity thresholds. *Mathematical Biosciences*, Vol. 106, pp. 1–21, 1991.

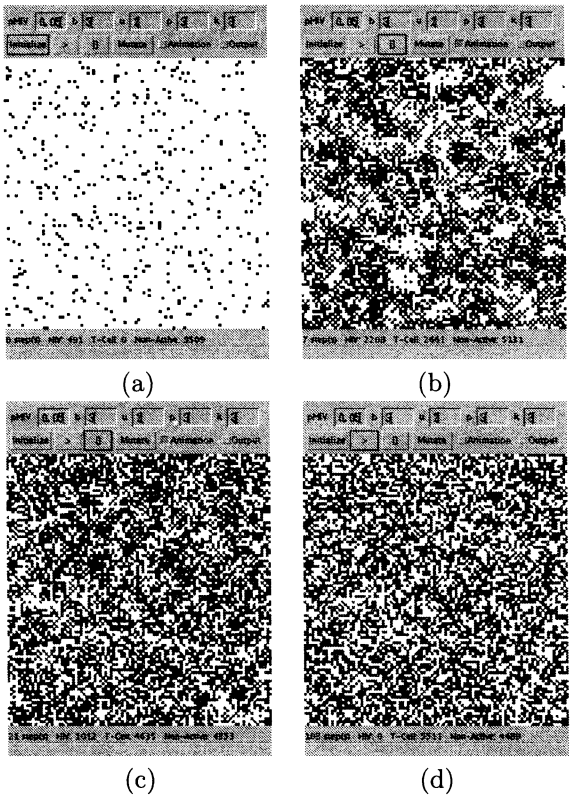


Figure 5: Snapshot of simulation 1. (a) – (d) correspond to 0, 7, 21, 93 steps respectively.

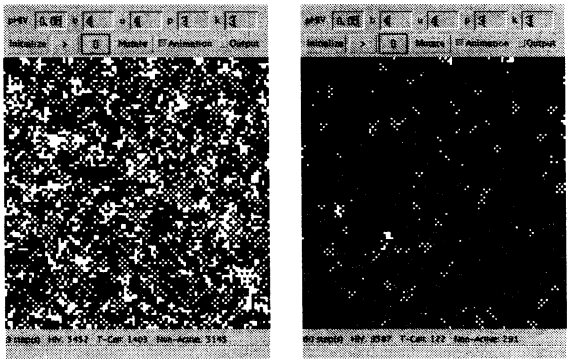


Figure 6: Snapshot of simulation 4. (a) , (b) correspond to 9, 60 steps respectively.

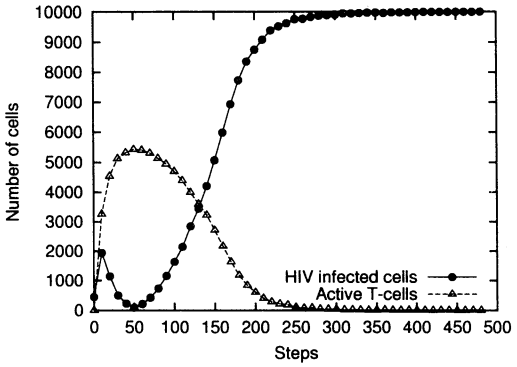


Figure 7: Number of cells versus steps in similar to simulation 1 with mutation at step 50. After mutation, sudden increase of HIV has occored.

[4] Martin A. Nowak and Andrew J. McMichael. How HIV defeats the immune system. *Scientific American*, pp. 58–65, August 1995.

[5] Hiroshi Ueda and Yoshiteru Ishida. A stochastic model on lattice spaces and antigenic diversity threshold. In *Proc. of The Seventh Int. Symp. on Artificial Life and Robotics*, pp. 205–208, 2002.

[6] Hiroshi Ueda and Yoshiteru Ishida. A stochastic model of initial HIV infection on lattice spaces. *Artificial Life and Robotics*, Vol. 7, , 2003. In press.

[7] Niels Kaj Jerne. The immune system. *Scientific American*, Vol. 229, No. 1, pp. 52–60, 1973.

[8] R. B. Pandey. A stochastic cellular automata approach to cellular dynamics for HIV: Effect of viral mutation. *Theory Bioscienc.*, Vol. 117, pp. 32–41, 1998.

[9] R.B. Pandey. Cellular automata approach to interacting cellular network models for the dynamics of cell population in an early HIV infection. *Physica A*, Vol. 179, No. 3, pp. 442–470, 1991.

[10] R.B. Pandey and D. Stauffer. Immune response via interacting three dimensional network of cellular automata. *J. Phys.*, Vol. 50, No. 1, pp. 1–10, 1989.

[11] Rita Maria Zorennon dos Santos and Sérgio Coutinho. Dynamics of HIV infection: A cellular automata approach. *Physical Review Letters*, Vol. 87, No. 16, pp. 168102–1–168102–4, 2001.

[12] Martin A. Nowak and C. R. M. Bangham. Population dynamics of immune responses to persistent viruses. *Science*, Vol. 272, pp. 74–79, 1996.

Proc. of The Ninth Int. Symp. on Artificial Life and Robotics (AROB 9th '04)
Beppu, Oita, Japan, 28-30 January, 2004

Statistical Approach for Function Classification of Proteins in the Biological Texts

°Dae-Won Park
Department of Computer Science
Pusan National University, Korea
bluepepe@pusan.ac.kr

Hyuk Gyu Cho
School of Computer and Information Engineering,
Youngsan University, Korea
hgcho3@ysu.ac.kr

Hyuk-Chul Kwon
Division of Computer Science & Engineering
Pusan National University, Korea
hckwon@pusan.ac.kr

Man-Hyung Lee
Department Mechanical & Intelligent System
Engineering, Pusan National University, Korea
mahlee@pusan.ac.kr

Abstract

Proteins are interacting and have relationships with other proteins. Many methods for extracting protein-protein interaction from large volumes of biological texts are introduced and being developed. In the interaction between proteins, the functions take an important role. Functionally related proteins may be interacting each other and have a close relationship with each other. The functions of protein can be used to extract the protein-protein interactions and other protein related information in biological literatures.

We assume that functions of protein will be determined by the terms of protein name and attempt to infer functions of protein and classify proteins into function classes using term features. In this paper, we represent a statistical approach with term features of proteins in biological texts. Term features make a function distribution and each feature have a probability of function. Term features are extracted from protein names and distributed the function classes according to the protein's function. The function of protein is inferred by the function probability of the term features. Each feature's functionality affects on the function of protein. We make a function distribution of term features with the functionally known proteins and infer functions of protein by the distribution.

Keywords : protein function, classification, function prediction, probability, term feature, protein

1 Introduction

Through various genome researches like the human genome project, many proteins are newly discovered and annotated [3][7]. There are many proteins still not assigned functions. There are many approaches for deducing the function of proteins. The sequence-based approach is to find out homologies between a protein and other proteins by sequence similarity and to deduce function of protein [11][13]. Several approaches have been made to predict protein functions using such data as gene expressions and protein-protein interactions [1][4][12].

Protein functions, protein-protein interactions and many other biological processes are being described and explained in biological text as the form of research paper. The biological texts are useful knowledge resource in research. With the accumulation of biological text, finding out proper information is not feasible and is time-consuming. Proteins take an important role in biology. Proteins are interacting and revealing with other proteins in biological processes. Many cellular processes and biological events are related with a group of proteins. With biological texts, several researches on protein name recognition [8] and protein-protein interaction extraction have been developed.

Proteins are interacting with other proteins in functional relation. Functions of protein play an important role to find out protein-protein interaction. Protein is annotated by its function with function prediction methods. We assume that functions of protein will be determined by the terms of protein name and attempt to classify proteins.

In this paper, we represent and experiment the functional classification of proteins using statistical approach. For the function classification of protein, we extract classification features from proteins. Term features extracted from proteins are representing genomic characteristics and are used as classification features. Classification features are distributed in the molecular function classes based on the GO molecular function. Functional distribution of term features is representing the functional probability in the classes.

2 Method

Our method for function classification of proteins is composed of two parts. The one is extracting term feature and constructing feature class set. According to the protein

functions, we construct feature vector for each function classes. The second part is to predict functions of proteins with comparing with feature vector.

2.1 Classification feature

Proteins are generally annotated by their functions that are assigned through gene analysis such as gene sequencing, structure sequencing and other annotation methods [7]. Protein name may be properly assigned to represent its functions. Since term is an important feature in text-based research such as information extraction and information retrieval [9], we use term as key feature to represent and predict protein function.

Protein name is composed of one or more terms. All terms of protein are not used as key feature. There are grammatical function words and numerals. These terms are trivial. Extraction of term as key feature from proteins is process of tokenizing and filtering. Terms are tokenized by several rules. We exclude numerals and grammatical function words.

2.2 Feature class

Each feature has its own functionality derived from protein. Term features are distributed in function classes based on protein functions. According to the functions of protein, term features are functionally divided. Term features of a class set feature vector. The feature vector of each class represent functional characteristic.

Each term feature has weight in the function class that occurred. The weight of term feature is influenced on the feature frequency and feature's functional distribution in function classes. Following equation is the basic weight function of a term feature.

$$P(C_i \mid t_k) = tf_{ki} / \Sigma_{(j=1, N)} tf_{kj}$$
$$W(C_i \mid t_k) = P(C_i \mid t_k) * idf_k$$

Ci : function class i
tf_{ki} : term feature k frequency in function class i
N : function class number
idf_k : inverted number of function class including term feature k

For instance, if term feature k is occurred 5, 2 and 3 times in function class 1, 2 and k, the term feature's function probability is 0.5, 0.2 and 0.3. In other word, the term feature k has three functionalities.

$$W(Ci \mid t_k) = (tf_{ki} + 1/N)/(\Sigma_{(j=1, N)} tf_{kj} + 1) * idf_k$$

The feature weight is modified using smoothing method. With the basic weight function, unknown class of term feature has zero weight. We apply a small value for unknown class.

2.3. Function Classification

The functional distribution of term feature shows the usage of term feature for representing protein function. The frequency of term feature in a class provides the functional probability. The process of functional classification of protein is composed of two steps : the one is the process of selecting candidate classes, the second step is selecting proper function classes from the candidate classes.

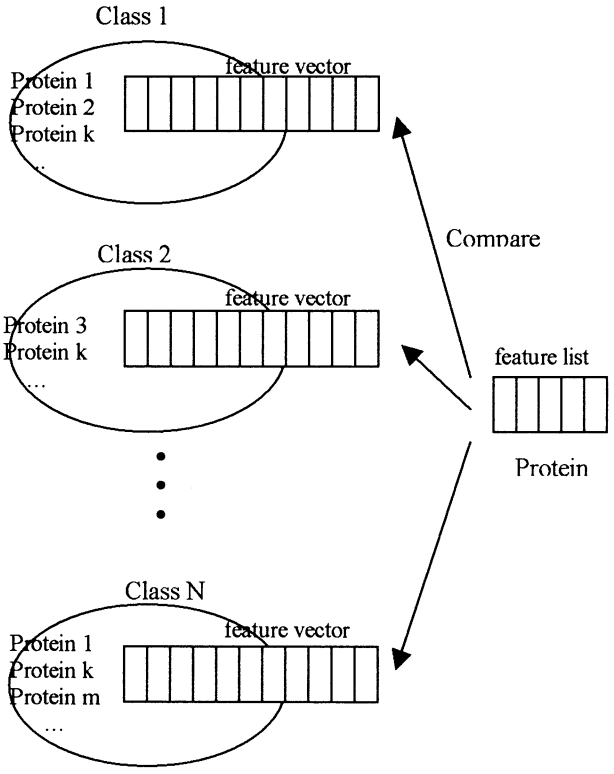


Fig 1. Statistical Similarity with feature vector
Each function class has feature vector constructed by protein's term features. Features of input protein are compared with the feature vector of each function class and the functional probability is calculated.

$$Sim(C_i \mid P) = \Sigma_{(j=1, k)} W(Ci \mid t_j)$$

Protein has functions and also term features extracted from protein have same functions as protein. Each class has feature vector constructed by term feature of protein and protein feature list. Function class with high similarity to protein is selected as candidate class. Feature vector represents functionality of the class, and each feature in the class has function probability. Since protein can have several functions, we select more than one candidate classes.

The second step of functional classification is protein feature alignment. Protein feature in function class is protein's feature index list. Features of protein are stored in protein feature list. Features are ordered by the location in protein. In the process of similarity estimation, we estimate protein similarity with each feature's functional weight. Protein feature alignment is process of comparing input protein and protein feature in the class. In the alignment of protein feature, feature's order is important. For the candidate class, we re-estimate protein's function probability and similarity with protein feature alignment.

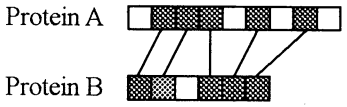


Fig 2. Feature Alignment
Protein is compared with protein features in the classes. If the class has similar feature pattern to the input protein, the class is selected as function class of protein.

3 Experiment

We apply our approach to infer the functions of human proteins. As we explained in the previous section, we divide protein data into two groups. The one is a training dataset for constructing feature distribution and the other is a testing dataset for estimating our method. With precision, recall, and f-score, our method is estimated.

3.1 Protein Dataset

We use GO assignments for the proteins of the non-redundant human proteome set. These data is provided in the GO. From these GO association data sets, we extract protein name and GO ID that indicates functions of protein. GO ID is mapping to the molecular function classes that is used in our method. We exclude symbols and synonyms of proteins.

3.2 Function Class

The GO(Gene Ontology) is a large hierarchy of molecular biology concepts [5][6]. The GO has three organizing principles that are molecular function, biological process and cellular component. The GO molecular function describes gene products' activities. We use the GO molecular function for classifying proteins. The GO molecular function has 28 classes of the first level and each class has one or more activities. Some molecular function classes of GO have same activities, even though that describe different activities. For example, 'ATP-binding cassette (ABC) transporter activity' is belong to binding, catalytic activity, and transporter activity. For these activities belong to several molecular function classes, we make new molecular function classes that are functionally distinguished. We evaluate the molecular function classes on the basis of the GO molecular function. The function classes are divided into 56 classes that have completely different sub activities. We assign proteins to 56 these classes and predict protein function based on these new classes.

3.3 Results

Function classification is experimented with 10-fold protein datasets. 9 of 10 data folds are used for training and 1 data fold is for estimating our method. Training dataset and estimating dataset are completely disjointed each other. We use estimation measure as precision, recall and f-score. Experiment result is average value of 10-fold cross validation. Each fold has about 1,200 protein data.

Precision	Recall	F-Score	Precision	Recall	F-Score
0.7048	0.6445	0.6746	0.7250	0.6683	0.6967
0.7184	0.6697	0.6940	0.7163	0.6699	0.6931
0.7148	0.6500	0.6824	0.7295	0.6756	0.7026
0.7306	0.6698	0.7002	0.6468	0.7583	0.7026
0.6912	0.6451	0.6682	0.6488	0.7661	0.7075

Table 1. Classification Result

Our method show that average Precision is 0.7026, Recall is 0.6817 and F-Score is 0.6922. In our method, Precision and Recall is close. As shown in result (Table 1), precision is shown between 0.6468 and 0.7306, and recall is between 0.6445 and 0.7661.

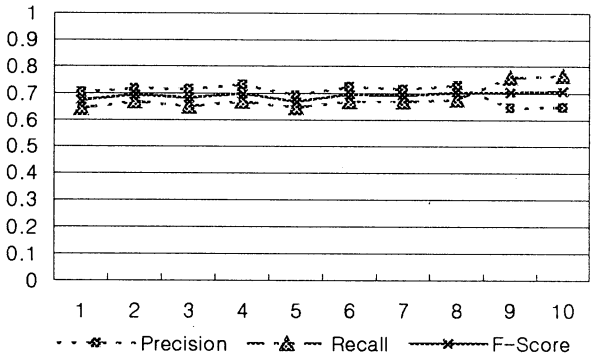


Fig 3. Estimation Result

Protein can interact with several proteins in the different function classes. Therefore, in the predication and classification of protein function, recall is also important. Our method using feature probability and feature alignment may be well performing in the protein-protein interaction.

4 Conclusion

Our approach of the function classification is for extracting information related with proteins from biological texts. For extracting protein-protein interaction, functions of protein have not been used. We attempt to infer functions of protein and classify protein by function with known function proteins. From the functionally known proteins, the function distribution of features is set and it applies to classification. As a group of proteins are functional related and interacted, functions of protein will be applied as metadata for extracting interactions.

Our function classification method is not well performed for unknown feature, as same as most of statistical methods have. And also feature with low frequency is being refined as smoothing. We will more concern feature weighting method for improving function classification. Especially, term feature frequency in function class is characteristic. Low frequency feature is more popular and most of features are appeared in the particular function classes. The count of features in class and characteristic of feature frequency are being used.

We will apply natural language processing method for extracting features and genome lexicon dictionary for extracting more proper term feature. In the next our research, we will focus on extracting interaction of proteins related aging from the biological texts.

Acknowledgements

This work was supported by National Research Laboratory Program (Contract Number : M10203000028-02J0000-01510) of KISTEP.

References

1. Alexi Vazguez, Alessandro Flammini, Amos Maritan, Alessandro Vespignani,, *Global protein function prediction from protein-protein interaction networks*, Nature biotechnology letter, 2003
2. Jiro Araki, *Construction of Database for Protein Classifications*, Genome Informatics 12, 2001
3. Jensen LJ, Gupta R, Staerfeldt HH, Brunak S., *Prediction of human protein function according to Gene Ontology categories.*, Bioinormatics., March 2003.
4. Letovsky S, Kasif S., *Predicting protein function from protein/protein interaction data : a probabilistic approach.*, Bioinformatics. July 2003.
5. Alexa T. McCray, Allen C. Browne, Oliver Bodenreider, *The Lexical Properties of the Gene Ontology(GO).*, Proceedings of the AMIA 2002 Annual Symposium, 2002
6. Gene Ontology Consortium (http://www.geneontology.org)
7. Rajesh Nair, Burkhard Rost, *Annotating protein function through lexical analysis.*,, AI Magazine, 2003.
8. Kazuhiro Seki, Javed Mostafa, *A Probabiistic Model for Identifying Protein Names and their Name Boundaries.*, Proceedings of the Computational Systems Bioinformatics, 2003.
9. Goran Nenadic, Simon Rice, Irena Spasic, Sophia Ananiadou, Benjamin Stapley, *Selecting Text Features for Gene Name Classification : from Documents to Terms,*, Proceeding of ACL, 2003
10. Liviu Badea, *Functional Discrimination of Gene Expression Patterns in Terms of the Gene Ontology,* Pac Symp Biocomput, 2003
11. Edward M. Macrotte, Matteo Pellegrini, Ho-Leung Ng, Danny W. Rice, Todd O. Yeates, David Eisenberg, *Detecting Protein Function and Protein-Protein Interactions from Genome Sequences*, SCIENCE, 1999
12. Minghua Deng, Kui Zhang, Shipra Mehta, Ting Chen, Fengzh, *Prediction of Protein Function using Protein-Protein Interaction Data,* IEEE CSB Conference, 2002
13. Altschul, S.F. Madden, T.L., A.A., Zhang, J., Zhang, A., Miller, W. and Lipman, D.J., *Gapped BLAST and PSI-BLAST : a new generation of protein database search programs.* Nucleic Acids Research 25, 1997

Proc. of The Ninth Int. Symp. on Artificial Life and Robotics (AROB 9th '04)
Beppu, Oita, Japan, 28-30 January, 2004

Chemotaxis of an Eukaryotic Cell in Complex Gradients of Chemoattractants

Shin I. Nishimura
Graduate School of Information Science
Nagoya University
Nagoya 464-8601, Japan
shin@sasai.human.nagoya-u.ac.jp

Masaki Sasai
Graduate School of Information Science
Nagoya University
Nagoya 464-8601, Japan
sasai@info.human.nagoya-u.ac.jp

Abstract

We study chemotaxis of an eukaryotic cell by constructing a mathematical model that takes into account chemical kinetics as well as the cellular shape. A cell is defined as a certain single domain on discrete two-dimensional grids. In the cellular domain each grid contains three kinds of molecule, activator and inhibitor of the actin polymerization, and polymerized actins. The external signal promotes production of both activator and inhibitor and thus changes the amount of polymerized actins. If the amount of polymerized actins in a grid of the cell border (as cellular membrane) is larger than a certain threshold, then a new grid adjacent to the border is assigned to a cellular grid. Upon this change of the cellular shape, constraints are imposed to preserve the cellular volume and to make the length of the cellular border as small as possible. The cell moves in the grid space driven by this change of the cellular shape. We succeeded in reproducing chemotaxis in a linear gradient. For two more complex gradients, behavior of our cell is consistent with experimental results.

keywords: chemotaxis, eukaryotic cells, complex gradients.

1 Introduction

Chemotaxis is crucial for proper functioning of biological systems. Unicellular organisms use chemotaxis in order to discover their foods. Multicellular organisms recruit immune cells which migrate to invaded tissues following chemoattractants[1]. There might be many different mechanisms for implementation of chemotaxis. For example, it has been hypothesized that some bacterium species detect the temporal change of chemical concentration[2]: If the concentration decreases, bacterium changes its moving direction, which makes the bacterium arrive at the point of maximal concentration. Many researchers have believed, on the other hand, that eukaryotic cells do not use such an indirect method but can directly detect the spatial difference in chemical concentration. Its mechanism, however, has been long secreted. Recently, the mechanism has been partially elucidated[3, 4, 5, 6] and a set of differential equations have been developed that may explain how cells can detect and amplify a small difference in chemical concentrations at the cellular "front" and "rear"[7]. However, the mechanism how eukaryotic cells can crawl in dynamically changing gradients has not been known. Since blood or body fluid flows in either vessels or tissues, crawling cells (e.g. leukocytes in vertebrates) have to reach proper tissues in not static but in dynamically changing concentration of chemoattractants. How do eukaryotic cells resolve such "difficult" problems? Here, we present a model that may explain cell's ability of chemotaxis in complex gradients. The cell in the model succeeds in moving up static gradients in the simulation. We discuss motion of the cell in more complex patterns of chemical gradients.

2 Model

Our model has discrete two-dimensional grids on which some concentrations of molecules are defined. A cell is defined on the grids as a domain. We adopt hexagonal grids for convenience. A grid is either external or in the cellular domain. When the grid is in the cellular domain, three real numbers are defined on the grid, which indicate densities of activator, inhibitor and actin filaments.

We give four rules in order to move the cell: Kinetics, Diffusion, Actin filaments extending the cellular domain and Keeping the cell. The following paragraphs explain those rules.

(1) **Kinetics**: Both activator and inhibitor are produced by the stimulation of the external signal[7]. The activator enhances polymerization of actins, whereas

the inhibitor suppresses the polymerization. First, this rule selects a grid in the cellular domain randomly. If densities of activator, inhibitor and actin filaments at the selected grid i are expressed as A_j, I_j and F_j, respectively, those variables are changed obeying the following equations:

$$A'_j = A_j + \alpha * S_j - k_\alpha A_j \quad (1)$$

$$I'_j = I_j + \beta * S_j - k_\beta I_j \quad (2)$$

$$F'_j = \begin{cases} \gamma \frac{A}{I} - k_f F_j & (\frac{A}{I} > h) \\ -k_f F_j & (\text{otherwise}) \end{cases}, \quad (3)$$

where α, β, γ, k_α, k_β, k_f, γ and h are constants. S_j indicates the concentration of chemoattractants or the strength of the external signal at the jth grid. Grids at the border of the cellular domain are regarded as the cellular membrane. We say that a grid in the cellular domain is in the membrane if at least one of the six nearest grids is external. S_j is set to zero if the jth grid is in the cellular domain but not in the membrane. The functional form of S_j represents chemical gradients.

(2) **Diffusion**: Only the inhibitor diffuses into the whole cytoplasm[7]. This rule selects a grid from the whole cellular domain. At the selected jth grid and its nearest cellular lth grid, I_j and I_l obey the following equations:

$$I'_j = I_j - DI_j \quad (4)$$

$$I'_l = I_l + \frac{DI_j}{n}, \quad (5)$$

where D is the diffusion constant. n is the number of the nearest cellular grids. D should be smaller than 1 by definition.

(3) **Actin filaments extending the cellular domain**: The rule randomly selects a grid from the membrane. When F_j at the selected jth grid in the membrane reaches the threshold F_{th}, an external grid in the six nearest grids of the jth grid is turned into a cellular grid. When there are two or more than two external grids around the jth grid, a grid is randomly selected. If this grid is referred to as l, $F_l = F_j/2$ and other variables are set to zero. F'_j equals to $F_j/2$ by definition, where the prime indicates the value at the next time step.

(4) **Keeping the cell**: We also give a rule to prevent cell from breaking into pieces. The cellular volume is kept and the cellular surface length is constrained to be as small as possible. This rule randomly selects a grid from the membrane. Then the rule decides either to remove the grid or to add a new cellular grid around the grid. This rule checks the cellular "tension" by calculating energy of tension as:

$$E = (V - V_0)^2 + cl^2, \quad (6)$$

where V and l are the cellular volume and length of the membrane and V_0 and c are constants. When E' denotes the energy after either removing or adding a cellular grid, we define the probability P as follows:

$$P = \exp\left(-\frac{E' - E}{kT}\right), \quad (7)$$

where kT is a constant. We generate a random number between 0 and 1 and then compare the number with P. If the number is smaller than P, we "undo" the event of removing/adding. From the definitions of P and E, the volume of the cell tends to be V_0 and the length of the membrane becomes as small as possible. Note that if removing is chosen, the values of A, I and F in the removed grid are added into the nearest cellular grid.

We also give the "master" rule that randomly selects one of the above rules. Each rule has the probability of selection. The probabilities of selection for rules from (1) to (4) are written as P_1, P_2, P_3 and P_4. $P_1 + P_2 + P_3 + P_4$ should equal to 1. After the master rule selecting one of the four rules, the selected rule is executed. We iterate this process several millions times.

3 Results

First, we try to clarify what our cell does in a simple linear gradient. We select a set of parameters to make the cell go up the gradient as follows: $\alpha = 1.0$, $\beta = 0.1$, $k_\alpha = 0.9$, $k_\beta = 0.02$, k_f, $D = 0.45$, $h = 1.0$ $P_1 = 0.0419$, $P_2 = 0.03$, $P_3 = 0.03$, $P_4 = 0.898$, $V_0 = 900$, $c = 10^5$ and $kT = 100$. The initial diameter of the cell equals to 30 grids. Although we have not yet exhaustively tried different parameter sets, we expect that the cell behaviors are robust against the parameter change.

Signal S depends only on y-axis but not on x-axis: S is a linear function such that $S = ay + b$. Figure 1 shows snapshots of the cell moving. First, F increases on the whole membrane and then banishes except at the cellular front. After this polarization, the cell starts its chemotaxis. Figure 2 shows trajectories of cell's center of mass. All trajectories have the same initial condition except a different random number seed. Although trajectories are not parallel to the direction of the given gradient, the averaged direction approximately coincides with the gradient.

We observe behaviors in more complex gradients. We introduce two types of gradients: cliff and hill gradients. The cliff gradient has a sudden drop, whereas

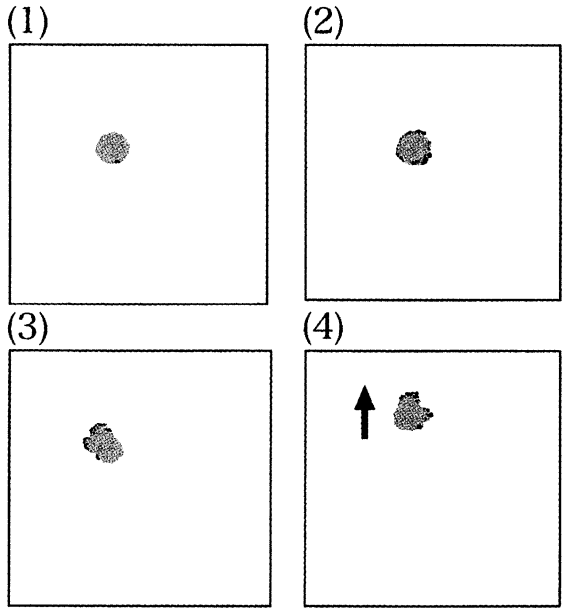


Figure 1: Snapshots of motion of the cell. The gray collared area is the region of cellular grids. Dark part of the cell indicates positions where F is larger than $F_{th}/2.0$. S increases in the upward direction.

the hill gradient has a top with left and right gradually dropped. Figure 3 shows trajectories of center of mass in the case of the cliff gradient. The cell cannot go beyond a drop as if a wall exists. Figure 4 shows the case of the hill gradient, in which the cell does not stop at a top but it tends to return after going down the gradient to some distance in contrast to the cliff gradient case.

The above two results are consistent with experimental results of Jeon et al[8]. They succeeded in constructing a new device that can generate spatially and temporally controlled gradients of chemotactic factors. They generated cliff and hill gradients and observed qualitatively same results as shown with our simulation.

4 Conclusions and Future Works

We constructed a model that can explain cellular locomotion and chemotaxis. We tested three gradients, linear, cliff and hill gradients. Behaviors in these three gradients were consistent with experimental results.

For future works, we will investigate behaviors of our "artificial cells" in more complex gradients or conditions. We believe that eukaryotic cells always face difficult situations. For example, sources of chemotactic factors might spatially and/or temporally move or change. If gradients are not smooth but jaggy, cells should avoid local minima. Our future goal is to elucidate mechanisms underlying these abilities.

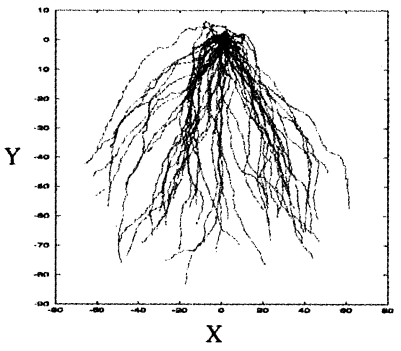


Figure 2: Behavior of the cell in the linear gradient. Each curved line is a trajectory stared with a different random seed. The S increases in the downward direction. ($a = -1$ and $b = 30$)

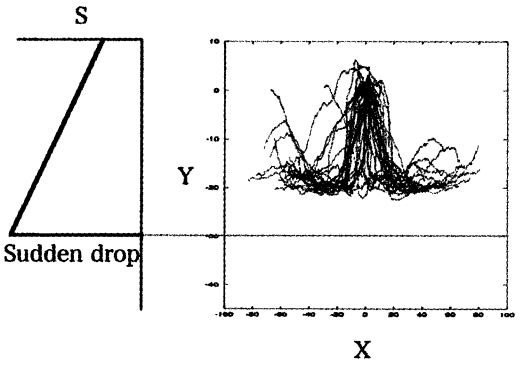


Figure 3: Behavior of the cell in the cliff gradient (at right) and a schematic picture of the cliff gradient (at left). The sudden drop is at $y = -30$.

Acknowledgments

This work is supported by ACT-JST program of Japan Science and Technology Agency.

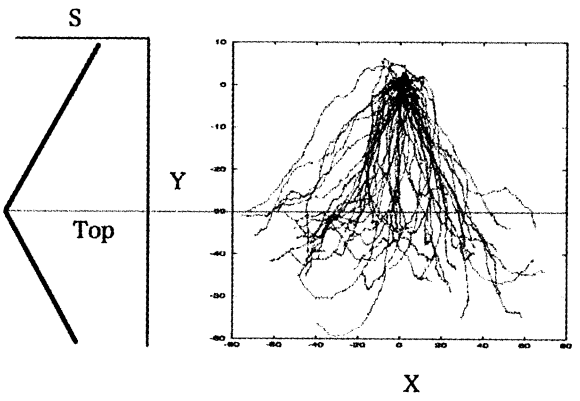


Figure 4: Behavior of the cell in the hill gradient and a schematic picture of the hill gradient. The top of the hill is at $y = -30$.

References

[1] Roitt I, Brostoff J, and Male D (1998), *Immunology*. Mosby International Ltd.

[2] Spiro PA, Parkinson JS, and Othmer HG (1997), A model of excitation and adaptation in bacterial chemotaxis. *Proc. Natl. Acad. Sci. USA*, 94:7263–7268

[3] Pollard TD (2003), The cytoskeletion, cellular motility and the reductionist agenda. *Nature*, 422:741–745

[4] Pollard TD and Borisy GG (2003), Cellular motility driven by assembly and disassembly of actin filaments. *Cell*, 112:453–465

[5] Pollard TD Blanchoin L and Mullins RD (2000), Molecular mechanisms controlling actin filament dynamics in nonmuscle cells. *Annu. Rev. Biophys. Biomol. Struct.*, 29:545–76

[6] Iijima M, Huang YE and Devreotes P (2002), Temporal and spatial regulation of chemotaxis. *Dev. Cell*, 3:469–478

[7] Levchenko A and Lglesias PA (2002), Models of eukaryotic gradient sensing: Application to chemotaxis of ameobae and neutrophils. *Biophys. J.*, 82:50–63

[8] Jeon NL, Baskaran H, Dertinger SKW, Whitesides GM, Water L and Toner M (2002), Neutrophil chemotaxis in linear and complex gradients of interleukin-8 formed in a microfabricated device. *Nature Biotechnol.*, 20:826–830

Proc. of The Ninth Int. Symp. on Artificial Life and Robotics (AROB 9th '04)
Beppu, Oita, Japan, 28-30 January, 2004

Time Minimum Extrinsic Blood Clotting System as a cascade biosignal transmission.

Hirohumi HIRAYAMA
Department of Public Health, Asahikawa Medical College.
hirayama@asahikawa-med.ac.jp

Abstract

Control strategy of the extrinsic blood clotting system was analyzed by computational approach. The temporal changes in the concentrations of the inactive precursors and their activated forms in the system were expressed by 15 non linear differential equations. We have proposed the time minimum (the shortest time) optimization . The temporal changes in the concentrations of the species under the time minimum optimization were obtained by solving 15 non linear rate equations of the system simultaneously with another 15 non linear differential equations for the adjoin variables corresponded to the species through partial differentiation of Hamiltonian under the multiple boundary conditions.

The temporal changes in the concentrations of species under the time minimization differed from the non minimization case in the rapid and considerable larger increase than those under the non minimization case at near the end of the reaction.

1. Introduction

Blood clotting system is one of the most important host defense mechanism. Once the clotting system has been activated, a sequential cascade reaction proceeds to produce clot to cease bleeding. Only a small trigger stimulation results in an enormous clot. Therefore, the process of rapid and large production of clot itself is non linear system. By numerous experiments[1], we can have detailed mechanism and minute constitution of blood clotting system. On the other hand, a few investigation has been carried to disclose integrated properties of the clotting reaction as a whole dynamical system [2]. There has been, however, no investigation for the organization principle namely, what kind of control strategy dominate the clotting reactions. Nobody has challenged to disclose whether the clotting system operate under the optimality, nor if it existed, is it time minimum control or least square minimization control of the species in the system ? Unfortunately, even by the up to date experimental technique, it is impossible to identify the control principle of the clotting system.

In the present study, to solve this problem, we have made a theoretical approach founded on precise rate equations in which the exact values of rate constants were referred from reported experiments. We have hypothesized that the clotting system operates under the optimal principle, either of the time minimum or the least square minimization. For the simplicity, analysis was confined only to the extrinsic pathway.

2. Processes in Blood Coagulation.

The extrinsic blood clotting system is comprised of a cascade of sequential activation reactions (Fig 1) in clotting factors with feed back loops [1] [2]. The extrinsic clotting reaction is activated by tissue thromboplastin (Factor 3) leaked out from damaged tissue. In Figure 1, Fni is an inactive precursor of Factor " n" which serves as a substrate. Fna is an activated form of Fni to work as a proteolytic enzyme for the subsequent activating reactions. Every activating process follows a Michaelis-Menten mechanism [1],[2],[3] such as

$$\mathrm{Fni} + \mathrm{Fma} \underset{k\text{-}n}{\overset{kn}{\leftrightarrow}} \mathrm{Yn} \xrightarrow{kns} \mathrm{Fna} + \mathrm{Fma} \quad \text{----(1)}$$

where Yn is the enzyme substrate complex of the proteolytic enzyme Fma and the substrate Fni. kn, k-n and kns are the rate constants. The activating process proceeds from formation of a complex Yn to dissociation of the complex Yn to active Factor n (Fna) and Fma through transformation of Fni to Fna by Fma on the complex Yn. In the activating process, we have involved Calcium ion and Phospholipid as accessory factors [1],[2]. The complex Yn is formed with the rate constant kn timed by the concentrations of the accessory factors involved. The coagulation completes with formation of fibrin coagulant from fibrin monomer derived from fibrinogen.

— Fibrinogen ----> fibrin monomer -----> fibrin coagulant ---------(2)

3. Theoretical method.

3-1. The rate equations.

By applying the mass-action law to the reactions in Figure 1, following rate equations were obtained (' denotes differentiation with respect to time)

$X_1' = -k_1 U F_3 PL X_1 - k_3 X_4 X_1 - k_{13} Ca\ PL X_6 X_1 - k_{2a} X_{10} X_1$ ------(3)

$X_2' = k_1 U F_3 PL X_1 + k_3 X_4 X_1 + k_{13} Ca\ PL X_6 X_1 - k_4 X_2 X_5 - k_{2ad} X_2 + k_{2a} X_{10} X_1$ ------(4)

$X_3' = -k_2 X_2 X_3 - k_{14} X_6 X_3$ ------(5)

$X_4' = k_2 X_2 X_3 + k_{14} X_6 X_3 - k_{4ad} X_4$------(6)

$X_5' = -k_4 X_2 X_5$ ------(7)

$X_6' = k_4 X_2 X_5 - k_5 Ca\ PL X_6 X_9 X_8 - k_{14} X_3 X_6 - k_{13} Ca\ PL X_1 X_6 - k_7 X_7 X_6 - k_{6ad} X_6 - k_i\ ATIII$ ------(8)

$X_7' = -k_7 X_7 X_6 - k_8 X_{10} X_7$ ------(9)

$X_8' = k_7 X_7 X_6 + k_8 X_{10} X_7 - k_5 Ca\ PL X_6 X_9 X_8 - k_{8ad} X_8 - k_{i2}\ ATIII - k_{iAPC}\ APC$ ------(10)

$X_9' = -k_5 Ca\ PL X_6 X_9 X_8$ ------(11)

$X_{10}' = k_5 Ca\ PL X_6 X_9 X_8 - k_{10} Ca X_{10} X_{11} - k_{11} X_{10} X_{13} - k_8 X_{10} X_7 - k_{10ad} X_{10} - k_{i3}\ ATIII$ --(12)

$X_{11}' = -k_{10} Ca X_{10} X_{11}$ ------(13)

$X_{12}' = k_{10} Ca X_{10} X_{11} - k_{12ad} X_{12}$ ------(14)

$X_{13}' = -k_{11} X_{10} X_{13}$ ------(15)

$X_{14}' = k_{11} X_{10} X_{13} - k_{12} Ca X_{14} X_{12}$ ------(16)

$X_{15}' = k_{12} Ca X_{14} X_{12}$ --------(17)

Fig 1. Activating Pathway for the Extrinsic Clotting System.

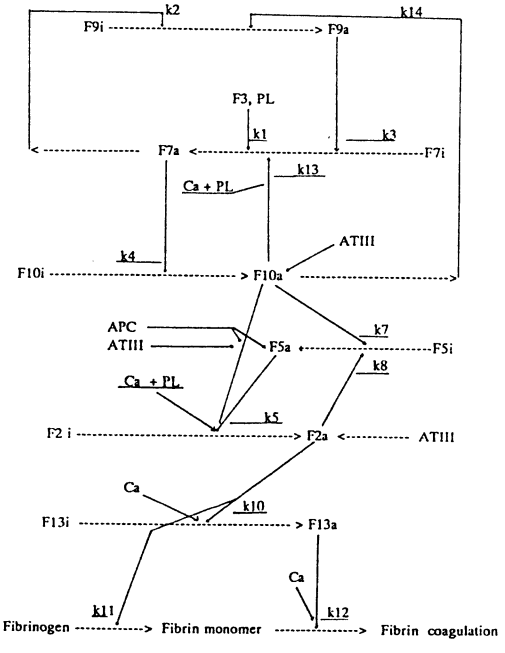


Table 1. List of the variables in the rate equations of the extrinsic clotting system of Fig. 1.

X1 : Inactive Factor 7
X2 : Activated Factor 7
X3 : Inactive Factor 9
X4 : Activated Factor 9
X5 : Inactive Factor 10
X6 : Activated Factor 10
X7 : Inactive Factor 5
X8 : Activated Factor 5
X9 : Inactive Factor 2 (Pro thrombin)
X10 : Activated Factor 2
X11 : Inactive Factor 13 (Fibrin-Stabilizing factor)
X12 : Activated Factor 13
X13 : Fibrinogen
X14 : Fibrin monomer
X15 : Fibrin coagulant
Ca : Calcium Ion
PL : Phospho Lipid
F3 : Factor 3. (Tissue Thrombo Plastin)
ATIII : Anti thrombin III.
APC : Thrombin activated protein C)

Xn denotes the concentration of species and are shown in Table 1. U is the trigger function to release the tissue thromboplastin (Factor 3) from the damaged tissue and is a control input. We have utilized the reported experimental data for rate constants. The values of kn, the initial concentrations of all the inactive precursors, Phospho Lipid (PL) , Calcium Ion (Ca) and Factor 3 are listed on Table 2 with references [4] to [24]. We have incorporated the inherent inhibitory effects by anti thrombin III [3],[20], [22] and thrombin activated protein C [21]. knad is the rate of degradation of Xn[2].

3-2. The time minimum optimal control.

Firstly, we propose the time minimum control as an optimal control strategy for the extrinsic clotting reaction. Because the ultimate purpose of the clotting reactions is to prevent the blood loss as soon as possible and minimize the damage. We have sought the shortest time course of the extrinsic clotting reaction based on the optimal control theory [25]. The cost function for the time minimum optimization is

$$J = \int_0^{te} 1 \, dt \quad \text{----------(I)}$$

Hamiltonian is

$$H = \lambda 0 + \lambda n \, Xn(t) \quad \text{----------(18)}$$

where λn is the adjoin variable for Xn(t). The optimized differential equations for the adjoin functions are obtained by differentiating Hamiltonian with respect to corresponding state variables Xn(t).

$$\lambda 1' = -\partial H/\partial X1 = -[\lambda 1(-k1\,U\,F3\,PL) + \lambda 1(-k3\,X4) + \lambda 1(-k13\,Ca\,PL\,X6) + \lambda 1(-k2a\,X10) + \lambda 2(k1\,U\,F3\,PL + k3\,X4 + k13\,Ca\,PL\,X6 + k2a\,X10) + \lambda 6(-k13\,Ca\,PL\,X6)] \quad \text{--(19)}$$

$$\lambda 2' = -\partial H/\partial X2 = -[\lambda 2(-k4\,X5 - k2ad) + \lambda 3(-k2\,X3) + \lambda 4(k2\,X3) + \lambda 5(-k4\,X5) + \lambda 6(k4\,X5)] \quad \text{--(20)}$$

$$\lambda 3' = -\partial H/\partial X3 = -[\lambda 3(-k2\,X2 - k14\,X6) + \lambda 4(k2\,X2 + k14\,X6) + \lambda 6(-k14\,X6)] \quad \text{--(21)}$$

$$\lambda 4' = -\partial H/\partial X4 = -[\lambda 1(-k3\,X1) + \lambda 2(k3\,X1) + \lambda 4(-k4ad)] \quad \text{--(22)}$$

$$\lambda 5' = -\partial H/\partial X5 = -[\lambda 2(-k4\,X2) + \lambda 5(-k4\,X2) + \lambda 6(k4\,X2)] \quad \text{--(23)}$$

$$\lambda 6' = -\partial H/\partial X6 = -[\lambda 1(-k13\,Ca\,PL\,X1) + \lambda 2(k13\,Ca\,PL\,X1) + \lambda 3(-k14\,X3) + \lambda 4(k14\,X3) + \lambda 6(-k5\,Ca\,PL\,X9\,X8 - k14\,X3 - k13\,Ca\,PL\,X1 - k7\,X7 - k6ad) + \lambda 7(-k7\,X7) + \lambda 8(k7\,X7 - k5\,Ca\,PL\,X9\,X8) + \lambda 9(-k5\,Ca\,PL\,X9\,X8) + \lambda 10(k5\,Ca\,PL\,X9\,X8)] \quad \text{--(24)}$$

$$\lambda 7' = -\partial H/\partial X7 = -[\lambda 6(-k7\,X6) + \lambda 7(-k7\,X6 - k8\,X10) + \lambda 8(k7\,X6 + k8\,X10) + \lambda 10(-k8\,X10)] \quad \text{--(25)}$$

$$\lambda 8' = -\partial H/\partial X8 = -[\lambda 6(-k5\,Ca\,PL\,X6\,X9) + \lambda 8(-k5\,Ca\,PL\,X6\,X9 - k8ad) + \lambda 9(-k5\,Ca\,PL\,X6\,X9) + \lambda 10(k5\,Ca\,PL\,X6\,X9)] \quad \text{--(26)}$$

$$\lambda 9' = -\partial H/\partial X9 = -[\lambda 6(-k5\,Ca\,PL\,X6\,X8) + \lambda 8(-k5\,Ca\,PL\,X6\,X8) + \lambda 9(-k5\,Ca\,PL\,X6\,X8) + \lambda 10(k5\,Ca\,PL\,X6\,X8)] \quad \text{--(27)}$$

$$\lambda 10' = -\partial H/\partial X10 = -[\lambda 1(-k2a\,X1) + \lambda 2(k2a\,X1) + \lambda 7(-k8\,X7) + \lambda 8(k8\,X7) + \lambda 10(-k10\,Ca\,X11 - k11\,X13 - k8\,X7 - k10ad) + \lambda 11(-k10\,Ca\,X11) + \lambda 12(k10\,Ca\,X11) + \lambda 13(-k11\,X13) + \lambda 14(k11\,X13)] \quad \text{--(28)}$$

$$\lambda 11' = -\partial H/\partial X11 = -[\lambda 10(-k10\,Ca\,X10) + \lambda 11(-k10\,Ca\,X10) + \lambda 12(k10\,Ca\,X10)] \quad \text{--(29)}$$

$$\lambda 12' = -\partial H/\partial X12 = -[\lambda 12(-k12ad) + \lambda 14(-k12\,Ca\,X14) + \lambda 15(k12\,C1\,X14)] \quad \text{--(30)}$$

$$\lambda 13' = -\partial H/\partial X13 = -[\lambda 10(-k11\,X10) + \lambda 13(-k11\,X10) + \lambda 14(k11\,X10)] \quad \text{--(31)}$$

$$\lambda 14' = -\partial H/\partial X14 = -[\lambda 15\,k12\,Ca\,X12 - \lambda 14\,Ca\,X12] \quad \text{--(32)}$$

$$\lambda 15' = -\partial H/\partial X15 = 0 \quad \text{----------(33)}$$

The time minimum temporal changes in the concentration of the species was obtained by solving equations (3) to (17) simultaneously with equations (19) to (33). The initial conditions Xn(t=0) were given in Table 2 while the terminal conditions for the adjoin variables were set to $\lambda n(Te) = 0$ (n= 1 to 14) and $\lambda 15\,(Te) = -1.0$ [26] . Thus, total 30 non linear differential equations were solved numerically under these two points boundary value constraint. Due to the complex nature of the present system, it is impossible to obtain the switching function in an analytical form. So, we set U, 1.0, 0.5, -0.5 and -1.0 [27]. Positive U indicates the system is driven and negative one indicates the system is inhibited.

3-3. Least square minimization of the changes in the concentrations of species.

3-3-1. Linearization of the system.

For analyzing the temporal behavior of the system under the least square minimization, we have linearized the non linear equations (3) to (17) in order to apply the linear system analysis. Firstly, we have solved these non linear differential equations. In the second, we compared the temporal changes in concentrations (μ mole/ml 10^5) of two species composing the non linear terms in the rate equations. The left part of Fig 2 shows examples of comparison. From these figures, it can be seen that X2 >> X5 (Fig 2-a), X9 >> X6, X8 (Fig 2-b) and X11 >> X10 (Fig 2-c). Thus, we set X1 (F7i), X3 (F9i), X5 (F10i), X7 (F5i) , X9 (F2i) and X11 (F13i) and X13 (Fibrinogen) as constant. As a result, all the non linear terms were linearized and we obtained 6 linearized differential equations. The right half of Fig 2 shows examples of comparing the temporal changes in the concentrations of F10a (Fig 2-d), F2a (Fig 2-e) and Fibrin monomer (Fig 2-f) obtained by solving the non linear differential equation (NL in figures) and by solving the linear ones (L in the figures). Both of them were not optimized in this stage. Because the rate equations were highly stiff, there were inevitable discrepancies between non linear and linearized solutions.

3-3-2. The performance function for the least square minimization.

Finally, based on the optimal control theory [25], we have optimized this linearized system such that the feed back law U = - K X minimizes the cost function (II).

$$J = \int_0^t [X\,Q\,X + U\,R\,U]\,dt \quad \text{----------(II)}$$

where Q and R are the weighting matrixes comprised of 6 * 6 elements to characterize the relative potency of minimizing the concentrations of the species and U. For the standard state, all the values in Q and R were set to unity. After this optimization, we have solved the linear differential equations under the same initial conditions as in the case (Table 2) of the time minimum optimization.

4. Results.

Fig 3 shows the minimum time courses of concentrations F7a (μ mole/ml 10^3, Fig 3-a), F5a (μ mole/ml 10^2 , Fig 3-b) and F10a (μ mole/ml 10, Fig 3-c). For U=+1.0 and +0.5, these species increased while for U=-1 and -0.5, they decreased.

Fig 4 shows the time specified comparison of the temporal changes in concentrations of the species in the non linear system under the time minimum optimized and non optimized one. F2a (μ mole/ml 10^5, Fig 4-a), F13a (μ mole/ml 10^5, Fig 4-b) and Fibrin coagulant (μ mole/ml 10^2, Fig 4-c) under the time minimum optimization increased rapidly particularly at near the end of reactions than those of non optimized system.

Fig 5 shows the influence of the least square minimization (described by the performance function (II)) on the temporal changes in the concentrations (μ mole / ml 10^5) of the species, F 10a, F13a, Fibrin coagulant. Fig 5-d, Fig 5-h are the gathered data of all the species in the linearized system under the same initial conditions with those of the time minimum optimization (I). The left half of Fig 5 is those without any optimization while the right half of Fig 5 is those under the least square minimization. The concentration of the optimized species (the right half of Fig 5) increased and disappeared rapidly but with considerable lower peak value than those of the non optimized linearized cases (the left half of Fig 5).

5. Discussion.

The present investigation was intended to disclose the control strategy of the extrinsic blood clotting system. The concentrations of the activated clotting factors and fibrin coagulant under the time minimum optimization increased rapidly than those without time minimum optimization. The least square minimization of the system resulted in irrational responses of the species. Thus the extrinsic clotting system must be controlled under the time minimum optimal control strategy rather than the least square minimization.

1. Computational approach and modeling of the clotting system.

The extrinsic clotting system is comprised of a complicated sequential reactions with multiple feed backs and cross link to the intrinsic clotting system [1],[2]. Thus, experimental approach can never disclose the entire properties and the inherent control strategy of the system. Therefore, computational approach based on a rigorous theory with exact values of the system parameters is the only was to solve above problems. In the previous work [2], by solving the non linear system equations, we have shown the validity of computational approach through presenting the successful simulations for the reported experimental data of temporal changes in the concentrations of the species in clotting system. Unfortunately, however, the lack for investigation disclosing the strategy or principle of the clotting system made our understanding of the system incomplete. In the present study as the second step, we have hypothesized the optimal control principle for the extrinsic clotting system.

2. Optimal control strategy.

The temporal changes in the concentrations under the time minimization showed a marked difference between the non minimization case, 1) the increase at early stage (before t=0.7 min in Fig 4) was gradual and lower concentration than non minimization case but 2) at near the end of the reaction time (t = 1.0 min), the time minimization reactions increased rapidly in considerably larger amount than those under the non minimization case. From the teleological stand point, these behaviors under the time minimization are consistent and rational to the ultimate purpose of the clotting reaction, namely to prevent the blood loss as soon as possible with sufficient amount of coagulant.

On the contrary, the onsets of the reactions of the species under the least square minimization (Fig 5-e, 5-f, 5- g and 5- h) were rapid and terminated considerably earlier than those of non least square minimization (Fig 5-a, 5-b, 5- c and 5- d). Apparently these prompt reactions seemed to be adequate for clotting reactions. The peak concentration of responses, however, was considerably smaller than the responses without least square minimization. Since sufficient amount of fibrin coagulant is required to bleeding, these results ((Fig 5-e, 5-f, 5- g and 5- h) suggested that the least square minimization is inconsistent to the ultimate purpose of the clotting reaction.

Present investigation has challenged to disclose the unknown feature of the extrinsic clotting system which had been impossible to investigate by experimental approach. Improvements in experimental technique will make comparison to our theoretical results possible.

6. Conclusion

The organization principle of the extrinsic clotting reaction must be the time minimum optimal control rather than the least square minimization for the concentrations of species.

7. References

[1] C.M. Jackson, " Blood coagulation, " Ann. Rev. Biochem. vol. 49 , pp. 765-811, 1980

[2] H. Hirayama , K. Yoshii , H. Ojima , N. Kawai , S. Goto and Y. Fukuyama , " Linear Systems Analysis of Blood Clotting System," I.E.I.C.E.. Transactions on fundamentals of electronics, communications and computer sciences. vol. E 78-A, pp.1419-1931, 1995

[3] G.M. Willems and H.C. Hemker, "Simulation model for thrombin generation in Plasma," Haemostasis, vol. 21, pp.197-207, 1991

[4] S.A. Silverberg, Y. Nemerson and M. Zur, "Kinetics of the activation of Bovine coagulation factor X by components of the extrinsic pathway," J. Biol. Chemistry, vol. 252, pp. 8481-8488, 1977.

[5] M. Zur and Y. Nemerson , "The esterase activity of coagulation factor VII, " J. Biol. Chemistry,vol. 253, pp. 2203-2209,1978.

[6] S.A Morrison and J. Jesty, "Tissue factor-dependent activation of tritium-labeled factor IX and factor X in human plasma, " Blood, vol. 63, pp. 1338-1347, 1984.

[7] J. Jesty and S.A. Silverberg, "Kinetics of the tissue factor dependent activation of coagulation factors IX and X in a Bobive plasma system, " J. Biol. Chemistry, vol. 254,pp. 12337-12345, 1979.

[8] S.P. Bajaj , S.I. Rapaport and W.A. Russell , "Redetermination of the rate limiting step in the activation of factor IX by factor XIa and by factor VIIa / tissue factor, " Biochemistry, vol .22, pp. 4047-4053,1983.

[9] M. Zur and Y. Nemerson, "Kinetics of factor IX activation via the extrinsic pathway, " J. Biol. Chemistry, vol. 255, pp. 5703-5707, 1980.

[10] R. Radcliffe and Y. Nemerson, "Activation and control of factor VII by activated factor X and thrombin, " J. Biol. Chemistry, vol. 250, pp. 388-395, 1975.

[11] B.J. Warn-Cramer and S.P. Bajaj , "Intrinsic versus extrinsic coagulation, " Biochem. J, vol. 239, pp. 755-762, 1986.

[12] L.V.M Rao, S.P. Bajaj and S.I. Rapaport, "Activation of human factor VII during clotting in vitro, " Blood, vol . 65, pp. 218-226, 1985.

[13] J. Pieters, T. Lindhout and H.C. Hemker, " In situ-generated thrombin is the only enzyme that effectively activates factor VIII and factor V in thromboplastin -activated plasma, " Blood, vol 74, pp. 1021-1024, 1989.

[14] J. Jesty , "Analysis of the generation and inhibition of activated coagulation factor X in purified systems and in human plasma, " J. Biol. Chemistry, vol. 261, pp. 8695-8702, 1986.

[15] D.D. Monkovic and P.B. Tracy, "Activation of human factor V by factor Xa and thrombin, " Biochemistry,vol. 29, pp. 1118-1128, 1990.

[16] T. Lindhout, C. Hemker and J. Rosing , "Factor Va-factor Xa interaction, " Biochemistry, vol. 21, pp. 5494-5502, 1982.

[17] W.B. Foster , M.E. Nesheim and K.G. Mann KG, " The factor Xa catalyzed activation of factor V, " J. Biological Chemistry, vol .258, pp. 13970-13977, 1983.

[18] T. Lindout and H.C. Hemker , "Thrombin generation and inactivation in the presence of antithrombin III and heparin, " Biochemistry, vol. 25, pp. 5962-5969, 1986.

[19] W. Kisiel and W.M. Canfiled, Method of Enzyme, vol. 80, pp. 246, 1980.

[20] G.F. Smith, Fibrinogen- The specific thrombin substrate ; in Machovich R (ed) : The Thrombin. Boca Raton, CRC Press, vol . 1, pp. 55-82, 1984.

[21] S. Solymoss, M.M. Tucker and P.B. Tracy, "Kinetics of inactivation of membrane -bound factor Va by activated protein C, " J. Biol. Chem. vol. 263, pp. 14884-14890, 1988.

[22] P. Schoen , T. Lindhout , G.M. Willems and H.C. Hemker, "Antithrombin III-dependent anti-prothrombinase activity of heparin and heparin fragments, " J. Biol. Chem. vol . 264,pp. 10002-10007,1989.

[23] J. Rosing , H.C. Hemker, "The role of phospholipids and factor Va in the prothrombinase complex, " J. Biol. Chem. vol. 255, pp. 274-283, 1980.

[24] L.V.M. Rao, S.I. Rapaport and S.P. Bajaj, "Activation of human factor VII in the initiation of tissue factor-dependent coagulation, " Blood. vol. 68, pp. 685-691, 1986.

[25] L.S. Pontryagin, " The mathematical theory of the optimal process, " J. Wiley. Inc. 1962.

[26] A.S. Perelson and G.F. Oster, " Optimal strategies in Immunology. J. Mathematical Biology, vol. 3. pp. 325-367, 1976.

[27] M Athans and P.L. Falb. Minimum time control of linear systems. Sec 6-5. In. Optimal Control. New. York. McGraw-Hill. 1966.

Table 2. The rate constants from reported experimental data.

k1 = 3.3 mM	[5]
k2 = 254 nM - 540 nM	[8], [9], [11]
k3 = 2.6- 3.1 mM	[12] [24]
k4 = 0.45 (μM)	[4] [6] [14] [19]
k5 = 210 (nM)	[16], [23]
k2a = 5.8 mM	[10]
*k6 =0 (damy data)	
k7 = 10 nM	[15], [17]
k8 = 72 nM	[13] [15]
*k9 = 0 (damy data)	
k10 = 20 μM	[19]
k11 = 2 μM	[20]
k12 = 10 mM	[2], [19]
k13 =0.6 mM	[12] [24]
k14=0.85 μM	[6] [7]

k-1 = k-2 = k-3 = k-4 = k-5 = k-6 = k-7 = k-8 = k-9
= k-10 = k-12 = k-13 = k-14 = 10^{-6}nM [2]

k2ad = k4ad = k6ad = k8ad = k10ad = k12ad = 10^{-6}nM [2]

ki1 = 0.25 /min	[3]
ki2 = 0.05 /min	[14], [18], [22]
ki3 = 1.3/min	[18], [20]
kiapc2 = 24 /min	[21]

Fig 2-a

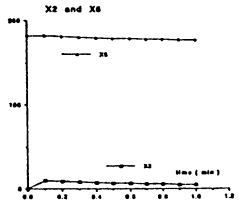


Fig 2-d

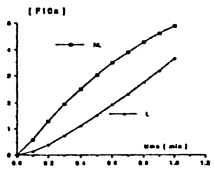


Fig 2-b

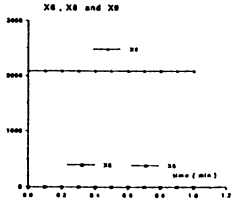


Fig 2-e

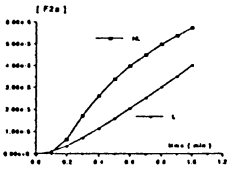


Fig 2-c

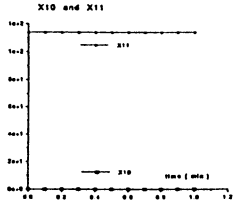


Fig 2-f

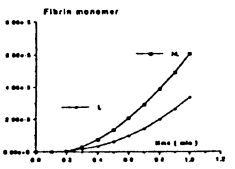


Fig 3-a

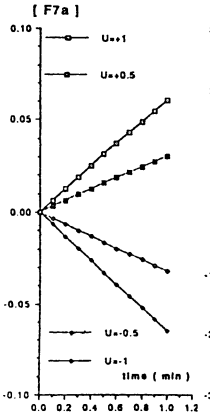


Fig 3-b

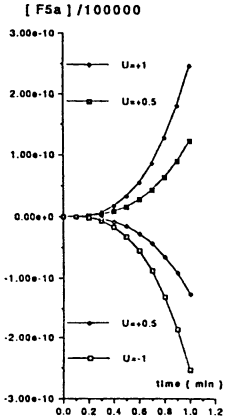


Fig 3-c

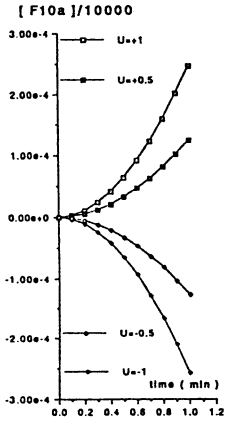


Table 3.

Initial conditions of inactive precursors for clotting factors and the accessory factors (μg/ml) [1]

F7i	0.5 (μg/ml)	5.0 10^4 (mole)
F9i	5.0 (μg/ml)	5.5 10^5 (mole)
F10i	10.0 (μg/ml)	5.5 10^4 (mole)
F5i	10.0(μg/ml)	3.3 10^6 (mole)

Tissue thromboplastin (Factor 3) 0.1 (μg/ml)

F2i	40(μg/ml)	7.2 10^4 (mole)
F13i	10 (μg/ml)	8.8 10^4 (mole)

Fibrinogen 3600(μg/ml)

Ca 3.76 - 5.04 mg /dl

PL 145-256 mg/dl

Fig 4-a

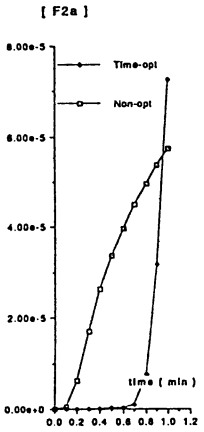


Fig 4-b

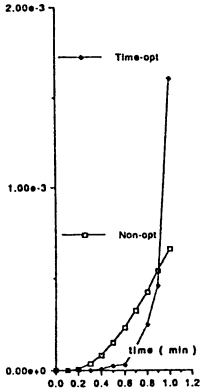


Fig 4-c

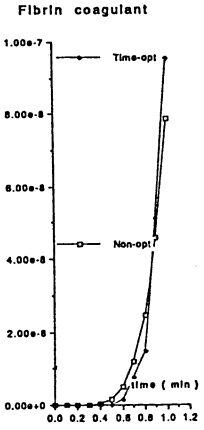


Fig 5-a

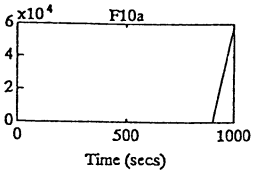


Fig 5-e

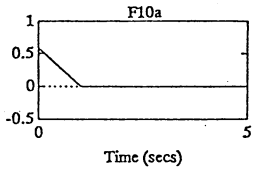


Fig 5-b

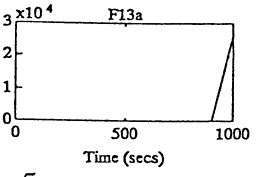


Fig 5-f

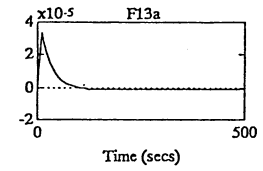


Fig 5-c

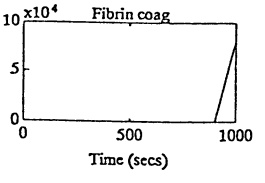


Fig 5-g

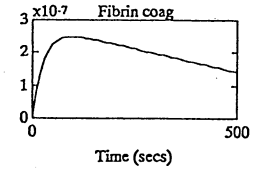


Fig 5-d

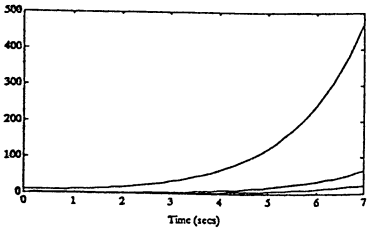
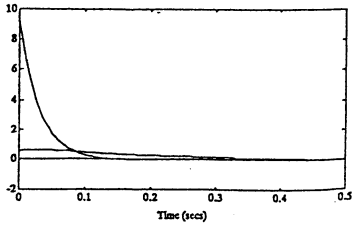


Fig 5-h



Proc. of The Ninth Int. Symp. on Artificial Life and Robotics (AROB 9th '04)
Beppu, Oita, Japan, 28-30 January, 2004

Finding evolutional mechanism in financial time series by means of correlation dimension analysis

Mieko Tanaka-Yamawaki and Hiroto Tanaka
Department of Information and Knowledge Engineering, Tottori University, Tottori, 680-8552 JAPAN

Abstract

We apply correlation dimension analysis to show that tick-wise movements of price fluctuation has stronger deterministic element in comparison to lower frequency motions like the daily close values, which are known to be random walks.

1.Introduction

Financial time series are known to be highly random. This fact makes prediction very hard. At the same time the same property gives every trader a chance to win in the market on which the fairness of the market is guaranteed. In the context of financial engineering, this situation is usually written as follows:

$$X_n = X_{n-1} + \Delta X \qquad (1)$$

where the increment is a Gaussian noise added by appropriate income coming from interest rate r.

$$\Delta X \approx N(0,\sigma^2) + r\Delta t \qquad (2)$$

However, recent knowledge on high frequency price motions much faster than the daily base has altered the above view in many aspects. Mentioning a few of them we have:

(1) Probability distributions of price increments have fat tails, indicating deviation from the pure random walk. [1]

(2) Correlation between two price increments at different moments diminishes very soon as they separate more than a few ticks. [2]

(3) Correlation of volatilities at different moments lingers for a large scale.

(4) Conditional probabilities in regard to the signs of tick-wise price increment are far from the coin-tossing and keep almost the same values for several years. [3]

Plenty of works are currently ongoing [4] and we expect to have more established view on the property of high frequency data in the near future.

Suppose if we write instead of Eq.(2) the price fluctuation by denoting Levy's stable distribution of mean value x, index α and scale parameter γ by $L(x,\alpha,\gamma)$,

$$\Delta X \approx L(0,\alpha,\gamma) + r\Delta t \qquad (3)$$

this is not a whole story. Already in Ref.[1] the real data were not on a single distribution function and only the center part of the distribution was consistent with Levy's stable distribution of α=1.4.

In predicting the immediate future of financial time series, we rather use autoregressive process (AR) and fit the parameters in the linear expression.

$$X_n = a_0 + a_1 X_{n-1} + \cdots + a_p X_{n-p} \qquad (4)$$

More generally we look for a map f in

$$X_n = f(X_{n-1}, X_{n-2}, \ldots, X_{n-p}) \qquad (5)$$

In case if f in Eq.(5) is a chaos map we expect a random-like time series as an output of Eq.(5), and by reconstructing an attractor from the output time series would show fractal property, which may be detected by performing the correlation dimension analysis and the resulting correlation dimension would have a non-integer value.

There are still other sources to cause randomness in financial time series, such as many-body effect in the process of determining a price, and even a pure coin-toss effect that always affect human decisions. Taking all of them as noise factor η, we write

$$X_n = f(X_{n-1}, X_{n-2}, \ldots, X_{n-p}) + \eta \qquad (6)$$

i.e., the next price is determined by a certain deterministic map f and the noise η term.

Menna, Rotundo and Tirozzi recently analyzed about three thousand data points of daily closure prices of Italian car industry shares and concluded that the major portion of the price movements is stochastic [5].

We examine this issue in more detail by means of analyzing correlation dimensions of two set of tick-wise data, price of in individual stock (A) and foreign exchange rate (B) which are expected to have more deterministic

elements than those of daily data (A', and C).

2. Estimating correlation dimensions

If the time series $X = \{X_0, X_1, X_2, ...\}$ is generated as a result of a certain chaos map, the reconstructed attractor has self-similarity and the correlation dimension should have a non-integer value. We adopt a simple method known as GP algorithm [6,7] to estimate the correlation dimension as a saturation point of the local slopes of log-log plot of correlation integral as a function of m-dimensional distance r between two points, as m increases. Namely taking points at every time delay parameter τ from the time series $X = \{X_0, X_1, X_2, ...\}$ we reconstruct a trajectory in m-dimensional vector space

$$\vec{X} = (X_n, X_{n+\tau}, ..., X_{n+(m-1)\tau}) \qquad (7)$$

Correlation integral C(r) is computed by counting the number of pairs of points that are found within distance r.

$$C(r) = \lim_{n\to\infty} \frac{1}{N(N-1)} \sum_{\substack{i,j=1 \\ i\neq j}}^{N} H(r - |\vec{X}_i - \vec{X}_j|) \qquad (8)$$

The scaling behavior

$$C(r) \propto r^D \qquad (9)$$

indicates the fractal property. The index D, correlation dimension, is estimated as the saturation point of local slopes in log-log plot of Eq. (8).

3. Comparison of daily data vs. tick data

3.1 Individual stock price (tick to daily)

Following the method explained in section 2, we compared tick data of the first 100,000 ticks of IBM stock price corresponding to the interval from January 1, 1998 to late February in 1998, with the corresponding daily data. We also compare the intermediate time scale by taking every 10 points from the tick-wise data (total 10,000 points), and every 100 points (total 10,000 points by adding A the following days toward the end of the same year.)

The embedding dimension M runs from 1 to 10, and the time delay parameter τ from 1 to 4. We took a fixed value τ =2 to draw the following figures, based on the observation that the most stable result is obtained around this value.

Fig.1a shows the correlation integral of the tick data A, and Fig.1b is the local slopes of each line in Fig.1a. Note that a stable plateau can be seen in the range 0.5<r<1.5 for M=4-10. The plateau for M=4-10 in Fig.1b is enlarged and is shown in Fig.1c.

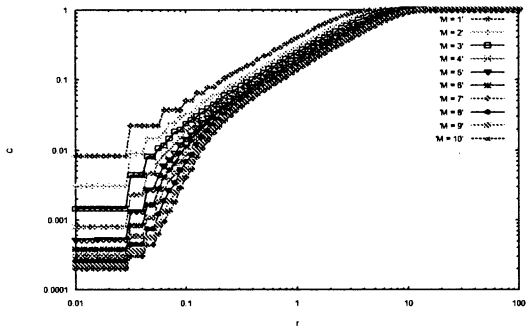


Fig.1a Correlation integral C(r) as a function of distance r (0.01<r<100) computed for tick data A is shown in log-log plot.

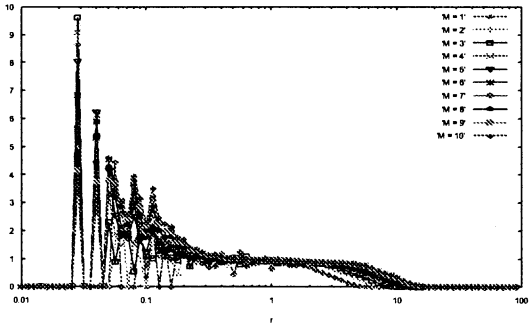


Fig.1b Local slopes of the correlation integral logC(r) vs. log(r) in Fig.1a. Horizontal axis is the same as Fig.1a. Note that a stable plateau is observed in the range of 0.5<r<1.5.

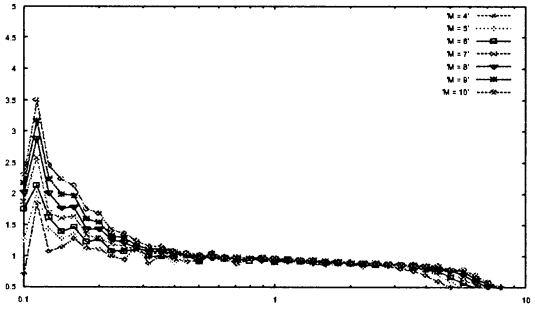


Fig.1c The enlarged portion of plateau of Fig. 1b (0.1<r<10) for M=4-10, which may support a view that the tick-wise price moves are driven by a certain map.

Next we will see how this plateau shrinks as we increase the time resolution toward the daily base. First we use the same tick data as in Figs.1 but take every 10 points. Fig.2a shows the correlation integral C(r) in log-log plot. Fig.2b shows the local slopes of log C(r). For further comparison we show the result of taking every 100 points in Fig.3a and Fig.3b.

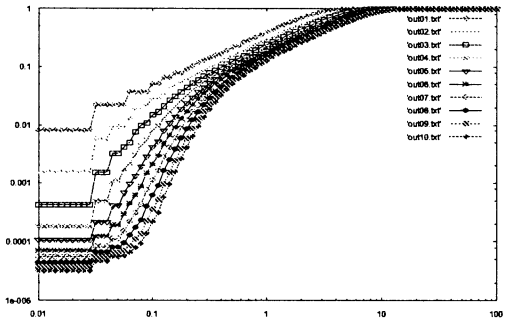


Fig.2a The correlation integral C(r) for the tick data A rougher resolution (data points taken every 10 points from the original data).

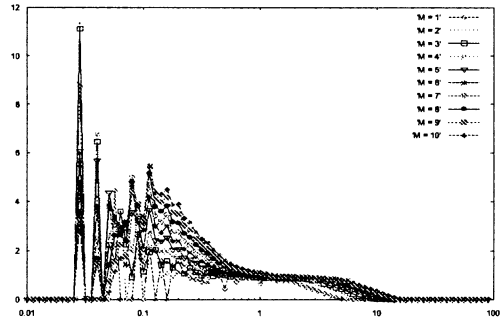


Fig.2b Local slopes of the correlation integral logC(r) vs. log(r) in Fig.2a. Horizontal axis is the same as Fig.1a. The region of stable plateau has shrunk considerably compared to the tick-wise motion in Fig.1b, indicating the random factors began dominating the time series.

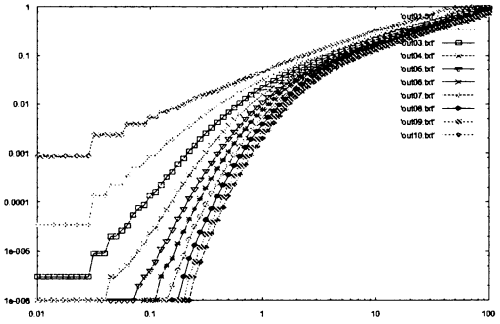


Fig.3a The correlation integral C(r) for the tick data A in much rougher resolution (data points taken every 100 points from the original data).

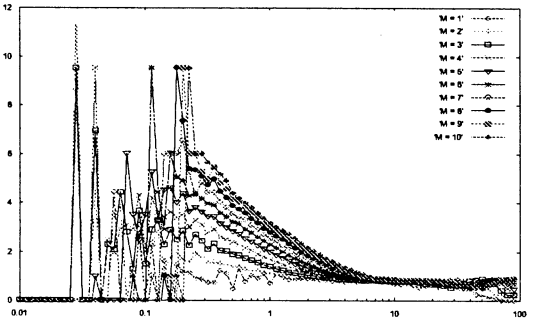


Fig.3b Local slopes of the correlation integral logC(r) vs. log(r) in Fig.3a. The region of stable plateau has shrunk further, indicating more randomness dominates the time series.

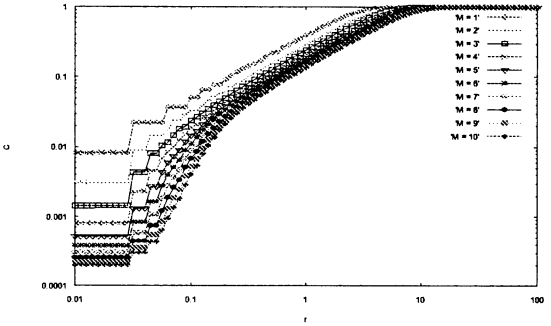


Fig.4a Correlation integral C(r) as a function of distance r ($0.01<r<100$) computed for daily close data of the same stock A, having 756 data points) is shown in log-log plot.

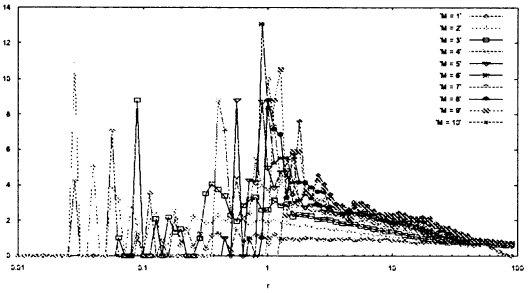


Fig.4b Local slopes of the correlation integral log C(r) vs. log(r) in Fig.4a. No stable region can be seen, and the data can be interpreted as a random data.

3.2 Foreign exchange rate (tick vs. daily)

We show the result of the same analysis on foreign exchange rate. We use the first one million ticks of U.S.Dollar vs. Japanese Yen taken from CQG terminal from January 2, 1995 to April 30, 2001, which we call B (tick data). We compare those results with the corresponding daily data of U.S.Dollar vs. Japanese Yen taken separately from a web page which we call C(daily data), extending January 2,

1985 to January 2, 2002, having 4,400 data points.

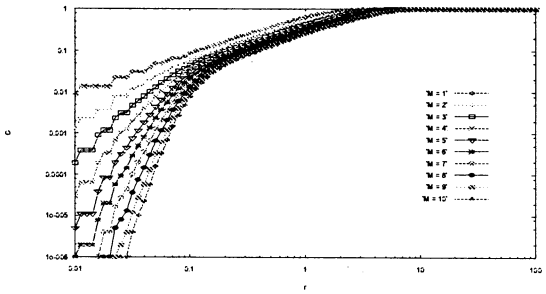


Fig. 5a Correlation integral C(r) for range 0.01<r<100 computed for tick-wise motion of foreign exchange rate (B) is shown in log-log plot.

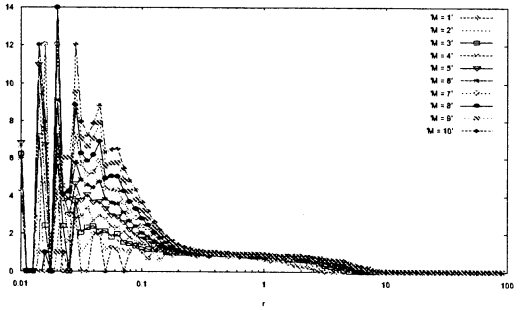


Fig.5b Local slopes of log C(r) vs. log(r) in Fig.5a. Note that a stable plateau is observed in the range of 0.5<r<1.0

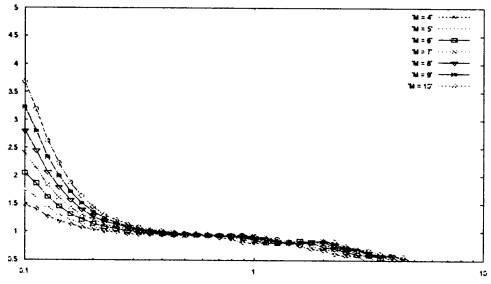


Fig.5c The enlarged plateau of Fig. 5b (0.1<r<10) for M=4-10, which may support a view that the tick-wise price moves are driven by a certain map.

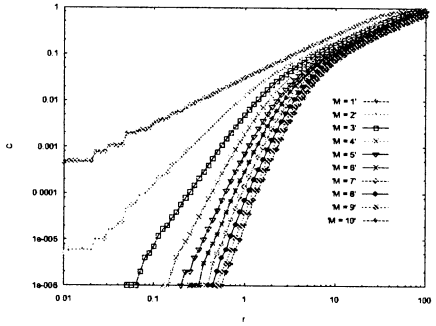


Fig 6a Correlation integral C(r) as a function of distance r (0.01<r<100) computed for daily close value of foreign exchange rate, C (4,400 data points), is shown in log-log plot.

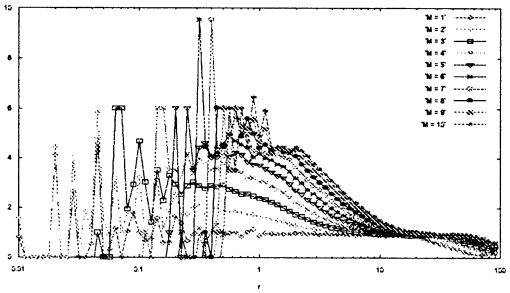


Fig.6b Local slopes log C(r) vs. log(r) in Fig.6a.

4. Conclusion

We have shown by analyzing tick data and daily data of price movements that very fine motions have definite values of correlation dimension showing the existence of deterministic mechanism, while longer frequency movements have no definite values of correlation dimension thus equivalent to random walks.

Acknowledgments

This work is supported in part by Scientific Grant-in -Aid by the Ministry of Education, Culture, Sports, Science and Technology of Japan (C2:14580385)

References

[1] R.N. Mantegna and H.E. Stanley(1995), "Scaling Behavior in the Dynamics of an Economic Index" Nature, 376:46-49

[2] e.g., M. Tanaka –Yamawaki(2002), "A study on the predictability of high frequency financial data, Sugisaka M (ed), Proceedings of the International Symposium on Artificial Life and Robotics (AROB7th), Beppu, Oita Japan, Jan 16-18, pp.74-77

[3] M. Tanaka- Yamawaki and S. Komaki(2003), "Characteristic features of high frequency financial time series", Sugisaka M(ed), Proc. International Symposium on Artificial Life and Robotics (AROB8th), Beppu, Oita Japan, Jan 28-30: 74-77

[4] e.g., http://irene.ike.tottori-u.ac.jp/mieko/econo

[5] M. Menna, G. Rotundo and G. Tirozzi(2002), International Journal of Modern Physics C, 13: 1-9.

[6] T. Ikeguchi, T. Yamada, M.Komuro, "Fundamentals and Applications of Chaos Time Series Analysis" (Sangyo Tosho, 2000, in Japanese)

[7] P. Grassberger and I. Procaccia(1983), "Characteristics of Strange Attractors", Physical Review Letters 50:346-349

Proc. of The Ninth Int. Symp. on Artificial Life and Robotics (AROB 9th '04)
Beppu, Oita, Japan, 28-30 January, 2004

Gene expression modelling with the use of Boolean network

Tomasz Kubik† Masanori Sugisaka*

† Institute of Cybernetics Engineering, Wroclaw University of Technology,
Janiszewskiego 11/17, Wroclaw 50-372, Poland
E-mail: tkubik@ict.pwr.wroc.pl
* Department of Electrical and Electronic Engineering, Oita University,
700 Dannoharu, Oita 870-1124, Japan
E-mail: msugi@cc.oita-u.ac.jp

Keywords: gene expression modelling, Boolean networks

Abstract

In this paper we concern a method of gene networks modelling. A gene network is a mass of genes interacting with one another through expression. The level of expression of each gene can be measured indirectly, by estimating how many mRNA copies are present in the cell. The measurements can be made at different time steps and in different environmental settings. Such data can be collected in order to infer a gene expression mechanism.

In our approach we have tried to automate a process of interaction identification employing a Boolean network model. We have shown that large data can be handled efficiently with the aid of already developed methods and algorithms. Thanks to them drawing a meaningful inferences from large gene expression data may converted into a simple tasks. We hope that such an analysis can help in genetics engineering, for example, assisting to distinguish the most important (controlling) genes in a large set of other genes.

1 Introduction

In the biological science gene expression is understood as the study on, which of genes are "expressed," or active, at any given time in a particular cell or tissue. By the central dogma, the gene expression corresponds to the functional state of an organism. Thus, measuring the levels of gene expression and identifying interactions between genes can give valuable insight into the dynamics of life. The level of expression of each gene can be measured indirectly, by estimating how many mRNA copies are present in the cell. The measurements can be made at different time steps and in different environmental settings. Resulting time series serve as a base for the gene regulation mechanism investigation.

To collect gene expression data several technological solutions has been already proposed[1]. One of the most productive is called *DNA microarray* (or *DNA microarrays*, or *DNA chips*, or *gene chips*, etc.)

In this paper we focus on the investigation of gene regulation mechanisms based on time series of gene expression patterns. The time series can be regarded as the state transition tables of a finite state system or as a collection of input-output pairs of an unknown Boolean function. A Boolean network model and its variations in the context of network inference from state transition tables were already studied [2, 3, 4]. In particular, Liang, Fuhrman and Somogyi [3] proposed an algorithm named REVEAL for the Boolean networks inference. In our approach Boolean network model is used to determine the Boolean function from an input-output data.

2 Microarrays as a source of data

Microarrays use the preferential binding of complementary single-stranded nucleic acid sequences. They are usually glass slides on which DNA molecules are attached at fixed locations (spots). There are different ways how microarrays can be used to measure the gene expression levels. In general the measuring starts with the mRNA extraction from the cells, followed by fluorescent labelling. Then labelled cDNA samples are washed over the microarray and the amount of nucleic acid bound to each spot is measured by a level of (excited by a laser) fluorescence emitted. This gives the raw data that must be processed the image analysis software. The final data are produced after some scaling procedures. Measurements are repeated over the time, so different times series are obtained for different environmental settings.

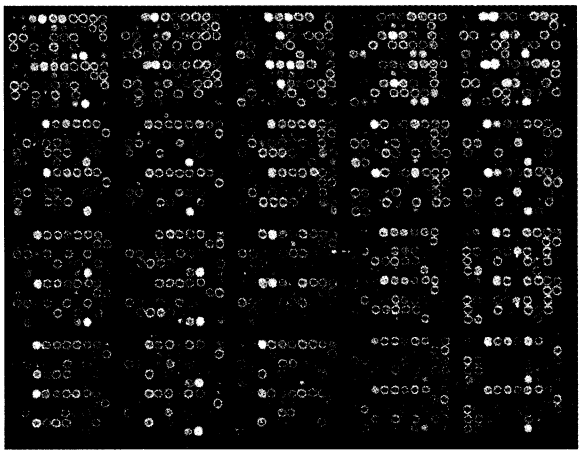


Figure 1: Part of an illuminated microarray

3 Boolean networks

The roots of the Boolean networks lie in the automata theory that was a subject of Turing and von Neumann work. This theory, primarily employed in the system engineering, was adapted by Kauffman [5] for a genetic regulatory networks modelling.

Description: In brief, a Boolean network is a system of N interconnected binary elements - nodes. Each node takes input from some specified number of other nodes. The number of inputs may vary or be the same for all nodes in the network. It is common to express number of inputs by the variable K. There is a Boolean activation function assigned with each node. This function evaluate the truth or falsity of its arguments, specifically, it compute node output based on the binary values of node inputs.

Representation: Boolean network can be represented as:

- a pair $G(V,F)$, where $V = \{v_1, v_2, \ldots, v_N\}$ is a set of nodes, and $F = \{f_1, f_2, \ldots, f_N\}$ is a set of Boolean functions associated with nodes. The output of a node i at the time step T is represented by binary value $v_i(T) \in B$, $B = \{0,1\}$. $v_i(T+1)$ is calculated from based on the node's inputs at the time step T, $v_i(T+1) = f\left(v_{i1}(T), v_{i2}(T), \ldots, v_{ik_j}(T)\right)$. The number of arguments k_i of f_i equals to the number of particular node's inputs (outputs from other nodes or itself), thus $f_i : B^{k_i} \rightarrow B$.

- a wiring scheme and set of rules, that declares, respectively, for each node a set of input nodes and an updating rule. Let set V' be a copy of V. Then, a wiring scheme is a graph, $G'(V'', E)$, where $V'' = V \cup V'$, and E is a set of edges. Set E consist of links connecting such nodes $v_j \in V$ with a given node $v'_i \in V'$, whose indexes $j = i_1, \ldots, i_{k_i}$ correspond to the indexes of inputs to v_i.

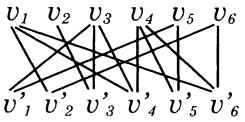
- a truth table that consists of all possible variations of the N inputs and outputs.

Lets consider a Boolean network consisting of six nodes: $v_1, \ldots, v_6$ with the truth table and the wiring scheme defined as in the Table 1 and Table 2. Such a network is fully defined. The wiring scheme can be constructed from the truth table with the use of Boolean minimization algorithms (reverse engineering task), and the truth table can be constructed from the wiring scheme.

Table 1: Truth table of 6 node Boolean network

64 inputs-outputs pairs (not all are shown)		
inputs (outputs at the time step T-1)	v_1	000000000000..111111111111111111
	v_2	000000000000..001111111111111111
	v_3	000000001111..110000000011111111
	v_4	000011110000..110000111100001111
	v_5	001100110011..110011001100110011
	v_6	010101010101..010101010101010101
outputs (at the time step T)	v_1	000000000011..110000000000110011
	v_2	010101010101..111111111111111111
	v_3	000000001111..111111111111111111
	v_4	000000000000..000000000000000000
	v_5	111100111111..111111001111110011
	v_6	010111110101..111111111111111111

Table 2: Set of rules and wiring scheme

set of rules:	wiring scheme:
$v'_1 = v_3 \& v_5$	
$v'_2 = v_1 \vert v_6$	
$v'_3 = v_2 \vert v_3$	
$v'_4 = !v_1 \& v_3 \& v_4$	
$v'_5 = !v_4 \vert v_5$	
$v'_6 = v_1 \vert v_4 \vert v_6$	

The most useful information regarding the Boolean network behavior is stored in the wiring scheme and the set of rules. In the gene expression modelling with the use of Boolean network the rules and wiring scheme are subjects of investigations.

4 Boolean network model of gene expressions

The model we use is based on the assumption that: each gene can be either in "on" or "off" state; the time occurs in discrete, clocked moment: $T = 1, 2, 3, \ldots$; state of each gene (binary output) at the next time step is determined by a Boolean function of its inputs at the current time step, and each node updates its state synchronously; genes may have different number of inputs. Hence, each gene can be treated as a node of a certain Boolean network. The properties of this network reflect properties of cells. For a real living cell the topology of the gene network is not known *a priori*. It must be synthesized first. This reverse engineering task can be defined as follows: given a (large) set of gene expression observations find a wiring diagram and transition rules (Boolean functions), such that the network fits to these observations. In most approaches the problem of network synthesis was tackled with small or even without referring to the achievements of electrical engineering, where the same problem, known as Boolean function minimization, has been solved.

Table 3: Time series examples

	series 1				series 2				
T	1	2	3	4	1	2	3	4	5
v_1	0	0	0	0	0	0	0	0	1
v_2	0	0	1	1	0	0	1	1	1
v_3	1	1	1	1	0	0	0	1	1
v_4	1	1	1	1	1	0	0	0	0
v_5	0	0	0	0	0	0	1	1	1
v_6	0	1	1	1	0	1	1	1	1

Let assume that the Boolean network (Table 1, Table 2) represents expressions of 6 genes and that the wiring scheme is not known. The only data we have are the observations time series. We can simulate these observations and generate the time series as in Table 2. These series must serve as a base for reverse engineering task, i.e. from them the gene interference pattern (wiring scheme and rules) must be constructed.

5 Boolean function minimization - reverse engineering of Boolean networks

Minimization of Boolean function has a long history in electrical engineering. It has been involved in the process of digital circuit design that realize desired input-output while optimizing some cost criteria[6, 7, 8]. Nowadays, several highly efficient cost optimization algorithms exist. Some of them, like ESPRESSO, [9], are publicly available. They can be exploit when modelling gene expressions by Boolean networks, even that some assumptions on which these algorithms rely do not necessarily make biological sense.

5.1 Two-level Boolean Minimization

Boolean function minimization belongs to the family of NP-hard problems. Two-level minimization is one of the methods that provide solution in the most efficient way. Such a minimization may lead to the discovery of wirings schemes and rules for Boolean network models of gene expression. Some of cost functions used in minimization, as types of Boolean functions, number of inputs per node (gene), reuse of inputs from important nodes (regulators), etc., would allow the networks to be biased towards biologically plausible features.

The two steps in two-level Boolean minimization are: 1) generation of the set of prime product-terms for a given function; 2) selection of a minimum set of prime terms to implement the function. State-of-the art logic minimization algorithms are all based on the Quine and McCluskey method. The method reduces a function in sum-of-products form to a set of *prime implicants* from which as many variables are eliminated as possible. These *prime implicants* are then examined to see if some of them are redundant. The method makes repeated use of the law $v+!v = 1$ in the reduction phase.

The sum-of-products is also known as the *minterm canonic form* - function in that form is a logical sum of *minterms* (logical products of variables where each variable is used once and once only.) In example $f(v_1, v_2, v_3, v_4) = v_1 \& v_2 \& v_3 \& !v_4 | !v_1 \& v_2 \& v_3 \& v_4$ is a function in the form of sum-of-products, and $v_1 \& v_2 \& v_3 \& !v_4$ and $!v_1 \& v_2 \& v_3 \& v_4$ are minterms (& - logical AND, | - logical OR, ! - logical NOT). The set of minterms for which f evaluates to 1 (0) is called the ON-set (OFF-set). DC-set (don't care) is a set of minterms, for which Boolean function is not specified, so |ON-set| + |OFF-set| + |DC-set| = 2^N. Lets consider the example of Boolean network (Table 1 and Table 2) assuming that the only available data are two time series of gene expressions (Table 3). Thus, there are only 9 input-output pairs available (Table 4) while 64 are necessary to fully specify Boolean network. The Boolean minimization algorithms must deal with this

Table 4: Input-output pairs

inputs/outputs (series 1)	inputs/outputs (series 2)
001100/001101	000100/000001
001101/011101	000001/010011
011101/011101	010011/011011
011101/011101	011011/111011
	111011/111011

fact. If we restrict the minimization only to the pairs provided, the solution of minimization is:

$$v'_1 = v_2\&v_3\&!v_4\&v_5\&v_6$$

$$v'_2 = !v_1\&!v_2\&!v_3\&!v_4\&!v_5\&v_6|!v_1\&v_2\&!v_4\&v_5\&v_6| v_2\&v_3\&!v_4\&v_5\&v_6|!v_1\&v_3\&v_4\&!v_5\&v_6$$

$$v'_3 = !v_1\&v_2\&!v_4\&v_5\&v_6|v_2\&v_3\&!v_4\&v_5\&v_6| !v_1\&!v_2\&v_3\&v_4\&!v_5|!v_1\&v_3\&v_4\&!v_5\&v_6$$

$$v'_4 = !v_1\&!v_2\&v_3\&v_4\&!v_5|!v_1\&v_3\&v_4\&!v_5\&v_6$$

$$v'_5 = !v_1\&!v_2\&!v_3\&!v_4\&!v_5\&v_6|!v_1\&v_2\&!v_4\&v_5\&v_6| v_2\&v_3\&!v_4\&v_5\&v_6$$

$$v'_6 = !v_1\&!v_2\&!v_3\&!v_4\&!v_5\&v_6|!v_1\&v_2\&!v_4\&v_5\&v_6| v_2\&v_3\&!v_4\&v_5\&v_6|!v_1\&!v_2\&v_3\&v_4\&!v_5| !v_1\&v_3\&v_4\&!v_5\&v_6|!v_1\&!v_2\&v_4\&!v_5\&!v_6$$

If the missing pairs are treated as a DC-set, the solution has a form:

$$v'_1 = v_3\&v_5 \ ; \ v'_2 = v_6 \ ; \ v'_3 = v_3\&!v_5|v_2$$
$$v'_4 = v_3\&!v_5 \ ; \ v'_5 = !v_4 \ ; \ v'_6 = 1$$

As we can see, the solutions obtained differ from the real Boolean network (Table 2). In general, hidden Boolean multiple input - multiple output function can not be evaluated for any arbitrary input. Because the input patters are determined by the environment settings and the internal state of the cells, some of the patterns can not be observed at all. Thus, even with a good tool for reverse engineering there is a chance that obtained model will not reflect accurately a real gene expression network.

6 Conclusions

When modelling gene expressions it must be considered that real gene expression levels tend to be continuous rather than binary. Moreover, because genes spend a lot of their time at intermediate values, some temporal aspects have to be taken into account as well. Nevertheless, the Boolean network model together with the use of Boolean minimization algorithms may help to understand basic functions and interconnections between genes. The model's advantages, as simplicity and large scale modelling ability, make it very attractive, especially for implementation on computers.

As we have shown, the Boolean network model provides a simple way for reverse engineering of gene networks. The accuracy of the model depends on the amount of experimental data (variations of input-output pairs.) If the data samples covers widely solutions space, then there is a chance that the Boolean network will reflect reality well.

References

[1] A. Brazma and J. Vilo: "Gene expression data analysis," *FEBS Letters*, **480**, pp. 17–24, (2000)

[2] T. Akutsu, S. Miyano, and S. Kuhara: "Identification of genetic networks from a small number of gene expression patterns under the boolean network model," in *Pacific Symposium on Biocomputing'99*, (Singapore), pp. 17–28, World Scientific Publishing Co., (1999)

[3] S. Liang, S. Fuhrman, and R. Somogyi: "Reveal, a general reverse engineering algorithm for inference of genetic network architectures," in *Pacific Symposium on Biocomputing*, **3**, p. 18, (1998)

[4] A. Wuensche: "Genomic regulation modeled as a network with basins of attraction," in *Pacific Symposium on Biocomputing*, **3**, p. 89, (1998)

[5] S. A. Kauffman: "Metabolic stability and epigenesis in randomly connected nets," *J. Theor. Biol.*, **22**, pp. 437–467, (1969)

[6] M. Karnaugh: "The map method for synthesis of combinational logic circuits," *AIEE Transactions, Part I Communication and Electronics*, **72**, pp. 593–598, (1953)

[7] E. McCluskey: "Minimization of boolean functions," *Bell Syst.Tech. J.*, **35**, pp. 1417–1444, (1956)

[8] J. Gimpel: "A method of producing a boolean function having an arbitrarily prescribed prime implicant table," *IEEE Trans. Computers*, **14**, pp. 485–488, (1965)

[9] R. Brayton, G. Hatchel, C. McMullen, and A. Sangiovanni-Vincentelli: *Logic minimization algorithm for VLSI minimization.* Kluwer Academic, (1985)

Proc. of The Ninth Int. Symp. on Artificial Life and Robotics (AROB 9th '04)
Beppu, Oita, Japan, 28-30 January, 2004

Chemical Genetic Programming – Evolutionary Optimization of the Translation from Genotypic Strings to Phenotypic Trees

Wojciech Piaseczny[1] Hideaki Suzuki[1] Hidefumi Sawai[2]

[1]ATR Human Information Science Labs. {wojtek, hsuzuki}@atr.co.jp
[2]Communications Research Laboratory sawai@crl.go.jp

Abstract

A new method of genetic programming, named chemical genetic programming (CGP), which enables evolutionary optimization of the mapping from genotypic strings to phenotypic trees is proposed. A cell is evolved, and includes a DNA string that codes the fundamental mapping from DNA code to computational functionality. Genetic modification of a cell's DNA allows the DNA code and the genotype-to-phenotype translation to coevolve. Building an optimal translation table enhances evolution within a population while maintaining the necessary diversity to explore the entire search space.

Keywords: *genetic programming, coevolution, chemical reaction, rewriting rules, genotype-to-phenotype mapping*

1 Introduction

In biological cells [1], symbol-to-function, or genotype-to-phenotype, translation is determined by the DNA, and is therefore subject to change when a cell undergoes genetic modifications. DNA is translated into functional units (amino acids) and transfer RNAs (tRNAs); the translated elements react together to form the translation set (aminoacyl-tRNAs) for determining the cells genotypic structure. Since code structure and code translation are both stored in the DNA, a cell is able to evolve both through genetic mutations.

Borrowing these mechanisms, the authors recently proposed a new method of genetic algorithms named chemical genetic algorithms (CGA) [3, 4]. CGA introduced a dynamic relationship between genotypic and phenotypic information and optimized the genotype to phenotype translation. This translation determines the performance of evolution, and by allowing it to be created through evolution rather than by human design, the system is allowed to build an optimal translation set.

Genetic programming (GP) [2] has been successfully applied to various engineering problems. Starting with a population of randomly generated programs composed of predetermined programming ingredients, conventional GP evolves a population over a series of generations by breeding the fittest programs using genetic operations. The population has no knowledge of which ingredients are productive to evolution, and which hinder progress.

Based upon these previous studies, here we propose a new method of genetic programming called *chemical genetic programming* (CGP). CGP aims to model biological cells by allowing the set of programming ingredients to change during evolution. By reproducing beneficial functions and eliminating destructive functions, CGP can create good programs with a higher probability. Artificial cells in chemical genetic programming are represented with a numerical string (DNA), transcription units (tRNAs), a rule set (amino acids), and a translation table (aminoacyl-tRNAs), enabling coevolution between the codes on DNA and their functionality. Cells are evolved using mutation, crossover, and molecular exchange operations, and evaluated against a given target function. The effectiveness of chemical genetic programming is demonstrated by observing distinguishing characteristics in solving a symbolic regression problem.

This paper presents the model and initial results of CGP. Following a detailed description of the CGP algorithm in Section 2, the experimental analysis is given in Section 3. Section 4 summarizes the results of this paper and describes further research involving CGP.

I→N	N→(NON) N→R N→Z	R→x R→Z R→Z.Z R→N^N	Z→D Z→ZZ	O→+ O→- O→* O→/	D→0 D→5 D→1 D→6 D→2 D→7 D→3 D→8 D→4 D→9

Figure 1: The initial set of aminos contains 6 non-terminal symbols, namely I, N, O, R, Z, and D, and 16 terminal symbols, namely x, ; +, -, *, /, and the digits 0 to 9. All translations begin with the symbol I, and end when all non-terminal symbols have been replaced.

2 Model

Evaluating a cell requires translation from DNA to executable program. This process is briefly explained, followed by a detailed explanation of the CGP algorithm.

2.1 Translation

As explained below, CGP creates new amino rewriting rules by combining existing aminos. The initial set of aminos is presented in Fig. 1. Each amino is a grammatical rewriting rule, or translation, that can be applied to alter an existing expression. Starting from the initial expression, I, translations are continually applied to the non-terminal symbols in the current expression, in the left-to-right order in which they appear in the DNA, until all non-terminal symbols have been replaced. A non-terminal symbol is any symbol that can be further translated. A demonstrative example, using the initial amino set, is shown in Fig. 2.

Each amino in the initial set is syntactically valid, therefore all aminos created by translating elements from this set must also be valid. Using this property, CGP is able to ignore the entire class of solutions that do not form executable structures.

2.2 Algorithm

CGP is a method for evolving a population of individuals towards a target. Figure 3 shows the basic mechanism used to evaluate an individual and to select the content of successive generations. Each operation is described in detail below.

Initialization: A set of random individuals is created, each containing an empty translation table. Every individual starts with the initial amino acid library shown in Fig. 1. The DNA codes, or rule numbers,

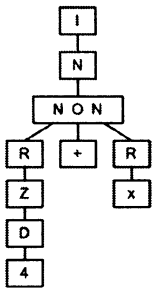


Figure 2: An example phenotypic tree showing the possible translations in generating the function 4+x.

used to fill the DNA strings are selected at random from the initial amino acid library.

Evaluation: Determining the fitness of an individual is a multi-step process that uses feedback to build the individual's phenotypic tree. The DNA is first translated, using the existing translation table, into a set of amino acids, and transcribed into a set of tRNAs. A mechanism has been added to allow for all initial aminos to re-enter an individual. This follows the biological analogy of a cell living inside another medium, and being able to accept aminos from this medium. The amino acid and tRNA sets react to form new aminoacyl-tRNA units that are added to the translation table in place of randomly chosen units. Using this updated translation table, the DNA is translated again, this time to form the phenotypic tree. When evaluated, this tree produces an expression that is compared against the predetermined target function using a comparison function.

Selection: Comparing a generated function against the target function produces a fitness value for each individual. This value is used as the probability that the individual will be selected into the next generation, using roulette wheel selection. This selection method creates a wheel, with size equal to the sum of fitness values from the entire generation of individuals, where each individual represents an area on the wheel equal to its fitness value. The population of the next generation is the set of random selections from this wheel.

DNA Mutation: Once individuals have been selected into a generation, they are genetically modified according to conventional GP methods. Each individual is mutated immediately upon being selected to continue evolving. Each of its DNA codes are ran-

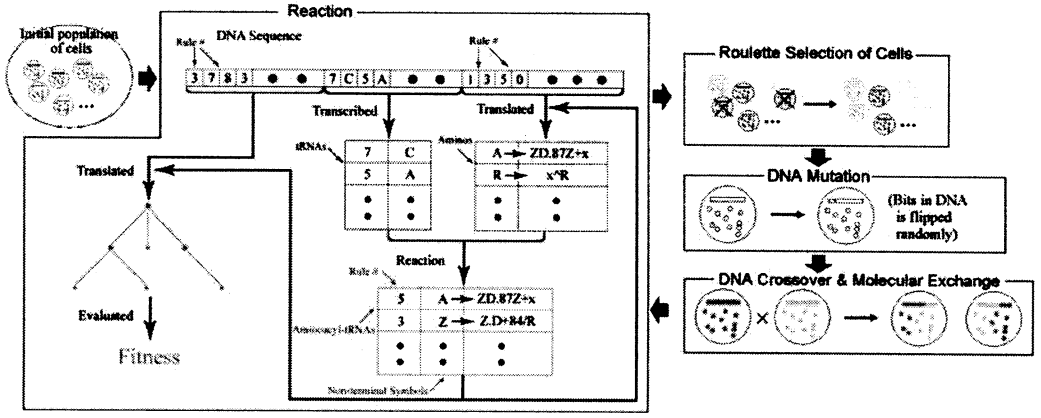


Figure 3: The CGP reaction algorithm. A detailed description is provided in Sect. 2.2.

domly replaced with another valid code with probability p_m.

DNA Crossover and Molecular Exchange: After mutation, individuals have probability p_c of being involved in a crossover operation. Single point crossover is performed between randomly selected pairs of DNA units. Half of each molecular unit, namely the translation table, tRNA pool, and amino pool, is exchanged between the two individuals during this operation.

Through evolution, beneficial aminos will be propagated throughout the population, while destructive aminos will be eliminated. The diversity of aminos will gradually decrease, while the diversity of aminoacyl-tRNAs increases. The complexity of aminoacyl-tRNAs will grow in time, as productive combinations of aminos can be merged into a single aminoacyl-tRNA. Combining well-chosen parameters together with maintaining the initial amino set allows CGP to escape local optima, regardless of proximity to the global solution.

3 Experimental Results

To verify the effectiveness of CGP, we apply it to a symbolic regression problem. We chose a single variable mathematical expression to evolve. Specifically our target function is:

$$f(x) = 2x^6 + 3x^4 + 4x^2 + 100,$$

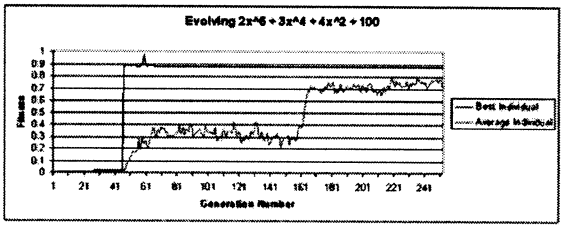


Figure 4: The best and average normalized fitness values over the first 250 generations of evolution. The best individual appears in generation 58.

over the domain [-5, 5]. An individual's fitness value is defined as

$$fitness = exp(6 * exp(-d/25000000)),$$

where d is the sum of the differences between the generated function and target function squared at a finite set of points over the desired interval. The parameter values for these experiments were influenced by those of successful CGA runs. The mutation rate, p_m, and crossover rate, p_c, were set to 0.007 and 0.7 respectively. The population size was 143. The parameter values were selected to minimize population size while maintaining the necessary diversity and guaranteeing the conservation of beneficial information in DNA. The results of a single representative CGP run are presented here. Fig. 4 plots the normalized best and average fitness values from the start of evolution until a final solution was found. The best individual

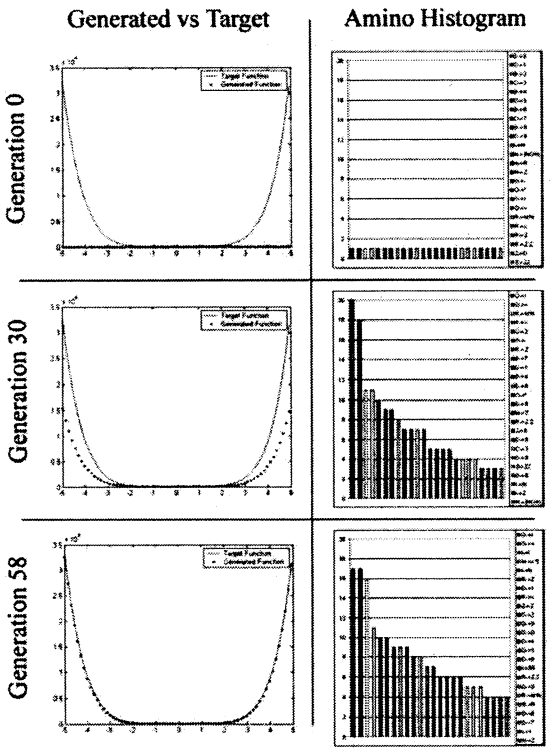


Figure 5: For the best individual in generations 0, 30, and 58, a plot of generated vs target functions is shown on the left, and the amino frequency histogram is shown on the right.

of all generations appeared in generation 58, approximately 20 minutes into evolution when running on a Pentium 4 3GHz desktop computer. CGP was able to maintain diversity after this result was found and continue to explore different solutions. Of equal importance is that the CGP was also able to retain a good solution to propagate to future generations. This indicates that the amino library is capable of being optimized to produce good individuals without converging to a single solution. To illustrate this point, Fig. 5 shows the amino library and difference plot of the best individual in selected generations before and after reaching a final solution.

4 Conclusion and Discussion

We developed a new genetic programming method, called *chemical genetic programming*. By coevolving the DNA and fundamental genotype-to-phenotype translation table, CGP created an adaptive cell in which the final functional tree is created by the translation of symbol sequences in DNA using a set of evolved amino rewriting rules.

CGP uses feedback to determine optimal content of the translation table. During its evolution, complex translations for creating subtrees may be combined into a single amino translation, allowing for more frequent use of productive rewriting rules. This causes the number of translation required for a phenotypic tree to reach a complex solution to decrease over time, while the contents of the translation table become more complex. CGP is able to maintain diversity at any stage in evolution, which helps it find an initial local optimum, as well as to escape from local optimums later in evolution.

Further research will include applying CGP to more complex problems, comparing it against other competent GP methods, and developing a measure of evolvability that might be enhanced through evolution.

Dr. K. Shimohara of ATR actively supports this study. The first and second authors' work was funded in part by the Telecommunications Advancement Organization of Japan. The second author's work was also supported by Doshisha University's Research Promotion Funds.

References

[1] Alberts, B., Bray, D., Lewis, J., Raff, M., Roberts, K., Watson, J.D.: 1994. *Molecular Biology of the Cell, The Third Edition.* New York: Garland Publishing (1994)

[2] Koza, R.: 1994. *Genetic Programming II.* London: MIT Press (1994)

[3] Suzuki, H., Sawai, H.: Chemical genetic algorithms - Coevolution between codes and code translation. In: Standish, R.K., Bedau, M.A., Abbass, H.A. (eds.): *Proceedings of the Eighth International Conference on Artificial Life (Artificial Life VIII)* (2002) 164-172

[4] Suzuki, H., Sawai, H., Piaseczny, W.: Evolvability enhancement by the optimization of a chemical translation system - a case study. In: Dittrich, P., Kim, J.T. (eds.): *The 7th European Conference on Artificial Life (ECAL) Workshop Proceedings* (2003) 146-155

Proc. of The Ninth Int. Symp. on Artificial Life and Robotics (AROB 9th '04)
Beppu, Oita, Japan, 28-30 January, 2004

Efficient method for collecting useful Web pages with the feature of the Web structure

Jun Matsukubo Yukio Hayashi
Knowledge Science
Japan Advenced Institute of Science and Technology, Hokuriku
Nomi, Ishikawa, Japan, 923-1292

Abstract

In this report, we propose a search method for useful Web pages preferentialy, and discuss about the link structure of the pages collected during search with the proposed method. Our method is that to collect appropriately preferentially the un-searched page with the most in-coming links, maximum in-degree on the local link structure consisted only of the collected pages. From search results, it is shown the tendency that the number of high-in-degree page collected with the proposed method is more than the number collected with breadth-first search (BFS). Moreover, it is shown the tendency that the connected frequency from arbitrary page to high-in-degree pages is higher with the proposed method than with BFS. Consequently, it is thought that the proposed method is performed via high-in-degree pages, which are seemed the cores of Web communities.

keywords: local search, Web, power-law distribution, scale-free network, meta-heuristic

1 Introduction

In this report, we propose a method to search preferentially for a useful Web page. In our method, the searching order of pages is determined by only the local link structure between the searched pages.

First, we describe the importance of preferential search for useful pages and the utility of a page. Collecting Web pages has been performed to improve retrieval accuracy at search engines. However, in the latest report[1], the total of Web pages is estimated to be 7 billion. And whereas, even Google said that it has the greatest cover rate in all search engines, the estimated cover rate is about 40%. Therefore, it seems difficult to reach Web pages more than a half of the whole Web page. Furthermore, because of rapidly increasing the number of Web page, it is actually difficult to cover all pages. Then, it is desired that the development of the search method for useful pages preferentially. Here, it is assumed that a useful page has high in-degree, the number of in-coming links from others to the page. It is because it is thought that the high-in-degree page is collecting much concern and interest. Henceforth, in consideration of the link direction of Web pages, the page with high in- and out-degree is called authority and hub, respectively.

On the scale-free (SF) networks as the Web, some search methods have been proposed, which apply the structural property. The methods have been proposed by Adamic, et al[2], Densmore[3], Kim, et al[4], and Tadic[5] to discover the path between arbitrary nodes with only the local link structure. In the methods, it traversed via high-degree nodes preferentially. However, since it is supposed that the degree of the nearest neighbor is known, it is difficult to apply these methods to search for Web pages directly.

Then, we propose a search method to determine approproately the search order of pages with only the local link structure of the Web pages discovered during search to collect useful pages efficiently. In the proposed method, the un-searched page with the most in-degree is preferentially searched for on the local link structure of Web pages discovered during search. Since the in-degree of page can be increased by founding the links from other pages when search progresses, the search order of a page changes in adaptation in the proposed method. Moreover, we performed the search experiment to compare the efficiency of collecting authorities with proposed method and the breadth-first search. Finally, we argue about the link structure of the Web page collected by the proposed method, and the collecting efficiency of authority.

2 Search on scale-free networks

In this section, we describe the existing search methods to discover the path between two arbitrary nodes, which utilize the property of the link structure of SF networks. The common feature of these methods is to search preferentially local high-degree nodes of the nearest neighbors.

Since the self-organized networks such as the Web, file sharing systems of GNUTELLA, and etc, are not only huge, but change rapidly, it is difficult to grasp always the whole link structures. Therefore, because it is difficult to discover the shortest paths between arbitrary nodes, the method is proposed to discover the paths efficiently using only local link structure. In [2] *sim* [5], it is experimentally shown that the shorter paths can be searched with these methods than with random walk. However, because of the supposition that the degrees of the nearest neighbors of each nodes are known, it is difficult to apply directly these methods to search Web pages.

3 Proposed method

In this section, we introduce the proposed method. In the above methods, it is supposed that the degrees of the nearest neighbors are known, it is actually difficult to count the in- and out-degree of the nearest neighbor during search on Web. Then, we propose the search method to determine appropriately the search order of pages using only the local link structure of the pages discovered during search. In the above method, only the nearest neighbors are set as candidates to be search, and whereas in the proposed method, the all un-searched pages discovered during search are set as those. Furthermore, since there is a non-searched page whose in-degree increases by discovering the link from others to the page when search progresses, the search priority of un-searched page changes in adaptation like meta-heuristics. Hereafter, the proposed method is called In-degree-first search; IFS.

Next, we discribe IFS in detail. First, IFS crawler, which is program to collect Web pages with IFS, downloads the source of a page and analyzes syntax of the page. Then, the crawler extracts the URLs to others, and stores the URLs in a non-searched list. Second, the crawler searches in the next step for the page of the URL with maximum in-degree within a non-searched list. The procedure is shown as follows.

1. Set a search start URL to p
2. Add p to the searched list Us
3. Download the source of page p
   Extract URLs from p not to duplicate the URLs
   Stores the URLs in the temporaril list Ut
4. Set the head URL in the list Ut to pt
   Delete pt in Ut

   IF pt is contained in Us THEN:
   Progress to (5)

   (a known URL is discovered)
   IF pt is NOT contained in Us THEN:
   IF pt is contained in Udup, URL list for duplication check THEN:
   Increase 1 in Din(pt), the in-degree of pt

   (a new URL is discovered)
   IF pt is NOT contained in Udup THEN:
   Add pt to the search queue Us
   Add pt to Udup
   Set 1 to Din(pt)
5. If Ut is not empty, return to (3)
6. Set p in Us with the maximum in-degree in Din (p) to the next search URL p
   Delete p in Din
7. Return to (2)

4 The comparison of Search efficiency

In this section, we compare the results of search experiments with in-degree-first search; IFS, and breadth-first search; BFS. The comparison items are degree distribution, cumlative authority number to collected page number, and connected correlation of degree between the collected pages. In the both cases of IFS and BFS, we started search experiments from the same URLs. We searched by 10 times using IFS and BFS, changing search-start pages considered to be separated mutually, such as the page of the White House, that of the royal library in Britain, and etc. Here, we set the number of pages which a crawler visits to 100,000. We show the search result from the homepage of JAIST (http://www.jaist.ac.jp/).

First, we show the page number distribution to in- and out-degree of collected pages in Fig. 1 and 2, respectively. In Fig. 1, horizontal and vertical axes are in-degree and page number in bi-logarithmic scale, respectively. The circles (o) and stars (*) correspond the results with IFS and BFS, respectively. Since both of the in-degree distributions have the portion which can be approximated with linear line, it shows that the distributions follow power-law. Moreover, the shift of the graph drawn with circles shows that the average link number is more on the result with IFS than with BFS. The circles drawn on the lower right part of Fig. 1 corresponds to authorities. At the upper left of Fig. 1, the distribution with IFS separated greatly from power-law. Since the distribution coincides the report of Pennock[6] that, to the pages with similar

topoics, the distribution follows log-normal distribution, it is considered it is relative to Web communities mentioned below. In addition, it is similar to out-degree. The marks on the lower right of Fig. 2 correspond to hubs.

Next, we show the cumlative the number of authority and hub to collected page number. Figs. 3 and 4 correspond to the cumlative authority and hub number, respectively. The authorities and hubs were decided with thresholds, which are 100th maximum in- and out-degree of the pages collected by IFS crawler. The solid and dashed lines in Fig. 3 and 4 correspond to the results of the number IFS and BFS, respectively. In Fig. 3 the cumlative authority number by IFS is about three times by BFS. And whereas in Fig.4 the cumlative hub number by IFS is about ten times. This result shows the tendency that IFS collects not only authorities, but also hubs.

Here, we consider why authorities and hubs are collected more with IFS than with BFS. Therefore, we show correlation between in-degree of a certain page and average in-degree of those which connects from the page. The correlation of IFS and BFS is shown in Fig. 5 and 6, respectively. First, in the both results, the connected correlation is high to the pages with high in-degree. Moreover, in the case of IFS, it seems that weak positive correlation has appeared. This shows that the frequency that the high in-degree pages connect to each other is high on the average.

Then, we consider behavior of IFS. In social networks, such as Web, acquaintance relation, sending-receiving relation of e-mails and etc, it has been clarified that the connected frequency between the high in-degree nodes is high[7]$\sim$[9]. It is thought that it relates to sparse and dense link structures are mixed on social networks. The dense one is called community structure. As Fig. 5 and 6 showed, the similar results was also obtained in the experiment. Moreover, on Web, it is known that the pages treating related topics connects densely, and form community structures. From above supposition, it is considered that IFS crawler searches on the Web via authorities and hubs, the cores of Web community.

5 Conclusion

Finally, we describe the conclusion. In this report, we proposed and impremented a new method to search appropreatelly preferentially un-searched pages with the most in-degree on the link structure of the pages discovered during search, in order to collect many pages which aggregate much interest and concern. By comparison of the results of proposed method and breadth-first search, it turns out that there is tendency that authorities are efficiently more collectable by the proposed method than by breadth-first search. This is considered that it is a cause that there are the high connection frequency between the high in-degree pages on the link structure of the pages collected by the proposed method. Moreover, from consideration, it is thought that the proposed method is searching one on the Web traversing authorities and hubs, which are the core nodes of Web communities, applying the feature that the link structure has positive connected correlation between the nearest neighbors.

References

[1] Yamana, H, "The inter-net leading it society(in Japanese)," Jour. of IEICE, Vol.86, No.5, pp.304-310,(2003).

[2] Adamic, L., Lukose, R., Huberman, B., "Local Search in Unstructured Networks," cond-mat/0204181,(2002).

[3] Densmore, O., "An Exploration of Power-Law Networks," http://backspaces.net/PLaw/

[4] Kim B.J., and et al., "Path finding strategies in scale-free networks," Phys. Rev. Lett., Vol.65, 027103,(2002).

[5] Tadic, B., "Adaptive random walks on the class of Web Graphs," Eur. Phys. J. B23, pp.221-228,(2001).

[6] Pennock, D., et al., "Winners don't take all: Characterizing the competition for links on the web," Proc. of the Nat. Acad. of Sci., Vol.99, No.8, pp.5207-5211,(2002).

[7] Newman, M.E.J., "Mixing patterns in networks," Phys. Rev. E, Vol.67, 026126,(2003).

[8] Newman, M., and Park, J., "Why social networks are different from other types of networks," cond-mat/0305612, (2003).

[9] Vázquez, A., "Growing network with local rules: Preferential attachment, clustering hierarchy, and degree correlation," Phys. Rev. E, Vol.67, 056104, (2003).

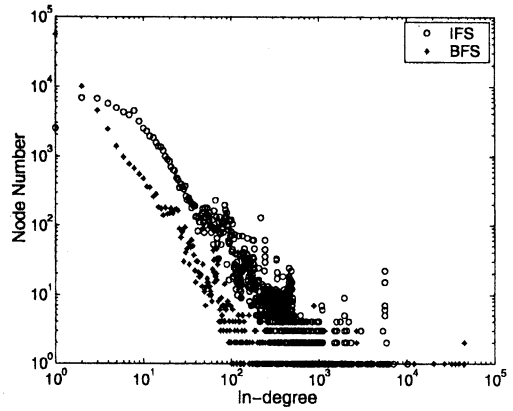


Figure 1: Comparison of node number distribution to in-degree

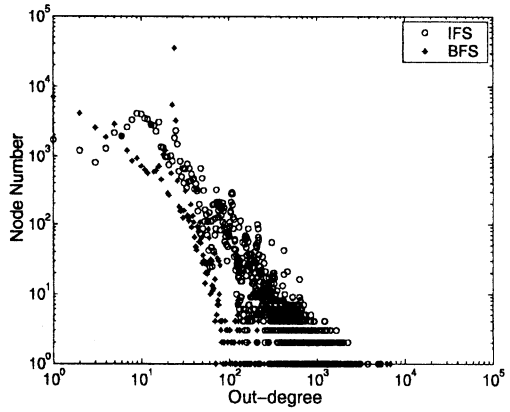


Figure 2: Comparison of node number distribution to out-degree

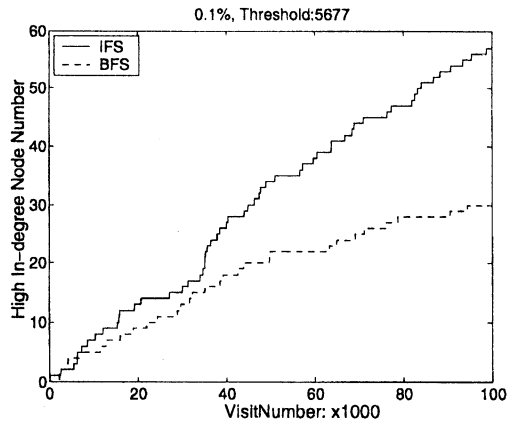


Figure 3: Comparison of a_{IFS}, cumulative authority number with IFS and a_{BFS} that with BFS to the number of pages by Web crawler

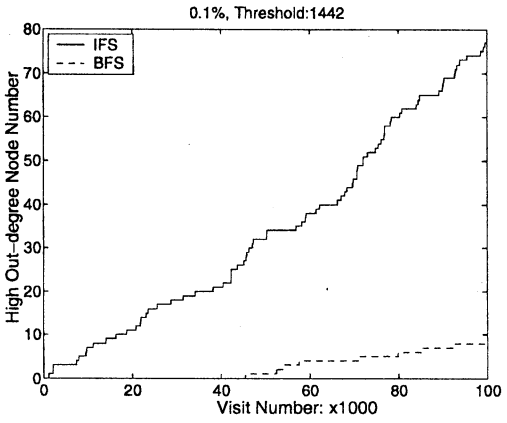


Figure 4: Comparison of h_{IFS}, cumulative hub number with IFS and h_{BFS} that with BFS to the number of pages by Web crawler

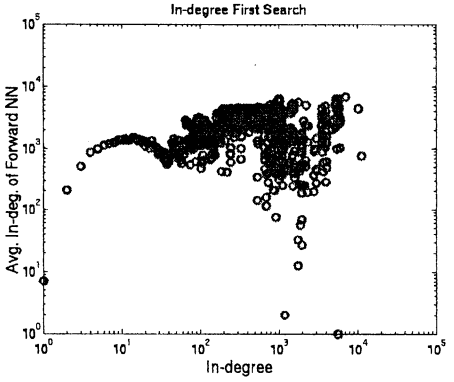


Figure 5: Indegree correlation between connected pages collected with IFS crawler

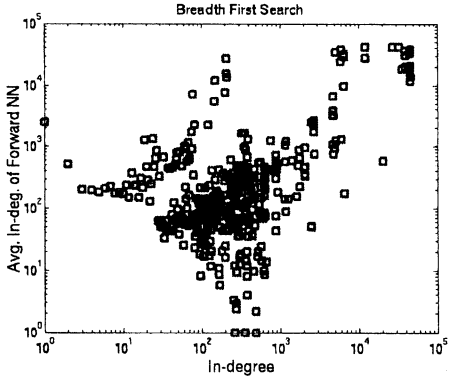


Figure 6: Indegree correlation between connected pages collected with BFS crawler

Proc. of The Ninth Int. Symp. on Artificial Life and Robotics (AROB 9th '04)
Beppu, Oita, Japan, 28-30 January, 2004

Toward the Consistent Simulation of Narrative Discourse Based on Narratology

Takashi Ogata
Department of Medicine and Engineering, Yamanashi University
Yamanashi, 400-8511 Japan
ogata@csi.yamanashi.ac.jp

Abstract

We discuss aspects of the narrative rhetoric based on narratology and a direction of their integration into a consistent narrative generation system. In traditional narratology, the typology of narrative rhetoric, the application to texts interpretation, implications to ideological and social thinking of texts interpretation, and so on are mainly treated. But we propose a new direction of narratology to be oriented toward so called an operational approach based on computational modeling and simulation of narrative generation process. In this paper, at first, we explain the computational re-definitions of four kinds of narrative rhetoric about narrative discourse aspect, and show a discourse transformation process using methods partially implemented.

1 Introduction: From Typological/ Interpretive Narratology to Operational Narratology

By the integration of cognitive and computational techniques and theories about narrative generation & understanding and literary knowledge based on literary theories and narratology, we have researched about, so to speak, a narrative generation mechanism supported by literary knowledge [1]. A central interest in traditional literary studies was the analysis and interpretation of literary texts and relating literary phenomena, but our approach aims at the conversion from such analytic and interpretive direction to literary theories for production and creation.

By adopting and expanding the basic idea of narratology, we divide a narrative generation process into three aspects of story, discourse, and representation or narration. Story means a temporal sequence of events to be narrated and a kind of narrative potential structure. Propp [2] proposed an influential literary theory about narrative potential structure and transformation based on it. As a starting point, we applied his theory to develop experimental story generation systems [3, 4]. On the other hand, narrative discourse is an aspect of how to narrate a story in various ways, and directly reflects the structure of surface text.

In this paper, we attempt a consideration toward the mechanism of a consistent process of the narrative discourse aspect by using Genette's theory [5] as a starting point. About this aspect in narratology (structural study on the aspect of narrative discourse is thought as narratology in the narrow sense by researchers), we have studied along following research process; (1) the computational re-definition of Genette's discourse elements. Namely, we have re-defined Genette's typological description as more precise and operational rhetorical techniques introducing the methods of computer modeling and simulation. (2) The integration of each discourse aspect and the composition of a consistent discourse simulation system. This paper considers about the approach to the second problem.

2 Narrative Techniqeus for Discourse Processing

Genette's discourse theory is composed of following three aspects; time or tense, mood, and voice. Time or tense means the set of temporal relations (speed or duration, order, and frequency) between story (narrative contents) and discourse. Mood, next major category, is the set of modalities, distance and perspective (point of view or focalization) regulating narrative information. Voice, last major category, treats the temporal and spatial relations between a narrator's narrative action and a narrated text. We have done the precise analysis and the implementation of experimental simulation systems of order & duration in time and distance & perspective in mood. Their detailed concepts found as operational narrative techniques are explained in next sections.

2.1 Temporal order's techniques

Order shows the order in which events occur and the order in which they are recounted. Genette has made a precise classification of the temporal order, and we have used it in our system by re-defining from the viewpoint of computation. We have called the temporal order processing based on Genette *structural discourse techniques of time*.

For example, structural transformation of temporal order is formally made by the substitution of some events in a sequence of events. But, a reader can not sometimes understand the existence of order transformation. Therefore, in real narrative texts, techniques that, so to speak, compensate for the structural discourse techniques are frequently used. For example, by the action of "recall" in a character, a temporal changing of order occurs, and simultaneously the recognition of a reader on introducing of a structural discourse techniques of time is helped. *The techniques of operational discourse of time* are the techniques in the level which makes a reader recognize the use of temporal structure's changing. We have proposed a computational modeling of time in

which blends these two types of narrative techniques [6].

Operational discourse techniques of time are operated by two kinds of subjects; character and narrator. It also has two directions; introducing or inserting the past into the present and introducing or inserting the future into the present. It has various sub-categories, namely concrete operations. Originally, we acquired these operations through the analysis of movie films, but here classify the operations into more abstract groups of operations; (1) Introducing the past and the future into the present by character-action: For example, the action in which a character recalls or dreams a past event is inserted into the present. As other ways, transmission is also used. There are predictions, premonition, planning, and so on in ways for introducing the future into the present. (2) Introducing the past and the future into the present by character-voice: In the voice, there are monologue and dialogue. (3) Introducing the past and the future into the present by narrator-action: In all narratives, the concept of narrator that comprehends characters exists. A narrator directly can insert a scene of the past or the future which a character does not know. (4) Introducing the past and the future into the present by narrator-voice: Similarly, a narrator introduce the past or the future into the present by narration. (5) Introducing the past and the future into the present by objects: This is the case that the past or future events are indicated by the existence of objects such as newspaper, ring, and scar.

2.2 Perspective's techniques

Perspective is the perceptual position in terms of which the narrated situations and events are rendered. It is divided into three types; zero perspective, internal perspective, and external perspective.

We define perspective as the problem of selection and removing in a story's information, and make a simple mechanism that transforms or edits the conceptual expression of a given story to different conceptual expressions based on different types of perspectives [7]. We think simply that the processing of perspective is the problem of deciding the range of information inside a story to be transformed to narrative discourse. We divide Genette's classification of perspective into two categories; first is a group of basic perspectives and second is a group of applicable ones. The applicable perspectives can be defined by the combinations of basic perspectives so is strongly related with strategic knowledge.

Basic perspectives have three sub types; zero perspective, internal fixed perspective, and external perspective. Zero perspective is he type which can narrate all information in a story. Internal fixed perspective is the type which narrates narrative information about a certain character and information the character perceives such as mental state and the stream of consciousness. External perspective is the type which narrates only external aspects about characters.

Applicable perspectives have internal variable perspectives and internal multiple perspectives which are two applications of the internal fixed perspective. Moreover, as another type's category, alteration means a temporary transgression to the perspective adopted consistently, and has paralipsis and paralepsis. The internal variable perspective is the type which narrates a story while changing the character chosen as the subject of a perspective (focalized character). Internal multiple perspective is the type which narrates a same event using different characters' internal fixed perspectives. The paralipsis is the technique that does not intentionally (perhaps) narrate the narrative information which should be narrated, and the paralepsis is one that dare narrate the narrative information which should be overlooked.

We implemented a first experimental system by Allegro Common Lisp which transformed variously conceptual data expressing a story based on the specification of perspectives. A user gives a sequence of events, the information related to their events, and a particular type of perspective. And then, the system outputs a sequence of transformed events. The conceptual expression of each event in a story has an event concept as first item and pairs of some slots like actor, object, place, and their values. Each element in an event concept is linked to a particular element in persona-frames, object-frames, and place-frames. Each slot in a persona-frame corresponds to name, sex, external-aspect, internal-aspect and perception. The perception slot stores an event that a character currently perceives. Object-frame and place-frame respectively have a name slot and an external-feature slot.

2.3 Distance's techniques

The concept of distance is originated with Plato. Plato called the state that narrates in the name of a poet (author) itself a story "diegesis" (pure narrative discourse), and the state that a story is narrated without the intervention of any poets or authors "mimesis" (imitation). Genette defined these relations as the problem of "distance" between a narrator and a story or the information to be narrated. From the viewpoint, the state of diegesis means longer distance, and the one of mimesis means shorter distance. In the state of longer distance, we can find various characteristics or narrative techniques; the compression of information in a story, the emphasis of a narrator's existence or the exposure of a narrator itself, the insertion into discourse of the narration by a narrator itself, the usage of indirect speech in language expression, and so on. On the other hand, in the state of shorter distance too, we can find many discourse methods; descriptive and dramatic narration, excessively detailed description of events and objects, the usage of internal monologue, the usage of direct speech in language expression, and so on. Genette also describes the law of "the degree of a narrator's existence in a story + (descriptive quantity about the) story = equal".

Genette's proposition is a very conceptual idea, but we try to give the operational and precise definition in a distance's computational system [8]. Input data into the system are a sequence of events, and for each event, a user inputs the value of distance from 0 to 10. The system interprets that if the value is nearer 0, the degree of mimesis is higher, and if it is nearer 10, the degree of

diegesis is higher. Based on these data, the system processes next four kinds of operations.

At first, we prepare the mechanism renews an events sequence using a story tree. All leaves and nodes in the tree correspond to events, and higher level's nodes mean more abstract events, and lower level's ones mean more concrete events. A sequence of events as input data correspond to node(s) or leaf (leaves) in the story tree that the system preliminary holds. However, child nodes under a same parent are all included in the sequence of events or is not all included in the sequence. When the values of distance in events with a same parent are sufficiently high, the system removes all child events from the sequence of events, and moves up the hierarchy in the tree by one step, and then substitutes the child events into the place where the parent event existed. On the contrary, if the values of distance of a parent event in a sequence of events are sufficiently low, the system removes the parent event from the sequence of events and replaces the same place by the child events. Going up in a hierarchy means more abstract processing, namely longer distance. On the contrary, going down means more concrete processing, namely shorter distance.

Second, the system uses the function of event slot removing. It removes slot or slots in each event in the sequence of events after above operation. The number of slot in an event to be removed is determined by the rate based on the value of given distance. For example, if the value of distance is "4", forty percent slots are removed. The selection of the slot(s) to be removed is (are) decided at random.

Above two tasks are operations of distance inside a story's content itself, but distance is closely related with the problem of narrator's appearance and intervention. First, the system transforms the value of distance of each event to correspondent percentage, and interprets it as the probability for generating narrator's events. Next, the system determines original narration by the narrator. After the generation of narrator's events was determined, the system uses a knowledge frames network for determining narrative objects that does not have any relations with the story itself. The knowledge frames network is a knowledge structure that has events and various concepts linked to them like characters, places, objects, human relations, etc. Using this, the system decides the number of links to search according to the value of distance, and selects the slots in the knowledge frame that it finally reached as the object of narrator's event. At the same time, the system generates the narrator's mental actions like opinion and imagination using specially prepared slot's values in the event frame.

2.4 Duration's techniques

Duration means relations between temporal passage in a story and the quantity of the description. It is the flow of time like "slow" and "speedy" in a narrative. Genette divided duration into four types techniques; pause, scene, summary, and ellipsis. But he did not show more detailed or concrete classification. We have considered about lower level's techniques of these duration's categories utilizing the analysis of a novel and other documents too.

In pause, temporal progress in a narrative stops, and the discourse time is longer than story time. We can think, for example, next techniques for really doing it; (1) Explanation: the conceptual narration about narrative elements such as character, event, object, and so on. (2) Digression: the narration not having the relation with the story to be narrated. (3) Description: the detailed and concrete narration about character, event, object, and so on.

In scene, discourse time is equal to story time. The expression of scene is made by a narrator or a character. The expression by a narrator has next techniques; (1) A scene's, so to speak, simultaneous description or a kind of live announce or reporting: the narration about things occurring currently. (1-1) The narration (simultaneous description or reporting) about the mental situation or state in a narrator itself or other character(s) in the current scene. (1-2) The narration about the external situation or state in character(s) and other object(s) in the current scene. (2) The utterance by a character or characters. (2-1) Dialogue means the conversation among some characters. (2-2) Monologue means the utterance doing by only one person. (3) Thought or thinking is the internal monologue. The themes or contents introduced by these techniques include opinion, anticipation, desire, daydream, question, and so on.

In summary, discourse time is shorter than story time. (1) Report is narrating the result and the passage in an event. (1-1) Report on an event which had finished means a kind of recall of a past finished event. (1-2) Report on an event which has finished means the narration about an event continuing from a point in the past to current time.

In ellipsis, there is no part of the narrative text corresponding to a story. On this category, Genette himself showed some sub categories; explicit ellipses, implicit ellipses, and hypothetical ellipsis.

3 A Discourse Process by Narrative Discourse Techniques

The extreme purpose of my research about the expansion of narrative discourse is blending its aspects into a consistent computational system and combining with other narrative phases, namely story, expression, social or marketing, literary works, and so on, to create a whole narrative generation system. We consider on a consistent narrative discourse process using an incomplete trace of narrative discourse process. Some narrative discourse techniques we explained above were implemented as experimental simulation systems, but they are partial attempts inside each aspect and here we think about how to compose a consistent narrative discourse simulation by showing the mutual transformation relation between input text and output text in each technique.

Following list is the first input text which is really generated by the simulation program based on the literary theory of Propp [3]. This is a simple skeleton of a

story, and aspects of discourse are omitted. Real output is conceptual representation, but in following example, we use conveniently simple Japanese and English natural languages representation.

男の子の父は家から森へ男の子のために出かけた. (A boy's father went to a forest from a house for the boy.)/男の子の母は男の子を家に監禁した. (The boy's mother confined the boy in the house.)/男の子は家から脱出した. (The boy escaped from the house.)/司祭はお姫様に金の鳥を質問した. (A priest asked a princess about a golden bird.)/お姫様は司祭に金の鳥を教えた. (The princess taught the golden bird to the priest.)/司祭は王様に乱暴した. (The priest used violence to a king.)/王様は金の鳥に反応した. (The king reacted to the golden bird.)/司祭は金の鳥を食べた. (The priest ate the golden bird.)/男の子は家の近くから森へ向かって出立した. (The boy left from near the house toward the forest.)/男の子は森で蛇と闘った. (The boy fought with a snake in the forest.)/男の子は蛇を殺害した. (The boy murdered the snake.)/死者は男の子を捕えた. (A dead caught the boy.)/男の子は死者を供養した. (The boy held a memorial service for the dead)/死者は男の子に鋼の肉体を贈った. (The deadpresented the boy with a body of steel.)/死者は男の子を森から王国へ案内した. (The dead showed the boy to the kingdom from the forest.)/男の子は王国で司祭と闘った. (The boy fought with the priest in the kingdom.)/男の子は司祭に勝った. (The boy won the priest.)/男の子は王様に金の鳥を譲渡した. (The boy transferred the golden bird to the king.)/司祭は自殺した. (The priest committed suicide.)/男の子はお姫様と結婚した. (The boy married the princess.)

3.1 Temporal order's processing

The mechanism for temporal order's transformation first accepts the above sequence of events and transforms it into a different sequence of events using basically structural discourse techniques of time and operational discourse techniques of time. The system decides the kinds of structural discourse techniques, event(s) to be inserted and the place(s), and other necessary information, and changes the narrative structure considering some constraints. And the system applies operational discourse techniques to the transformed part. At last, the system outputs a sequence of symbolic description. Next text is an example of the transformation, and in it, the order events appear is changed, and indications for modifying it like "dream" are used.

お姫様は「男の子が男の子が蛇を殺害した夢を見る気がする」とつぶやいた. (A princess mumbled "I feel that a boy will dream that the boy murdered a snake.")/男の子の母は男の子を家に監禁した. (The boy's mother confined the boy in the house.)/熊は「男の子は死者を供養することになるぞ」とつぶやいた. (A bear mumbled "The boy will hold a memorial service for a dead.")/男の子は家から脱出した. (The boy escaped from the house.)/司祭はお姫様に金の鳥を質問した. (A priest asked the princess a golden bird.)/男の子は熊に「私は男の子が蛇を殺害した夢を見る予定だ」と話した. (The boy talked "I will dream the boy murdered the snake" to the bear.)/司祭は王様に乱暴した. (The priest used violence to the king)/男の子は男の子が蛇を殺害した夢を見た. (The boy dreamed the boy murdered the snake.)/王様は金の鳥に反応した. (The king reacted to the golden bird.)/司祭は金の鳥を食べた. (The priest ate the golden bird.)/男の子は家の近くから森へ向かって出立した. (The boy left from near the house toward a forest.)/男の子は森で蛇と闘った. (The boy fought with the snake in the forest.)/死者は男の子を捕えた. (A dead caught the boy.)/男の子は死者を供養した. (The boy held a memorial service for the dead.)/司祭はなぜか男の子が司祭に勝つ夢を見た. (The priest dreamed the boy won the priest somehow.)/死者は男の子に鋼の肉体を贈った. (The dead presented the boy with the body of steel.)/死者は男の子を森から王国へ案内した. (The dead showed the boy to the kingdom from the forest.)/男の子は王国で司祭と闘った. (The boy fought with the priest in the kingdom.)/男の子は蛇を殺害した. (The boy murdered the snake.)/男の子は司祭に勝った. (The boy won the priest.)/侍女たちは「男の子は蛇を殺害したらしい」と噂し合った. (The lady's maids mutually rumored "the boy seemed to murder the snake".)/お姫様は司祭に金の鳥を教えた. (The princess taught the golden bird to the priest.)/男の子は王様に金の鳥を譲渡した. (The boy transferred the golden bird to the king.)/男の子は家から脱出した. (The boy escaped from the house)/司祭は自殺した. (The priest committed suicide.)

3.2 Perspective's processing

Zero perspective can narrate all narrative information included in a story, and the system simply outputs the information inputted into the story as it is. Internal fixed perspective, first, outputs three kinds of information; information about action(s) in event(s) that a particular person who functions as the center of the perspective (focalized person) makes, external information described in the event(s), and internal information of the focalized person. Next, if this focalized person knows other's event, the system removes the internal information in the other's persona-frame because focalized person cannot perceive the other's internal information, and outputs the action's information and external information in the event(s). External perspective outputs only external action(s) which appear(s) outside and the information of external aspects among the narrative information included in the story data. And then, it removes mental action(s) (which does not appear outside, for example thinking and considering) of person and internal information.

For the use of internal fixed perspective, first, we give mental states into "boy" in above text. (In following description of examples, Japanese are omitted.)

The boy's mother confined the boy in the house. -> A boy's mother confined the *excited* boy in the house. / The boy escaped from the house. -> The *excited* boy

escaped from the house. / The boy talked "I will dream the boy murdered the snake" to the bear.) -> The *calm* boy talked "Anxious I will dream the *excited* boy murdered the snake" to the bear. / The boy dreamed the boy murdered the snake. -> The *anxious* boy dreamed the *excited* boy murdered the snake. / The boy left from near the house toward a forest. -> The *tense* boy left from near the house toward a forest. / The boy fought with the snake inthe forest. -> The *excited* boy fought with a snake in the forest. / A dead caught the boy. -> A dead caught the *scared* boy. / The boy held a memorial service for the dead. -> The *calm* boy held a memorial service for the dead. / The dead presented the boy with the body of steel. -> The dead presented the *calm* boy with a body of steel. / The dead showed the boy to the kingdom from the forest. -> The dead showed the *happy* boy to the kingdom from the forest. / The boy fought with the priest in the kingdom. -> The *desperate* boy fought with the priest in the kingdom. / The boy murdered the snake. -> The *excited* boy murdered the snake. / The boy won the priest. -> The *desperate* boy won the priest. / The boy transferred the golden bird to the king. -> The *flesh* boy transferred the golden bird to the king. / The boy escaped from the house. -> The *excited* boy escaped from the house.

Next text is an example that paralipsis is used to one of boy's events ("The *excited* boy murdered the snake.") processed by internal fixed perspective.

A princess mumbled "I feel that a boy will dream that the boy murdered a snake."/ A boy's mother confined the *excited* boy in the house. / A bear mumbled "The boy will hold a memorial service for a dead."/ The *excited* boy escaped from the house. / A priest asked the princess a golden bird. / The *calm* boy talked "Anxious I will dream the *excited* boy murdered the snake" to the bear. / The priest used violence to the king. / The *anxious* boy dreamed the *excited* boy murdered the snake. / The king reacted to the golden bird. / The priest ate the golden bird. / The *tense* boy left from near the house toward a forest. / The *excited* boy fought with a snake in the forest. / A dead caught the boy. / The *calm* boy held a memorial service for t he dead. / The priest dreamed the boy won the priest somehow. / The dead presented the *calm* boy with a body of steel. / The dead showed the *happy* boy to the kingdom from the forest. / The *desperate* boy fought with the priest in the kingdom. / *The boy murdered t he snake.* / The *desperate* boy won the priest. / The lady' s maids mutually rumored "the boy seemed to murder the snake" . / The princess taught the golden bird to the priest. / The *flesh* boy transferred the golden bird to the king. / The *excited* boy escaped from the house. / The priest committed suicide.

3.3 Distance's processing

We use distance operation to only a part in previous text, and show the concept of distance. First, an event is transformed into more concrete form using the moving of a story tree for realizing nearer distance. For example, we hypothesize that there is a small story tree of *"murder"*; *(murder (invite sleeping-pil-in-a-cup-of-wine sleep cut die))*. In this case, an event in the original text "The boy murdered the snake" is transformed into a more detailed sequence of events; *"The boy invites the snake. / The boy gave sleeping pil in a cup of wine. / The snake slept. / The boy cuts the snake's body. / The snake died."*.

Next, a narrator's event, *"Now my mother came home. / We wait continuing narration until my mother come to this room. / My mother entered into my room. / I start to narrate."*, is inserted into the point between, for example, "The boy's mother confined the boy in the house." and "A bear mumbled 'the boy will hold a memorial service for a dead."" for realizing very far distance.

3.4 Duration's processing

In this text, the figure of the princess in first event is described at little detailed way, and while this description is working, temporal progress of the event is paused.

A princess mumbled "I feel that a boy will dream that the boy murdered a snake."/ *The princess has blue eyes. / The princess has black hair. / The princess is tall. / The princess is wearing a white dress.* / A boy's mother confined the excited boy in the house. / Now my mother came home. / We wait continuing narration until my mother come to this room. / My mother entered into my room. / I start to narrate. / A bear mumbled "The boy will hold a memorial service for a dead."/ The excited boy escaped from the house. / A priest asked the princess a golden bird. / The calm boy talked "Anxious I will dream the excited boy murdered the snake" to the bear. / The priest used violence to the king. / The anxious boy dreamed the excited boy murdered the snake. / The king reacted to the golden bird. / The priest ate the golden bird. / The tense boy left from near the house toward a forest. / The excited boy fought with a snake in the forest. / A dead caught the boy. / The calm boy held a memorial service for the dead. / The priest dreamed the boy won the priest somehow. / The dead presented the calm boy with a body of steel. / The dead showed the happy boy to the kingdom from the forest. / The desperate boy fought with the priest in the kingdom. / The boy invites the snake. / The boy gave sleeping pil in a cup of wine. / The snake slept. / The boy cuts the snake' s body. / The snake died. / The desperate boy won the priest. / The lady' s maids mutually rumored "the boy seemed to murder the snake" . / The princess taught the golden bird to the priest. / The flesh boy transferred the golden bird to the king. / The excited boy escaped from the house. / The priest committed suicide.

4 Conclusions

In this paper, we treated the aspect of narrative discourse which is one of the most important and complex element in narrative generation, and tried to

show an approach toward a consistent computer simulation. We have many problems for the final goal, and show some of them.

- The problem of data structure like input and output data: As we independently consider and decide the mechanism and specification about each discourse techniques until now, data structures (mainly, input & output data and internal knowledge representations) used in each technique are respectively different. Thus, we can not still make a consistent computer simulation of discourse transformation. But, as it is related to the problem of how to define or distinguish the range of each phase (especially, story and discourse) in a narrative generation process, is difficult to easily decide. In principle, we think that story phase generates a story world (the story in the wide sense) to include all information which have potential possibility to be narrated and a sequence of events along temporal order (the story in the narrow sense). In the case of non sequential novel like hypertext novel, the generation of the story in the narrow sense may not be necessary. Therefore, narrative discourse processing is limited to pure transformation processing of story information. On the contrary, for deciding the kind of information which should be generated in story phase, the analysis of narrative discourse mechanisms and their organizational integration are necessary.
- The order of processing: We can think the order for applying narrative discourse techniques to text. For example, there is the sequential order which discourse techniques are applied in a fixed order like above process (temporal order -> perspective -> distance -> duration). We can also think a kind of distributed discourse processing in which various discourse techniques are executed as occasion arises to a part of text.
- Levels of narrative discourse techniques: As discourse techniques classified by Genette's are comparatively higher level's rhetoric and their many techniques do not have sufficient or direct operational functions, we have to expand Genette's model as the set of lower level's operational functions. Through narrative analysis, we could acquire or define more concrete techniques. For example, there are many lower level's techniques such as "description", "explanation", "simultaneous reporting", and so on. Many techniques of them are general operations which can be commonly utilized under some Genette's techniques. From a viewpoint, Genette's typology may mean a kind of literary rhetoric and lower level's techniques which give more concrete operations to it may mean cognitive or linguistic procedures. Integrating both elements means both cognitive/ computational expansion of literary theories and literary expansion of cognitive science/ artificial intelligence (we have insisted on "expanded literary theory" [1]).
- The blending of technical knowledge and strategic knowledge: Narrative discourse techniques explained in this paper do not include strategic knowledge on how to use them like the timing to be executed. Such knowledge affects the aspect of narrative structure and the aspect of cognitive effect in readers such as interestingness and emotional response. We currently want to avoid including easily psychological element into literary research, but it is necessary and important to introduce the strategic knowledge related to narrative structure from the viewpoint of at least literary effect. We want to start from the consideration of ad hoc and fragmentary description about strategic narrative knowledge in [5].
- The integration into a narrative generation mechanism: This is related to first problem. Based on narratology, narrative generation process is divided into two phases of story and discourse, but we divides discourse into two aspects; discourse in the narrow sense and surface expression from the point of computational symbol processing. Therefore, we have to decide the range in each processing of story, discourse, and expression. Especially, we think that story also has two distinguished aspects; story world (story in the wide sense) and a sequence of events (story in the narrow sense). Story world is a knowledge structure in which all information occurred in the fictional or virtual world, and may mean a kind of chronicle, and story in the narrow sense is a selective arrangement of in story world's information. It may include diverse types of knowledge and cover wide range, but we will be able to acquire various knowledge types through the functional analysis of each narrative discourse techniques.

References

[1] Ogata, T.: Expanded Literary Theory: Cognitive/Computational Expansion of Literary Theories and Narratology, *Proc. of 17th Congress of the International Association of Empirical Aesthetics*, 163-166, 2002.

[2] Propp, V. (Пропп, В. Я.): *Морфология сказки, Изд, 2е.* Москва: Наука, 1969.

[3] Ogata, T. & Terano, T.: Explanation-Based Narrative Generation Using Semiotic Theory, *Proc. of National Language Processing Pacific Rim Symposium 91*, 321-328, 1991.

[4] Hosaka,Y. & Ogata,T.: A Study of Story Generation and Representation - A Simulation of V.Propp Theory as a Starting Point -, *The 4th International Conference on Cognitive Science* (*Abstracts*, 64), 2003.

[5] Genette, G.: Discours du recit, essai de methode, *Figures III*, Paris: Seuil, 1972.

[6] Mukouyama, K., Shinohara, K., Kanai, A. & Ogata, T.: Rhetorical Analysis and Automatic Editing of the Film, *Proceedings of 17th Congress of the International Association of Empirical Aesthetics*, 571-574, 2002.

[7] Ueda, K. & Ogata, T.: Classification and Combination of Perspective in Narrative, AROB2004, 2004.

[8] Ogata, T. & Yamakage, S.: A Computational Mechanism of the "Distance" in Narrative: A Trial in the Expansion of Literary Theory, Unpublished (1-6), 2003.

Proc. of The Ninth Int. Symp. on Artificial Life and Robotics (AROB 9th '04)
Beppu, Oita, Japan, 28-30 January, 2004

Extraction of Meaningful Tables on the Internet*

Sung-Won Jung
Dept. of Computer Engineering
Pusan National University
Busan, Korea, 609-735
swjung@pusan.ac.kr

Jae-ho Kang
Dept. of Computer Engineering
Pusan National University
Busan, Korea, 609-735
jhkang@pusan.ac.kr

Kwang Ryel Ryu
Dept. of Computer Engineering
Pusan National University
Busan, Korea, 609-735
krryu@pusan.ac.kr

Hyuk-Chul Kwon
Dept. of Computer Engineering
Pusan National Univerisity
Busan, Korea, 609-735
hckwon@pusan.ac.kr

Abstract

The information retrieval system currently in use fails to consider the structural information of documents but uses extracted indexes from documents instead. Structural information such as the font face, font size, indentation, tables, and etc. demonstrate the author's meaning and is clearly the prime means of documentation. This paper pays special attention to tables because tables are commonly used within many documents to make the meanings clear, which are well recognized because web documents use tags for additional information. On the Internet, tables are used for the purpose of the knowledge structuring as well as design of documents. Thus, we are firstly interested in classifying tables into two types: meaningful tables and decorative tables. However, this is not easy because HTML does not separate presentation and structure. Therefore, this paper proposes a method of extracting meaningful tables using a modified k-means and compares it with other methods. The experiment results show that classifying on web documents is promising.

1 Introduction

The ultimate goal of an information retrieval system is to offer the most suitable information to its users. Performance is measured by its ability to find documents with useful information for the user. The related works have, therefore, focused mainly on the method of improving recall and precision. Special attention was given to web documents where an increasingly large number of users produce un-verified documents. An efficient retrieval method is required to improve the accuracy of such systems.

To make a high precision system, we must analyze the semantics of html documents. However, it is very difficult with present technology to apply semantics to an internet retrieval system. Another method, by which we grasp the author's intention, is to analyze the structural information of html documents.

* This work was supported by National Research Laboratory Program (Contract Number : M10203000028-02J0000-01510) of KISTEP.

This paper examines tables in several informational structures in html documents. The table form is more obvious than the plane text form, because we use a structured table in documents to convey our subject clearly. A performance improvement of an information retrieval system can be expected through the analysis of the tables because it is easy to find the tables and easy to extract the meanings in the web documents. This method can also be applied on the ranking models of current information retrieval systems like the vector space model, the P-norm model [1,2,3,4,5] etc.

2 The Challenge

Current information retrieval systems rank related documents based on similarities between documents and the users' query [1,2]. Such systems place great importance on index words and have the following limitations.

Firstly, current systems do not draw the meaning from html documents. To retrieve information more accurately, semantics of html documents should be considered. These information retrieval systems measure the similarity between html documents and the users query based on the 'term frequency' and 'document frequency'. Furthermore, these systems accept the assumption that documents are related to the index word in proportion to the 'term frequency' of the documents. However, this assumption is only of limited validity.

Secondly, current systems do not distinguish relatively weighted indexes or keywords from general indexes in html documents. Because there can be more important keywords, even in the document, people tend to remember the important part when they read a certain document. If all keywords in a document are given the same weight, it is difficult to retrieve exactly what the users want. The systems consider the 'term frequency' and 'document frequency' of the indexes by an alternative method but it does not increase the matching accuracy sufficiently enough to satisfy all users.

Lastly, the current systems do not reflect structural information in html documents. We can grasp the writer's intention to some degree if we consider the structural information of the documents. As the writer uses titles for each paragraph, indentations and tabular forms to convey his intention clearly, they have significance in a document. These information retrieval systems, however,

ignore the structural information when they extract index words from these documents.
In addressing these limitations the devised system aims to analyze and process tabular forms. For an author writing a document it may be more effective, therefore, to represent the document with a tabular form rather than to describe it in the usual methods. Related works [9, 10, 11, 12, 13] that study the extraction of table information handle a special tabular form, and extract information using abstraction rules. Similarities exist with this and our previous work [8]. The defect of such methods, however, is that it is difficult to apply them to various web document formats. In order to address this problem a method of extracting meaningful tables using decision trees and applying their results to an information retrieval system has been developed.

3 Implementation

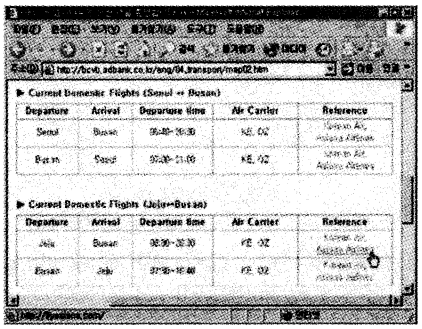
3.1 The classification of tables on the Internet

Various kinds of tables exist on the Internet. In general, a table is a printed or written collection of figures, facts, or information, arranged in orderly rows across and down the page which conveys an author's meaning more clearly. The <table> tag is supported in HTML for use on the web in a table. However, tables on the web are used not only for the purpose of the original goal but also to make the information clearer by lining it up. The task of deciding which tables are meaningful on the web is necessary before the information in a table can be extracted. To achieve this, the tables on the web have been classified into two types:
First, it is important to know which tables can be processed by the information retrieval system from amongst the meaningful tables on the web to extract the required table information. Figure 1.a is a web page from the Busan Convention and Visitor Bureau [7]. In this paper this kind of table is called the 'meaningful table', which can be defined as having the following criteria:

- The index of the table is located in the first row and the first column.
- The contents of a cell extracted by a combination of rows and columns have specific information.
- The term and document frequency cannot represent a relation between row index, column index and the content of a cell in a table.

Besides the tables having the above characteristics, we can often usually see a web page like the one in Figure 1.b. The <table> tags are used all over the HTML source of this document. However, the tables of Figure 1.b are not illustrating the owners' meaning but are offering a well-arranged display to the users. This kind of table is defined as the 'decorative table' and the following criteria:

- The table does not have table indexes in the first row and the first column.
- The table has no repeatability of cell form, and is not structural.
- The contents of the table have complex contents such as long sentence, image, etc.



a. Meaningful table



b. decorative table

Fig. 1. The types of table on the Internet

3.2 Institution of table features

It is unusual to encounter a document which includes meaningful tables on the web. Nevertheless, the meaningful tables should be extracted from amongst the others for effective information retrieval; however, it is impossible to extract them manually due to the large number of internet documents. Therefore, the tables should be defined automatically, to identify if they are meaningful or not on the basis of the characteristics which were obtained previously by analyzing meaningful tables in the training data. For example, several characteristics could be acquired from Figure 1: presence of pictures, presence of background colors and the table size.
The whole features used in the devised system are as follows:

1. The presence of <caption> tag
2. The presence of <th> tag
3. The presence of <thead> tag
4. The classification of the cells on the first rows
5. The difference of the background color option between the row with the index and the next row, or the difference of the background color option between the column with the index and next column

6. The difference of the font color option between the row with the index and next, or the difference of the font color option between column with index and next column
7. The difference of the font face between the row with the index and next row, or the difference of the font face between column with the index and the next column
8. The presence of the border option
9. The ratio of empty cells
10. The ratio of cells including <a href> tag
12. The ratio of cells consisting of text only
13. The presence of rows or columns consisting of numeric data only
14. The ratio of cells consisting of only symbols
15. The presence of other tables in the table
16. The table size
17. The number of sentences with more than 40 characters in a cell
18. The type of table shape
19. The difference of the font size between the row with index and next row, or the difference of the font size between the column with the index and the next column
20. The index word type
21. The number of meaningful index column

3.3 Application of Proposed Learning Algorithm

We convert the features, which have been extracted from a table, to vector of 21 dimensions. These vectors are input data of machine learning algorithms. Our previous work[14] applies this data to ID3 algorism using information gain. The limitation of our previous method is that it has nominal values as results. Thus, we were unable know which degree of ambiguity a table shows. Therefore, modified k-means algorithm is used in this work because we need continuous value. Compared with decision tree algorithm, our new algorithm has following advantages:

1. This method can be used to determine the level of ambiguity existing in a table.
2. We can get representable types of tables.
3. This method can apply to the extraction table information.
4. This method can easily combine other information retrieval methods.

Figure 2 illustrates our proposed method. Let's observe the process step by step. Firstly, each feature value is changed into its frequency ratio by numeric formula of step 1. This ratio means classification power of each feature. For the test we change our extract data from tables into a modified one with continues value. This modified learning data set, is foundation data for proposed method. Secondly, data set is divided into two subsets, meaningful tables and decorative tables. Each subset is clustered by k-means algorithm and we get centroids of clusters which are representable type of each subset.

Step 1. Making Learning Data Set

$$S=\{V_1,V_2,\cdots,V_n\} \quad V_i=\{v_1,v_2,\cdots,v_{21}\} \quad v_i=\{a_{i,1},a_{i,2},\cdots,a_{i,m}\}$$

$$\Rightarrow\ p(a_{i,j})=\frac{S(a_{i,j})}{N}\ \Rightarrow$$

$$\hat{S}=\{\hat{V}_1,\hat{V}_2,\cdots,\hat{V}_n\} \quad \hat{V}_i=\{w_1\hat{v}_1,w_2\hat{v}_2,\cdots,w_{21}\hat{v}_{21}\} \quad \hat{v}_i=\{p(a_{i,1}),p(a_{i,2}),\cdots,p(a_{i,m})\}$$

S : real data set

$\hat{S}$: modified real data set

V_i : a real datum with vecotr of 21 demenstion, i.e. a table

$\hat{V}_i$: a modified real datum

v_i : attribute of vector

$\hat{v}_i$: modifined attribute of vector

w_i : coefficent of modifined attribute

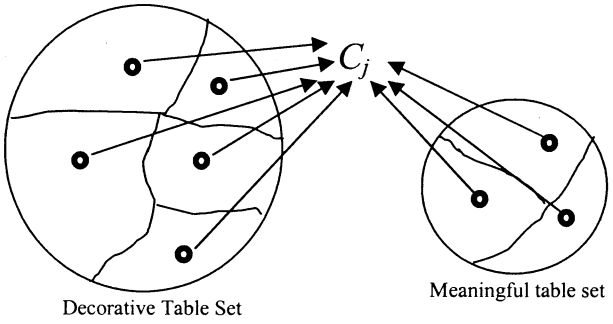
$a_{i,j}$: value of i attribute

$p(a_{i,j})$: frequent ratio of $a_{i,j}$

$S(a_{i,j})$: Number of $a_{i,j}$ in learing data set

N : Number of learing data

Step 2. Get centroids of representable type



Step 3. Get coefficient for classification

$$M(\hat{V}_i)=\begin{cases}1:\hat{V}_i \text{ is meaningful table}\\ 0:\hat{V}_i \text{ is decorative table}\end{cases}$$

$$E(\hat{V}_i)=\begin{cases}1:\underset{C_j}{\operatorname{argmax}}\,D(\hat{V}_i,C_j),M(\hat{V}_i)=M(C_j)\\ 0:\underset{C_j}{\operatorname{argmax}}\,D(\hat{V}_i,C_j),M(\hat{V}_i)\neq M(C_j)\end{cases}$$

$$\arg\max R(\hat{S})=\underset{w_1,w_2,\cdots,w_{21}}{\arg\max}\sum_i E(\hat{V}_i)$$

Fig. 2 Proposed Learning Algorithm

3.4 The System implementation

Figure 3 is a system implementation procedure. The whole procedure of the task is summarized as follows. Firstly, the sample data to be analyzed is collected and is then classified by tables and the others by hand. We investigate 100,000 documents to establish the sample data for this system. Secondly, we implement the system which extracts the features of each table automatically after the table information is extracted from the parsing of HTML documents. The sample data is generated from the merging of the former and latter results. Using this sample data, our system implements our proposed

method and creates a table information dictionary. Finally, the system uses this dictionary for the information retrieval system.

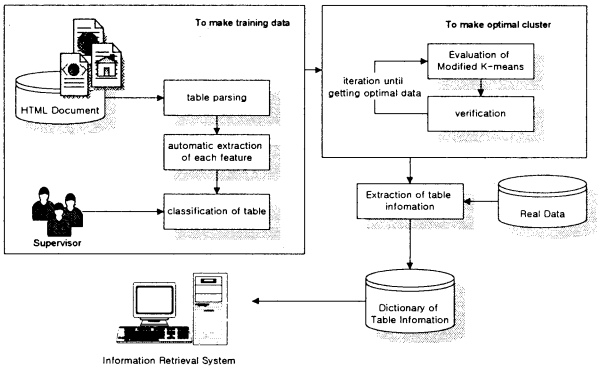


Fig. 3 The process of the system implementation

4 Experimental Result

We implemented the system with an Intel Pentium IV that has a 2GHz CPU and 256 MBytes main memory. Sample data was extracted in about 100,000 internet documents and test data was chosen from about 5 millions internet documents that were collected in Artificial Intelligence Laboratory in Pusan National University.

Table 1 shows error rates according to variation of cluster number. The cluster number coincides with the number of representable type for each class. From Table 3, we set MN for 2 and DN for 3, because we judge one class with only one cluster to overfit.

Table 1. Error Rate for Number of Cluster

No. of Table : 9769		No. of Decorative Table Cluster(DN)				
		1	2	3	4	5
No. of Meaningful Table Cluster(MN)	1	247	106	60	40	48
	2	199	92	53	54	54
	3	131	113	98	71	54
	4	111	119	96	99	86

Table 2 is a result from the application of the modified k-means to test data. The data is 5,000 web documents collected on the Internet. For the results a recall of 84.58% and a precision of 75.52% were obtained

Table 2. The application of the modified k-means

Number of tables	Decision Tree		Modified k-means	
	Recall	Precision	Recall	Precision
4283	81.54	55.21	86.92	79.58
8020	52.91	55.56	83.60	72.15
6341	67.47	39.72	78.31	62.50
9108	86.11	63.70	85.65	83.33
9769	95.83	38.33	91.67	68.75
37521	73.36	54.45	84.58	75.52

5 Conclusions and Future Work

The devised information retrieval system requires making estimates to show correct information to the user. For the system to extract information from a table, it must classify whether it is a meaningful table or a decorative table. If a meaningful table is extracted, it is easy to process the information in the table to other data forms. For example, when a user inputs a query such as the "Temperature of Busan", the system should output the correct result using abstracted table information. This work can process data of a general information retrieval system or a specific domain that has many tables. The work needs a more accurate algorithm for classifying and learning a table thereafter.

Future work will seek to identify the correlation between documents and tables. The rationale behind this work will research the link between tables and documents i.e. if a table can supply the contents of a document, how relevant tables can affect the importance of a document.

References

1. M. Kobayashi, K. Takeda, "Information Retrieval on the Web", ACM Computing Surveys, pp. 144-173, 2000
2. G. Salton, M. J. McGill, "Introduction to Modern Information Retrieval", McGraw-Hill, 1983
3. E. A. Fox, "Extending the Boolean and Vector Space Models of Information Retrieval with P-norm Queries and Multiple Concept Types", Dissertation Cornell University, 1983
4. M. E. Smith, "Aspects of the P-norm Model of Information Retrieval : Syntactic Query Generation, Efficiency, and Theoretical Properties", Dissertation Cornell University, 1990
5. G. Salton, E. A. Fox, H. Wu "Extended Boolean Information Retrieval", ncstrl.cornel, pp. 82-511, 1982
6. T. M. Mitchell, "Machine Learning", McGraw-Hill, pp. 53-79, 1997
7. http://www.busancvb.org/eng/home.html
8. S.W. Jung, K. H. Sung, T.W. Park, H.C. Kwon, "Effective Retrieval of Information in Tables on the Internet" IEA/AIE June pp. 493-501, 2002
9. J. Hammer, H. Garcia-Molina, J. Cho, R. Aranha, and A. Crespo, "Extracting Semistructured Information from the Web", SIGMOD Record, 26(2), pp. 18-25, 1997
10. Y. Huang, G.Z. Qi, F.Y. Zhang "Constructing Semistructed information extractor from the Web document", Journal of Software 11(1) pp. 73-75, 2000
11. N. Ashish, C. Knoblock "Wrapper Generation for Semi-structed Internet Sources", SIGMOD Record, 26(4) pp. 8-15, 1997
12. D. Smith, M. Lopez, "Information Extraction for Semi-structed Documents, In Proceedings of the Workshop on Management of Semistructed Data", Conjunction with PODS/SIGMOD, Tucson, AZ, USA, May, 12, 1997
13. G. Ning, W. Guowen, W. Xiaoyuan, S. Baile, "Extracting Web table information in cooperative learning activites based on abstract semantic model, Computer Supported Cooperative Work in Design, The Sixth International Conference on 2001 (2001) 492-49

Proc. of The Ninth Int. Symp. on Artificial Life and Robotics (AROB 9th '04)
Beppu, Oita, Japan, 28-30 January, 2004

Spatial Strategies on a Generalized Spatial Prisoner's Dilemma

Y. Ishida and K. Mori
Department of Knowledge-Based Information Engineering
Toyohashi University of Technology
Toyohashi, Aichi, Japan 441-8580

Abstract

Many strategies such as tit-for-tat have been proposed in Iterated Prisoner's Dilemma (IPD) which performs Prisoner's Dilemma (PD) repeatedly two players. Spatial version of the Iterated Prisoner's Dilemma (SPD) has been studied where the player placed at each site plays IPD game with the players in the neighbor. However, strategies studied in SPD are those considering past actions of only single opponent's. We studied *spatial* strategies that depend on the configuration of actions taken by the neighbors (as opposed to convenient *temporal* strategies). Since the generosity can be considered for the spatial strategies, we first investigate the generosity required when the action error is involved. We also propose several spatial strategies that outperform many others.

1 Introduction

Many strategies have been proposed in Iterated Prisoner's Dilemma (IPD) which performs Prisoner's Dilemma (PD) repeatedly two players[1, 2]. Axelrod reported Tit-For-Tat (TFT) has been outperformed on average in a tournament of strategies. IPD can be extended to n players and the extension lead to a spatial version of IPD where players with possibly distinct strategies are placed at each node in a network (called distributed PD[5]) or at each cite in a lattice (spatial version of PD [3, 4]). In most frameworks of Spatial Prisoner's Dilemma (SPD), however, strategies studied are limited to usual IPD which depend on the past action of the opponent player. IPD is played with the neighbor players and these scores are added to evaluate the strategy. Only few (e.g., [5]) focuses on spatial strategies (as opposed to convenient temporal strategies) that depend on action patterns of the neighbor's.

By spatial strategies, not only strategies similar to those studied in IPD such as TFT or its generalization with different level of generosity, but those not defined in IPD (such as Majority startegy that follow the majority action looking around the neighbor's actions) can be introduced. Also, arguments on the required generosity when action error is involved can be similarly made. Further, since effective spatial strategies remain undiscovered, we propose several strategies that outperform most spatial strategies.

2 SPD with Spatial Strategy

The PD is a game played just once by two players with two actions (cooperation, C, or defect, D). Each player receives a payoff (R, T, S, P) where $T > R > P > S$ and $2R > T + S$. In IPD, each player (and hence the strategy) is evaluated. In SPD, each site in a two-dimensional lattice corresponds to a player. Each player plays PD with the neighbors, and changes its action by the total score it received. Our model generalized SPD by introducing spatial strategy. Each player placed at each lattice of the two-dimensional lattice. Each player has an action and a strategy, and receives a score. Spatial strategy determines the next action dependent upon the spatial pattern of actions in the neighbors. Each player plays PD with the neighbors, and changes its strategy to the strategy that earns the highest total score among the neighbors.

Table 1 is the Payoff matrix of PD. In our simulations, R, S, T, and P are respectively set to 1, 0, $b(1 < b < 2)$ and 0 in simulations below following the Nowak-May's simulations.

Table 1: The Payoff Matrix of the Prisoner's Delemma Game. R, S, T, P are payoff to the player 1. $(1 < b < 2)$

		Player 2	
		C	D
Player 1	C	R(1)	S(0)
	D	T(b)	P(0)

Our SPD is done in the following way with n (a size of the lattice, 40x40 in our simulations) players with

$k(2 \leq k \leq n)$ distinct strategies.

1. Initial arrangement : Action and strategy of each player are determined at random.

2. Renewal of action : Next action will be determined by its strategy based on neighbors' (and player itself's) actions.

3. Score : Score for each player is calculated by summing up all the scores received from PD with 8 neighbor players and the player itself (the "self-interaction" is involved to make our simulation comparable to the Nowak-May's model[3]), and then add the sum to the current score of the player. (The score will be added until the strategy is renewed.)

4. Renewal of strategy : After (2) - (3) is repeated r (=1 in our simulations) times, the next strategy will be chosen from the strategy with the highest score among the neighbors and the player itself. (2) - (4) are counted as one time step.

2.1 Spatial strategies and their code expressions

In our model, each player determines the next action by the current action of itself and the eight neighbors. The strategy may be regarded as "spatial strategy" in contrast to "temporal strategy" in IPD.

To specify a spatial strategy, actions of the eight neighbors and the player itself must be specified, hence 2^9 rules are required. For simplicity, we restrict ourselves on a " totalistic spatial strategy" that depend on the number of D (defect) action of the neighbor, not on their positions. To represent a strategy, a bit sequence is used whose l-th element is 1 (0) if the action C (D) is taken when the number of D of the neighbor players is $l(l = 0, 1, \cdots, 8)$. For example, All-C is [111111111], All-D is [000000000]. The number of strategies is $2^9 = 512$. As a typical strategy, we define kD that takes D if $l > k$ and C otherwise. For example, 2D is [110000000]. This kD can be regarded as a spatial version of TFT where k seems to indicate the generisoty (how many D actions in the neighbor are tolerated.). The strategy kC can be similarly defined: it takes C if if $l > k$ and D otherwise. For example, 7C is [000000011]. The number k in the strategy kC seems to indicate the contrariness that would cooperate even if k players in the neighbor defect.

Further, $k_1D - k_2C$ is a combination of k_1D and k_2C. For example, 2D-7C is [110000011].

The binary code expression above does not reflect the action of the player itself. The code expression is extended to represent the action relatively to the current own action. The symbols s and r are used to express *stay* and *reverse* the next action from the curent action. For example, the Majority strategy is [1111s0000]. Including the relative (relative to the current own action) code other than the absolute binary code broaden the number of strategies to 4^9, hence strategies with higher performance can be found than those restricted in the binary code.

3 Frameworks for Computer Simulations

The strategy with the highest score survives in our model. The strategy whose proportion (the number of players with the strategy / total number of players) becomes eventually high can be considered to be a winner. In a matchup with m strategies, an initial configuration with m strategies assigned randomly to all the players (1600 players). The initial proportion of these m strategies is equal for these strategies. Initial actions (C or D) are assigned randomly to all the players, and the initial proportion of these actions is equal for all the players, too. Parameter b is varied from to see the influence.

Computer simulations are conducted in the following two frameworks.

- Evolutionary Framework: In renewing strategies, a single bit of the strategy code is changed with a rate b; and the code of the player itself and that of the neighbor's player with the highest score are "crossed over" with a rate c.

- Deterministic Framework: Stochastic parameters above (mutation rate b and cross over rate c) are suppressed to be 0.

Evolutionary framework has been mostly used to find a strategy with high performance. In the following, we focus on the deterministic framework, although other stochastic factor (errors in action) is involved in the next section. We also conducted simulations in a framework to find "collectively stable" strategy. That is, an initial configuration with a single player of one (mutated) strategy and the rest of players of another (original) strategy. However, this result is omitted in this paper.

In a matchup with several strategies, All-C and 5D 6D 7D are ranked high in a situation advantageous

to C (e.g. b=1.1). In contrast, All-D and 1D 2D 3D are ranked high in a situation advantageous to D (e.g. b=1.9). Noticeably, in Matchup with two strategies, clusters of cooperative collectives with cooperative strategy have been formed that reject the invasion of the opposite strategy.

4 Generosity in Spatial Strategies

In real world, actions are not taken in a deterministic fashion on the basis of strategy, but errors are involved in taking actions. Nowak and Sigmund pointed out that generosity is required in their stochastic framework and TFT could not win the generous strategy[2]. Grim pointed out that further generosity is required when the Nowak-Sigmund model is spatialized[4].

Our model reduces to the Nowak-May's model [3] when the parameter r is set $r = 1$ and that only two strategies All-C and All-D are considered. Figure 1 shows the performance among the four spatial strategies (0D, 1D, 3D, and 6D) without error in actions (above) and with error (below). When the action error rate is set to be a, the action is reverted with the probability a. The parameter b of the payoff matrix is set to be $b = 1.9$, which is advantageous for the action D. Hence, the strategy 0D (All-D) outperforms the generous strategy 6D with no error in actions. However, 6D outperforms 0D when the action error is involved as observed in Figure 1. Involvement of the action error has an effect of favoring more generous strategies for the parameter $b = 1.4, 1.5, 1.6, 1.7$ except $b = 1.8$ which is at the *chaotic region*[3].

In sum, the action error has an effect to favor more generous spatial strategies in the sense that more D actions should be forgiven in the neighbor's actions.

5 Round-Robin Tournament

A tournament on a round-robin basis has been conducted among five representative strategies expressed by a binary code. Five strategies include the following three with All-D and All-C.

1. [111000011] (3D-7C)
2. [100011111] (1D-4C)
3. [111111000] (6D)

The above three strategies outperform many other strategies within those expressed by the binary strategy code. All-D and All-C are included for comparison reason.

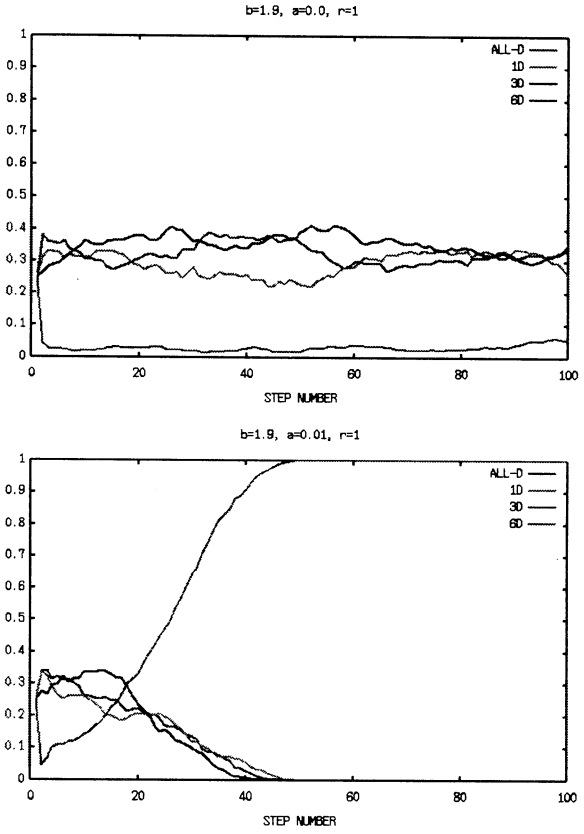


Figure 1: Time Evolution of the Proportion of Four Strategies without Error in Actions (above) and with Error (below).

In a matchup between i-th versus the j-th strategy, i-th strategy wins if the proportion of i-th strategy exceeds 0.5 at the time step 100.

Table 2 shows the result of the tournament where the number $q_{ij}(Q_{ij})$ in i-th row and j-th column indicates the result of the match between i-th versus the j-th strategy. The number $q_{ij}(Q_{ij})$ is 1 when i-th strategy wins j-th strategy with the parameter $b = 1.4$ ($b = 1.9$); and 0 when it loses. There has been no draw in this tournament. The parameter b of the payoff matrix sets the environment: small b sets the cooperative (C-favored) environment.

As observed from the result, 3D-7C wins the rest except All-C in the C-favored environment ($b = 1.4$). This fact suggests both mild generosity and contrari-

Table 2: A Round-Robin Tournament among Five Strategies.

	3D-7C	1D-4C	6D	All-D	All-C
3D-7C		1(1)	1(1)	1(1)	0(1)
1D-4C			1(1)	1(0)	1(1)
6D				1(1)	0(1)
All-D					0(1)
All-C					

ness may be required. Thus, the combined strategy $k_1D - k_2C$ is expected to outperform where the parameters k_1 and k_2 depend on the environment. In the binary strategy code, the first and the last few bits must be 1 with the middle bits 0. Specifically, the last bit must be 1 to avoid "lock-in" to D actions in the neighbor including the player, and the first bit must be 1 to keep the C actions.

Since the extended strategy code can refer to the information of the current action of the player, the strategy expressed in the extended code is likely to outperform the strategies limited in the binary code. Another round-robin tournament has been carried out with the following three with All-D and All-C.

1. $[s11rrr0rs]$ (A)
2. $[01rrrrr10]$ (B)
3. $[ss1ssss1r]$ (C)

These three strategies A, B and C outperform many other strategies within the extended strategy code. However, we have not thoroughly investigated and other strategies are likely to be found to outperform these three strategies.

Match up between two strategies has been conducted in the same way as the above tournament.Table 3 shows the result of the tournament. As known from the result, strategies A, B and C all outperform All-C and All-D. Strategies A, B and C can be ranked in this order based on the result of this tournament.

Table 3: A Round-Robin Tournament among Five Strategies Including Ones Expressed by the Extended Code.

	A	B	C	All-D	All-C
A		1(1)	1(1)	1(1)	1(1)
B			1(1)	1(1)	1(1)
C				1(1)	1(1)
All-D					0(1)
All-C					

6 Conclusion

We studied *spatial* strategies (as opposed to the convenient *temporal* strategies) in a spatial version of Prisoner's Dilemma (SPD) game. Spatial strategies depend on the spatial pattern of actions taken by the neighbor players. Both "generosity" and "contrariness" can be considered in spatial strategies, and they are shown to play an important role in SPD. For spatial strategies also, more generosity is required when the error is involved in taking actions.

We carried out two round-robin tournaments. In the tournament with five strategies expressed by the binary strategy code, we proposed a combined strategy involving both "generosity" and "contrariness" that would outperform many other strategies when these two properties are appropriately set.

In the extended strategy code that can refer to the current action of the player itself, stronger spatial strategies remains to be discovered, although we suggest some strategies that seem to outperform many other strategies.

Acknowledgements

We thank Mr. Kosaka for his contribution to computer simulations, which has been carried out in his Master thesis. This work was partly supported by the 21st Century COE Program "Intelligent Human Sensing" from the Ministry of Education, Culture, Sports, Science and Technology of Japan.

References

[1] R. Axelrod, *The Evolution of Cooperation*, Basic Books, New York, 1984.

[2] M. A. Nowak and K. Sigmund, "Tit for tat in heterogeneous populations," *Nature*, Vol. 355, pp. 250-252, 1992.

[3] M. A. Nowak and R. M. May, "Evolutionnary games and spatial chaos," *Nature*, Vol. 359, pp.826-829, 1992.

[4] P. Grim, "The greater generosity of the spetialized prisoner's dilemma," *J. theor. Biol.*, Vol. 173, pp. 353-359, 1995.

[5] K. Matuo and N. Adachi, "Metastable Antagonistic Equilibrium and Stable Cooperative Equilibrium in Distributed Prisoner's Dilemma Game," *Proc. Int. Symp. Syst. Res., Infor. Cybern.*, 1989.

Proc. of The Ninth Int. Symp. on Artificial Life and Robotics (AROB 9th '04)
Beppu, Oita, Japan, 28-30 January, 2004

Transformation of Story in the Story Generation System based on Narratology

Takashi Ogata
Department of Medicine and Engineering,
Yamanashi University
Yamanashi, 400-8511 Japan
ogata@esi.yamanashi.ac.jp

Yoshinori Hosaka
Yamanashi University
Yamanashi, 400-8511 Japan

Abstract: This paper shows an approach for thinking the problem of story's variation in Propp's theory based on our experimental story generation system. We pay attention to the concept of "move" which means a structural unit in story, and by interpreting cases and incomplete rules for combing moves by Propp, we define more precise and general rules for operating moves. And then we show an example of story transformation process using these rules and propose a simple story grammar with move's function. This kind of transformation means the method to extend a story itself, while the transformation in narrative discourse rhetoric means the method to make variations in a story.

1 Introduction

We have been trying to integrate narratology & literary theories and computational & cognitive sciences toward the building a narrative generation system by integrating various aspects of narrative, such as story, discourse, and narration [1]. In the phase of story generation, we started from the computational reconsideration of Propp's theory [2], which proposed a method of describing the form of story and composing a story (in Russian magic-tale) [3]. On his famous literary theory, we think there is a fixed idea; all stories have a fixed structure. But, through the precise analysis of his theory by computational method, we have discovered that the description about the aspect of variation from a structural form of story was very rich. Of course, we can treat such problem as the one of rhetorical techniques of narrative discourse which Genette proposed [4] and we have expanded from the viewpoint computational rhetorical system [5]. But, Propp's variation we are going to describe here has different features from narrative discourse theory in the narrow sense. The study of Propp's story variation is essentially related to some interesting directions such as the changing of genres and a kind of narrative evolution.

This paper shows an approach for thinking the problem of story's variation in Propp's theory based on our experimental story generation system. We pay attention to the concept of "move" which means a structural unit in story, and by interpreting cases and incomplete rules for combing moves by Propp, we define more precise and general rules for operating moves. And then we show an example of story transformation process using these rules and propose a simple story grammar with move's function. This kind of transformation means the method to extend a story itself, while the transformation in narrative discourse rhetoric means the method to make variations in a story.

2 A Computational Approach to Propp Theory

Story phase in a narrative generation process has two aspects; the making of a sequence of events and the background knowledge or story world. Propp showed very rich approaches to these two directions. Especially, in [3], methods and concepts for the former as shown in following description were explored. In our first researches based on Propp ([2, 6]), we mainly studied the cases of 1, 2, 3 and 4. In this paper, we think about the problem of 10. Move is a unit of story which is composed of the selective and sequential arrangement of thirty one functions and their sub-functions.

1. Thirty one functions and their fixed order.
2. Seven types of character's roles.
3. The selection of sub-functions.
4. The correspondent relations among functions and sub-functions.
5. Schema of prototypes.
6. Eight story types.
7. The setting of names and other characteristics to character's roles.
8. The transformation of names and other characteristics of character's roles.
9. The inversion of functions and changing places.
10. Methods to combine moves.
11. Assimilation of functions.
12. Polysemy of a function.
13. Trebling.
14. The setting of preliminary part.
15. The setting of the situation introducing a story.
16. Connective incident.

3 Story Transformation Mechanism

Our experimental system [7] has mainly two parts; the mechanism to make sequences of story's flow and the one to transform a story move. These mechanisms are implemented using ANSI Common Lisp. The

input parameters of the system are agent's names & types and place names. Those names are selectable in an initial data set. In this system, we prepared the data set of agent-name and object-name borrowing from the data of the Propp's study, and prepared about 170 event concepts remade for usefulness in story (or discourse) representation part.

Propp listed eight types (breeds) of typical story schema as the case of analysis. It is construable that those types are species or derivation of the prototype folktale. A type has a simple single-move, and the other is complicated with multi-moves, and so on. On the definition of the move operation, Propp himself described "the way which stories are combined" [3] and proposed several patterns of combining moves. We had considered those patterns and divided them into a group of basic operations and a group of applied operations from the viewpoint of organization of operational knowledge about story generation. It is possible to simulate the almost patterns written by Propp with combinations of basic operations, and to simulate more complicated stories with applied operations and basic operations. In following sections, we show a basic mechanism for story transformation based on the concept of Propp's move.

3.1 Types of moves by Propp

Propp showed eight patterns of typical story in Russian magic-tale. Their three patterns are stories with only one move, but other five patterns are more complicated stories with two or more moves. We show five examples with some moves based on [3] (part. II).

1. A tale with one beginning and two moves and develops via two functions; "battle" and "victory".

$\alpha\beta^1\gamma^2\xi^1\eta^3\delta^2\theta^3A^1$ I $\{B^4C\uparrow D^1\bar{E}^1\bar{F}\}$ $D^1\bar{E}^1\bar{F}$

II $B^4C\uparrow D^1E^1$ $H^1—I^1K^4\downarrow$

2. A tale with two moves, and first one develops via "battle" and "victory" and second one develops via "difficult task" and "solution".

I $\alpha\uparrow D^9\bar{E}^9\bar{F}$

$D^9\bar{E}^9\bar{F}$

$D^9E^9F^9$

$D^9\bar{E}^9$

$D^9\bar{E}^9$

$D^9E^9F=G^{\overset{5}{6}}A^{\frac{1}{2}}B^4C\uparrow H^1—I^1$

$H^1—I^1$

$H^1—I^1K^4J^2w^1\downarrow$

III $*A^1D^9E^9F^{\frac{1}{1}}G^1OLM—N\bar{Q}TUQW*$

3. A tale with four moves.

I $\alpha*D^4f^9E^4A^9\eta^3\theta^3A^{12}O$

II $F^1A^{16}B^1C\uparrow F^{\frac{1}{1}}H^1—I^1K^4J\downarrow L$

III $a^6B^2C\uparrow$

IV $A^{14}B^4C\uparrow$ $\}f^1K^9\downarrow ExQUW*$

4. A complex tale with complicated five moves.

I $\alpha F^1\beta^2a^1MC\uparrow N$

$M—NW*$

II $\beta^3\eta^3\theta^3A^6$

III A^{ii}

IV $F^{\overset{6}{9}}a^1C\uparrow G^2K^1Pr^1—Rs^1\downarrow\overline{W}*$

V $A^{18}BCD^9—E^9K^4$

II F^2K^5U

IV $W*$

III $C\uparrow F^9K^4w^2$

5. A tale with two heroes.

I $\alpha a^2B^3C\uparrow D^2E^2F^1\downarrow$

II $a^2B^3C\uparrow D^2E^2F^1\downarrow$

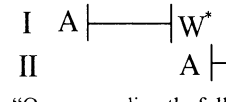
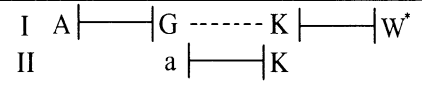
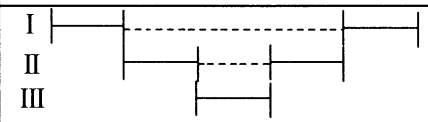
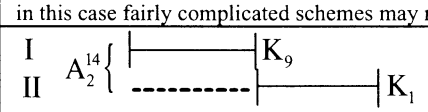
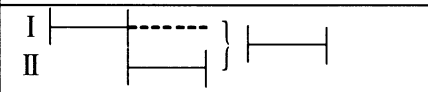
III $\uparrow S\wedge G^2W*F^5$

IV $A^{17}C\uparrow H^1—I^1J^2LQExUW*$

III $\beta^3\eta^3—\theta^3A^{14}B^4C\uparrow G^2\eta^3—\bar{\theta}^3K^9\bar{U}$

At the same time, Propp showed six cases of combinations in which moves are combined (table.1). Propp thought that variants with some moves are made by these operations.

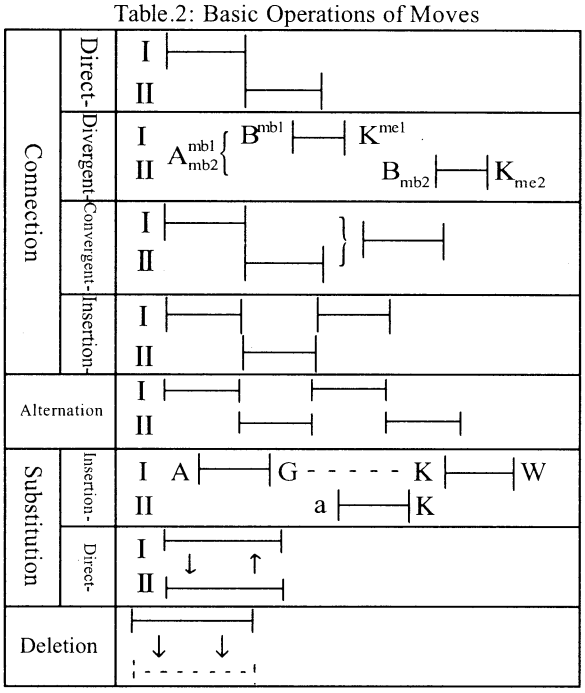
Table.1: Ways for Combining Types by Propp

1	 "One move directly follows another."
2	 "A new move begins before the termination of the first one."
3	 "An episode may also be interrupted in its turn, and in this case fairly complicated schemes may result."
4	 "A tale may begin with two villainies at once, of which the first one may be liquidated completely before the other is."
5	 "Two moves may have a common ending."
6	 "Sometimes a tale contains two seekers."

3.2 Operations for combing moves

We think that Propp's operations of move are not the definition in a same level and some are thought the combination of some primitive operations. Therefore, we defined a set of more primitive and general operations or rules of move combination for transforming or extending a story. These rules contain two categories; basic operations and applicable operations. Table.2 shows basic operations.

Table.2: Basic Operations of Moves



1. *Connection*: this group connects between moves.
   I. *Direct connection* connects first move and second move.
   II. *Divergent connection* connects in an order if a function affected in the multi directions.
   III. In *convergent connection*, if different moves have common endings, first move's sequence is differed by other moves and first move restarts from the convergent point with a function in second move sequence.
   IV. In *insertion connection*, first move sequence is deferred from second move, and restarts after completion of the second move.
2. *Alternation*: two moves alternatively develop.
3. *Substitution*: this group has two ways.
   I. *Insertion substitution* is the case that first move sequence is deferred by second move, and restarts after completion of the second move.
   II. *Direct substitution* is a move for another move.
4. *Deletion*: the deletion of a move.

The kinds of applicable operations of moves are shown in table.3 and table.4.

Table.3: Applicable Operations of Moves

Increase	The iteration of connections.
Decrease	The iteration of deletions.
Reverse	The replacement the connection order of moves.

Table.4: Other Applicable Operations

Distribution	Multi-moves are interwoven.

3.3 An example of move operations

We trace fourth tale (a complex tale with complicated five moves) shown in section 3.1

```
;; (a) First original pattern (first material).
(defvar *prototype-schema-of-russian-magic-tale-2*
  '(A B C Dep D E F G O L M J N K Ret Pr Rs Q Ex T U
W))
;; (b) Second original pattern (second material).
(defvar *prototype-schema-of-russian-magic-tale-4*
  '(A B C Dep D E F G K Ret Pr Rs Q Ex T U W))
;; W <- W*
;;; STEP. 1
;;; The system transforms (a) to generates move1.
'(alp F-1 bet-2 Aa-1 M C Dep N W-*)
;;; STEP. 2
;;; The system repeats the part of M-N and deletes
 second "C Dep".
'(alp F-1 bet-2 Aa-1 (<++> (M C Dep N) (M N)) W-*)
;;; STEP. 3
;;; The system uses "direct connection".
;;; Move2 = (b)' s transformation = (2 (bet-3 eta-3
tht-3 A-6 F-2 K-5 U))
'(){
  (1 (alp F-1 bet-2 Aa-1 (<++> (M C Dep N) (M N)) W-*))
  (2 (bet-3 eta-3 tht-3 A-6 F-2 K-5 U)))
;;; STEP. 4
;;; The system uses "insertion connection" to insert
 move3 between move2 and A-6.
;;; Move3 = (b)' s transformation = (3 (A-2a C Dep F-9
K-4 W-2s))
'(){
  (1 (alp F-1 bet-2 Aa-1 (<++> (M C Dep N) (M N)) W-*))
  (2 (bet-3 eta-3 tht-3 A-6 (} 2-1 (F-2 K-5 U))))
  (3 (A-2a C Dep F-9 K-4 W-2s ({ 2-1))))
;;; STEP. 5
;;; The system uses "insertion connection" to insert
 move4 between A-2a in move3 and C.
;;; Move4 = (b)' s transformation
;;;          =(4 (F-9u6 Aa-1 C Dep G-2 K-1 Pr-1 Rs-1 Ret
(^ W-*) W-*))
'(){
  (1 (alp F-1 bet-2 Aa-1 (<++> (M C Dep N) (M N)) W-*))
  (2 (bet-3 eta-3 tht-3 A-6 (} 2-1 (F-2 K-5 U))))
  (3 (A-2a (} 3-1 (C Dep F-9 K-4 W-2s))))
  (4 (F-9u6 Aa-1 C Dep G-2 K-1 Pr-1 Rs-1 Ret (^ W-*)
W-* ({ 3-1) ({ 2-1))))
;;; STEP. 6
;;; The system uses "insertion connection" to insert
move5 between (^ W-*) in move4 and W-*.
```

```
;;; Move5 = (b)' s transformation = (5 (A-18 B C D-9
E-9 K-4))
' () (
  (1 (alp F-1 bet-2 Aa-1 (<++> (M C Dep N) (M N)) W-*))
  (2 (bet-3 eta-3 tht-3 A-6 () 2-1 (F-2 K-5 U))))
  (3 (A-2a () 3-1 (C Dep F-9 K-4 W-2s))))
  (4 (F-9u6 Aa-1 C Dep G-2 K-1 Pr-1 Rs-1 Ret (^ W-*)
() 4-1 (W-*))))
  (5 (A-18 B C D-9 E-9 K-4 ([ 4-1) ([ 3-1) ([ 2-1))))
;;; STEP.7
;;; The alternation of move2 and fragments of
 move3' second part : 2-1 -> 3-1
;;; The alternation of move2 and fragments of move4' s
second part : 2-1 -> 4-1
' () (
  (1 (alp F-1 bet-2 Aa-1 (<++> (M C Dep N) (M N)) W-*))
  (2 (bet-3 eta-3 tht-3 A-6 () 2-1 (F-2 K-5 U))))
  (3 (A-2a () 3-1 (C Dep F-9 K-4 W-2s))))
  (4 (F-9u6 Aa-1 C Dep G-2 K-1 Pr-1 Rs-1 Ret (^ W-*)
() 4-1 (W-*))))
  (5 (A-18 B C D-9 E-9 K-4 ([ 2-1) ([ 4-1) ([ 3-1)))
```

3.4 A story grammar with move operations

```
RUSSIAN-MAGIC-TALE →
   (<< INTRODUCTION {MOVE} )
INTRODUCTION → a
{MOVE} →
   (<< PRELIMINARY-PART
      ( BEGINNING
        PRELIMINARY-TRIAL
        TRIAL---RETURN
        ENDING
        ) )
PRELIMINARY-PART →
   β (// (=> ( γ δ ) ( ε ζ ) ) ( η θ ))
BEGINNING →
   (// A a ) {%} B C ? {%}
PRELIMINARY-TRIAL →
 D E F {%} G {%}
TRIAL---RETURN →
   (// Struggle-Sequence
       Difficult-Task-Sequence )
Struggle-Sequence →
   H J I {%} K {%} Return O {%} L {%}
Difficult-Task-Sequence →
   L {%} M J N {%} K {%} Return
Return → Ret {%} (=> Pr Rs) {%}
ENDING →
   (=> Q Ex) {%} T U {%} W {%}
--- --- --- --- --- --- --- --- --- --- --- --- --- --- ---
{%} → {MOVE}

;; (<< X Y) : X is calculated after Y
;; (// X Y ) : Alternative selection
;; (=> X Y) : Y continues after X with high probability.
```

Figure.1 : Story Grammar with Move

Propp showed some segments of folktale's construction. The segments contain "introduction", "preliminary-part", "beginning", and so on. We define a story grammar (figure.1) with these elements in this paper. We already proposed a precise story grammar containing all functions and all sub-functions which Propp defined and all event-concepts which Propp showed as examples [8], but the story grammar here in figure.1 is simpler. But, it is extended in the point that has move operations. The position of move operations is assigned with {%} mark. We defined the position by picking out all positions in tales of [3].

4 Conclusions

Until now an aspect in Propp theory as the theory showing the structural constraint of stories has been emphasized, but in this paper we pointed out the richness of mechanisms of transformation or variation which create at least surface diversity of stories, and proposed a kind of rhetorical rules or techniques for operating moves to develop complicated stories. We think that narratology perhaps needs to be approached in two directions; structural constraint exists in spite of surface diversity and surface diversity exists in spite of structural constraint. As a future direction, we are thinking about a framework of extended story grammar by which can flexibly edit fragmentary knowledge elements of story and narrative without a fixed structure.

References

[1] Ogata, T.: Expanded Literary Theory: Cognitive/Computational Expansion of Literary Theories and Narratology, *Proc. of 17th Congress of the International Association of Empirical Aesthetics*, 163-166, 2002.

[2] Ogata, T. & Terano, T.: Explanation-Based Narrative Generation Using Semiotic Theory, *Proc. of National Language Processing Pacific Rim Symposium 91*, 321-328, 1991.

[3] Propp, V. (Пропп, В. Я.): *Морфология сказки, Изд, 2е.* Москва: Наука, 1969. (*Morphology of the Folktale*, University of Texas Press, 1988.)

[4] Genette, G.: Discours du recit, essai de methode, *Figures III*, Paris: Seuil, 1972.

[5] Ogata,T.: Expansion of Techniques for Narrative Generation Using Literature Theory, *Proceedings of the International Conference on Cognitive Science '97*, 299-300, 1997.

[6] Ogata,T. & Terano,T.: Plot Generation and Expansion in Explanation-Based Narrative Generator, *Proceedings of First Singapore International Conference on Intelligent Systems*, 549-554, 1992.

[7] Hosaka,Y. & Ogata,T.: A Study of Story Generation and Representation - A Simulation of V.Propp Theory as a Starting Point -, *The 4th International Conference on Cognitive Science* (*Abstracts*, 64), 2003.

[8] Ogata, T.: Toward the computational model of story generation (in Japanese), *Japanese Cognitive Science Society Technical Report 93-No22*, 52-67, 1993.

Proc. of The Ninth Int. Symp. on Artificial Life and Robotics (AROB 9th '04)
Beppu, Oita, Japan, 28-30 January, 2004

Classification and Combination of Perspective in Narrative

Koji Ueda
Graduate School of Engineering
Yamanashi University
Yamanashi, 400-8511 Japan
e-mail g03mk004@ccn.yamanashi.ac.jp

Takashi Ogata
Department of Medicine and Engineering
Yamanashi University
Yamanashi, 400-8511 Japan
e-mail ogata@esi.yamanashi.ac.jp

Abstract

In this paper, we propose a simple and basic computational modeling of perspective in narrative using a perspective's typology in narrative discourse theory by Genette. First, after we describe the perspective's typology of Genette and our one from the viewpoint of computational modeling, we show the framework of a simple operation system of perspective's processing. Next, we show an image that a sequence of text is variously transformed by applying different perspective's techniques, and explain concrete mechanisms of some kinds of perspectives using examples of the system's input and output.

1 Introduction

Until now, the study of narrative understanding and generation has held energetic. But, the study which innovated the knowledge accumulated in literary theories and narratology has not been done. The theme of this paper - the problem of perspective in literary texts has been also progressed by many researchers, but approaches based on computer modeling and computer simulation have not been done.

In this paper, we propose a simple and basic computational modeling of the perspective in narrative applying a perspective's typology in narrative discourse theory by Genette. Genette is a literary theorist based on structuralism, and proposed a typological theory [1] about narrative discourse processing. We have re-defined his typological theory from the viewpoint of operational techniques using the method of computer simulation [2]. In following description, at first, we show Genette's classification of perspective, and then we divide it into basic perspectives and applicable perspectives as combinations of the former. At last, we explain simple computer programs to operate basic and applicable perspectives to formulate computational mechanism of perspective.

2 Genette's Typology of Perspective and Our Re-classification

Genette originally divided narrative perspective [3] into three categories; zero perspective, internal perspective, and external perspective. The internal perspective has internal fixed perspective, internal variable perspective, and internal multiple perspective as the sub types. He defined alteration which means a temporary transgression to the perspective adopted consistently. It has paralipsis and paralepsis.

Based on above idea, we divided the Genette's classification of perspective into two groups; a group of basic perspectives and a group of applicable ones. The second group can be defined in the combinations of basic perspectives so it is strongly related to strategic knowledge.

Basic perspectives have three sub categories; zero perspective, internal fixed perspective, and external perspective. Zero perspective can narrate all information in a story. Internal fixed perspective narrates the information about characters of limited number and perceived by them. External perspective narrates only the information about external aspects of characters such as external characteristics and actions.

Next group, applicable perspectives have internal variable perspective and internal multiple perspective. They are two applications in the internal fixed perspective. There is alteration as another type's category. As described above, applicable perspectives are simply defined by the combinations of basic perspectives. The internal variable perspective narrates a story while changing the character chosen as the subject of the perspective (focalized character). Internal multiple perspective is a type which narrates a same event using different characters' internal fixed perspectives. The paralipsis is a special technique that doesn't intentionally (perhaps) narrate the narrative information which should theoretically be narrated, and the paralepsis is one that theoretically dare narrate the narrative information which should be overlooked.

3 Overview of the System

We implemented a simple experimental system by Allegro Common Lisp that transforms given information of a story based on the particular perspective [4]. A user gives some sequences of events, the information related to their events and a particular type of perspective. The system outputs a sequence of transformed events. Figure.2 shows an image that different perspectives transform a story's information into various forms (input and output of implemented system aren't natural language, but conceptual representation).

The conceptual expression of each event in a story has an event concept as first item and pairs of some slots like actor, object and location, and their values. Each element in the event concept is linked to a particular element in persona-frames, object-frames, and location-frames. A persona-frame has name, sex, external aspect, internal aspect, direction, and perception as slots, and a perception slot stores an event that the person currently

percepts. An object-frame and a location-frame have respectively a name and external features. We show an image of input information in Figure.1.

System's algorithm is as follows; (1)A user inputs the information shown in above description. (2)System transforms one event data by inputted perspective's processing. (3)It puts transformed event data to a list of transformed events. (4)It checks whether all events were transformed. (4-1)If all events were not processed, go to (2). (4-2)If all events were processed, it outputs data getting in a list of transformed events.

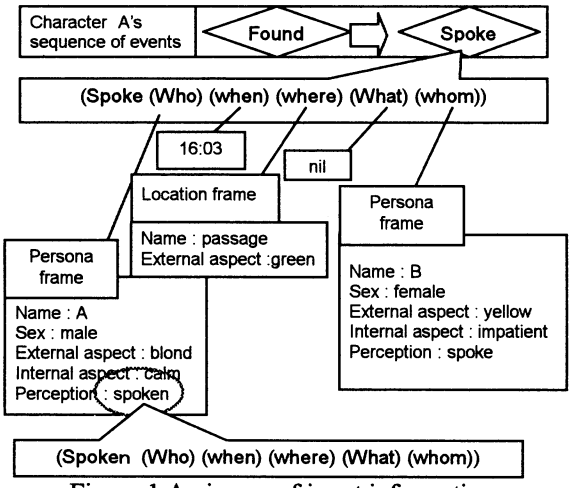


Figure.1 An image of input information

4 Perspective's Operations

In this section, we explain mechanisms that the system operates various perspectives. We use real examples except for some types. Following list is input information, and in sub sections, operations to this list will be shown. This list includes two events; "blond and calm A finds out yellow and impatient B" and "yellow and impatient B thinks".

```
[1] Event = Find1
Time      : 1600
Act       : Find
Actor     : (Persona (Name A) (Sex male) (External-aspect blond)
(Internal-aspect calm) (Perception (Event (Time 1600) (Act think) (Actor
(Persona (Name B) (Sex female) (External-aspect yellow) (Internal-aspect
impatient) (Perception nil))) (Object nil) (Location (Location (Name
passage) (External-aspect green))) (Direction nil))))
Object    : (Persona (Name B) (Sex female) (External-aspect yellow)
(Internal-aspect impatient) (Perception nil))
Location  : (Location (Name passage) (External-aspect green))
Direction : nil
[2] Event = Think1
Time      : 1600
Act       : think
Actor     : (Persona (Name B) (Sex female) (External-aspect yellow)
(Internal-aspect impatient) (Perception nil))
Object    : nil
Location  : (Location (Name passage) (External-aspect green))
Direction : nil
```

4.1 Zero perspective

Zero perspective can narrate all narrative information included in a story, and the system simply outputs the information inputted into the story as it is.

4.2 Internal fixed perspective

First, internal fixed perspective outputs three kinds of information; information about action(s) in event(s) that a particular person who functions as the center of the perspective (focalized person) makes, external information described in the event(s), and internal information of the focalized person. Next, if this focalized person knows other's event, the system removes the internal information in the other's persona-frame because focalized person cannot perceive the other's internal information, and outputs the action's information and external information in the event(s). We show a result which processed the story data shown previously with internal fixed perspective's processing. This list means the event of "blond and calm A finds out yellow B", and the mental or internal state of B ("impatient") is removed.

```
[1] Event = Find1
===<<< Focused Person >>>===
— Self —
Time      : 1600
Act       : Find
Actor     : (Persona (Name A) (Sex male) (External-aspect blond)
(Internal-aspect calm) (Perception (Event (Time 1600) (Act think) (Actor
(Persona (Name B) (Sex female) (External-aspect yellow) (Internal-aspect
///removed///) (Perception nil))) (Object nil) (Location (Location (Name
passage) (External-aspect green))) (Direction nil))))
Object    : (Persona (Name B) (Sex female) (External-aspect yellow)
(Internal-aspect ///removed///) (Perception nil))
Location  : (Location (Name passage) (External-aspect green))
Direction : nil
— Other —
Act       : think
Actor     : (Persona (Name B) (Sex female) (External-aspect yellow)
(Internal-aspect ///removed///) (Perception nil))
Object    : nil
Location  : (Location (Name passage) (External-aspect green))
Direction : nil
```

4.3 External perspective

External perspective outputs only external action(s) which appear(s) outside and the information of external aspects among the narrative information included in the story data. And then, it removes mental action(s) (which doesn't appear outside, for example thinking and considering) of person and internal information. We show a result which processed the story data shown previously with external perspective. In next list, A's internal aspect ("calm"), B's one ("impatient"), and B's internal action ("think") are removed.

```
[1] Event = Find1
Time      : 1600
Act       : Find
Actor     : (Persona (Name A) (Sex male) (External-aspect blond)
(Internal-aspect ///removed///) (Perception (Event (Time 1600) (Act
think) (Actor (Persona (Name B) (Sex female) (External-aspect yellow)
(Internal-aspect ///removed///) (Perception nil))) (Object nil) (Location
(Location (Name passage) (External-aspect green))) (Direction nil))))
Object    : (Persona (Name B) (Sex female) (External-aspect yellow)
(Internal-aspect ///removed///) (Perception nil))
Location  : (Location (Name passage) (External-aspect green))
Direction : nil
[2] Event = nil
```

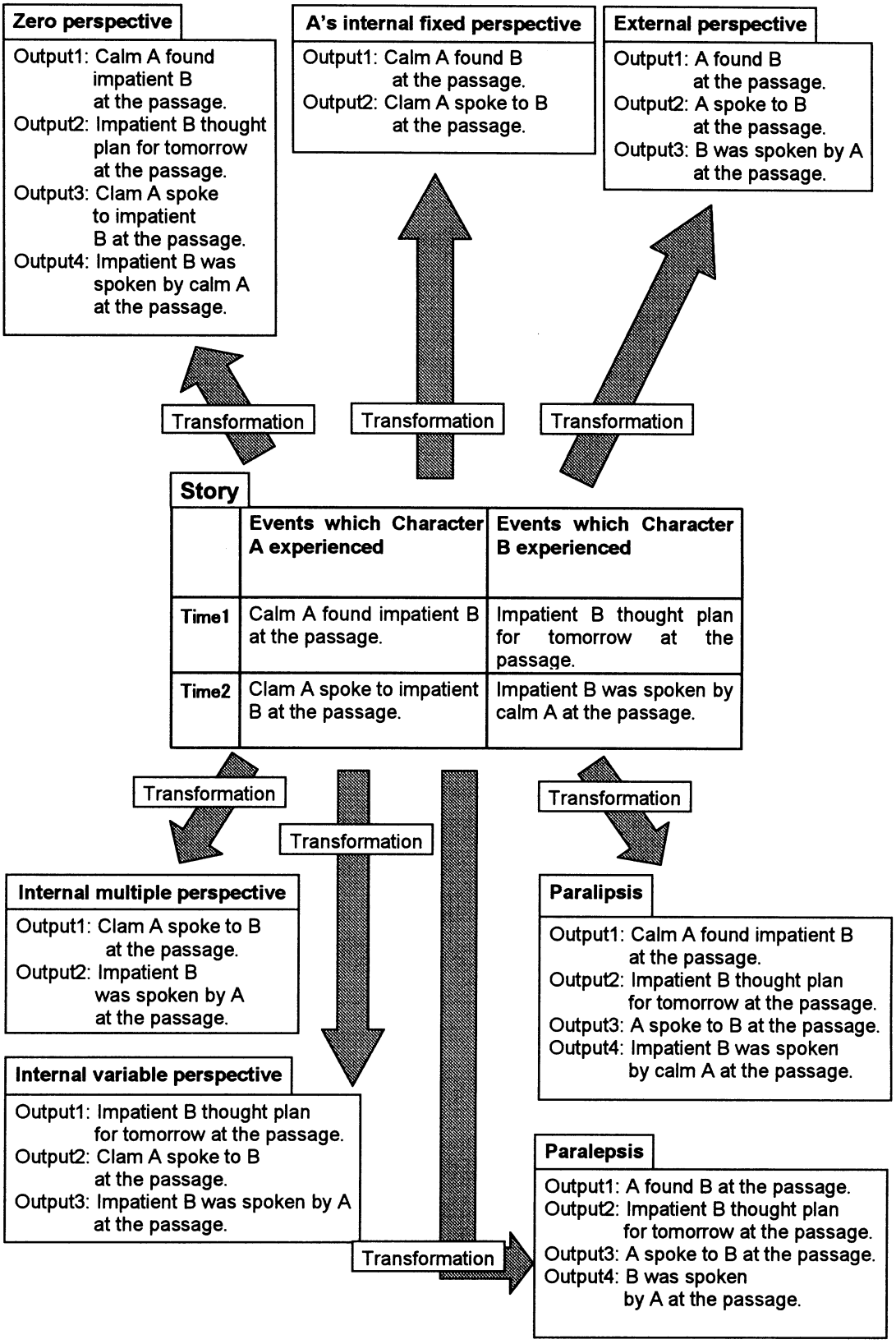


Figure. 2 An image of various transformations by different perspectives

4.4 Internal variable perspective

As internal variable perspective's processing requires that a focalized person changes, the system rearranges event sequences so that the same actor doesn't continue. And then, the system processes the rearranged event sequence with internal fixed perspective of the person who has caused the event.

4.5 Internal multiple perspective

Internal multiple perspective cannot do multiple narration, unless several persons know the certain event(s). That is to say, this needs the event(s) which several persons perceive. For this reason, the system checks the perception slot of a persona-frame as first processing. When the event(s) which several persons perceive exist(s), the system processes it (them) with internal fixed perspectives of the persons who perceive the event(s).

4.6 Paralipsis

Paralipsis doesn't intentionally narrate the narrative information which should be narrated. For this reason, the system decides an event which doesn't narrate the narrative information be narrated, implements the operation of reducing the quantity of narrative information about that event, and processes other event(s) according to the consistent type of perspective. Describing concretely, the system makes the consistent perspective's type of zero perspective, and decides at random an event which processes with external perspective. We show an example of the event which was transgressed with external perspective. This example shows that explicit information decreases for the transgression by external perspective. A's internal aspect ("calm") and B's internal aspect ("impatient") which should originally be narrated are intentionally removed.

```
[1] Event = Find1
Time      : 1600
Act       : Find
Actor     : (Persona (Name A) (Sex male) (External-aspect blond)
(Internal-aspect ///removed///) (Perception (Event (Time 1600) (Act
think) (Actor (Persona (Name B) (Sex female) (External-aspect yellow)
(Internal-aspect ///removed///) (Perception nil))) (Object nil) (Location
(Location (Name passage) (External-aspect green))) (Direction nil))))
Object    : (Persona (Name B) (Sex female) (External-aspect yellow)
(Internal-aspect ///removed///) (Perception nil))
Location  : (Location (Name passage) (External-aspect green))
Direction : nil
```

4.7 Paralepsis

Paralepsis dare narrate the narrative information which should be overlooked. For this reason, the system decides an event which narrates narrative information be overlooked, implements the operation of increasing the quantity of narrative information about that event, and processes other event(s) according to the consistent type of perspective. Describing concretely, the system makes the consistent type of perspective of external perspective, and decides at random an event which dare narrate the narrative information not be narrated. And then, the system outputs that event with zero perspective, outputs all events except that event with external perspective. We show an example of event which was transgressed with zero perspective. This example shows that explicit information increases for the transgression by zero perspective. A's internal aspect ("calm") and B's internal aspect ("impatient") which shouldn't originally been narrated are intentionally narrated.

```
[2] Event = Think1
Time      : 1600
Act       : think
Actor     : (Persona (Name B) (Sex female) (External-aspect yellow)
(Internal-aspect impatient) (Perception nil))
Object    : nil
Location  : (Location (Name passage) (External-aspect green))
Direction : nil
```

5 Conclusions

In this paper, we re-defined Genette's typology of perspective, and showed a simple operating model for perspective's processing. We simplified the problem of perspectives as the operations of prepared necessary information. By this kind of processing, we can treat various processings of perspective in the combinations of simplified processings, and moreover, the integrated usage with other discourse techniques will become easy for the simplification.

Of course, as this attempt is a starting point for computational processing of narrative perspective, we have various problems and future works. First, in this system, a perspective is firstly given, but for more flexible processing, the system should have a mechanism to control perspectives by inputted different parameters of perspective at any time. Next problem isn't a one relating directly to the processing of perspective itself, but is very important for the architecture of the narrative generation system. In this research, we prepare directly by hand simulation the information about a story or narrative content to be used as input data, but the information should be generated or prepared inside a mechanism of story generation.

References

[1]Genette, G., *Discours du recit in Figures III*, Seuil,1972.

[2]Ogata, T., Expanded Literary Theory: Cognitive/Computational Expansion of Literary Theories and Narratology, *Proceedings of 17th Congress of the International Association of Empirical Aesthetics*, pp.163-166, 2002.

[3]Tsuchida, T., Aoyagi, E., & Ito, N., *Gendai bungaku riron* (In Japanese), Shinyousha, pp.54-56, 1996.

[4]Ueda, K., "Shiten" ni yoru monogatari henkan shisutemu no kousatsu (In Japanese), Graduation thesis (Yamanashi University), 2003.

Proc. of The Ninth Int. Symp. on Artificial Life and Robotics (AROB 9th '04)
Beppu, Oita, Japan, 28-30 January, 2004

A Robotic Approach to Emotion from a Selectionist Perspective

Tomoko KATO Takaya ARITA
Graduate School of Information Science, Nagoya University
Furo-cho, Chikusa-ku, Nagoya 464-8601, Japan
E-mail:{tomo@create, ari@info}.human.nagoya-u.ac.jp

Abstract

This paper reports on the current state of our efforts to synthesize emotion in robots from a selectionist perspective. As a first step, we describe a minimal model of emotion in robots in somewhat behavioristic view, which is based on Dietrich Doerner's theory on human emotions. From this perspective, we define five emotions of robots in terms of four modulators. Next, we conduct a robotic experiment in order to test that humans can identify a set of basic emotions in a mobile robot synthesized based on our definition This paper reports on the result of this evaluation test, and also discusses adaptive properties of each emotion by assuming illustrative examples in which a robot moves around an environment with various physical conditions.

Keywords: Emotional robots, Artificial life, Behavior modulation, Evolutionary psychology

1 Introduction

The study of emotions has become a hot research area during recent years [1]. Many researchers have focused on the functions of emotion, and typical explanations of them are based on flexibility of behavior response to reinforcing signals, communications which transmit the internal states, or social bonding between individuals, which could increase fitness in the context of evolution. Among them, Masanao Toda has developed a theoretical framework termed the urge theory in which human activities may be modelized, and has focused on the functional aspect of emotion systems [2].

The first purpose of our study is to explore the origin and the adaptations of emotion by synthesizing an emotion system "as it could be" in robots (Fig. 1). We believe that the possession of emotion is an adaptive "trait" also to robots conducting their assigned tasks in environment with or without humans, which is parallel with a selectionist view that emotion in humans is the product of adaptive evolution.

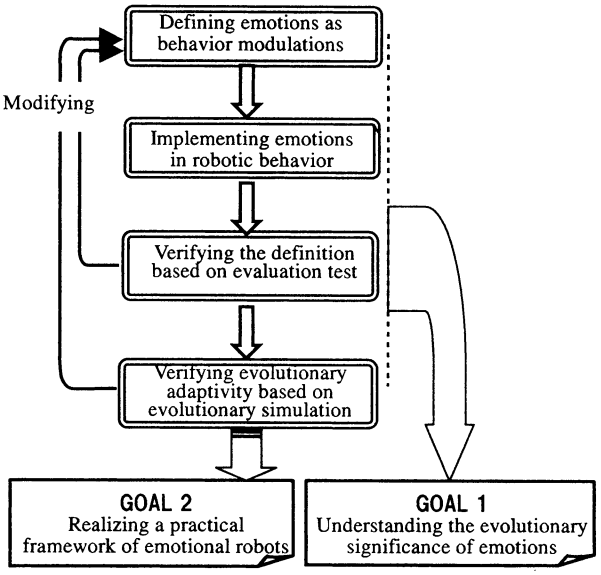


Fig. 1 Study scheme.

The second purpose is to realize an efficient robotic system in which robots perform tasks flexibly and effectively by using their emotional system. Although there is a possibility that our emotion system is rapidly becoming obsolete as our life environment has changed at a much faster rate than evolution, the emotion system in robots can be optimized according to given tasks by evolutionary algorithms.

As a first step, we describe a minimal model of emotion in robots, which is based on Dietrich Doerner's theory on human emotions, which is, in short, that emotions are seen as behavior modulations [3][5][6]. We define five emotions of robots in terms of

four modulators based on his claim. Next we conduct a robotic experiment in order to test whether humans can identify a set of basic emotions in robots implemented based on the definition, which might remind of the impressive work of Valentino Braitenberg, in which, as thought experiments, he designed many simple vehicles and described them as possessing fear, love and aggression [4]. Our model of emotions in robots is functionalistic, and supposed to lead to evolutionary grounding. For this purpose, we discuss adaptive properties of each emotion by assuming illustrative examples in which robots move around an environment with various physical conditions.

2 Emotions as Behavior Modulations

We describe a minimal model of emotion in robots in somewhat behavioristic view in Section 3, which is based on the Dietrich Doerner's theory on human emotions. Doerner's claim is, in short, that emotions are seen as behavior modulations [3][5][6]. The theory identifies four different modulators that describe goal-directed behavior at any given time, a) activation, b) externality, c) precision, and d) focus.

a) **Activation**
The amount of nonspecific activation that is involved while pursuing a goal. This modulator has the extremes of hypoactivation (a lack of energy) and hyperactivation (a surplus of energy).

b) **Externality**
The proportion of time spent in external activity. This modulator has the extremes of introversion (devoted mainly to information processing) and extroversion (devoted mainly to action).

c) **Precision**
How much care or precision a goal is pursued with. This modulator has the extremes of imprecision and precision.

d) **Focus**
The amount of attention that is allocated to the current task rather than to the surveillance of the background. This modulator has the extremes of broadened senses and of narrowed senses.

Following analogy might help our understanding of emotions as behavior modulations [6]. For example, a television can be adjusted for brightness, contrast and so on. These adjustments determine a "behavior modulation" for the television such as how bright, how much contrast and so on. The point here is they are all independent of the TV program actually showing. Similarly, human behavior can be described by emotions as behavior modulations. We can notice a striking difference between the behavior of an angry person and that of a sad person even if they take the same action. The volume control and so on in televisions correspond to activation, externality, precision, and focus in the emotion systems. The variations of the behavior on these four aspects define the modulations of human behavior. Each modulation pattern is associated with a particular emotion as shown in Tab. 1.

Tab. 1 Modulation patterns of six emotions [6].

	Modulation pattern in terms of modulators			
Emotion	Activation	Externality	Precision	Focus
None	0.50	0.50	0.50	0.50
Anger	1.00	1.00	0.00	1.00
Anxiety	1.00	0.00	1.00	1.00
Contentment	0.25	0.25	0.75	0.00
Excitement	0.75	0.75	0.25	0.00
Sadness	0.00	0.00	1.00	1.00

3 Introducing Emotions to Robots

We conducted a robotic experiment in order to test whether humans could identify a set of basic emotions in a robot synthesized based on the above-described Doerner's theory on emotions by using a mobile robot "AmigoBot" (Fig. 2). The robot moved on a particular path from the start point to the goal point in a field where there existed some obstacles and walls as shown in Fig. 3. We defined following four modulators in behavior of the robot to synthesize emotional behaviors (Fig. 4).



Fig. 2 AmigoBot.

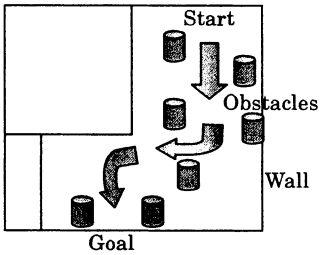


Fig. 3 Environment and Robot Task.

a) **Activation**
How long each behavior cycle is. The robot sets

its behavior (motor speed) every behavior cycle.

b) **Externality**
How fast it moves through the path.

c) **Precision**
How long it deviates from the route at curves.

d) **Focus**
How much degree it deviates from the route. If it concentrates its task, it moves to the goal directly along the route. If not, it deviates from the route.

Fig. 5 shows the typical trajectories of a robot with emotions defined by 4 modulators and the modulation patterns shown in Tab. 1.

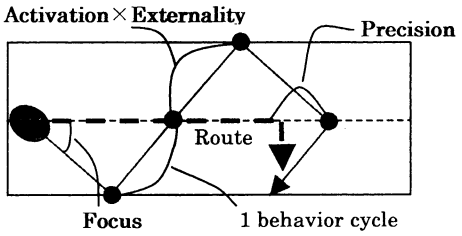


Fig. 4 Modulations of the robot behavior.
(Dashed line: Route, Solid line: Trajectory of a robot).

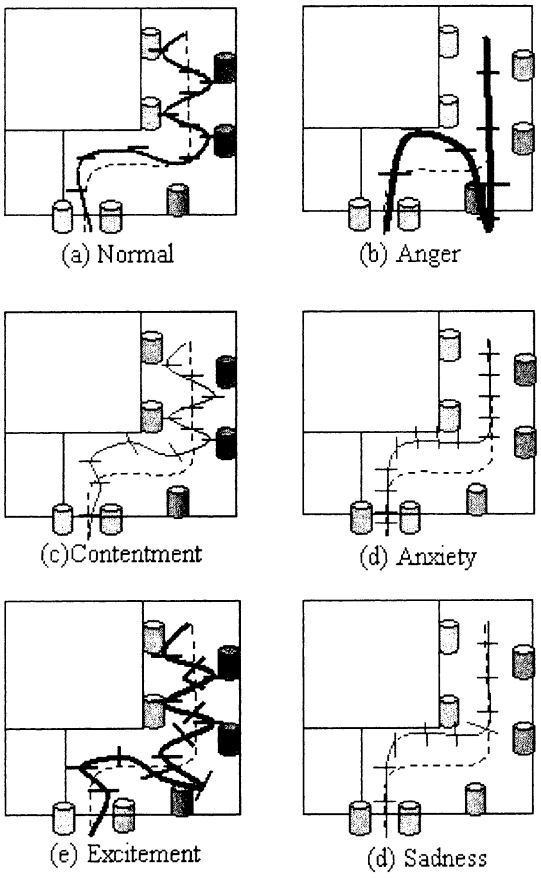


Fig. 5 A sketch of the robot trajectories with 6 emotions. (width of trajectories: robot velocity expressed by **externality**, length of each fragment:**activation*externality**).

4 Evaluation Test

We conducted an evaluation test in which the robotic behavior was estimated by more than 1000 subjects (visitors to a scientific museum) in order to test whether humans could identify a set of basic emotions in robots as described in the previous section. We captured five emotional behaviors and one behavior without emotion on movie files, and then human experimental subjects were required to assign five emotions to these five movie files after seeing and comparing them on the computer display (Fig. 6).

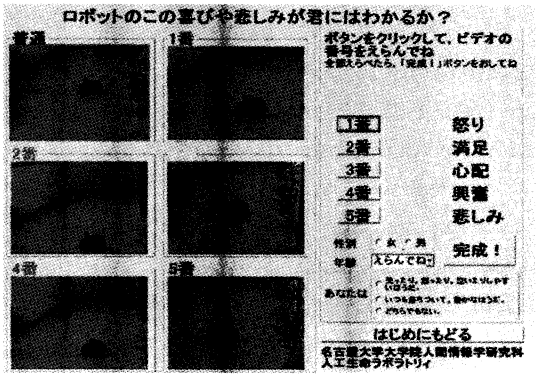


Fig. 6 A screen shot of the evaluation software.

Tab. 2 Human ratings of emotions.
(bold-type: the most frequently associated emotions).

Shown Emotions \ Ratings	Anger	Content-ment	Anxiety	Excite-ment	Sadness	None	Total
Anger	**335**	119	102	220	182	155	1113
Contentment	151	**382**	237	121	110	112	1113
Anxiety	132	153	**268**	164	245	151	1113
Excitement	204	147	215	**310**	88	149	1113
Sadness	135	168	170	136	**331**	173	1113
Total	957	969	992	951	956	740	5565

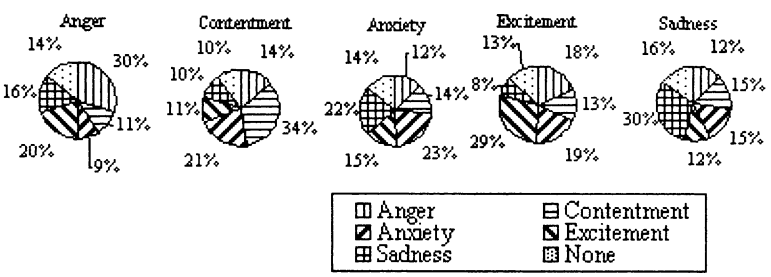


Fig. 7 Pie chart of human ratings of emotions.

The result of the experiment (Tab. 2 and Fig. 7) showed that subjects had a tendency to identify all of the basic emotions in the robot. The chi-square analysis showed significant relationship between the modulation pattern and the rating of the subjects ($\chi 2$: 189.88, df: 16, P: 1.8044E-159), although the evaluation test was not conducted under the strict conditions. It was shown that three emotions: anger, contentment and sad were clearly distinguished from the other emotions, while anxiety was least identified. Also, anxiety and sadness which have similar modulation patterns tended to be confused, which seems rather reasonable.

5 Discussion

Here we discuss adaptive properties of some emotions in robots from a selectionist perspective by using illustrative examples. Suppose that a robot moves from the start point to the goal point in an environment with various physical conditions as shown in Fig. 8.

In this figure, Zone A is a hazard area, in which the robot suffers serious damage every second. So, it is adaptive for the robot to get angry when entering the zone, because most activation and most externality make the robot get out the zone in a rush even though least precision might cause dissipation of its some energy. Also, anger might be adaptive when moving the narrow path (Zone B). It would be difficult for a robot with careful moving to get out these zones. In contrast, tough actions of angry robot could go through such a path while bumping against walls at times.

Next, suppose that a robot moves in contentment. Its focus is least and activation and externality are low. Its relaxed move might have a tendency to let the robot find a light source and fill in its energy (Zone C). In case that a robot enters a poorly-lighted area (Zone D), it would be adaptive for a robot to become anxious, because accurate move with concentrated attention could let the robot find and clear the obstacles. Also, to be anxious might become adaptive in Zone E, as the robot could respond to irregular emergence of obstacles.

6 Conclusion

We have synthesized an emotion system "as it could be" in robots based on the view of emotions as behavior modulations. We conducted an evaluation test which looks something like the famous Turing test, and showed that humans could identify the five basic emotions from the emotional behaviors of a robot defined by modulation patterns. Adaptive properties of emotional behavior were also discussed based on illustrative examples. Our next step is to conduct evolutionary simulations to verify this sort of evolutionary adaptivity with the scenario of the origin and the evolution of human emotions in mind as shown in Fig. 1.

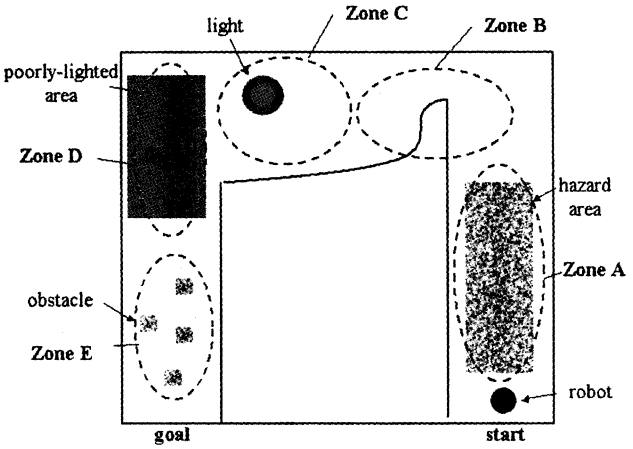


Fig. 8 An environment with various physical conditions.

References

[1] R. Treppel, P. Petta and S. Payr, *"Emotions in Humans and Artifacts"*, The MIT Press, 2003.

[2] M. Toda, "The Urge Theory of Emotion and Cognition", Chukyo University School of Computer and Cognitive Sciences, *Institute for Advanced Studies in Artificial Intelligence Technical Report*, 94-1-01, 1994.

[3] D. Doerner, H. Schaub, T. Staeudel and S. Strohschneider, "Ein system zur handlungs- regulation oder die interaktion von emotion, kognition und motivation", *Sprache & Kognition*, Vol. 4, pp. 217–232, 1988.

[4] V. Braitenberg, *"Vehicles: Experiments in Synthetic Psychology"*, The MIT Press, 1984.

[5] D. Doerner and K. Hille, "Artificial souls: Motivated emotional robots", *Proceedings of the International Conference on Systems, Man and Cybernetics*, pp. 3828-3832, 1995.

[6] K. Hille, "Synthesizing Emotional Behavior in a Simple Animated Character", *Artificial Life*, Vol. 7, No. 3, pp. 303-313, 2001.

Proc. of The Ninth Int. Symp. on Artificial Life and Robotics (AROB 9th '04)
Beppu, Oita, Japan, 28-30 January, 2004

Model based recognition for artificial brain

Xin Wang*,** Masanori Sugisaka** Wenli Xu*

*Department of Automation, Tsinghua University, Bejing 100084, China

**Department of Electrical and Electronic Engineering, Oita University, Oita 870-1192 Japan

Abstract

Image information is very important to the research on artificial brain machine or intelligent agent. This approach represent a compromise object-dependent technique to track a known static target in an image sequence from a moving platform, and its information is similar to the optical flow, but it is based on correspondence of interest points between inter-frame time intervals in image sequence. These time intervals cannot be short enough for well-known optical flow computation that is object-independent analysis method. We have noticed that though a point is environment sensitive, grouped points energy changes have their own statistical similarities. In our approach, we build a contour model of a static target to get some of low-energy points, use auto-relation relation to give the behavior of orientation in a local window, and decide corresponding point pairs between the local windows. Those detected corresponding relations are used to recover corresponding low-energy points in new frame. These new low-energy points then give a description about the target for machine recognition.

Keywords: *tensor feature, correspondence, image sequence*

1. Introduction

In recent year, interest in motion processing has increased with advances in motion analysis methodology and processing capabilities. The usual input to a motion analysis system is a temporal image sequence, with a corresponding increase in the amount of processed data. Motion analysis is often connected with real-time analysis. Another common motion analysis problem is to obtain comprehensive information about moving and static objects present in a scene. A set of assumption can help to solve motion analysis problem-prior knowledge helps to decrease the complexity of analysis. Prior knowledge includes information about the camera motion, mobile or static, and information about the time interval between consecutive images, especially whether this interval was short enough for the sequence to represent continuous motion. This prior information helps on the choice of an appropriate motion analysis technique.

Generally, there are three groups of motion-related problems from the practical point of view: motion detection, moving object detection and location and derivation of 3D object properties. We will deal with the second group, etc. moving object detection and location.

The notable algorithms of objective from a moving platform using a vision sensor camera use temporal or spatial disparities estimated from the image sequence for detection purpose. These algorithms can be grouped into three classes: (1) methods using optical flow; (2) methods using qualitive estimates of motion; (3) methods using velocity field. Object motion parameter can be derived from computed optical flow vectors [1][2]. But in reality, estimates of optical flow or object- independent point correspondence are noisy et al., the interpretation of motion is ill-conditioned. Motion field analysis relies on distinctive characteristics in different frames and can be concluded into the point or area correspondence analysis. Comparing with traditional motion field or velocity field in optical flow computation, we mean it is based on images acquired at intervals that are not short enough to ensure small changes due to motion and can be also acquired if the number of images in a sequence is small. Motion filed computations represent a compromise technique: information is similar to the optical flow, but it is based on images acquired at intervals that are not short enough to ensure small changes due to motion. The velocity field can also be acquired if the number of image in a sequence is small. We discuss motion analysis problem based on tracking correspondence features in image sequence from a moving platform.

One of important differences between motion in moving camera or moving platform and static camera is that every pixel is moving in the former case and only object pixels are moving in the later. We discuss the case of moving platform and static target/object on the assumptions that motion is with maximum velocity constraint and mutual correspondence that each point of an object corresponds to exactly one point in the next image in sequence in this paper.

We defined the final converged control points of an active contour about a target as *kernel*. Our approach consist of building a contour model of a target/object, finding corresponding key areas or points in consecutive image which kernels appeared in the model, getting a corresponding relation, and recovering the kernels in frames.

In the next section, some notations and general process of this method are given. Section 3 describes the principle of an active contour model, introduces our tensor model and how to use this model to detect interest points. The method to manipulate these cor-

responding relations is explained in Section 4. Our experimental results are illustrated in the related sections.



Fig. 1: Frames selected from a image sequence.

2. Notations and processes

We denote $I(\mathbf{x})$ intensity function of an image, {$\mathbf{x}$=(x, y): $\mathbf{x} \in \mathcal{R}^2$}, as any a frame in an image sequence and the i_{th} $(i = 1, 2, \ldots, n)$ frame as $I_i(\mathbf{x})$. *kernel* state space is $\breve{A}_m$, *tracking windows* are A'_m and A'_n, input state spaces and output state spaces of interest point are A_m, A_n respectively. $\widetilde{A}_r^m$ and $\widetilde{A}_r^n$ are the sets of detected correspondence pairs space in A_m and A_n. There are the relations of $A_m \subset A'_m \subset I_i(\mathbf{x})$, $A_n \subset A'_n \subset I_j(\mathbf{x})$. All interest points and detected points are indicated by the symbol "+" where they are white background around in the relative figures.

Two target frames $I_i(\mathbf{x})$, $I_j(\mathbf{x})$, in which the target is, are sampled by their appeared orders in an image sequence. Assume the input frame be $I_i(\mathbf{x})$, the output $I_j(\mathbf{x})$. Intuitively, we sample points in $I_i(\mathbf{x})$ by a prior knowledge. After executing the algorithm described in Section 3, the contour converges to low-energy positions and a contour model is formed. Consequently, the *kernel* state space $\breve{A}_m$ are those maximally likely low-energy states. There are N *kernels* in the state space $\breve{A}_m$. A'_m gives a *tracking window* in $I_i(\mathbf{x})$. We compute the possible interest points around these *kernel* points in the *tracking window*, and build another *tracking window* A'_n including a corresponding output state spaces A_n={$\mathbf{y}_n$} in $I_j(\mathbf{x})$. An input state spaces A_m (see Section 4), A_m={$\mathbf{x}_m$}, are constructed around those *kernels* in $\breve{A}_m$. The size of A'_n is up to the maximum distance D_{max} (Section 5.1). Finally, the corresponding relations are established by application of the algorithm presented in Section 5. A target's position in $\widetilde{A}_r^n$ is described by the points which is in the *coding chain* in $\widetilde{A}_r^m$. In $\widetilde{A}_r^m$, we can get some new *kernels* to form a new input space state, and track the target in consecutive image sequence by repeating the same steps as before.

3. Model and tensor features

3.1. Active contour model

The traditional active contour model is also called sanke, it is defined as an energy minimizing spline–the snake energy depends on its shape and location within an image. The energy functional to be minimized may be written as:

$$E_s^* = \int_0^1 (E_{int}(\mathbf{v}) + E_{ext}(\mathbf{v}))ds. \quad (1)$$

where $\mathbf{v}$=$v(s)$=[$x(s)$, $y(s)$], x(s), y(s) are x, y co-ordinates along the contour and $s \in$[0, 1], $v(s)$ can be approximated as a B-spline. $E_{int}(\mathbf{v})$ represents the internal energy of the spline due to bending. External energy $E_{ext}(\mathbf{v})$ includes image forces $E_{im}(\mathbf{v})$ and external constraint forces $E_{cst}(\mathbf{v})$:

$$E_{ext}(\mathbf{v}) = E_{im}(\mathbf{v}) + E_{cst}(\mathbf{v}). \quad (2)$$

$E_{im}(\mathbf{v})$ is derived from the image data over which the snake lies. $E_{cst}(\mathbf{v})$ come from external constraints which may force the snake toward or away from particular features. The functional to be minimized is (1).



(a)



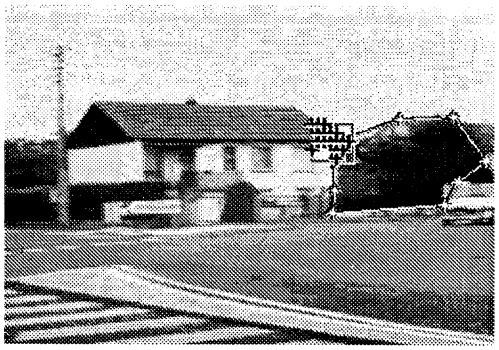
(b)

Fig. 2: Snake contour model (a) and line contour model (b) based on (a).

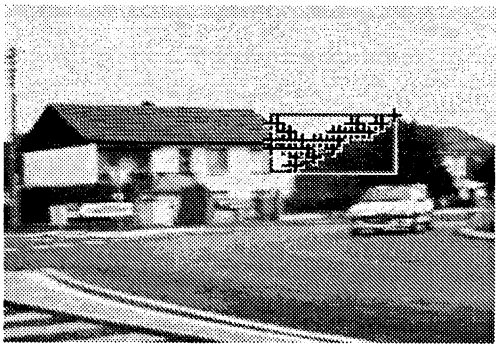
This minimizing condition can reduce to

$$\frac{\partial v(s,t)}{\partial t} - \frac{\partial}{\partial s}[\alpha(s)\frac{\partial v(s,t)}{\partial s}] + \frac{\partial^2}{\partial s^2}[\beta(s)\frac{\partial^2 v(s,t)}{\partial s^2}] - \nabla E_{ext}[v(s,t)] = 0. \quad (3)$$

where $\alpha(s)$, $\beta(s)$ specify the elasticity and stiffness of the snake.



(a)



(b)

Fig. 3: Interest points of a selected image area. (a): the input frame; (b): the output frame.

More details can be found in the research [3]. we only give some results here. Fig.2a shows an original snake contour by the described model, Fig.2b gives the line contour used in our algorithm.

3.2. Representation

The statistics of the gradient in an image neighborhood can yield a useful description of the neighborhood. Within a widow [6], there is a rough taxonomy of four qualitative types of image window :

- *constant window* : gray level is approximately constant;
- *edge window* : there is a sharp change in image change that runs along a single direction;
- *flow widow* : there are several fine parallel stripes;
- *and 2D window* : there is some form of 2D texture.

These cases correspond to different kinds of behavior on the part of the image gradient. In *constant windows*, the gradient vector is short; *in edge windows*, there is a small number of long gradient vectors all pointing in a single direction; *in flow widows*, there many gradient vectors all pointing in two directions; and in *2D windows*, the gradient vector swings. We build up a transform relation $H(\mathbf{x})$ in a local window about a point $\mathbf{x}$ as follows:

$$H(\mathbf{x}) = \Re(\mathbf{x}) * \sum \{(\nabla I(\nabla I)^T\}$$

$$= \Re(\mathbf{x}) * \sum \begin{Bmatrix} (G_x * I)^2 & (G_x * I)(G_y * I) \\ (G_x * I)(G_y * I) & (G_y * I)^2 \end{Bmatrix} \quad (4)$$

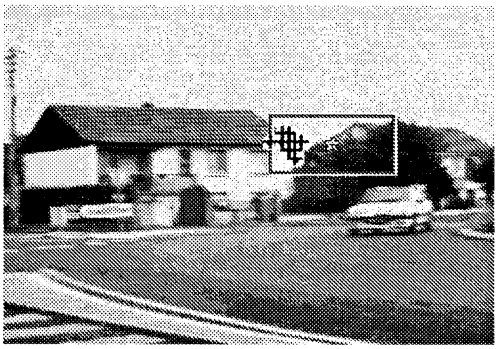
where $I=I(\mathbf{x})$, $*$ is the convolution operation. G is a Gaussian with standard deviation one, $G_x=\partial G/\partial x$, $G_y=\partial G/\partial y$. $\Re(\mathbf{x})$ is a weight mask to weight the derivatives over the window. This matrix captures the local structure. The eigenvectors of this matrix are the principal curvatures of the auto-correlation function. Its rank one indicates an edge and rank zero a homogeneous region. Two significant values indicate the presence of an interest point. We consider a cost function $M(\mathbf{x})$:

$$M(\mathbf{x}) = t_1 det[H(\mathbf{x})] + t_2 trace[H(\mathbf{x})]. \quad (5)$$

where t_1, t_2 are preset constants which are used to control the number of interest points. The interest points are decided by selecting a threshold about $M(\mathbf{x})$. Fig.3 shows our detected results for Fig.1 (upper two frames) by this method. A_m and A_n are detected in A'_m and A'_n respectively. We are subject to same constraints but different scales i.e. window sizes, which result from the computing cost and the demands of the algorithm.



(a)



(b)

Fig. 4: Detection of correspondences: 13 points in (a) correspond with 10 points in (b). The *star* in (b) indicates the same position of the kernel in (a).

4. Decision of corresponding pairs

After the process of interest point detection, we have to decide relations of those interest points between A_m and A_n because the interest points cannot tell us anything about their correspondences.

4.1. Probability relations

A_m=$\{\mathbf{x}_m\}$ is the set of all interest points in the first starting image that is input state space, and A_n = $\{\mathbf{y}_n\}$ the interest points in the second image that is output state space. Let $\mathbf{c}_{mn}$ be a vector connecting points $\mathbf{x}_m$ and $\mathbf{y}_n$. Two points $\mathbf{x}_m$ and $\mathbf{y}_n$ can be considered potentially corresponding if their distance satisfies the assumption of maximum velocity, $|\mathbf{x}_m - \mathbf{y}_n| \leq d_{max}$, d_{max} is the maximum distance a point may move in the time interval between two consecutive images. Two correspondences of points $\mathbf{x}_m\mathbf{y}_n$ and $\mathbf{x}_k\mathbf{y}_l$ are termed consistent of $|\mathbf{c}_{mn} - \mathbf{c}_{kl}| \leq c_{dif}$, c_{dif} is a preset constant derived from prior knowledge. Consistency of corresponding point pairs will increases the probability that a correspondence pair is correct. We construct a data structure as follows:

$$[\mathbf{x}_m, \{\mathbf{c}_{mn}, P_{mn}\}, (NV^*, NP^*)], n = 1, 2, \ldots, CN. \quad (6)$$

where P_{mn} is defined as the probability of correspondence of points $\mathbf{x}_m$ and $\mathbf{y}_n$, NV^*, and NP^* are special symbols indicating that no potential correspondence was found. $CN.$ is a constant.

We initialize the probabilities P_{mn} as $P_{mn}^{(0)}$ as follows:

$$P_{mn}^{(0)} = \frac{1}{1 + k_p \omega_{mn}} (1 - P_{(NV^*, NP^*)}^{(0)}). \quad (7)$$

where $P_{(NV^*, NP^*)}^{(0)}$ is the initialized probability of no correspondence, k_p is a constant and

$$\omega_{mn} = \sum_{\Xi} [I_m(\mathbf{x}_m \pm \Xi) - I_n(\mathbf{y}_n \pm \Xi)]^2. \quad (8)$$

Ξ defines a neighborhood for image match testing –a neighborhood consists of all points ($\mathbf{x}$+Ξ), Ξ is defined as a symmetric neighborhood around $\mathbf{x}$. We iteratively determine the probability of correspondence of a point $\mathbf{x}_m$ with all potential points $\mathbf{y}_n$ as a weighted sum of probabilities of correspondence of all consistent pairs $\mathbf{x}_k\mathbf{y}_l$, $\mathbf{x}_k$ are neighbors of $\mathbf{x}_m$ and the consistency of $\mathbf{x}_k\mathbf{y}_l$ is evaluated according to $\mathbf{x}_m$, $\mathbf{y}_n$. A quality q_{mn} of the correspondence pair is defined as

$$q_{mn}^{(s-1)} = \sum_k \sum_l P_{kl}^{(s-1)}. \quad (9)$$

where s denotes an iteration step, k refers to all points $\mathbf{x}_k$ that are neighbors of $\mathbf{x}_m$, and l refers to all points $\mathbf{y}_l \in A_n$ that form pairs $\mathbf{x}_k\mathbf{y}_l$ consistent with the pair $\mathbf{x}_m\mathbf{y}_n$.

The probabilities of correspondence are updated for each point pair $\mathbf{x}_m$, $\mathbf{y}_n$:

$$\hat{P}_{mn}^{(s)} = P_{mn}^{(s-1)}(k_a + k_b q_{mn}^{(s-1)}). \quad (10)$$

where k_a and k_b are preset constants. They deal with the convergent speed of P_{mn}. Normalize

$$P_{mn}^{(s)} = \frac{\hat{P}_{mn}^{(s)}}{\sum_j \hat{P}_{mj}^{(s)}}. \quad (11)$$

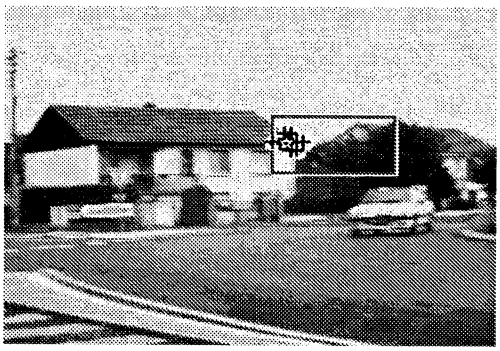
Those interest points that hold high probabilities that obviously differ from those interest points without correspondences finally. Repeat (9) (10) and (11) until all $P_{mn}^{(s)} > P_{thr}$ (threshold) are found for all points $\mathbf{x}_m$, $\mathbf{y}_n$. Fig.4 shows the results after detection of correspondences.

4.2. Directive chain

We select two *tracking windows* with different scales, A'_m and A'_n (Section 4.) for the *kernel*'s geometric characteristics. The *tracking windows* are made around every selected *kernel* which original position is the center of mass in A'_m. If some of corresponding elements of A'_m in A'_n are decided, the corresponding position of the *kernel* in $I_j(\mathbf{x})$ can be estimated. If some of new *kernels* are found in A'_n, we can also estimate the target in this new frame by prior knowledge. The relations between A'_m and A'_n are extrapolated by directive *chain codes* with their neighborhoods. More details can be found in the research [5].



(a)



(b)

Fig. 5: Nine interest points in (a) coincide with nine interest points in (b). The *star* in (b) indicates the new kernel position.

4.3. Reliability

Theoretically, if we know a corresponding pair ($\overrightarrow{V}_{ss}^{(m)}$, $\overrightarrow{V}_{ss}^{(n)}$) in $\widetilde{A}_r^m$ and $\widetilde{A}_r^n$, we can decide the corresponding *kernel* in $\widetilde{A}_n^n$, ss=$1, 2, \ldots, n''$. Good results should be that the elements in $\widetilde{A}_r^m$ and $\widetilde{A}_r^n$ have one and only one corresponding relations. To improve the reliability,

we assume that the number of detected corresponding elements is n', and there are n'' possible unexpected pairs. We define the following criterions:

$$\frac{n'-n''}{n'} > P^{(1)}_{nthr};\ n' > P^{(2)}_{nthr}. \quad (12)$$

and

$$\mathbf{Re}(\overrightarrow{V}^{(m)}_{ss} - \overrightarrow{V}^{(n)}_{ss}) < \varepsilon_1;\ \mathbf{Im}(\overrightarrow{V}^{(m)}_{ss} - \overrightarrow{V}^{(n)}_{ss}) < \varepsilon_2. \quad (13)$$

where ε_1, ε_2, $P^{(1)}_{nthr}$ and $P^{(2)}_{nthr}$ are preset threshold constants. (12)(13) give valid constraints to enforce suppressing redundant additivity and noise resulting from random factors to ensure the reliability. These constraints are very valid. This can be seen by comparison of Fig.4 and Fig.5.

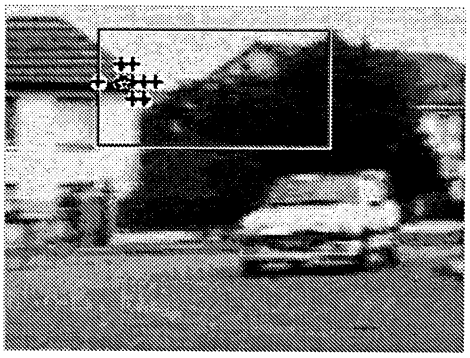


Fig. 6: More larger Fig.5b.

5. Experiments

In this section, we discuss the experimental results based on the presented method. We use the 3rd and the 8th frames in Fig.1 (up) to execute our experiments. We apply the presented algorithm to illustrate the case of one of the kernels because the others are with the same principle. The active contour model and line contour model have been shown in Fig.2a and Fig.2b. There are eight kernel elements in $\breve{A}_m$. A'_m and A'_n, 17 interest points detected in A'_m and 37 elements in A'_n are shown in Fig.3a and Fig.3b. Fig.4a and Fig.4b show us those corresponding results of Section 5.1. There 13 elements in $\widetilde{A}^m_r$ and 10 in $\widetilde{A}^m_r$. Further, the perfect relations are established by using the constraints of (12)(13). In Fig.5, nine interest points in (a) coincide with nine interest points in (b); The new corresponding kernel is also drawn in (b) with the symbol star. Fig.6 gives the amplified Fig.5b.

In this experiment, the parameters are N=8, α=0.6, β=0.01, γ=25, $\mathbf{E}_{im}(\mathbf{v})$=-$|(\nabla I(\mathbf{x}))|^2$, $\mathbf{E}_{cst}(\mathbf{v})$=0. We select pixel distance in a time interval D_{max}=37.5 pixels, D_{dif}=1 pixel, s=10, P_{thr}=0.70. The correspondence points are decided with errors less than 5 pixels because our calculating image unit is 5 pixels. Fig.6 gives the more clear new kernel's position. Then the new kernel in Fig.5b becomes the input for the next frame. Similarly, we can get the other new kernels related to the others in $\breve{A}_m$.

6. Conclusions

We proposed three processes of the method to track a static target from a moving platform: active contour model, which uses estimation of kernel points at the contour position; an interest point detection, which uses kernel's area, along with measures of auto-correlation transform, as the system input measurement; and a probabilistic relaxation method, which uses correspondence pairs detection, as the former system output and the next system input. Because even a subset of feature points can present a target correctly and a line is constituted by points, we are sure that feature points have more power to present the target than other methods, for example the detection of line, contour et al., if we give the system some of prior knowledge.

This approach also takes us another advantage to occlusion problems, because a target can be estimated by parts of its features. A simple example is, if we define a target rectangle as RT={ shape: rectangle; points: aa, bb, cc, dd}, to a unidentified target with UT={shape: rectangle; points: aa, bb, dd}, it is still possible for a machine to know UT is RT in spite of $UT \subset RT$.

In future work, we hope to rationalize the selection of visual cues used for target tracking based on prior image knowledge. Another interesting question is to efficiently apply the described method to machine with artificial brain and intelligent agent.

Acknowledgement

This research is also done at the Department of Electronics, Oita Institute of Technology.

References

[1] A. Kumar, A. Tannenbaum, and G. Balas, "Optical flow: a curve evolution approach," *IEEE Trans. Image Processing*, vol. 5, no. 5, pp. 598-610, 1996.

[2] R. Green, D. Gray, and J. Powers, *Artificial Vision*, Academic Press, London, 1997.

[3] X. Wang, M. Sugisaka M and W Xu, "Active contour model-based tracking analysis," *Proc. of the sixteenth Int. Conf. on Systems Engineering*, Vol. 2, pp. 730-735, 2003.

[4] G. Carneiro, and A. Jepson, "Phase-based local features," *Computer Vision - ECCV 2002, Part I*, pp. 283-296, 2002.

[5] X. Wang, M. Sugisaka M and W Xu, "Recognizing static target in video frames taken from moving platform," *Proc. of 2003 Int. Conf. on Control, Automation, and Systems Engineers*, 2003.

[6] D. A. Forsyth, J. Ponce, *Computer Vision*, Prentice Hill, USA, 2003.

[7] W. Kropatsch, R. Klette, F. Solina, and R. Albrecht, *Theroetical foundations of computer vision*, Springer Wien, New York, 1996.

Proc. of The Ninth Int. Symp. on Artificial Life and Robotics (AROB 9th '04)
Beppu, Oita, Japan, 28-30 January, 2004

Non-intrusive Eye Gaze Estimation under Large Head Movement using Property of Projective Transform

Dong Hyun Yoo
Dept. of EECS
Korea Advanced Institute
of Science and Technology
373-1, Guseong-dong, Yuseong-gu,
Daejeon, Korea

Myung Jin Chung
Dept. of EECS
Korea Advanced Institute
of Science and Technology
373-1, Guseong-dong, Yuseong-gu,
Daejeon, Korea

Abstract

In this paper, an eye gaze estimation system is proposed. The proposed system consisted of five IR LEDs and a CCD camera. The direction of the user's eye gaze can be computed without the geometrical relation among the eye, the camera, and the monitor in 3D space. Our method is comparatively simple and fast.

1 Introduction

Eye gaze estimation system estimates the direction of the eye gaze. In other words, these systems find where a person looks. The gaze is an important cue to understand a person's intention. The eye gaze can be used as an interface between human and a device such as a computer, a robot, and so on. The interface using the eye gaze is an active interface different from the passive interface like a mouse or a keyboard.

Sugioka [2] formulated equations that computed the eye-gaze direction from the positions of the pupil and a bright spot made by the reflection of infra-red light and obtained coefficients of the equation by calibration. He used the distance measured by an ultrasonic sensor to allow head movement. However, the accuracy of the system is not good because the distance measured by an ultrasonic sensor is inaccurate.

T. Ohno, et. al. [5] proposed a head-free eye gaze tracking system. They developed the eye gaze tracking system using three cameras and one IR LED. They said the 3D position of the center of the cornea curvature can be computed using one camera and Purkinje image. However, the distance between the eye and the camera is required to get the position. So, they utilize a stereo camera system to detect user's head and to measure the distance. However, the system is heavy and expensive. They didn't describe any result when the head's position varies.

In the previous methods, the methods require the position of the eye or the head in 3D space. They need other information like the distance between the camera and the user's eye. To measure the distance, stereo camera or ultrasonic sensor is utilized. These devices make the eye gaze systems complex, so that the complicated system needs complex calibration processes. The user cannot use these systems easily.

The method proposed in this paper is also a non-intrusive method based on the reflection of light. However, our system consists of five IR LEDs and two CCD cameras. To estimate where the user looks, we use the projective relation between the four glints made by the reflection and the center of the pupil in images and the monitor and the gaze point. We utilize a property of projective space. This method using the projective property is simple, fast, and accurate under large head motion.

Our new eye gaze estimation system is introduced in Section 2, and the eye gaze estimation method using the proposed system is described in Section 3. Experiment results are shown in Section 4. Finally, conclusions are given Section 5.

2 System Description

For unrestricted head movement, our method needs five IR LEDs and two CCD cameras as depicted in Fig.1. Four IR LEDs are attached to the corners of the monitor to cause the reflections on the surface of the cornea, and the other one is located at the center of the camera's lens to make the bright-eye effect(see Fig.2). The four IR LEDs on the monitor are turned on and off together, and the one of the camera is activated independently. The switching of the LEDs is

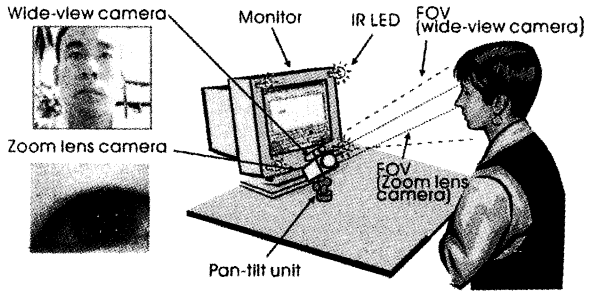
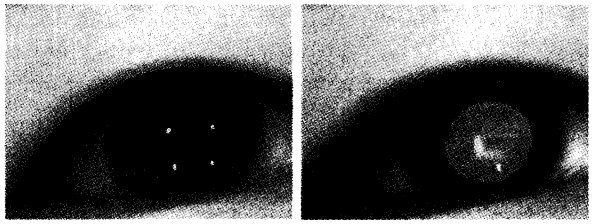


Figure 1: System configuration; a monitor with four IR LEDs attached to the corners and a CCD camera with an IR LED)



(a) (b)

Figure 2: Input images captured from a camera((a)dark eye image(corneal reflection) (b)bright eye image)

synchronized with the image capture to get two images like Fig.2. The LEDs of the monitor make the reflections on the cornea, and four glints are shown in the captured image. These glints are used to estimate the eye-gaze direction by linear mapping from image space to monitor screen. The LED of the camera makes the diffusion of light on the retina to generate the bright-eye effect, and one glint on the cornea. This glint is on the closest surface of the cornea to the camera. Actually, the five IR LEDs and one camera are needed to estimate the eye gaze. Therefore, this system is simple, fast, and inexpensive. This is a merit of this method.

3 Estimation of an gaze point

To understand our estimation method, the detail investigation about the geometric relation is needed. To help understanding, let's simplify the problem to 2-dimensional case(see Fig.3). Assume that there are a monitor with three IR LEDs, a camera, and an eye that is in front of the monitor. The user looks at one gaze point(x_g) of the screen. In this figure, the points

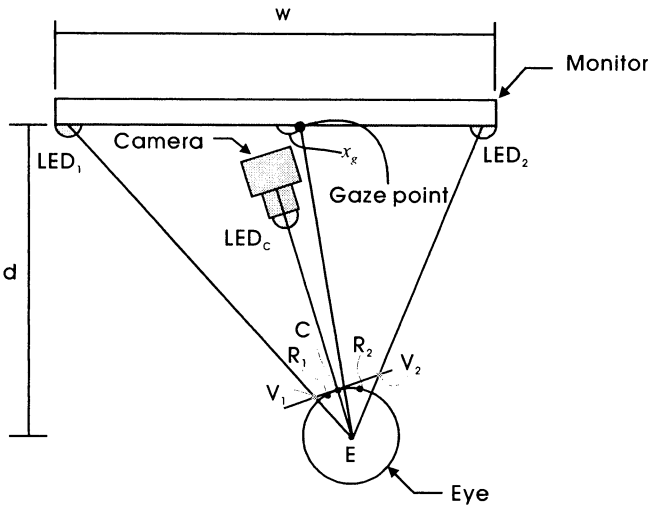


Figure 3: Geometrical relation of the reflection.

R_1, R_2, and C are the glints made by LED_1, LED_2, and LED_C respectively on the surface of the cornea. If the positions of the reflections in images are u_{R_1}, u_{R_2}, and u_C respectively, then they are generated by the reflection of light. Therefore, these features are not suitable to use the property of the projective space.

To resolve the problem, the virtual projection points made by the projection are computed. A virtual line is tangent to the cornea at the point C. The points V_1 and V_2 on the tangent line are the cross points of the tangent line and the line from the LEDs to the center of the eye. The point C is on the line connecting the optical center of the camera and the center of the eye because the LED of the camera is located on the center of the lens. The three points are the cross points of the tangent line and the lines crossing the same vanishing point. Therefore, the relation is considered to two projections: from the monitor to the line tangent to the eye, from the tangent line to the image plane of the camera. Therefore, the gaze point can be estimated by the invariant value of the projective space. This concept can be applied to 3-dimensional case.

3.1 Computation of the virtual projection point

The virtual projection points should be computed in order to utilize the property of the projective space. It is not easy to compute the virtual points from the real reflected points because the relation is too complicated. The closed-form solution cannot be formulated. Fortunately, the range of the head movement can be

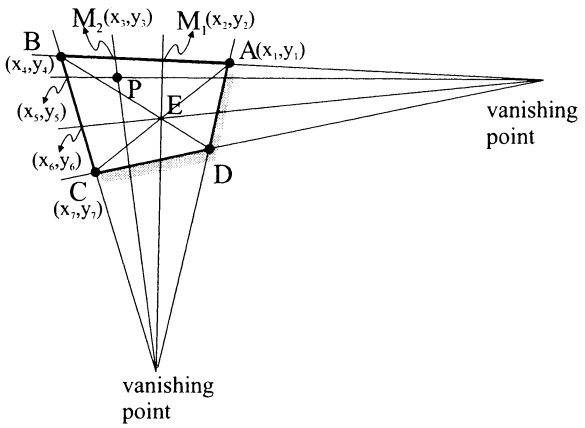


Figure 4: How to compute a cross ratio in an image. A, B, C, and D are the virtual projection points on the cornea. P is the center of the pupil in the image. E is an intersection of diagonal lines of the polygon ABCD.

confined to a specific region in the situation that a user in front of a monitor looks at the monitor. By confinement of the head movement, the virtual projection points can be computed approximately by the following equation:

$$u_{V1} = u_{R_1} + \alpha(u_{R_1} - u_E), \tag{1}$$

where α is a constant close to 2. The value is decided through a simple calibration process.

3.2 *Estimation of an eye gaze point by cross ratio*

The gaze point is estimated using the cross ratio that is invariant to the projective transform. Fig.4 shows how to compute the cross ratio in the image. The points A,B,C,and D are the virtual projection points computed by the method described in the previous section. P is the center of the pupil, and E is the cross point of the line $\overline{AC}$ and the line $\overline{BD}$. $(x_i, y_i)(i = 1, 2, \cdots, 7)$ are coordinates of each point in the image.

The x-coordinate of the eye gaze point is computed by the following method. At first, a vanishing point should be computed by line $\overline{AD}$ and line $\overline{BC}$ allowing the two points M_1 , M_2 to be calculated. M_1 is a crossing point of line $\overline{AB}$ and a line that connects two points E and the vanishing point. E is an intersection of the diagonal lines of the polygon $ABCD$. M_2 is the point at which the line $\overline{AB}$ and the line that connects P and the vanishing point cross. Two points M_1 and M_2 are needed to compute the cross ratio. The cross ratio of the four points on the line $\overline{AB}$ is the following equation:

$$CR_x = \frac{(x_1y_2 - x_2y_1)(x_3y_4 - x_4y_3)}{(x_1y_3 - x_3y_1)(x_2y_4 - x_4y_2)}. \tag{2}$$

In a similar way, the cross ratio of the monitor screen is computed through an equation like the following:

$$CR_x = \frac{(w - \frac{w}{2})\hat{x_g}}{(w - \hat{x_g})\frac{w}{2}} = \frac{\hat{x_g}}{w - \hat{x_g}}. \tag{3}$$

where w is the width of the monitor screen and $\hat{x_g}$ is the x-coordinate of the estimated eye gaze point $P'(\hat{x_g}, \hat{y_g})$.

These cross ratios are equal because the cross ratio is invariant in projective space. Then, we can get the x-coordinate of the estimated eye gaze point.

$$\hat{x_g} = \frac{w \cdot CR_x}{1 + CR_x}. \tag{4}$$

The y-coordinate of the eye gaze point is computed by the same way. Then,

$$\hat{y_g} = \frac{h \cdot CR_y}{1 + CR_y}. \tag{5}$$

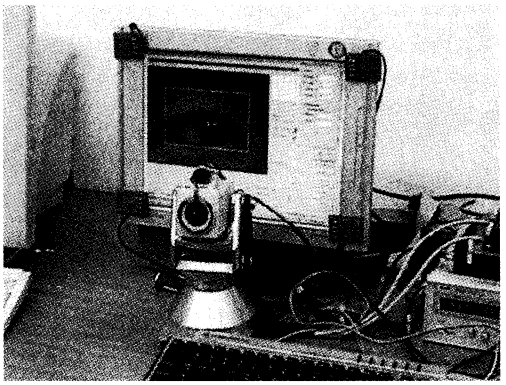


Figure 5: Experimental setup: A monitor with four IR LEDs and two cameras mounted on a pan-tilt unit. A small wide-view camera is attached to the top of the high-zoom camera.

4 Experimental Results

Some experiments were carried out to show the feasibility of the proposed method. Fig. 5 is the experi-

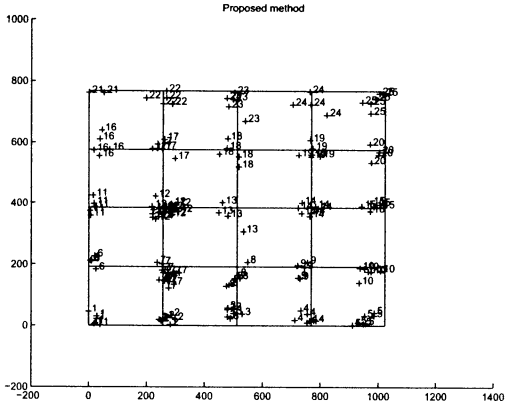


Figure 6: Experimental result. The resolution of the screen was 1024×768 and the screen was divided into 5×5 blocks.

Table 1: The average, standard deviation, and maximum of the estimation error using the proposed method

Error (mm)	Average	Standard deviation	Maximum
X	8.6	6.5	33.7
Y	7.2	5.9	29.3

mental setup. The camera was a near infra-red CCD camera and the image size was 640×480 pixels. The computer used was a Pentium IV-1.4GHz system and the monitor had a 17-inch screen. The resolution of the screen is 1024×768 pixels. There are 5×5 points in the screen of the monitor. The user sat 30cm~40cm in front of the screen and looked at one of the target points. This system estimated which point the user looked at. About 200 trials were carried out in large head motion and the results are shown in Fig.6. In this figure, x- and y-axes are coordinates of the screen, and dots were the estimated eye gaze points. In Table 1, average, standard deviation, and maximum of the estimation error are listed. The cross means the estimated result, and the number means the target number. The accuracy of the proposed method in degree are 0.98° and 0.82° in x and y coordinates respectively.

5 Conclusions

In this paper, a novel method to estimate the eye gaze point of the human eye was suggested. Four IR LEDs were attached to a computer monitor, and light from these LEDs was reflected on the surface of the cornea. This reflection generated bright spots in images captured by a camera. We assumed the screen was projected to a polygon whose vertices were the glints. To estimate the eye gaze point, the pupil's center position and the bright spots of the corneal reflection were detected in images and the cross ratio was used. To use the cross ratio, the virtual projection points are is suggested. The advantage of the proposed method is that it doesn't need any geometrical knowledge about the LEDs, the monitor, the camera, and the eye. Also, it doesn't require any complicate calibration process. This method works well under large head movement in real-time, and consists of simple devices.

References

[1] D. Cleveland, "Method and Apparatus for Locating Image Features", *U.S.Patent 5,231,674*, July, 1993.

[2] A. Sugioka, Y. Ebisawa, and M. Ohtani, "Noncontant Video-based Eye-gaze Detection Method Allowing Large Head Displacements", *IEEE Int. Conf. on Medicine and Biology Society*, pp.526-528, 1996.

[3] Y. Ebisawa, "Improved Video-Based Eye-Gaze Detection Method", *IEEE Trans. on Instrument and Measurement*, Vol. 47, No. 4, pp.948-955, 1998.

[4] R. Newman, Y. Matsumoto, S. Rougeaux, and A. Zelinsky, "Real-time Stereo Tracking for Head Pose and Gaze Estimation", *Fourth IEEE International Conference on Automatic Face and Gesture Recognition*, 122 -128, 2000.

[5] T. Ohno, N. Mukawa, and A. Yoshikawa, "FreeGaze: A Gaze Tracking System for Everyday Gaze Interaction", *Proceeding of Eye Tracking Research & Applications Symposium*, pp.125-132, 2002.

[6] D. H. Yoo, J. H. Kim, D. H. Kim, and M. J. Chung, "A Human-Robot Interface using Vision-based Eye Gaze Tracking System", *IEEE/RSJ International Conference on Intelligent Robots and System*, pp.1196-1201, 2002.

Proc. of The Ninth Int. Symp. on Artificial Life and Robotics (AROB 9th '04)
Beppu, Oita, Japan, 28-30 January, 2004

Developing a Benchmarking Framework for Map Building Paradigms

J.J. Collins, Malacy Eaton, Mark Mansfield, and David Haskett.
Dept. of Computer Science and Information Systems
University of Limerick, Limerick
Limerick, Ireland.
Email:[j.j.collins/mark.mansfield/david.haskett/malachy.eaton]@ul.ie

Shane O'Sullivan
IBM Software Group
Santry,
Dublin 9, Ireland.
Email:osushane@ie.ibm.com

Abstract

This paper presents a benchmarking suite to empirically evaluate map-building algorithms in the field of intelligent autonomous mobile robots. We suggest that one of the more crucial tasks currently facing researchers is the provision of a common task, or set of tasks, as a means of evaluating different approaches to robot design and architecture, and the generation of a common set of experimental frameworks to facilitate these different approaches. Map building is seen as a key component in the evolution of robot control software architecture, and forms the basis upon which higher order behaviours such as pursuit and evasion can be designed. This paper outlines a set of benchmarks for map-building and briefly evaluates their usefulness across a sample set of paradigms.

1. Introduction

In the field of mobile robots, a variety of simultaneous localisation and map-building (SLAM) approaches can be adopted for model construction. The maps themselves generally fall into two categories [1]:

- Metric maps, in which the environment is decomposed into a 2D or 3D lattice of grids or cells, with each cell representing the probability of occupancy, as depicted in figure 2 for an environment shown in figure 1.
- Topological maps are graph-oriented models with nodes representing structural features of the environment, and vertices capturing adjacency and ordering information, as depicted in figure 3. Topological maps are computable from a metric map.

A considerable range of map building paradigms have been documented in the literature, ranging from probabilistic and Bayesian frameworks, to artificial neural networks, to the Cartesian symbolic-oriented approach. While empirical results of individual paradigms have been presented consistently, very little work has been done on developing a benchmarking framework to cross compare and contrast sets of map-building algorithms.

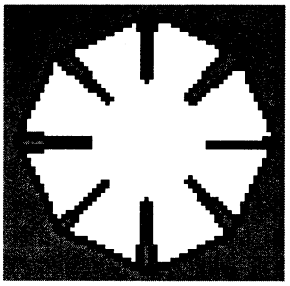
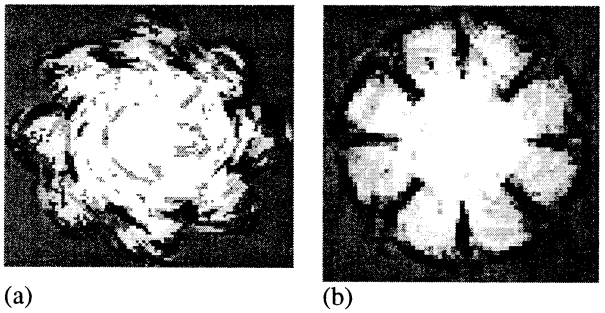


Figure 1. The ideal map of a star environment.



(a) (b)

Figure 2. Occupancy grid maps generated for figure 1.

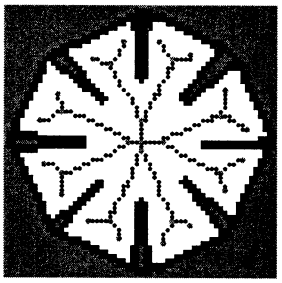


Fig 3. Star ideal map with inscribed Voronoi graph of all possible paths in the environment.

Map-building in static environments is difficult due to the following:

1. Specular reflections from sonar range sensors introduce and propagate noise into the model.

2. Map-building relies on localisation. Dependence on odometry is insufficient in itself to guarantee self-localisation.
3. The selection of the sonar model itself impacts significantly upon the paradigm used to compute occupancy values.
4. Independence assumptions introduced into some of the paradigms for reasons of computational tractability are only approximations of the true theoretical model.

These difficulties are depicted in figure 2, illustrating the difference in quality of the maps generated by alternative paradigms when a robot is deployed in an environment that corresponds to that shown in figure 1.

The evaluation of ideal versus generated maps based on correlation techniques from the image processing domain focus primarily on a cell-by-cell comparison. These metrics fail to take into account that [2]:

1. Maps are artefacts primarily used for navigation
2. Discrepancies between occupancy values in ideal and generated maps will have varying degrees of significance.

This paper presents a benchmarking framework for map-building based on:

1. Baron's cross correlation coefficient [3].
2. Martin and Moravec's map score [4].
3. An extension of Thrun's [5] loss metric based on the computation of Voroni diagrams from the ideal map, estimation of the universe of unique paths, and determining their feasibility in the generated maps.

2. In Benchmarking

One of the more important tasks currently facing researchers in the fields of artificial life and embodied intelligence is the provision of common benchmarks for performance evaluation. Current benchmarks, while useful, have their problems. We advocate the generation, from the bottom up of a common set of experimental frameworks, for performance evaluation and benchmarking of bio-inspired robots.

A current *de facto* standard in this field is RoboCup annual challenge. RoboCup operates in four categories: simulated teams, a small size league, a middle size league, and legged robots. An example small size robot is Khephera, a typical middle sized robot is Pioneer (1/2) and The Sony artificial dog fits in the third category. There is also a humanoid league. RoboCup tests skills at the individual, the inter-individual, the collective and at the competition level. [6]

Individual skills to be mastered include navigation and localisation on the field of play, including the selection of optimal paths. Inter-individual skills include the coordination of movements with playing partners in order to pass accurately. At the top level the tasks of strategy generation and recognition of opponents' strategies are crucial.

Criticisms of RoboCup stem from the controlled environment in which the robots operate, and the fact that soccer playing skills are quite specific and may lead to the development of highly focused robots of little use for any other task. Also, the self-localisation problem is somewhat constrained by the used of landmarks that completely reduce dependence on dense sensor matching-oriented paradigms. Also, considering the complexity of the task facing the robot teams, how does one assign credit to individual components within the software architecture, given that there is only one reinforcement signal per episode – win or loss.

So while RoboCup may currently be a useful testing bed for approaches to Artificial Intelligence and Artificial Life, problems exist. One potential approach, which we espouse, involves the provision of a set of specifically designed experimental frameworks, and involving tasks of increasing complexity, rigorously defined to facilitate experimental reproducibility and verification.

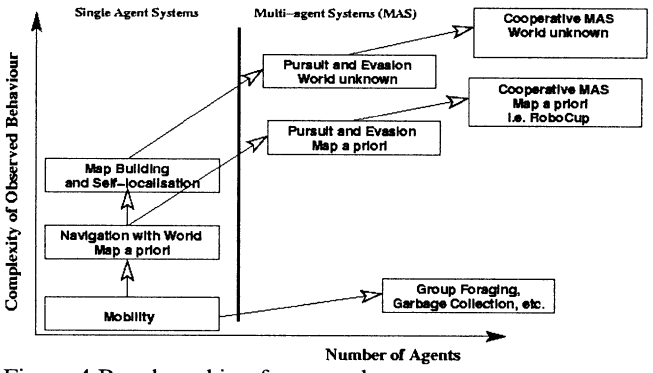


Figure 4 Benchmarking framework.

The authors advocate, and shown in figure 4, that issues of map-building and self-localisation are fundamental to the progressing robotic-based research [7]. It is also argued that that pursuit and evasion should be undertaken prior to RoboCup type applications, primarily because the modelling of behaviour and interaction can be constrained to just two players. Secondly, pursuit and evasion have strong biological and game theoretic foundations, and thus provide a framework in which scientific modelling of the system can be performed, and later validated through experimentation [8]. Figure 4 strongly hints that current

robot competitions should be focused on map building and, pursuit and evasion with a map a priori.

3. Metrics for Map Building Paradigms

3.1 Cross Correlation Between Maps

One possible fitness measure of the map generated by the system is calculated using Baron's *cross correlation coefficient* [1]:

$$C_N(y) = \frac{\langle I_T T \rangle - \langle I_T \rangle \langle T \rangle}{\sigma(I_T)\sigma(T)}$$

This is based on *template matching*, where $C_N(y)$ is the cross correlation coefficient, I_T is the map to be matched, T is the original map being matched against, and <> is the average operator. There are two fundamental problems with this approach:

1. Maps must be anchored precisely along the same coordinate system.
2. This metric makes no allowance for freespace readings in the ideal map that are occupied in the generated, and vice-versa.

3.2 Map Score

Martin and Moravec [39] developed a map comparison measure called *Map Score* in order to facilitate the automatic learning of sensor models. Unlike correlation, map scoring compares two maps on a cell-by-cell basis. Given two maps, M and N, the score between them is calculated as the sum of the squared differences between corresponding cells:

$$Match = \sum_{m_{X,Y} \in M, n_{X,Y} \in Y} \left(m_{X,Y} - n_{X,Y}\right)^2$$

where $m_{X,Y}$ is the value of the cell at position (x,y) in map M and likewise for $n_{X,Y}$. This formula is equivalent to the well-known sum of squared error metric used widely in machine learning paradigms. This formula works well with the application for which it was designed, learning a sonar model, since the only requirement is to minimise the score/fitness on a single map.

In order effectively use the map score metric as a benchmark, it is necessary to normalise it. The ideal map only has three possible values, 0, 0.5, and 1, or empty, unknown and occupied respectively. A naïve method of finding the worst map would be to set each empty cell to 1, each occupied cell to 0, and each unknown cell to either 0 or 1. One could then compute the map score between the ideal and worst possible map, and use this as a normalising factor. However, this still does not take cognizance of the fact that there are places in the map that the robot cannot go, for example there may be a large expanse of unknown area with no access to it. It therefore is logical to create the worst possible map of an environment based on where the robot *can* go. This is done by setting the empty cells to 1, as above, but only change the value of an unknown or occupied cell if it is proximal to an empty cell and is detectable from that empty cell.

Another weakness of the *Map Scoring* technique is that mapping algorithms that overestimate the empty regions of space. To redress the balance, a second *score* test is used that only compares the occupied cells in both maps. For any two maps M and N, if either the value $m_{X,Y} > 0.5$ or $n_{X,Y} > 0.5$, then the squared difference between those two cells is added to the final score. Otherwise they are ignored.

3.3 Path Analysis

Most quantitive analysis presented on the grid maps focus on techniques similar to those discussed in the earlier part of this chapter – namely comparing the values in the cells to each other. When training a sonar model in a small area this is quite a good approach to take, but to properly evaluate the worth of a map, one must get away from the idea of a map being an isolated The purpose of a map is, after all, to enable a robot to get from point A to point B as quickly and as safely as possible. However, many researchers ignore the fact that a map need not *perfectly match* the ideal map of an environment to be *perfectly usable* in that environment. It is not necessary for a map to be an exact replica of the surrounding environment, it is just necessary for it to be an abstraction of that environment which, when combined with an appropriate path planning algorithm, generates a true real world path for the robot to follow. It is the quality of these paths that truly give the value of the map, a value based on the use to which the map will be put rather than a metric based on techniques that can be seen as an extension of human vision such as map matching and image correlation. To get the true worth of a map, two elements of the map must be tested:

1. The degree to which the robot should be able to plan a path from one position to another using the generated map, but cannot – false negatives.
2. The degree to which paths calculated in the generated map would cause the robot to collide with an obstacle, and are therefore invalid – false positives.

Both of these are tested using only the map to guide the robot's movement.

There are four steps required to calculate the two above items of information from a generated map.

- **Step 1**: Calculate all possible paths, in the ideal map P^I, by generating a Voronoi graph. Record the end-

points of each path, E^I. For each pair of endpoints in E^I that have a path between them in the ideal map, attempt to create a path in the generated map between those two endpoints using a path-planning algorithm.

- **Step 2**: Count the number of paths between endpoints in E^I that could not be completed in the generated map due to obstacles existing in that map where they do not exist in the ideal map – false negatives. The percentage of false negatives is then:

$$\frac{\sum \text{incomplete paths in generated map}}{\sum \text{ edges in the Ideal map}}$$

- **Step 3**: Calculate all possible paths in the generated map, once again using a Voronoi diagram. Superimpose each Voronoi edge from the generated map onto the ideal map, and count the percentage of edges that pass through occupied spaces, and would therefore cause the robot to crash – false positives.

4. Results

The following three occupancy-grid map-building paradigms and extensions were evaluated using the benchmarking suite:

- Moravec and Elfes probability-based framework with a Gaussian sonar model [9].
- Mathias and Elves Bayesian-update framework with a Gaussian sonar model [10].
- Konolige's Bayesian update framework with Normal-distribution sonar model, pose buckets and dynamic mixture models [11].

The extension also evaluated is O'Sullivan's linear feature predictor [2] used to identify specular reflections. The results demonstrate that path analysis approach is a more intuitive and reliable metric that captures the accuracy and reliability of the maps generated. Path analysis clearly demonstrated that a framework that incorporates a Normal distribution sonar model, pose buckets, and linear feature prediction clearly outperforms all other combinations.

5. Discussion and Conclusion

The benchmarking suite is now being extended with metrics that capture the difficulty posed by an environment for map-building paradigms. These metrics are based on cycles in the environment, total path distance, number and acuteness of corners responsible for specular reflections, etc.

.

In addition to this, our current focus is on extending the benchmarking suite to robot pursuit and evasion. Typical metrics captured are tag rates, and some recent work has focused on the informational aspect to PE based on a measure of entropy. These metrics are behavioural in that results are based on observation of external behaviour. It is difficult in PE contests there to relate behaviour to the underlying mechanics responsible for the agent's actions. This is further exacerbated by virtue of the fact that an agent is deployed in a world characterised by uncertainty. Current work is focused on introspective metrics for PE that facilitates the assignment of credit to paradigms responsible for the generation of behaviour.

[1] Thrun, S. (2002). Robotic Mapping: A Survey. CMU Technical Report CMU-CS-02-111, Carnegie Mellon University, Pittsburgh, Pennsylvania.

[2] O'Sullivan, S. 2003. An Empirical Evaluation Of Map Building Methodologies in Mobile Robotics Using The Feature Prediction Sonar Noise Filter And Metric Grid Map Benchmarking Suite. MSc Thesis, University of Limerick, Ireland.

[3] Baron, R. J. (1981). Mechanisms of human facial recognition." International Journal of Man Machine Studies 15: 137-178.

[4] Martin, M. C., Moravec, H.P. (1996). Robot Evidence Grids. CMU Technical Report CMU-RI-TR-96-06, Robotics Institute, Carnegie Mellon University, Pittsburgh, Pennsylvania.

[5] Thrun, S. (1998). Learning Metric-Topological Maps for Indoor Mobile Robots. Artificial Intelligence 99(1):21-71, February 1998.

[6] Kitano H, Asada M, Kuniyoshi Y., et al (1995) RoboCup: The Robot World Cup Initiative, IJCAI-95 Workshop on Entertainment and AI/Alife, 1995.

[7] Eaton, M. Collins, J., and Sheehan, L (2000). Towards a benchmarking framework for research into bio-inspired hardware-software artefacts. In Proc. of the 5th Int. Symp. On Artificial Life and Robotics, Oita, Japan.

[8] Mansfield, M, Collins, J.J., Eaton, M., Haskett, D. (2004). Developing a Statistical Baseline for Robot Pursuit and Evasion using a Real-World Control Architecture. To appear in Procs. Of the 9th Int. Sym. On Artificial Life and Robotics, Oita, Japan.

[9] Moravec, H. P., Elfes, A. (1985). High Resolution Maps from Wide Angle Sonar. In Procs. of the 1985 IEEE Int. Conf. on Robotics and Automation.

[10] Matthies, L., Elfes, A. (1988). Integration of Sonar and Stereo Range Data Using a Grid-Based Representation. In Procs. of the 1988 IEEE Int. Conf. on Robotics and Automation.

[11] Konolige, K. (1997). Improved Occupancy Grids for Map Building. Autonomous Robots 4:351-367.

Proc. of The Ninth Int. Symp. on Artificial Life and Robotics (AROB 9th '04)
Beppu, Oita, Japan, 28-30 January, 2004

Developing a Statistical Baseline for Robot Pursuit and Evasion using a Real World Control Architecture

Mark Mansfield, J.J. Collins, Shane O'Sullivan, Malachy Eaton, David Haskett and Thomas Collins
Dept.of Computer Science and Information Systems
University of Limerick,
Limerick. Ireland.
Email: mark.mansfield@ul.ie

Abstract

The canonical robotic pursuit and evasion (PE) contest is one where two agents, an evader and a pursuer, aim to maximise or minimise contact and distance of separation between each other. This paper highlights the need for a greater understanding of such contests and details a method of developing a statistical baseline against which the utility of various pursuer and evader agents can be measured. Also described is an extensible real world control architecture that allows pursuit and evasion capabilities to be integrated with other requirements for a robotic agent operating in the real world. Initial results and future research directions are also discussed.

1 Introduction

PE scenarios receive a lot of attention in robotics because they are highly dynamic contests in an ever-changing environment, that require a tightly coupled sensory-motor loop to facilitate the necessary real-time control. As PE experimentation is relatively new to the field of embodied autonomous robotics, many of the results reported so far have been independent of other results, as there is no common benchmarking system in place. This makes it difficult to assess the overall relevance of much work. For this reason there exists a requirement for some standard characterisation of agent behaviour within PE contests. Also, it is noticable that the majority of results are based on how agents behave. It may be significant to classify agents according to their informational content or internal workings. To this end some work has been carried out by Ficici and Pollack [1, 2] using information theoretic tools to characterise internal dynamics. Results reported in this paper are based on their experimental framework.

Another noticeable trait of some robotic PE research is that it is not grounded in robotics. Simulations take place in unbounded two-dimensional planes meaning that the problems inherent in embodied robotics such as sensor and odometry error are sometimes ignored. It is hoped that by including PE capabilities in an overall global robot control architecture, this work will have a greater and more relevant impact than research that is distinct from any robotic platform.

The next section outlines the motivations for studying PE with section 3 describing the real world control architecture that has been developed. Section 4 details the experimental framework and section 5 describes some preliminary results of these experiments before the penultimate section mentions possible future research directions before the concluding remarks.

2 Pursuit and Evasion Motivation

There are several reasons why there is currently much interest and research into PE scenarios not only within the field of robotics but in other scientific areas also. In a series of papers by Cliff and Miller [3, 4, 5] some of these reasons are outlined. They suggest that PE is the perfect domain in which to study co-evolution where two hostile populations compete in a co-evolutionary arms race to complexity because it is the simplest situation in which co-evolution seems to occur. In addition PE contests are a common setting for protean behaviour. Protean behaviour, also termed adaptive unpredictability, is often observed in predator-prey situations in the animal world where fleeing animals are frequently observed to zig-zag unpredictably when predators are within extremely close range. Proteanism serves to confuse competition as it is the opposite to predictability, and predictability is a weakness that can be exploited by opponents.

The modelling of PE also has implications for a range of sciences including Ethology. Studies of animal behaviour such as Holley's study of PE habits of brown hares and foxes [6] would be complemented by a PE simulation environment where various theories could be tested and perhaps outcomes explained. Endowing robots with the characteristics of specific prey and predators would allow many more situations to be observed and manipulated.

From a robotics point of view PE contests are an interesting case because they require a tight sensory-motor loop, as the introduction of another agent makes the environment highly dynamic meaning that a change of environmental state may require an immediate change of direction or action. While this falls under the umbrella of reactive control there is also a requirement for some deliberation as the robot moves. The robot may have some overall pursuit or evasion strategy that is too complex to compute in real-time. This need for both reactive and deliberative control makes PE an interesting case for the robotics community.

The experimental setup described in this paper is based on research undertaken by Ficici and Pollack [2]. In this work the authors realise the lack of a rigorous metric for PE agent behaviour and use methods from information theory to characterise this. They develop an artificial recurrent neural network to control an evolving evader. There are no inputs to the network with the evader effectively being blind. The only output indicates the angle that the robot is to turn to for the next move. The evader can be seen to be evolving as it learns over generations, based on fitness returns. Using tools from information theory, hand built pursuers develop a statistical model of an evader based on a period of observation of ten thousand time steps. The model is built using n^{th} order statistics. The order of a pursuer describes the number of movement observations made when computing the probability of sequences of moves occuring. A 0 order pursuer makes a single observation before recalculating probabilities while a 10^{th} order pursuer updates probabilities based on 11 observations.

Simulation takes place in a 2-D plane where both agents move at a rate of one bodylength, in a particular direction, per time-step. The pursuer perceives the evader to be moving in one of eight directions and develops a statistical model approximating the evader's movement patterns. The pursuer uses its model to predict the movement of the evader for a specified number of time-steps. If the pursuer can get to any point on the predicted path before the evader, then it will move directly to that point in order to intercept the evader. Otherwise the pursuer moves to the first point on the path.

Fitness for the evader is determined by the average distance it can maintain between itself and the pursuer over the course of the game while the pursuer aims to maximise the number of times it comes within one body length of the evader.

Results are based on observation of simulated PE contests and show that higher order pursuers are more successful, while evaders evolved against higher order pursuers develop more unpredictable movement patterns. Results based on the accuracy of pursuer modeling capabilities are reported in a later section of this paper.

3 A Real World Control Architecture

In order to deploy an embodied agent with the abilities to pursue and evade it has been necessary to develop a real world control architecture that takes into account both the needs of real-time control as well as time-consuming deliberation. The extensible architecture diagrammed in figure 1 shows the significant classes for an architecture that allows robots to build maps as well as pursue and evade. Client controllers take readings from the physical robot and pass these to the *serviceControl* module. The *serviceController* is where the inherent extensibility of the system is realised. It is endowed with different queues for distinct types of data. This is necessary because map building and PE contests require the manipulation of different types of data. Map building work by O' Sullivan [7] has required the use of sonar data while PE uses data concerning the position and orientation of robots. The *serviceControl* module queues data, which is popped from its queues by the robots client services that are the classes *Mapping* and *Referee* in this case. The clients can then manipulate the data as they see fit. The *mappingModules* build maps useful for navigation while the *Pursuer* and *Evader* modules decide on long-term policies for robot motion. Effectively the *serviceController* is a store for data with the client controllers and mapping and PE services being clients that register with it.

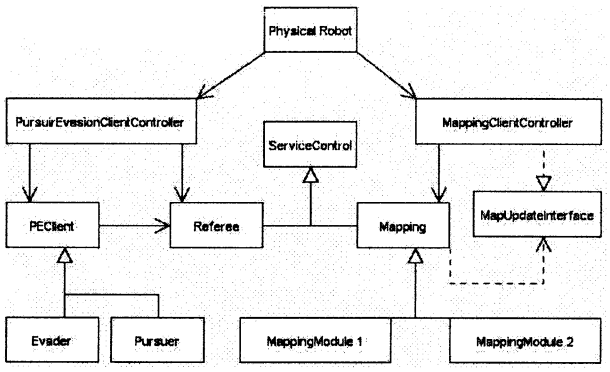


Figure 1: Extensible Control Architecture

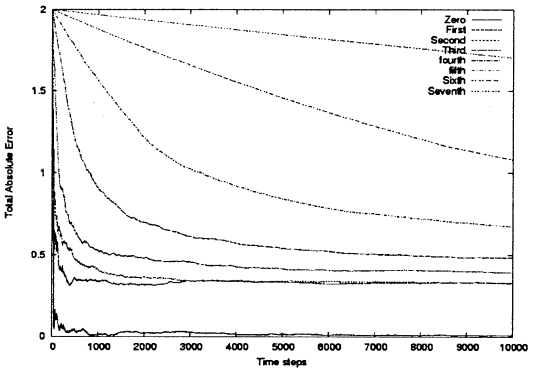


Figure 2: Total Absolute Error

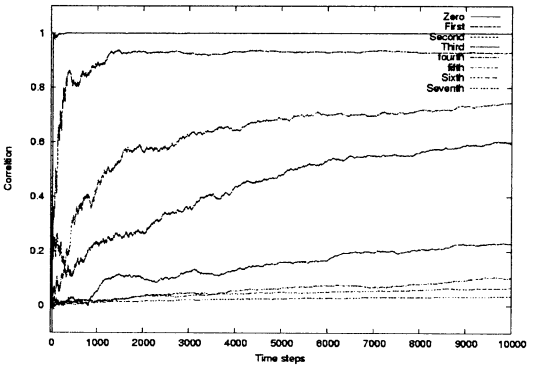


Figure 3: Baron's Correlation Coefficient

4 Experimentation

4.1 Setup

For the work described here, the evolving evader of Ficici and Pollack has been replaced by an evader that bases its moves on a predefined probability distribution, which is created using n^{th} order statistics. A 0-order evader effectively behaves in a random fashion with actions having an impact for only one time step into the future, whereas a 7^{th} order evader commits to movements for eight time steps into the future. The pursuers however, are replicas of those described above, computing their model of the evader using a sliding-window mechanism. From the pursuers point of view it is irrelevant that the neural network generator has been replaced by a probability distribution because the evader is only able to observe the movement of the evader and not its decision process.

4.2 Simulation Suite

As already stated these experiments are being deployed in a real world robotic environment. Testing is taking place using the Saphira/Aria software robot simulation suite. Testing in an environment such as this is considered necessary, as much previous simulation in this domain has taken place in unbounded two-dimensional planes where real world error is not considered. Also a software simulation suite is suited to the code-debug-test cycle and there is no chance of damage to physical robots. One Saphira time step is 100ms in duration. This has lead to some difficulty because a robot takes more that 100ms to turn and move in a real world environment as is necessary for these experiments.

5 Preliminary Results

Preliminary results regarding the accuracy of pursuer prediction capabilities have been recorded. Experiments by Ficici and Pollack have used agents up to an order of 12 that can move in any one of 8 directions. It has become apparent that an observational period of 10,000 time steps is not sufficient to give a clear indication of the probability model of the evader, as a 12^{th} order evader would have 8^{13} potential move sequences. For evaders of higher order it is suggested that an extended observational period is required. Evaders up to an order of 7 that can move in 4 directions have been modelled. Figure 2 shows the total absolute error for evaders of order 0 to 7. With a maximum of 2, it is clear that for a 0 order evader, the error rapidly drops but for evaders of higher order there is a slow gradual decrease in error. For a 7^{th} order evader the error drops approximately 12.5%.

Figure 3 shows the Baron cross correlation coeffi-

cient for the eight evaders calculated by:

$$C_N(y) = \frac{< I_T T > - < I_T >< T >}{\sigma(I_T)\sigma(T)} \quad (1)$$

where $C_N(y)$ is Baron's cross correlation coefficient, $I_T T$ is the evaders probability distribution, T is the pursuers estimation, σ is the standard deviation over the distributions and $<>$ is the average operator. This results in a value between -1 and 1, with values close to 1 meaning there is a high correlation between the two distributions. Figure 3 shows that zero order pursuers are able to make a good approximation of evader characteristics quite rapidly, while 10000 time-steps is not long enough for higher order pursuers to develop an accurate model of an evader. Both of these diagrams relate to experiments using agents of the same order.

6 Future Work

Once the information theoretic experiments described above have been completed, there appears to be two promising avenues for future work. The first is the study of co-evolution using PE as mentioned earlier. The second is the application of Reinforcement Learning (RL) to PE. Smart and Kaebling [8] suggest that RL may be well suited to robotics because a RL robot is given a task specification that it must learn to accomplish itself rather than instructions on how to complete the task. This makes sense because autonomous embodied robots are often deployed in unpredictable environments that can be difficult to model and specify in advance. Work by Asada et al [9] has shown that with a suitable descretisation of the state space, simple robotic tasks are achievable, while Ono et al [10] show that effective PE is a real possibility using RL. Future work involves replacing the neural network controlled evolving evader with a RL agent and observing how these compare when inserted into the co-evolutionary framework.

7 Conclusion

Currently there exist few metrics to characterise the behaviour of pursuit and evasion agents. This paper has described previous and current investigation into this area, reasons for simulating PE in robotics and a real world control architecture that has been developed for use in PE contests. Clearly there are useful insights to be gained into co-evolutionary dynamics among other things from the study and simulation of PE contests. The introduction of RL into this setting may provide agents that can learn the best ways to pursue and evade. This is the subject of future work.

References

[1] Ficici, S.G. and Pollack J.B.(1998) Coevolving Communicative Behavior in a Linear Pursuer-Evader Game. From Animals to Animats 5, pp 505-514. MIT Press.

[2] Ficici, S.G. and Pollack, J.B. (1999). Statistical Reasoning Strategies in the Pursuit and Evasion Domain. Proc. of the Fifth European Conference on Artificial Life, pp 70-88. Springer.

[3] Miller G.F. and Cliff D. (1994) Protean Behaviour in Dynamic Games: Arguments for the co-evolution of pursuit-evasion tactics. From Animals to Animats 3, pp 411-420. MIT Press.

[4] Miller G.F. and Cliff D.T. (1994) Co-Evolution of Pursuit and Evasion I: Biological and Game-Theoretic Foundations. Technical Report CSRP311. University if Sussex (1994).

[5] Cliff D. and Miller G.F. (1996) Co-Evolution of Pursuit and Evasion II: Simulation Methods and Results. In From Animals to Animats 4, pp 506-515. MIT Press.

[6] Holley A.J.F. (1993) Do Brown Hares Signal to Foxes? Ethology 94, pp 21-30.

[7] O'Sullivan (2003) An Empirical Evaluation of Map Building Methologies in Mobile Robotics using The Feature Prediction Sonar Noise Filter and Metric Grid Map Benchmarking Suite. (2003) Masters Thesis, University of Limerick.

[8] Smart, W.D. and Kaelbling L.P. (2002) Effective Reinforcement Learning for Mobile Robots. International Conference on Robotics and Automation.

[9] Asada, M., Noda, S. et al (1994) Coordination of Multiple Behaviors Acquired By A Vision-Based Reinforcement Learning. In Proceedings of the IEEE International Conference on Intelligent Robots and Systems, pp917-924.

[10] Ono, N., Fukomoto K. et al (1996) Collective Behavior by Modular Reinforcement Learning Animats. In From Animals to Animats 4, pp 618-624. MIT Press.

Proc. of The Ninth Int. Symp. on Artificial Life and Robotics (AROB 9th '04)
Beppu, Oita, Japan, 28-30 January, 2004

Controlled balanced growth of robot populations

D. J. G. James[1] and V. G. Rumchev[2]

[1] Control Theory and Applications Centre, Coventry University, Coventry, CV1 5FB, UK. E-mail: g.james@coventry.ac.uk
[2] Department of Mathematics and Statistics, Curtin University of Technology, GPO Box 1987, Perth, WA 6845, Perth, Australia. E-mail: rumchevv@maths.curtin.edu.au

Abstract

Adopting cohort-type population models to represent the dynamics of autonomous intelligent robot communities the problem of achieving a desired total size of the robot population under a balanced growth (contraction) and the problem of maintaining this desired size are studied. Properties of positive discrete-time systems are used to develop the results, which are illustrated using simple examples.

Key-words: Autonomous robots, positive systems, balanced growth.

1 Introduction

In the robotics research literature, over the recent decade, significant interest has been shown in societies of autonomous intelligent robots or colonies of robots [1]. These multi-robot systems are seen as essential for undertaking tasks such as space station exploitation, planetary exploration and undersea exploration /exploitation, in which they are required to complete tasks without human controls. Clearly such robots will be required to have a degree of autonomy, implying an ability to interact with their environment, make necessary decisions and take appropriate actions including improving individual and collective performances. Although the field of autonomous systems is still in its infancy there is the expectation of rapid progress over the next decade or so. In this paper the problem of robot population evolution is considered under the assumption that they are capable, both by reinforced learning and by interacting with the environment, of continual self-evolution. The robot population is categorised into generations or cohorts and its dynamics formulated as a cohort population model with migration, this being a specific discrete-time positive dynamic system with the duration of a single time period corresponding to the basic cohort span. In [2] on the basis of this model properties such as reachability and controllability, which are fundamental for the robot population dynamics, are considered. At the same time, balanced growth (contraction) of robot populations also seem to be quite important for the controlled evolution. The balanced growth (contraction) is defined as a growth (contraction) of the population, in which the (desired) relative sizes (the ratios of the number of robots within a generation to the total number of robots in the population) of different generations remain constant during their evolution. In this paper, the problem of balanced growth (contraction) is formulated and studied in full and some interesting results are obtained. Among them, the relationship between the growth factor and such essential characteristics as 'survival' and 'birth' rates seem to be quite important for the controlled evolution of the robot population. An interesting phenomenon is identified, namely not any desired distribution of the relative sizes of the robot generations can be maintained during the evolution; only those of them that belong to a specific set (polyhedral cone) induced by the parameters of the population can be preserved in a balanced growth (contraction). A method of achieving and maintaining a desired total size of the robot population is also developed. Simple numerical examples are included to illustrate the theoretical results.

2 The model

A robot population is categorized into n generations (or cohorts) G_i, $i = 0,1,2,..., n-1$, with $x_i(t) \geq 0$, $t = 0,1,2,...$, denoting the *size* (the number of robots) *of generation* G_i at time period t, where a single time period corresponds to the time between the release of new generations of robots (say, for example, 2 years). The *total size of the robot population* in time period t is, then,

$$y(t) = \sum_{i=0}^{n-1} x_i(t) \qquad (1)$$

Each new generation of robots exhibits incremental evolution in relation to the previous generation, with G_0 representing the newest generation (i.e. robots developed during the last time period $(t-1, t)$) and G_{n-1} representing the oldest active generation, becoming obsolete at the end of the current time period $(t, t+1)$. It is assumed that *controlled migration*, from other robot communities, is allowed to, at least, some of the generations G_i. Let $J = \{j_1, ..., j_s, ..., j_m\}$ with

$j_1 < \ldots < j_s < \ldots < j_m$, $m = |J| \le n$, denotes the index set of all such generations; it is clear that $J \subseteq N = \{0, 1, 2, \ldots, i, \ldots, n-1\}$, where N is the index set of all robot generations $\{G_i\}$. Then,

$$u_s(t) = \begin{cases} u_s(t), & \text{if } s \in J \\ 0, & \text{if } s \notin J \end{cases} \qquad (2)$$
$$s = 0,1,2,\ldots, n-1,\ t = 0,1,2,\ldots$$

denotes the migration to generation G_s.

During one time period $(t-1, t)$ the cohort constituting the ith generation simply moves up to the $(i+1)$th generation, subject to attenuation due to some of the robots becoming non-functional and obsolete. Thus

$$x_{i+1}(t+1) = \beta_i x_i(t) + u_{i+1}(t), \begin{cases} i = 0,1,2,\ldots,n-2 \\ t = 0,1,2,\ldots \end{cases} \qquad (3)$$

where β_i is the *survival rate* of the ith generation during one period,

$$0 \le \beta_i \le 1, \qquad (4)$$

and $u_{i+1}(t)$ is as in (2).

It is assumed that, at least some, robots within each generation are able to contribute to the development of a new generation of robots. Under this assumption, and recognising the possibility of controlled external (migration) inflows, the number $x_0(t+1)$ of new generation robots (that is the size of G_0) developed during the time interval $(t, t+1)$ is given by

$$x_0(t+1) = \alpha_0 x_0(t) + \alpha_1 x_1(t) + \ldots + \alpha_{n-1} x_{n-1}(t) + u_0(t)$$
$$t = 0,1,2,\ldots \qquad (5)$$

where $\alpha_j \ge 0$ is the *production rate* of the jth cohort of robots, $j = 0, 1, \ldots, n-1$.

Together (3) and (5) constitute the discrete-time model for the robot population dynamics and may be expressed in a matrix-vector form as

$$\boldsymbol{x}(t+1) = \boldsymbol{A}\boldsymbol{x}(t) + \boldsymbol{B}\boldsymbol{u}(t),\ t = 0,1,2,\ldots \qquad (6)$$

with

$$\boldsymbol{A} = \begin{bmatrix} \alpha_0 & \alpha_1 & \alpha_2 & \cdots & \alpha_{n-1} \\ \beta_0 & 0 & 0 & \cdots & 0 \\ 0 & \beta_1 & 0 & \cdots & 0 \\ \vdots & & & & \vdots \\ 0 & 0 & 0 & \cdots \beta_{n-2} & 0 \end{bmatrix} \ge 0$$

$$\boldsymbol{B} = [\boldsymbol{e}_{j_1} \vdots \boldsymbol{e}_{j_2} \vdots \cdots \vdots \boldsymbol{e}_{j_m}] \ge 0,\ \boldsymbol{u}(t) \ge 0 \qquad (7)$$

where $\boldsymbol{x}(t) = (x_0(t)\ x_1(t)\ \ldots\ x_{n-1}(t))^T \ge 0$ is the state vector (which components are the sizes of the robots generations at time period t), $\boldsymbol{u}(t) = (u_{j_1}, \ldots, u_{j_m})^T \ge 0$ is the control (migration) vector, the columns $\boldsymbol{e}_{j_s}$ of (control) matrix $\boldsymbol{B}$ ($j_s \in J$, $s = 1, 2, \ldots, m$) are linearly independent unit basis vectors, T denotes the transpose and the notation $\boldsymbol{A}, \boldsymbol{B} \ge 0$ ($\boldsymbol{x}, \boldsymbol{u} \ge 0$) is used for nonnegative (element-wise) matrices (respectively, vectors); all matrices and vectors in (6) have suitable dimensions.

The system (6) - (7) representing the robot population dynamics is a positive linear system, see [3, 4]. Reachability and controllability (fundamental properties of dynamic systems) of different classes of robot populations (totally sterilized, totally fertile, fertile with generations becoming obsolete during robot life span and others) have been studied in [2]. In this paper the problem of achieving a desired total size of the robot population under a balanced growth (contraction) and the problem of maintaining the desired total size are studied in sections 3 and 4 respectively.

3 Achieving a desired total size by constant growth (contraction)

The *balanced growth* (contraction) is defined as a growth (contraction) of the population, in which the relative sizes (the ratios of the number of robots within a generation to the total number of robots in the population) of different generations remain constant during their evolution. Such balanced growth (on a ray) may be specified by:

$$\boldsymbol{x}(t+1) = \delta\,\boldsymbol{x}(t) \text{ or } \boldsymbol{x}(t) = \delta^t \boldsymbol{x}(0) \qquad (8)$$

where $\delta > 1$ denotes a balanced growth and δ is called a constant growth factor (or simply constant growth). If $0 < \delta < 1$ then the system contracts at a constant rate, and for $\delta = 1$ maintains the initial state in time.

A substitution of (8) into (6) yields

$$(\delta \boldsymbol{I} - \boldsymbol{A})\,\boldsymbol{x}(t) = \boldsymbol{B}\,\boldsymbol{u}(t) \qquad (9)$$

For $\delta > \rho(\boldsymbol{A})$, where $\rho(\boldsymbol{A})$ is the dominant eigenvalue of $\boldsymbol{A} \ge 0$, the matrix $\delta\boldsymbol{I} - \boldsymbol{A}$ is a non-singular M-matrix that has a non-negative inverse [5, 6] . So from (9), since it is satisfied for any $t = 0,1,2,\ldots$, one can obtain

$$\boldsymbol{x} = (\delta\boldsymbol{I} - \boldsymbol{A})^{-1}\boldsymbol{B}\,\boldsymbol{u} \quad \text{with } \boldsymbol{u} \ge 0 \qquad (10)$$

The state $\boldsymbol{x}$ is, clearly, non-negative for any non-negative migration (decision) vector $\boldsymbol{u}$ since $(\delta \boldsymbol{I} \quad \boldsymbol{A})^{-1} \geq 0$ and $\boldsymbol{B} \geq 0$. The system (10) has non-negative solutions if and only if the initial state $\boldsymbol{x}_0$ belongs to the cone spanned by the columns of the non-negative matrix $(\delta \boldsymbol{I} \quad \boldsymbol{A})^{-1} \boldsymbol{B}$, i.e.

$$\boldsymbol{x}_0 \in cone\,((\delta \boldsymbol{I} \quad \boldsymbol{A})^{-1} \boldsymbol{B}) = \{\boldsymbol{x} / \boldsymbol{x} = \sum_{j=1}^{m} u_j col_j\,(\delta \boldsymbol{I} - \boldsymbol{A})^{-1} \boldsymbol{B}, \; u_j \geq 0,\ j = 1,\ldots,\ m\} \tag{11}$$

where $col_j\,(\delta \boldsymbol{I} - \boldsymbol{A})^{-1} \boldsymbol{B}$ are the generators of the cone. The cone $cone\ ((\delta \boldsymbol{I} \quad \boldsymbol{A})^{-1} \boldsymbol{B})$ is finitely generated and, hence, it is a polyhedral cone [4]. This cone is, clearly in the nonnegative orthant of the n-dimensional real vector space.

Given an admissible initial state $\boldsymbol{x}_0$, such that $\boldsymbol{x}_0 \in cone\ ((\delta \boldsymbol{I} \quad \boldsymbol{A})^{-1} \boldsymbol{B})$, one can find a (constant) decision vector

$$\boldsymbol{u}^* = (\boldsymbol{B}^{\mathrm{T}} \boldsymbol{B})^{-1} \boldsymbol{B}^{\mathrm{T}} (\delta \boldsymbol{I} - \boldsymbol{A})\, \boldsymbol{x}_0 \geq 0 \tag{12}$$

that guarantees a desired constant balanced growth δ of the system since for the robot population the control matrix $\boldsymbol{B}$ given in (7) is of full column rank m.

It is well known, that a nonnegative matrix $\boldsymbol{A} \geq 0$ always has a real non-negative eigenvalue $\rho(\boldsymbol{A}) \geq 0$ called a dominant (or maximal) eigenvalue, such that the moduli of all the eigenvalues of $\boldsymbol{A}$ are not greater than ρ. Then, the following evaluation takes place [6]

$$\min_i \sum_{j=1}^{n} a_{ij} \leq \rho(\boldsymbol{A}) \leq \max_i \sum_{j=1}^{n} a_{ij} \tag{13}$$

where $a_{ij} \geq 0$ are the entries of $\boldsymbol{A}$, with equalities holding on both sides if and only if all the row sums are equal; the evaluation is true also for reducible nonnegative matrices but the equality sign either on the left side or on the right side could hold in the case when not all the row sums are equal.

The evaluation (13) specified for the cohort matrix $\boldsymbol{A}$ given in (7) yields

$$\min\{\beta_i, \sum_{j=0}^{n-1} \alpha_j\} \leq \rho(\boldsymbol{A}) \leq \max\{1, \sum_{j=0}^{n-1} \alpha_j\} \tag{14}$$

since, as indicated in (4), the survival rates of robot generations are $\beta_i \leq 1$ for $i = 0, 1, \ldots, n-1$.

3.1 Totally sterilized robot population

In totally sterilized robot populations the robot generations cannot contribute to the development of the new robot generation [2], so that the production rates are zero, i.e. $\alpha_j = 0$, $j = 0, 1, \ldots, n-1$, and the system (cohort) matrix in (7) becomes

$$\boldsymbol{A}_s = \begin{bmatrix} 0 & 0 & 0 & \cdots & 0 \\ \beta_0 & 0 & 0 & \cdots & 0 \\ 0 & \beta_1 & 0 & \cdots & 0 \\ \vdots & & & & \vdots \\ 0 & 0 & 0 & \cdots \beta_{n-2} & 0 \end{bmatrix} \geq 0 \tag{15}$$

The cohort matrix $\boldsymbol{A}_s$ of totally sterilized robot populations has an eigenvalue $\lambda = 0$ with algebraic multiplicity n, that is all the eigenvalues are zeros, and, hence, the dominant eigenvalue $\rho(\boldsymbol{A}_s) = 0$. It readily follows from this that a totally sterilized robot population can experience balanced growth or contraction with any growth (respectively, contraction) factor $\delta > 0$ for any initial state $\boldsymbol{x}_0 \in cone\ ((\delta \boldsymbol{I} \quad \boldsymbol{A}_s)^{-1} \boldsymbol{B})$, since $(\delta \boldsymbol{I} \quad \boldsymbol{A}_s)$ is a non-singular M-matrix. The inverse of $(\delta \boldsymbol{I} \quad \boldsymbol{A}_s)$ is

$$(\delta \boldsymbol{I} \quad \boldsymbol{A}_s)^{-1} = \frac{1}{\delta} \begin{bmatrix} 1 & 0 & 0 & \cdots & 0 & 0 \\ \frac{\beta_0}{\delta} & 1 & 0 & \cdots & 0 & 0 \\ \frac{\beta_0 \beta_1}{\delta^2} & \frac{\beta_1}{\delta} & 1 & 0 & \cdots & 0 \\ \vdots & \vdots & \ddots & \ddots & \cdots & \vdots \\ \frac{\beta_0 \beta_1 \cdots \beta_{n-2}}{\delta^{n-1}} & \frac{\beta_1 \beta_2 \cdots \beta_{n-2}}{\delta^{n-2}} & \cdots & \cdots & \frac{\beta_{n-2}}{\delta} & 1 \end{bmatrix} \geq 0 \tag{16}$$

so given $\boldsymbol{B}$ one can easily find the generators (edges) of the polyhedral cone $cone\ ((\delta \boldsymbol{I} \quad \boldsymbol{A}_s)^{-1} \boldsymbol{B})$.

Let

$$y^* = \sum_{i=0}^{n-1} x_i^* \tag{17}$$

be the *desired* (total) *size* of the robot population in steady-state, and let $\boldsymbol{x}_0 \in cone\ ((\delta \boldsymbol{I} \quad \boldsymbol{A})^{-1} \boldsymbol{B})$ be the initial state. The initial robot population size is

$$y_0 = \sum_{i=0}^{n-1} x_i(0) \tag{18}$$

The *objective* is to achieve the desired population size in finite time by balanced growth if $y_0 < y^*$ or balanced contraction if $y_0 > y^*$; if $y_0 = y^*$, the problem is to maintain the desired total size.

A substitution (component-wise) of (8) in (1) leads to

$$y(t) = \sum_{i=0}^{n-1} \delta^t x_i(0) = \delta^t\ y_0,\ t = 1,2,\ldots. \tag{19}$$

It is easy to see from (19) that the desired robot population size can be achieved by balanced growth (contraction) in

$$t^* = \left[\frac{\ln \frac{y^*}{y_0}}{\ln \delta}\right] \qquad (20)$$

time periods, where $[a]$ denotes the (positive) integer closest to the real number $a \geq 0$. If it is required to achieve the desired population size y^* from a given initial size y_0 in a specified time t one can find from (20) the growth (respectively, contraction) factor δ needed to meet the objective,

$$\delta = \sqrt[t]{\frac{y^*}{y_0}} \qquad (21)$$

A totally sterilized robot population is controllable and, therefore, the transition from any initial size y_0 to any desired total size y^* can be achieved in finite time if the survival rates $\beta_i > 0$ for $i = 0, 1, \ldots, n-1$ and a new generation of robots is produced. In the case when robots of, say, from generation G_k become obsolete, i.e. $\beta_k = 0$ for some k, $0 < k < n$ 1, during the whole life-span of the robot community, migration into G_k from other communities in addition to building new generation robots is needed to exercise a complete control over its evolution [2].

Example 1

Consider a totally sterilized robot population consisting of three generations with survival rates $\beta_0 = 0.9$ and $\beta_1 = 0.8$ (recall that the oldest active generation G_2 becomes obsolete at the end of the time period) and migration inflows allowed into generations G_0 and G_1 only, so that index set $J = \{0, 1\}$ and, hence,

$$\boldsymbol{B} = \begin{bmatrix} 1 & 0 \\ 0 & 1 \\ 0 & 0 \end{bmatrix}$$

It is desired to achieve a total population size $y^* = 120$ from an initial state $\boldsymbol{x}_0 = (4, 6, 4)^T$ (the initial total size is $y_0 = 14$) by constant balanced growth with growth factor $\delta = 1.2$.

Since

$$(\delta \boldsymbol{I}-\boldsymbol{A})^{-1}\boldsymbol{B} = \begin{bmatrix} \frac{5}{6} & 0 \\ \frac{5}{8} & \frac{5}{6} \\ \frac{5}{12} & \frac{5}{9} \end{bmatrix}$$

the edges (generators) of the cone

$$cone((\delta \boldsymbol{I}-\boldsymbol{A})^{-1}\boldsymbol{B}) = cone(\boldsymbol{r}_1, \boldsymbol{r}_2) = \{\boldsymbol{x} \mid \boldsymbol{x} = c_1 \boldsymbol{r}_1 + c_2 \boldsymbol{r}_2, c_1, c_2 \geq 0\} \qquad (22)$$

are, respectively, $\boldsymbol{r}_1 = (\frac{5}{6}, \frac{5}{8}, \frac{5}{12})$ and $\boldsymbol{r}_2 = (0, \frac{5}{6}, \frac{5}{9})$.

For a constant balanced growth (on a ray) the initial state must belong to the cone (22), see (11). One of the ways to check this is to represent the cone (22) by its external representation (in terms of the bounding planes). Note, firstly, that this cone lies on the plane

$$cone(\boldsymbol{r}_1, \boldsymbol{r}_2) \in plane(\boldsymbol{r}_1, \boldsymbol{r}_2) = 2x_2 - 3x_3 = 0 \qquad (23)$$

and that the edge $\boldsymbol{r}_2$ is on the (x_2, x_3)-plane with an equation $x_1 = 0$. Secondly, the plane $3x_1 - 4x_2 = 0$ passes through the edge $\boldsymbol{r}_1$ and contains the x_3 – axis. Thus, the external representation of the cone (22) is given by

$$cone(\boldsymbol{r}_1, \boldsymbol{r}_2) = \{(x_1, x_2, x_3) \mid 2x_2 - 3x_3 = 0, 4x_2 \quad 3x_1 \geq 0, x_1 \geq 0) \qquad (24)$$

It is easy to verify that $\boldsymbol{x}_0 = (4, 6, 4) \in \{(x_1, x_2, x_3) \mid 2x_2 - 3x_3 = 0, 4x_2 \quad 3x_1 \geq 0, x_1 \geq 0\}$, so a constant balanced growth with the given growth factor $\delta = 1.2$ is possible. The controlled migration needed for this growth can be determined directly using (12),

$$\boldsymbol{u}^* = (\boldsymbol{B}^T\boldsymbol{B})^{-1}\boldsymbol{B}^T(\delta \boldsymbol{I} - \boldsymbol{A})\boldsymbol{x}_0 = \begin{bmatrix} \frac{6}{5} & 0 & 0 \\ -\frac{9}{10} & \frac{6}{8} & 0 \end{bmatrix}\begin{bmatrix} 4 \\ 6 \\ 4 \end{bmatrix} = \begin{bmatrix} \frac{24}{5} \\ \frac{18}{5} \end{bmatrix}$$

and the number of time periods required to achieve the desired population size $y^* = 120$ from (20),

$$t^* = \left[\frac{\ln(\frac{120}{14})}{\ln 1.2}\right] = [11.8] = 12$$

Alternatively if it is desired to achieve the desired population in 8 time periods then the growth factor must be selected to be as in (21), giving

$$\delta = \sqrt[8]{(120/14)} = (120/14)^{1/8} = 1.31$$

Clearly, adopting a new value for the growth factor, one has to check again the cone condition (whether the

initial state belongs to the new cone) before proceeding to find the new control.

3.2 Fertile robot populations with low productivity

A robot population is called a population with low productivity if the sum of production rates is less than unity, i.e.

$$\sum_{j=0}^{n-1} \alpha_j < 1 \tag{25}$$

Clearly a totally sterilized robot population is a population with zero productivity

If there exists some attenuation (due to some of the robots becoming non-functional) in each generation, i.e. $\beta_i < 1$ for $i = 0, 1, \ldots, n-1$, and the oldest generation G_{n-1} is able to contribute to the development of new-generation robots G_o, i.e. $\alpha_{n-1} > 0$, then the cohort matrix A given in (7) is irreducible and its dominant eigenvalue is bounded above by unity,

$$\rho(A) \le \max_i \{\beta_i, \sum_{j=0}^{n-1} \alpha_j\} < 1 \tag{26}$$

In this case, since $\rho(A) < 1$, the robot population can experience either a *balanced growth* or *contraction* with constant growth (respectively, contraction) factor $\delta > \rho(A)$. Thus, given an initial robot population size y_o, a desired (total) size y^* in steady-state and $\delta > \rho(A)$ one can find the time needed to achieve y^* by balanced growth (contraction) using formula (20). Alternatively, when the transition time t from y_o to y^* is specified one can find the corresponding growth (contraction) factor from (21) provided that $\delta > \rho(A)$.

If generation G_{n-1} does not contribute to the development of a new generation of robots then the production rate $\alpha_{n-1} = 0$ and, therefore, the cohort matrix A is no longer an irreducible matrix but still, since the survival rates $\beta_i < 1$ for $i = 0, 1, \ldots, n-1$, the dominant eigenvalue $\rho(A) < 1$, so that the robot population can experience some contraction. If A is a reducible matrix ($\alpha_{n-1} = 0$) and at least one of the survival rates is equal to unity, say $\beta_k = 1$, the equality sign on the right hand side in (14) could hold, that is $\rho(A) = 1$, and the inequality $\delta > \rho(A)$ is to be verified for every particular fertile robot population with low productivity.

Example 2

Replacing the totally sterilized robot population of Example1 by a fertile robot population with productivity rates $\alpha_0 = 0.2$, $\alpha_1 = 0.3$, and $\alpha_2 = 0.4$ leads to a model having system (cohort) matrix A_f and control matrix B given by

$$A_f = \begin{bmatrix} 0.2 & 0.3 & 0.4 \\ 0.9 & 0 & 0 \\ 0 & 0.8 & 0 \end{bmatrix}, B = \begin{bmatrix} 1 & 0 \\ 0 & 1 \\ 0 & 0 \end{bmatrix}$$

Again it is desired to achieve a total population size $y^* = 120$ from an initial state $x_0 = (4, 6, 4)^T$ by constant balanced growth factor $\delta = 1.2$ (which is such that $\delta > \rho(A_f) = 0.88$).

With this value for the growth factor the edges (generators) of the cone

$$cone((\delta I - A_f)^{-1}B) = cone(r_3, r_4) = \{x \mid x = c_3 r_3 + c_4 r_4,\ c_3, c_4 \ge 0\} \tag{27}$$

are respectively $r_3 = (1.74, 1.30, 0.87)$ and $r_4 = (0.82, 1.45, 0.97)$.

For a constant balanced growth the initial state must belong to this cone. Proceeding as in Example1 the cone (27) lies on the plane

$$cone(r_3, r_4) \in plane(r_3, r_4) = 2x_2 - 3x_3 = 0$$

and by determining the two planes which contain an edge and its projection on the (x_1, x_2) plane the external representation of the cone (27) is given by

$$cone(r_3, r_4) = \{(x_1, x_2, x_3) \mid 2x_2 - 3x_3 = 0,\ 4x_2 \quad 3x_1 \ge 0,\ 1.45\, x_1 \quad 0.82x_2 \ge 0,\ x_1 \ge 0,\ x_2 \ge 0\} \tag{28}$$

It is readily verified that the initial state $x_0 = (4, 6, 4)^T$ is contained within the cone (28) and so a constant balanced growth with the given growth factor $\delta = 1.2$ is possible.. From (12) the controlled migration required for this growth is

$$u^* = (B^T B)^{-1} B^T (\delta I - A_f) x_0 = (0.6\ 3.6)^T$$

and from (20) the number of time periods required to achieve the desired population size $y^* = 120$ is $t^* = 12$.

3.3 Fertile robot populations with high productivity

A fertile robot population is called a population with low (high) productivity if the sum of production rates is less (greater) than unity, i.e.

$$\sum_{j=0}^{n-1} \alpha_j > 1 \tag{29}$$

In this case the dominant eigenvalue of the cohort matrix A can be greater than unity, so balanced contraction may not be achievable. If the desired total population size y^* is greater than the initial size y_o, i.e. $y^* > y_o$, then it can be achieved by balanced growth provided that $x_o \in cone\ ((\delta I \quad A)^{-1} B)$. The transition time t^* and the balanced growth factor δ can be found from (21) and (22), respectively. The fertile robot population with high productivity is not controllable [2] in finite time since at least one production rate $\alpha_j > 0$, and, therefore, the transition from y_o to y^* may not be possible for any y_o and y^*.

4. Maintaining a desired total size

Let t^* be the time when the desired total size y^* is achieved by balanced growth or contraction with constant factor δ^* and let x^* be the corresponding state. Since the objective is to maintain y^* it is possible to do this by maintaining the state x^*, i.e.

$$x(t) = x^*, \quad t = t^* + 1, t^* + 2,... \tag{30}$$

The state x^* is, clearly, in the polyhedral cone $cone\ ((\delta^* I \quad A)^{-1} B)$ for $\delta^* > \rho(A)$. Thus, if $\rho(A) < 1$, then a constant migration of robots (control) from other robot colonies

$$u^* = (B^T B)^{-1} B^T (I - A) x^* \geq 0 \tag{31}$$

maintains the state $x(t) = x^*$ for $t = t^* + 1, t^* + 2,...$, and the size y^* of the robot population.

A different approach to maintaining the desired size is based on changing the parameters of robot population – the survival and production rates. By improving robots maintenance the generation survival rates can be increased and by regulating the contributions of robot generations to the development of new generation of robots the survival and production rates can be made to satisfy the following relations

$$\begin{aligned} &\alpha_s + \beta_s = 1, \text{ for } s = 0, \ldots, n-2 \\ &\alpha_{n-1} = 1 \end{aligned} \tag{32}$$

so that the cohort matrix A becomes a column stochastic matrix , i.e. $A = P$ with $e\,P = e$, where $e = (1, 1,..., 1)$. Then, if no migration is allowed ($u(t) = 0$ for $t = t^*, t^* + 1, t^* + 2,...$) the evolution of the robot population is described by the equation

$$x(t + 1) = P\,x^*(t), \text{ for } t = t^*, t^* + 1, t^* + 2,.... \tag{33}$$

Pre-multiplying both sides of (33) by e and taking into account (17) yields

$$y(t + 1) = e\,x^* = y^* \text{ for } t = t^* + 1, t^* + 2,... \tag{34}$$

so the desired total robot population size is maintained after it is achieved.

The robot population size y^* can also be maintained after it is achieved by observing the state $x(t)$, for $t = t^*, t^* + 1, t^* + 2,....$, and controlling the migration flows on the bases of these observations. Thus, by using a linear state-feedback of the form

$$u(t) = K\,x(t), K = [k_{ij}]_{m \times n} \geq 0 \tag{35}$$

the open-loop positive linear system (6) can be reduced to the closed-loop positive linear system

$$x(t + 1) = A_c x(t), \quad t = t^*, t^* + 1, t^* + 2,.... \tag{36}$$

where the closed-loop system matrix A_c is given by

$$A_c = A + BK \geq 0 \tag{37}$$

Taking into account the structure of the control matrix B, see (7), the inequality (37) can be rewritten in the flowing form

$$\begin{aligned} &a_{s,*}^{(c)} = a_{s,*} + k_{s,*} \text{ for } s \in J \\ &a_{s,*}^{(c)} = a_{s,*} \qquad \text{for } s \notin J \end{aligned} \tag{38}$$

where $a_{s,*}$, $k_{s,*}$ and $a_{s,*}^{(c)}$ are the s^{th} rows of, respectively, the cohort matrix A given in (7), the controller K and the closed-loop system matrix A_c.

Provided that an inflow into the new generation of robots G_0 is allowed, that is $k_{1,*} \neq 0$, one can find from (38) a controller K that makes A_c a column stochastic matrix, i.e. $e\,A_c = e$, and, then, pre-multiplying (37) by e and taking into account (17) one can obtain for $x(t) = x^*$, $t = t^*, t^* + 1, t^* + 2,....$, once again the equality (34). Note that negative values of the control gains can be interpreted as reductions in the corresponding productivity rates.

5 Concluding remarks

Two major problems of robot population evolution are formulated and studied in this paper – the problem of achieving a desired total population size from a given initial state under balanced growth or contraction and the problem of maintaining the total size during periods of the controlled evolution. The results of the study reveal the important relationships that exist between the growth /contraction factor and the time of achieving the desired total size on the one hand and such, essential for the robot population evolution,

parameters as production and survival rates as well as the immigration policy on the other. A somewhat surprising result is obtained namely a balanced growth or contraction cannot be experienced from any initial state. They can only be achieved from those of the states which belong to a certain region (polyhedral cone) in the state space. The ability to maintain a desired total size, after it is achieved, is also strongly affected by the immigration policy and the survival and production rates – it might not be possible to maintain the size without changing the policy or/and the rates. All the results obtained in this paper once again expose the fundamental importance of reachability and controllability properties of the robot population for its controlled evolution.

Acknowledgments

The authors thank the Australian Research Council for providing support (under grant A00001126) for this work.

References

[1] Agah A, (1996) Robot teams, human work groups and animal socio-biology: a review of research on natural and artificial multi-agent autonomous systems, Adv. Robotics, 10:523-545.

[2] James DJG, Rumchev VG (2000) Robot populations and their controlled evolution, Artificial Life and Robotics, **14:** 137-142.

[3] Luenberger D (1979) Introduction to dynamical systems: theory, models and applications, Wiley, New York.

[4] Farina L, Rinaldi S (2000) Positive linear systems: theory and applications, JohnWiley & Sons, New York.

[5] Berman A, Plemmons R (1994) Nonnegative matrices in mathematical sciences, SIAM, Philadelphia.

[6] Rumchev VG, James DJG (2003) Controlled balanced growth of positive linear discrete- time systems, Proceedings of ICSE ' 2003, Coventry University, UK, ISBN 0-905949-91- 9, vol. 2, pp. 597-601.

[7] Minc H (1988) Nonnegative matrices, Wiley, New York.

Proc. of The Ninth Int. Symp. on Artificial Life and Robotics (AROB 9th '04)
Beppu, Oita, Japan, 28-30 January, 2004

Leak Detection in Pipelines Based on Non-negative Matrix Factorization*

Rong Hu
Dept. of Automation, Tsinghua Uinv.
Beijing, 100084, P .R. China
hr02@mails.tsinghua.edu.cn

Hao Ye
Dept. of Automation, Tsinghua Uinv.
Beijing, 100084, P .R. China
haoye@tsinghua.edu.cn

*Supported by the National Natural Science Fund of China and the 863 Program of China

Abstract

Leak detection in oil pipelines is important for safe operation of pipelines. A new approach based on the non-negative matrix factorization (NMF) method to detect leaks of oil pipelines which simulates the process of human's visual perception is proposed in this paper. Experimental results show that the method can successfully detect many leak faults from a pressure curve which might not be effectively detected by a traditional signal processing based method but can be recognized easily by human visual perception.

Keywords: Non-negative matrix factorization; visual pattern recognition; leak detection

1. Introduction

Leak detection in oil pipelines is important for safe operation of pipelines. Among a great deal of approaches for leak detection and location, the so-called negative pressure wave based approach has been widely adopted in real applications [1].

The basic idea of the negative pressure wave based methods is that, when leak occurs, there is a negative pressure wave propagating from the leak point toward the upstream and downstream ends and so that we can detect leaks by detecting the pressure changes at the both ends, and further locate the leak by calculating the time difference between the arrival times of the negative pressure wave at each end. The key problems of leak detection and location are how to sensitively detect the pressure changes caused by the negative pressure wave and accurately determine the difference between its arrival times.

Ye, et al. [2] have proposed a negative pressure wave based approach which uses Wavelet Transform to detect the pressure changes. However, the method has a high possibility of false alarm for the case of strong noise in the pressure measurement records and has a high possibility of miss detection with a small or slow leak. It is also a common problem in almost all of the negative pressure wave based approaches.

However, the fact that even an ordinary operator who is not an experienced expert of the oil enterprise can easily recognize a lot of leaks from the pressure curve gives us an implication to solve this problem from a new point of view, i.e. the leak detection can be realized based on a method which simulates the process of human's visual perception.

Inspired by the successful application of the so-called Non-negative Matrix Factorization (NMF) method in face and object recognition and its unique advantage compared with Principal Components Analysis (PCA) [3], in this paper, we propose to use NMF to recognize the negative pressure waves in a pressure wave curve, which has not been used in leak detection.

NMF is distinguished from the other methods such as PCA due to the use of non-negativity constraints [3], and the method can learn the parts of objects that resemble intuitive notions in an unsupervised way, which is consistent with human visual perception. So in this paper, a new method for leak detection which can simulate the process of human's visual perception is proposed.

2. Brief Introduction of NMF Technique

This section provides a brief introduction of Non-negative Matrix Factorization (NMF) [3,

4].Given a non-negative n×m matrix V, where a column of V denotes the measured values of all variables at a time instant, and a row of V denotes the measured values of one variable at all time instants, then the NMF finds the non-negative n×r matrix W and the non-negative r×m matrix H such that

$$V_{i\mu} \approx (WH)_{i\mu} = \sum_{a=1}^{r} W_{ia} H_{a\mu} \quad (1)$$

The rank r of the factorization is generally chosen to satisfy $(n+m)r < nm$, and the product WH can be regarded as a compressed form of the data in V. Each column of W can be regarded as a basis vector, and each column of H can be regarded as a group of weights. So the product of the μ^{th} column in H and the r basis vectors in W actually approximate the μ^{th} column in V. Different from PCA, which allows the matrices similar to W and H to be of arbitrary sign, NMF does not allow negative entries in the matrix factors W and H which permits the combination of multiple bases images to represent an object. So NMF has the characteristic of parts-based representation which is appealing because of the intuitive notion of combining parts to form a whole.

NMF can be implemented by the update rules for W and H given in the next equations,

$$W_{ia} \leftarrow W_{ia} \sum_{\mu} \frac{V_{i\mu}}{(WH)_{i\mu}} H_{a\mu}, \quad (2)$$

$$W_{ia} \leftarrow \frac{W_{ia}}{\sum_{j} W_{ja}}, \quad (3)$$

$$H_{a\mu} \leftarrow H_{a\mu} \sum_{i} W_{ia} \frac{V_{i\mu}}{(WH)_{i\mu}}. \quad (4)$$

Iteration of these update rules converges to a local maximum of the objective function

$$F = \sum_{i=1}^{n} \sum_{\mu=1}^{m} [V_{i\mu} \log(WH)_{i\mu} - (WH)_{i\mu}] \quad (5)$$

subject to the non-negative constraints described above.

3. Detection of Negative Pressure Wave Based on NMF

3.1 Basic Idea

In this paper, pressure curves are regarded as pressure images, and as an object recognition method, NMF is used here to recognize the negative pressure wave in a pressure image.

Based on the principle of NMF, the basic procedure of the detection includes two phases:

(1) Training phase: In this phase, the history pressure curves in which we already know there exist or there doesn't exist negative pressure waves are used to determine the different values of the basis matrix W (i.e. W^1 and W^2) corresponding to the 'Abnormal' case (Negative pressure wave exists) and the 'Non-leak' (No negative pressure wave exists) case respectively.

(2) Detecting phase: In this phase, a pressure image to be detected is projected onto W^1 and W^2 respectively first, then the projections are used to reconstruct two pressure images respectively, and finally the original pressure image is classified to be 'Normal' or 'Abnormal' according to the reconstruction errors corresponding W^1 and W^2 respectively.

3.2 Training Samples and Detection Samples

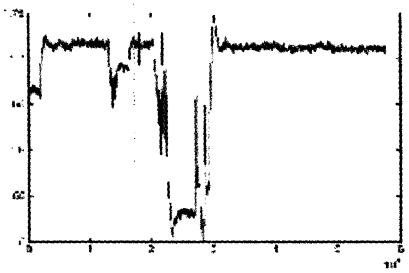
Let $p(k)$ denote the sampled data of the pressure at an upstream or downstream end at time instant k. In this paper, a sample S_i at instant i for training or detection is defined as a data segment which consists of 2000 continually sampled pressure data $p(k)$ for $k = i - 2000 + 1, \cdots, i$ and the sample time between $p(k)$ and $p(k+1)$ is 60 ms.

In order to simulate the process of human's visual perception and detect the negative pressure wave using the NMF based object recognition method, each training sample or detection sample is further converted into a 30×30 image before it is used for training or detection.

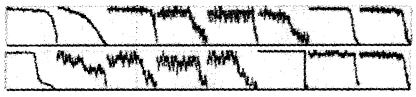
In this paper, the training samples are obtained from the real history data of an oil pipeline whose length is 32 Km, and the conclusion that whether each sample has negative pressure wave or not is already known based on the history record or experienced human's judgment. The approach is just tested off-line, so the detection samples are also chosen from the history data of the same pipeline as the one mentioned above.

We have collected 9,637 samples in the paper, of which 931 contain negative pressure waves. Among all the samples, 7,160 samples are selected randomly as training samples, and the others are used as test samples.

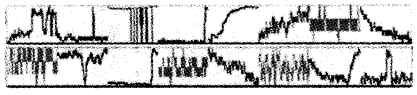
For convenience, we call a sample which contains negative pressure wave an 'Abnormal Sample', and a sample which doesn't include a negative pressure wave a 'Non-leak sample'.



(a) Pressure data for 1 hour



(b) Abnormal Samples



(c) Non-leak Samples

Fig.1 Examples of samples.

Fig. 1 (a) shows the pressure data of 1 hour, and an abnormal sample is further generated based on the data in the rectangle. Fig.1 (b) and Fig. 1 (c) give some examples of abnormal samples and non-leak sample respectively.

From Fig.1 (c), it can be seen that the non-leak actually can be further divided into several classes, such as the horizontal curve, the ascending curve, and the noisy curve etc.

3.3 Learning bases component

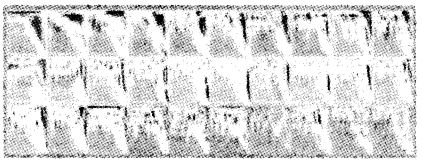
Let $V^i = [S_1 \ \cdots \ S_{m_i}]$ denote the matrix of training samples corresponding to case i, where i=1,2,3,4 represents the abnormal case, horizontal curve case, ascending curve case and noisy curve case respectively, and m_i is the number of samples of case i, let W^i denote the basis matrix in NMF corresponding to case i. Then the basis matrix W^i, i=1,2,3,4 can be learned according to (2), (3) and (4), i.e.

$$W_{ia}^i \leftarrow W_{ia}^i \sum_{\mu} \frac{V_{i\mu}^i}{(W^i H^i)_{i\mu}} H_{a\mu}^i \tag{6}$$

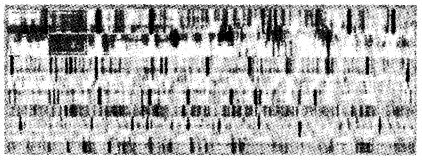
$$W_{ia}^i \leftarrow \frac{W_{ia}^i}{\sum_j W_{ja}^i} \tag{7}$$

$$H_{a\mu}^i \leftarrow H_{a\mu}^i \sum_i W_{ia}^i \frac{V_{i\mu}^i}{(W^i H^i)_{i\mu}} \tag{8}$$

Fig.2 (a) and (b) show some examples of the basis components W after training corresponding to the abnormal and non-leak cases respectively.



(a) W after training for abnormal case



(b) W after training for non-leak case

Fig.2 Examples of the basis components W after training

3.4 Recognition of the negative pressure wave

For a sample S_i to be detected, the algorithm of negative pressure curve recognition involves the following steps:

(1) Project S_j into W^i for i=1,2,3,4 respectively, i.e.

$$h_j^i = (W^{iT} W^i)^{-1} W^{iT} S_j . \quad (9)$$

(2) Reconstruct the pressure image by

$$f_j^i = W^i h_j^i \quad (10)$$

(3) Calculate the ratio of Signal-to-Noise [5] according to

$$R^i{}_{SN} = 10\lg\left(\frac{\| S_j \|^2}{\| S_j - f_j^i \|^2}\right) \quad (11)$$

(4) The equation (12) can be used to determine the presence of negative pressure wave curve.

$$R_{SN1} = \max\{R_{SN1}, R_{SN2}, ..., R_{SNi}\} . \quad (12)$$

3.5 Test Results

2477 samples which are not included in the training set are used to test the approach, among which 249 samples are abnormal containing negative pressure waves. The results of detection by our approach are shown in Table 1. It can be seen that the method based on NMF can effectively detect the negative pressure wave with an acceptable miss detection rate and false alarm rate respectively.

Table 1 Test results

	Test Sample	Recognize correctly	Recognize wrongly
Abnormal Samples	249	229	20
Non-leak samples	2228	2226	2

According to the test, many detection samples which can not be classified correctly by the traditional wavelet based method [2] due to the strong noise have been correctly recognized by the NMF based method in this paper. Fig. 3 (a) and (b) show 2 samples which lead to the miss detection and false alarm in the traditional method respectively. However, the NMF based method in this paper has correctly recognized both of them.



(a) (b)

(a) Sample leads to miss detection

(b) Sample leads to false alarm

Fig.3 Samples lead to wrong results in traditional method

4. Conclusion

In this paper, a new method based on Non-negative Matrix Factorization (NMF) to detect the negative pressure wave is proposed, which is a key phase in the whole leak detection and location procedure. In fact, the approach with intuitive notion is consistent with the process of human visual perception, and the experimental results show the leak can effectively be recognized with little computation. It is also able to detect the slow and small leaks with strong noise.

However, the problem of operations in the upstream and downstream which might also lead to the pressure changes is not discussed in this paper.

References

[1] Wang, K. F., G. Z. Wang, Jun Yang, C. Z. Fang (1992), A method of leak diagnosis based on negative wave propagation in Pipeline. Information and Control Vol.21, No. 4, pp. 217-221 (In Chinese).

[2] Ye, H., G. Z. Wang and C. Z. Fang (1995), Application of Wavelet Transform to Leak Detection and Location in Transport Pipelines. Engineering Simulation Vol. 13, pp. 1025-1032. OPA, Netherlands.

[3] D. Lee and H. Seung (1999), Learning the parts of objects by non-negative matrix factorization. Nature 401:788-791, 1999.

[4] D. Lee and H. Seung (2000), Algorithms for non-negative matrix factorization. *NIPS*, 2000.

[5] Zhaoqi Bian, Xuegong Zhang (2000), Pattern Recognition (Second Edition) [M]. Tsinghua University Press, Beijing, 1999. (In Chinese).

Proc. of The Ninth Int. Symp. on Artificial Life and Robotics (AROB 9th '04)
Beppu, Oita, Japan, 28-30 January, 2004

Acrobot Control by Learning the Switching of Multiple Controllers

Masaya NISHIMURA† Junichiro YOSHIMOTO‡,† Shin ISHII†,‡

† Nara Institute of Science and Technology
8916-5 Takayama, Ikoma, Nara 630-0192, JAPAN
‡ CREST, Japan Science and Technology Agency
E-mail: {masay-ni, juniti-y, ishii}@is.aist-nara.ac.jp

Abstract

Reinforcement learning (RL) has recently been applied to constructing controllers for nonlinear systems. Although the RL has some merits which the traditional control theory does not have, it needs appropriate function approximators to represent a value function and a large number of trials, especially when the state and action are continuous. For this reason, it is difficult to apply RL methods to tasks with strong nonlinearity and/or high dimensionality. In order to overcome this problem, we propose an RL scheme by incorporating the control theory. We then apply it to swinging-up and stabilization task of an acrobot with a limited torque, which is a typical but very difficult non-linear control problem. The simulation result showed that our method was able to realize stable learning and to achieve a fairly good control.
keywords reinforcement learning, acrobot, nonlinear control

1 Introduction

Reinforcement learning (RL) has recently been extensively applied to constructing controllers for nonlinear systems. In contrast to methods based on the traditional control theory, RL methods have abilities to adapt to dynamic environments though exact dynamics models of target plants are not directly required. Especially when a task can be formulated as a Markov decision process (MDP) with finite states and actions, it is known that RL methods, such as TD-learning and Q-learning [1], are able to construct semi-optimal controllers. Some studies suggested that these methods are applicable even to MDP tasks with continuous states and actions by using function approximators [2]. However, successful applications so far are still limited to tasks with weak non-linearity and low dimensionality, like inverted pendulum control or cart-pole balancing.

Typical RL methods have problems when applied to continuous-state tasks. If the target plant has strong non-linearity and high dimensionality, it is difficult to determine an appropriate class of function approximators. Selecting inadequate function approximators suffer from unstable learning. It is also difficult to apply to tasks in the real world because a large number of trials are often necessary.

On the other hand, dynamical property of the task plant may partly be known in a priori in many real situations. In such a situation, using the knowledge, it is possible to design local controllers by applying the control theory to the linearized dynamics, even though designing a global controller is difficult.

In this study, we propose a new RL scheme by incorporating the control theory, so that we construct a global controller for a non-linear target plant. We deal with a control problem of an acrobot as an application of our scheme, though possible applications of our scheme are not limited to this task.

2 Learning Scheme

2.1 Architecture

In this section, we describe the basic concept of our approach. We assume a situation where the dynamical property of a target plant is known but it is difficult to construct a controller to achieve the whole task due to the nonlinear dynamics of the plant. A typical example is to control under-actuated robots like an acrobot.

In order to construct a global controller, we divide our approach into two phases. In the first phase, the design phase, multiple incomplete controllers are constructed based on the locally linearized dynamics of the target plant and/or heuristic techniques. Here, an "incomplete controller" refers to a controller that is

able to play a specific role, e.g., stabilizing the system in a state subspace or gaining the kinetic energy [3], while not to achieve a global control only by itself. Since constructing such incomplete controllers depends on the task, actual instances are described in section 3 within a specific application.

After the design phase, let N incomplete controllers be designed, each labeled by n ($n = 1, \ldots, N$). In the second phase, the RL phase, an RL method is applied in order to determine what incomplete controller is used at each state. The implementation is described in the subsequent section.

Figure 1 summarizes the architecture assumed in our approach. Dash box denotes the adaptive component obtained by RL while solid boxes denote fixed controllers designed based on a priori information.

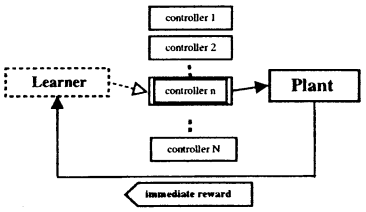


Figure 1: our architecture using multiple incomplete controllers

In the traditional non-linear control theory, a global controller is often constructed by combining some local controllers. In such a case, it is crucial but very difficult to select appropriately the boundary for switching a local controller with another. Our model tries to solve this switching problem autonomously by introducing the RL method. If we regard our approach as an instance of RL methods, on the other hand, it is expected that stable and fast learning is realized because the task of the RL is to select appropriate meta-rules (incomplete controllers in this case), which have been prepared in advance. Accordingly, our model combines the merits of RL with those of the control theory.

2.2 Reinforcement Learning

In this section, we formulate the RL phase as a Markov decision process (MDP) and introduce an RL method to solve it.

Let $x(t)$ and $a(t) \in \{1, \ldots, N\}$ be a state of the target plant and a selected incomplete controller, respectively, at time t. According to the traditional control theory, we have the following assumptions.

1. Once the incomplete controller $a(t)$ is selected, a control $\tau(t)$ is given by a fixed feedback rule $\mu_{a(t)}$ depending on $a(t)$, i.e., $\tau(t) = \mu_{a(t)}(x(t))$.

2. The state transition has a Markov property, namely, the next state $x(t+1)$ is selected from a stationary distribution dependent only on the current state $x(t)$ and the control $\tau(t)$.

If a policy that selects an incomplete controller is represented by a function $\pi : x(t) \mapsto a(t)$, we have $\tau(t) = \mu_{\pi(x(t))}(x(t))$. Since μ_n for any n is fixed, $\tau(t)$ is uniquely determined by $x(t)$ and $a(t)$, so that the next state $x(t+1)$ is selected from a stationary distribution dependent on the current state $x(t)$ and a fixed policy π. Accordingly, our RL phase can be formulated as an MDP with respect to the state $x(t)$ and the action $a(t)$, by defining an immediate reward $r_{t+1} \equiv r(x(t), a(t))$, where r is the reward function.

The objective of our RL method in this MDP is to find the policy π that maximizes the following discounted return:

$$V^{\pi}(x) = E_{\pi}\{\sum_{t=0}^{\infty} \gamma^k r_{t+1} | x(t) = x\}. \quad (1)$$

$\gamma (0 \leq \gamma < 1)$ is a discount factor to prevent equation (1) from diverging. E_{π} denotes the expectation under Markov chains produced by the policy π. We define the Q-function as

$$Q^{\pi}(x, a) = r(x, a) + \gamma E_{\pi}\{V^{\pi}(x(t+1))\}, \quad (2)$$

where $x(t) = x$ and $a(t) = a$ are assumed. From equations (1) and (2), the exact Q-function must satisfy the consistency:

$$Q^{\pi}(x(t), a(t)) = r(x(t), a(t)) + \gamma Q^{\pi}(x(t+1), \pi(x(t+1))). \quad (3)$$

The error between the left-hand and right-hand sides is called the Bellman residual. By reducing the expected Bellman residual through experience, it is known that the Q-function for a given policy π can be obtained. Based on the estimated Q-function, the policy π is improved as follows:

$$\pi(x) \leftarrow \operatorname*{argmax}_{a} Q^{\pi}(x, a). \quad (4)$$

This learning method is called SARSA, which is known to converge to the optimal policy under some conditions [4][1].

3 Application

In this section, we show an application of our learning scheme to the control problem of an acrobot. The acrobot is an under-actuated robot with two links, depicted in figure 2. It is analogous to gymnast swinging on a high bar. The second joint (corresponding to the gymnast's waist) exerts torque but the first one (corresponding to the gymnast's hand) does not. Since its dynamics has strong non-linearity, it is difficult to construct a global controller for balancing an acrobot.

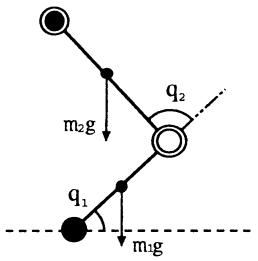


Figure 2: acrobot

Here, we define some notations. q_1 is the angle of the first link from the horizon and q_2 is the angle between the first and second links. $\dot{q}_n$ and $\ddot{q}_n$ is the angular velocity and acceleration, respectively, of the n-th link. A state of the acrobot can be represented as $x \equiv (q_1, q_2, \dot{q}_1, \dot{q}_2)$.

Since an acrobot is one of the well-known plants in the field of non-linear control, some local controllers have already been devised. If the state is very close to the unstable equilibrium state (at the upright position), an LQR controller derived from the locally linearized dynamics will be able to stabilize the state. Spong proposed two controllers to swing up an acrobot from the stable equilibrium state (at the bottom) based on the zero dynamics [5]. One is called a Σ_1 controller, which tries to rotate the second link quickly by exerting a very large torque. The other is called a Σ_2 controller, which oscillates the second link, synchronizing with the first one so that the kinetic energy increases. Although the Σ_1 and Σ_2 controllers have different strategies, both are able to swing the first link up but not to stabilize it. By making the Spong's idea be opposite, we can also construct a brake controller that attenuates the kinetic energy.

In this application, we aim to execute a swinging-up and stabilization control from the stable equilibrium state (at the bottom) by combining these four controllers with a τ_0 controller which always outputs zero torque. Computer simulation was conducted as follows. The system parameters of the acrobot were set to those in figure 3 and the torque was limited within the range between $-20(Nm)$ and $20(Nm)$. As the design phase, we constructed LQR, Σ_1, Σ_2, brake, and τ_0 controllers. As the RL phase, the immediate reward was given by a Bell-shape function that takes the maximum value at the objective upright state. The Q function was represented by the CMAC piling up 20 types of tables. An entry of each table corresponded to a state quantized by a $15 \times 15 \times 20 \times 20$ mesh grid with a random offset. A single episode was for 20 seconds and the initial state was generated from a normal distribution around the upright position, whose variance was gradually spread as the learning episode proceeded. The learning was conducted by repeating these episodes.

After about 10000 learning episodes, our scheme was able to achieve the task. Figure 4 shows the control process by the acquired controller from the bottom position. Figures 5 and 6 show the sequences of states and selected incomplete controllers, respectively, within the control sequence in figure 4. These figures show that our scheme was able to select sequentially appropriate incomplete controllers such to complete the task. Figure 7 shows the learning curve. The horizontal axis denotes the number of learning episodes, and the vertical axis denotes the performance of the acquired controller, which was evaluated by the successful rate from 100 different initial states. Here, a "success" means that the controller was able to stabilize the acrobot at the upright position within 30 seconds, starting from an initial state randomly selected within the range between $(q_1, q_2, \dot{q}_1, \dot{q}_2) = (-\pi/2, -\pi/2, -4\pi, -4\pi)$ and $(q_1, q_2, \dot{q}_1, \dot{q}_2) = (\pi/2, \pi/2, 4\pi, 4\pi)$. These results show that our scheme was able to realize stable learning and obtain a fairly good control in this task.

	first link	second link
mass(kg)	1.0	1.0
length(m)	1.0	2.0
center of mass(m)	0.5	1.0
friction coefficient	0.05	0.05
moment of inertia($kg \cdot m^2$)	0.083	0.33

Figure 3: The physical parameters of the acrobot

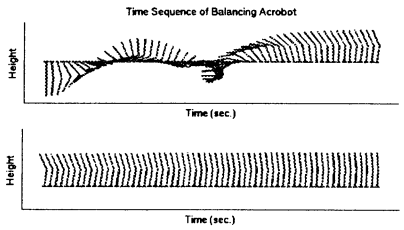


Figure 4: A typical control process by the acquired controller

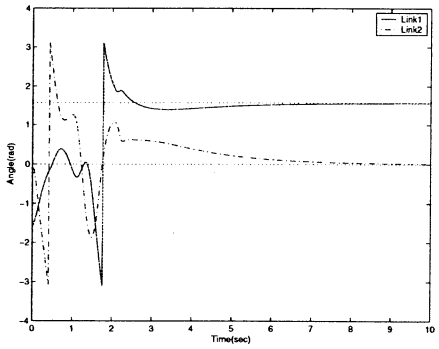


Figure 5: The sequences of q_1 and q_2 within the control shown fig.4

4 Summary

In this study, we proposed a new RL model by incorporating the control theory. We applied our model to swinging-up and stabilization control of an acrobot. The simulation result showed that our model was able to achieve the task, as well as to realize a stable learning.

However, our model still requires a large number of learning episodes. This is a critical problem when applied to tasks in a real world. In order to overcome it, we will improve the model by introducing a hierarchical structure in our future work. In addition, our scheme will be applied to the control of a real acrobot in a near future.

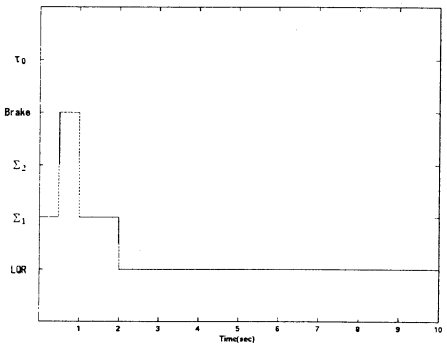


Figure 6: The sequence of selected incomplete controllers within the control shown fig.4

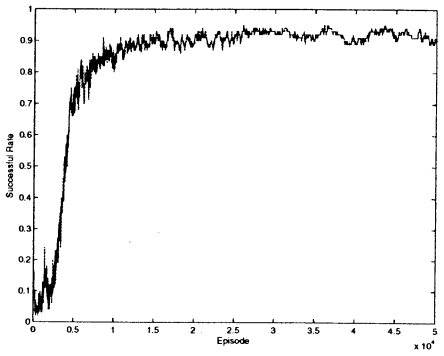


Figure 7: Learning curve

References

[1] R. S. Sutton and A. G. Barto: "Reinforcement learning", MIT Press (1998).

[2] K. Doya: "Reinforcement learning in continuous time and space", Neural Computation, **12**, pp. 219–245 (2000).

[3] G. Boone: "Minimum-time control of the acrobot", IEEE International Conference on Robotics and Automation, pp. 3281–3287 (1997).

[4] R. S. Sutton: "Learning to predict by the methods of temporal differences", Machine Learning, **3**, pp. 9–44 (1988).

[5] M. W. Spong: "The swing up control problem for the acrobot", IEEE Control Systems Magazine, **15**, pp. 49–55 (1995).

Proc. of The Ninth Int. Symp. on Artificial Life and Robotics (AROB 9th '04)
Beppu, Oita, Japan, 28-30 January, 2004

Real Time Implementation of Visual Feedback Control for Industrial Robot Manipulator

Sung Hyun Han
Division of Mechanical & Automation Eng.,
Kyungnam Univ.,
Masan, Korea, 631-701.

Dong Yean Jung, Hong Rae Kim
Dept. of Mechanical Design,
Kyungnam Univ.,
Mansan, Korea, 631-701.

Hideki Hashimoto
Institute of Industrial science
Univ. of Tokyo,
7-22-1, Roppongi, Minato Tokyo 106 Japan.

Abstract

This paper presents how it is effective to use many features for improving the speed and the accuracy of the visual servo systems. Some rank conditions which relate the image Jacobian and the control performance are derived. It is also proven that the accuracy is improved by increasing the number of features. Effectiveness of the redundant features is evaluated by the smallest singular value of the image Jacobian which is closely related to the accuracy with respect to the world coordinate system. Usefulness of the redundant features is verified by the real time experiments on a Dual-Arm Robot manipulator made in Samsung Electronic Co. Ltd..

Key words : Visual Servoing Control, Redundant Feature, Feature-Based Visual Tracking, Real Time Control.

1. Introduction

Recently, robots can perform assembly and material handling jobs with speed and precision yet, compared to human workers robots, are hampered by their lack of sensory perception. To address this deficiency considerable research into force, tactile and visual perception has been conducted over the past two decades.

Visual servoing is the fusion of result from many elemental areas including high-speed image processing, kinematics, dynamics, control theory, and real-time computing. It has much in common with research into active vision and structure from motion, but is quite different from the often described use of vision in hierarchical task-level robot control systems. Many of the control and vision problems are similar to those encountered by active vision researchers who are building robotic heads. However the task in visual servoing is to control a robot to cope with its environment using vision as opposed to just observing the environment.

Most visual servoing problems can be considered as nonlinear control problems with the gray level of each two dimensional pixel array being an observation. The difficulty of the problem is the size and the nonlinearity. The size of the observation is larger than ten thousand and they have nonlinear interaction with each other. A few researches based on the stochastic models of the two-dimension observation are found, but most visual servoing schemes uses the features of the image as the observation. To manipulate objects with complex shapes, it is important to deal with complex features such as spheres and cylinders. However, the time extracting complex features will become too long based on limited hardware. Accordingly, visual servoing scheme which utilizes many features effectively is required. Furthermore exploiting the information carefully from the features will give robust and accurate control performance [4], [5], [6].

Sanderson et al. proposed a feature-based approach and defined the Jacobian of ideal inverse interpretation which was considered as the infinitesimal change of the relative position and orientation between the camera and the object in the environment.

Newman et al. proposed an adaptive control law based on a single input single output model and a feature selection criterion were proposed [10], [11], [12]. The criterion addressed the choice of which feature should be used to control each actuator, where the number of selected features is equal to the number of the actuator. Feddema et al. [3], [4], [5], [6] also studied the selection method of the features to make the Jacobian good condition. Real time experiment of gasket tracking showed that the proper selection of features is necessary to minimize the effect of image noise.

Papanikolopoulos et al. [5], [6], [7] experimentally examined many control algorithms including Proportional-Plus- Integral, pole assignment and linear quadratic gaussian. Some adaptive control schemes were also examined in [8]. These approaches do not consider to use the redundant features which are defined as the features whose number is more than the degrees of freedom of the robot manipulator.

Chaumette el al. [8] and Espiau el al. [9] derived the interaction matrix, and introduced the concept of task function. Chaumette [2] extended the task function approach to the complex features. Jang and Bien [10] mathematically defined the "feature", and derived the feature Jacobian matrix. The authors [12] derived the image Jacobian, and used its generalized inverse and PD control to generate the hand trajectory. These schemes are based on the generalized inverse of the Jacobian. Redundant features

can be used. However, the parameters to improve the control performance are very limited and the controllability of the redundant features are not discussed.

The authors proposed a linearized dynamic model of the visual servo system and linear quadratic control scheme for redundant features [11], [13]. The controllability problem was discussed but the performance improvement by utilizing the redundant features was not presented.

This paper presents how the control performance of the feature-based visual servoing system is improved by utilizing redundant features. Effectiveness of the redundant features is evaluated by the smallest singular value of the image Jacobian which is closely related to the accuracy in the world coordinate system. Usefulness of the redundant features is verified by the real time control experiments. To illustrate the accuracy of the redundant visual servo system, real time experiments on the Dual-Arm robot with eight joints are carried out. Translation and rotation step response with three, four and five features are examined in this experiment.

2. System Modeling and Formullation

The object image moves with the joint angle to the object image, which is composed of the kinematic model and the camera model as shown in Fig.1. Suppose that a camera is mounted on the robot hand and the object does not move. The kinematic model is a map from the joint angle to a position of the camera. Since the camera is on the robot hand, the camera position is uniquely defined by the joint angle θ based on the kinematic structure of the robot. The camera model is a map from the position of the camera to the camera to the image of the object. The object image is generated by the perspective of the relative position between the camera and the object. The perspective projection is a map between two different representations of the position of the object, i.e., the representations in the camera coordinate system $[XYZ]^T$ and in the image plane $[xy]^T$.

The perspective projection with f being the focal length of the lens is given by

$$[x \;\; y]^T = [X \;\; Y]^T (f/z) \tag{1}$$

Suppose that there are n feature points, namely $p_i = [X_i Y_i Z_i]^T \;\; (i = 1,....,n)$, on an object and the corresponding positions in the image plane are $\xi_i = [x_i y_i]^T \;\; (i = 1,....,n)$. Assume that the shape and the size of the object are known and constant (i.e., the object is a rigid body). Then ξ_i for $i = 1,....,n$ become functions of the joint angle θ. Let us define a $2n$ dimensional feature vector by $\xi \cong [\xi_1^T \cdots \xi_n^T]^T$. Then the system model for n feature points is defined by the map $\psi : \mathbf{R}^m \rightarrow \mathbf{R}^{2n}$ from the joint angle θ to the feature vector ξ as follows:

$$\psi(\theta) \cong \xi \tag{2}$$

where m is the number of the joints of the robot.

Since the task must be carried out in the nonsingular region of the robot, the nonsingular region is called the operation region $\mathrm{M}_\theta \subset \mathbf{R}^m$. We restrict the robot motion in the operation region. Thus the robot Jacobian J robot is invertible in the working area. It is useful to introduce the feature manifold M, which is defined by

$$\mathrm{M} = \{\xi \in \mathbf{R}^{2n} : \xi = \psi(\theta), \theta \in \mathrm{M}_\theta\} \tag{3}$$

The features on the feature manifold is called the admissible features. If the features are admissible, then the robot Jacobian is invertible by definition. In equation (3), θ represents joint angle.

Differentiation of the system model yields

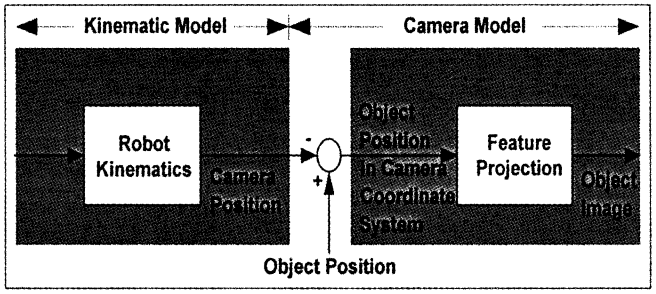


Fig. 1. System Modeling

$$\dot{\xi} = J\dot{\theta} \tag{4}$$

where the $2n \times m$ matrix J is defined by

$$J \cong \begin{bmatrix} J_{im}^{(1)} \\ \vdots \\ J_{im}^{(n)} \end{bmatrix} {}^{c}J_{ARM} \tag{5}$$

The matrix $J_{im}^{(i)}$ is given by [12]

$$J_{im}^{(i)} \cong \begin{bmatrix} -\frac{f}{z_i} & 0 & \frac{x_i}{Z_i} & \frac{x_i y_i}{f} & -\frac{x_i^2 + f^2}{f} & y_i \\ 0 & -\frac{f}{z_i} & \frac{y_i}{Z_i} & \frac{y_i^2 + f^2}{f} & \frac{x_i y_i}{f} & -x_i \end{bmatrix} \tag{6}$$

and called the image Jacobian [12]. ${}^{c}J_{ARM}$ is the robot Jacobian expressed in the camera coordinate system. Since

the vector ${}^{c}J_{ARM}\dot{\theta} \in \mathbf{R}^6$ is the linear and angular velocities of the camera expressed in the camera coordinate system, $J_{im}^{(i)}$ becomes the infinitesimal change of the position of the camera. Moreover, $J(i) \cong J_{im}^{(i)}\,{}^{c}J_{ARM}$ becomes the infinitesimal change of the features according to the infinitesimal change of the joint angles.

The degenerated features are the features for which the extended image Jacobian is not full rank. The degenerate features should be avoided because the inverse map (the map from ξ to θ) becomes singular. Thus, when the number of joints is m,

$$rank\, J(\theta) = m \quad \forall \theta \in \mathrm{M}_\theta \tag{7}$$

is required for all admissible features. To satisfy this condition $n \geq m/2$ is an obvious necessary condition, but it is not sufficient for some cases.

For example, consider a general six degree of freedom $(m = 6)$. In this case, $n \geq 3$ is necessary. If $n = 3$, $rank\, J < 6$ the camera lies on the cylinder(Fig. 2) which includes the three points and the axis of which is perpendicular to the plane containing these points. For any attitude of the camera, J is singular. Thus $n = 3$ is not sufficient and $n \geq 4$ is desirable. For the case of $n = 4$, we have the following theorem.

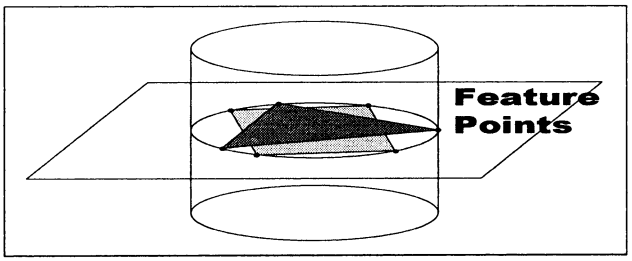


Fig. 2. Singular Cylinder

Theorem 1: Suppose that there are four points on a plane and the corresponding feature vector is admissible. Then the extended image Jacobian is full rank if any three feature points out of them are not collinear in the image plane.

Proof: Let the plane on which the four points exist be $Z = pX + qY + r$. Then Z_i satisfies $Z_i = pX_i + qY_i + r$ for $i = 1, \cdots, 4$. Substituting (1) into this yields

$$\frac{f}{Z_i} = \frac{f - px_i - qy_i}{r} \tag{8}$$

And substituting this into (6) yields

$$J_{im}^{(i)} = M_i N \tag{9}$$

where M_i and N are defined by

$$M_i = \begin{bmatrix} f & 0 & x_i & y_i & 0 & 0 & x_i^2/f & x_i y_i/f \\ 0 & f & 0 & 0 & x_i & y_i & x_i y_i/f & y_i^2/f \end{bmatrix},$$

$$N = \frac{1}{r}\begin{bmatrix} -1 & 0 & 0 & 0 & -r & 0 \\ 0 & -1 & 0 & r & 0 & 0 \\ p & 0 & 1 & 0 & 0 & 0 \\ q & 0 & 0 & 0 & 0 & r \\ 0 & p & 0 & 0 & 0 & -r \\ 0 & q & 1 & 0 & 0 & 0 \\ 0 & 0 & -p & 0 & -r & 0 \\ 0 & 0 & -q & r & 0 & 0 \end{bmatrix} \tag{10}$$

Then we obtain $J = MN\,{}^{c}J_{ARM}$, where $M = \begin{bmatrix} M_1^T & M_2^T & M_3^T & M_4^T \end{bmatrix}^T$. It is straightforward to see that

$$\det M = \begin{vmatrix} 1 & x_1 & y_1 \\ 1 & x_2 & y_2 \\ 1 & x_3 & y_3 \end{vmatrix} \bullet \begin{vmatrix} 1 & x_2 & y_2 \\ 1 & x_3 & y_3 \\ 1 & x_4 & y_4 \end{vmatrix} \bullet \begin{vmatrix} 1 & x_3 & y_3 \\ 1 & x_4 & y_4 \\ 1 & x_1 & y_1 \end{vmatrix} \bullet \begin{vmatrix} 1 & x_4 & y_4 \\ 1 & x_1 & y_1 \\ 1 & x_2 & y_2 \end{vmatrix} \tag{11}$$

Thus M is invertible because any three feature points are not collinear. On the other hand, if $p^2 + q^2 \neq 0$, the first six rows of N is linearly independent. If $p = q = 0$, the first four and the last two rows are linearly independent. Thus rank $N = 6$. finally, since all features are admissible, ${}^{c}J_{ARM}$ is invertible. Therefore, the extended image Jacobian J is full rank.

3. Analysis of Visual Servoing System

For evaluating the performance of the feature-based visual servo system, it is useful to discuss the ratio of the joint angle error to the feature vector. The following theorem shows that increasing the number of the feature point is an effective way to improve the performance.

Let the joint error be $\Delta\theta = \theta - \theta_d$ and the feature error be $\Delta\xi = \xi - \xi_d$. Define the worst joint/feature error ratio ER, called sensitivity, as follows:

$$ER = \sup_{\|\Delta\xi \neq 0} \frac{\|\Delta\theta\|}{\|\Delta\xi\|} = \frac{1}{\beta_{\min}(J)} \tag{12}$$

where $\beta_{\min}(J)$ is the minimum singular value of J. Then the sensitivity ER decreases strictly by increasing the number of non-degenerated features on the object.

Let J_n be the image Jacobian for n feature points and J_{n+1} be the image Jacobian obtained by adding an extra

feature point to the already existing feature points.

Then we have

$$J_{n+1} = \begin{bmatrix} J_n \\ J^{(n+1)} \end{bmatrix} \tag{13}$$

where $J^{(n+1)}$ is the $2 \times m$ image Jacobian corresponding to the newly added feature point. It is straightforward to see that

$$\beta_{\min}(J_n) \leq \beta_{\min}(J_{n+1}) \tag{14}$$

The equal sign holds only if each row of $J^{(n+1)}$ is linearly dependent to J_n, i.e., only if J_{n+1} is not full rank. Since we assumed that the features are not degenerated, the equal sing should be dropped. Thus adding extra feature points strictly increases the minimum singular value.

This theorem says that we can reduce the joint angle error by increasing the number of feature points.

Linearizing the model (2) with the feature vector being the state vector yields an uncontrollable model because ξ can not move arbitrarily in $\mathbf{R}^{2n}$ [13]. A simple way to avoid this problem is to map $\xi \in \mathrm{M}$ onto the tangent space of M by using the following transformation.

$$z = J_d^T(\xi - \xi_d) \tag{15}$$

where $J_d = J(\theta_d)$ is the image Jacobian at the desired point. Note that z and θ are one-to-one in the neighborhood of θ_d. The dynamics of the feature error on the tangent space of the manifold M is given by

$$\dot{z} = J_d^T J(\theta)\dot{\theta} \tag{16}$$

Thus, for a simple continuous time control law $\dot{\theta} = -Kz$ with a positive definite constant matrix K yields an asymptotic stability if $J_d^T J(\theta)$ is positive definite. It is shown that this condition is satisfied fairly large region about θ_d [13].

4. Experiments and Discussion

As shown in Fig.3, the objects are white boards with three, four and five black marks. Three points are arranged to make a regular triangle with edge length 120mm. Four points are on corners of a square with edge length 120mm. All marks are on a plane except the one of five points at the center of the square, which has height 60mm. Dual-Arm robot holds the objects and a camera(Fig.4). The world coordinate system $\omega_X - \omega_Y - \omega_Z$ is at the base of the Dual-Arm robot. A nominal camera position is almost in front of the plane on which the marks exist. To avoid the singular cylinder(Fig.2) the optical axis and the normal axis of the object plane are not aligned. The distance is about 1000mm. The features are the x and y coordinates of the center of the image of each mark. Computing their minimum singular values at the reference position gives

$$\begin{aligned} \beta_{\min} &= (J_3) = 0.35, \\ \beta_{\min} &= (J_4) = 0.65, \\ \beta_{\min} &= (J_5) = 3.60 \end{aligned} \tag{17}$$

Thus accuracy of the position control of the camera in the 3D work space will be improved by using 5 features. We carried out many step tests to this observation.

The first experiment is a step motion in vertical axis. The object is moved upward for 120mm (i.e., in ω_Z direction). The camera is controlled to keep the features at the initial positions. Thus the initial values and the reference values are the same. The object motion is considered as a disturbance for the plots of the features in the image plane. On the other hand, the object motion becomes the step change of the reference position for the plots of the camera motion in the world coordinate system. Since Dual-Arm robot has only 6 degrees of freedom, the orientation of the object changed slightly. Thus, the reference orientation is [2.8, 0, -1.8] degrees expressed in the Euler angles, say p, η, ϕ.

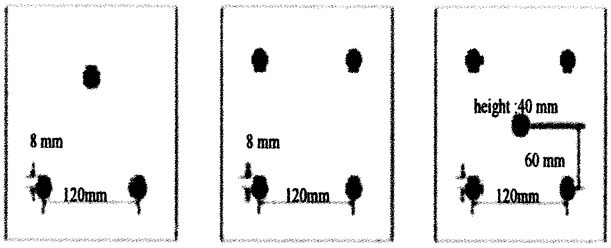


Fig. 3. Configuration of Feature Points

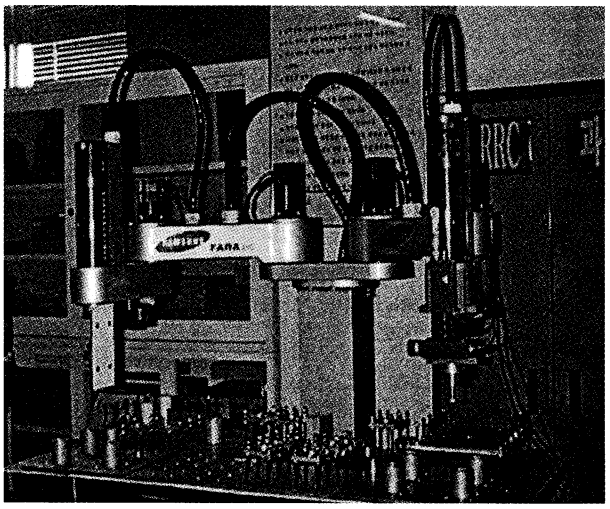


Fig. 4. Experimental Setup

Table 1. Specification of Dual Arm Robot

Content		Unit	Spec.	Remark
Workspace	1st Arm	deg	180	
	2nd Arm	deg	450	
	Z Axis	mm	150	
	R Axis	deg	±180	
Maximum Reach		mm	(350+260)	
Payload		Kg	2.5	High-speed
Max. Resultant Vel.		m/sec	5.4	1,2 Axis
Position Repeatability	Plane	mm	0.05	1,2 Axis
	Z Axis	mm	0.02	
	M Axis	deg	0.05	
Weight		Kg	200	
Coincident Control Axis No.		EA	8Axis (4+4)	

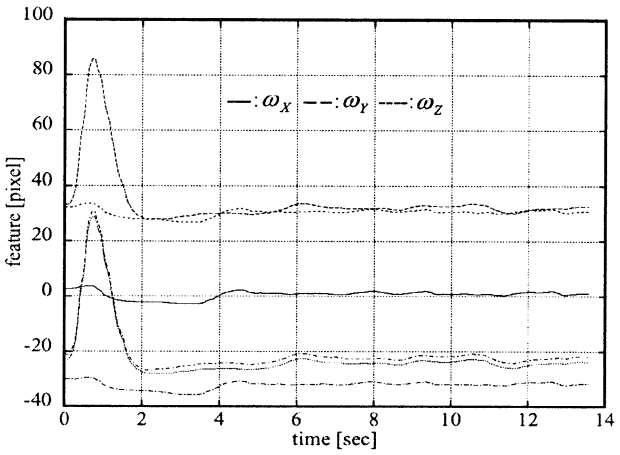


Fig. 5. Response in Image Plane for 3 Points (Vertical Step)

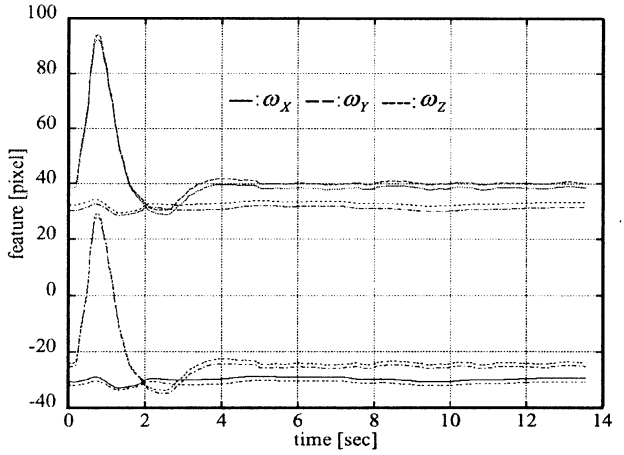


Fig. 6. Response in Image Plane for 4 Points (Vertical Step)

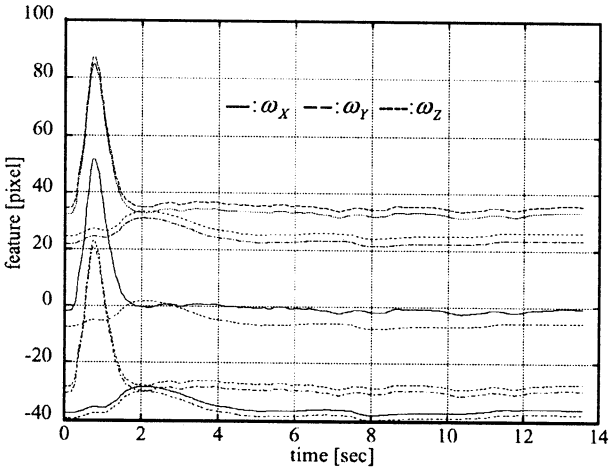


Fig. 7. Response in Image Plane for 5 Points (Vertical Step)

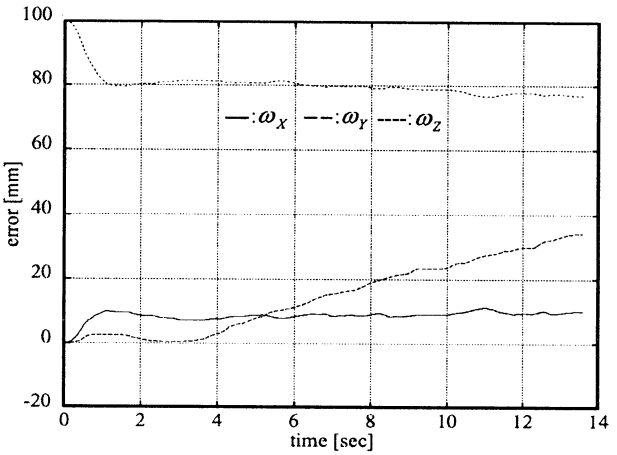


Fig. 8. Error in 3D for 3 Points (Vertical Stop)

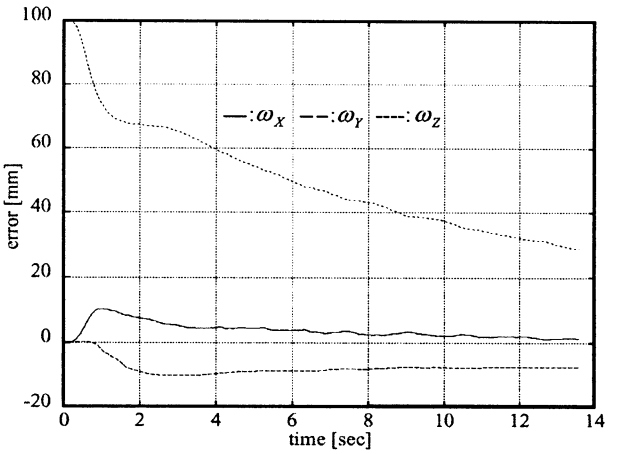


Fig. 9. Error in 3D for 4 Points (Vertical Step)

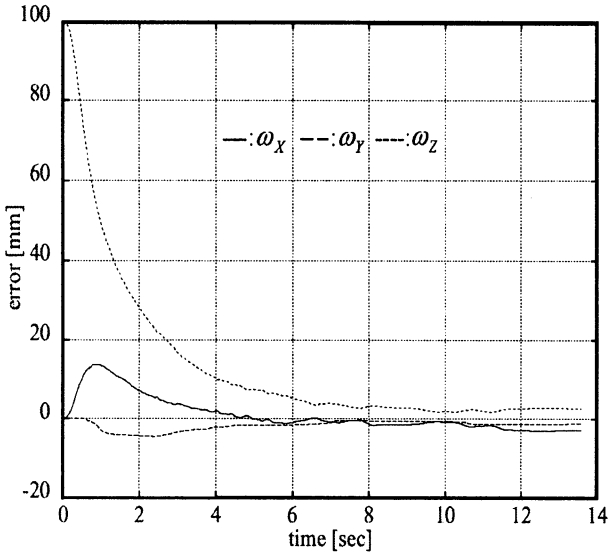


Fig. 10. Error in 3D for 5 Points (Vertical Stop)

Fig. 5 has six curves which show the x and y coordinates of the three feature points in the image plane. The horizontal axis is the time. The curves disturbed largely are the y coordinates and the others are the x coordinates. They are almost stabilized in two seconds. Fig.7 depicts the image coordinates of five points. All responses in the image plane are similar to each other.

The plots in Fig.8 depicts the position errors of the camera for three feature points (measured in the world coordinate system). The error in ω_Y direction is diverging. However, as shown in Fig.9, the response of the camera position with four feature points is stabilized. It is sluggish, and it takes more than 20 seconds to stabilize the disturbance. Fig.10 is the response with five feature points. It is improved very much for both speed and accuracy. The steady state errors are smaller than 5mm for all directions

5. Conclusions

In this paper, it has been presented how the control performance of the feature-based visual servo system is improved by utilizing redundant features. Effectiveness of the redundant features is evaluated by the smallest singular value of the image Jacobian which is closely related to the accuracy in the world coordinate system. It shows that the accuracy of the camera position control in the world coordinate system was increased by utilizing redundant features. Real time experiments on dual-arm-robot were carried out to evaluate the improvement of the accuracy and speed by utilizing the redundant features. The results verifies that the minimum singular value of the extended image Jacobian plays an important role for performance improvement of the feature-based visual servoing.

References

[1] K. Hashimoto et al., "Image-based dynamic visual servo for a hand-eye manipulator," in *MTNS-91*, Kobe, Japan, pp. 609~614, 1991.

[2] Sung Hyun Han, Man Hyung Lee, Hideki Hashimoto, "Image-Based Servoing Control of a SCARA Robot" *KSME International Journal*, Vol. 14, No. 7, pp. 782~788, 2000.

[3] P. K. Allen, A. Timcenko, B. Yoshimi, and P. Michelman, "Automated tracking and grasping of a moving object with a robotic hand-eye system," *IEEE Trans. Robotics and Automation*, vol. 9, no. 2, pp. 152~165, 1993.

[4] K. Hashimoto, T. Ebine, and K. Kimura, "Visual servoing with hand-eye manipulator—optimal control approach," *IEEE Trans. on Robotics and Automation*, vol. 12, no. 5, pp. 766~774, 1996.

[5] K. Hashimoto. T. Ebine, K. Sakamoto, and H. Kimura, "Full 3D visual tracking with nonlinear model-based control," in *American Control Conference*, San Francisco, Calif., pp. 3180~3184, 1993.

[6] L. E. Weiss, A. C. Sanderson, and C. P. Newman, "Dynamic sensor-based control of robots with visual feedback," *IEEE J. Robotics and Automation*, vol. RA-3, no. 5, pp. 404~417, 1987.

[7] J. T. Feddema and O. R. Michell, "Vision guided servoing with feature-based trajectory generation," *IEEE Trans. Robotics and Automation*, vol. 5, no.5, pp. 691~ 700, 1989.

[8] K. Hashimoto et al., "Manipulator control and with image-based visual servo," in *IEEE Int. Conf. Robotics and Automation*, Sacramento, Calif., pp. 2267~ 2272, 1991.

[9] W. Jand and Z. Bien, "Feature-based visual servoing of an eye-in-hand robot with improved tracking performance," in *IEEE Int. Conf. Robotics and Automation*, Sacramento, Calif., pp. 2254~2260, 1991.

[10] B. Espiau, F. Chaumette, and P. Rives, "A new approach to visual servoing in robotics," *IEEE Trans. Robotics and Automation*, vol. 8, no. 3, pp. 313~ 326, 1992.

[11] F. Chaumette, "Visual servoing using image features defined upon geometrical primitives," in *Proc. 33rd Conf. Decision and Control*, Lake Buena Vista, Florida, pp. 3782~3787, 1994.

[12] J. T. Feddema, C. S. G. Lee, and O. R. Michell, "Automatic selection of image features for visual servoing of a robot manipulator," in *IEEE Int. Conf. Robotics and Automation*, Scottsdale, Ariz, pp. 832~837, 1987.

[13] N. Papanikolopoulos and P. K. Khosla, "Adaptive robotic visual tracking: theory and experiments," *IEEE Trans. Automatic Control*, vol. 38, no. 3, pp. 429~445, 1993.

Proc. of The Ninth Int. Symp. on Artificial Life and Robotics (AROB 9th '04)
Beppu, Oita, Japan, 28-30 January, 2004

Quality of Cascade Operations Control Based on Uncertain Variables

D. Orski
Institute of Control and Systems Engineering
Wroclaw University of Technology
Wyb. Wyspianskiego 27, 50-370 Wroclaw, Poland
E-mail: donat.orski@pwr.wroc.pl

Abstract

The paper concerns a problem of control quality evaluation for a control plant composed of cascade operations. Execution time of each operation is described by an expert in a form of inequality containing unknown parameter. All unknown parameters are assumed to be values of uncertain variables characterized by certainty distributions. The paper contains formulation and solution of knowledge-based control problem, proposition of a control quality index, a comprehensive example illustrating the presented approach and results of simulations.

Key words: knowledge-based control, uncertain variables, operation systems

1 Introduction

A theory of uncertain variables has been developed as a tool for modeling expert's knowledge in knowledge-based decision systems ([1], [2]). During the last years many applications of uncertain variables to analysis and control in knowledge-based systems has been discussed, in particular – to control problems formulated for complex plants consisting of parallel operations (e.g. [3], [4]). The operations are considered to be resource-consuming activities, characterized by their execution times. In a traditional formulation the relationship between an amount of resource allocated to an operation and its execution time is described by a function, and the control problem consists in finding resource allocation to particular operations, minimizing execution time of the whole set of operations. In the formulation of knowledge-based control problem exact functional relationship is unknown, and instead the approximate description given by an expert and containing parameters assumed to be values of uncertain variables is used. Quality of the solution is directly connected with the accuracy of expert's description, thus evaluating quality of control based on uncertain variables seems to be important, especially, from the practical point of view. In some considerations done recently for simple control plants ([5], [6]) an approach to quality analysis employing real-life plant or its simulator, and based on evaluation of actual result of control was considered.

The purpose of this paper is to present how this approach may be applied for a more complex plant – composed of cascade operations.

In Sec. 2 a description of a set of cascade operations is introduced, and the formulation and solution of cascade operations control based on uncertain variables is presented. In Sec. 3 a method for control quality evaluation using quality index is suggested. Sec. 4 contains an illustrative example together with selected results of simulations.

2 Resource allocation in a set of cascade operations

Let us consider a complex operation plant (Fig. 1) consisting of m operations to be performed in a sequence, i.e. the execution of operation O_i begins after the execution of operation O_{i-1}, $i = 2, 3, ..., m$.

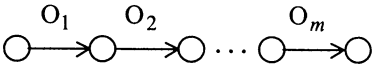


Fig. 1. Set of cascade operations.

The execution time T of the whole set of operations is given by the following formula

$$T = T_1 + T_2 + ... + T_m \tag{1}$$

where T_i, $i = 1, 2, ..., m$, denotes the execution time of the i-th operation, dependent on the amount of resource u_i allocated to the operation. The total amount of resource to be allocated is denoted by U, i.e.

$$u_1 + u_2 + ... + u_m = U. \tag{2}$$

In a traditional formulation the relationships between amounts of resource allocated to operations and their execution times are described by functions. In knowledge-based approach with uncertain variables it is assumed that although such exact deterministic descriptions exist, they are unknown. Instead we use approximate descriptions given by an expert.

Typically, they have a form of inequalities

$$T_i \le \varphi_i(u_i, x_i), \quad i \in \overline{1,m} \tag{3}$$

where the parameters x_i are unknown and assumed to be values of uncertain variables $\bar{x}_i$ described by certainty distributions $h_{xi}: R^1 \to [0,1]$ (Fig. 2.). For the particular value x_i the function $h_{xi}(x_i)$ represents the certainty index of the soft property "$\bar{x}_i$ is approximately equal to x_i", denoted by $v(\bar{x}_i \cong x_i)$.

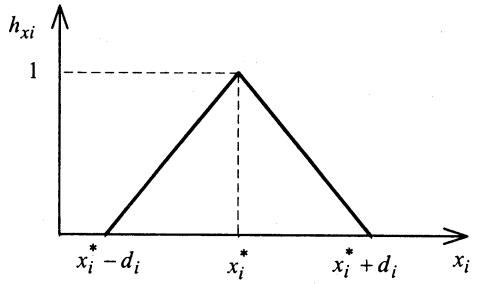


Fig. 2. Example of the certainty distribution.

In general we have a vector of uncertain variables $\bar{x} = [\bar{x}_1, \bar{x}_2, ..., \bar{x}_m]$. The user's requirement concerns the maximal possible execution time of the whole set of operations and is presented in the form of inequality $T \le \alpha$ where $\alpha > 0$.

The **allocation problem** is then formulated as follows [7]: For the given φ_i, h_{xi}, U and α find the allocation $u^* = (u_1^*, u_2^*, ..., u_m^*)$ maximizing the certainty index

$$v(u) = v\{D_y(u;\bar{x}) \tilde{\subseteq} [0,\alpha]\} = v[y(u;\bar{x}) \tilde{\le} \alpha] \tag{4}$$

that the user's requirement is approximately satisfied, where

$$D_y(u;x) = \{y \in R^1 : y(u;x) \le \alpha\}$$

and

$$y(u;x) = \varphi_1(u_1, x_1) + \varphi_2(u_2, x_2) + ... + \varphi_m(u_m, x_m)$$

denotes the maximum possible value of the execution time (1).

The solution may be found in two steps:

1. Based on the general method for calculating certainty indexes [1], on condition that $\bar{x}_1, \bar{x}_2, ..., \bar{x}_m$ are independent, one should determine $v(u)$ according to the formula

$$v(u) = \max_{x \in D_x(u;\alpha)} \min_i h_{xi} \tag{5}$$

where

$$D_x(u;\alpha) = \{x \in R^m : y(u;x) \le \alpha\}. \tag{6}$$

2. One should maximize (5) with respect to u, subject to constraints (2) and

$$u_i > 0, \quad i = 1, 2, ..., m. \tag{7}$$

3 Quality of control based on expert's knowledge

Let us assume that the exact deterministic descriptions of the operations have a form of the equations

$$T_i = k_i u_i^{-1}, \quad i = 1, 2, ..., m \tag{8}$$

where u_i is the amount of a resource allocated to the i-th operation. If the parameters k_i are known, it is easy to determine the optimal decisions $\bar{u}_i$ ($i = 1, 2, ..., m$), minimizing the execution time (1) and satisfying the constraints (2) and (7). The results are as follows

$$\bar{u}_i = \sqrt{k_i}\left(\sum_{i=1}^{m} \sqrt{k_i}\right)^{-1} U,$$

and the minimal execution time (1) is

$$\bar{T} = \left(\sum_{i=1}^{m} \sqrt{k_i}\right)^2 U^{-1}. \tag{9}$$

If the values k_i are unknown we may use the description given by an expert and apply the non-optimal decisions u_i^* introduced in the previous section. Consequently, the execution time is the following

$$T^* = k_1 (u_1^*)^{-1} + k_2 (u_2^*)^{-1} + ... + k_m (u_m^*)^{-1}.$$

For the evaluation of the result of control based on expert's knowledge a quality index

$$\frac{T^*}{\bar{T}} \triangleq Q \tag{10}$$

is proposed. The value Q evaluates the control based on the knowledge in the form of the inequalities (3) and the certainty distributions h_{xi} (i.e. the knowledge given by an expert) and consequently, evaluates the quality of an expert.

The considerations may be extended to a more general case where the operations are described by the equations

$$T_i = k_i u_i^{-a_i}.$$

The solution may be complicated from the computational point of view and may require a special numerical procedure. In the case when $a_1 = a_2 = ... = a_m \triangleq a$ the values of $\bar{u}_i$ and $\bar{T}$ are as follows:

$$\bar{u}_i = \sqrt[a+1]{k_i}\left(\sum_{i=1}^{m} \sqrt[a+1]{k_i}\right)^{-1} U,$$

$$\bar{T} = \left(\sum_{i=1}^{m} \sqrt[a+1]{k_i}\right)^{a+1} U^{-a}.$$

The quality evaluation based on the value of the quality index Q may be obtained for the given values k_i. Hence, it can be used to investigate the influence of the parameters in h_{xi} on the quality based on the expert's knowledge for the fixed values k_i and to compare the results of the control based on the knowledge given by different experts.

4 Example and results of simulations

According to the general formulation of the optimal control problem the optimal resource allocation $u^* = (u_1^*, u_2^*, ..., u_m^*)$ should maximize the certainty index (5), where $D_x(u,\alpha)$ is determined according to (6), subject to constraints (2) and (7).

Let us consider a complex of $m = 2$ cascade operations with execution times (8) characterized by an expert in a form of inequalities

$$T_1 \le x_1 u_1^{-1}, \qquad T_2 \le x_2 u_2^{-1}$$

where unknown parameters x_1, $x_2 > 0$ are described by triangular certainty distributions (Fig. 2), $x_i^* - d_i \ge 0$. In the first step of the procedure described in the previous section we obtain

$$D_x(u,\alpha) = \{(x_1,x_2): \ \frac{x_1}{u_1} + \frac{x_2}{u_2} \le \alpha\},$$

and, since $u_2 = U - u_1$, it may be shown that the certainty index (5) is given by the following formula

$$v(u_1) = \begin{cases} 1 & \text{for} \quad e(u_1) \le 0 \\ \frac{1}{d_1}[g(u_1) - x_1^*] + 1 & \text{for} \quad c(u_1) \le 0 \le e(u_1) \\ 0 & \text{for} \quad c(u_1) \ge 0 \end{cases}$$

where

$$c(u_1) = \alpha u_1^2 + (x_2^* - d_2 - x_1^* + d_1 - \alpha U)u_1 + (x_1^* - d_1)U,$$

$$e(u_1) = \alpha u_1^2 + (x_2^* - x_1^* - \alpha U)u_1 + x_1^* U,$$

$$g(u_1) = \frac{-\alpha d_1 u_1^2 + (x_1^* d_2 - x_2^* d_1 + \alpha d_1 U)u_1}{(d_2 - d_1)u_1 + d_1 U}.$$

Taking into account the different possible placements of the roots of quadratic equations $c(u_1) = 0$ and $e(u_1) = 0$ we obtain

$$v(u_1) = \begin{cases} 1 & \text{for} \quad u_1 \in D_{ue} \\ \frac{1}{d_1}[g(u_1) - x_1^*] + 1 & \text{for} \quad u_1 \in D_{uc} - D_{ue} \\ 0 & \text{otherwise} \end{cases} \quad (11)$$

where

$$D_{ue} = [\underline{u}_e, \overline{u}_e] \cap (0,U), \qquad D_{uc} = [\underline{u}_c, \overline{u}_c] \cap (0,U),$$

$$\underline{u}_e = (x_1^* - x_2^* + \alpha U - \sqrt{\Delta_e})(2\alpha)^{-1},$$

$$\overline{u}_e = (x_1^* - x_2^* + \alpha U + \sqrt{\Delta_e})(2\alpha)^{-1},$$

$$\underline{u}_c = (x_1^* - x_2^* - d_1 + d_2 + \alpha U - \sqrt{\Delta_c})(2\alpha)^{-1},$$

$$\overline{u}_c = (x_1^* - x_2^* - d_1 + d_2 + \alpha U + \sqrt{\Delta_c})(2\alpha)^{-1},$$

$$\Delta_e = (x_2^* - x_1^* - \alpha U)^2 - 4\alpha x_1^* U,$$

$$\Delta_c = (x_2^* - d_2 - x_1^* + d_1 - \alpha U)^2 - 4\alpha(x_1^* - d_1)U.$$

In the second step, after maximization of (11) with respect to u_1 we obtain the following result:

1. If $D_{ue} \ne \varnothing$ then $v(u^*) = 1$ for any $u_1 \in D_{ue}$.
2. If $D_{ue} = \varnothing$ and $D_{uc} \ne \varnothing$ then

$$v(u^*) = \frac{1}{d_1}[g(u_1^*) - x_1^*] + 1,$$

and

(i) for $d_1 = d_2$

$$u_1^* = \frac{\alpha U + x_1^* - x_2^*}{2\alpha},$$

(ii) for $d_1 \ne d_2$

$$u_1^* = \frac{2\alpha d_1 U - \sqrt{\Delta_g}}{2\alpha(d_1 - d_2)}$$

where

$$\Delta_g = 4\alpha U[(x_1^* d_2 - x_2^* d_1)(d_2 - d_1) + d_1 d_2 \alpha U].$$

3. If $D_{uc} = \varnothing$ then $v(u^*) = 0$ for any $u_1 \in (0,U)$.

For example, for the numerical data: $k_1 = 36$, $k_2 = 49$, $U = 1$, $\alpha = 120$, $x_1^* = 29$, $x_2^* = 49$, $d_1 = 20$, $d_2 = 24$, we obtain $\overline{T} = 169$ and

$$\Delta_e = -3920 < 0, \quad \Delta_c = 6496 > 0,$$

$$\underline{u}_c \approx 0.1 > 0, \quad \overline{u}_c \approx 0.77 < U,$$

$$D_{ue} = \varnothing, \quad D_{uc} = [\underline{u}_c, \overline{u}_c],$$

$$\Delta_g = 16^2 \cdot 30 \cdot 3529,$$

$$u_1^* \approx 0.42, \quad u_2^* \approx 0.58, \quad v(u^*) \approx 0.62,$$

$$T^* \approx \frac{36}{0.42} + \frac{49}{0.58} \approx 170, \qquad Q \approx \frac{170}{169}.$$

A series of simulations has been performed for the control of two operations described by deterministic models and by expert's knowledge, the same as in the example. The purpose of simulations was to investigate the influence of parameters in certainty distributions given by an expert on the quality of control. Selected results, related to case 2, obtained

for $k_1 = 36$, $k_2 = 49$, $U = 1$, $x_2^* = 49$, $d_2 = 24$ and for the different values of parameters x_1^* and d_1 in h_{x1} are presented in Fig. 3 and Fig. 4, respectively.

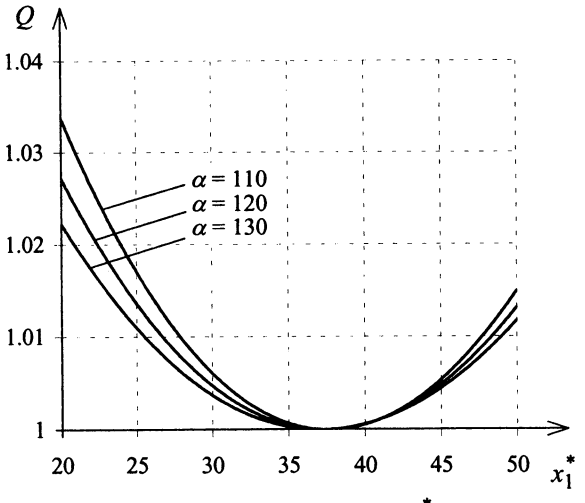


Fig. 3. Relationship between Q and x_1^* for $d_1 = 20$.

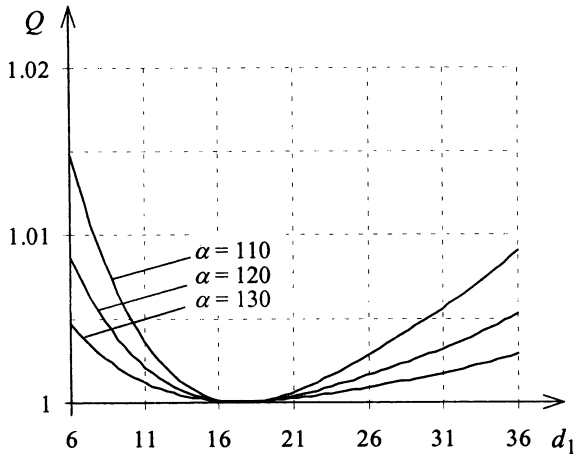


Fig. 4. Relationship between Q and d_1 for $x_1^* = 36$.

It may be observed that for wide intervals of x_1^* and d_1 quality of the knowledge-based control is high enough to be accepted (i.e. $Q \leq 1.02$). However, one can note that within these intervals parameters influence the quality index quite strongly, and that there exist optimal values of parameters, for which $Q \approx 1$. Therefore, further improvement is still possible. Another observation is that the less realistic user's requirement is, the poorer quality of control will be achieved. However, unrealistic values of α do not influence quality of control based on knowledge of a good expert, i.e. expert giving near-optimal values of parameters. Finally it should be pointed out that for $\alpha > \overline{T}$ (case 1) results of knowledge-based control may be even worse than in case 2, because there is no procedure for choosing the best control decision from the set D_{ue}.

5 Conclusions

In the paper a method for evaluating quality of control of cascade operations described by an expert in the form of inequalities and certainty distributions has been presented. In the presented example considerably good quality of control was achieved. However, the determination of the optimal decision based on uncertain variables may be very complicated for more than two operations.

The quality index proposed in the paper may be used for the investigation of the influence of parameters in certainty distributions on the control quality. It can be also used for the adaptation consisting in the minimization of Q by *step by step* changing of the parameters in certainty distributions, starting from the values given by an expert.

Interesting research problems to be taken into account during further studies could include application of the presented approach to more complex operation plants [7], e.g. to a plant of cascade-parallel structure, application of an adaptation process [6], and application of other definitions of uncertain variable [1].

References

[1] Bubnicki Z. (2002) Uncertain Logics, Variables and Systems. Springer-Verlag, Berlin-London-New York.

[2] Bubnicki Z. (2003) Analysis and Decision Making in Uncertain Systems. Springer-Verlag, Berlin-London-New York.

[3] Bubnicki Z. (2002) "Application of uncertain variables to decision making in a class of distributed computer systems." In: Proc. of 17th IFIP World Computer Congress, Montreal, 2002, pp. 261-264.

[4] Bubnicki, Z. (2002) "Application of uncertain variables in allocation problem for a complex of parallel operations." *Foundations of Computing and Decision Sciences* 27(1): 3-15.

[5] Bubnicki Z., Orski D. (2002) "A comparison of descriptive and prescriptive approach for a class of uncertain and fuzzy controllers." *Systems Science*, 28(3):19-30.

[6] Orski D. (2003) "Quality analysis and adaptation in control systems with a controller based on uncertain variables." In: Proc. of the 16th International Conference on Systems Engineering, Coventry, 2003, vol. 2, pp. 525-528.

[7] Bubnicki Z. (2003) "Application of uncertain variables to a project management under uncertainty." In: Proc. of the 16th International Conference on Systems Engineering, Coventry, 2003, vol. 1, pp. 94-99.

Proc. of The Ninth Int. Symp. on Artificial Life and Robotics (AROB 9th '04)
Beppu, Oita, Japan, 28-30 January, 2004

On the Sub-optimal Control of Certain Nonlinear Systems

William R. Wells

Mechanical Engineering Department

University of Nevada, Las Vegas

Las Vegas, Nevada 89154-4027 USA

wcube@egr.unlv.edu

Abstract

This paper considers practical means of obtaining sub-optimal solutions to the control design of a subset of nonlinear systems which are relevant to the study of robotics. Such systems are modeled by equations containing nonlinear terms as well as state dependent time delays (retarded systems). The method chosen considers the adaptation of design methods associated with linear and non retarded systems in such a way that useful results can be obtained without solving the original nonlinear system. For instance, in the case of the nonlinear regulator problem, sub-optimal nonlinear feedback gains can be computed by adapting the form of the Riccati equation for the analogous linear problem. Control designs obtained in this way are usually referred to as being based on the state-dependent Riccati equation method. For the nonlinear time-delay system a sub-optimal control law will be designed for asymptotic stability in the sense of Krasovskii using recent results obtained for the analogous linear system design. In each situation an asymptotically stable system is obtained.

Key words: nonlinear control, sub-optimal control, time-delay systems

1 Introduction

Considerable attention has been given recently to the problem of designing sub-optimal feedback control laws for certain nonlinear systems utilizing a method referred to as the State Dependent Riccati Equation (SDRE) method [1], [2]. This method is based on the concept that useful design results may be obtained for certain nonlinear systems by adapting the same structure for the feedback control law as that obtained for an analogous linear quadratic regulator (LQR) problem. The gains obtained for the nonlinear problem are state dependent and are computed from a state-dependent form of the algebraic Riccati equation.

2 Overview of SDRE technique

The nonlinear system is expressed as

$$\dot{x} = f(x) + g(x)u \tag{1}$$

where $x \in R^n$, $u \in R^m$ and $f(\cdot)$ and $g(\cdot)$ are sufficiently smooth functions and $f(0) = 0$, $g(x) \neq 0$ for all x.

The performance index to be minimized with respect to the state x and control u is

$$J = \tfrac{1}{2}\int_0^\infty [x^T Q(x)x + u^T R(x)u]dt \tag{2}$$

where $Q(x) = C^T(x)C(x) \geq 0$ and $R(x) > 0$ for all x.

In order to use the SDRE method, equation (1) is written in the state dependent coefficient (SDC) form [3].

$$\dot{x} = A(x)x + B(x)\,u \tag{3}$$

where, in general, $A(x)$ is non unique and the pair $\{A(x), B(x)\}$ is point wise controllable in the linear sense for all x in a region Ω in state space and the pair $\{C(x), A(x)\}$ is point wise observable in the linear sense for all x in Ω.

The state dependent Riccati equation design for the sub-optimal feedback controller for the nonlinear regulator problem [1], [2] is given as

$$u = -R^{-1}(x)B^T(x)P(x)x \tag{4}$$

where $P(x) \geq 0$ satisfies the algebraic state-dependent Riccati equation

$$A^T(x)P(x) + P(x)A(x) + Q(x)$$

$$-P(x)B(x)R^{-1}(x)B^T(x)P(x) = 0 \qquad (5)$$

The closed-loop matrix

$$A_c(x) = A(x) - B(x)R^{-1}(x)B^T(x)P(x) \qquad (6)$$

is Hurwitz at every $x \in R$ from Riccati theory.

3 Systems with time-delay

The mathematical model of many control systems contain state variables delayed by a constant time θ, [4]. Linear models of this type have been considered previously, for example [5], [6]. The purpose of this paper is to explore the possibility of applying SDRE methods to nonlinear problems of this type. First, some results for the control design using a linear quadratic regulator for a time-delay system are summarized.

3.1 The linear regulator problem

Consider the state equation

$$\dot{x}(t) = Ax(t) + Bx(t-\theta) + Gu(t) \qquad (7)$$

with initial function $x(t) = g(t)$, $t \in [-\theta, 0]$ and where $x \in R^n$, $u \in R^m$ and A, B and G are constant matrices. The problem is to determine the control u which minimizes the performance index

$$J = \tfrac{1}{2}x^T(t_f)M\,x(t_f) + \tfrac{1}{2}\int_0^{t_f} u^T R u\,dt \qquad (8)$$

where the final time t_f is fixed and $M = \phi^T\phi$ is a symmetric semi-positive definite matrix of rank $k \leq n$ and R is a symmetric positive definite matrix of rank m. From [5], the solution for the optimal control u for the system is

$$u = -R^{-1}(\phi\Lambda G)^T\,\phi\Lambda(t_f,t)x$$

$$-R^{-1}(\phi\Lambda G)^T\,\phi\int_t^{t+\theta}\Lambda(t_f,\sigma)x(\sigma-\theta)d\sigma \qquad (9)$$

where the adjoint matrix $\Lambda(t_f,t)$ satisfies

$$\dot{\Lambda}(t_f,t) = -\Lambda(t_f,t)A - \Lambda(t_f,t+\theta)B \qquad (10)$$

$$\Lambda(t_f,t) = 0,\ t > t_f,\ \Lambda(t_f,t_f) = I_n$$

and P satisfies the Riccati equation

$$\dot{P} = P(\phi\,\Lambda G)R^{-1}(\phi\,\Lambda G)^T P \qquad (11)$$

$$P(t_f) = I_k$$

In general, the systems given by equations (7)-(11) cannot be solved for an analytical closed form expression. Instead, numerical schemes are used.

3.2 Nonlinear SDRE approach

The analogous nonlinear form of equation (7) is written in state dependent coefficient form are

$$\dot{x} = A(x)x + B(x)x(t-\theta) + G(x)u \qquad (12)$$

$$x(t) = g(t),\ t \in [-\theta, 0].$$

The conditions on $A(x)$, $B(x)$, and $G(x)$ should be the same as those for the non-delayed problem. The performance index to be minimized is

$$J = \tfrac{1}{2}x^T(t_f)M[x(t_f)]x(t_f) + \tfrac{1}{2}\int_0^{t_f} u^T R(x) u\,dt \qquad (13)$$

The suggested form of a sub-optimal solution for the control u is the same as that given by equations (10)-(12) with the constants A, B, G, M, and R replaced with state dependent functions. Details of this approach have yet to be developed.

3.3 Other Feedback Control Design

Recently the control design or linear time-delay systems was reported in [7]. The system considered was of the form

$$\dot{x}(t) = Ax(t-\theta) + Bu(t) \tag{14}$$

with initial function $x(t) = g(t)$, $-\theta \le t \le 0$ and where $x \in R^n, u \in R$ and A and B are constant,

$B = (0,0,\cdots 0,1)$ and

$$A = \begin{pmatrix} 0 & 1 & 0 & \cdot & 0 \\ 0 & 0 & 1 & \cdot & 0 \\ \cdot & \cdot & \cdot & \cdot & 0 \\ 0 & 0 & 0 & \cdot & 1 \\ a_1 & a_2 & \cdot & \cdot & a_n \end{pmatrix}$$

A control law is sought which will stabilize the state vector to the origin and expressed as

$$u = Lx(t-\theta) \tag{15}$$

resulting in the closed loop system

$$\dot{x}(t) = (A + BL)x(t-\theta) \tag{16}$$

with characteristic equation

$$p(s) = \det\{sI - (A + BL)e^{-s\theta}\} = 0 \tag{17}$$

This system is said to be (α, r)-stable if all the solutions lie in the semi-plane $\{s : \mathrm{Re}(s) \le -\alpha, \alpha > 0\}$ defined

by the intersection of the sets

$\{s : \mathrm{Re}(s) \le -\alpha, \alpha > 0\}$ and $\{s : |s| \ge r > 0\}$.

In reference [8] it is shown that a sufficient condition to stabilize the state to the origin is to choose L according to

$$L(\alpha, \beta) = -L_0 - L_1(\alpha, \beta) \tag{18}$$

where $L_0 = [a_1 \; a_2 \; \cdots \; a_n]$ and

$$L_1(\alpha, \beta) = [\beta^n e^{-n\alpha\theta} C_n^n \cdots \beta^2 e^{-2\alpha\theta} C_n^2 \; \beta e^{-\alpha\theta} C_n^1]$$

with $\alpha, \beta > 0$ and $C_n^p = \dfrac{n!}{p!(n-p)!}$.

A possible extension of the two concepts discussed earlier would be to utilize the results given by equations (4), (15), and (18) to design a controller for the system

$$\dot{x}(t) = A(x)x(t) + \bar{A}x(t-\theta) + u \tag{19}$$

with initial conditions $x(t) = g(t), -\theta \le t \le 0$ by letting

$$u = Bv + \bar{B}w \tag{20}$$

where v is chosen to minimize the performance index

$$J = \tfrac{1}{2}\int_0^\infty [x^T Q(x)x + v^T R(x)v]dt \tag{21}$$

subject to the constraint

$$\dot{x} = A(x)x + Bv \tag{22}$$

and w is chosen to stabilize the origin of the system

$$\dot{x}(t) = \bar{A}x(t-\theta) + \bar{B}w \tag{23}$$

with initial conditions $x(t) = g(t), t \in [-\theta, 0]$ subject to the constraint of equations (15), (18), and (19).

4 Remarks

Suggestions are made as to how sub-optimal control designs for nonlinear dynamic systems can be obtained from the concepts of analogous linear systems. In particular, the systems discussed were those typically modeled by nonlinear equations containing time delays (retarded systems). The two methods chosen for discussion were the method referred to as the state-dependent Riccati equation method to handle the nonlinear terms and a design methodology recently developed to stabilize the origin of a system with time delay.

References

[1] J. Cloutier and D. Stanbey. The capabilities and art of state-dependent Riccati equation - based design. In *Proceedings of the American Control Conference,* May, 2002.

[2] M.Xin and S. Balakrishnan. A new method for sub-optimal control of a class on nonlinear systems. In *Proceedings of the 41st IEEE Conference on Decision and Control*, December 2002.

[3] P. Menor, T. Lam, L. Crawford and V. Chang. Real -time computational methods for SDRE nonlinear control of missiles. In *Proceedings of the American Control Conference*, May 2002.

[4] M. Oguztoreli. Time-lag control systems. Academic Press, 1966.

[5] G. Slater and W. Wells. A computational approach to optimal time delay systems. In *Proceedings of the 12th Automatic Control Conference of the American Automatic Control Council*, 1971.

[6] E. Jafarov. Robust sliding mode control of multivariable time-delay systems. In *Proceedings of the 16th International Conference on Systems Engineering*, September 2003.

[7] D. Tingey, K. Busawon, S. Danaher and G. Waterworth. A control design for linear time-delay systems. In *Proceedings of the 16th International Conference on Systems Engineering* , September 2003.

Proc. of The Ninth Int. Symp. on Artificial Life and Robotics (AROB 9th '04)
Beppu, Oita, Japan, 28-30 January, 2004

An evolutionary model for 3D agents integrating continuous and plastic development

Artur Matos
Graduate School of Human Informatics
Nagoya University
Nagoya, 464-8601, Japan

Takaya Arita
Graduate School of Information Science
Nagoya University
Nagoya, 464-8601, Japan

Abstract

Most of the current research in generative encodings for artificial creatures has only focused on the final matured genotypes, and doesn't take into account the developmental process itself. In this paper, we introduce a grammar based approach for generating agents with both 3D morphology and neural networks that leads to more natural developmental processes than previous approaches. This new model is based on Lindenmayer systems, but with added extensions for dealing with continuous development of limbs, and for simulating chemical interactions between development and the surrounding environment. This paper includes a detailed description of the model, as well as some results of our preliminary experiments for evolving agents that exhibit walking or other similar behaviors.

1 Introduction

Since Karl Sims' seminal work [5] on virtual creatures, significant research has been done for evolving agents with both integrated 3D morphology and neural systems. Most of the research currently being done in the field has been focusing on generative encodings, where the genotype is interpreted as instructions for building the phenotype, instead of directly mapping traits to it. Regarding these generative encodings, two distinct approaches can be observed in the current literature: the first one uses formal grammars or high-level structures for representing developmental processes (*grammar based approaches*), for example, Lindenmayer systems (LSystems). On the other hand, *cell chemistry approaches* attempt to simulate the low level interactions between cells during development, for instance, gene regulation and targeting. Although at a first glance these two approaches appear to be distinct and even opposite to each other, this division is largely artificial, and it should be possible to incorporate concepts from one approach to the other. So in this paper, we present a developmental system that although being grounded on developmental grammars, attempts to bridge between these two approaches, by introducing concepts that can easily be modeled on cell chemistry systems but that are usually not found in the grammar based ones. This new model, based on a previous one by Hornby and Pollack [1], integrates two different LSystems: Differential LSystems (Prusinkiewicz, Hammel and Mjolsness [4]) for modeling continuous processes, for instance, elongation of limbs; And Open LSystems (Mech and Prusinkiewicz [2]), for simulating chemical interactions between the developmental process and the environment.

2 The 3D agents and the environment

The agents in our model have both a 3D morphology and a simulated nervous system to control it. The 3D morphology for each agent is made of rectangular parallelepipeds connected by hinge joints, that restrict the movement of the connecting parts in one degree of freedom. The nervous system actuates on the joints by changing the speed of actuating motors present on each joint. The nervous system is a simple free form neural network, and includes sensors for the environment and joint positions, processing nodes and actuators for the joints. The processing nodes include sigmoids, linear transfer functions and sinusoid oscillators. The nodes in the neural network use standard propagation functions on the incoming connections, that is, the weighted sum of all the connections values, and are constantly active (no activation function is considered). For the sinusoid oscillator, the computed weighted sum of the incoming connections works as frequency modulator for the sinusoid, mapping the frequency in the interval $[0, 2\pi]$.

The environment simulates all physical interactions, including gravity and collision with objects. A flat ground is also simulated, extending indefinitely in the XZ plane. The simulation may include other objects

depending on the behavior that is being evolved.

3 The developmental process

Each step for the developmental process is represented by a sequence of commands indicating the morphology and neural system for the agent. The commands themselves are changed by the LSystem associated with each agent through developmental time. The commands used are similar to the ones by Hornby and Pollack [1], but extended for allowing continuous values, in order to use differential Lindenmayer Systems. The developmental commands for the morphology work as a turtle constructor, and they include: *forward(n)* for moving the turtle forward n units in the currently defined direction, creating a new stick, and connecting it to the previous existing one by a joint; *backward()* for moving the turtle cursor back to the parent stick; *right(n)*, *up(n)*, *clockwise(n)* for allowing to control the direction of the turtle, rotating in the specified direction n units, with 1 corresponding to $\frac{\pi}{2}$. Negative values can also be used for moving in the opposite direction. Finally, *revolute-1()*, *revolute-2()*, *twist-90()* and *twist-180()* change the kind of joint to be created between two successive forward commands. The revolute commands create joints over the current turtle's Z axis, with hinge stops between [0, $\frac{\pi}{2}$] for *revolute-1()*, and [$-\frac{\pi}{2}$, $\frac{\pi}{2}$] for *revolute-1()*, and *revolute-2()*, respectively. The twist commands work in a similar way, but for the X axis. The developmental commands for the nervous system work as edge encoding commands, and they are described in table 1. There are also stack commands (*push()* and *pop()*), for pushing a retrieving the current state of the turtle and neural constructor, allowing to create branched morphologies.

3.1 Representing continuous development

DLSystems are based on parametric Lindenmayer systems, but they add a differential component for modeling continuous changes. Due to space constraints, parametric LSystems themselves will not be explained here and we will focus on dLSystems instead. For a good introduction to LSystems, the reader is referred to to Prusinkiewicz and Lindenmayer [3].

The first major difference concerning dLSystems is that development doesn't occur in discrete steps, instead there is a continuous developmental time frame t. As in PLSystems, the development is iterative, but it progresses by an user specified time step, Δt. This time step is completely detached from the underlying model, so it is possible to use a different Δt in order to observe the developmental process with more or less detail, as desired.

For specifying the changes occurring as t progresses through the developmental space, two different kinds of successors are used. Continuous changes are specified by using differential equations, that relate the changes in parameters' values to the step Δt. Structural changes, or adding new limbs or nodes to the agent are specified by sequence of tokens, as in PLSystems. Discrete transitions are applied on the same way as in PLSystems, the token being replaced by the matched sequence. Depending on the time step ΔT, the LSystem interpreter may need to subdivide the interval for taking into account both continuous and discrete transitions. An example dLSystem can be seen in figure 1. In this example system, for $\Delta T = 1$, the following sequence, starting from ω would be derived: $B(1), A(0,0)$; $B(2), A(2,1)$; $B(3), B(4), C(2)$. A smaller Δt (for instance 0.5), would yield $B(1), A(0,0)$; $B(1.5), A(1,0.5)$, $B(2), A(2,1)$.

ω :	$B(1)A(0,0)$			
$B(x)$:	$x < 4$	$\rightarrow$	**solve** $\frac{dx}{dt} = 1$	(1)
	$x >= 4$	$\rightarrow$	$A(2,2), B(1)$	(2)
$A(x,y)$:	$y < 2$	$\rightarrow$	**solve** $\frac{dx}{dt} = 2$	(3)
			solve $\frac{dy}{dt} = 1$	
	$y >= 2$	$\rightarrow$	$B(x), C(2)$	(4)

Figure 1: An example dLSystem

3.2 Evolving dLSystems

Currently, our model uses a standard Genetic Algorithm for evolving dLSystems that exhibit specific behaviors, for instance, walking or jumping. Each agent is created from a random Lindenmayer System as described before, undergoes the developmental process, and then it is evaluated for the task at hand. Each genotype contains a starting axiom and an LSystem, both constrained in order to exhibit only viable growth processes. This is assured both by the random generation process and by the GA operators.

In order to model continuous development there are two different sets of commands present in the system. The first set, corresponding to the commands explained before, are used for modeling already sta-

ble processes. Another set of commands mirrors exactly the same functionality, but are used for modeling maturing processes that are still changing in developmental time. This maturing set of commands has the same name as their matured counterpart, prefixed by an "m". This separation is needed most of the times for modeling growing phenomena by using Lindenmayer Systems as pointed out by Prusinkiewicz, Hammel and Mjolsness [4].

For assuring continuity, the generated rules are always instances of the same template, working as follows: if matched, a maturing command grows linearly, until it reaches a certain threshold. After this threshold has been reached, the token is replaced by its matured counterpart, possibly with some more additional tokens added. Only linear differential equations are used. Additional constraints may be present depending on the command. An example rule for the *mforward(a)* command can be seen in figure 2.

$$
\begin{array}{lll}
mforward(x): & x < 2 & \rightarrow \quad \textbf{solve } \frac{dx}{dt} = 1 \\
& x >= 2 & \rightarrow \quad forward(a), push(), \\
& & \quad\; right(-1), \\
& & \quad\; mforward(0)
\end{array}
$$

Figure 2: An example branching pattern

In addition to this, each genotype also maintains a set of control tokens, that can be used for controlling development at a higher level. These set of control tokens (starting alphabetically from A) are not used by the morphology or neural system constructor, but they can be used for generating higher level rules of development. The rules, if generated, follow the same template as described before.

Random genotypes are first created by generating random rules and successors. Mutations occur by replacing tokens in discrete successors by random ones, by changing conditions values, tokens in the starting axiom, or by adding or deleting new rules. Crossover occurs by choosing a token from all the available commands at random, and by exchanging rules alphabetically on that point.

3.3 Interactions with the environment

We also added plasticity to this developmental model by using another LSystem extension, Open LSystems (Mech and Prusinkiewicz [2]). This extension simulates chemical inflows and outflows with the surrounding environment, allowing the developmental process to both affect or be influenced by the surrounding environment. For this, we extended our current model for the environment by adding an unary array for representing chemical concentrations, that can be read and changed both by the developmental process and by the neural controller of the matured phenotype.

Summarily, OLSystems exchange information with the environment by using special tokens called *environmental symbols*, that are processed after each developmental step takes place. In our current model, these are of the form $?E(x, y, z)$, where x stands for the kind of command used (0 for setting a chemical concentration in the environment, 1 for setting a value), y for a index in the chemical concentration array, and z for the concentration value, if in set mode. After each LSystem iteration, any generated environmental symbols are processed in sequence, and allowed to change and retrieve the values in the environment. For any commands of the form $?E(1, y, z)$, the system replaces z with the value present in the environment at that time, in order to allow the productions to access that value on the next iteration. By using these commands as left or right context in rules, it is possible to trigger different developmental paths depending on the surrounding environment.

4 Preliminary experiments

Currently, the above described system has been used for evolving developmental processes for interacting tasks, like walking or jumping. One example of an evolved creature can be seen in figure 3. The fitness function used was the distance moved by the agents in the XZ plane. The developmental process, as can be seen from a) to c), works by generating two linear branches. The final evolved creature behaves like a snake, coiling itself in the ground. The system is implemented in Java, using Open Dynamics Engine for simulating physics and collisions. The renderings are done by using Art of Illusion (a free modeler and animation tool).

Other experiments are being planed and conducted for studying developmental plasticity in the implemented model, modeling of developmental interactions between predator and preys (cyclomorphosis) and canalization.

Command	Description
offset-weight(n)	Adds or subtracts n to the weight of the current link
duplicate(n)	Duplicates the current link
loop(n)	Creates a self connecting link from the current head neuron
merge(n)	Replaces the current link and connecting neurons with the head neuron. All connections from both neurons are copied into this neuron.
next(n)	Changes the head neuron to its nth sibling if it exists
parent(n)	Changes the head neuron to its nth parent, if it exists
output(n)	Creates a new output neuron, connected to the current joint. Creates a link from this new neuron to the previous head neuron.
reverse()	Reverses the current connection
split(n)	Creates a new sigmoid neuron, creates a connection from the current head to this new neuron, and from the new neuron to the current tail. Sets the current connection to the new one.
setNodeType(n)	Changes the node type of the current neuron. 0 → linear, 1 → sigmoid, 2 → oscillator
cut	Removes the current connection

Table 1: Commands for behavior

5 Conclusion

In this paper, we introduced a new developmental model that attempts to bridge between the two main approaches previously found in the literature. It is our hope that this model will demonstrate the advantages of both approaches, and will allow to model developmental processes more naturally in simulations. The added Open LSystems component should be important for studying developmental plasticity and other issues related with development, and hopefully this should be clear with future experiments.

Acknowledgments

This research is funded with a Japanese MEXT scholarship (400000357010989).

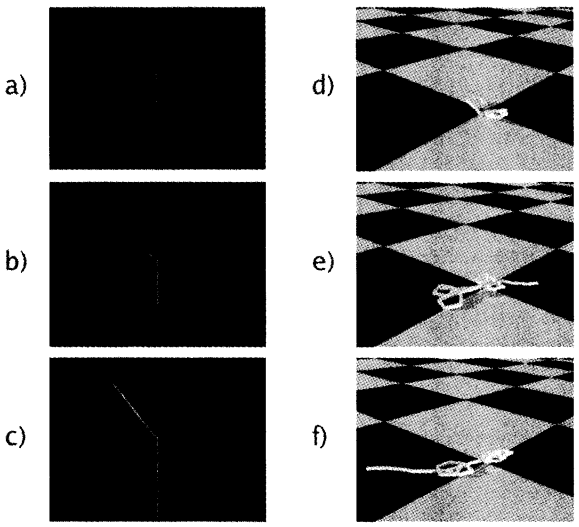


Figure 3: Development and interaction for a sample creature. a) to c) development seen from above for $t = 0.54$, $t = 0.99$ and $t = 2.33$, respectively. d) to f) The same creature, after development, interacting in the environment.

References

[1] Hornby G. and Pollack J. Creating high level components with a generative representation for body-brain evolution. *Artificial Life*, 8:223–246, 2002.

[2] Radomir Mech and Przemyslaw Prusinkiewicz. Visual models of plants interacting with their environment. In *Proceedings of SIGGRAPH 96*, pages 397–410. ACM SIGGRAPH, 1996.

[3] Prezemyslaw Prusinkiewicz and Aristid Lindenmayer. *The algorithmic beauty of plants*. Springer Verlag, 1996.

[4] Przemyslaw Prusinkiewicz, Mark Hammel, and Eric Mjolsness. Animation of plant development. In *Proceedings of SIGGRAPH 93*, pages 351–360. ACM SIGGRAPH, 1993.

[5] Karl Sims. Evolving virtual creatures. In *Siggraph '94 Proceedings*, pages 15–22. ACM SIGGRAPH, 1994.

Proc. of The Ninth Int. Symp. on Artificial Life and Robotics (AROB 9th '04)
Beppu, Oita, Japan, 28-30 January, 2004

An Evolved Learning Mechanism for Teaching a Robot to Foveate

Gabriel Gómez[1]
[1]Artificial Intelligence Laboratory
University of Zurich
Zurich, Andreasstrasse 15, CH-8050
gomez@ifi.unizh.ch

Peter Eggenberger Hotz[1,2]
[2]Emergent Communication Mechanisms
Information Sciences Division, ATR
Kyoto 619-0288, Japan
eggen@ifi.unizh.ch

Abstract

We showed in a previous work that an artificial evolutionary system (AES) whose task was to track a light source was able not only to evolve and grow a neural network, but was also able to evolve learning mechanisms. The evolved neural network was then transferred to a robotic system consistent of a camera mounted on the gripper of a robot arm with results comparable to the ones achieved by the simulation (Eggenberger et al.[1]). In this paper we continued testing the evolved controller in the real-world increasing the sensory-motor capabilities and the robot's task as follows: (a) The visual system was enhanced to detect color and movement in the environment and a proprioceptive system was added to have feedback of the arm movements. (b) The number of degrees of freedom (DOF) of the robot was increased from two to three. (c) The position of the cameras was fixed and the same underlying principles were used to teach the robot arm in front of the cameras to move a colored object from an initial location at the periphery of the visual field to the center of it. The arm could solve the task not only for two DOF, but also for three DOF.

1 Introduction

In evolutionary robotics the standard approach is to take a particular robot and use a genetic algorithm to evolve a control architecture for a particular task. Changes in the sensory-motor capabilities of the robot or in its task imply that a new control architecture must be evolved. Most of these approaches use direct genotype-to-phenotype encodings, where each synaptic weight is represented by a genetic parameter. As such an encoding scheme scales quadratically with network size, considerable effort has been put into the development of indirect encoding schemes, where the genome is a developmental program specifying processes which in their turn grow the neural structures and fine-tune the synaptic weights according to the tasks specified by the designer. Here, a more biological approach is propose to evolve large neural networks, which are able to grow and learn; in this method the genetic information no longer directly encodes for specific properties (in this case a neural network), but controls developmental processes generating the functioning structures. This will be explained in the following section. In section 3 the robustness of the learning mechanism is tested, the neural structure and its connections to the robot are described, then the experiments and results are shown in section 4 and we conclude with a discussion in the last section.

2 Evolutionary methods and developmental processes

To be able to explore both, growth and learning, the concept of selective recognition between entities, we call it "ligand-receptor interactions" played a crucially important role (Eggenberger[2]). This concept allows (a) a neuron to recognize more or less specifically another partner neuron, (b) an axon to follow cues in the environment and (c) a neuromodulator to diffuse in the environment and influence specific synapses to change their weights. In this way learning rules can be evolved and have not to be pre-specified by the designer of the system.

2.1 Growth mechanisms

By varying axonal receptor types different influences can be easily explored by the evolutionary strategy (ES) and growth patterns resulting in topological maps between interneurons and the sensory input emerged. Figure 1 illustrates the mechanisms by which the gene activities of the cells will determine the types of receptors expressed on their axons and finally determine if a source of signaling molecules has an at-

tracting or repelling influence. Similar ligand-receptor interactions will control which cells will stick together or which will build up synapses or which neuromodulator will change the synaptic weight. By varying the expression of different ligand-receptor interactions the ES can easily explore different connectivity patterns with a small load of genetic information.

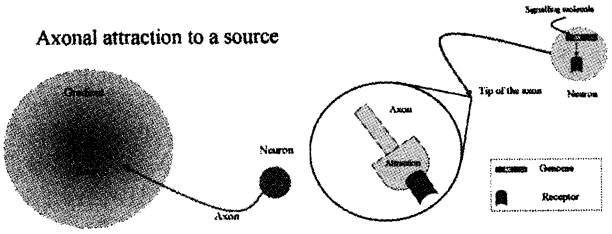


Figure 1: Overview of the most important biological mechanisms used in the proposed artificial evolutionary system.

To illustrate the proposed evolutionary approach a retinal structure was evolved, the task of the system was to evolve a neural network that could move the eye in such a way that an incoming peripheral sensory stimulus falls in the center of the "eye". The fitness function depended on the number of cells, on the movements, and on the precision of the movements measured by the deviation of the position of a stimulus from the center of the eye after peripheral stimulation. More details about how this controller was evolved and transferred to the robot can be found in the following references: Eggenberger[3] and Eggenberger et al.[1]. Figure 2 gives a schematic overview of the neural network at different stages of evolution.

2.2 Learning mechanisms

The exploration of learning mechanisms is based on the expression of artificial receptors on the synapses

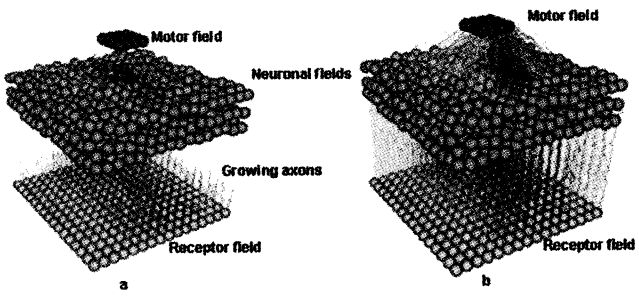


Figure 2: Schematic overview of the growing neural network. (a) Growing neural network. (b) The final neural network controlling a foveating retina.

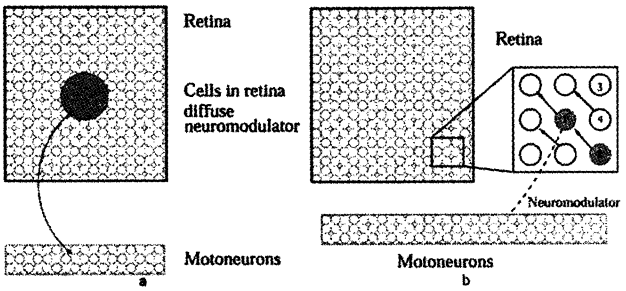


Figure 3: Two different evolved foveating systems.

and the interactions with signaling molecules.(In Ishiguro et al.[4], this concept was also explored by us to simulate the evolution of a biped robot). In general the change of the weights depends on the activity of different ligand-receptor complexes. By varying the place and time of these interactions, the ES is able to explore learning mechanisms without the need of the designer to declare a set of learning rules (e.g., Hebbian, Anti-Hebbian), because such rules can be evolved. The following example gives a solution of how a Hebbian learning rule could be evolved: Neurons can link the emission of a signaling molecule to their neural activity. Depending on their specific differentiation, the cells produce and emit signaling molecules, the synaptic weight changes if ligands emitted from other cells have a strong enough impact on the synapse. Let us suppose that a neuron emits a substance and the emitted transmitter has an affinity to one of two receptors on a particular synapse and a second neuron emits a substance for a second receptor on that synapse, then the weight will be increased in an AND fashion, a Hebbian learning rule is found. The AES evolved two neuromodulatory systems able to teach the robot about the success of its exploratory movements. The first mechanism localized in the center of the retina cells able to emit neuromodulators when they where activated. This had the effect that the system could learn to move the camera correctly (see figure 3 a). The second mechanism was more sophisticated and efficient: the neuromodulator was emitted if at any given position the movement of the robot brought the light source closer to the center (see figure 3b). This evolved mechanism is quite similar to a value system (Edelman[5], Friston et al.[6] and Sporns et al.[7]). In contrast to their hand-designed methods, where the value system is located in other brain parts, our evolved value system is located directly in the network performing the task.

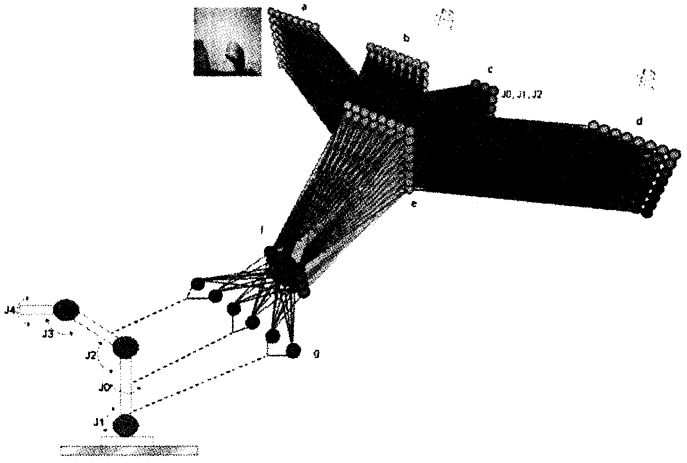


Figure 4: Neural structure and its connections to the robot arm. Neuronal areas: (a) RedColorField. (b) RedMovementToRightField. (c) ProprioceptiveField. (d) RedMovementToLeftField. (e) NeuronalField. (f) MotorField. (g) MotorActivites.

3 Testing the robustness of the learning mechanism

There is an intimate linkage between the neural controller, the sensory-motor system and the task-environment. Therefore to test the robustness of the learning mechanism we increased the sensory-motor capabilities of the robot as well as its task-environment.

3.1 Increasing the complexity of the robot's task

At the beginning of each experiment the active vision system was initialized looking at the center of the visual scene and the position of its motors were held still. The robot arm was placed at a random position at the periphery of the robot's visual field and a colored object was put on its gripper. The robot's task was then to learn how to move the arm in order to bring the object from the periphery of the visual field to the center of it.

3.2 Increasing the neural structure

In figure 4 a somewhat geometric looking overview of the evolved neural net is given, because the paths of the axons searching for their targets are omitted. The neural network was enhanced to couple with more sensory input and with more degrees of freedom of the motor system.

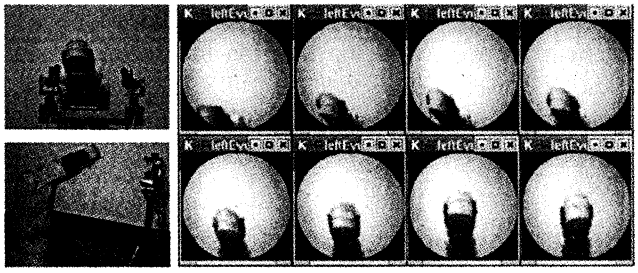


Figure 5: Robotic setup performing an experiment: moving an object from the bottom-left corner of its visual field to the center of it.

3.3 Increasing the sensory-motor capabilities of the robot

In the previous work the sensory input consisted of the intensity channel (i.e., $I = (r + g + b) / 3$) and two degrees of freedom were used. In these set of experiments we augmented the sensory-motor capabilities to use visual and proprioceptive feedback as follows: (a) A "broadly" color-tuned channel was created for red: $R = r - (g + b) / 2$. This channel yields maximal response for the fully-saturated red color, and zero response for black and white inputs. The negative values were set to zero. Each pixel was then mapped directly to neuronal units of area *redColorField* (see figure 4a) which activity was calculated as:

$$S_i = \begin{cases} 1.0 & : \ if \ R_i > \theta_1 \\ 0.0 & : \ otherwise \end{cases} \quad (1)$$

Where S_i is the activity of the i-th neuron on area *RedColorField*; R_i is the value of the red color-tuned channel for the pixel i-th; and θ_1 is a threshold value. (b) Motion detectors were created to detect movements of red objects in the environment. These motion detectors are based in the well-known elementary motion detector (EMD) of the spatio-temporal correlation type (Marr[8]). Motion detectors reacting to red objects moving to the right side of the image were mapped directly to neuronal units of the area *RedMovementToRightField* (see figure 4b) and the motion detectors reacting to red objects moving to the left side of the image were mapped directly to neuronal units of the area *RedMovementToLeftField* (see figure 4d). The activities of the neurons in these areas were calculated as:

$$S_i = \begin{cases} 1.0 & : \ if \ |EMDOutput_i| > \theta_2 \\ 0.0 & : \ otherwise \end{cases} \quad (2)$$

Where S_i is the activity of the i-th neuron; $EMDOutput_i$ is the output of the motion detector

at position i-th; and θ_2 is a threshold value.
(c) Sensors to encode the position of the joints: J0 ("shoulder"), J1 ("shoulder") and J2("elbow") of the arm were also created. See figure 4c.

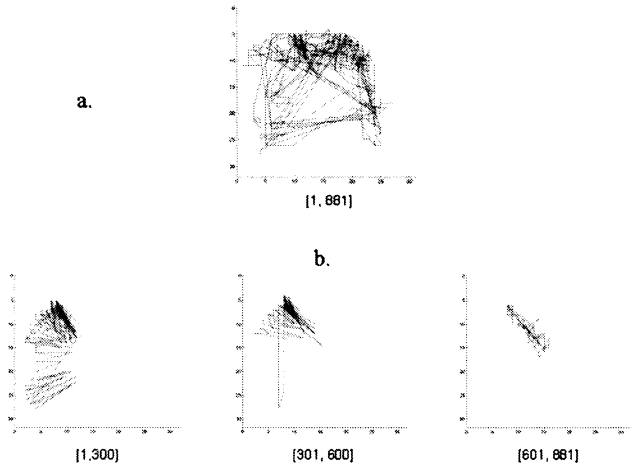


Figure 6: Position of the center of the object in the visual field during the experiments. (a) Random exploration. (b) Sensory-motor coordinated experiment.

4 Experiments and results

Our experiments were performed using the experimental setup showed in figure 5. In order to compare the effects of the learning mechanism different sets of experiments were performed. The result of a non-sensory motor coordinated experiment can be seen in figure 6a, in this experiment the learning mechanism was not activated and therefore the robot arm made only random movements without being able to solve the task. In contrast when the learning mechanism was activated, the robot was engaged in a sensory motor coordinated loop, as can be seen in the figure 6b. In this experiment the robot was able to solve the task bringing the object to the target position several times in a stabilized trajectory.

5 Discussion

With the above results we could show that the evolved learning mechanism can be transferred to a robot arm and that the task could be learned by the robot and that the eyes can teach the robot arm to bring an object to the center of the visual field. These results point to a new direction of how to overcome the reality gap: the goal should be to evolve learning mechanisms (not fixed neural networks) that can control the performance of a robot interacting with the real-world.

Acknowledgments

Gabriel Gómez was supported by the grant number 11-65310.01 of the Swiss NSF and the EU-Project ADAPT (IST-2001-37173). Peter Eggenberger was sponsored by the EU-Project HYDRA (IST-2001-33060).

References

[1] Peter Eggenberger, Gabriel Gómez and Rolf Pfeifer. Evolving the morphology of a neural network for controlling a foveating retina - and its test on a real robot. In *Artificial Life VIII: Proceedings of The Eight International Symposium on Artificial Life*, pp. 243-251, 2002.

[2] Peter Eggenberger. Evolving Neural Network Structures Using Axonal Growth Mechanisms. In *International Joined Conference on Neural Networks*, 2000.

[3] Peter Eggenberger. On Evolving a Simulated Foveating Retina. In *3D Forum: The Journal of Three Dimensional Pictures*, Vol. 15, pp. 164-169, 2001.

[4] Akio Ishiguro, Akinobu Fujii and Peter Eggenberger Hotz, "Neuromodulated Control of Bipedal Locomotion Using a Polymorphic CPG Circuit" , *Adaptive Behavior*,Vol. 11, pp. 7-17, 2003.

[5] Gerald M. Edelman. Neural Darwinism. *New York:Basic Books*, 1987.

[6] K. J. Friston, Guilio Tononi, G. N. Reeke, Olaf Sporns and Gerald M. Edelman., "Value-dependent selection in the brain: Simulation in a synthetic neural model" , *Neuroscience*,Vol. 59, pp. 229-243, 1994.

[7] Olaf Sporns and William H. Alexander, "Neuromodulation and plasticity in an autonomous robot" , *Neural Networks*,Vol. 15, pp. 761-774, 2002.

[8] David Marr. Vision. A Computational Investigation into the Human Representation and Processing of Visual Information. *W.H. Freeman & Company*, 1982.

Proc. of The Ninth Int. Symp. on Artificial Life and Robotics (AROB 9th '04)
Beppu, Oita, Japan, 28-30 January, 2004

LQ-learning Based on Self-Organizing Classification of Sequences

H. Y. Lee
Dept. of Elec. & Comm. Eng.
Tohoku Univ.
Sendai, 980-8579, Japan

H. Kamaya
Dept. of Elec. Eng.
Hachinohe Nat'l Col. of Tech.
Hachinohe, 039-1192, Japan

K. Abe
Dept. of Elec. & Comm. Eng.
Tohoku Univ.
Sendai, 980-8579, Japan

Abstract

In POMDP environments, the learning agent cannot observe the environment directly, thus partially observed states appeared. In order to overcome this partially observable problem, we had proposed a new RL algorithm, called "*Labeling Q-learning*". Unlike the original LQ-learning, for an advanced LQ-learning, some knowledge about the environment is prepared ahead of learning process. The knowledge is a kind of self-organizing clasification of sequences. It provides the classfied sequence which consist with passed states, here it is called "group". New LQ-learning agent assumes the transitions of groups tp be a landmark-like labeling situation.
In this paper, we try to extend the previous LQ-learning based on initial knowlege in more extended environment. In order to demonstrate LQ-learning based self-organizing classification of sequences, we apply it to "route-searching" in Grid-World problems shown in many literatures as a POMDP environment.

1 Introduction

Reinforcement Learning (RL) is one of Machine Learning methods and an RL agent autonomously learns the action selection policy by interactions with its environment. Unfortunately in practical problems, the agent suffers from the incomplete perception: the agent observes the state of the environments, but these observations include incomplete information of the state. This problem is formally modeled by *"Partially Observable MDP"*(POMDP)[1].
One of the possible approaches to POMDP is using the historical information of state transition to estimate states. As a simple way to add memory to the agent for state representation, the agent defines a finite-width window of history including recent observations and, if needed, actions.
Another approach is to use a hierarchical RL algorithm. Wiering and Schmidhuber[2] had proposed the interesting method, called *"Hierarchical Q-learning"*(HQ-learning). In HQ-learning, a non-Markovian task is automatically decomposed into simpler subtasks solvable by usual memoryless Q-learning. However, in order to perform, hierarchical method maintaining the learning mechanism also in a simple problem, it is considered to be a thing with much futility. We also had proposed a new type of reinforcement learning algorithm for POMDP, called "LQ-learning (Labeling Q-learning)". It has no hierarchical structure, but adopts a characteristic internal memory mechanism called "Labeling". It makes the agent define a finite-length of history sequences including recent observation and if needed, actions as a state representation. In this way, LQ-learning agent can distinguish the states that perceived as the same even though they are quite different. In previous LQ-learning, the labeling situations should be decided by the designer of systems in advance. Therefore, as the environment would be changed, the labeling situations should be changed accordingly. Actually in LQ-learning, we designed the landmark-like situation as when the two consecutive state transitions are observed different each other. This predefinition was the demerit of LQ-learning on which aim for the autonomous learning.
In the current LQ-learning based on self-organizing classification of sequences, instead of predefinition by designer, we provided the knowledge about state transitions classified by Kohonen's Self-Organizing Map (SOM).

2 Review of RL

In RL process, a learning agent receives a scalar reinforcement signal, *reward*, as a feedback performance from its environment, and updates its parameters so as to act optimally in environment. Namely, the aim of the agent is to construct an optimal action policy that maximizes the discounted cumulative reinforcement in

future:

$$\sum_{t=0}^{\infty} \gamma^t r_t, \tag{1}$$

where r_t is the reward received at step t , and γ $(0 \leq \gamma \leq 1)$ is a discount factor.
In the widely used RL approaches[1], such as *Q-learning*, *TD*, and *SARSA*, the action selection at each step is based on Q-values which are related to the goodness of actions. The Q-values are used to predict the discounted cumulative reinforcement for each state-action pair given the agent is in that state and executes that action. An environment is defined by a finite set of states S, and the agent has a finite set of actions A. In the Q-learning approach, the Q-values are estimated based on the *Temporal Difference* (TD) method. At step t, the agent observes $s_t \in S$ and executes an action $a_t \in A$. Then, as a result, the agent receives a reward r_t and the environment transits to the next state $s_{t+1} \in S$. A standard form of updating the Q-values is expressed as

$$\begin{aligned} \delta &\leftarrow r_t + \gamma Q(s_{t+1}, a_{t+1}) - Q(s_t, a_t), \\ Q(s,a) &\leftarrow Q(s,a) + \alpha \delta_t e(s,a), \quad \text{for all } s,\ a, \end{aligned} \tag{2}$$

where α is a learning rate, γ is a discount factor, and $e(s,a)$ is *Eligibility Traces*. Modified eligibility traces, known as *Replacing Traces*[1] are used here.

3 Labeling Q-learning

Here, we define the episodic (separated trial) learning task[2]. Namely, the agent is assumed to have a lifetime, T_{max}, separable into trials (or episodes). Each trial consists of at most S_{max} steps. Each trial ends in a special state called a goal "G", followed by a reset to a standard starting state "S".
In each trial, let o_t be an observation at step t. In LQ-learning process, an integer $\theta_t \in \Theta$ is attached to each observation o_t based on current and past observations, say historical memory, where $\Theta = \{0, 1, 2, \cdots, M-1\}$ (M: the number of labels). Thus, the LQ-learning agent gets an observation $\tilde{o}_t = (o_t, \theta_t) (\in \tilde{O} = O \times \Theta)$, as a new type of perception. It means that the LQ-learning agent gets the observation in its own way. Regarding the $\tilde{o}$ as a state relative, then the Q-values on $\tilde{O} \times A$ (an finite set of actions) are updated by conventional Q-learning.
In LQ-learning, the agent attached a new label when a landmark-like situation (i.e. noticeable state transition) occurred. Therefore it is very important to decide which state transition is decided as a landmark-like situation. In the previous LQ-learning, landmark-like situations are tuned by hand.

The landmark-like situation was predefined by the labeling condition parameter, *CHANGE*. *CHANGE* is defined as follows;
Let $\sigma_t = o_1 o_2 \cdots o_{t-1} o_t$, a history (string) of current and past observations, and $\tilde{\sigma}_t = \tilde{o}_1 \tilde{o}_2 \cdots \tilde{o}_{t-1} \tilde{o}_t$, a history of current and past *labeled* observations. Then we define the Boolean variable *"CHANGE"* on this history space of observations. On the other hand, the labeling function h is defined as a function on the history space of labeled observations. Then, by using *CHANGE* and LF(indicated by "h" in Eq.(3)), our labeling process is expressed simply below.

$$\begin{aligned} \theta(o_t) &\leftarrow h(\tilde{\sigma}_t) \quad \text{if } \textit{CHANGE} \text{ is True}, \\ \theta(o_t) &\leftarrow \theta(o_t) \quad \text{if } \textit{CHANGE} \text{ is False}, \\ \tilde{o}_t &\leftarrow (o_t, \theta(o_t)). \end{aligned} \tag{3}$$

In Eq.(3), the Boolean variable *CHANGE* and LFs are defined on the whole history from the initial observation at the starting state to the current observation. But we will, here, consider the case in which they are defined only on a fixed-width finite history, as stated below. $\theta(o)$ is regarded as a function from the observation space O to the label space Θ. But the value $\theta(o)$ is initialized with a default value, say "0" at starting of each trial, and labels are renewed whenever *CHANGE* is true during a trial. This means that the value of $\theta(o_t)$ is the latest label attached to the observation $o = o_t$, before time step t.
Here we used one of LF, h.

$$\text{LF} \quad h(\tilde{\sigma}_t) = min(M-1, \theta(o_t)+1). \tag{4}$$

Here M is the number of labels.
In practical problems, unfortunately, it is difficult to decide beforehand what kind of state transitions are considered as the noticeable events that serve as landmarks. In order to overcome this problem, it is necessary to find some methods of automatically acquiring the landmark-like situation, and it should be solved by introducing a method which can classify the state transition of the environment. In the next section, we will propose a new idea of LQ-learning with this classified information.

4 LQ-learning with Self-Organizing Classification

As shown in Fig.1 which shows how the sequences of state transitions are classified. Each sequence consists of 5 consecutive observations. (they are made on the basis of possible transitions in the Grid-1 shown in

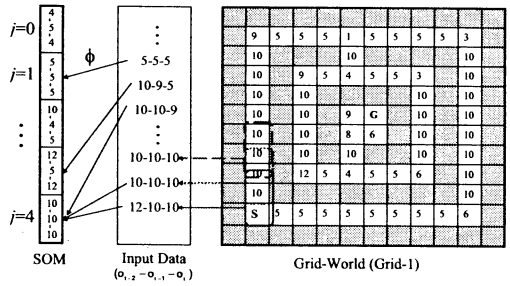


Figure 1: Example of how the sequences are classified from the environment, into groups from Grid-1; Grid-1: 12×12 maze; The number indicated in each cell means the observation value. Once the agent reaches the goal, it receives a reward of 10. Otherwise the reward is zero; the numbers written in SOM means the winner of each group.

Fig.1). During making input data, all actions of agent are selected at random except reject action which means an action such as goes back to the last state. There is no action selection rule, therefore, all input data are made from random moving of agent.
In previous paper[3], we were able to see that prior knowledge makes LQ-learning more efficient and applicable. In order to investigate availability of LQ-learning based on classified sequences, we made the self-organizing classified group, SOM_{5s}. It is composed by 5 consecutive state transitions, i.e. at step t, $o_{t-4} - a_{t-3} - o_{t-2} - a_{t-1} - o_t$.
Classification takes 100 trials to make whole input data, and in addition, each trial consists of 1000 steps (1 step is equivalent to 1 state transition). SOM algorithm computes the input data so that they optimally describe the domain of observations. In SOM_{5s}, we set the number of winner to "5", i.e., all sequences are classified to 5 groups. In order to make classified sequences, we used *SOMPAK* which is available from the site of Kohonen's laboratory. In SOMPAK, the parameters are set to as follows;

- Initialization: The size of map is 5 × 1; neighborhood function is taken to be a step function.
- Learning: At the first learning, the number of times of learning is 1000; the learning rate (notation of α in SOMPAK) is 0.05 (it decreases monotonically with the learning steps); the radius is 3. At the secondary learning, the number of times of learning is 10000; the learning rate is 0.02; the radius is 1.

From result of SOMPAK, we can see that the state transitions which completely seem to be different belonged to the same group. There would be some relevance among the elements belonging to the same group. Unlike original LQ-learning, each group has a corresponding Q-table. Let ϕ be the mapping from the sequence of observations to the groups for each sequence of observation with fixed length, the group, j is decided as follows;

$$j_{5s}(t) = \phi(o_{t-4}, o_{t-3}, o_{t-2}, o_{t-1}, o_t). \quad (5)$$

In order to formulize a new type of observation including the information about group, j, let $\bar{o} = (o, j)$ be a new observation for new LQ-learning. Therefore the observation with label, $\tilde{o}$, is newly defined by $\tilde{o} = (\bar{o}, \theta)$.
The most remarkable point of this algorithm is we define the $CHANGE$ is true, when

$$CHANGE \equiv ((j(t-2) \neq j(t-1)) \wedge (j(t-1) \neq (j(t)) \quad (6)$$

It showes that the landmark-like situation is defined only by transitions of groups. Indeed, it means that LQ-learning agent decides the labeling situation based on autonomously acquired knowledge of environments. The labeling functions for a new LQ-learning are defined like Eq.s (7).

$$\text{LF} \quad \theta(\bar{o}_t) = \min(M-1, \theta(\bar{o}_t) + 1). \quad (7)$$

5 Experiments

As mentioned above, we got the input sequences for classification in the Grid-1. In order to demonstrate the efficiency of LQ-learning, we apply it to *"route-searching problems"* in two Grid-Worlds.

5.1 Environments

We tested our LQ-learning on discretized 2-dimensional maze, called *Grid-World*. Grid-Worlds are not restricted in arrangement of obstacles, starting, and goal points, therefore huge complexity may be realized. Fig.1 and Fig.2 present Grid-1 and Grid-2 used in experiments, respectively.
In each Grid-World, shaded cells mean obstacles, and the agent can occupy any other cells in the maze. At each step, the agent can only see which of the adjacent cells are obstacles. The scalar observation value is computed by adding the value of shaded cells next to the agent, where the value of the northern, eastern, southern and western shaded cell are, 1, 2, 4, and 8, respectively.

5.2 Action Selection

The agent has four actions: go north, go east, go south, and go west, except any action that would move

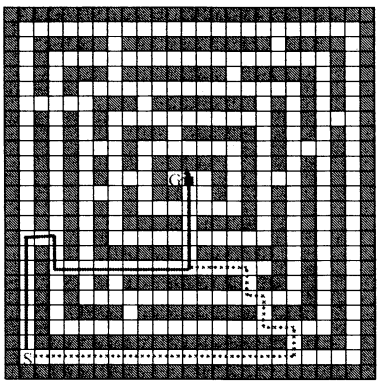


Figure 2: Grid-2; 25×25 maze; the optimal step is 28. The solid line shows the optimal route, and the dotted line means the shortest route which the agent actually learned, 38 steps

the agent into a shaded cell. We further introduce *"reject action"*, which means an action such as goes back to the last state.
The agent selects actions by ϵ-greedy rule that involves the random action selections. The value of epsilon is set to

$$\epsilon_T = (1 - \frac{T}{T_{max}})\epsilon_0, \quad (8)$$

at Tth trial, where ϵ_T is the ϵ at trial T, and ϵ_0 is the maximum value of ϵ fixed at 0.1 in our simulations.

6 Results

All results are presented by the average of 30 experiments. All LQ-learning agents learn the near-optimal routes in Grid-1. The route takes 38 steps in average. Although the optimal route is 27 steps, the LQ-learning agent decided the route with 38 steps autonomously.

In order to verify the availability of classified sequences, we applied it to a more extended and complex environment problem, Grid-2 shown in Fig.2. As shown in Fig.4, all LQ-learning agents learn the route, though learned route is far from the optimal, 212 steps. However, in Grid-2, there are many data which don't belong to any groups of SOM, then these are assumed to belong to the first group.

7 Conclusion

In this paper, we proposed a new type of LQ-learning based on self-organizing classification of sequences. In original LQ-learning, the predefinition of landmark-like situations may weaken the performance of LQ-learning in applying to general Grid-World problems. In the new LQ-learning with initial

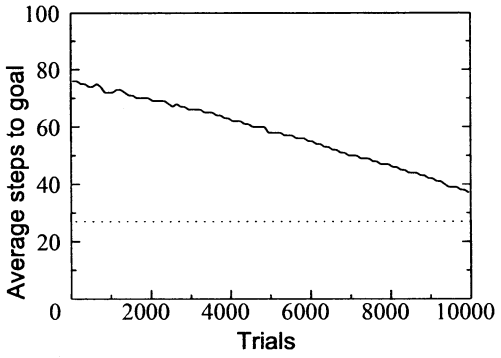


Figure 3: Result of LQ-learning in Grid-1: $T_{max} = 10000, S_{max} = 100$; The broken line shows the steps for optimal route.

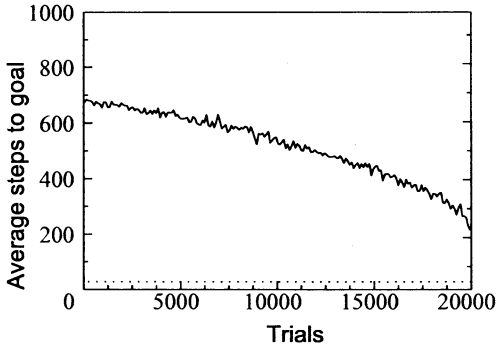


Figure 4: Result of LQ-learning in Grid-2: The broken line shows the optimal path.

knowledge of environment, it is not needed to predefine the landmark-like situation. Instead, the state transitions are classified by SOMs (in this paper) in advance. Further we can see that new LQ-learning would have possibility to adopted on a distinct environment, work well in a rather big environment. By introducing initial knowledge of environment, it would be expected to be more adaptable for learning in unknown environments.

References

[1] R. S. Sutton and A. G. Barto, "Reinforcement learning : an introduction," Cambridge, MA: MIT Press, 1998.

[2] M. Wiering and J. Schmidhuber, "HQ-learning," *Adaptive Behavior* Vol.6, no.2, 1997.

[3] H. Y. Lee, H. Kamaya, and K. Abe, "Labeling Q-learning with SOM," *Proc. of (ICCAS 2002)*, pp. 105–109, 2002

[4] T. Kohonen, "Self-Organizing Maps", Springer, 1995.

Proc. of The Ninth Int. Symp. on Artificial Life and Robotics (AROB 9th '04)
Beppu, Oita, Japan, 28-30 January, 2004

Occurrence of state confusion in the learning of communication using Q-learning

Masanobu Nakanishi, Masanori Sugisaka, Katsunari Shibata
Dept. of Electrical and Electronic Engineering, Oita University
700 Dannoharu Oita 870-1192 Japan

Abstract

The learning of one-way communication between two agents using Q-learning was investigated. A transmitter agent learned what communication signals should be transmitted and a receiver agent learned to generate appropriate actions from the signals. We discovered that when there exists a non-looped branch in the receiver's state transition, and the optimal action in a detour is the same as the optimal one in a state closer to the goal on the optimal path, there is a possibility that the receiver cannot take the optimal path because of state confusion. The main reason why the receiver agent falls into the state confusion can be considered that it is not reinforced for the transmitter agent to learn to transmit the state value to the receiver agent.

1. Introduction

Communication has a very important role in collision avoidance, cooperative action and the supplement to insufficient observation in multi-robot and multi-agent systems. In order to learn a purposive communication autonomously, evolutionary method[1] or reinforcement learning[2][3][4] has been used. A kind of simulation that shows autonomous acquisition of one-way communication to supply the receiver's insufficient observation was employed. However, it was not examined what kind of information should be transmitted, or whether the optimal communication can be acquired in any cases.

We have investigated what communication signals a transmitter agent should learn to transmit and whether a receiver agent can learn to generate appropriate actions from the signals. We discovered the case in which a receiver agent falls into POMDP(Partially Observable Markov Decision Process) and its action does not become optimal one because of state confusion that is caused by the communication signal obtained by reinforcement learning. In this paper, some simulation results are introduced, and it is considered empirically why and on which condition the state confusion happens and blocks to learn the optimal path.

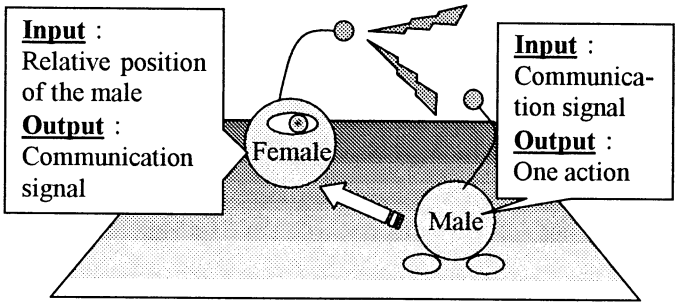


Fig.1 Learning of one-way communication

2. Learning of one-way communication

2-1 Task description

In this paper, the learning of one-way communication that supplies the receiver's insufficient observation is focused on. The simulation environment was decided referring to [1][2]. Fig.1 shows the image of one-way communication learning. Two agents called a male and a female are assumed in a discrete environment. The male can move, but does not have sight. On the other hand, the female can't move, but can transmit some signals to the male. The female's input is the relative position of the male, and it's output is a communication signal. The male's input is the communication signal and its output is an action. If the male touches the female, a reward is given to the both agents. The meaning of the communication signal is not given to either agent at all beforehand. Therefore, a transmitter agent has to learn what communication signal should be transmitted and a receiver agent has to learn to generate appropriate actions from the signal. If some common language can be built up between the male and the female, the contact can be repeated efficiently.

2-2 Learning method for the both agents

For the learning of the both agents, Q-learning is used. In Q-learning, the state-action pair is evaluated, and the evaluation value is called Q-value. An agent chooses an action with the probability calculated from the Q-values. It is performed on a discrete environment and action space.

The algorithm of Q learning is as follows.

(1) An agent observes a state.
(2) The agent selects and executes an action.
(3) The agent observes the state after the transition.
(4) A reward r_{t+1} is received from the environment.
(5) Q-value is modified as

$$Q(s_t,a_t) \leftarrow (1-\alpha)Q(s_t,a_t) + \alpha\left[r_{t+1} + \gamma \max_a Q(s_{t+1},a)\right] \quad (1)$$

where α is a learning rate $(0 < \alpha \leq 1)$
γ is a discount factor $(0 \leq \gamma < 1)$

(6) t -> $t+1$, and it is returned to the step(2).

For the female, the state s is the male's relative position, and the action a is the communication signal. For the male, the state s is the communication signal, the action a results in a state transition, and α is 0.1, γ is 0.9 and all the initial Q-values are 0 here.

2-3 Action selection

An action is selected using Boltzmann selection here. When the state is x, the probability of the action a is calculated as,

$$p(a \mid x) = \frac{\exp(Q(x,a)/T)}{\Sigma_{i \in A} \exp(Q(x,i)/T)} \quad (2)$$

where A is a set of actions, and T is a temperature coefficient. An action is selected randomly when T is large. As opposite to it, when T is close to 0, a little difference of Q-value has great influence on the action selection, in other words, the action selection is almost greedy. In this simulations, the initial value of T is 1.0, and it is gradually decreased exponentially to 0.01 in 80% of trials. In the rest of trials, it was fixed at 0.01.

2-4 Flow of the learning

These agents act in accordance with the following cycle.

(1) The female detects the male's state.
(2) The female's Q-value at t-1 is modified.
(3) The female transmits a signal to the male.
(4) The male receives the female's signal.
(5) The male's Q-value at t-1 is modified.
(6) The male makes an action.
(7) If the both agents touch each other, the trial finishes, and they get a reward. In that case they learns their Q-value at t with $\max Q(s_{t+1},a) = 0$ according to Eq.(1) and the flow returns to (1). If the trial finished, t=0, otherwise t->t+1.

The step(2)(5) is not executed when t=0.

3. Simulation

3-1 Case1

At first, an example, in which the agent could not learned the optimal path, that we found, is introduced.

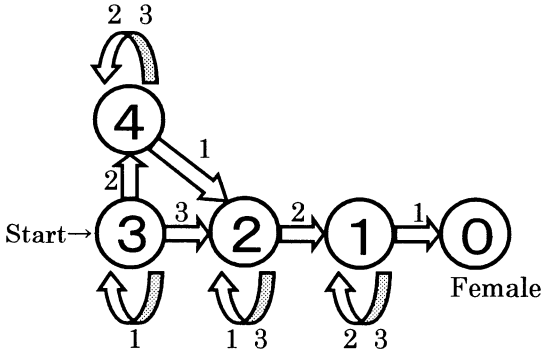


Fig.2 Simulation environment 1

The diagram of the male's state transition is shown in Fig.2. A number in the circle indicates the state, and an arrow indicates a state transition that is always deterministic. The male can take one of three actions(1,2,3), and the number along the arrow indicates the taken action. The female's input is the male's present state(one of from 0 to 4), and the female's signal has four kinds(from 1 to 4). On the other hand, the male's input is the communication signal from the female. Therefore, the number of the signals is more by one than that of the actions. The male's initial state is 3, and the state 0 is the goal where the female exists. If the male reaches the state 0, a reward is given to the both agents, and then the male is located on the initial state 3 again. A trial is defined as a sequence from the initial state to the goal.

Q-values of the both agents after 10000 trials of learning are shown in Table 1. The maximum Q-value for each state is hatched in the table. From the table, it can be seen that the female transmits the signal 2 on the state 1 or 4, and it transmits the signal 1, 3 or 4 on the state 2 or 3. On the other hand, the male selects the action 2 on the signal 1, 3 or 4, and it selects the action 1 on the signal 2.

Since, the male selects the action 2 on the state 3, the optimal action could not be learned even though the number of the signals is more than that of the male's actions. Even when the number of the communication signals is increased, the agents still could not learn the optimal path, because one of the communication signal

was assigned to the action 1, and the other signals are all assigned to the action 2 in the male. The process that the agents learned non-optimal action has been considered as shown in Fig.3.

Table 1 Q-value after learning

Female's Q-value [state][signal]	Male's Q-value [signal][action]
f_q[1][1]=0.610	m_q[1][1]=0.677
f_q[1][2]=1.000	m_q[1][2]=0.754
f_q[1][3]=0.727	m_q[1][3]=0.678
f_q[1][4]=0.670	m_q[2][1]=0.849
f_q[2][1]=0.900	m_q[2][2]=0.699
f_q[2][2]=0.794	m_q[2][3]=0.680
f_q[2][3]=0.900	m_q[3][1]=0.678
f_q[2][4]=0.900	m_q[3][2]=0.757
f_q[3][1]=0.729	m_q[3][3]=0.678
f_q[3][2]=0.653	m_q[4][1]=0.677
f_q[3][3]=0.729	m_q[4][2]=0.758
f_q[3][4]=0.729	m_q[4][3]=0.683
f_q[4][1]=0.726	
f_q[4][2]=0.810	
f_q[4][3]=0.729	
f_q[4][4]=0.728	

State 1 When the female transmits a signal A, the male learns to select the action 1 and reaches the goal, then the female also learns to transmit the signal A.

↓

State 4 Female learns to transmit the signal A because the male chooses the action 1 when the female transmit the signal A.

↓

State 4 The value of the state 4 increases for the male because it receives the same signal at the state 1.

↓

State 3 The male learns to choose the action 2 because the value of the action 2 is higher than the action 3.

↓

Agents could not learn the optimal path.

Fig.3 Considered process by which non-optimal path was learned.

From this, the main problem is that the signal which represents the state value was not reinforced. Furthermore, all the signals except for the one signal are assigned to the action 2 in the male. The reason is considered as follows.

(1) State 2: When the female transmits a signal B which is not A in Fig.3, the male chooses the action 2, and learns to move to the state 1.

(2) State 3: The female learns to transmit another signal C except for A or B because the female wants the male to take the action 3.

(3) State 3: The male learns to choose the action 2 even if it receives the signal C because the evaluation value of the state 4 is higher than that of the state 2 due to the state confusion as shown in Fig.3.

(4) State 3: The Q-value for the signal C goes down, and the female comes to transmit the signal D.

Then, the male learns to allocate all the signals except for the signal A to the action 2 by repeating (2), (3), (4).

3-3 Case 2

Next, an example in which the optimal actions can be learned in a similar environment to that in the case 1 is shown in Fig.4. Some important Q-values are also shown.

Female's Q-value f_q[state][signal]	Male's Q-value m_q[signal][action]
f_q[2][1]=0.900	m_q[1][1]=0.667
f_q[2][2]=0.793	m_q[1][2]=0.743
f_q[2][3]=0.900	m_q[1][3]=0.671
f_q[2][4]=0.900	m_q[3][1]=0.667
f_q[3][1]=0.770	m_q[3][2]=0.743
f_q[3][2]=0.616	m_q[3][3]=0.672
f_q[3][3]=0.742	m_q[4][1]=0.667
f_q[3][4]=0.748	m_q[4][2]=0.743
	m_q[4][3]=0.674

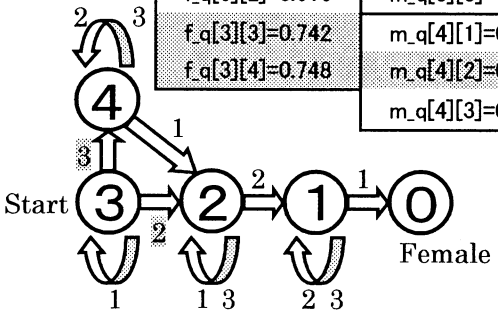


Fig.4 Simulation environment 2

Between the case 1 and case 2, only the state transition from the state 3 is different. In this environment, when the male selects the action 2, it moves to the state 2. When it selects the action 3, it moves to the state 4. The action and state transition pair is inverted from the environment 1 as shown in Fig.2.

Though there is non-looped branch in the receiver's state transition and the optimal action in the state 4 on the detour is the same as the optimal one in the state

1 that is closer to the goal on the optimal path, the male could learn the optimal path to the goal. The reason why the agent could learn is that the optimal action in the state 3 is the same as the optimal one in the state2 that is closer to the goal on the optimal path.

From the above, it is suggested that the agent sometimes can learn the optimal actions even if there exists a non-looped branch in the receiver's state transition and the optimal action in a detour is the same as the optimal one in a state closer to the goal on the optimal path.

3-2 Case 3

Finally, the case in which non-looped branch does not exist.

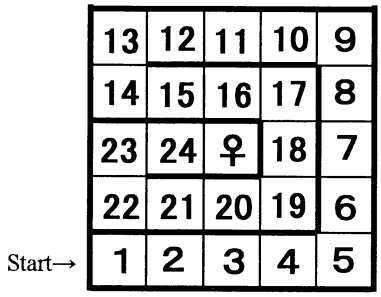


Fig.5 Simulation environment 3

Here, a simulation environment consisting of 25 discrete states as shown in Fig.5 is assumed. A bold line shows a wall. The male starts at the state 1, and female in the center square. The male's action has four kinds, and the male moved to the next cell in each of 4 directions. When the action to go to the wall is selected, the agent does not move.

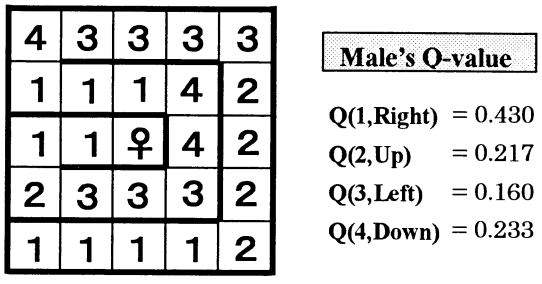


Fig.6 Result of simulation environment 3

The number in each square in Fig.6 is the communication signal assigned by the female after learning. These signals became correspond to the optimal action to the goal, such that the agent should go to the right when the signal is 1. This environment becomes POMDP for the male due to the state confusion.

After learning the Q-values of non-optimal action in each state becomes almost 0, and the optimal path could be learned. The reason might be that if the agent selects a looped branch, it will return to the state again, and that results in the decrease of the Q-value corresponding to the looped branch. Therefore, it can be thought that if there is no branch except for a loop the optimal actions could be learned, even if the state value that is closer to the goal is smaller due to the state confusion.

4. Conclusion

In this paper, it was shown that when there exists a non-looped branch in the receiver's state transition, and the optimal action in a detour is the same as the optimal one in a state closer to the goal on the optimal path, there is a possibility that the receiver cannot take the optimal path because of the male's state confusion. Then, the main factor for this problem might be that the transmitter agent's signal is not reinforced to represent the state value. It was also suggested that there is a possibility that the optimal action could be learned even if state confusion happened on the optimal path, if there is no branch except for a loop even if it happens that the evaluation value of a state that is closer to the goal is smaller due to the state confusion.

The method by which the transmitter learns to send a signal representing the state value has to be developed in the future research.

Acknowledgement

This research was partially supported by the Japan Society for the Promotion of Science, Grants-in-Aid for Scientific Reearch, #14350227 and #15300064.

Bibliography

[1] G.M. Werner & M. G. Dyer : Evolution of Communication in Artificial Organizing System, Proc.of Artificial life II, 1-47(1991)

[2] N.Ono, T. Ohira, and A. T. Rahmani: Emergent Organization of Interspecies Communication in Q-Learning Artificial Organism,*Advances in Artificial Life*, pp. 396-405 (1995)

[3] K. Shibata and K. Ito: Learning of Communication for Negotiation to Avoid Some Conflicts of Interests-Learning of Dynamic Communication Using a Recurrent Neural Network-Trans. of SICE Vol.35, No.11, 1346-1354 (1999) (in Japanese)

[4] K. Shibata and K. Ito Emergence of Communication for Negotiation by a Recurrent Neural Network, Proc. of ISADS '99, pp, 294-301. (1999)

Proc. of The Ninth Int. Symp. on Artificial Life and Robotics (AROB 9th '04)
Beppu, Oita, Japan, 28-30 January, 2004

Molecular basis underlying social behaviors of honeybees

Hideaki Takeuchi

Department of Biological Sciences, Graduate School of Science, University of Tokyo,

Bunkyo-ku, Tokyo, 113-0033, Japan

E-mail: takeuchi@biol.s.u-tokyo.ac.jp

Abstract

Mushroom bodies (MBs) are insect brain structures that are important for memory, learning, and higher-order sensory processing for different sensory modalities. Honeybee MB function is believed to be closely associated with their social behaviors for the following reasons: 1) Honeybee MBs are more prominent compared with those of other insects. 2) Honeybee MBs have a high degree of structural plasticity and the volume of the neuropil varies according to the division of labor. To clarify the molecular basis underlying the honeybee MB neural function, we utilized molecular biology methods (Differential display method, DNA microarray and MALDI-TOF MS) and identified genes selectively expressed in the MBs in the honeybee brain.

Keyword: Honeybee, social behavior, molecular biology, mushroom body

1. Introduction

The honeybee *Apis mellifera* L. is a social insect, and colony members perform various exquisite communications and division of labor to maintain colony activities. For example, workers inform the other foragers of information related to both the distance and direction of a food source using dance language. The honeybee has three types of adults; queens (reproductive caste), workers (labor caste), and drones. Female honeybees have a genetically equal potential to differentiate into two castes (queens or workers) and nutritional factors (the amount of royal jelly and honey fed in the early larval stage) determine their differentiation fate into these two castes. In the honeybee colonies, queens and drones are fed by the workers and have unique specializations, particularly in association with reproduction. The workers are sterile and perform diverse tasks to maintain their colony activity. The life span of a worker bee is usually 30 to 40 days and their functional role changes dependent on their age after eclosion (age-polyethism). Young workers (nurse bees) labor at in-nest jobs such as cleaning,

brooding, and nursing, while older ones (forager bees) forage for nectar and pollen. The molecular basis of honeybee social behavior, however, is largely unknown.

Mushroom bodies (MBs) are involved in higher-order sensory processing for different sensory modalities and are important structures for memory formation in the insect brain. The MBs of the aculeate *Hymenoptera*, including the honeybee, are more prominent compared with most other insects. In the honeybee, each MB has two calyces composed of 170000 Kenyon cells, the intrinsic MB neurons. In contrast, in the fruit fly there are only approximately 2500 Kenyon cells per hemisphere. The honeybee MBs are composed of two morphologically distinct large- and small-type Kenyon cells (6–7 and 4–5 μm in diameter, respectively). The dendritic projection pattern are also different among these Kenyon cell types. The large-type Kenyon cells receive projections from olfactory and optic neurons at the lip or collar zone, respectively, of the calyces. The small-type Kenyon cells receive projections at the basal ring and collar zones. The honeybee MBs have a high degree of structural plasticity and the volume of the neuropil varies according to the division of labor. These observations suggest that MB function is closely associated with honeybee social behavior. In our research, to identify genes involved in the intrinsic function of the MBs, we searched for genes expressed preferentially in the MBs of the worker honeybee brain.

2 Summary

2.1 Identification of mushroom bodies selective genes using differential display method

To clarify the molecular basis underlying the honeybee MB neural function, we performed differential display/ DNA microarray analysis and identified 36 genes preferentially expressed in the honeybee MBs. Five of them encoded components of the Ca^{2+}-signaling pathway [1], [2], which is involved in neural plasticity. Based on these findings, we proposed that the Ca^{2+}-signaling function and thus the synaptic plasticity of the MB neurons are enhanced in the honeybee brain. We also identified a novel gene, termed *Mblk-1*, encoded a transcription factor with two DNA-binding motifs [3]. Its structure is conserved among the animal kingdom. The transcriptional activity of Mblk-1 can be modulated by ras/ MAPK signaling pathway, which is also involved in neural plasticity. Most of the identified cDNA clones corresponded to 3'-untranslated regions, and identification of proteins encoded by these genes is now in progress. These MB-preferential genes would be promising candidates for genes involved in neural/ behavioral plasticity and associated with honeybee social behaviors.

2.2 Neuropeptides in the honeybee mushroom body

From nematoda to vertebrate, neuropeptides are important for the modulation of social behaviors. In nematoda, the *npr-1* gene, which encodes a G-protein-coupled receptor that is structurally related to the mammalian neuropeptide Y receptor, is involved in social feeding behavior. In vertebrates, nine-amino-acid peptides (nonapeptides), which includes oxytocin and vasopressin, are involved in the regulation of social behavior and/or sex-specific behavior. However no neuropeptide in the honeybee brain has not been identified. To search for possible neuropeptides modulating honeybee MB function, we used matrix-assisted laser desorption/ionization with time-of-flight mass spectometry (MALDI-TOF/ MS) and identified tachykinin-related neuropeptides (*Am*TRPs) from the honeybee MB regions [4]. Although *in vivo* function of insect TRPs remains unclear, TRPs have been identified in various insects. Interestingly in blowfly, locust, cockroach, and fruit fly brain, localization of TRPs in the intrinsic MB neurons (Kenyon cells) has not been reported. *In situ* hybridization of *AmTRP* gene demonstrated preferential expression of the *Am*TRP gene in the MB (Kenyon cells) in the honeybee brain, suggesting that its MB expression might be characteristic of the honeybee. Next, to examine whether the expression of *AmTRP* gene changes depending on the age-polyethism, we performed Northern blot analysis of RNA from the head of nurse and forager bees. It showed that expression of the prepro-AmTRP gene in the head changes depending on age/division of labor of the honeybees. Considering that *Am*TRP gene expression was enhanced in the MBs, which are believed to be associated with social behavior, and the prepro-*Am*TRP transcript levels vary according to age and/or division of labor of the workers, *Am*TRP is a good candidate neuropeptide involved in the social behavior of honeybees.

Footnote

This paper is a review originally based on the previous published papers.

Acknowledgements

I thank Drs. A Yasuda, Y Yasuda, and T Nakajima (Suntory Institute for Bioorganic Research) for MALDI-TOF/MS analysis; A Kato, and A Tsujimoto (DNA chip research Inc.) for DNA microarray analysis. I thank very much R Paul, T Fujiyuki, K Shirai, Y Matsuo, Y Hayashi, E Kage, M Sawata, S Hori, T Kunieda and T Kubo (University of Tokyo) for their collaboration.

References

[1] Kamikouchi A, Takeuchi H, Sawata M et al. Concentrated expression of Ca^{2+}/ calmodulin-dependent protein kinase II and protein kinase C in the mushroom bodies of the brain of the honeybee *Apis mellifera* L. (2000) J. Comp. Neurol. 417: 501-510

[2] Takeuchi H, Fujiyuki T, Shirai K et al. Identification of genes expressed preferentially in the honeybee mushroom bodies by combination of differential display and cDNA microarray. (2002) FEBS lett. 513: 230-234

[3] Takeuchi H, Kage E, Sawata M et al.Identification of a novel gene, *Mblk-1*, that encodes a putative transcription factor expressed preferentially in the large-type Kenyon cells of the honey bee brain. (2001) Insect Mol. Biol. 10: 487-494

[4] Takeuchi H, Yasuda A, Yasuda-Kamatani Y et al.. Identification of a tachykinin-related neuropeptide from the honeybee brain using direct MALDI-TOF MS and its gene expression in worker, queen, and drone heads. (2003) Insect Mol. Biol. 12: 291-298

Proc. of The Ninth Int. Symp. on Artificial Life and Robotics (AROB 9th '04)
Beppu, Oita, Japan, 28-30 January, 2004

Random-walk evolution of protein-sequences analyzed in multi-dimensional pseudo-euclidean sample space spanned by principal coordinate axes. A study towards constructing multi-dimensional evolutionary tree

[1]Koji Ohnishi and [2]Naotaka Furuichi .
[1,2]Center for Transdisciplinary Research ([1]Dept .of Biology, Fac. of Science, and [2]Dept. of Agrobiology, Fac. of Agriculture), Niigata Univ., Niigata, 950-2181, Japan.
[1]E-mail: ohnishi@sc.niigata-u.ac.jp

Abstract

Principal coordinate analysis (PCOA) [1-3] and its applicability to amino acid (aa) sequence comparison in molecular evolutionary study [4, 5] was theoretically considered from an aspect of evolutionary random-walk movement in multi-dimensional pseudo-euclidean orthogonal sample space. By using an appropriate evolutionary distance, evolution was found to be analyzed as a random-walk aa substitution movement in this multidimensional space. Based on this background, PCOA was successfully applied to α crystallins and RUBISCOs, resulting in giving some new findings. This study established a theoretical backgrounf of efficient method for constructing multidimensional evolutionary tree in pseudo-euclidean sample space spanned by pricipal coordinate axes.

1. Introduction

Principal coordinate analysis (PCOA) was first described by Togerson [1] and Gower [2,3] as a useful method for mapping n samples in n –1 dimensional orthogonal (pseudo-euclidean) space, based on distance data among samples. PCOA is applicable for analyzing evolutionary distance-relationship among protein or base-sequences, and for constructing multidimensional evolutionary tree, as has been reported [4-6].

In the present paper, recent protein sequence data was analyzed by PCOA from an aspect of random-walk evolutionary movement in (pseudo-)Euclidean space..

2. Principal coordinate analysis: Theoretical background

We start from a distance matrix

$$\mathbf{D} = (d_{ij})_{n,n}, \qquad \text{(Eq1)}$$

where d_{ij} denotes evolutionary distance obtained (observed or calculated) between samples (or OUT's, operational taxisonomic

units) P_i and P_j (i, j = 1, 2, ..., n). A symmetric matrix, $\mathbf{B} = (b_{ij})$, can be calculated by

$$b_{ij} = \frac{1}{2}\{\frac{1}{n}\sum_{k=1}^{n} d_{kj}^{\,2} + \frac{1}{n}\sum_{k=1}^{n} d_{ik}^{\,2} - \frac{1}{n^2}\sum_{k=1}^{n}\sum_{k'=1}^{n} d_{kk'}^{\,2} - d_{ij}^{\,2}\} \quad \text{(Eq.2)}$$

We can find an orthogonal matrix $\Lambda = (\delta_{ij}\lambda_j)_{n,n}$ (δ_{ij}: Kronecker's delta; λ_j : eigenvalues of **B**) and an orthogonal matrix $\mathbf{V} = (v_{ij})$ satisfying $\mathbf{V'BV} = \Lambda$, and $v = (v_{ij}, v_{2j}, ..., v_{nj})$ is an eigenvector of B, corresponding to λ_j and satisfies $\sum_{i=1}^{n} v_{ij}^{\,2} = 1$.

Thus we further have

$$\mathbf{A} = \mathbf{V}\Lambda^{1/2} \quad \text{(Eq.3)}$$

and $$\mathbf{B} = \mathbf{AA'}, \quad \text{(Eq.4)}$$

because $\mathbf{AA'} = (\mathbf{V}\Lambda^{1/2})(\mathbf{V}\Lambda^{1/2})' = (\mathbf{V}\Lambda^{1/2})(\Lambda^{1/2}\mathbf{V'}) = \mathbf{V}\Lambda\mathbf{V'} = \mathbf{V(V'BV)V'} = \mathbf{(VV')B(VV')} = \mathbf{IBI} = \mathbf{B}$.

Eq.3 means

$$a_{ik} = \sqrt{\lambda_k} \cdot v_{ik} \quad (k=1,2,...,n-1) \quad \text{(Eq.5)}$$

and that P_i (a_{i1}, a_{i2}, ..., $a_{i,n-1}$) gives a principal coordinate of sample point P_i (OTU_i) in an n-1 dimensional orthogonal space.

From Eq.4, we obtain

$$\sum_{k=1}^{n-1}(a_{ik} - a_{jk})^2 = b_{ii} + b_{jj} - 2b_{ij} = d^2_{ij}$$

, which proves that d_{ij} equals to pseudo-euclidean distance between P_i and P_j. If all eigenvalues are non-negative (i.e., **B** is positive semi-definite), n sample points can be mapped in a real euclidean space E^n., and d_{ij} denotes euclidean distance. If some eigenvalues are negative, the corresponding a_{ik} is purely imaginul number, and the corresponding axis is a purely immaginal axis. Variance of a_k is given by

$$Var[a_k] = \lambda_k / n. \quad \text{(Eq.6)}$$

Note that thus defined variance is negative for purely imaginal axes (where λ_k is negative).

Since $\sum_{i=1}^{n} a_{ik} = 0$, centroid of the n sample points is **O**(0, 0 ..., 0).

The n eigenvalues (λ_1 λ_2 ..., λ_n) can be re-numbered so that

$$\hat{\lambda}_1 \geq |\hat{\lambda}_2| \geq |\hat{\lambda}_3| \geq ..... \geq |\hat{\lambda}_{n-1}| \geq \hat{\lambda}_n = 0 \quad \text{(Eq.7)}$$

is satisfied, since rank(**B**) = n-1. Here, $|\ |$ denotesabsolute value.

By letting

$$x_{ik} = \hat{a}_{ik} = \sqrt{\hat{\lambda}_k} \cdot \hat{v}_{ik}, \quad \text{(Eq.8)}$$

P_i is mapped as P_i (x_{i1}, x_{i2}, ..., $x_{i,n-1}$) in an n-1 dimensional orthogonal space spanned by n-1 axes, x_1, x_2, ..., x_{n-1}. In Eq.8,

$$\hat{v} = (\hat{v}_{1k}, \hat{v}_{2k}, ..., \hat{v}_{n-1,k})'$$

is an eigenvector of B, corresponding to the eigenvalue $\hat{\lambda}_k$ From Eqs.6 and 7,

$$Var[x_k] = \hat{\lambda}_k / n \quad \text{(Eq.9)}$$

and

$$Var[x_1] \geq |Var[x_2]| \geq |Var[x_3]| \geq ...$$
$$.. \geq |Var[x_{n-1}]| \geq Var[x_n] = 0. \quad \text{(Eq.10)}$$

Thus x_k denotes the k-th principal coordinate axis, which explains

$$v_k = |Var[x_k]| / \sum_{i=1}^{n-1} |Var[x_i]| = |\lambda_k| / \sum_{i=1}^{n-1} |\lambda_i| \quad \text{(Eq.11)}$$

of total sum of variances. Mapping in an m-dimensional space spanned by 1st to m-

th axes can explain $v_{(1,m)} = \sum_{k=1}^{m} v_k$ of total sum of variances.

Let m be noted for the number of negative eigenvalues of B, then P_i (x_{i1}, x_{i2}, ..., $x_{i,n-1}$) give a mapping in an n – 1 dimensional pseudo-euclidean space, $\Psi^{(n-1,m)}$ spanned by n-m-1 real-number axes and m purely imaginal number axes. For those cases where m = 0, $\Psi^{(n-1,m)}$ denotes an n – 1 dimensional real euclidean space $\mathbf{E}^{n-1}$.

3. Evolutionary random-walk in multidimensional space spanned by principal coordinate axes

Principal coordinate axes in PCOA are eigenvectors of $\mathbf{B} = (b_{ij})$, and covariance of any two different axes are 0, meaning that pricipal coordinate axis are independent to one another.

Consider a hypothetical ancestral amino acid (aa) sequence P_o, from which contemporary sequences P_α and P_β have evolved by random aa replacements (See Figure).

Let Δ_{ij} denote the fraction of amino acid (aa) difference between two aligned aa sequences P_i and P_j. Estimated number of random aa substitutions required for changing from P_i to P_j, or from P_j to P_i [5] is given by

$$K_{aa(i,j)} = \ln\frac{1}{1-\Delta_{ij}}. \qquad \text{(Eq.12)}$$

PCOA is then applied by letting

$$d_{ij} = \sqrt{K_{aa(i,j)}} \qquad \text{(Eq.13)}$$

in Eq.1. Since n-1 coordinates in pseudo-euclidean space, $\Psi^{(n-1,m)}$, are independent with one onother, evolution in this space is considered to have occurred by random walk whose unit-length in the k-th coodinate is proportional to $\sqrt{Var[x_k]}$. The expected number of random-walk steps required for evolving from P to P is given by

$$N_{ij} \propto {d_{ij}}^2 = K_{aa(i,j)}. \qquad \text{(Eq.14)}$$

Accordingly, application of PCOA to aa sequence comparison by Eq.13 brings about Eq.14, which gives a useful tool for analyzing evolutionary history as evolutionary randomwalks in $\Psi^{(n-1,m)}$.

Fig.1 shows the PCOA result of the above-mentioned three sample sequence points, P_o

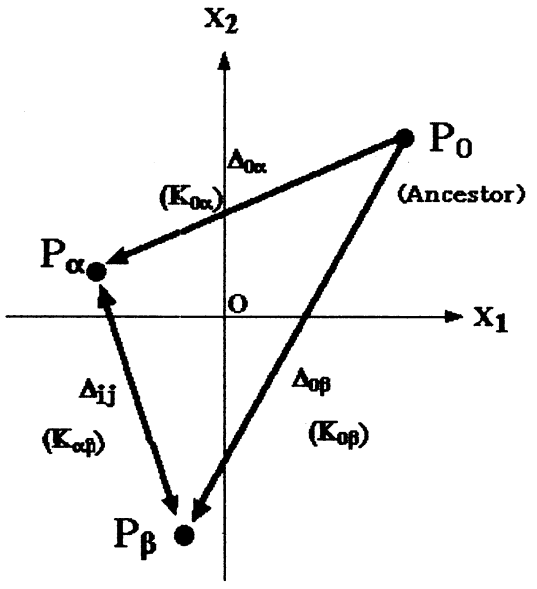


Fig. 1. PCOA of an ancestral aa sequence (P_0) and its descendant sequences (P_α and P_β), by letting $d_{\alpha\beta}^2 = K_{\alpha\beta}$, where is (pseudo-)Euclidean distance between sequences (sample points) P_α and P_β.

(latest common ancestor), P_α and P_β (descendants) by using Eq.13. Based on the above consideration, we easily find

$$K_{0\alpha} + K_{0\beta} = cd_{0\alpha}{}^2 + cd_{0\beta}{}^2 \quad \text{(Eq.15)}$$

$$K_{\alpha\beta} = cd_{\alpha\beta}{}^2, \quad \text{(Eq.16)}$$

where c is a constant. It should be noted that we cannot find any reason for explaining Kimura's statement (ref.[5], pp.68-70),

$$K_{\alpha\beta} = K_{\alpha 0} + K_{0\beta}, \quad \text{(Eq.17)}$$

because P_0 is an "unknown determined point, and Eq.17 is based on an assumption that P_0 be an "undetermined' ancestral point.

4. PCOA of aa sequences of mammalian α crystallin A and plant RUBISCO molecules

PCOA was employed for analyzing aligned aa-sequences of mammalian α crystallin A (Fig.2), and rbcL proteins (ribulose 1,5-bisphosphate carboxylase (RuBisCO) large subunit (rbcL) (Fig.3).

Recent molecular phylogenetic analyses based on evolutionary tree constructions suggest an earliest branching-off of Nymphaeaceae from other groups of Angiospermae (= Magnoliophyta = Anthophyta) 6], which, however, does not seem to be supported by traditional morphological classification. In order to answer to this problem, rbcL aa sequences of 21 representative species of vascular plants were analyzed by PCOA,via employment of Eqs. 12 and 13. The resulting three-dimensional projection is shown in Fig.2. In this geometrical mapping, Most species of Magnoliophyta are located in the area relatively near to Gymnosperms. However, *Ceratop-hyllum* (Nyphaeaceae) is not located in the direction to gymnosperms, but is located distantky in the opposite direction. This strongly suggests that the distant relationship of Nymphaeaceae to other angiosperms is most plausibly the result of specialization, and not of its primitiveness.

PCOA of mammalian α crystallin A gave a reasonable results shown in Fig. 2. Most of major clustering of eutherian species well coincide with recent molecular taxonomy [7, 8]. Detailed discussions will be published elsewhere.

Acknowledgement: This work was partly supported by a project of Transdisciplinary Research Institute of Niigata University. Useful discussions are acknowledged to Prof. Tatsuyoshi Morita, Niigata Univ.

References

[1] Togerson, W.S.: *Psychometrica* 17: 401, 1952.

[2] Gower, J.C.: *Biometrica* 53: 325 1966.

[3] Gower, J.C.: *Statistician* 17: 13 1967.

[4] Ohnishi, K., *Dev. Comp. Immunol.* 5 (Suppl. 1) : 123-128, 1980.

[5] Kimura,M.: *The Neutral Theory of Molecular Evolution.* Cambridge Univ. Pr., London, 1983.

[6] Soltis, P.S., Soltis, D.E., Chase, M.W.: Nature 402: 402-404. ; Qiu, Y. et al.: Nature 402: 404-07.

[7] Murphy,W.J. et al.:Science294:2348-51, 2001.

[8] Madsen et al.: Nature 409: 610-614.

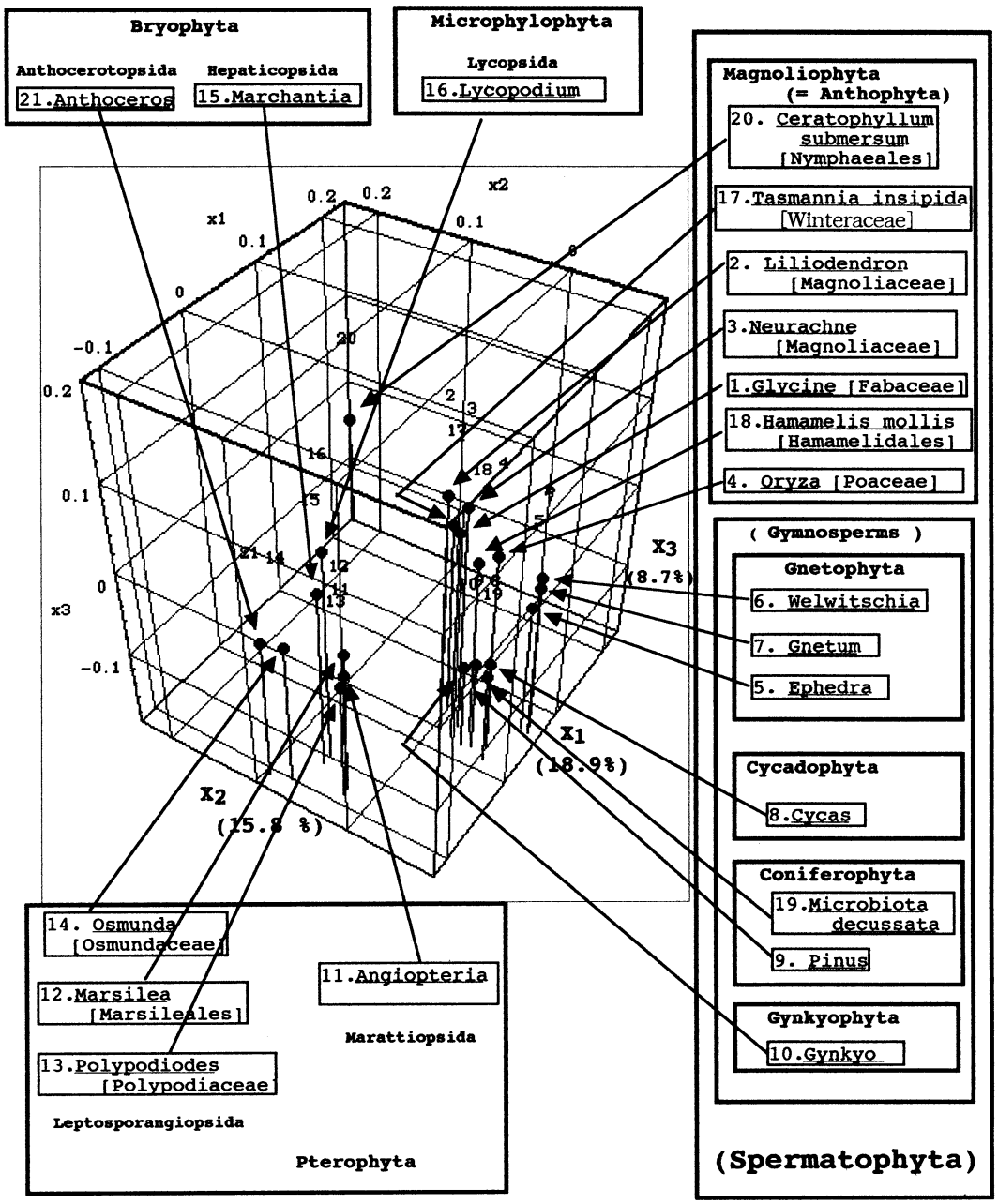


Fig.2. Principal coordinate analysis (PCOA) of 21 RubisCO L subunit amino acid (aa) sequences from vascular plant chloroplasts. PCOA is employed by letting $d_{ij} = [\ \ln \{1 / (1 - \Delta_{ij})\}]^{1/2}$ (Eq.13), where Δ_{ij} denotes ratio of aa difference in the aligned region (corresponding to *Ceratophyllum submersum* RubisCO L aa's 12-420), and d_{ij} denotes 20-dimensional (real) euclidean distance in $\mathbf{E}^{20}$ spanned by 20 principal coordinate axes. X_1, X_2, and X_3 represent the 1st, 2nd and 3rd principal coordinates (given in Eq.8), which explains 18.9%, 15.1%, and 8.7% (sum = 44.2%) of the total sum of variances along 21 principal coordinate axes. The 21 principal coordinate axes are real number-valued since corresponding eigenvalues of **B** are positive. Data are obtained from SwissProt/GenBank database.

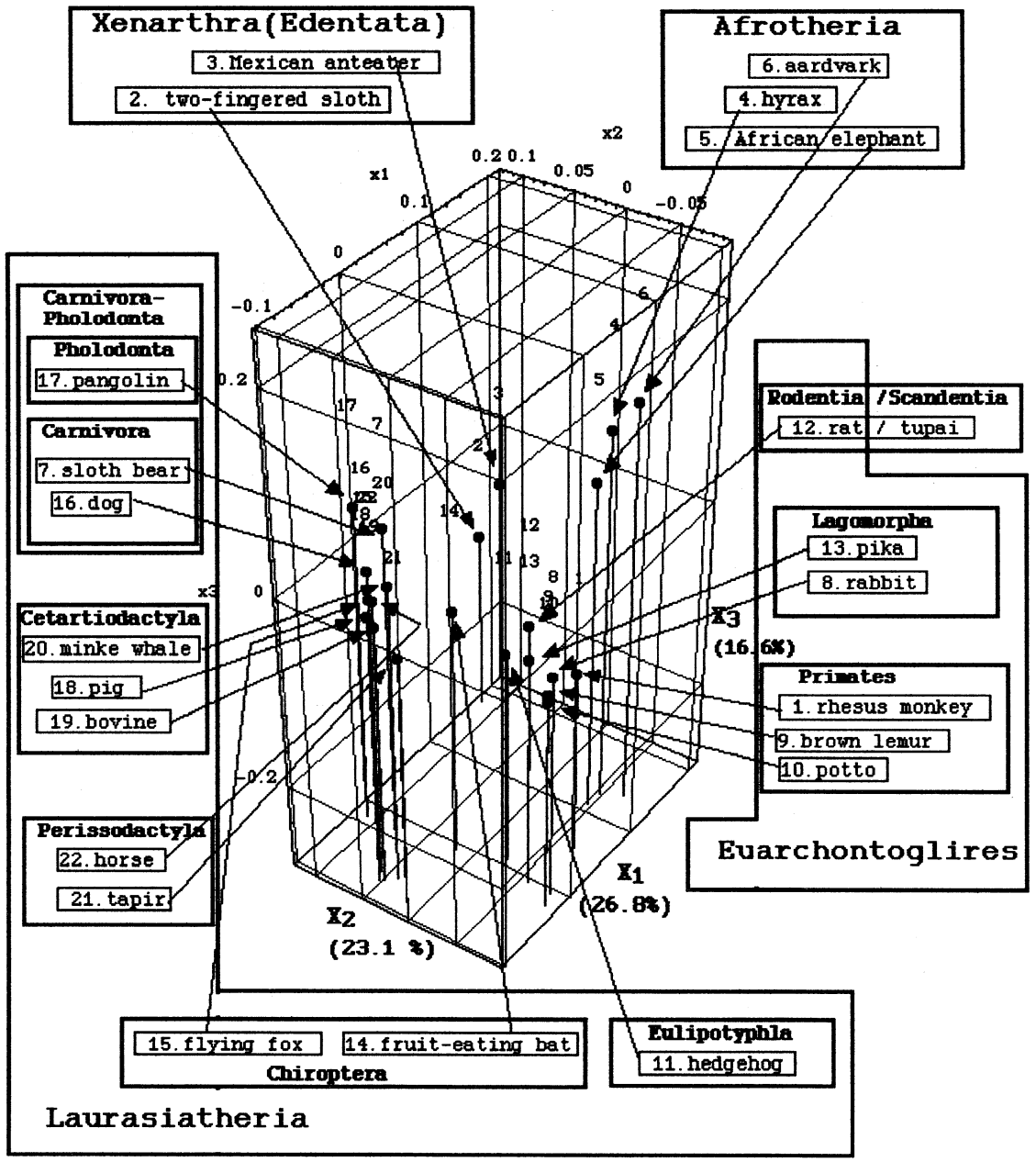


Fig. 3. Principal component analysis (PCOA) of 22 mammalian α crystalline A chain aa sequences. PCOA was employed by letting $d_{ij} = [\ \ln \{1 / (1 - \Delta_{ij})\}]^{1/2}$ (Eq.13), as similarly as in the legend of Fig.2, based on the aa sequence difference in the aligned region (corresponding to the dog sequence aa's 61-173). All of the 21 principal coordinate axes are real numbe axes. X_1, X_2, and X_3 represent the 1st, 2nd and 3rd principal coordinates (given in Eq.8), which explain 26.8%, 23.1%, and 16.6% (sum = 66.5%) of the total sum of variances. Note that eutherian major four groups (Afrotheria, Xenarthra, Euarchontoglires, and Laurasiatheria) make their respective clusters, although some Laurasiatherians (such as Chiroptera and Eulipotyphla) are located in the region between Euarchontoglires and other Laurasiatherians.

Proc. of The Ninth Int. Symp. on Artificial Life and Robotics (AROB 9th '04)
Beppu, Oita, Japan, 28-30 January, 2004

Early genesis and evolution of mRNAs and 16S rRNA from poly-tRNA ribozymes

[2] Yuka Ishimoto, [2]Madoka Ohshima, [2]Shouken Hokari,
[1,3]Naotaka Furuichi, and [1,2,]*Koji Ohnishi
[1]Center for Transdisciplinary Research ([2]Dept .of Biology, Fac. of Science, and
[3]Dept. of Agrobiology, Fac. of Agriculture), Niigata Univ., Niigata, 950-2181, Japan.
E-mail : ohnishi@sc.niigata-u.ac.jp (*K.O.)

Abstract

The origin of mRNA and genetic code as well as 16S rRNA was analyzed from the aspect of the (*trrnD*-type) poly-tRNA theory [1-3]. The *trrnD*-operon in *Bacillus subtilus* (BSU) has a structure, (5') [16SrRNA-23SrRNA-5SrRNA-$(tRNA)_{16}$](3'), where $(tRNA)_{16}$ is called *trnD* tRNA gene cluster. A hypothetical 16-amino acid (aa) peptide in the ordering of *trnD* tRNA aa specificities is called "*trrnD*-peptide (or *trnD*-peptide), which would have been synthesized by the so-called "*trrnD*-poly-tRNA model". Protein sequences similar to the *trnD*-peptude were searched for, and their coding DNA regions were analyzed by making multi-alignment with the $tRNA^{His-Gln-Gly-Cys-Leu}$ region and related tRNA clusters. Detailed analyses revealed that the $tRNA^{His-Gln-Gly-Cys}$ is homologous to *pgtB*, *GlyS*, F_0-a, F_1-γ, and lectin Bra-3 genes. 16S rRNAs are homologous to the $tRNA^{Gly-Cys-Leu}$.

1. Alignment of *trrnD*-mRNA-related genes against the *B. subtilis trnD*-tRNA cluster

Poly-tRNA theory hypothesized that the poly-tRNA transcript from the BSU *trrnD* operon and *rrnB* operon are both evolutionary relics of early peptide-synthesizing poly-tRNA molecules[1-3]. In the previous paper, the DNA region of the *E. coli* glycyl-tRNA synthetase (GlyRS) α was found to be most plausibly homologous to the hexa-tRNA region of the BSU *trnD*-tRNA cluster. However, because of low levels of aa- and base-sequence identity to the hexa-tRNA region, exact alignment of GlyRS and its homologous sequences (such as ATP-synthase subunits F_0-a, F1-γ, PgtB, etc.) against *trnD*-poly-tRNA region is yet considerably difficult in several low-base-identity regions, even if homology is very evident in high-base-identity (core-homology) regions.

Aa sequence similarity search by FASTA [4] in SWISSPROT database revealed that 3-phospho-glycerate transporter protein B (pgtB) and C-type lectin Bra-3 showed most significant levels of similarity (E value =0.64, 0.71, respectively, using PAM40 matrix) to the trrnD-peptide. Eubacterial Glycyl-tRNA synthetase α subunit (GlyRSα) was

found to show most significant level of aa similarity to the lectin Bra-3(aa's 107-112). Based on the sequence homologies among these sequence regions, GlyRSα, lectin Bra-3, pgtB, and the *trrnD*-peptide were aligned with one another. As shown in Fig.1, the DNA regions coding for these proteins were further aligned against the *trnD*-tRNA gene cluster including the *trrnD*-mRNA region. For an observed m-base match in n-base aligned pair of sequences, similarity levels were statistically evaluated by $P_{nuc}(m,n)$ value, wich gives, an m or more base-matching probability by chance [2,3]. The result is given in Table 1, showing close homology relationship of F1-γ and lectin Bra-3 to the $tRNA^{Gly}$-$tRNA^{Cys}$ region of the *trrnD*-opero. Thus, the sequences aligned in Fig.1 are considered to be truly homologous to one another, supporting the poly-tRNA hypothesis of mRNA-origin.

2. *B. subtilis trnD*-tRNA cluster as an ancient poly-tRNA of the latest common ancestor of living organisms

The poly-tRNA theory postulates that the *B.subtilis trrnD*- and *rrnB*-poly-tRNA structures would have been both possessed by an organism comm.only ancestral to all living organisms [2,3]. In order to determine whether or not we could find some evidence for such oldness of these poly-tRNA structure, tRNA gene clustere found in hitherto sequenced complete genomes (in GenBank Database) were compared with each other. Representative tRNA gene clusters more or less similar to the *trrnD*-operon in diverge phyla in eubacteria and eukaryotes are schematically shown in Fig. 2. Archaebacteria do not have similar tRNA clusters.

Evident homologues of the B. subtilis *trrnD*-operon or its *trnD*-tRNA gene cluster are widely distributed amng Gram-positive bacteria (Phylum Firmicutes) *including Lactobacllus, Clostridium, and Thermoanaerobacter.* The "16S rRNA-23S rRNA-5S rRNA-$tRNA^{Asn}$ " is also found in *Fusobacterium*(Phylum Fusobacteria). The existence of a pseudo-tRNA gene cluster[5], a homologue of "NSEVMDFTYW" region of the *B. subtilis rrnB*-operon strongly suggests that the B.S. trrnD-operon must have emerged earlier than the branching time-point of Firmicutes and Gamma-Proteobacteria. On the other hand, a tri- or di-tRNA gene cluster, $tRNA^{Gly}$-$tRNA^{Cys}$, (-tRNALeu) in Gamma-Proteobacteria and *Aquifex* suggest that the "GCL" tri-tRNA region must have been commonly ancestral to all living eubacteria. These observations seems to support that the *Bacillus trnD*-cluster is most plausibly more primitive than the tRNA-clusters in non-Bacillus-type Firmicutes tRNA-clusters shown in Fig.2. In order to further confirm this evolutionary direction, it is important, in future studies, to find out evolutionary relics of tRNA-deletions in non-Bacillus Firmucutes tRNA clusters.

Fig. 1. Alignment of the tRNA^{His}-tRNA^{Gln}-tRNA^{Gly}-tRNA^{Cys}-tRNA^{Leu} region of the *Bacillus subtilis* (BSU) *trrnD* operon with other tRNA gene clusters and protein-encoding DNA regions. Base-matches to B. subtilis trrnD-operon are indicated by asterisk (*), and those to GlyRS gene (GlyS) are boxed and indicated by "+". Proto-tRNA viroid is also shown.

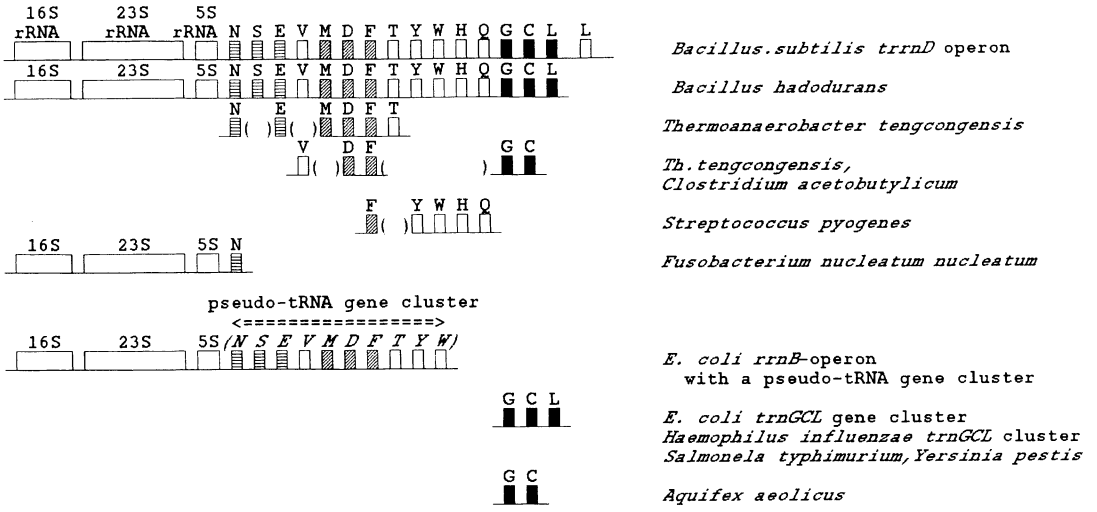


Fig. 2. tRNA gene clusters possibly related to the *trrnD*-operon or *trnD* tRNA gene cluster in *Bacillus subtilis*. Gene clusters found in "sequenced complete genomes" of GenBank Database are shown. Spaces needed to be introduced for aligning tRNA-clusters are indicated by ( ).

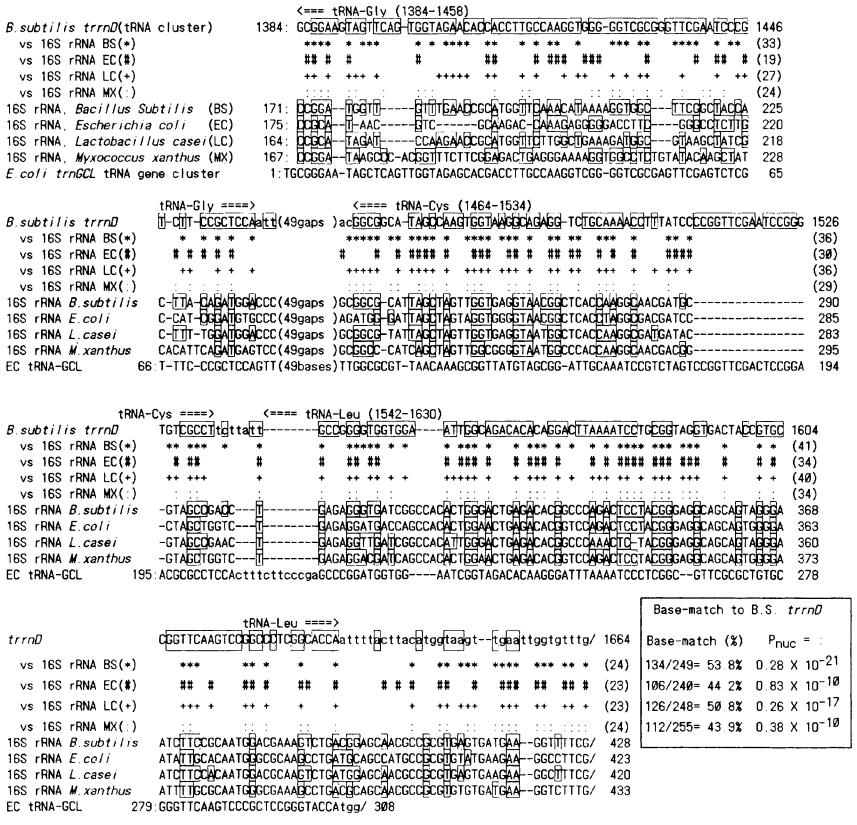


Fig. 3. Alignment of eubacterial 16S rRNAs against the $tRNA^{Gly}$-$tRNA^{Cys}$-$tRNA^{Leu}$ region of the *B. subtilis trnD* tRNA gene cluster. Base-match levels and P_{nuc} values are given in the lower-right box

Table 1. Statistical evaluation of base-sequence similarities by $P_{nuc}(m,n)$*

	(1) Comparison with GlyRSα		(2) Comparison with trnD-poly-tRNA	
	Base-match (%) (m/n)	$P_{nuc}(m,n)$	Base-match (%) (m/n)	$P_{nuc}(m,n)$
GlyRSα			50.0% (159/318)	9.1E-22
pgtB	48.2% (79/164)	1.3E-10	44.1% (71/161)	1.0 E-7
Bra-3	50.2% (115/229)	2.2E-16		
F1-γ (Syn.)	63.1% (113/179)	6.0E-27	48.3% (84/174)	3.1E-11
F0-a (Syn.)	57.2% (99/173)	2.2E-19	47.0% (79/168)	5.6E-10

* $P_{nuc}(m,n)$ is given by, $P_{nuc}(m,n) = \Sigma_{(i=m,n)} C_{n,i} (1/4)^{1} (3/4)^{n-i}$, where $C_{n,i} = n ! / [i ! (n - i) !]$, and $\Sigma_{(i=m,n)}$ denotes summation over m to n.

3. Origin of 16S rRNA

In order to study the origin of 16S and 23S rRNAs, dot-matrix method (Harr Plot) was employed for finding similar base-sequence region between these rRNAs and the *trrnD*-poly-tRNA region (*ttrnD*-tRNA cluster). Detailed analysis elucidated that 16S rRNAs possess a base-sequence region significantly similar to the $tRNA^{Gly}$-$tRNA^{Cys}$-$tRNA^{Leu}$ region of the *B. subtilis trrnD* operon. The 16S rRNA portion thus found are aligned against the tri-tRNA region of the *B. subtilis trnD*-tRNA cluster, and against the E. coli trnGCL. Cluster, as shown in Fig. 3. This portion of the *B. subtilis* 16S rRNA was found to show a 58.3% base-match, giving Pnuc(134,249) = 0.28×10^{-21} (See Fig.3), which most probably confirms the origin of the 16S rRNA from the tri-tRNA region.

Thus we have reached an important conclusion that the $tRNA^{Gly}$-$tRNA^{Cys}$-$tRNA^{Leu}$ region of the *B. subtilis trrnD* operon.is the origin of both an earliest mRNA (trrnD-mRNA-derived mRNAs) and the 16S rRNA.

4. REFERENCES

[1] Ohnishi, K.: In: *Endocytobiology V.*, ed. by S. Sato,. Ishida and H. Ishikawa, pp. 407-414, Tubingen University Press, Tubingen, 1993.

[2] Ohnishi et al.: Viva Origino 30: 63-72, 2002.

[3] Ohnishi, K. et al.: Genome Informatics 13: 71-81, 2001.

[4] Mount, D.W.: Bioinformatics: Sequence and Genome Analysis. Cold Spring Harbor Lab. Press, Cold Spring Harbor, NY, 2001.

[5] Ohnishi, K. et al.: Genome Infoematics 11: 325-326, 2000.

Proc. of The Ninth Int. Symp. on Artificial Life and Robotics (AROB 9th '04)
Beppu, Oita, Japan, 28-30 January, 2004

Defence mechanisms of potato :Regulation of RiCDPK, the Ca^{2+}-dependent protein kinase, by the elicitor and suppressor of *Phytophthora infestans*

[1, 2]Naotaka Furuichi, [2]Tomoo Okuta , [2]Amjad Hassan,
[1]Koji Ohnishi and [2]Noriyuki Hatsugai.
[1]Center for Transdisciplinary Resarch, and [2]Graduate School of Science and Technology,
Niigata University, Niigata 950-2181, Japan. [1]E-mail: nfuru@agr.niigata-u.ac.jp

Abstract

To investigate the role of CDPK in hypersensitive reaction (HR) of potato, the proteins encoded by RiCDPK-1, and -2 from potato were expressed in *E. coli* and the effect of HWC and suppressor of HR from Pi on the auto-phosphorylation of the RiCDPK-1- and -2-His were examined. In the present report, the suppressor from Pi stimulated the auto-phosphorylatioh of the RiCDPK-1-His and -2-His in the early period *in vitro*. With Ca^{2+} and Mg^{2+} , the auto-phosphorylation of RiCDPK-1-His and -2-His was stimulated. These data suggest that RiCDPK-1, and -2 may play an important role in the signaling cascade caused by HWC and suppressor in potato cell, leading to and in the inhibition of HR in the compatible response between potato and Pi.

1. Introduction

Plants respond to invading pathogens with hypersensitive response (HR). The HR result from the incompatible interaction between the plant and the pathogen [1-5]. The mechanisms underlying HR are still not fully understood; hence it is necessary to elucidate the signals involved in cascade resulting in HR. The potato and an oomycete *P. infestans* (Pi) combination are the model system for HR. Potato cells responded to the attack of incompatible races of *Pi* resulting in HR cell death [2,6-10]. Infection with an incompatible race of *Pi* caused a rapid cell death within 10 min after the infection [10].

2. Cloning and expression of RiCDPKs.

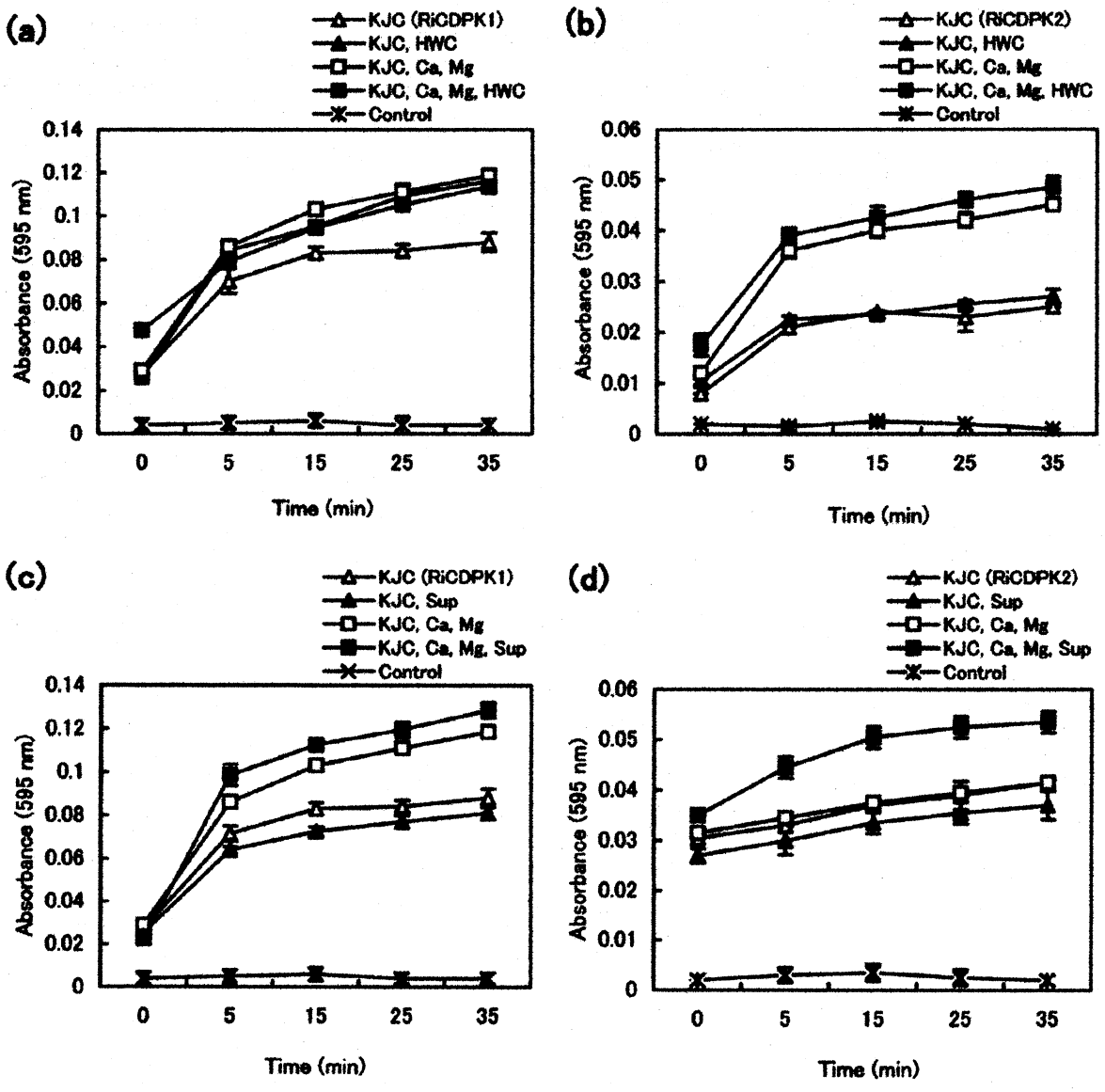
Sequence analyses showed that two different members of CDPK family existed in potato (R_1). The CDPK cDNA from cv. Rishiri, contains a myristoylation site in the N-terminal domain and shows 73.8% identity of amino acids with AK1

(AtCDPK1) from *Arabidopsis thaliana* [11] was designated as *RiCDPK1*. The cDNA has 67.4 % identity with *AK1* gene from *Arabidopsis* [11,12] is designated as *RiCDPK2* (Fig. 1). Since the N-terminal native start codon of *RiCDPK-1* and *RiCDPK-2* is determined, it is likely from the present result that *RiCDPK1* is myristoylated to plasma membrane of potato cells. Analysis of the deduced amino acid sequence revealed that *RiCDPK2* contains in a single polypeptide chain, a kinase domain followed by a 31 amino acid auto-inhibitory domain that presumably functions as a pseudo-substrate inhibiting phosphorylation reactions in the absence of Ca^{2+} [11,12] and a calmodulin-like Ca^{2+}-binding regulatory domain at the C-terminus.

3. Effect of HWC and suppressor on auto-phosphorylation of RiCDPK

The KJC of RiCDPK2-His in the presence of Ca^{2+} and Mg^{2+} was treated with HWC and suppressor *from Pi*. The HWC caused 18 % stimulation in auto-phosphorylation of KJC in the presence of Ca^{2+} and Mg^{2+} just after the addition as compared to the KJC as a control in the presence of Ca^{2+} and Mg^{2+} (Fig. 1b). RiCDPK1-His caused 39% stimulation of auto-phosphorylation of the fusion when it was treated with HWC in the presence of Ca^{2+} and Mg^{2+} (Fig. 1a). As shown in Figure 1, suppressor treatment stimulated the auto-phosphorylation of KJC of RiCDPK2-His in the presence of Ca^{2+} and Mg^{2+} up to 25 % just after the addition as compared to the KJC in the presence of Ca^{2+} and Mg^{2+} without suppressor. In the experiments, suppressor stimulated 12% of the auto-phosphorylation of RiCDPK1-His (Fig. 1c). In the present results, suppressor of *Pi* did not stimulated the activity of RiCDPK2-His in the absence of Ca^{2+} and Mg^{2+} (Fig. 1d). It was observed that the suppressor of Pi effectively regulates the auto-phophorylation of RiCDPK2-His in the presence of Ca^{2+} and Mg^{2+}. Keeping these observations from RiCDPK2 (Fig. 1d) and RiCDPK1-His (Fig. 1c) into the consideration, the suppressor seems possible to transduce the signal with greater amplification for the inhibition of HR in case of RiCDPK1-His in the presence of Ca^{2+} and Mg^{2+} than RiCDPK2-His. It was suggested that the HWC and suppressor caused auto-phophorylation of KJC in the presence of Ca^{2+} and Mg^{2+}.

Fig. 1. Effect of HWC and suppressor from *Phytophthora infestans* (Pi) on the kinase activity of the RiCDPK1-His and -2-His (KJC) in the presence or absence of Ca^{2+} and Mg^{2+}. The concentration of the KJC were 1.5 μg, and Ca^{2+} and Mg^{2+} (100 μM and 1mM). HWC and suppressor glucan were treated to the concentration of 2 μg. Data are shown as the mean ± SD.



4.GFP imaging of RiCDPK

Sub-cellular localization of RiCDPK1-GFP was investigated under the CCD camera. Potato cells were transformed by RiCDPK1-GFP by particle gun. Then, the cells were treated with HWC from Pi. It was observed that the transient RiCDPK1–GFP expression after the HWC treatment at 35 min after the treatment. The results showed that the expression of RiCDPK1-GFP contents in the cells were induced and increased rapidly within 10 min, and that the RiCDPK1-GFP localized in the plasma membrane of potato cells. In the present study, the HWC and suppressor of Pi stimulated auto-phosphorylation of RiCDPK1- and RiCDPK2-His. The action of HWC leads to a resistant and that of suppressor to a susceptible reaction of the host. It was found that at least a single copy of *RiCDPK* gene exists in four different cultivars of potato with R_1-, R_1R_3- and r-gene to *Pi* (unpublished). In several other plant species, more than one CDPK genes have been identified [11-13] suggesting the role of CDPKs in intracellular signaling. Stimulation of the kinase activity of the RiCDPK with the HWC and suppressor *in vitro* indicates that RiCDPK1 and RiCDPK2 may be involved in the regulation of compatible signaling pathways in the host and *Pi* interaction.

Acknowledgements: We acknowledge A. Shirata (NIAS) and T.L. Graham (Ohio State Univ.) for discussion and correcting the manuscript. We thank to J. F. Harper (Scripps Insti.) for CDPK cDNA. This work was supported by Grants-in-Aids of the Ministry of Education, Science and Culture, Japan to N. F.

References

[1] Doke, N., Sakai, S. Tomiyama, K. (1979a) Ann. Phytopath. Soc. Japan 45, 386-393.

[2] Doke, N., Tomiyama, K., Furuichi, N. (1982) in: Plant Infection: The physiological and Biochemical Basis, pp. 79-96 (Asada, Y., Bushnell, W.R., Ouchi, S. and Vance, C.P., Eds.) Japan Sci. Soc. Press, Tokyo/Springer-Verlag, Berlin.

[3] Furuichi, N.,Suzuki, J. (1990a) Annals of Phytopathological Society of Japan 56, 457-467.

[4] Goodman, R.N., Novacky, A.J. (1994), pp. 243 APS Press, St. Paul, Minnesota.

[5] Tomiyama, K. (1982) in: Plant Infection: The Physiological and Biochemical Basis, pp. 329-344 (Asada, Y., Bushnell, W.R., Ouchi, S. and Vance, C.P., Eds.) Japan Sci. Soc. Press, Tokyo.

[6] Doke, N., Furuichi, N. (1982) Physiological Plant Pathology 21, 23-30.

[7] Doke, N. ,Tomiyama, K. (1980) Pysiological Plant Pathology 16, 177-186.

[8] Furuichi, N., Tomiyama, K., Doke, N. (1979) Phytopathology 69, 734-736.

[9] Kitazawa, K.,Tomiyama, K. (1969) Phytopathologische Zeitschrift 22, 317-324.

[10] Kitazawa, K., Inagaki, H., Tomiyama, K. (1973) Phytopath. Z. 76, 80-86.

[11] Harper, J.F., Binder, B.M.,Sussman, M.R. (1993) Biochemistry 32, 3282-3290.

[12] Harmon, A.C., Yoo, B.-C., McCaffery, C. (1994) 33, 7278-7287.

[13] Harmon, A.C., Gribskov, M.,Harper, J.F. (2000) Trends in Plant Science 5, 154-159.

Proc. of The Ninth Int. Symp. on Artificial Life and Robotics (AROB 9th '04)
Beppu, Oita, Japan, 28-30 January, 2004

Extraction of User's Interests by ICA and GA for Information Filtering

Hidekazu Yanagimoto
Department of Computer and Systems Sciences
Osaka Prefecture University
1-1, Gakuencho, Sakai
Osaka 599-8531, Japan

Sigeru Omatu
Department of Computer and Systems Sciences
Osaka Prefecture University
1-1, Gakuencho, Sakai
Osaka, 599-8531, Japan

({hidekazu, omatu}@cs.osakafu-u.ac.jp)

Abstract

We propose an information filtering system using ICA and GA. In this paper ICA extracts independent components (topics in documents) from observed data (documents). We cut off some independent components which represent noise and reconstruct document vectors with remaining independent components. To extract user's interests we use GA with Kullback Leibler divergence. Finally we describe the experiments to evaluate a proposing method and discuss the effectiveness of it.

Keyword: Independent Component Analysis (ICA), Genetic Algorithm, Kullback Leibler Divergence

1 Introduction

Users can have access to vast store of information through the Internet recently, as the Internet becomes widespread. When they search information they desire with search engines, they get a lot of search results and hardly find ones they desire truly. To cope with this situation, many researchers have paid attention to developing information filtering systems. The information filtering systems automatically select information depending on user's interests (user profile). To select information correctly, the systems must keep appropriate user's interests.

In this paper, we propose extraction of user's interesting by ICA and GA for information filtering. We try to extract independent components from documents using ICA and cut off some independent components which represent noise. We regard document vectors as probability distribution and calculate the similarity between user profile and documents by Kullback Leibler divergence. Our aim is the improvement of accuracy with these approaches. To evaluate a proposing method, we discuss the effectiveness of the proposing method in the viewpoint of selection ability.

2 Previous work

Independent Component Analysis (ICA) is the technique that separates observed signals which mix source signals linearly on the basis of the independence of signals. FastICA is the algorithm which separates source signals and solves many problems in signal processing, image processing and so on. FastICA was proposed by Hyvärinen[1] Some researchers try to apply ICA to information retrieval to improve the accuracy of information selection[2][3].

GA is the algorithm which simulates the biological evolution and is proposed by Holland[4]. GA is often applied to combinational optimization problems. NewT[5] is a information filtering system using GA and use GA to create user profile.

To deal with documents on computers, Vector Space Model (VSM) is proposed by Salton et al[6]. In the VSM all documents are represented as vectors and the distance between documents is defined as inner produce between the documents.

3 Methodology

In this section we explain the key concepts of a proposing method. They are the similarity using Kullback Leibler divergence in SVM and GA and ICA.

3.1 Vector Space Model

In Vector Space Model (VSM) a document written with natural language is represented as a vector to deal with it on computers. The vector is called a

document vector below. The element of the document vector denotes a word included in a document and is calculated by TF-IDF.

$$w_j^i = tf_j^i \ log\frac{N}{df_j} \tag{1}$$

where w_j^i is the weight of a term T_j in a document Doc_i, tf_j^i is a term frequency of T_j in Doc_i, df_j is a document frequency of T_j and N is the total number of documents.

In VSM the similarity between two documents can be defined by a distance between them. The distance is generally calculated by inner product. We propose a Kullback Leibler divergence (KL divegence) to calculate the distance. KL divergence is a divergence to compare two probability distributions and is defined as below.

$$Div = \sum_{k=1}^{n} q_k \ log\frac{q_k}{q_k} \tag{2}$$

where q_k and p_k are probabilities of kth word in probability distributions of q and p. KL divergence ranges between 0 and 1 and does not become negative. If two distributions is same, KL divergence is 0. And if two distributions are different, KL divergence is 1. The document vector calculated by TF-IDF is not a probability distribution. The document vector needs to be transformed into a probability distribution with the next formula.

$$Pr(T_j^i) = \frac{w_j^i}{Z_i} \tag{3}$$
$$Z_i = \sum_j w_j^i$$

where T_j^i is jth term T_j in ith document Doc_i.

In this paper user profile, which represents user's interest, is the same vector as a document vector. As the user profile represents user's interest, it is close to the document vector of an interesting document and far from the one of an uninteresting document. Recommending documents according to user's interest, our proposing method selects documents depending on the similarity calculated between user profile and documents.

3.2 Genetic Algorithm

We make user profile using a genetic algorithm since to make the user profile is to find the vector which maximizes the similarity between a gene and interesting document vectors and minimizes the similarity between a gene and uninteresting document vectors.

Given initial genes at random. For $t = 0, \cdots, T$:
- ·Select two genes as parents.
- ·For $n = 0, \cdots, N$
  - ·Produce two child genes using UNDX.
    - $\mathbf{C}_1 = \mathbf{m} + z_1\mathbf{e}_1 + \sum_{k=2}^{n} z_k\mathbf{e}_k$
    - $\mathbf{C}_2 = \mathbf{m} - z_1\mathbf{e}_1 - \sum_{k=2}^{n} z_k\mathbf{e}_k$
    - $\mathbf{m} = \frac{(\mathbf{P}_1+\mathbf{P}_2)}{2}$
    - $z_1 \sim N(0, \sigma_1^2)$, $z_k \sim N(0, \sigma_2^2)$
    - $\sigma_1 = \alpha d_1$, $\sigma_2 = \frac{\beta d_2}{\sqrt{n}}$
    - $\mathbf{e}_1 = \frac{(\mathbf{P}_1-\mathbf{P}_2)}{|\mathbf{P}_1-\mathbf{P}_2|}$, $\mathbf{e}_i \perp e_j (i \neq j)$
- ·Select two genes as survivors from all child genes.

Figure 1: The GA algorithm.

In the genetic algorithm, a gene represents the user profile and real valued vector.

To carry out a genetic algorithm a fitness function must be defined. The fitness function is

$$F_k = \sum_{D_j \in U} Div_{D_j}^k - \sum_{D_i \in I} Div_{D_i}^k \tag{4}$$

where $Div_{D_i}^k$ is KL divergence between a document vector for D_i and kth gene, I is a set of interesting documents and U is a set of uninteresting documents. This fitness function denotes that the fitness value becomes maximum balue when a gene selects documents according to their ratings.

Our crossover is unimodal normal distribution crossover (UNDX) proposed by Ono et al [7]. The UNDX is one of crossover techniques implemented for real-coded genetic algorithms and explores a search space depending on a distribution of genes. Pseudocode for GA is shown in Fig. 1.

3.3 Independent Component Analysis

ICA is a statistical technique for revealing hidden signals from a set of observed signals. In ICA it is assumed that observed signals combines some source signals linearly and the source signals is statistically independent. This model denotes

$$X = AS \tag{5}$$

where X is the observed signals, S is the source signals and A is mixed matrix. The aim of ICA is to estimate the source signals from the only observed signals. In other words, the aim is to find a separation matrix W in Eq. (6).

$$S = WX \tag{6}$$

Table 1: The 206 documents in the experiment.

	documents	words	unique words
Task 106	64	1566	771
Task 139	142	2731	1020
Total	206	4297	1705

FastICA is proposed by Hyvärinen to estimate the separation matrix.

In this paper the observed signals are document vectors and the source signals are topics included in the documents. We assume that a document consists of some topics and each topic is statistically independent. Since a document is generally categorized by a topic according to frequency of the words in the document, this assumption is not overly restrictive. Independent components revealed from documents by ICA include some noise components since documents have the ambiguities of term usage. The document vectors is reconstructed with the topics got rid of noise components.

4 Experiment

4.1 Data

To evaluate a proposing method, we choose 206 documents from NTCIR2 test collection which consist of documents on information retrieval (task number is 106) and documents on sick house syndrome (task number is 139). Now the 206 documents are test data and we regard the documents on information retrieval as interesting documents. Test data are shown in Table 1

In each experiment a set of training samples consists of 100 documents drawn at radom from 206 documents. A set of test samples consists of 106 remaining samples.

4.2 Simulation and Result

To discuss the similarity calculated with KL divergence, we compare it with the similarity calculated with inner product. The similarity calculated with inner product is defined below.

$$sim_{ij} = doc_i \cdot doc_j \tag{7}$$

where sim_{ij} is the similarity between two documents, doc_i is a document vector of a document Doc_i and $\cdot$ denotes inner product. The fitness function is defined below.

$$F_i = \sum_{D_j \in U} Gene_i \cdot doc_j - \sum_{D_i \in I} Gene_i \cdot doc_j \tag{8}$$

where $Gene_i$ is ith gene. The parameters of GA for these two methods are shown in Table. 2

Table 2: The Parameters of GA.

Genes	Generations	Crossover
5000	50000	20

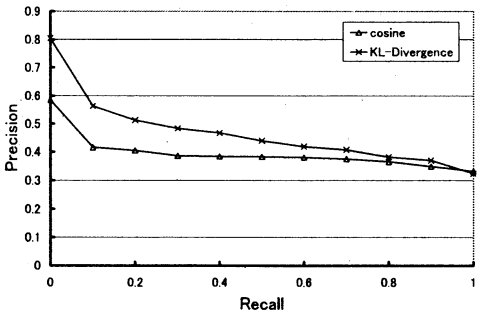


Figure 2: The interpolated precision for KL divergence fitness function and inner product fitness function.

The graph of interpolated precision for these two methods is shown in Fig. 2. Precision on every recall is the average of 10 precision of 10 experiments.

In Table 3 11-point average precision is shown. The 11-point average precision is calculated with 11 precision data on 11 recall data in Fig. 2.

We reconstruct 206 document vectors with 100 independent components (topics) to consider the effectiveness of ICA. A set of training samples consists of 100 documents drawn at radom from 206 documents and a set of test samples consists of 106 remaining samples. To make user profile GA with KL divergence function is used. This result is shown in Table 4.

4.3 Discussion

In Fig. 2 we realize that GA with KL divergence is superior to GA with inner product. So KL divergence can express the difference of user profile and a document vector correctly and select documents depending on user's interests.

In Table 3 GA with KL divergence is superior to GA with inner product, too. The difference of 11-point average precision is about 7% in Table 3. Now we carry

Table 3: The 11-point average precision.

KL divergence($\hat{\mu}_{KL-DIV}$)	cosine($\hat{\mu}_{COSINE}$)
47.0%	39.7%

Table 4: The 11-point average precision with ICA.

GA with ICA	GA
50.4%	46.8%

out test of significance to consider whether this difference is significant. In this case a null hypothesis H_0 is $\mu_{KL-DIV} = \mu_{COSINE}$ where μ_{KL-DIV} is expectation of 11-point average precision for GA with KL divergence and μ_{COSINE} is expectation of 11-point average precision for GA with inner product. First, the difference of the 11-point average precision is transformed with next formula.

$$t = \frac{\hat{\mu}_{KL-DIV} - \hat{\mu}_{COSINE}}{s\sqrt{\frac{1}{n_{KL-DIV}} + \frac{1}{n_{COSINE}}}} \quad (9)$$

where s is standard deviation of all 11-point average precisions, n_{KL-DIV} is the number of 11-point average precision for GA with KL divergence ($n_{KL-DIV} = 10$) and n_{COSINE} is the number of 11-point average precision for GA with inner product ($n_{COSINE} = 10$). In this experiment, t is 2.118. Since t is 2.101 in the level of significance of 5%, the null hypothesis H_0 is rejected. We confirm that GA with KL divergence improves the ability of selection.

In Table 4 the user profile created from document vectors reconstructed with ICA is superior to the user profile created from original document vectors. We think that the reduction of noise in document vector leads to this improvement. Since this experiment is small scale experiments, we need to discuss the effectiveness of applying ICA to documents more strictly.

5 Conclusion

In this paper we proposed extraction of user's interest by ICA and GA for information filtering. We introduced KL divergence to calculate the similarity between two documents or between user profile and a document. The GA with KL divergence fitness function was superior to GA with inner product fitness function and improves about 7% on 11-point average precision. We confirmed that the difference of 11-point average precision was significant with significance test.

We discussed the effectiveness of pre-processing for document vectors with ICA. The transformed document vectors, which are reconstructed with the documents got rid of some independent components (topics), improved the accuracy.

We will apply this proposing method to other situations and evaluate the proposing method in detail.

Acknowledgements

This study is supported by Grants-in-Aid for Scientific Research. We would like to thank MEXT for the supports.

References

[1] A. Hyvärinen, J. Karhunen and E. Oja(2001), Independent Component Analysis, Jhone Wiley-Sons, New York

[2] C. Isbell and P. Viola(1998), Restructuring Sparse High Dimensional Data for Effective Retrieval, Advances in Neural Information Processing Systems, Vol.11

[3] T. Kolenda, L. K. Hansen and T Mitchell(2000), Text Classification from Labeled and Unlabeled Documents Using EM, Machine Learning, Vol.39, No.2/3, pp.103–134

[4] J. H. Holland(1962), Outline for a Logical Theory of Adaptive Systems, Journal of the Association for Computing Machinery, vol.3, pp.297–314.

[5] B. Sheth and P. Maes(1993), Evolving Agents for Personalized Information Filtering, Proceedings of the Conference on Artificial Intelligence Application, Vol. 9, pp.345-352.

[6] G. Salton and M. McGill(1983), Introduction to Modern Information Retrieval, McGrwa-Hill Book Company, New York

[7] I. Ono and S. Kobayashi(1997), A Real-coded Genetic Algorithm for Function Optimization Using Unimodal Normal Distribution Crossover, Proceedings of 7th International Conference on Genetic Algorithms, pp.246–253

Proc. of The Ninth Int. Symp. on Artificial Life and Robotics (AROB 9th '04)
Beppu, Oita, Japan, 28-30 January, 2004

Recommendation of News Articles by Consecutive Revision with a Genetic Algorithm

Motonao Ikeda
Computer and Systems Science
Osaka Prefecture University
1-1 Gakuencho Sakai-City
Osaka 599-8531
m_i3@sig.cs.osakafu-u.ac.jp

Hidekazu Yanagimoto
Computer and Systems Science
Osaka Prefecture University
1-1 Gakuencho Sakai-City
Osaka 599-8531
hidekazu@cs.osakafu-u.ac.jp

Sigeru Omatu
Computer and Systems Science
Osaka Prefecture University
1-1 Gakuencho Sakai-City
Osaka 599-8531
omatu@cs.osakafu-u.ac.jp

Abstract

This paper proposes recommendation of news articles by consecutive revision with a genetic algorithm. Up to this time, there is a problem that a user-profile is not correctly reflected by interest of a user because in making the user-profiles the changing interest of the user and importance of past data as time goes on are not taken into account. To solve this problem, we propose to revise a user-profile consecutively by combining the previous user-profile and a new one treating the importace of past data. The effectiveness of proposing method compared to the genetic algorithm and relevance feedback is evaluated by simulations.
Keywords: genetic algorithm, information filtering system, user-profile

1 Introduction

Now personal computers are used all over the world and anybody can make use of the Internet and send information through his/her homepage. Therefore the number of computerized documents is increasing exponentially with the spread of the Internet. As a result, it is difficult to find the needed information of users, because a lot of results are returned to them and they have to spend much time to find the truly needed information. In such a circumstance, a phenomenon of information flood is seen, that the needed information is covered with much unneeded information.

To deal with this problem, many information filtering systems are proposed, which provide only information needed by the users through filtering the results. As one of such filtering methods, we have proposed a recommendation method which exstracts a user-profile(interests of a user) with a real-coded genetic algorithm. But in the recommendation method there is a problem that a user-profile is not correctly reflected by the interests of a user because in creating a user-profile the changing interest of the user and importace of past data as time goes on are not taken into account. In order to slove this problem, we propose a method to revise a user-profile consecutively by combining the previous user-profile and a new one made by articles of the day. We perform simulations with our proposing method and evaluate it by a recomendation accuracy with the genetic algorithm and relevance feedback.

2 Pre-Study

Information retrieval systems usually use vector space model(VSM)[1] to deal with documents on computer. In VSM, the user-profiles and the documents are made into vectors. And each element of the document vectors is assigned with a weight of each term appearing in the documents.

Up to now, various methods are used in order to filter information. To take examples of the algorithms, relevance feedback(RFB)[2], support vector machine(SVM)[3], genetic algorithm and the like.

Relevance feedback is usually used in order to clarify search requests of a user. It uses feedback information from the user to make his/her user-profile close to interesting document vectors and far away from uninteresting document vectors.

SVM constructs a pattern classification machine with linear classification functions and categorizes documents. It optimizes a separating hyperplane by maximizing a margin and concludes the process of optimization with solving a quadratic programming problem.

Genetic algorithm extracts user's preference by searching with genetic manipulation such as selection, crossover and mutation.[5] The feature is that it can search a solution in a broad domain efficiently.

3 Proposing Method

We have proposed a method to recommend articles for users with user-profiles made by the genetic algorithm. It makes out user-profiles by extracting users' interests from the evaluated articles.

In order to extract user's interests, it uses a real-coded genetic algorithm with a unimodal normal distribution crossover(UNDX)[4]. In this chapter, we explain the document vector. After that, we explain the pre-study with the genetic algorithm to make out a user-profile and propose a method to forget past data.

3.1 Document vector

A document vector is the vector that expresses the feature of the document by weighting for each term after morphological analysis. In order to calculate a weight of each element of document vectors, we use tfidf using the following formula.

$$w_k^i = tf_k^i \log \frac{N}{df_k} \tag{1}$$

where w_k^i means the weight of the term T_k in the document D_i, tf_k^i means the frequency of the term T_k in the document D_i, df_k means the frecuency of the documents including the term T_k and N means the number of all the documents.

Because a document vector and a user-profile are defined in VSM, it is possible to calculate a distance of them called similarity. It is defined as an inner product of a document vector and a user-profile using the following formula.

$$s = D_i \cdot U \tag{2}$$

where D_i means the ith document vector and U means the user-profile. Our method determines the recommendation of documents by plus or minus of the similarity.

3.2 Real-coded genetic algorithm

In creating user-profile, we use UNDX as the crossover of the real-coded genetic algorithm which can search a solution effectively in a function whose variables are dependent on each other.

1. Make initial vectors randomly within a domain of the value in genetic locus.
2. Choose two parents in the group randomly.
3. Applie UNDX N_c times to the parents and makes $2N_c$ children.
4. Substitute two parents with two survived children. The one child is the best gene in the parent and the other child is chosen from the child group except the best gene by a roulette sellection.
5. Repeat 2. to 4. until reaching the final generation.

After finishing the learning, the best gene becomes the user-profile.

3.3 Consecutively revised user-profile

In order to forget past data, we approach through revising a user-profile consecutively by combining a day-old user-profile and a new user-profile made by articles of the day with α which is a forgetting rate of past data. The update rule is as follows.

$$U(n+1) = \alpha U(n) + (1-\alpha)U'(n+1) \tag{3}$$

where $U(n+1)$ means $(n+1)$th user-profile, $U'(n+1)$ means a temporary user-profile made by articles on only $(n+1)$th day, $U(n)$ means nth user-profile made by articles until nth day and α means a coefficient matching the forgetting rate of past data. The domain is $0.0 \leq \alpha \leq 1.0$. By a pilot study, the coefficient α produces an excellent result within 0.4 to 0.6.

4 Simulation and Result

We perform simulations to confirm whether the recommendation accuracy by our proposing method is better than those by genetic algorithm without α and relevance feedback. All the recommendation accuracies are evened off by one user.

4.1 Environment of Simulation

We perform the simulations with 5 methods. They are a method with the real-coded genetic algorithm which doesn't forget past data(RGA1), our proposing method(RGA2), our proposing method with domain changed for each term(RGA3), a relevance feedback which doesn't forget past data(RFB1) and a relevance feedback which deals with forgetting past data(RFB2). Because RGA1, RGA2 and RGA3 use the real-coded genetic algorithm, there are small differences of the recommendation accuracy every simulation. Therefore, we use average amounts of recommendation accuracies after performing each method 5 times.

We use news articles in Yomiuri On-Line[6] on the Internet as collection data. About the data collection,

the time frame is from Jul. 21st to Aug. 2nd in 2003, and 10 articles a day are evaluated by 10 users. The articles are selected in 5 fields such as Society, Sports, International news, Politics and Economy. So, each field presents 2 articles per day and a total of 120 articles are used in the simulations.

The users read articles on each day and determine with or without interests on them, after that we compare the interests of the users with the evaluations calculated from the user-profiles and compute the recommendation accuracy. We use a correct rate to evaluate the recommendation accuracy. The formula is as followings.

$$c = \frac{n}{N} \tag{4}$$

where n is the number of articles that user's with or without interests on articles are consistent with those evaluated by a user-profile and N is the number of all articles.

Table1 shows the parameters in detail of the real-coded genetic algorithm to create user-profiles.

Table 1: The Parameters.

Population	50	Crossover	100
Generation	25000	Domain	$[-v_k, v_k]$

In Table1, v_k is a value of a domain of each.With RGA1 and RGA2 use [-3.0, 3.0]. And with RGA3, we make each domain $[-v_k, v_k]$. v_k is defined as the following formula.

$$v_k = \left| \sum_{D_i \in I} w_k^i - \sum_{D_j \in O} w_k^j \right| \tag{5}$$

where I means the group of interesting articles and O means the group of uninteresting articles. We define broad domains for important terms and narrow domains for unimportant terms. The weight of a term by the tfidf is calculated for articles and the domain of a term is calculated for each user apart.

The performance function is set as a following formula to prioritize separating interesting articles from uninteresting ones.

$$f = 10000 \times s + \sum_{D_i \in I} D_i \cdot U - \sum_{D_j \in O} D_j \cdot U \tag{6}$$

where s means the number of separating articles by a gene.

We explain update rules of a user-profile with each method. RGA1 revises user-profiles without α as follows. Forgetting past data is not taken into account.

$$U(n+1) = U(n) + U'(n+1) \tag{7}$$

RGA2 and RGA3 use the equation(3). The update rule of user-profiles with RFB1 is as following. Forgetting past data is not taken into account without α.

$$U(n+1) = U(n) + \left| \frac{1}{|I|} \sum_{D_i \in I} D_i - \frac{1}{|O|} \sum_{D_j \in O} D_j \right| \tag{8}$$

The update rule of user-profiles with RFB2 is as following. Forgetting past data is taken into account with α.

$$U(n+1) = \alpha U(n) + (1-\alpha) \left| \frac{1}{|I|} \sum_{D_i \in I} D_i - \frac{1}{|O|} \sum_{D_j \in O} D_j \right| \tag{9}$$

4.2 Simulation 1

We perform a simulation to confirm how the correct rates transit for 11 days with each method. We decide the coefficient α is 0.5 with every method. The result of this simulation is shown at Fig.1 and Table2.

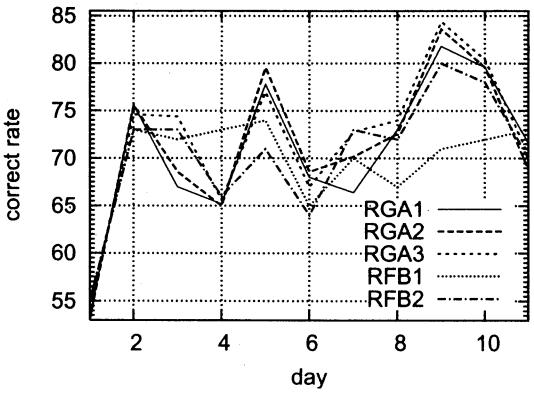


Figure 1: The transition of correct rates for 11 days.

Table 2: Average correct rate for 11 days.

	RGA1	RGA2	RGA3	RFB1	RFB2
correct rate	70.8	71.4	72.3	69.5	70.5

4.3 Simulation 2

Secondly, we calculate the average recommendation accuracy for n days with each method. In this simulation we can confirm which method averagely works out as time goes on.

1. Acquire a series of data of articles and evaluations of users for $n+1$ days.

2. Calculate average correct rates of all the users for n days and even them off by one day for each data up above.

3. Even off the values of each data up above by one data.

4. Perform 1. to 3. from n=1 to n=11.

The result of this simulation is shown at Fig.2.

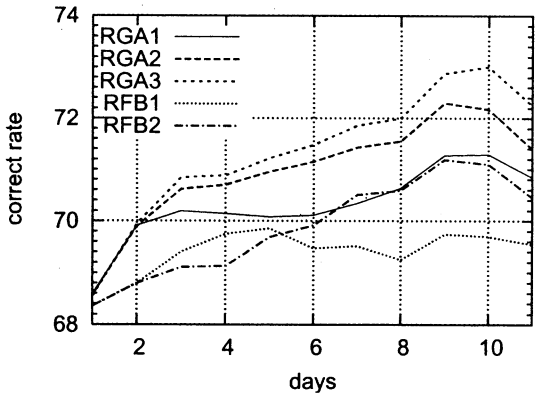


Figure 2: The transition of average correct rates.

5 Discussion

According to Fig.1 and Table.2, for 11 days proposing methods RGA2, RGA3 and RFB2 have averagely better correct rates than RGA1 and RFB1 without the coefficient α. The good tendencies are noticeable on 7th day and 9th day when every proposing methods show better results than those without α. Because the news articles on previous days are very similar to those of the current days, therefore the 3 methods significantly affected by a previous day can easily recommend the news compared to the methods without α using all the before. It should be considered that α forgetting past data is effective. On 3rd day RGA1 and RGA2 has low correct rates but RGA3, RFB1 and RFB2 keeps the correct rates. It means that it is effective to change the domains of terms for each user apart with the genetic algorithm.

According to Fig.2, each proposing method averagely advances the correct rate as time goes by until 9 days. Compared to it, RGA1 and RFB1 are flagging from 2 days to 8 days which should be considered that user-profiles of RGA1 and RFB1 can't forget past news without the coefficient α. The proposing method RGA2 and RGA3 have good result of them all and we can confirm the effectiveness.

6 Conclusion

In our research, we propose to apply rivising user-profiles with a coefficient matching user's changing interest. As the result of the simulations, we found our proposing method is more useful than previous ones with both the genetic algorithm and the relevance feedback. After this, we have a plan to perform a simulation with longtime data collection and improve the perfomance function of GA and the equation of similarity.

References

[1] G.Salton, M.J.McGill, "Introduction to Modern Information Retrieval", McGraw-Hill Book Company, 1983

[2] J.Rocchio, "Relevance feedback in information retrieval", The SMART Retrieval System *Experiments in Automatic Document Processing*,pp.313–323,1971

[3] Vapnik.V, "The Natureof Satistical Learning Theory", Springer-Verlag, 1995.

[4] I. Ono and S. Kobayashi(1997), A Real-coded Genetic Algorithm for Function Optimization Using Unimodal Normal Distribution Crossover, Proceedings of 7th International Conference on Genetic Algorithms, pp.246–253

[5] B. Sheth and P. Maes(1993), Evolving Agents for Personalized Information Filtering, Proceedings of the Conference on Artificial Intelligence Application, Vol. 9, pp.345-352.

[6] Yomiuri On-Line, http://www.yomiuri.co.jp/

Proc. of The Ninth Int. Symp. on Artificial Life and Robotics (AROB 9th '04)
Beppu, Oita, Japan, 28-30 January, 2004

The Proposal for the Way to Recommend Information with ICA

Takeru Yokoi
Computer and Systems Science
Osaka Prefecture University
1-1 Gakuencho Sakai-City
Osaka 599-8531
takeru@sig.cs.osakafu-u.ac.jp

Hidekazu Yanagimoto
Computer and Systems Science
Osaka Prefecture University
1-1 Gakuencho Sakai-City
Osaka 599-8531
hidekazu@cs.osakafu-u.ac.jp

Sigeru Omatu
Computer and Systems Science
Osaka Prefecture University
1-1 Gakuencho Sakai-City
Osaka 599-8531
omatu@cs.osakafu-u.ac.jp

Abstract

We propose an information filtering system with Independent Component Analysis(ICA). Document-word matrix is generally sparseness. It also have ambiguity of synonyms. In Addition, they are affected by noises easily because of the sparseness. To solve these problems, our proposing method transforms document vectors with components extracted by ICA. An independent component generated by ICA is considered as a topic. Concretely speaking, at first we map the document vectors into the space constructed by topics. Secondly, we create the user profile from transformed data with a genetic algorithm and relevance feedback. Finally, we recommend documents by the user profile and evaluate the accuracy by interpolated precision. We also consider the meaning of the components in this experiment.

Keywords: Independent Component Analysis, Information Filtering System, User Profile

1 Introduction

Recently an information technology has proceeded very much and a plenty of information are served by the technology such as the Internet. However, the larger amount of information become, the more difficultly we can find the information that we demand by the retrieval systems with database. Finally, the information flood that the necessary information is buried in a lot of other information has happened. To solve the problem, information retrieval systems with user's interests which select information according to user's interests have been studied. In our research, to select user's necessary information with better precision, we use ICA[1] for pre-processing to make the user profile which discribes user's interests. ICA is recently used for signal processing, image processing, and so on. With ICA for pre-processing, we get topics included in documents. Here the topic means the category where documents belong and we assume each topic is statistically independent. This assumption isn't overly restrictive because each topic has different words and importance of the words are also variant. Then we map the input data into the space constructed by the topics and make user profile in the space. Finally we recommend interesting documents with the user profile. In addition we can solve problems which synonyms causes with ICA so the accuracy of the recommendation is expected to become better.

2 Pre-Study

In an information filtering system, vector space method[2] is often used. Using this method, documents and user profile are represented as vectors. The elements of the vector are weights of the words that appear in documents. The more documents we treat, the more dimensions the vectors need. The vectors are affected by the noise easily and have ambiguity of synonyms. If there are synonyms, some documents includeing the synonyms for the keeword can't be serched.

There are some pre-study of information filtering system method. Firstly, the most popular method is relevance feedback(RFB)[3] which Rocchio proposed. This method makes user profile that becomes close to interesting document vectors and becomes far away from uninteresting document vectors. This is often used for compared method for other information filtering methods. Secondly it is reported that Support Vector Machine (SVM)[4] also left good results. SVM is often used in solving classification problem. This method constructs the hyperplane that divides sample vectors called support vector as the margin becomes maximum. Collaborative Filtering method[5] is also popular filtering method. It serves user's interesting

document selected depending on the interests of the someone familiar with the user. In fact the technique is used in e-commerce service.

As another method for preprocessing, there is Latent Semantic Analysis (LSA)[6]. LSA is the analysis way that uses singular valued decomposition. LSA removes the small singular values to cut off including noises. The process also helps to solve the synonym problems.

3 Independent Component Analysis

In this chapter we explain ICA.

3.1 Model of ICA

ICA is the method to find statistically independent signal sorces from only observed signals. In ICA the observed signals are described with the combination of some statistically independent signals. Now if the observed signal is X and some statistically independent signal is S, we get the next equation.

$$X = AS \tag{1}$$

where A is mixed matrix. The aim of ICA is to find S from X based on equation (1) . In the other word, we estimate W in the next equation.

$$S = WX \tag{2}$$

3.2 Fast ICA

In our research we used Fast ICA that found independents elements by negentropy. In the below, we introduce the algorithm of Fast ICA.

1. Centering income signal X.

$$X' = X - E[X] \tag{3}$$

2. Whitening with PCA, and Rot denotes transfered matrix.

$$\begin{aligned} E[X^T X] &= V^T D V \\ Rot &= V^T D^{\frac{1}{2}} V \qquad (4) \\ Y &= RotX \qquad (5) \end{aligned}$$

where $D^{1/2} = diag[eig^{1/2}...]$.

3. Generating the weight vector w at random, and the norm of w is 1.

4. Changing w into w' with next update rule,

$$\begin{aligned} w' &= E[Yg(w^T Y)] - E[g'(w^T Y)]w \qquad (6) \\ g(u) &= ue^{-\frac{u^2}{2}} \end{aligned}$$

5. Normalizing w'.

6. If the inner product between w' and w is close to 1, finish the calculations, and otherwise go back to 4 and modify w again.

7. If the weight vector is first one, go back to 3 and find next one. Otherwise making the vectors orthgonal from previous ones with Schmidt's orthogonal method.

8. Until getting the n weight vectors, repeating the algorithm after 3.

9. With the n weight vectors w_i, making $B = [w_1...w_n]$ and get the Z with next equation,

$$Z = BY \tag{7}$$

where Z is the independent component that we demand.

In our research income signal X is the matrix whose rows are document vectors. Z is considerd to show topics. To represent document with topics, we do next operation.

$$X" = Z^T X \tag{8}$$

This operation means to make original document vectors mapped to the space constructed by independent components which mean topics. And the mapped vectors are used in an experiment.

4 Vector Space Model

To use documents with computers, we describe document vectors in vector space method. The elements of a document vector are calculated by tf-idf method. The calculation is following next equation.

$$w_j^i = tf_j^i \cdot log\frac{N}{df_j} \tag{9}$$

where w_j^i means the weight of the word T_j in the document D_i, tf_j^i means the frequency of word T_j in the document D_i and df_j means the frecuency of the documents including the word T_j. N means the number of all documents.

5 Simulation and Result

In this chapter we mention the simulations and the results.

5.1 Environment of Simulation

The documents used in our research are 625 documents of test collection NTCIR2. These documents are concerned with the information retrieval. Table1 shows data in detail.

Table 1: The Input Data.

	all	set1	set2	set3	set4	set5
interesting	34	7	13	5	3	6
uninteresting	591	118	112	120	122	119

Now in our research document vectors consists of 1145 words. And we make user profile with them. In addition, we used cross validation to evaluate the ability in this experiment.

Here firstly the 625 documents are divided into 5 document sets. Each document set includes 125 documents. Secondly making all document sets which are three out of five samples and the other documents tests. If we make document set for all combination, we get 10 combinations of sample document set and test document sets. We test four kind of method to make user profile and compare with the results, ICA+GA, GA, ICA+RFB and RFB.

To evaluate the result we used interpolated precision. The interpolated precision is precision calculated at each recall. The flow of the simulation is,

1. Make the document vectors from the documents.
2. Carry out ICA.
3. Make experiment data with cross validation.
4. Make user profile.
5. Recommend the interesting documents with the user profile and evaluate the result by 11-point average precision.

5.2 Making User Profile with Genetic Algorithm

Here we make user profile with a genetic algorithm. Now our fitness function of the genetic algorithm is next equation,

$$f = \sum_i \alpha_i U D_i \qquad (10)$$

where α_i depends on the ratio between the number of interesting documents and the one of uninteresting documents. The crossover is two points crossover. Other parameters of the genetic algorithm are shown in Table2. The result is shown at Fig.1.

Table 2: Parameter of Genetic Algorithm.

	Generation	Cross Ratio	Mutation Ratio
GA	10000	1	0.005
ICA+GA	5000	1	0.05

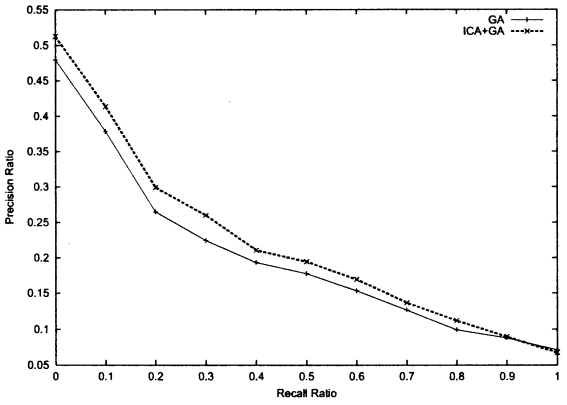


Figure 1: Imputation Precision with GA.

5.3 Making User Profile with Relevance Feed Back

We also use relevance feedback to make user profile. The formula used in our research is

$$U = a \sum_{D_i \in I} D_i + b \sum_{D_j \in J} D_j \qquad (11)$$

where I means interesting documents set and J means uninteresting documents set. The coefficients a, b are decided by the same rule as the genetic algorithm. The 11-points average precision is shown at Fig.2.

5.4 The Independent Component

Here we introduce two examples of the independent component in Table3 and Table4. Table3 is the independent component which shows a topic such as the information retrieval. For the meanwhile, Table4 is also an independent components which isn't considerd to have a sence very much.

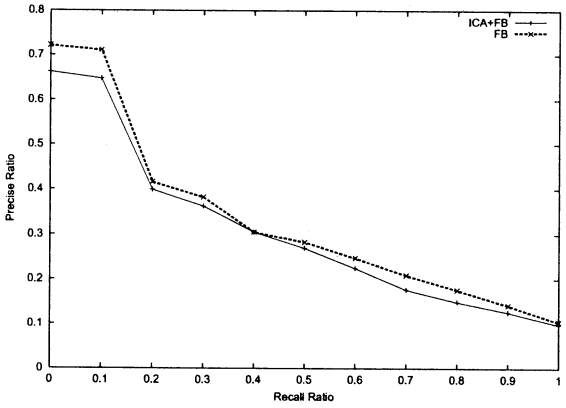


Figure 2: Imputation Precision with RFB.

6 Discussion

According to Fig.1 and Fig.2, while ICA didn't effect for relevance feedback, concerning with GA, ICA is useful to improve the accurancy of precision. Seeing the Table4, this component is considerd to be noise, because the words which have no concern with each other have similar weights. This noise component is found based on forth cumurant. Forth cumurant is defined by next formula.

$$cum = E[x^4] - 3\{E[x^2]\}^2 \qquad (12)$$

where x means independet component. The noise component has low cumurant. Here we used all independent component so didn't remove the noise very much. Therefor if we remove the noise component well, the result is expected to become better.

In addition, we confirm the independent component shows the topic included in documents. In Table3 ,the component includes some words concernd with the information retreival such as "character string search" and "relevance feedback" . So this component is supposed to mean "Information Retrieval".

Seeing Table3, the synonym problem is also solved, because the synonyms in the different documents originally such as "character string search" and "text retrieval system" get together in the same component.

7 Conclusion

In our research, we propose to use ICA for preprocessing to make user profile. At the result, we found the ICA can apply any method and for GA our proposal is especilly useful. In additon, if we remove the noise components, the result is expected to become better. We confirm that the independent component shows the topic.

Table 3: The example of Independent Component.

morphological analysis	16.90419
character string search	0.444585
morphological	0.259996
media	0.089577
relevance feedback	0.087687
multi	0.08351
content constitution	0.080829
text retrieval system	0.06526

Table 4: The noise independent Component.

score synthetic	5.941926
vector	5.860551
dynamic image	5.309139
oblique direction	5.030985
bit	4.659333
local city	4.566391
file	4.283691
television	4.251266

References

[1] Aapo Hyvārinen, Erkki Oja: Independent component analysis: A tutorial. Neural Network, Vol. 13, pp. 411–430, 2000.

[2] G.Salton, M.J.McGill, "Introduction to Modern Information Retrieval", McGraw-Hill Book Company, 1983

[3] J.Rocchio, "Relevance feedback in information retrieval" , The SMART Retrieval System *Experiments in Automatic Document Processing*,pp.313–323,1971

[4] Vapnik.V, The Natureof Satistical Learning Theory, Springer-Verlag, 1995.

[5] J.A.Konstan, B,N.Miller, D.Maltz, J.L.Herlocker, L.R.Gordon and J.Riedle, "GroupLens:Applying Collaborative Filtering to Usenet News" *Communications of the ACM*, Vol.40,No.3 pp.77–87,1997.

[6] Deerwester.S, Dumais.T, Landauer.T, Furnas.W, Harshman.A, Indexing by Latent Semantic Analysis, *Journal of the Society for Information Science* Vol.41, No.6, pp.391–497

Proc. of The Ninth Int. Symp. on Artificial Life and Robotics (AROB 9th '04)
Beppu, Oita, Japan, 28-30 January, 2004

Construction of a Classifier Using AdaBoost for Information Filtering

Hidekazu Yanagimoto
Department of Computer and Systems Sciences
Osaka Prefecture University
1-1, Gakuencho, Sakai
Osaka 599-8531, Japan

Sigeru Omatu
Department of Computer and Systems Sciences
Osaka Prefecture University
1-1, Gakuencho, Sakai
Osaka, 599-8531, Japan

(hidekazu, omatu@cs.osakafu-u.ac.jp)

Abstract

We propose an information filtering system using AdaBoost. AdaBoost is a method for improving the accuracy of any learning algorithms. This paper explains AdaBoost and a genetic algorithm which creates weak learners for AdaBoost. Finally we describe the experiments of information filtering service and discuss the effectiveness of our proposing method.
Keyword: Information Filtering, AdaBoost, genetic Algorithm

1 Introduction

Users can have access to vast store of information through the Internet recently, as the Internet becomes widespread. When they search information they desire with search engines, they get a lot of search results and hardly find ones they desire. To cope with this situation, many researchers have paid attention to developing information filtering systems. The information filtering systems automatically select information depending on user's interests (user profile). To select information correctly, the systems must keep appropriate user's interests.

In this paper, we propose that the information filtering system using AdaBoost to make appropriate interests. Since user's interest is generally complex, the user profile needs to have richly expressive power. The hypothesis learned with AdaBoost can express complex hyperplain and improve the accuracy of a classifier. To evaluate a proposing method, we discuss the effectiveness of the proposing method in the viewpoint of selection ability.

2 Previous work

The proposing system consists of an information filtering, AdaBoost and GA to create user profile. We describe related works in detail.

The information filtering system is the system which selects information depending on user's interests. A content-based filtering system[1] chooses information analyzing the content of information. The content-based filtering system generally selects texts. A social filtering system[2] is the system which selects information using the relationship between user and information creators. Since social information is used without analyzing information, the information filtering systems can be expanded to the systems which deal with non-text data. A collaborative filtering system[3] is the system which selects information depending on ratings voted by many other users. The system calculates the similarity among users and recommends information for a user which other user who has the same interests is interested in. The system is applied to text, graphical data, music and so on since the system deal with the content of information.

AdaBoost is one of ensemble learning algorithms and is proposed by Freund et al[4]. The AdaBoost combines classifiers called weak learners which are better than random classification and makes final classifier. AdaBoost solves many difficult problems in pattern recognition, machine learning and information Retrieval. Boostexter[5] is the system which classifies texts using Probabilistic TF-IDF, Sleeping-experts, Naive-Bayes and Rocchio to learn weak learners.

GA is the algorithm which simulates the biological evolution and is proposed by Holland[6]. GA is often applied to combinational optimization problems. NewT[7] is an information filtering system using GA.

3 Methodology

Our aim is to develop the content-based information filtering system using AdaBoost. We use GA to learn weak learners for AdaBoost. In this section we describe the methodology of our proposing method in detail.

3.1 Vector Space Model

In Vector Space Model (VSM) documents written with natural language is represented as vectors to deal with them on computers. The vector is called a document vector below. The element of the document vector denotes a word included in a document and is calculated by TF-IDF.

$$w_j^i = tf_j^i \ log\frac{N}{df_j} \tag{1}$$

where w_j^i is the weight of a term T_j in a document Doc_i, tf_j^i is a term frequency of T_j in Doc_i, df_j is a document frequency of T_j and N is the total number of documents.

In VSM the similarity between two documents can be defined by a distance between them. The distance is generally calculated by inner product.

$$sim_{ij} = doc_i \cdot doc_j \tag{2}$$

where sim_{ij} is the similarity between two documents, doc_i is a document vector of a document Doc_i and $\cdot$ denotes inner product.

In this paper user profile, which represents user's interest, is the same vector as a document vector. As the user profile represents user's interest, it is close to the document vector of an interesting document and far from the one of an uninteresting document. Recommending documents according to user's interest, our proposing method selects documents depending on the similarity between user profile and documents.

3.2 AdaBoost

Pseudocode for AdaBoost is shown in Fig. 1. This algorithm takes as input a training set $(x_1, y_1), \cdots, (x_m, y_m)$ where each x_i belongs to instance space X, and each label y_i belongs to label set Y. AdaBoost carries out weak or base learning algorithm repeatedly in a series of rounds $t = 1, \cdots, T$. A distribution or set of weights over the training set is decided on each round. The weight on training sample i is denoted $D_t(i)$ on round t. Initially, all weights are set equally, but the weights of incorrectly classified samples are

Given:$(x_1, y_1), \cdots, (x_m, y_m)$
where $x_i \in X$, $y_i \in Y = \{-1, +1\}$
Initialize $D_1 = \frac{1}{m}$
For $t = 0, \cdots, T$:
·Train weak learner using distribution D_t.
·Get weak hypothesis h_t:$X \rightarrow \{-1, +1\}$ with error
$\epsilon_t = Pr_{i\sim D_i}[h_t(x_i) \neq y_i]$
·Choose $\alpha_t = \frac{1}{2} ln(\frac{1-\epsilon_t}{\epsilon_t})$
·Update:

$$D_{t+1}(i) = \frac{D(i)}{Z_t} \times \begin{cases} e^{-\alpha_t} & \text{if } h_t(x_i) = y_i \\ e^{\alpha_t} & \text{if } h_t(x_i) \neq y_i \end{cases}$$

where Z_t is a normalization factor.
Output the final hypothesis:
$H(x) = sign(\sum_{t=1}^{T} \alpha_t h_t(x))$.

Figure 1: The AdaBoost algorithm.

increased so that the weak learner is forced to learn such samples in training set. In this paper the training sample x_i is a rated document vector and label y_i is a rating of the document vector.

The weak learner finds a weak hypothesis h_t for the distribution D_t. In this paper the weak hypothesis is created using a genetic algorithm. The ability of a weak hypothesis is measured by its error ϵ_t. Now we assume that the error of the weak hypothesis is less than 1/2. This assumption means that the weak hypothesis is better than random selection and is not overly restrictive.

Once the weak hypothesis h_t is created, AdaBoost calculates a parameter α_t. Intuitively, α_t measures the importance assigned to the weak hypothesis h_t. Note $\alpha_t \geq 0$ if $\epsilon_t \leq 1/2$ and that α_t is larger as ϵ_t is smaller.

The distribution D_t is updated depending on whether the training samples are classified correctly or not. This update rule is shown in Fig. 1. This rule causes that the weight of correctly classified sample is decreased and the one of misclassified sample is increased. The weights of "hard" samples are increased and the weak hypothesis focuses on such samples.

A final Hypothesis H is the weighted sum of T weak hypotheses. α_t is the weight assigned to h_t.

3.3 Genetic Algorithm

To learn weak learners for AdaBoost is to create user profile since the user profile has positive distance for interesting documents and negative distance for uninteresting documents. Now we make such user profile using a genetic algorithm. In the genetic algorithm, a gene represents the user profile and has the

Given initial genes at random. For $t = 0, \cdots, T$:
·Select two genes as parents.
·For $n = 0, \cdots, N$
·Produce two child genes using UNDX.
$\mathbf{C}_1 = \mathbf{m} + z_1\mathbf{e}_1 + \sum_{k=2}^{n} z_k\mathbf{e}_k$
$\mathbf{C}_2 = \mathbf{m} - z_1\mathbf{e}_1 - \sum_{k=2}^{n} z_k\mathbf{e}_k$
$\mathbf{m} = \frac{(\mathbf{P}_1+\mathbf{P}_2)}{2}$
$z_1 \sim N(0, \sigma_1^2)$, $z_k \sim N(0, \sigma_2^2)$
$\sigma_1 = \alpha d_1$, $\sigma_2 = \frac{\beta d_s}{\sqrt{n}}$
$\mathbf{e}_1 = \frac{(\mathbf{P}_1-\mathbf{P}_2)}{|\mathbf{P}_1-\mathbf{P}_2|}$, $\mathbf{e}_i \perp e_j (i \neq j)$
·Select two genes as survivors from all child genes.

Figure 2: The GA algorithm.

same feature as the user profile.

The fitness function is

$$F_i = \sum_{Doc_j \in C_i} D_t(j) - \sum_{Doc_k \in N_i} D_t(k) \qquad (3)$$

where F_i is a fitness value for the ith gene $Gene_i$ and $D_t(i)$ denotes the weight of ith documents Doc_i on round t. C_i and N_i are defined below.

$$\begin{aligned} C_i &= \{Doc_j | Doc_j \in I \text{ and } Gene_i \cdot doc_j \geq 0 \\ &\quad \text{or } Doc_j \in U \text{ and } Gene_i \cdot doc_j \leq 0\} \\ N_i &= \{Doc_j | Doc_j \in I \text{ and } Gene_i \cdot doc_j \leq 0 \\ &\quad \text{or } Doc_j \in U \text{ and } Gene_i \cdot doc_j \geq 0\} \end{aligned}$$

where I is a set of interesting documents and U is a set of uninteresting documents. When a gene selects documents according to their ratings, the fitness value becomes maximum value.

Our crossover is unimodal normal distribution crossover (UNDX) proposed by Ono et al [8]. The UNDX is one of crossover techniques implemented for real-coded genetic algorithms and explores a search space depending on a distribution of genes. Pseudocode for GA is shown in Fig. 2.

4 Experiment

We carry out expriments in the ability of our proposing method. We use NTCIR2 test collection as training data and test data. We compare the user profile created with the proposing method to the one created with only GA.

4.1 Data

To evaluate a proposing method, we choose 206 documents from NTCIR2 test collection which consist of documents on information retrieval (task number is 106) and documents on sick house syndrome (task number is 139). Now we regard the documents on information retrieval as interesting documents. Test data are shown in Table 1

Table 1: The 206 documents for the experiment.

	documents	words	unique words
Task 106	64	1566	771
Task 139	142	2731	1020
Total	206	4297	1705

Table 2: The Parameters of AdaBoost and GA.

	AdaBoost	GA
Genes	100	5000
Generations	100	10000
Crossover	20	20
T for AdaBoost	50	-

In each experiment a set of training samples consists of 100 documents drawn at random. A set of test samples consists of 106 remaining documents.

4.2 Simulation and Result

To evaluate a proposing method we compare it with the method using only GA. Parameters of the proposing method and comparing method are shown in Table 2.

This simulation is repeated 10 times since the genetic algorithm is a probabilistic method. Recall and Precision are used to compare abilities of two methods. Recall (R) and Precision (P) are calculated below.

$$\begin{aligned} R &= \frac{\text{Retrieved interesting documents}}{\text{All interesting documents}} \\ P &= \frac{\text{Retrieved interesting documents}}{\text{Recommended documents}} \end{aligned} \qquad (4)$$

Interpolated precision is shown in Fig. 3. The precision for each recall is an average of 10 results.

11-point average precision is shown in Table 3. The 11-point average precision is the average of 11 values of precision on 0, 0.1, $\cdots$, 1.0 of recall.

4.3 Discussion

In Fig. 3, we realize that AdaBoost is superior to GA on every values of recall. AdaBoost learns more appropriate hypothesis than GA because of the combination of weak hypotheses.

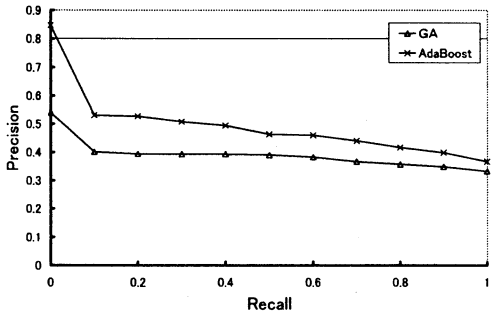


Figure 3: The interpolated precision for GA and AdaBoost.

Table 3: The 11-point average precision for AdaBoost and GA.

AdaBoost($\hat{\mu}_{Ada}$)	GA($\hat{\mu}_{GA}$)
49.6%	39.2%

In Table 3, AdaBoost improve 12% on 11-point average precision. To consider this difference of performance, we carry out test of significance. In this case a null hypothesis H_0 is $\mu_{Ada} = \mu_{GA}$ where μ_{Ada} is expectation of 11-point average precision for AdaBoost and μ_{GA} is expectation of 11-point average precision for GA. First, the difference of the 11-point average precision is transformed with next formula.

$$t = \frac{\hat{\mu}_{Ada} - \hat{\mu}_{GA}}{s\sqrt{\frac{1}{n_{Ada}} + \frac{1}{n_{GA}}}} \tag{5}$$

where s is standard deviation of all 11-point average precision, n_{Ada} is the number of 11-point average precision for AdaBoost ($n_{GA} = 10$) and n_{Ada} is the number of 11-point average precision for GA ($n_{GA} = 10$). In this experiment, t is 2.917. Since t is 2.101 in the level of significance of 5%, the null hypothesis H_0 is rejected. We confirm that the AdaBoost improves the ability of selection.

5 Conclusion

In this paper we propose construction of a classifier using AdaBoost and discuss the effectiveness. The proposing method is superior to comparative method and improves about 10% on 11-point average precision. We confirm that the difference of 11-point average precision is significant with significance test.

We will apply this proposing method to more training data and test data and evaluate the proposing method in more detail. We will discuss an algorithm for weak learners and improve the accuracy.

Acknowledgements

This study is supported by Grants-in-Aid for Scientific Research. We would like to thank MEXT for the supports.

References

[1] T. W. Malone, K. R. Grant and F. A. Turback(1987), The Information Lens: As Intelligent System for Information Sharing in Organizations, Proceedings of ACM CHI'86, pp.1–8.

[2] P. Maes(1994), Agents that Reduces Work and Information Overload, Communication of ACM, Vol. 37, No. 7, pp.30–40

[3] J. A. Konstan, B. N. Miller, D.Maltz, J. L. Herlocker, L. R. Gordon and J. Riedl(1997), GroupLens: Applying Collaborative Filtering to Usenet News, Communications of the ACM, Vol. 40, No. 3, pp.77–87.

[4] Y. Freund and R. E. Schapire(1997), A Decision-theoretic Generalization of On-line Learning and an Application to Boosting, Journal of Computer and System Sciences, Vol. 55, No.1, pp.119–139.

[5] R.E. Schapire and Y. Singer(2000), Boostexter: A Boosting-based System for Text Categorizasion, Machine Learning, Vol. 29, No.2/3, pp.135–168.

[6] J. H. Holland(1962), Outline for a Logical Theory of Adaptive Systems, Journal of the Association for Computing Machinery, vol.3, pp.297–314.

[7] B. Sheth and P. Maes(1993), Evolving Agents for Personalized Information Filtering, Proceedings of the Conference on Artificial Intelligence Application, Vol. 9, pp.345-352.

[8] I. Ono and S. Kobayashi(1997), A Real-coded Genetic Algorithm for Function Optimization Using Unimodal Normal Distribution Crossover, Proceedings of 7th International Conference on Genetic Algorithms, pp.246–253

[A]
Abe K. 347,659
Adachi S. 61
Abo F. 61
Amemiya Y. 400
An K. 37
Arai F. I-24
Arita T. 601,651
Assal S. 539

[B]
Bae H. 91
Bakri A. 148
Ban T. 295
Ban X. 107
Berry R. 160
Binder A. 45
Brooks R. 482
Browne M. 494
Bubnicki Z. 396
Bui V. 367
Buller A. 166
Byun K. 233

[C]
Cao T. 371
Cao X. 367
Casti J. I-19
Chang Y. 17
Chen R. 425
Chistaller T. 494
Cho H. 551
Choi J. 128
Choi Y. 1
Chung M. 37,610
Collins J. 111,410,414,614 618
Collins T. 618

[D]
Dao H. 367
Do T. 515
Dong L. I-24

[E]
Eaton M. 111,410,414,614 618
Endo S. 67
Endo Y. 49

[F]
Fan X. 287
Fard M. 355
Finkelstein R. 274
Freund R. 45
Friedlander D. 482
Fukuda T. I-24
Furuichi N. 671,677,682

[G]
Gofuku A. 140
Gómez G. 655
Goto R. 253
Guirnaldo S. 523

[H]
Ha T. 519
Habib M. 99,507
Han C. 21
Han L. 152
Han S. 476,637
Hart J. 160
Hashimoto H. 637
Haskett D. 410,414,614,618
Hassan A. 682
Hatanaka T. 406
Hatsugai N. 682
Hayashi E. 95
Hayashi Y. 575
Hemmi H. 166
Heo J. 33
Heo K. 233
Herrmann J. 494
Higashi K. 13
Hirasawa Ka. 211
Hirasawa Ko. 132,333
Hirayama H. 543,559
Hoang Tha. 367
Hoang Thi. 367
Hoang V. 371
Hokari S. 677
Homma N. 347
Honda H. 5
Hong S. 17
Horio K. 498
Hosaka T. 443
Hosaka Y. 593
Hoshino K. 79,83
Hotz P. 655
Hu J. 132,333
Hu R. 629
Hua X. 178,182
Hussein A. 333
Hwang C. 225

[I]
Ibrahim Z. 241,299
Ikeda M. 690
Imai J. 380
Imajo S. 380
Inooka H. 355
Inoue K. 190
Inoue Y. 468
Iravani P. I-32
Ishibuchi H. 263
Ishida Y. 57,271,547,589
Ishii S. 329,633
Ishikawa S. 29
Ishimoto Y. 677
Isokawa T. 61
Ito K. 140
Itoh T. 437
Izumi K. 523,527,531,535 539
Izumi T. 259

[J]
James D. 622
Jeong J. 229

Jin T. 216
Joachimczak M. 166
Johnson J. I-32
Joo Y. 237
Jordan N. 111
Jung D. 476,637
Jung S. 585

[K]
Kadota H. 325
Kai T. 174
Kamaya H. 659
Kameda A. 303,388
Kamimoto N. 452,456
Kamisato S. 83
Kanai A. 162
Kanemoto K. 329
Kang H. 249
Kang J. 585
Kanoh H. 283
Kashiwagi H. 41
Kashiwamura S. 303
Katai O. 202,384
Kato T. 601
Kawakami H. 384
Kawamura H. 325
Kawamura K. 274
Kawamura T. 119
Khairah N. 148
Khalid M. 241,299
Kim H. 476,637
Kim J. 225
Kim M. 33
Kim Sang-K. 115,429,433
Kim Sangju 221
Kim Su. 91
Kim T. 229
Kim Y. 91
Kimoto M. 136
Kimura H. 287,419
Kimura T. 267
Kimura Y. 406
Kinjo H. 75
Kitamura M. 452,456
Kitayama N. 207
Kitazoe T. 174
Klimenko V. 156
Ko B. 21
Kobayashi F. 170
Kobayashi M. 269
Kobayashi T. 5,13
Kobele G. 482
Kogeichi Y. 464
Kondo K. 317
Konishi M. 380
Kono M. 178,182,194
Kosaka T. 460
Kose A. 194
Kou Z. 295
Kubik T. 490,567
Kurata K. 71
Kurino R. 144
Kuroda S. 211
Kwon H. 551,585

[L]
Le M. 371
Le T. 515
Lee D. 225,229
Lee Hae. 659
Lee Ho. 237
Lee Jae. 128,221
Lee Jang-M. 216,221
Lee Jia. 61
Lee Jin. 115
Lee Jung-Ju 33
Lee Kw. 115,429,433
Lee Ky. 21
Lee Ma. 17,91,551
Lee Mu. 17
Lee Sang-He. 21
Lee Sang-Hy. 91
Lee So. 21
Lee Y. 429,433
Li D. 132
Li Y. 41
Liu J. 166
Lund H. I-1,I-7

[M]
Maeshiro T. 279
Makino T. 190
Mansfield M. 111,410,414,614
618
Maru N. 321,468
Marti P. I-1
Marui E. 245
Mashiko S. 61
Matos A. 651
Matsui N. 61
Matsukubo J. 575
Matsuno F. 140
Mayer N. 494
Mbaitiga Z. 511
Meng Q. 502
Mine Y. 198
Miyachi H. 445
Mizoguchi F. 9,198
Mokhtar N. 392
Mori H. 95
Mori K. 589
Mori T. 57
Motoyama T. 313
Murakami J. 87

[N]
Naitoh K. 440,449
Nakanishi M. 351,663
Nakashima T. 263
Nakayama K. 202
Nakayama S. 279
Nakazono K. 75
Nassiraei A. 494
Nawata T. 363
Nguyen C. 519
Nguyen Dinh-K. 519
Nguyen Dinh-T. 371
Nguyen Du. 367
Nguyen Ho. 515
Nguyen Hu. 371
Nguyen Manh. 515

Nguyen Minh-C. 519
Nguyen Minh-T. 87
Nguyen Quoc. 515
Nguyen Tha. 367,519
Nguyen Thi-K. 515
Nguyen Thi-T. 515
Nguyen Thi-Hi. 515
Nguyen Thi-Hu. 371
Nguyen Thi-M. 519
Nguyen Thi-M-H. 367
Nguyen Van-C. 371
Nguyen Van-L. 515
Nguyen Viet. 519
Niitsuma S. 186
Nishi T. 380
Nishikawa K. 452,456
Nishimura M. 633
Nishimura S. 555
Nishiyama H. 9,198
Nose Y. 539

[O]
Obayashi M. 9,198
Odo S. 79,83
Ogata T. 49,162,170,579 593,597
Ohira T. 443
Ohkawa H. 5
Ohmi T. 211
Ohnishi Koji 671,677,682
Ohnishi Kouhei 75
Ohshima M. 677
Ohuchi A. 303,325,388
Okabe H. 190
Okamoto K. 321
Okuta T. 682
Omatu S. 460,464,686,690 694,698
Omori T. 317,341
Ono O. 241,299
Oohira T. 341
Orski D. 643
Oshiro N. 71
O'Sullivan S. 410,414,614,618
Oswald M. 45
Oya M. 5,13

[P]
Palma V. I-1
Park ChangHe 25
Park ChangHy 233
Park D. 551
Park Gi. 1
Park Gu. 17
Park Jin-B. 237
Park J-H. 1
Park Jin-W. 216
Park Y. 249
Peper F. 61
Pfeifer R. I-13
Pham H. 367
Pham T. 519
Pham Van-C. 515
Pham Van-T. 367
Piaseczny W. 571

[R]
Ray T. 472
Ren F. 502
Riggle J. 482
Rim K. 128
Rizon M. 148,287
Rumchev V. 622
Rusli N. 148
Ryu K. 585

[S]
Saad P. 148
Saeki K. 123
Sagara S. 337,375
Saijo K. 140
Sakai M. 347
Sakamoto M. 190
Sakamoto Naohisa 445
Sakamoto Naoya 283
Sakira S. 148
Sano A. 267
Sapaty P. 156,274
Sasai M. 555
Sasano N. 123
Sato Y. 253
Sawai H. 571
Sekine Y. 123
Shibata K. 144,351,486,663
Shibata T. 103
Shibuya K. 337
Shimizu T. 136
Shimohara K. 53,166,202,279
Shinchi T. 174
Shiose T. 384
Sim K. 225,229,233
Stabler E. 482
Stefanski A. 166
Sugata K. 136
Sugisaka M. I-28,144,156,274 287,392,419,425 486,490,511,567 605,663
Sugiyama H. 182
Suh J. 429,433
Suzuki H. 571
Swiatek J. 291
Syam R. 527

[T]
Taira Y. 375
Takahashi Na. 388
Takahashi No. 194
Takahashi T. 269
Takamatu Y. 95
Takata H. 363
Takaya T. 325
Takeuchi H. 667
Tamaki S. 83
Tamano Y. 535
Tamura M. 337
Tan J. 29
Tanaka F. 211
Tanaka H. 563
Tanaka-Yamawaki M. 136,207,313,563
Tanev I. 53,472
Tani K. 119

Tanie	K.	103
Taniguchi	S.	190
Taylor	C.	309,482
Teranishi	M.	460
Tokunaga	K.	186
Toma	N.	67
Tomita	N.	359
Tran	D.	367
Tran	T.	367
Truong	C.	371
Tsuboi	Y.	241,299
Tu	X.	107,152
[U]		
Ueda	H.	271,547
Ueda	K.	597
Uemura	T.	174
Ueno	K.	498
Uosaki	K.	406
[V]		
Vallejo	E.	309
Vesisenaho	M.	I-7
Vo	V.	519
[W]		
Wada	Ka.	103
Wada	Ki.	132,333
Wada	M.	5,13
Wang	D.	502
Wang	J.	419
Wang	X.	605
Watanabe	K.	523,527,531,535 539
Wells	W.	647
[X]		
Xu	W.	605
[Y]		
Yamada	H.	119
Yamada	K.	67,79,83
Yamada	Y.	452,456
Yamagishi	H.	384
Yamaguchi	I.	29
Yamaguchi	K.	321
Yamaguchi	T.	531
Yamakawa	T.	498
Yamamoto	H.	245
Yamamoto	M.	303,325,388
Yamauchi	K.	317,341
Yamazaki	W.	198
Yanagimoto	H.	686,690,694,698
Yang	Z.	140
Yano	M.	359
Ye	H.	629
Yin	Y.	107
Yokoi	T.	694
Yokomichi	M.	174,178,182
Yokose	Y.	259
Yonezawa	Y.	400
Yoo	D.	37,610
Yoon	K.	25
Yoshida	T.	263
Yoshimoto	J.	329,633
Yoshimura	H.	136
Yuki	K.	486
[Z]		
Zeng	G.	107
Zhang	C.	295
Zhang	L.	502
Zhang	Y.	I-28
Zhao	H.	392
Zhuang	L.	295

SANWA INSATSU SYUPPAN Co. Ltd.
4323-22 1Takaenishi, Oita, 870-1117, Japan
Tel : 097-596-7700 Fax : 097-596-7888
E-mail : sanwa@d-sanwa.com
http://www.d-sanwa.com